American Society of Biomechanics
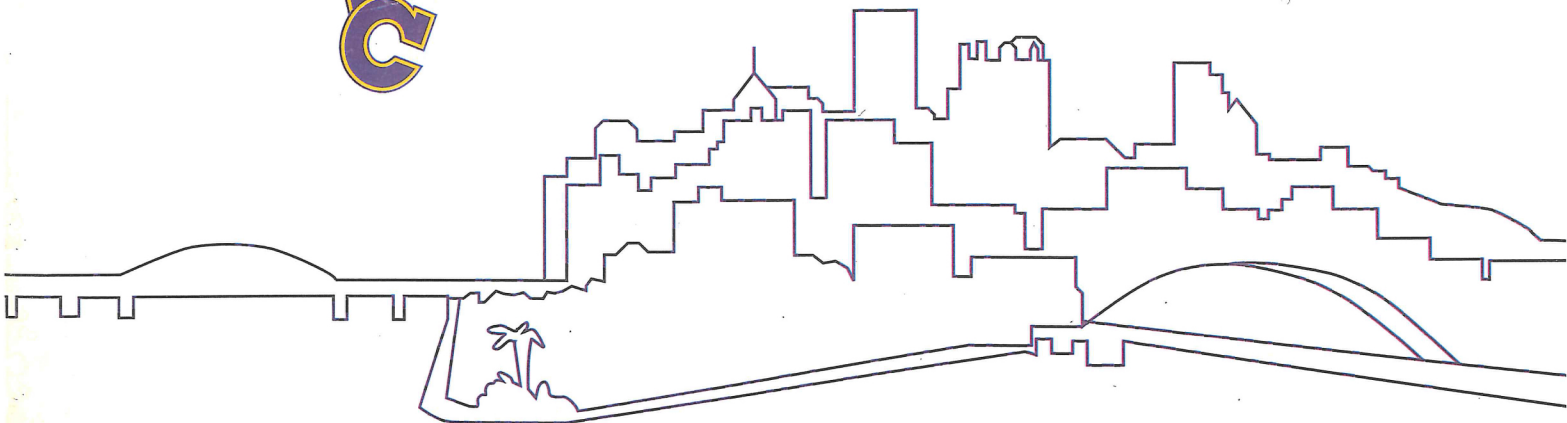
ASB founded 1977
AMERICAN SOCIETY OF BIOMECHANICS

UNIVERSITY OF PITTSBURGH
VERITAS 1787 VIRTUS

MSRC

23rd Annual Meeting
October 21-23, 1999
UPMC Health System
Pittsburgh, PA

Abstract Book

Committees

ASB Executive Board Members

R. Bruce Martin - President
Thomas S. Buchanan
Scott L. Delp
Mark D. Grabiner
Joseph E. Hale
Gerald Smith
Savio L-Y. Woo

Eadric Bressel
J.J. Trey Crisco
Lars G. Gilbertson
M. Melissa Gross
Robert Shapiro
Suzanne D. Smith

Local Organizing Committee

Savio L-Y. Woo - Co-Chair
Steven D. Abramowitch
Chris Celechovsky
Diann DeCenzo
Kenneth J. Fischer
Akihiro Kanamori
Chris A. Phillips
Jonathan Sakai
Kathryne Stabile
James H-C. Wang
Jennifer Zeminski

Lars G. Gilbertson - Co-Chair
Ezequiel Cassinelli
Richard E. Debski
Todd C. Doehring
Mary Gabriel
Colleen M. O'Hara
Theodore W. Rudy
Serena S. Chan Saw
Danyel Tarinelli
Eric K. Wong

Program Committee

Thomas S. Buchanan - Chair
J.J. Trey Crisco
Kurt Manal

Thomas A. Abelew
Richard E. Hughes
William C. Whiting

Awards Committee

Mark D. Grabiner - Chair
Bruce Beynnon
David B. Burr

Thomas J. Armstrong
Richard A. Brand
Paul DeVita

MSRC Awards Committee

Mark D. Grabiner - Chair
R. Bruce Martin

M. Melissa Gross
Y.C. Fung

Exhibitors

Aircast Foundation
Innovative Sports Training
Microstrain, Inc.
MTS Systems Corp.
Novel Electronics, Inc.
Run Technologies, Inc.

AMTI, Inc.
Kistler Instrument Corp.
Motion Analysis
Noraxon Inc.
Peak Performance Technologies Inc.
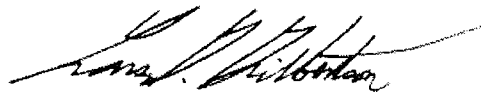Tekscan, Inc.

Welcome!

On behalf of the Local Organizing Committee, we extend to you our warmest welcome to the 23rd Annual Meeting of the American Society of Biomechanics! We have put our hearts (and elbow grease!) into the preparations for hosting this meeting, and we sincerely hope that you will find everything to your satisfaction. If there is anything we can do to make your participation in this meeting more rewarding or to make your stay in Pittsburgh more enjoyable, please let us know, and we will do our best to help you. In the meantime, we look forward to meeting new friends at this meeting and to being reunited with our many friends from meetings past.

Welcome to Pittsburgh--Let's have some fun!

Savio L-Y. Woo, Ph.D., D.Sc.
Meeting Co-Chair

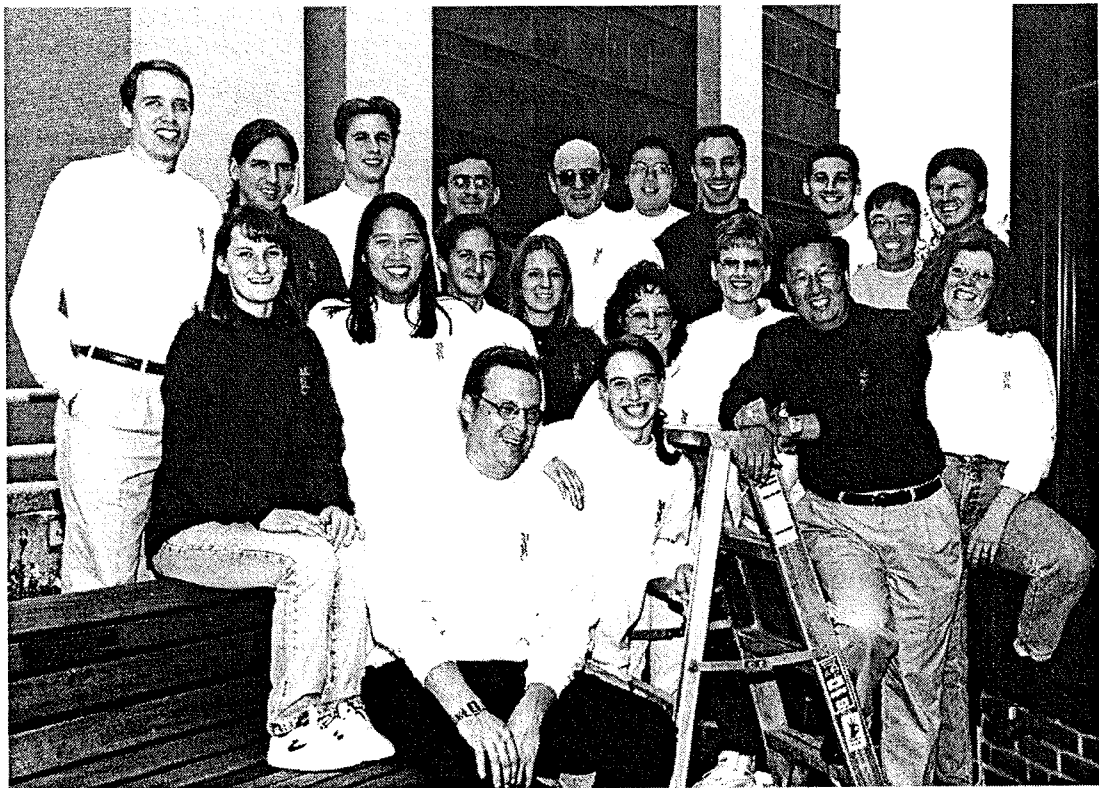Lars G. Gilbertson, Ph.D.
Meeting Co-Chair

Table of Contents

Symposia

Symposia #4: A Tribute to Thomas A. McMahon   26
Session Chair: Art Kuo

Podium Sessions

Thursday, October 21

10:15 am - 11:45 am   **Page**

Podium Session #1: Upper Extremity
Session Co-Chairs: Glenn Fleisig and Ken Fischer

Podium Session #2 Gait
Session Co-Chairs: Debra Hurwitz and Scott Lephart

Finalist, Journal of Biomechanics Award

Poster Session #1

Thursday, October 21

1:15 pm - 3:30 pm   **Page**

Clinical Biomechanics

Modeling

 # Winner, Young Scientist Pre-Doctoral Award   ** Finalist, Clinical Biomechanics Award*

Orthopaedics

Podium Sessions

Thursday, October 21

4:00 pm - 5:30 pm   Page

Podium Session #3: Motor Control
Session Co-Chairs: Mark Latash and Mark Redfern

Podium Session #4: Orthopaedics
Session Co-Chairs: Tim Norman and Patrick McMahon

Thematic Poster Presentation

Friday, October 22

8:00 am - 9:45 am   **Page**

Sport
Session Co-Chairs: Joseph Hamill and Thay Lee

* Finalist, Journal of Biomechanics Award

Podium Sessions

Friday, October 22

8:00 am - 9:45 am **Page**

Podium Session #5: Bone
Session Co-Chairs: Louis Draganich and James Wang

Friday, October 22

10:15 am - 11:45 am **Page**

Podium Session #6: Foot & Ankle Mechanics
Session Co-Chairs: Jonathan Dingwell and Jennifer Wayne

Podium Session #7: Movement
Session Co-Chairs: Rodger Kram and Michael Boninger

Podium Sessions

Saturday, October 23

10:15 am - 11:45 am   **Page**

Podium Session #8: Knee Mechanics
Session Co-Chairs: Wendy Murray and Richard Debski

Podium Session #9: Spine
Session Co-Chairs: Lars Gilbertson and Mark Miller

\# Winner, Young Scientist Post-Doctoral Award   ** Winner, Microstrain Award*

Poster Session #2

Saturday, October 23

1:15 pm - 3:30 pm	Page

Gait & Movement

Motor Control

Posture & Balance

Tissue Mechanics

Podium Sessions

Saturday, October 23

Podium Session #10: Methods/Instrumentation
Session Co-Chairs: Stephen Piazza and Douglas Adams

* Finalist, Journal of Biomechanics Award

Podium Session #11: Clinical Biomechanics
Session Co-Chairs: Kurt Manal and Glen Livesay

* Finalist, Journal of Biomechanics Award

Symposia

THE FUNCTIONAL BIOMECHANICS OF THE ANTERIOR CRUCIATE DEFICIENT KNEE

Thomas P. Andriacchi[1], Eugene J. Alexander[1], and Debra Hurwitz[2]
[1]Division of Biomechanics, Stanford University, Stanford, CA 94305-3030
[2]Department of Orthopaedic Surgery, Rush-Presbyterian-St. Luke's Medical Center,
1653 West Congress Parkway, Chicago, IL 60612

INTRODUCTION

The anterior cruciate ligament is one of the four major ligaments of the knee. It provides primary restraint to anterior displacement of the knee, as well as rotational stability (3). It is also the most frequently injured major ligament of that joint. Rupture of the anterior cruciate ligament (ACL) of the knee is a common sports injury(4).

Treatment of the ruptured anterior cruciate ligament is often complicated by the difficulty in predicting from passive physical examination of the knee which patients will be functionally impaired by the loss of this ligament and which patients will have minimal symptoms. The neuromuscular system can play an important role in providing dynamic stability through altering patterns of muscle firing during locomotion (2). Thus, a functional test that provides a measure of dynamic stability during walking or other activities would be important in assessing function in the ACL deficient knee. The purpose of this study was to develop and apply a dynamic measurement method for evaluation of dynamic anterior – posterior (AP) stability during walking. The method was applied to the study of normal subjects and patients with anterior cruciate deficient knees.

MATERIALS AND METHODS

The AP motion of the knee was measured using a point cluster method to determine the six degree of freedom motion of the femur with respect to the tibia (1). The position of the origin of the femoral coordinate system described above was used to quantify AP translation of the femur with respect to the tibial coordinate system (1). The AP displacement of the femur on the tibia during the gait cycle was quantified by the displacement of point Fp (midpoint of transepicondylar axis) (Figure 1.)
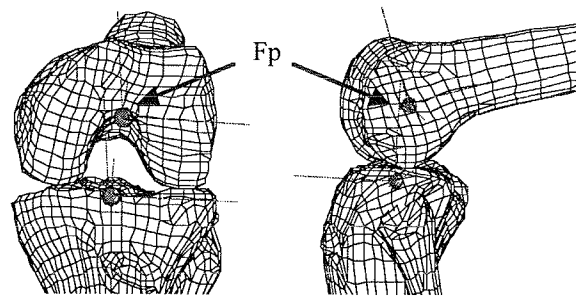
Figure 1. The location of the femoral and tibial origins used to quantify AP motion of the femur relative to the tibia.

Seven ACL-deficient knees and seven normal knees were tested in the gait laboratory. No patient had radiographic evidence of degenerative joint disease in either knee. None of the patients had developed the neuromuscular adaptations associated with a reduced the quadriceps moment during walking.

Knee kinematics (6 degrees of freedom) were measured using the previously described point-cluster method as subjects walked at self-selected speeds of slow, normal, and fast.

RESULTS

The pattern of AP movement of the femoral origin relative to the tibia had several characteristics common to all subjects. At heel strike AP_{hs} the femur is located posterior on the tibia. At mid-stance the femur moves anterior as the knee flexes and continues to move anterior as the knee extends to terminal extension (t_3). The maximum anterior position (AP_{max}) typically occurs during swing phase. The maximum AP displacement during the gait cycle was significantly greater (p<.002) for the injured group (2.2 ± 0.5cm) than for the control group (1.3 ± 0.4cm). The heel strike stance phase displacement (AP_{hs}) was also significantly greater (p<0.04) for the injured group (1.4 ± 0.4) than for the control group(1.0 ± 0.3).
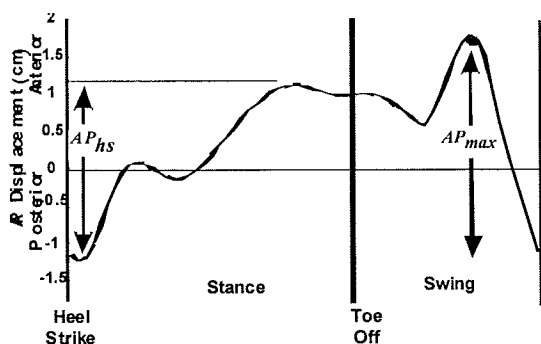
Figure 2. The curve depicts the typical characteristics of the AP motion of the femur with respect to the tibia.

DISCUSSION

The physical interpretation of the anterior-posterior position of femur with respect to the tibia provides some interesting insights into the relative tibiofemoral contact movement over the gait cycle. At heel strike the results of this study demonstrate that the femur is posterior displaced with respect to the tibia. This finding is reasonable in the context of the loads that occur at heel strike. Typically, as the foot strikes the ground there is an anteriorly directed force on the tibia at the heel. Simultaneously prior to heel strike, the quadriceps muscles are firing which will also produce an anterior force on the tibia with the knee at full extension. The swing displacement is important since it is primarily caused or controlled by muscle contraction.

These findings provide a basis for the dynamic evaluation of anterior-posterior stability of the knee joint. In addition, it points out the importance of relating knee kinematics to the particular dynamic function when attempting to describe tibiofemoral kinematics.

REFERENCES
1. Andriacchi TP, Alexander GJ, Toney MK, Dyrby CO, Sum JA: A Point Cluster Method for In Vivo Motion Analysis: Applied to a Study of Knee Kinematics. Journal of Biomechanical Engineering, 1998
2. Andriacchi, T. P., Hurwitz D., Bush-Joseph, C., Bach, B.: Clinical Implications of Functional Adaptations in Patients with ACL Deficient Knees. Sportorthopadie-Sporttraumatologie 13(3):153-160, 1997.
3. Butler, D.L., Noyes, F.R., and Grood, E.S.: Ligamentous Restraints to Anterior-Posterior Drawer in the Human Knee. J Bone Joint Surg 62A:259-270, 1980.
4. Caborn, DN and Johnson, BM: The Natural History of the Anterior Cruciate Ligament-Deficient Knee. A Review. Clin.Sports Med., 12: 625-636, 1993.

IN VIVO MEASUREMENT OF ACL STRAIN BIOMECHANICS

Braden C. Fleming, Bruce D. Beynnon

Dept of Orthopaedics & Rehabilitation
McClure Musculoskeletal Research Center
University of Vermont, Burlington VT 05405
Email: fleming@salus.med.uvm.edu   Web: www.vtmednet.org/~g136911/

Many factors have been associated with destruction of articular cartilage of the knee joint; however, only trauma such as that associated with disruption of the anterior cruciate ligament (ACL) has been shown to initiate osteoarthritis. At this time, the diagnosis, treatment, and rehabilitation of an ACL injury remain an enigma. Thus, it is important to study the function of the ACL in an effort to optimize its treatment. Over the last ten years, we have developed a technique to measure ACL strain in human subjects to resolve some of the controversies about ACL function and rehabilitation. The focus of this presentation is to review the studies where the ACL strain response has been evaluated during passive loadings (no muscle activation), under weightbearing conditions, and under a variety of muscle controlled activities commonly prescribed following ACL injury or reconstruction.

Participants in these studies have been volunteers with normal ACLs who were undergoing diagnostic arthroscopy under local anesthesia. This permitted subjects full control of their musculature. All subjects had normal knees with no history of knee ligament trauma. After the surgical procedure was complete, a Differential Variable Reluctance Transducer (DVRT) was implanted on the anteromedial band of the ACL to measure it's displacement pattern and calculate strain behavior [1,2,4].

ACL strain was determined during various passive loading conditions: passive flexion-extension motion of the knee (PFE) [2], and under anterior-posterior directed shear loads [2,3], internal-external torques [6,10], and varus-valgus moments [10] applied externally to the tibia relative to the femur. It has been argued that the ACL is a restraint to all of these loading conditions. Our findings suggest that the ACL remains unstrained during PFE as the knee is extended from 90° to 10° with the thigh horizontal. This result was expected since the gravity vector contains a posteriorly directed component throughout most of this range of knee motion. PFE from 10° to full extension increased ACL strain. Anterior directed shear loading produced strain values that were greater when the knee was at 30° when compared to 90° [2,3]. These data verify that the ACL is a primary restraint to anterior tibial translation and explain the increased sensitivity of the Lachman test compared to the drawer test in detecting ACL injuries. We determined that significant ACL strains were produced with the application of internal torques but not external torques while neither varus nor valgus moments strained the ACL with the knee at 20° of flexion [10]. These data question the percieved role of the ACL in resisting these latter loads.

Knee joint stability is maintained by a force balance between the ligaments, muscles, articular contact, and body weight: therefore it is also important to study the ACL during weightbearing conditions [6,10]. Application of

bodyweight requires the activation of the leg musculature to maintain equilibrium in a flexed knee. Previous investigations have reported that weightbearing provides a protective mechanism to the ACL or ACL graft since the articulating condyles are forced together and muscle co-contraction is utilized. We found a significant increase in ACL strain with the application of the compressive load produced by bodyweight as compared to the unweighted condition with the knee at 30° and 20° of flexion. These findings suggest that the quadriceps muscles are dominant in maintaining equilibrium and have important clinical ramifications in the use and development of rehabilitation protocols following ACL injury or ACL reconstruction.

We have also evaluated the effects of muscle activation during commonly prescribed rehabilitation activities on ACL strain [5,7,8,9]. These exercises included quadriceps dominated activities, hamstrings dominated activities, and exercises that involved co-contraction of the quadriceps and hamstrings with and without weight bearing. Exercises that produced low strain values were dominated by the hamstrings muscle group, incorporated contraction of the quadriceps muscles with the knee flexed at 60° or more, or involved simultaneous quadriceps and hamstrings contraction. Quadriceps dominated activities with the knee between 50° and full extension produced higher strains. We recently determined that the maximum ACL strain values produced during squatting; a closed-kinetic-chain exercise, were similar to those produced during active extension of the knee; an open-kinetic-chain exercise [7]. The similarity of ACL strain response during these two common rehabilitation exercises calls into question whether or not we should consider exercises to be either safe or unsafe for an ACL graft based on the commonly

used closed- and open-kinetic-chain terminology. In addition, we determined that the ACL strains produced by squatting were unaltered with the application of elastic resistance (the Sport Cord) designed to increase the muscle activity about the knee. This finding demonstrates that increasing resistance in an effort to strengthen the leg muscles during the squat exercise does not produce a significant increase in ACL strain values. This is in contrast to our earlier investigations that revealed increasing resistance during open-kinetic-chain, active flexion-extension of the leg created a significant increase in ACL strain values [5].

A method has been developed to investigate the contribution of the ACL in knee joint function. Although these measurements have been performed on subjects with normal ACLs, these data provide useful insight into the effect that various forces have on a properly positioned ACL graft. Thus, these data have been helpful in designing prospective randomized clinical studies evaluating the effects of different rehabilitation programs on graft healing.

REFERENCES

1) Howe et al: *Arthroscopy* 6:198, 1990; 2) Beynnon et al: *Int Orthop* 16:1, 1992; 3) Fleming et al: *J Biomech* 26:51, 1993; 4) Fleming et al: *J Orthop Res* 12:789, 1994; 5) Beynnon et al: *Am J Sports Med* 23:24, 1995; 6) Beynnon et al: *Am J Sports Med* 25:353, 1997; 7) Beynnon et al: *Am J Sports Med* 25:823, 1997; 8) Fleming et al: *Am J Sports Med* 26:109, 1998; 9) Fleming et al: *Arthroscopy* 15:185, 1999; 10) Fleming et al: *Proc of the ASB*, 1999.

ACKNOWLEDGEMENTS

ROLE OF NEUROMUSCULAR CONTROL IN FEMALE ACL INJURIES

Scott M. Lephart, Susan L. Rozzi, C. Buz Swanik, Brian L. Riemann, Freddie H. Fu
Neuromuscular SportsMedicine Research Laboratory, Musculoskeletal Research Center,
Department of Orthopaedic Surgery, University of Pittsburgh
Email: lephart+@pitt.edu

INTRODUCTION

The incidence of non-contact anterior cruciate ligament (ACL) injuries in females has attracted attention to the dynamic restraint mechanism and its role in protecting capsuloligamentous structures from excessive joint loads (Ireland, 1997). The capacity of the dynamic restraint mechanism is dictated by several neuromuscular characteristics including proprioception, preparatory and reactive muscle activation, muscle stiffness, muscle force production and flexibility (Beard, 1993, Branch, 1989, McNair 1992, Wojtys, E., Huston, 1994). There is also reason to believe that an interaction between factors such as joint laxity and fatigue may alter the neuromuscular system and influence the dynamic restraint mechanism. However, little objective data exists to support that any of the proposed mechanisms definitively influences ACL injuries in the female. The purpose of our series of studies was to develop a neuromuscular profile of these characteristics in healthy and pathologic joints of both female and male athletes in an attempt to identifying aberrations of the dynamic restraint mechanism that preclude joint stability. Once the roles of these neuromuscular characteristics are defined relative to joint stability, appropriate intervention programs can be initiated for the prophylaxis, and reconditioning of a pathological joint.

PROCEDURES

Four groups were studied and included: 17 healthy female (mean age $18.9 \pm .9$ years) and 17 healthy male (mean age 20.4 ± 1.7 years) intercollegiate basketball and soccer players; 12 functionally stable ACL deficient female athletes (ACLD) (mean age $= 25.2 \pm 7.3$ years) and 12 control females (mean age $= 22.7 \pm 4.0$ years). The neuromuscular profile included assessment of kinesthesia and joint position sense using a specially designed proprioception testing devise; anterior knee joint laxity assessed by KT-1000; electromyographic (EMG) activity of the hamstrings, gastrochnemious, and quadriceps during functional landing and hopping tasks and during gait, as well as EMG recorded latencies in response to sudden joint perturbation; active hamstring muscle stiffness by modeling the lower extremity after single degree of freedom mass spring system; isometric and isokinetic peak torque and time to peak torque; and hamstring flexibility. The group of healthy female and male athletes were subjected to a fatigue protocol that included three bouts of knee flexion and extension isokinetic exercise until which time that 3 consecutive repetitions fell below 25% of the knee extensor peak torque.

RESULTS

Significant ($p<0.05$) mean differences between the healthy female and male athletes were revealed for anterior knee joint laxity (females 6.05 ± 1.46; males $4.80 \pm$

1.53); proprioception testing during kinesthesia assessment of knee extension (female 2.95°± 1.4, males 2.11° ± .63); peak lateral hamstring EMG during landing (female 156.0 ± 72.6, male 84.8 ± 43.4), and area of lateral hamstring EMG (female 10.8 ± 8.3, male 2.8 ± 2.6) during landing. Muscular fatigue resulted in significant (p<0.05) delays in kinesthesia and onset time for the medial hamstings and lateral gastrochnemius in both the male and female groups. Fatigue also resulted in significant increases in the area of EMG activity in the vastus medialis and vastus lateralis of both groups. There were not significant between group differences. The ACLD females exhibited significantly (p<0.05) increased area of preparatory muscle activity in the lateral hamstring prior to landing and lower hamstring muscle stiffness. The ACLD group also demonstrated greater flexion peak torque and torque at .2 seconds for isometric and isokinetic knee flexion when compared to controls (p<0.05). In addition, less time was required to attain peak torque in knee flexion and ACLD females had significantly less hamstring flexibility. No significant differences were identified in the area of reactive muscle activity during landing or the onset time of reflexive muscle activity after joint perturbation.

DISCUSSION

These studies demonstrate that female athletes participating in high-risk sports for ACL injuries inherently possess excessive laxity and diminished proprioceptive qualities compared to matched male athletes. Additionally, these results suggest that the females possess dynamic characteristics that are different than males in an attempt to stabilize the knee during functional activities. Following injury these adaptations appear to be heightened in the absence of mechanical stability. The significant increase in preparatory activity of the lateral hamstring suggests that ACLD females use feed-forward processing to preprogram muscle activation strategies. Isometric and isokinetic strength results suggest that ACLD subjects possess adaptations to the hamstring muscle group that permit them to produce greater force, in a shorter period of time, therefore increasing dynamic restraint. While we continue to hypothesize that there may be a gender by fatigue interaction related to the incidence of ACL injury these studies did not demonstrate that fatigue had a selective effect by gender. However, since the female athletes appear to be more reliant on dynamic mechanisms for stability during functional activities the effects of fatigue may be more pronounced than in the males. The role of fatigue related to neuromuscular mechanisms of joint stability warrants further investigation.

REFERENCES

Beard, D.J. et al. (1993). *J. Bone Joint Surg.* **75-B**, 311-315.

Branch,et al. (1989). *Am. J. Sports Med.* **17**, 35-41.

Ireland, M.L.,et al. (1997). *J. Sports Rehabil.* **6**, 97-110.

McNair, P.J. et al. (1992). *Clin. Biomechanics*, **7**, 131-172.

Wojtys, E., Huston, L. (1994). *Am. J. Sports Med.* **22**:89-104.

EFFECTS OF VASTUS MEDIALIS STRENGTH VARIATION
ON THE PATELLOFEMORAL JOINT BIOMECHANICS

Thay Q. Lee, Matthew D. Sandusky, Arshya Adeli, Patrick J. McMahon

Orthopaedic Biomechanics Laboratory
Comprehensive Rehabilitation Service, VA Medical Center, Long Beach, California
Department of Orthopaedic Surgery, University of California, Irvine, Orange, California
Email: tqlee@med.va.gov

INTRODUCTION

The etiology of patellofemoral disorders, a common knee problem, has been attributed to excessive stresses associated with abnormal patellofemoral joint mechanics and patellofemoral contact pressures. Selective strengthening of the Vastus Medialis (VM) muscle is a form of conservative treatment utilized to address some of these problems. The objective of this study was to examine the effects of varying VM strength on patellofemoral joint kinematics, contact pressures and areas at different knee flexion angles.

METHODS

Five fresh-frozen cadaveric knees were used, dissected free of all soft tissue except the joint capsule and quadriceps mechanism. All knees were mounted and tested on a custom knee jig which allows variation of the knee flexion angle tibial rotation with 5 degrees of freedom (3 translational and 2 rotational). Anatomically based loading of the quadriceps was utilized (1). In the 100% VM condition the muscles were loaded as follows: Vastus Medialis 67N, Vastus Lateralis (VL)) 98N, Rectus Femoris/Vastus Intermedius (RF/VI) 111N, Iliotibial Band (ITB) 27N. Subsequent VM conditions were taken as a percentage of the force used on VM at the 100% VM condition (0%, 50%, 75%, 125%, and 150%) while keeping the forces on the VL, RF/VI, and ITB constant.

Contact area and pressure were measured using pre-scale pressure sensitive Fuji film (super-low). Patellofemoral kinematics were measured using a Flock of Birds system, which provided three-dimensional motion tracking of the patella relative to the femoral epicondylar axis (2). Data was collected at 0, 30, 60, and 90° of knee flexion. All results were compared to the 100%VM condition using multivariate ANOVA.

RESULTS

For patellofemoral contact pressures, an increase of 50% or a decrease of 100% in VM strength resulted in a statistically significant ($p<0.05$) increase in pressure when all knee flexion angles were grouped together (Figure 1). When looking at the 5% peak pressure significance was shown only when the VM strength was decreased by 100% and the knee flexions were grouped together. There was no statistical significant differences shown in the patellofemoral contact areas ($p>0.8$). The patellar medial to lateral translation showed significance at 0% VM for 0°, 30°, 60°, and 90° of knee flexion and when all knee flexions were grouped together (overall), at 50% VM for 0° and overall, at 150% VM for 30° and 60° of knee flexion (Figure 2). The anterior translation showed significance at 0% VM for 30°, 60°, and overall, at 50% VM and 150% VM for 60° of knee flexion. There was no significance for anterior translation at 0° or 90° of knee flexion. The superior

translation showed significance at 0% VM for 0°, 60°, and overall, at 50% VM for overall, at 150% VM for 30° and overall, and at 75% VM for 30° of knee flexion. There was no significance in superior translation at 90° of knee flexion.

DISCUSSION

The findings from this study showed that statistically significant changes in patellofemoral contact pressures can only be achieved by decreasing the force on the VM by 100% or increasing by 50%. The peak patellofemoral contact pressures required a complete removal of the VM force as in VM paralysis to show a statistical difference from 100% VM condition. The results also indicate that an increase or decrease in VM force of 50% is required to statistically change patellar kinematics (medial, anterior, or superior). The kinematic data was influenced by knee flexion angle, for example when looking at anterior to posterior translation no significance was seen at the 0° or 90°, but there was significance at 30° and 60° for 0%VM.

Clinically, isolated strengthening of the Vastus Medialis is prescribed in conjunction with Iliotibial band stretching and patellar mobilizations, focusing on stretching the lateral retincaculum, for the treatment of anterior knee pain. This study did not show significant changes in patellofemoral joint biomechanics with an increase or decrease of 25% in the VM strength, a minimum of 50% change in the VM strength was required to significantly alter the patellofemoral joint contact pressures and kinematics.

Total Contact Pressure
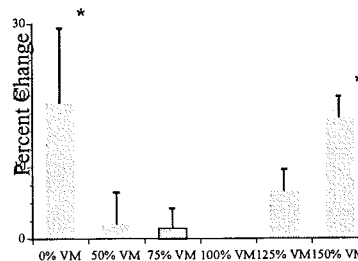
Figure 1: Histogram showing patellofemoral contact pressures with respect to % VM strength.

Medial Patellar Translation
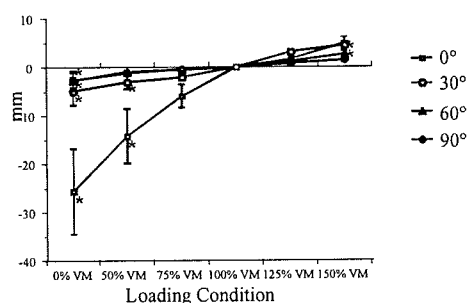
Figure 2: Graph showing medial patellar translation with respect to % VM strength.

REFERENCES

1. Powers, CM, Lilley, JC and Lee, TQ: The Effect of Axial and Multi-plane Loading of the Extensor Mechanism on the Patellofemoral Joint. Clin Biomech. 13: 608-615, 1998.
2. Glaser, FE, Gorab, RS and Lee, TQ: Edge Loading of the Patellar Component in TKA. J. Arthoplasty. 14(4): 493-499, 1999.

ACKNOWLEDGEMENTS

MALE-FEMALE BIOMECHANICAL DIFFERENCES IN SELECTED CUTTING AND LANDING MANEUVERS: RELATIONSHIP TO INJURY

Robert Shapiro

Biodynamics Laboratory, University of Kentucky, Lexington, Kentucky
Email: rshap01@pop.uky.edu   Web: http://home.image.uky.edu/biodynamics

INTRODUCTION

It has been documented that female athletes are at a higher risk of anterior cruciate ligament (ACL) injury than their male counterparts (Arendt & Dick, 1995). The mechanisms for these injuries are typically non-contact and often associated with rapid decelerations, as observed in landing from a jump or changes in directions associated with cutting maneuvers. A number of factors have been hypothesized as being linked to this increased risk including mechanical factors related to performance (Arendt & Dick, 1995). Given the high injury rate in the female athlete, it is important to evaluate potential factors that may suggest why this difference occurs. In a recently reported investigation, no kinematic differences between genders during straight line running and sidestep cutting were observed (McClean et al., 1999). However, it would appear that leg loading patterns and muscle function during the plant phase of the cut or during landing would also be of interest. Therefore, the purpose of these studies was to compare biomechanical parameters from male and female athletes executing cutting and landing maneuvers in an effort to see if any potential observed differences could be linked to ACL injury occurrence.

PROCEDURES

This presentation will review preliminary results from three studies in our laboratory. Consent was obtained from all subjects.

1) 18 female and 16 male collegiate basketball and soccer athletes executed 45° and 90° sidestep cuts (Shapiro et al., 1999; Chandler et al., 1999). Ground reaction forces (grf) and EMG output from the gastrocnemius, rectus femoris, semimembranosus, and gluteus medius muscles were measured. Comparisons of peak forces, loading rate, duration of force application, muscle onset, muscle offset and duration of muscle activity were made between groups. Approach velocity was not controlled.

2) 10 female and 9 male collegiate soccer athletes were taught a 180° degree cutting maneuver (Ford, 1997). The kinematics of the plant leg were determined from 3-d video. Vertical grf was measured for the plant leg. Muscle activity was monitored in the plant leg from the following muscles: vastus medialis, rectus femoris, vastus lateralis, biceps femoris, semimembranosus, gastrocnemius, tibialis anterior and gluteus medius. In addition, hip range of motion, playing experience and training were evaluated. Approach velocity was not controlled.

3) 10 female and 10 male high school basketball athletes executed landings from two different heights. One leg and two leg landings were evaluated. Lower leg kinematics and kinetics were evaluated utilizing 3-d videography. Grf and muscle activity from the external oblique (on the non-dominant side), rectus femoris, vastus lateralis, vastus medialis, medial hamstring, lateral

hamstring, medial gastrocnemius, lateral gastrocnemius, and tibialis anterior muscles were also measured. Ankle, knee and hip kinematics, and kinetics were compared by landing height and gender. Muscle onset and duration times were also compared.

RESULTS AND DISCUSSION

Several significant differences were observed when subjects executed the 90° cut. Males consistently produced a lower peak vertical grf and a lower loading rate. The females generated greater breaking and propulsive forces and higher loading rates than the males. There were no observed differences in the 45° cut in relation to grf. With respect to muscle activity, no differences were observed at either angle for onset times. However, at both 45° and 90° males demonstrated longer activity in the gluteus medius. At 90° they also demonstrated longer gastrocnemius activity. The combination of longer muscle activation times which may contribute to stability and the lower forces combined with lower loading rates may contribute to the lower rate of injury seen in male athletes.

In the 180° cut, no gender differences were observed in plant leg kinematics or muscle recruitment patterns as determined from onset times. This agrees with the results recently reported by McClean et al. (1999). Vertical ground reaction forces were significantly greater for the males with time to peak force being shorter for them as well. Significant differences were noted when the subjects were divided into two groups based on hip range of motion. The group with greater ROM landed in a more extended position at the knee and did not demonstrate as much knee flexion during the plant phase. These subjects all had comparable training and experience.

In examining the landings, no significant difference was observed in knee flexion at impact. All subjects tended to strike the ground at or near full leg extension at the knee. Females did tend to land in greater hip flexion and had a greater range of motion at the hip. Small differences were also observed in ankle kinematics. No significant muscle activity differences were observed. Males did generate greater peak vgrf, however, this may be a function of the height they landed from. These heights were adjusted for leg length.

SUMMARY

Results of these investigations do not provide support for the hypothesis that there are significant differences in deceleration mechanics between males and females. While some differences do exist they are not currently sufficient to explain the rate of injury. It appears that other factors such as experience or training may still provide the key to determining the observed difference in injury rates.

REFERENCES

Arendt, E. and Dick, R. (1995). *Am J Sports Med.* **23(6)**: 694-701.
Chandler, T.J. et al. (1999). *Med & Sci Spts Ex,* **31(3) supplement:**1381
Ford, K.R. (1997). Unpublished master's thesis, University of Kentucky.
McClean et al. (1999). *Med & Sci Spts Ex,* **31(7)**, 959-968
Shapiro, R. et al. (1999). *Med & Sci Spts Ex,* **31(3) supplement:**1380

ACKNOWLEDGMENTS

WHAT DOES THE NERVOUS SYSTEM KNOW ABOUT MECHANICS?

What internal mechanical states does the nervous system monitor in structural soft tissues?
Peter Grigg Ph.D.

Dr. Grigg will describe experiments in which mechanoreceptors in non-contractile soft tissues - like joint capsule and skin - are studied in relation to local tissue stresses and strains.

Does the nervous system know the internal structure of muscle?
Art English Ph.D.

Dr. English will review anatomical and developmental studies of the origins and central neural representations of muscle compartments, which are naturally occurring divisions of skeletal muscles.

What use is made by the nervous system of information about limb mechanical states?
Zev Rymer M.D., Ph.D.

Dr. Rymer will review the ways in which muscle sensory input is used by the CNS for the control of posture and movement, including proprioception, effort calibration, reflex action and force control.

The role of CNS internal models of body mechanics in sensorimotor control
Art Kuo Ph.D.

Dr. Kuo will review the roles of internal models in sensorimotor control, including the dynamics of all elements between the outgoing motor command and the resulting afferent return information. A great deal of evidence suggests that motor control requires knowledge about the dynamics of the body and muscles. The central nervous system appears to be aware of kinematic and task constraints on motion, dynamical constraints imposed by limb masses and inertial properties, and physiological constraints such as maximal muscle force. Another aspect of control is the use of sensors to determine the orientation of the limbs. Although mechanical sensors are often designed so that their internal dynamics are well separated from the dynamics of overall motion, biological sensors often tend to be much slower. Biological sensors are also usually subject to noise. The processing of sensory information from many sources must certainly account for the dynamics of the sensors, and ideally their noise levels as well. We will show evidence suggesting that the CNS adjusts its weighting of sensors based on both of these factors.

MICRO-MECHANICS OF THE BIOPROSTHETIC AORTIC HEART VALVE CUSP: EFFECTS OF CHEMICAL FIXATION AND FATIGUE

Michael S. Sacks

Department of Bioengineering, University of Pittsburgh, Pittsburgh, PA
email: msacks@engrng.pitt.edu
web: http://www.engrng.pitt.edu/~wwwbiotc/faculty/sacks.html

Billiar and Sacks, for the first time, generated biaxial mechanical data necessary for constitutive modelling of the bioprosthetic heart valve (BHV) cusp (1, 2). Similar to the natural cusps under biaxial load, the BHV cusp demonstrated complex, highly anisotropic behaviour. However, glutaraldehyde-fixation produced a more gradual stress-strain response (1). Billiar and Sacks subsequently developed a structural constitutive model to separate the effects of changes in fiber alignment from those due to changes in the properties of the collagen fibers themselves. The model predicted that glutaraldehyde fixation increases the effective collagen fiber stiffness (2).

Effects of Fatigue

Structural

Studies have examined the structural/mechanical changes that occur with fatigue of TSPV valve tissue. Sacks and Smith used SALS (Small Angle Light Scattering) to quantitatively assess the changes in collagen fiber architecture (e.g. fiber alignment and orientation) following 0–500 million in vitro accelerated test cycles. They demonstrated that the gross collagen fiber architecture remains largely unchanged during long-term cyclic loading (5). Histological analyses demonstrated that long-term cyclic loading is associated with progressive collagen fiber debonding and layer delamination (4, 5). The fact that major gross fiber damage is not observed raises the possibility that fatigue-induced damage occurs at the molecular level. This hypothesis was supported by a subsequent study by Vyavahare et. al. which demonstrated progressive fatigue-induced alterations in the molecular structure of type I collagen as assessed by Fourier transform IR spectroscopy (FTIR). Specifically, FTIR results suggested a progressive collagen denaturation: loss of the native triple helical structure of the molecule (6).

Mechanical

Sacks et. al. performed biaxial mechanical tests on valve tissue following 0–200 million in vitro accelerated test cycles. With increasing test cycles, they observed a decreasing radial extensibility (decreased ~15% by 200 million cycles) while circumferential extensibility was unchanged (4). When the structural model was applied to elucidate the cause of this unique mechanical behaviour, it was predicted that the effective fiber stiffness was significantly higher than the non-fatigued specimens. In addition, both cuspal directions demonstrated a substantial drop in ultimate tensile strength (UTS, tension at failure) following long-term cyclic loading. After 200 million cycles, UTS decreased by ~50% in the circumferential specimens and by ~33% in the radial specimens, suggesting that fatigued collagen fibers become more prone to failure. Overall, these mechanical results imply that long-term cyclic loading produces modest stiffening of the collagen, and that the in-plane tensile properties do

not drastically change with cyclic fatigue
(4).

Since cuspal flexure is implicated in valve failure, subsequent studies have investigated the bending properties of valve tissue using a custom-built three-point bending apparatus (3). Circumferential and radial strips of cuspal tissue were removed and bending tests were performed with and against the natural curvature of the cusp to simulate in vivo cuspal flexure. Since the collagen fibers are preferentially oriented along the circumferential direction, the bending stiffness of the valve is higher than compared to the radial direction. Furthermore, differences in bending properties with and against curvature occur as a direct result of the tri-layer structure of the aortic valve cusp. When the specimen is bent *against* the cuspal curvature, the fibrosa is stretched while the ventricularis is compressed. Conversely, when the specimen is bent *with* the natural curvature, it is the ventricularis that is stretched while the fibrosa is compressed.

To study the effects of fatigue on bending behaviour, Gloeckner et al. tested specimens taken from valves fatigued from 0–200 million in vitro test cycles. They observed a decrease in bending stiffness in both the radial and circumferential direction with increased cyclic loading. The greatest loss in stiffness was exhibited by circumferential strips bent against their natural curvature (bending stiffness index decreased ~80%), suggesting that the fibrosa experienced the greatest reduction in bending stiffness (3). Thus, in addition to representing the natural in vivo mechanics of the valve cusp, bending tests are also highly sensitive indicators of alterations that occur with long-term cyclic loading.

References

1. Billiar, K. L., and M. S. Sacks. Biaxial mechanical properties of the natural and glutaraldehyde treated aortic valve cusp: Part I experimental results. *Journal of Biomechanical Engineering* in press, 1999.
2. Billiar, K. L., and M. S. Sacks. Biaxial mechanical properties of the natural and glutaraldehyde treated aortic valve cusp: part II. A structurally guided constitutive model. *Journal of Biomechanical Engineering* submitted, 1999.
3. Gloeckner, D. C., K. L. Billiar, and M. S. Sacks. Effects of mechanical fatigue on the bending properties of the porcine bioprosthetic heart valve. *ASAIO Journal* 45: 59-63, 1999.
4. Sacks, M. S., K. L. Billiar, and F. J. Schoen. Effects of fatigue on the mechanical properties of the porcine bioprosthetic heart valve. *Journal of Biomedical Engineering*, submitted.
5. Sacks, M. S., and D. B. Smith. Effects of accelerated testing on porcine bioprosthetic heart valve architecture. *Biomaterials* 19: 1027-1036, 1998.
6. Vyavahare, N., M. Ogle, F. J. Schoen, R. Zand, D. C. Gloeckner, M. S. Sacks, and R. J. Levy. Mechanisms of bioprosthetic heart valve failure: Fatigue causes collagen denaturation and glycosaminoglycan loss. *Journal of Biomedical Materials Research* 46: 44-50, 1999.

BIOMECHANICS OF ABDOMINAL AORTIC ANEURYSM

David A. Vorp, M.L. Raghavan, and David H-J Wang
Departments of Surgery, Bioengineering, and Mechanical Engineering
University of Pittsburgh, Pittsburgh, PA
Email: VorpDA@msx.upmc.edu   Web: http://www.pitt.edu/~vorp

INTRODUCTION

Abdominal aortic aneurysm (AAA) is a focal, balloon-like dilation of the distal aorta. If left untreated, AAA can rupture, an event which is ranked as the 13th most common cause of death in the US. Associated with surgical repair of AAA are significant costs and risks to the patient. In the clinical management of AAA patients, it is desirable to determine when the risk of AAA rupture justifies surgical intervention and its related complications. Presently, there is no reliable criterion to predict the risk of AAA rupture. We believe that principles in mechanics may be used to predict the propensity of rupture for AAA. With the development of an aneurysm, the stress on the aortic wall increases progressively [1] until it reaches its gradually decreasing failure strength [2]. Comparison of locally acting AAA wall stress and local wall strength could be used as a reliable indicator of rupture. We present here a summary of our efforts to develop a method for the noninvasive estimation of AAA wall stresses, and to understand one factor that affects local AAA wall strength.

AAA WALL STRESSES

Our methodology to determine estimates of the in-vivo wall stresses for actual AAA is based on obtaining three critical inputs: the AAA geometry, the constitutive behavior of the AAA wall, and the boundary conditions.

AAA Geometry

Methods to obtain the in-vivo geometry of an intact AAA are detailed elsewhere [3]. In short, spiral CT cross-sectional images were obtained that span the entire AAA. Images were individually processed to provide coordinate values of a discrete number of data points on the AAA wall. The XYZ data recorded for each patient forms a point cloud when plotted in 3D space. A 3D reconstruction of each aneurysm, or a "virtual AAA", was obtained by first triangulating and then smoothing each point cloud surface.

Constitutive Relationship for AAA

We have recently developed a finite strain constitutive model for AAA wall, in which this material is assumed to be hyperelastic, homogenous, incompressible, and isotropic [4]. The appropriate functional form of the pseudo-strain energy function was determined from experimental stress-stretch ratio data, and is given as:

$$W = \alpha(I_B - 3) + \beta(I_B - 3)^2$$

where W is the strain energy density function, α and β are material parameters, and I_B is the first invariant the left Cauchy-Green deformation tensor. We have shown that utilization of population mean values of α and β provide reasonably accurate, individual stress distribution estimates for AAA [4].

Boundary Conditions

Quasi-static systolic pressure (individually measured for each patient) was applied as outward traction on the AAA wall surface. The two ends of the AAA model were constrained from displacing in the longitudinal direction to simulate anatomical tethering.

Finite Element Analysis (FEA)

We meshed each "virtual AAA" with 5000-6000 thin-walled quadrilateral shell elements and computed the wall stress distributions using FEA.

Results

All analyses reached convergence. Overall, it was noted that the stresses were complexly distributed with distinct regions of high and low stress. The regions of maximum stress occurred predominantly on the posterior surface of the AAA in the cases studied. The peak wall stress for the AAA varied from 29 to 50 N/cm^2 while that for a nonaneurysmal aorta was 12 N/cm^2.

Discussion

Our finding that high stress regions occur on the posterior surface is consistent with autopsy studies, which found that AAA rupture occurs predominantly on this surface [5]. In addition to being completely noninvasive, our methodology does not require any additional involvement or expense by the AAA patient than what is usually required (e.g., CT scanning is routinely performed to evaluate AAA patients). Therefore, there are no logistical constraints to its applicability in a clinical setting.

AAA WALL STRENGTH

Our laboratory has shown that the strength of aneurysmal tissue is significantly decreased as compared with normal tissue [2]. However, wall strength may also vary spatially within a single AAA. Using both computational and experimental techniques, we found that ILT attenuates diffusion of oxygen to the AAA wall, possibly causing hypoxia [6]. Therefore, we hypothesize that the strength of the AAA wall is regionally dependent on ILT thickness and decreases as ILT thickness increases.

Methods

Study subjects were six patients undergoing traditional AAA reconstruction. Upon resection, a longitudinally oriented strip of AAA wall spanning the apex to the distal neck of the aneurysm was cut with ILT intact. One 3x15 mm section of tissue was cut from the region of the wall where attached ILT was the thickest, and another was cut from the region where the attached ILT was thinnest or absent. The thickness of attached ILT was measured before cutting. Prepared specimens were tested to failure on a uniaxial tensile testing device, and Cauchy stress and strain were determined as described [2]. The stress-strain curve was plotted for each of the specimens tested and the strength was defined as the maximum stress prior to failure.

Results

The figure shows the strength of each pair of AAA specimens. The thickness of attached ILT for each specimen is labeled at the top of each bar. The strength of the wall specimens adjacent to thick ILT (light bars) is significantly less than that for the specimens adjacent to thin ILT (dark bars): 224 ± 40

N/cm^2 vs. 125 ± 16 N/cm^2, respectively ($p = 0.03$, by paired t-test).

Discussion

Our data suggests that local AAA wall strength is decreased in regions with thicker adjacent ILT. This may be due to hypoxic conditions set up in the wall due to ILT [5]. More experiments are needed before we can definitively correlate thickness of ILT with the strength of the AAA wall, however.
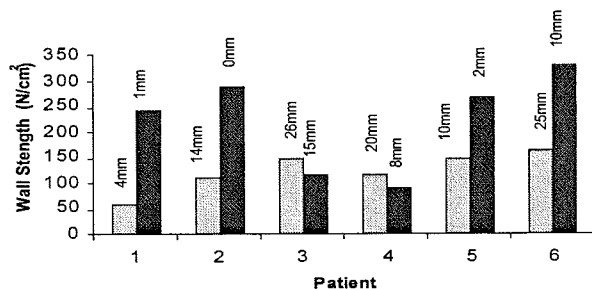
REFERENCES

1. Vorp et al., J. Vasc. Surg., 27:632-639, 1998
2. Raghavan et al., Ann. Biomed. Eng. 24:573-582, 1996.
3. Sacks et al., Ann Biomed. Eng., 27:469-479, 1999.
4. Raghavan et al., J. Biomech., in press.
5. Darling et al., Circulation 56, 161-164, 1977..
6. Vorp et al., J. Biomech. Eng., 120:579-583, 1998.

THE MICROMECHANICS OF THE AORTIC VALVE

Ivan Vesely
Department of Biomedical Engineering, Lerner Research Institute
The Cleveland Clinic Foundation, Cleveland, Ohio
Email: vesely@bme.ri.ccf.org Web: http://www.lerner.ccf.org/bme/valve/

INTRODUCTION

It is becoming appreciated that the aortic valve is an extremely complex, highly specialized structure. When it fails, there is no widely accepted means of repairing it; it needs to be replaced with a prosthesis.

A number of alternatives exist for replacing a disfunctioning aortic valve (Figure 1). Mechanical valves, consisting of carbon and metal components are very durable but require the patient to be on chronic anticoagulation therapy.
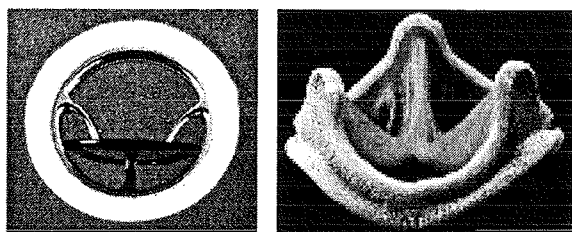
Figure 1: Images of mechanical (left) and bioprosthetic valves used in the aortic position.

Tissue valves or bioprostheses, typically consist of glutaraldehyde-treated porcine aortic valve tissue mounted on a supporting stent to enable convenient surgical implantation. Bioprostheses do not require chronic anticoagulation, but suffer from gradual degeneration by way of calcification and material wear. They eventually fail and need to be replaced. Tissue valves have the potential to become the ideal prosthesis, once their durability and functional life span is extended, so that they can be used for a wider range of patients, instead of just the elderly.

The objectives of our ongoing research into the structure and function of bioprosthetic valve tissue is to develop an understanding of what makes these materials naturally durable, and use this knowledge to improve the fabrication of alternative valve devices.

METHODS

Microscopic imaging, materials testing and mathematical modeling have been used to investigate the structure/function relationship in the native aortic valve.

Aortic valves have been shown to have an intricate network of elastin that partitions and links larger collagenous structures (Scott & Vesely, 1996). These features have been revealed by digesting the valve leaflets in 0.1 N NaOH at 75°C for 45 minutes, lyophilizing and viewing under scanning electron microcopy.

Materials testing was done typically on 5 mm wide strips of tissue tested along or across the major collagen fiber bundles, as well as on leaflets dissected apart to separate the major structural layers; the fibrosa and the ventricularis (figure 2).

Mathematical modeling involved applying an extension of Fung's Quasilinear Viscoelastic theory to uniaxial test data of valve tissue

strips. The extensions to QLV involved fitting a model of the loading and stress relaxation history to experimental data, and obtaining the elastic functions and relaxation spectrum from this model (Carew et al., 1999).

RESULTS

Morphologically, the aortic valve cusps are composed of three structurally distinct layers of tissue (figure 2). The fibrosa contains mainly collagen and is held in a wavy, corrugated configuration by way of its attachment to the underlying ventricularis, which is under tension.
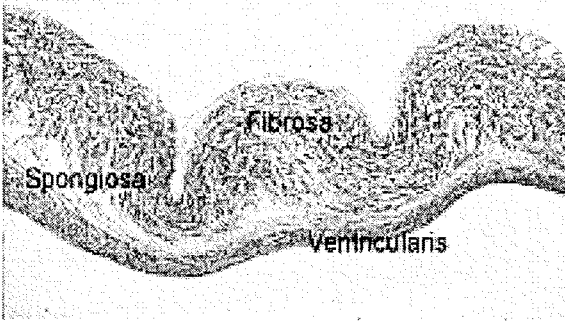
Figure 2: H&E stained sections of a porcine aortic valve cusp, showing the three layers.

Towards the edges, the fibrosa is organized in to bundles, each surrounded by a tube of elastin, all of them connected together by elastin struts (figure 3).
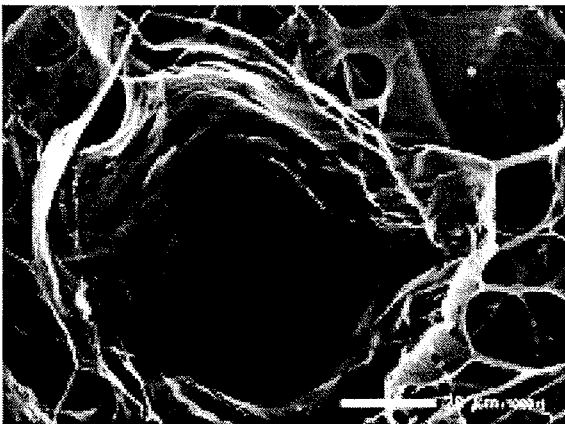
Figure 3: SEM image of elastin tubes in the fibrosa. Note the connectivity between tubes.

In spite of the complexity of the aortic valve cusps, some aspects of their mechanics can be modeled by QLV. Circumferential strips subjected to cyclic uniaxial testing generated data that was very close to the stress/strain response predicted by QLV (figure 4).
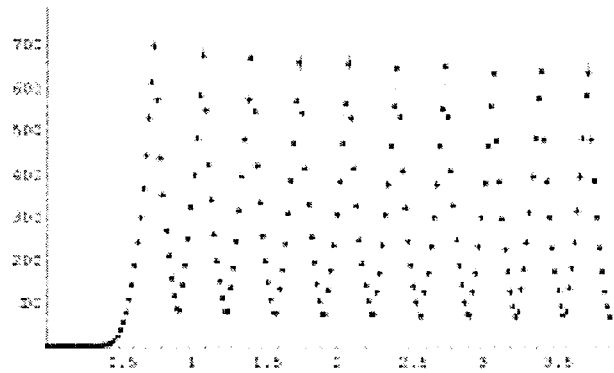
Figure 4: Solid line represents model prediction, dots are experimental data points.

CONCLUSIONS

These morphometric and mechanical studies have shown that the intricate morphology of the elastin relative to the collagen exists in order to return the collagen fiber geometry back to some neutral resting state between successive loading cycles. The sharing of function across a wide range of stress and strain may be one mechanism by which the aortic valve cusps attain their strength, compliance and remarkable durability. With the appropriate viscoelastic models, we may be able to relate external observations and measurements to internal stresses, and pave the way towards using biological materials in engineering design.

REFRENCES

Scott M.J., Vesely I., Morphology of porcine aortic valve cusp elastin. J.Heart Valve Dis., 5(5):464-471, 1996.
Carew E.O., Talman E.A., Boughner D.R., Vesely I., Quasi-linear viscoelastic theory applied to internal shearing of heart valve leaflets. J.Biomech.Eng., 1999 (In Press)

New Advances in Microvascular Research: 3-D Networks In Vivo

Christopher Ellis

University of Western Ontario

Abstract was not submitted

The Cleveland Clinic Rotary Pump

A Third Generation Blood Pump

Leonard A. R. Golding, M.D.

Introduction

The goal of permanent implanted blood pumps that can partially or completely replace heart function is rapidly approaching reality. The third generation blood pumps are demonstrating the potential for a minimum 5-year reliable function for patients with irreversible cardiac damage and rival the results obtained with heart transplantation. One such system is being developed at the Cleveland Clinic Foundation.

Result/Discussion

Utilizing a concurrent engineering approach with a multidisciplinary group an initial prototype pump was used as the basis of a completely implanted ventricular system. The unique rotodynamic pump has an inverted motor and a single moving part passively suspended rotor. The radial pump produces 5 liters/minute blood flow at 3,000 RPM and a delta pressure of 100 mm mercury.

Bench testing confirmed hydraulic function and animal studies demonstrated low damage to red cells. An initial problem with clot formation in the journal bearing was addressed by computational fluid dynamic analysis resulting in design modification. Surface characteristics were also modified.

The control logic for such devices was also developed and evaluated both in vitro and in vivo. Such control is important to allow adaption to varying blood flow needs.

Pump implant studies now routinely run for 30 days. Three month studies are being initiated.

Summary

The Cleveland Clinic Rotary Pump is the basis of a Third Generation Implanted Ventricular Assist System showing good potential for clinical use.

INTRAVASCULAR ULTRASOUND IN THE EVALUATION OF CORONARY ARTERY REMODELLING

D. Geoffrey Vince[1], Jon D. Klingensmith[1], E. Murat Tuzcu[2], J. Fredrick Cornhill[1]

[1]Department of Biomedical Engineering, The Cleveland Clinic Foundation, Cleveland OH
[2]Department of Cardiology; The Cleveland Clinic Foundation, Cleveland OH
E-mail: vince@bme.ri.ccf.org Web:http://www.lerner.ccf.org/pi/vince.html

Introduction

It has been shown that as atherosclerosis progresses, arteries undergo a compensatory response in which the overall vessel size increases to prevent significant luminal narrowing [1-5]. The exact mechanisms controlling this positive remodeling continue to be investigated. However, it is known that the ability of endothelial cells to sense and respond to changes in blood flow is central to the modulation of compensatory enlargement [6]. In addition to investigation of the molecular control mechanisms, the disease process and remodeling response in various human arteries, including the carotid [4], the femoral [2, 7], and the coronary arteries [1, 5, 8], has been studied. The impetus for these numerous investigations is the clinical relevance of compensatory enlargement. Studies have shown that the process of outward remodeling may cause a predisposition to plaque rupture, resulting from a structural weakening of the plaque [8].In our study, a novel 3D reconstruction technique, which circumvents the limitations of other techniques and accurately accounts for the 3D geometry of the vessel [8], was used to document compensatory enlargement in human coronary arteries.

Methods and Results

Seven human coronary arteries were reconstructed using intravascular ultrasound and biplane angiography, and vessel geometries were quantified. In all seven vessels, as plaque area increased, overall vessel area increased (R = 0.986, 0.933, 0.984, 0.678, 0.763, 0.963, and 0.830), but luminal cross-sectional area did not

significantly decrease. Focal compensatory enlargement was identified in each vessel, and in some cases this response appeared to occur until the vessel was 65% occluded. This finding is particularly noticeable in Figure 1, where enlarged regions of the vessel are separated by an area of apparently normal arterial wall. These data are consistent with those of others who have identified the focal nature of compensatory enlargement [2]. In Figure 1a (images 60 – 73) the wall area, plaque area, and luminal area appear to increase at a fairly uniform rate. At image 73, both the wall and plaque areas continue to rise, but the luminal area falls. It appears that at this point (58% occluded), the compensatory mechanism fails and luminal encroachment ensues. Luminal enlargement near the proximal ends was attributed to the natural taper of the vessel.

a)
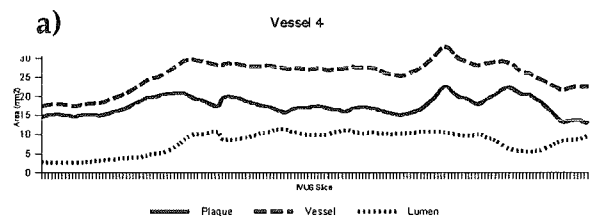
b)
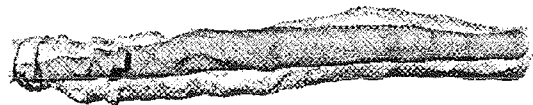
Discussion

Three-dimensional reconstruction of seven diseased coronary arteries using IVUS and biplane angiography revealed compensatory enlargement in vessels with significant atherosclerosis. Previous histological

studies by Glagov *et al* [1] have shown that compensatory enlargement occurs in response to atherosclerotic plaque formation. However, it has been demonstrated that tissue fixation and processing can affect the geometry of coronary arteries, which may consequently compromise the morphology data obtained. Siegel *et al* have documented that tissue processing on vessels with moderate to large amounts of disease tends to cause an underestimation of total arterial area of approximately 30% [9]. The IVUS procedure used in our study overcame this limitation, as IVUS studies demand no tissue preservation, and all imaging was performed on fresh unfixed vessels within hours of autopsy.

The quantitative techniques in other ultrasound studies have considerable subjective user interaction or planimetry, making them difficult to reproduce accurately. Previous studies by our group, investigating vascular compliance [10], have shown that small changes in wall or plaque diameter cannot be accurately quantified by manual tracing, as intra-operator variation in the procedure is often greater than the change in wall diameter. The three-dimensional reconstruction technique in our study used a semi-automated segmentation technique called "active surfaces" to outline the lumen and the medial-adventitial boundary]. The only user interaction required was the entering of a few control points for the initial surface. The three-dimensional snakes algorithm used volume data to achieve more accurate, automated, and reproducible segmentation and facilitated the analysis of over 900 IVUS images. Our data suggest that human left anterior descending coronary arteries enlarge in relation to an increase in plaque area and this process does not occur uniformly along the length of the vessel. 3D

reconstruction of coronary arteries, through combining visualization of accurate 3D geometry with image analysis over the entire length of the reconstructed vessel, provides a tool for quantitative assessment of vascular remodeling which can reveal information not previously available in the study of this mechanism. Comparing plaque and vessel volumes and rate of change in cross-sectional areas in different vessel segments, not available with histological or two-dimensional IVUS studies, will provide further insight into both positive and negative remodeling.

REFERENCES

1. Glagov S, Weisenberg E, Zarins CK, Stankunavicius R, Kolettis GJ. Compensatory enlargement of human atherosclerotic coronary arteries. New England Journal of Medicine 1987; 316:1371-5.

2. Losordo DW, Rosenfield K, Kaufman J, Pieczek A, Isner JM. Focal compensatory enlargement of human arteries in response to progressive atherosclerosis: in vivo documentation using intravascular ultrasound. Circulation 1994; 89:2570-7.

3. Zarins CK, Weisenberg E, Kolettis GJ, Stankunavicius R, Glagov S. Differential enlargement of artery segments in response to enlarging atherosclerotic plaques. Journal of Vascular Surgery 1988; 7:386-94.

4. Steinke W, Els T, Hennerici M. Compensatory carotid artery dilatation in early atherosclerosis. Circulation 1994; 89:2578-81.

5. Hermiller JB, Tenaglia AN, Kisslo KB, Phillips HR, Bashore TM, Stack RS, et al. In vivo validation of compensatory enlargement of atherosclerotic coronary arteries. American Journal of Cardiology 1993; 71:665-8.

6. Cowan DB, Langille BL. Cellular and molecular biology of vascular remodeling. Current Opinions in Lipidology. 1996; 7(2):94-100.

7. Pasterkamp G, Wensing PJ, Post MJ, Hillen B, Mali WP, Borst C. Paradoxical arterial wall shrinkage may contribute to luminal narrowing of human atherosclerotic femoral arteries. Circulation 1995; 91:1444-9.

8. Kearney P, Erbel R, Rupprecht HJ, Ge J, Koch L, Voigtlander T, et al. Differences in the morphology of unstable and stable coronary lesions and their impact on the mechanisms of angioplasty: an in vivo study with intravascular ultrasound. European Heart Journal 1996; 17(5):721-30.

9. Siegel RJ, Swan K, Edwalds G, Fishbein MC. Limitations of postmortem assessment of human coronary artery size and luminal narrowing differential effects of tissue fixation and processing on vessels with different degrees of atherosclerosis. Journal of the American College of Cardiology 1985; 5(2 pt 1):342-6.

10. Meier DS, Cothren RM, Vince DG, Cornhill JF. Automated morphometry of coronary arteries with digital image analysis of intravascular ultrasound. American Heart Journal 1997; 133:681-90.

The Legacy of Tom McMahon
Chair: Art Kuo (University of Michigan)

This symposium is a memorial for Harvard professor Tom McMahon, who was a major figure in the field of biomechanics and who passed away earlier this year. We will present a short tribute, followed by a technical program consisting of three talks, each discussing one of Tom McMahon's contributions in the areas of locomotion, scaling, and bone biomechanics. The speakers are R. McNeill Alexander, Andy Biewener, and Wilson Hayes.

Masses and springs modeling human movement
Presented by R McNeill Alexander, University of Leeds

Tom McMahon had a remarkable facility for devising simple models that revealed the basic principles of human movement far more clearly than more detailed models could have done. He and his colleagues explained the paradox that the forward swing of our legs, in walking, is largely passive, but is much faster than predictions from simple pendulum theory. They modeled running as a mass bouncing on a spring and explained the relationship between stride length and speed. They introduced the concept of the Groucho number, and their experiments and theories led to the design of an exceptionally fast running track.

Scale effects in biology: implications for biomechanical and physiological function.
Presented by Andy Biewener, Concord Field Station, Harvard University

Size is fundamental to the design and function of animals and plants. Various models have been proposed to explain empirical observations of scaling that have relevance to biomechanics and physiological function. These models can be tested using comparative studies of structure and function. Recently fractal branching networks have been proposed to explain the 3/4 power scaling of metabolic function and many other physiological variables upon which this scaling depends. Similarly, size-dependent changes in musculoskeletal loading (muscle force a $M^{3/4}$) to maintain peak stresses and safety factors constant across size within mammals may be linked to the scaling of metabolic energy supply. The scaling of musculoskeletal mechanics can also be related to changes in leg stiffness in running animals and to the energy cost of locomotion. Finally, other scaling patterns suggest that mechanical constraints may differ at different ranges of size.

The Legacy of McMahon's Bees: Bone, Biomechanics and Biology
Presented by Wilson C. Hayes, Oregon State University (formerly Director of the Orthopedic Biomechanics Laboratory at Harvard's Beth Israel Deaconess Medical Center)

Dr. Hayes will summarize Tom McMahon's contributions in solid mechanics, emphasizing in particular his work on falls, on age-related fractures of the hip and spine and their prevention, and on the mechanics of trabecular and cortical bone. The implications of this body of work and the legacy of his writings and students will be discussed.

May 13, 1999

Dear Tom,

One day you brought me a gift. You had promised it to me for several weeks, first rather vaguely and then with an increasing insistence that it was almost ready. That day, you were waiting for me in the library, sitting quietly, Tess at your feet. You sat there across the table, and at that distance I could see not only the twinkle in your eyes, but a hint of shyness, as if uncertain of your lines, and a little afraid to be on stage. When you lifted what you had brought out of its bag, you pinched it gently at both ends, carefully holding it horizontally, like a small level whose bubble would go unstable with the slightest tilt. It was ungainly, even ugly, all paperclips and rubber bands and scotch tape and strips of cotton fabric.

You said it was a tug-lock strap. "Watch", you said, as you gently and slowly pulled the ends apart. It was quite unremarkable. The thing just stretched, and as it did I worried that its paperclips and tape and rubber bands would break and you would be terribly disappointed. I worried for you sometimes. I worried mostly that you were lonely and that you couldn't, or wouldn't, ask for help. And so, as I sat there, worrying for your fragile contraption and your disappointment, I missed your achievement the first time around. I did see you give this thing a mighty tug and saw the look of triumph and relief that crossed your face. But I hadn't seen what happened. And so you patiently did it again. This time I saw that when you pulled it forcefully, it locked; it wouldn't stretch.

And then you told me how it worked, the words just tumbling out. It was not such an easy concept, especially at the levels you found so intriguing: dilatancy, critical shear rates, step changes in viscosity. But it was easy enough to see if you thought of it as a new kind of seat belt, one that locked when you pulled it quickly and stretched when you pulled it slowly. We did a duet then. Point and counterpoint and two part harmonies of applications: chin straps, protective garments and knee braces and special shoes for resisting ankle sprains. And then we soared together, from one dimension to two, to rate sensitive clutches, from two dimensions to three, to joy sticks and spherical connectors. We wrote the whole patent there that day.

You were like a catalyst; you fit to me, enhanced us, made our reaction go to completion. I came to think of us as the perfect pair, a Mutt and Jeff of invention and discovery, playing a Ping-Pong game of ideation and completion. You, with your flair for modeling and mathematics and your single-minded focus on the problem at hand; me, with a certain strength at making complex ideas accessible. You, who found such upset and discomfort in negotiations and self-promotion and me who found such challenge there. For most of the time that I knew you I assumed and found comfort in the thought that we were unique together, a special pair of travelers, walking down a road that only we walked. I now find greater comfort in the sense that you walked those special roads with so many others, catalyzing, finding fits.

You completed so many of us. We are all at a loss without you. Goodbye, dear friend. Travel well; we think of you often, with love.
Toby

Abstracts

OPTIMAL CONTROL OF CAVADER TENDONS PREDICTS MAXIMAL FINGERTIP FORCES IN PERIPHERAL NERVE INJURIES

F.J. Valero-Cuevas[1,2], J.D. Towles[1,2] and V.R. Hentz[1,3]
e-mail: valero@roses.stanford.edu

[1]Rehabilitation R&D Center, Veterans Affairs PAHCS, Palo Alto, California, U.S.A.
[2]Biomechanical Engineering Division & [3]Hand Surgery Division
Stanford University, Stanford, California, U.S.A.

INTRODUCTION

Peripheral nerve injuries in the upper extremity often result in functionally devastating reduction of pinch strength[1]. Because rehabilitation following peripheral nerve injuries includes multiple physical and psychological adjustments, objective estimates of paralysis-induced weakness would assist clinicians in setting realistic expectations for rehabilitation of grasp in these common neurologic injuries. Understanding weakness of individual digits is essential to understanding weakness in grasp. Therefore, this study establishes the reduction in finger strength that can be directly attributed to the paralysis of specific finger muscles associated with radial and ulnar palsies.

METHODS

We applied optimal control theory to cadaver forefingers to quantify the expected reduction of biomechanically possible fingertip force when both extensor muscles or all three intrinsic muscles are inactive (simulating radial and ulnar palsies, respectively). Six fresh cadaver hands (4 right, 2 left) were rigidly mounted to a tabletop and their forefingers placed in a standard functional posture (neutral ad-abduction, flexed 45° at metacarpophalangeal and proximal interphalangeal joints, and 10° at distal interphalangeal joint). The distal phalanx was rigidly coupled to a six-axis force sensor using polymethylmethacrylate and K-wires. The tendon of each finger muscle was excised and tied to a calibrated extensor spring via an inelastic string.

All components of fingertip force and torque were measured during the application of a force to each tendon equivalent to one-quarter of the maximal isometric force its muscle can produce[3]. Based on these measurements, Linear Programming algorithms[2] calculated the optimal combination of tendon forces to produce the maximal biomechanically possible magnitude of palmar force (analogous to pinch force, directed within 15° of a line normal to the mid-distal phalanx. See Figure 1). Optimal tendon force combinations to produce maximal palmar force were calculated for three conditions: nonparetic (all seven muscles available), radial palsy and ulnar palsy. Each optimal tendon force combination was applied and the resulting fingertip output measured.

RESULTS

Figure 1 shows an example of the three components of force at the fingertip measured during application of a force to each tendon equivalent to one-quarter of the maximal isometric force of its muscle. The palmar forces measured in the cadaver fingers were, on the average, within 6% of their predicted value. Furthermore, the maximal biomechanically possible palmar forces for radial and ulnar palsy conditions were, respectively, 75% and 51% of palmar

Figure 1: Fingertip force produced by each finger muscle

FP flexor profundus
FS flexor superficialis
EC extensor communis
EI extensor indicis
DI dorsal interosseous
PI palmar interosseous
LUM lumbrical
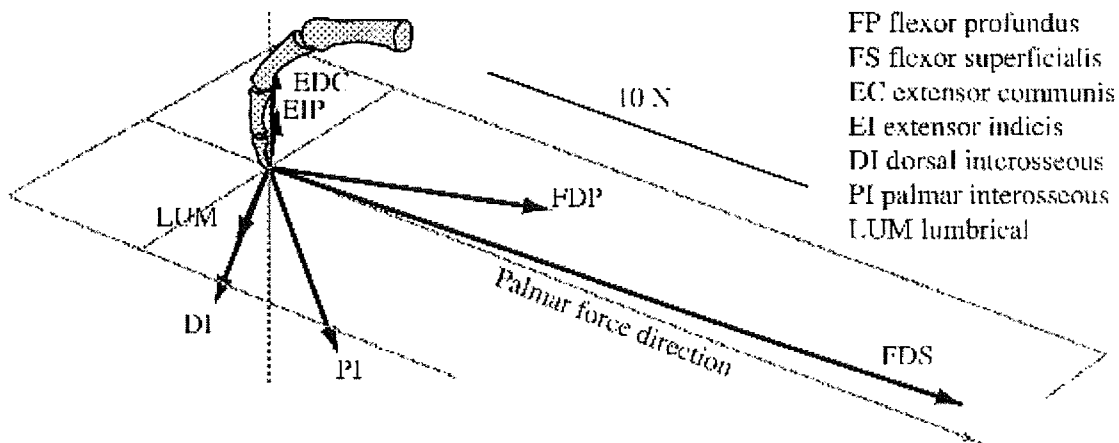
force for the nonparetic condition (n= 6, p<0.05). Figure 2 shows sample solutions for two conditions.

DISCUSSION

This novel combination of optimal control theory and cadaver preparations leads to rigorous, quantitative, 3D predictions of mechanical capabilities and muscle coordination patterns for actual fingers. These solutions specify the upper limit of fingertip force and elucidate the biomechanical consequences of paralysis following peripheral nerve injuries. Importantly, the optimal solution for nonparetic palmar force is functionally valid because it reproduces the use of extensor muscles and the lack of palmar interosseous muscle reported by EMG recordings and a biomechanical model for a similar task[3]. Furthermore, the nonintuitive weakness in pinch reported clinically for radial palsy[1] is here explained by the need to use extensor muscles to produce well-directed palmar force of large magnitude. This method will also be used to quantify hand function in other neurologic disorders, e.g., spinal cord injury, and to evaluate alternative surgical restoration strategies based on optimal, cadaver-simulated post-operative functional outcomes.

ACKNOWLEDGMENTS

REFERENCES

1. Brand, P. and Hollister, A., 1993, Clinical Mechanics of the Hand. St. Louis: Mosby.
2. Chvátal, V., 1983, Linear Programming. New York: W.H. Freeman and Company.
3. Valero-Cuevas, F.J., et al.,J Biomech, 31(8). 1998.

Figure 2: Maximal palmar force

FP FS EC EI
DI
100% Nonparetic

FP FS
DI
75% Radial palsy
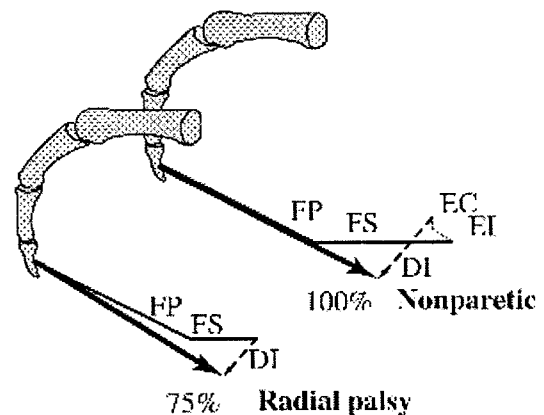
EFFECT OF ELBOW ANGLE AND ROTATIONAL VELOCITY ON IMPACT FORCE DURING OF A FALL ONTO AN OUTSTRETCHED HAND

Kurt M. DeGoede and James A. Ashton-Miller

Biomechanics Research Laboratory, Department of Mechanical Engineering
University of Michigan, Ann Arbor, Michigan
Email: degoede@umich.edu

INTRODUCTION

The wrist is the most common fracture site in the body (Donaldson et al. 1990). To determine the load likely to act on the hand while arresting a fall onto an outstretched hand a recent model analysis (Chiu, Robinovitch 1998) assumed a straight arm configuration upon initial impact with the ground. However, a study of untrained young males arresting self initiated falls from standing height found that initial ground contact occurred with an elbow angle of ~150°(Dietz et al. 1981), and impact forces were up to 60 % lower than those predicted with the above model. To resolve this discrepancy we developed a dynamic model of the upper extremity to test the hypothesis that both elbow angle and angular velocity can significantly alter the peak impact force when arresting a fall with the arms.

PROCEDURES

Each arm was modeled as two rigid links (length: L_1 and L_2) hinged at the elbow (Figure 1). The effective half-mass of the rest of the body, M=0.25BW, was connected at the shoulder through a spring and damper in parallel (K_1). At the ground, the interface between the hand and the landing surface was modeled with a non-linear element (K_2):

$$F_2 = kx^3(1 + b\dot{x}), \qquad (1)$$

used previously in a model of heal strike during running(Gerristen et al. 1995). A
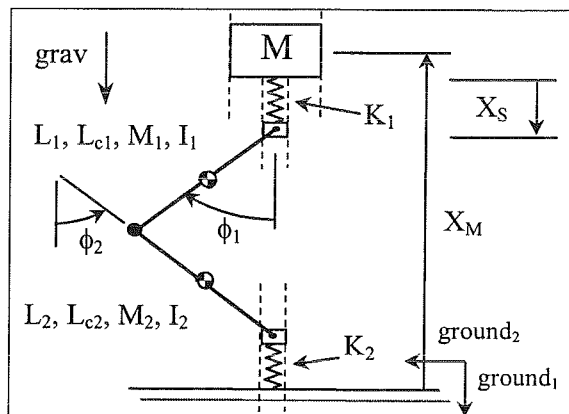
Figure 1: Rigid body dynamic model of the arm striking the ground while arresting a fall with outstretched arms

rotational spring and damper (not shown), in parallel, provide elbow restoring torque.

The model system had four degrees of freedom: X_M – the vertical position of torso, X_S – the position of the center of rotation of the shoulder, ϕ_1 and ϕ_2 – the absolute angle of the upper arm and forearm respectively, and is subject to one kinematic constraint:

$$L_1\dot{\phi}_1 \cos(\phi_1) + L_2\dot{\phi}_2 \cos(\phi_2) = 0. \qquad (2)$$

The parameter values for the shoulder and the hand-ground interface stiffness and damping were based upon data from tests conducted in 40 healthy subjects with a ballistic pendulum (unpublished data). The elbow parameters were selected such that the total elbow deflection matched the results from experimental trials with one healthy young subject measured using an Optotrak® camera system at 300 Hz.

RESULTS AND DISCUSSION

Simulations with the above model compared favorably with experimental data. The data from Deitz, et al., (1981) showed a peak force of approximately 1,100 N for a fall onto a stiff surface with an estimated impact velocity of 2.24 m/s (for the center of mass); additionally the elbow had an initial rotational velocity of 2 rad/sec. Model simulation under the same conditions yielded a peak impact force of 950 N (12 % error) for a 78 kg BW. To verify the overall nature of the response, a simulation of a fall with an impact velocity of 2.7 m/s was compared to the data from the young adult experimental trial (BW=72 kg) with the same impact velocity (Figure 2). The peak force from the experiment was 15 % lower than the peak force in the simulation, but in the experiment the force plate was padded with ¼" of neoprene.

Simulating a full fall to the floor (V_{impact}=3.0 m/s, BW=78 kg) onto a stiff surface, with no initial elbow velocity, produced a peak force of 1,350 N. The force increased to 1,640 N by changing the initial elbow angle from 150° to 179.9°, and decreased to 950 N when reducing it 120°. So, each degree decrement in initial elbow angle decreased impact force by 0.9%.

With the elbow fixed at an initial configuration of 150°, altering the initial rotational velocity of the elbow at ground contact further modified the peak force. Extending the elbow at impact with a velocity of just five times that observed in the self-initiated falls, as can occur when actively reaching for the ground prior to impact, resulted in a 40% higher peak impact force of 1,910 N. Flexing the elbow, by pulling the hands toward the body, with the same angular velocity lowered the peak impact force by 35 % to 875 N.
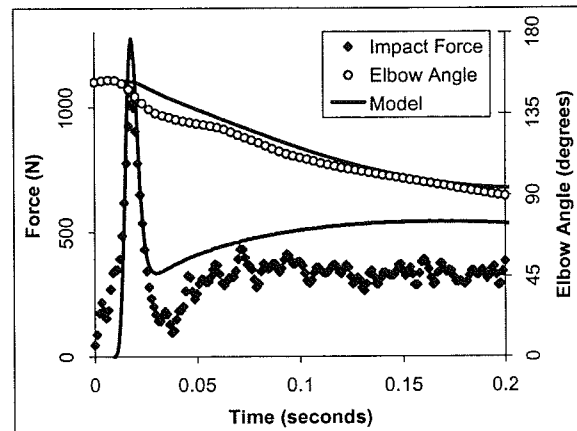
Figure 2: Experimental and simulated impact force and elbow angle data for the arrest of a forward fall with the arms.

SUMMARY

These results demonstrate that the peak impact force applied to the hands during the initial phase of a fall arrest can be modified significantly by altering the initial position and angular velocity of the elbow at ground contact. These findings suggest that it may be possible to affect the risk of wrist fracture in a fall, independent of the body's impact velocity and ground surface material properties.

REFERENCES

Chiu, J., Robinovitch, S.N. (1998). *J. Biomech.*, **31**, 1169-1176.

Dietz,V., et al. (1981). *J. Physiol.*, **311**, 113-125.

Donaldson, L.J., et al. (1990). *J. Epidemiol. Community Health*, **44**, 241-245.

Gerristen, K., et al. (1995). *J. Biomech.*, **28**(6), 661-668.

ACKNOWLEDGEMENTS

FRACTURE TOLERANCE OF THE MALE FOREARM: THE AFFECT OF PRONATION VERSUS SUPINATION

S. Duma, P. Schreiber, J. McMaster, J. Crandall, C. Bass, and W. Pilkey

Automobile Safety Laboratory, University of Virginia, Charlottesville, Virginia
Email: Duma@virgnia.edu   Web: http://cinderella.mech.virginia.edu/home.html

INTRODUCTION
It has been shown that there is a 40% increase in risk of serious (AIS 3) upper extremity injury to belted occupants with air bags versus those without air bags [NHTSA, 1996]. In order to design frontal air bags that minimize the risk of injuries to the upper extremities, the forearm fracture criteria must be known. A study by Pintar et. al. (1998) found a mean forearm failure bending moment of 94 Nm for all specimens; however, this study did not consider forearm orientation. Duma et. al. (1998) found that the female forearm is 21% stronger in the supinated versus pronated position.

METHODOLOGY
Ten male forearms, five matched pairs, were prepared by disarticulating the upper extremity at the shoulder and keeping the elbow joint intact. Dynamic three-point bending tests were performed using a 9.48 kg impactor released from a height of 2.0 m. These conditions were chosen to match radius and ulna strain rates as measured in cadaveric tests with driver side air bags [Bass, 1997]. In each matched pair, one limb was tested in the pronated position, and the other in the supinated position. The impact location was chosen as the distal third of the forearm, due to the local minimum in polar moment of inertia of both the ulna and radius at this point [Bass, 1997]. Peak strain and fracture time were observed from strain gages (Micro Measurements, model CAE-13-125UN-350) fixed on the radius and ulna.

RESULTS AND DISCUSSION
The average peak moment for the supinated forearms was 126 ± 13 Nm compared to 108 ± 8 Nm, a statistically significant difference (p = 0.03) (Table 1). There was no significant difference in timing between the ulna and radius fracture for the supinated test; however, the ulna fractured significantly earlier than the radius in the pronated tests (p = 0.05).

Post-test X-rays were used to assess fracture pattern and location. In the supinated group the radius fracture occurred proximal to the ulna fracture, while in the pronated group, the fracture locations were directly in line with the impactor.

These results suggest that the radius and ulna are being loaded sequentially in the pronated arm and the subsequent fractures are occurring directly beneath the impactor head. The ulna is loaded and fails before the radius starts to be significantly loaded. In the supinated position the impact force is more evenly distributed between the two bones. The tendons and muscle bellies of the forearm flexor compartment will also help distribute the impactor load in the supinated position, whereas in the pronated position the ulna is relatively exposed. The difference in fracture location suggests that the supinated forearms are breaking at weaker points rather than directly underneath the impactor as in the pronated forearms.

SUMMARY

Using five matched pairs of male forearms, it was determined that the forearm is 17% stronger in the supinated position, 126 ± 13 Nm, versus the pronated position, 108 ± 8 Nm. This difference and the difference in fracture time between the radius and ulna for pronated and supinated tests were statistically significant ($p < 0.05$). Additionally, two distinct fracture patterns were seen for the pronated and supinated groups.

To produce a conservative injury criterion, it is suggested that the pronated value of 108 Nm be used given that the forearm is weaker in the pronated position and that the driver forearm is typically in this orientation. Forearm fracture criteria that utilize tests in the supinated position may overestimate the tolerance.

REFERENCES

Bass C.R., Duma S.M., Crandall J.R., et al., The Interaction of Air Bags With Upper Extremities. SAE Paper 973324, 41st Stapp International Car Crash Conference, 1997.

Duma S.M., Schreiber P., McMaster J., et al., Dynamic Injury Tolerances for Long Bones in the Female Upper Extremity. International Research Council on the Biomechanics of Impact, 1998.

National Highway Traffic Safety Administration, Effectiveness of Occupant Protection Systems and Their Use, U.S. Department of Transportation, December 1996.

Pintar F.A., Yoganandan N., Eppinger R.H., Response and Tolerance of the Human Forearm to Impact Loading. SAE Paper 983149, 42th Stapp International Car Crash Conference, 1998.

Table 1: Supinated and Pronated Forearm Dynamic Three-point Drop Test Results.

		Radius		Ulna		Peak Moment	Time
Supinated		Peak Strain	Time	Peak Strain	Time	(Nm)	(ms)
Test	**Subject-Aspect**	(%)	(ms)	(%)	(ms)		
1	51 right	0.62	4.7	0.50	7.8	116	7.7
2	53 left	1.07	6.8	1.01	7.9	109	8.0
3	55 left	1.52	6.2	na	na	141	6.3
4	57 right	1.44	4.2	1.54	4.9	132	4.9
5	1000 left	1.21	7.6	1.03	8.1	132	7.8
Average		**1.17**	**5.9**	**1.02**	**7.2**	**126**	**6.9**
Std. Dev.		**0.36**	**1.4**	**0.42**	**1.5**	**13**	**1.3**
Pronated							
6	51 left	0.50	5.2	0.75	4.4	102	5.1
7	53 right	0.80	7.6	na	na	99	7.5
8	55 right	1.26	8.5	0.73	4.7	118	8.5
9	57 left	0.78	5.0	0.60	2.5	114	5.0
10	1000 right	1.05	7.4	0.70	6.0	107	7.3
Average		**0.88**	**6.7**	**0.70**	**4.4**	**108**	**6.7**
Std. Dev.		**0.29**	**1.6**	**0.07**	**1.4**	**8**	**1.6**

IN VIVO FLEXION AND EXTENSION CARPAL BONE KINEMATICS

Corey P. Neu[1], Joseph J. Crisco[1,2], Scott W. Wolfe[3]

[2]Department of Orthopaedics and [1]Division of Engineering, Rhode Island Hospital and Brown University, Providence, Rhode Island. [3]Department of Orthopaedics, Yale University School of Medicine, New Haven, Connecticut. Email: joseph_crisco@brown.edu

INTRODUCTION

Documentation of normal three-dimensional (3D) *in vivo* carpal kinematics is essential to the understanding of wrist and carpal mechanics and to provide unique insight into the effects of injury and treatment. It is also important to validate the wealth of cadaveric data, which is the only data base currently available. However, measuring 3D *in vivo* carpal kinematics is difficult due to the small size and tight articular spacing of the bones. Previous *in vitro* methods have used invasive techniques such as tracking radiopaque markers embedded in bones [e.g. 1,2]. These methods are technically demanding, and are not acceptable for *in vivo* studies.

To overcome these limitations, we developed an *in vivo*, non-invasive computed tomography (CT) technique to measure the 3D motions of the carpal bones. In this study, we report the motions of the capitate, scaphoid and lunate during wrist flexion and extension in male and female subjects.

MATERIALS AND METHODS

Both wrists of five healthy males and five healthy females (n = 20) were imaged in five wrist flexion positions (neutral, -30°, -60°, 30° and 60°) using a specially designed positioning jig. Institutional Review Board approval was obtained for all subject protocols. CT volume images (voxel size: $(0.2-0.9)^2 \times 1$ mm^3) from the distal radius through the proximal metacarpals were acquired at each position. Cortical bone surfaces were extracted and registered to neutral [3]. Capitate, scaphoid and lunate motions were described relative to a radially-based orthogonal coordinate system [1]. 3D motions were described as a rotation about and translation along a unique helical axis of

motion (HAM) axis. The error in this technique was estimated to be less than 2° rotation and 1.0 mm translation [3]. The intersection of the HAM axis with the sagittal plane was also calculated [4]. Radio-capitate motion was used as an indicator of wrist motion [1]. Gender differences in carpal volumes, HAM axis intersections with the sagittal plane, and rotations about the HAM axis were determined using Student's t tests (Instat, Graphpad, San Diego, CA).

RESULTS

CT volume images for a total of 98 positions were successfully acquired and used for analysis. Capitate flexion did not correlate with wrist flexion, measured by a protractor on the positioning jig.
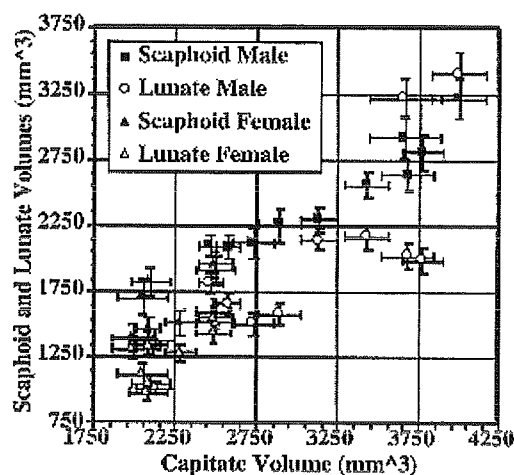
Figure 1. Scaphoid and lunate volumes plotted verses capitate volume. Error bars indicate variations in a subject's bone volume over five CT volume images.

Intra-subject variations in carpal bone volumes were less than 7% for a fixed resolution range (0.7-0.9 mm/pixel). Male

carpal bones were significantly larger than female carpal bones ($p < 0.05$). Scaphoid and lunate volumes increased linearly with capitate volume (Figure 1).
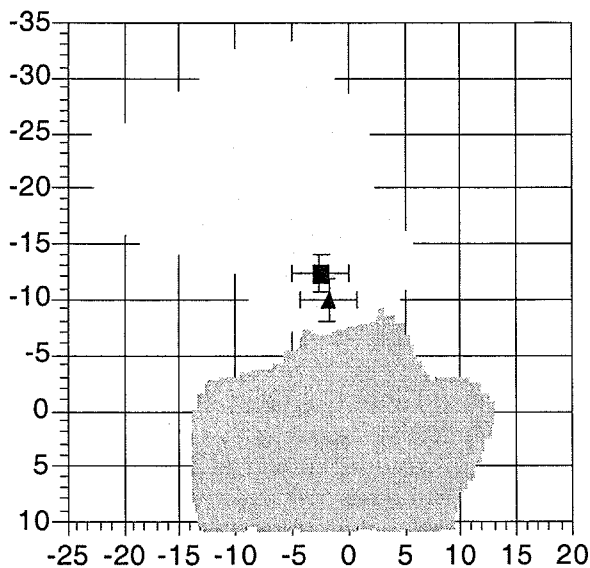
Figure 2. Mean and standard deviation of HAM intersections with the sagittal plane for the full range of capitate flexion-extension motion in males (square) and females(triangle). Data (mm) is plotted on a lateral projection of a single subject's capitate (light gray) and radius (dark gray) in neutral position.

The HAM axis intersections with the sagittal plane were significantly more distal in males than in females for the capitate (Figure 2) and scaphoid. Rotations out of the sagittal plane were generally less than 10%. Translation along each HAM axis was less than 3.0 mm.

Scaphoid and lunate rotations were not different in males and females at 30° and -30°. Scaphoid rotation closely tracked capitate rotation in extension, but rotated approximately 75% of the capitate rotation in flexion. Lunate rotation was approximately 75% of capitate rotation in extension, but was only 50% of capitate rotation in flexion (Figure 3).

DISCUSSION

This study documents *in vivo* 3D scaphoid and lunate kinematics in wrist flexion and extension. Scaphoid and lunate rotation patterns suggest that male and female carpal motion mechanics are not significantly

different. Differences in male and female HAM axis locations appear to be related to differences in carpal volumes.
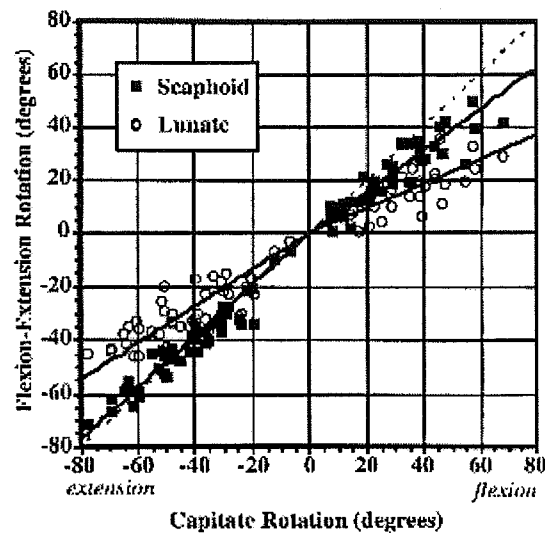
Figure 3. The scaphoid rotated more than the lunate in both flexion and extension. Solid lines indicate least-squares fits for scaphoid and lunate rotations. The dotted line is equal capitate rotation.

The scaphoid and lunate tracked more closely with the capitate than previously reported in cadaveric studies, possibly indicating less intercarpal motion *in vivo* than *in vitro* [e.g. 1,2].

These results are limited to capitate, scaphoid and lunate kinematics in wrist flexion and extension. In addition, the images were acquired statically and required extensive computation time. Further research on the complete 3D motion of all of the carpal bones is underway.

REFERENCES
[1] Kobayashi et al., *JOB*, 30(8), 787-793, 1998.
[2] Savelberg et al., *JOB*, 26(12), 1389-1402, 1993.
[3] Crisco et al., *JOR*, 17(1), 96-100, 1999.
[4] Panjabi et al., *JOB*, 14, 447-460, 1981.

WRIST FUNCTION AFTER THE BR-ECRB TENDON TRANSFER

Wendy M. Murray, Kevin L. Kilgore, Michael W. Keith
Biomedical Engineering Department and Cleveland FES Center
Case Western Reserve University and MetroHealth Medical Center
Cleveland, OH
Email: wmm@po.cwru.edu

INTRODUCTION

The ability to extend and flex the wrist is essential for providing functional use of the hand to persons with tetraplegia (quadriplegia). Wrist extension closes the hand and wrist flexion opens the hand, providing a means to grasp and release light objects. Individuals with a spinal cord injury at the fifth cervical segment (C5) have severely weakened or paralyzed wrist extensors, as well as paralyzed wrist flexors (Long and Lawton, 1955). Surgically attaching the distal tendon of the brachioradialis (Br), an intact elbow flexor, to the distal tendon of the extensor carpi radialis brevis (ECRB), a paralyzed wrist extensor, provides a means to voluntarily extend the wrist. Once active wrist extension is restored, gravity can assist passive wrist flexion.

The ability to extend the wrist does not always improve after the Br-ECRB tendon transfer (Freehafer and Mast, 1967). Also, a reduction in the passive range of motion at the wrist has been observed after transfer (Johnson et al., 1996). We hypothesize that surgical tensioning of the Br-ECRB transfer influences both active wrist extension and passive range of motion. We have developed a computer simulation of the transfer to test this hypothesis and to evaluate how surgical technique influences wrist function.

PROCEDURES

The Br-ECRB tendon transfer was simulated using an existing computer graphics-based model of the upper extremity (Murray et al., 1995; Gonzalez et al., 1997). The computer model allows the calculation of muscle lengths, forces, moment arms, and joint moments as a function of both elbow and wrist position. The model of the Br-ECRB transfer assumes that the transfer combines the elbow flexion moment arm of the brachioradialis with the wrist extension moment arm of the ECRB. We used the model to evaluate two different surgical techniques. The model of a *slack* transfer assumes the muscle fibers operate primarily on the ascending limb and plateau of the isometric force-length curve between full elbow extension (0°) and 130° elbow flexion. The model of a *tight* transfer assumes the muscle fibers operate at longer lengths for this range of motion, on the plateau and descending limb of the force-length curve.

To evaluate how surgical technique influences wrist function, the active and passive moment-generating capacities of the slack and tight transfers were compared to passive properties of the wrist joint. Wrist function was evaluated in arm postures where gravity opposes wrist extension. The gravitational wrist flexion moment imposed by the weight of the hand was estimated for a 50th percentile male based on regression equations (McConville et al., 1980), and was combined with measurements of the passive moment generated at the wrist by joint structures and muscles. Passive joint properties were measured in a subject with C5 level tetraplegia (Lemay and Crago, 1997).

RESULTS AND DISCUSSION

Given the passive wrist joint properties of an individual with C5 level tetraplegia without a Br-ECRB tendon transfer, the equilibrium position of the wrist (i.e., the position where the net passive moment is 0 Nm) is 26° flexion (Fig. 1). In more flexed wrist positions, the net passive moment is an extension moment. Thus, without the ability
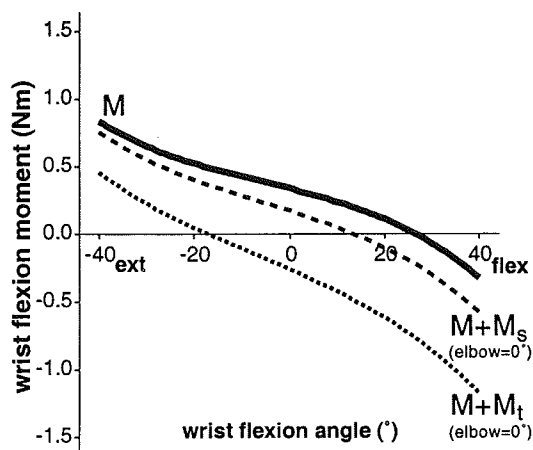
Figure 1. Net passive moment at the wrist joint without the Br-ECRB transfer (M), after a slack transfer (M+M$_s$), and after a tight transfer (M+M$_t$).

to actively generate a flexion moment, 26° flexion is the most flexed wrist posture that can be reached.

When the elbow is fully extended, both the slack and tight transfers generate a passive wrist extension moment which limits the attainable range of motion (Fig. 1). The passive extension moment generated by the slack transfer shifts the equilibrium position (and maximum flexion position) of the wrist to 12° flexion. The tight transfer shifts the equilibrium position to 18° wrist *extension*.

To maintain the wrist in a posture that is more extended than its equilibrium position, the Br-ECRB transfer must generate an extension moment to balance the net passive flexion moment at the wrist. The maximum isometric wrist extension moment generated by the transfer varies as a function of both wrist and elbow position. When the wrist is extended 40°, the moment-generating capacity of the slack transfer is not sufficient to maintain this wrist posture at elbow flexion angles greater than 108° (Fig. 2). However, the tight transfer can maintain 40° wrist extension up to 128° elbow flexion.

SUMMARY

Surgical tensioning of the Br-ECRB transfer influences the ability to actively extend the wrist and the passive range of motion of the

wrist. When tensioning the Br-ECRB tendon transfer, a surgeon should consider the balance between wrist extension (which provides *hand grasp*) and wrist flexion (which provides *hand opening*) that is necessary for functional use of the hand.

REFERENCES

Freehafer, A. A. and Mast, W. A. (1967). *J Bone Jt Surg*, **49-A**, 648-652.
Gonzalez, R. V. et al. (1997). *J Biomech*, **30**, 705-712.
Johnson, D. L. et al. (1996). *J Bone Jt Surg*, **78-A**, 1063-1067.
Lemay, M. A., and Crago, P. E. (1997). *IEEE Trans Rehab Eng*, **5**, 244-252.
Long, C. and Lawton, E. B. (1955). *Arch Phys Med Rehab*, **36**, 249-255.
McConville, J. T. et al. (1980). *Technical Report AFAMRL-TR-80-119*.
Murray, W. M. et al. (1995). *J Biomech*, **28**, 513-525.

ACKNOWLEDGEMENTS
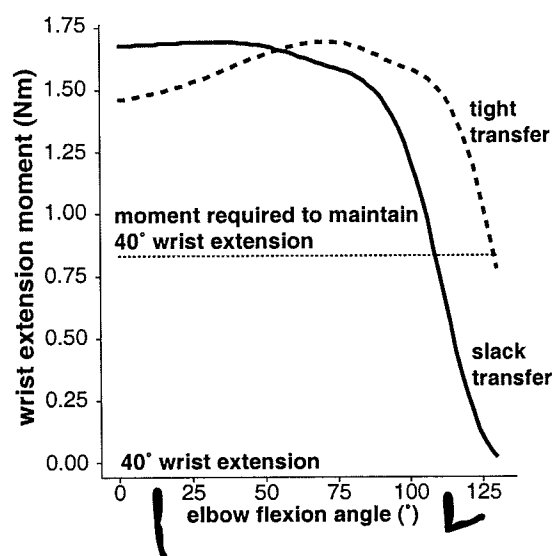
Figure 2. Comparison between the wrist extension moment generated by the slack and tight transfers when the wrist is extended 40° with the joint moment required to maintain that position.

A FIBER NETWORK THEORY MODEL TO DESCRIBE STRESS AND STRAIN IN THE INTEROSSEOUS LIGAMENT OF THE FOREARM

Jamie Pfaeffle[1], Theodore Manson[1], Kenneth Fischer[1], Jeffrey Weiss[2],
Matthew Tomaino[1], James Herndon[3], Savio L-Y Woo[1]

[1]Musculoskeletal Research Center, University of Pittsburgh, Pittsburgh, PA
[2]University of Arizona, Biomedical Engineering Program, Tucson, AZ
[3]Partners Department of Orthopaedics, Harvard Medical School, Boston, MA

Email: hjpst4@pitt.edu

INTRODUCTION

Ligaments are fibrous structures for which local levels of stress and strain vary spatially and change with joint position. Knowledge of the distribution of stress and strain in ligaments is needed to understand their function, mechanisms of injury, and efficacy of reconstruction techniques. Analysis of stress and strain in ligaments must account for a non-linear response, fiber direction, and allow fibers to collapse in compression.

While ligaments of the knee have received much attention, less is known about the interosseous ligament (IOL). It is a thin, wide ligament that connects the radius and ulna in the central forearm. The objective of this study was to develop a theory to describe stress and strain in the IOL that develops when load is applied to the hand. Since its local fiber orientation can be easily visualized, fiber network theory (Genensky and Rivlin, 1955, Steigmann and Pipkin 1991) is a suitable approach. Tension field theory (Steigmann, 1990) can account for the fact that ligament fibers cannot withstand compression.

MATERIALS AND METHODS

Soft tissues over the IOL were dissected away from a cadaveric forearm (58 year old male). Plexiglas registration blocks were attached to the bones close to the IOL insertions. CT scans were obtained, and in house software was used to build computer surface models of the radius, ulna, and IOL. Three adjacent sides of the registration blocks were used to define local coordinate systems (in CT coordinates) on the radius and ulna. Planes were fit to 100 points on each side using a least-squares technique. Intersection of the plane equations and the plane normals defined the position and orientation of the local coordinate systems to within 0.1 mm and 0.1° of accuracy.

A previously described experiment was performed to load forearms to 136N of compression (Pfaeffle, et al., 1997). Before and after application of load to the forearm, a Microscribe digitizer (Immersion Corp., San Jose, CA) was used to collect points on each registration block (from the same three sides used to define local coordinate systems in the CT data set). This experimental procedure was performed with the forearm in pronation, neutral rotation, and supination positions, respectively. After tests, the forearm was placed in neutral rotation, the registration blocks were digitized, and surface markers were placed on the IOL. Digital images were obtained before and after the IOL was cut out of the forearm and were used to measure the in-situ strain field.

Point data from the digitizer were used to define local coordinate systems on the bones using the method described for the CT data set. Thickness of the IOL and splines along the insertion sites were digitized on the computer models using TECPLOT (Amtec Engineering, Seattle, WA). A ruled surface representation of the IOL was defined in a Mathematica program (Figure 1).

CT GEOMETRY   **RULED SURFACE**
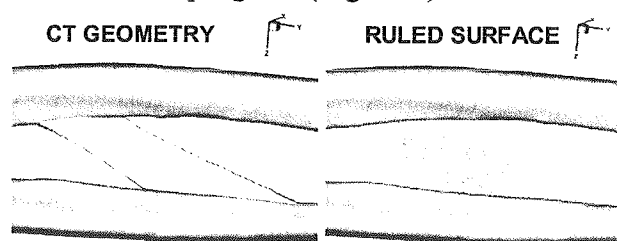
Figure 1. Ruled surface depiction of the IOL:

Using the local coordinate systems, the ruled surface was transformed to the configuration in which in-situ strains were measured, and fiber lengths were shortened based on the in-situ strain field to obtain the stress-free configuration. Rigid body kinematics from the loading experiment provided deformation of the ruled surface. An average stress-strain relation for the IOL determined from tensile tests of 18 specimens was expressed per unit width using the IOL thickness and used to predict the stress field. Kinematics of the bones were implemented in TECPLOT to visualize results in 3-D.

RESULTS

The loading experiment showed that the primary motion causing extension of the IOL fibers was lateral motion of the insertion sites away from each other, when load was applied to the hand. The network theory model predicted the net force in the IOL to be 27 N, 36 N, and 30 N in pronation, neutral rotation, and supination, respectively. These values are in the range of our experimental results for the net force in the IOL (Pfaeffle et al., 1998).

In-situ strain in the IOL was uniform across fibers at 2% strain. The network model results showed that the IOL displays non-uniform stress patterns that vary with forearm rotation (Figure 2). In pronation, levels of stress were relatively uniform, with a maximal stress in fibers near the elbow and only small variation across fibers.

In neutral rotation, stresses were the highest, with a maximal stress in fibers of the IOL near the elbow, and a larger gradient of stresses across fibers. In supination, stresses showed the greatest variation across fibers, with a maximal stress in fibers near the wrist and the lowest stress level observed for all positions in fibers near the elbow. Strains followed similar trends (Table 1).

	Pronation	Neutral	Supination
Min	3.3	3.7	2.1
Max	3.6	5.2	5.1

Table 1. Min and max fiber strains predicted by the network theory model (in percent).

DISCUSSION

In this work a network theory model for the IOL was successfully developed. The model shows that fibers of the IOL are not uniformly loaded, and is confirmed by experiment for net force in the IOL. It provides valuable information for surgeons regarding which parts of the IOL are taut in different joint positions. Future studies on experimental validation of IOL strain patterns, interactions between fibers and modeling non uniform stress-strain field along fibers are suggested.

ACKNOWLEDGMENT

REFERENCES

Genensky, S., Rivlin, R. (1955). *J. Rational Mechanics and Analysis*, 4:30-44.

Steigmann, D., Pipkin, A. (1991). *Phil. Trans.Royal Soc.of London*, **335**: 419-54.

Steigmann, D. (1990). *Proc. of the Royal Society of London*, **429**:141-73.

Pfaeffle, H.J., et al. (1997) *Trans ASME,* **BED 35**:173-174. .

Pfaeffle, H.J., et al., (1998) *Trans ORS* 1:287.

PRONATION
Min 20.8
Max 23.8

NEUTRAL
Min 23.3
Max 38.3

SUPINATION
Min 10.0
Max 40.0
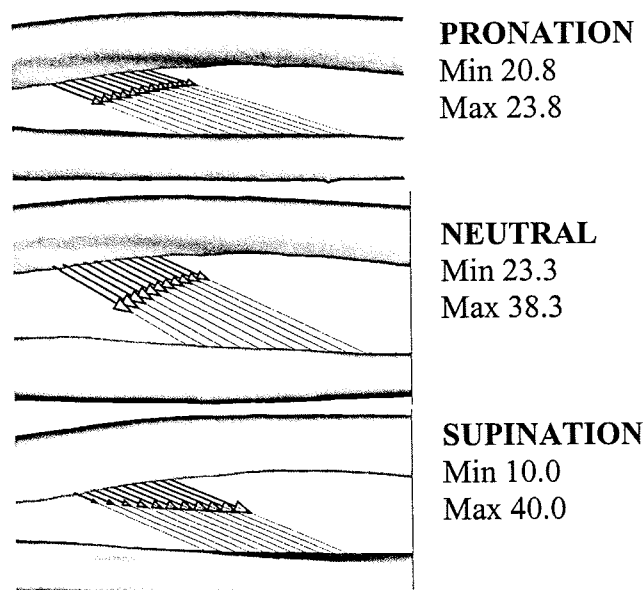
Figure 2 Fiber stresses in the IOL (MPa).

EFFECT OF GAIT SPEED ON OBSTACLE CROSSING OF THE TRAILING LIMB

Christina Kuo and Louis F. Draganich

University of Chicago, Section of Orthopedic Surgery and Rehabilitation Medicine,
Department of Surgery, Chicago, Illinois
Email: ldragani@surgery.bsd.uchicago.edu

INTRODUCTION

Our study was motivated by the serious problem of falls in the elderly. Tripping over obstacles has been cited as a frequent cause of falls in the elderly (Campbell et al., 1990). Previous studies on obstacle crossing of the trailing limb have examined the effects of toe-obstacle distance and obstacle height, but not the effect of gait speed on this activity (Chou and Draganich, 1997; Chou and Draganich, 1998). Our objective was to investigate the effect of walking speed on the biomechanics of the trailing limb during obstacle crossing. Gait speed is important because of the range of speeds commonly used in everyday life and the fact that in healthy adults, average gait speed peaks in the 30s and then decreases with age (Bohannon, 1997). Decreased gait speed has been associated with decreased muscular strength and falling in the elderly (Whipple et al., 1987). To obtain baseline data, we examined the trailing limb during obstacle crossing of 10 healthy young adults. We hypothesized that increased gait speed would significantly increase the motions and moments of the trailing limb while crossing an obstacle. If this is true, then the elderly should be careful not to walk too fast.

PROCEDURES

Gait analysis was performed on 10 healthy young adults (5 females, 5 males), having a mean age of 25 years (range, 22-39 years), an average height of 171 cm (range, 155 cm to 187 cm), and a mean weight of 643 N (range, 463 N to 904 N). All of them were right hand dominant. Subjects wore low-heeled shoes for the experiment. The obstacle was a white wooden rod 37 in. (94 cm) long and 0.03 in. (0.5 cm) in diameter, held 8 inches high (204 cm) by grooves in the two vertical arms of an aluminum frame. Subjects were asked to walk along the 9.5m long walkway, step over the obstacle with their right legs first and their left legs (trailing limbs) second, and continue walking to the end of the walkway. Each subject crossed the obstacle at a self-selected normal speed, self-selected slower than normal speed and self-selected faster than normal speed. The order of the slow and fast trials was random.

Ground reaction forces were measured with a multicomponent force platform in the center of walkway. Clusters of six or eight infrared light-emitting diodes were attached to the foot, shank, and thigh of the left lower limb and pelvis of the subject with elastic straps. Kinematic parameters were collected with the OPTOTRAK optoelectronic, three-dimensional digitizing system. Kinematic and force parameters were sampled at a rate of 100 Hz. The overall accuracy of the system was better than 0.5 mm.

The mean of three trials for each walking speed was used in formulating the results. SYSTAT was used to perform the statistical analysis. The effects of walking speed on the motions and moments of the trailing limb were tested using one-way analysis of variance with repeated measures. To account for multiple comparisons, an α level of 0.01 was used to determine statistical

significance. If a significant difference was detected, the polynomial test was performed at an α=0.05 level of significance to determine the trend (linear, quadratic, or cubic). The flexion-extension angles and external moments for the joints of the trailing limb are reported here.

RESULTS

When stepping over an obstacle in a self-selected manner, increasing gait speed significantly increased crossing velocity ($p \leq 0.0001$). Gait speed was not found to affect the flexion-extension angles of the joints. The peaks of five external flexion-extension moments about the hip, knee, and ankle increased linearly with gait speed (Fig 1). The largest increases from slow to fast speeds were 100% for hip flexion moment ($p \leq 0.0001$), 47% for knee flexion moment in late stance ($p \leq 0.0001$), and 63.3% for ankle plantarflexion moment ($p \leq 0.0001$).

DISCUSSION

Gait speed did not significantly affect the flexion-extension angles of the hip, knee or ankle of the trailing limb. Thus, flexion-extension angles are not key factors to crossing obstacles at increased gait speeds. However, five flexion-extension moment variables increased significantly with increased walking speed, so muscle strength is important to crossing obstacles at increased speeds. Studies have shown that muscle strength begins to diminish from the 5th decade until the 9th decade by 12-15% per decade, and that ankle and knee flexion-extension strengths are significantly weakened in a subset of elderly who suffer frequent falls (Whipple et al., 1987; Wolfson et al., 1985). The implication is that in frail older adults, the risk of tripping over obstacles is increased with faster gait.
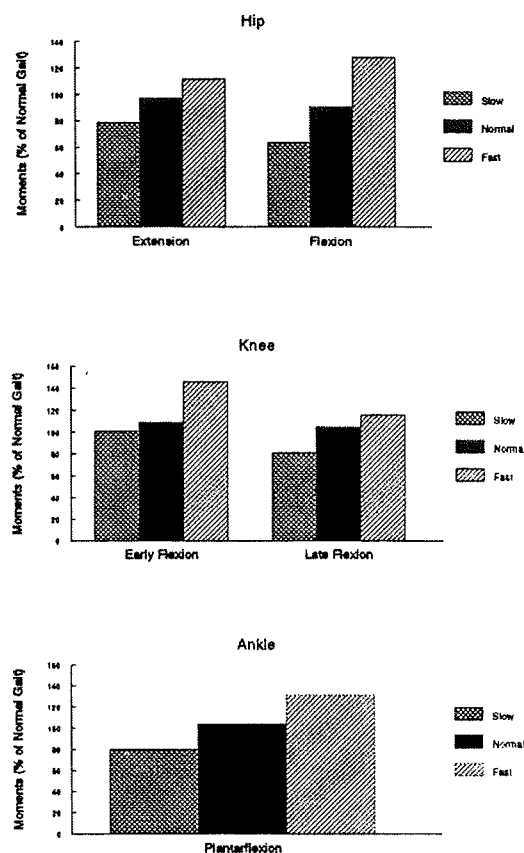
Figure 1. Hip, knee and ankle moments that increased linearly from slow to fast.

REFERENCES

1. Campbell, A.J. et al. (1990). *Age and Ageing,* **19**,136-141.
2. Chou, L.S. and Draganich, L.F. (1997). *J Biomechanics,* **30**, 331-337.
3. Chou, L.S. and Draganich, L.F. (1998). *J Biomechanics,* **31**, 685-691.
4. Bohannon, R.W. (1997). *Age and Ageing,* **26**, 15-19.
5. Whipple, R.H. et al. (1987). *J Am Geriatric Soc,* **35**, 13-20.
6. Wolfson, L.I. et al. *J Gerontology,* (1985). **50A**, 64-67.

TIBIAL ACCELERATION AS A PREDICTOR OF SKELETAL LOADING

Jennifer D. Lawson and Neil A. Sharkey

Center for Locomotion Studies and Department of Kinesiology
The Pennsylvania State University, University Park, PA
Email: celos@psu.edu   Web: www.celos.psu.edu

INTRODUCTION

Individuals who accumulate greater bone mass early in life may delay the onset of osteoporosis and associated fractures because they have more bone to lose later in life (Friedlander et al., 1995). It is known that the skeleton responds to increased mechanical usage by depositing more bone mass. During years of rapid growth (adolescence) habitual participation in activities that increase skeletal loading may build additional bone mass and help prevent osteoporosis and fractures in old age.

The daily stress stimulus theory proposes that bone remodeling and homeostasis can be predicted by multiplying the number of loading cycles (n) incurred at particular stress magnitudes by those magnitudes (σ) raised to an exponent (m), and then summing over the entire range of stress magnitudes encountered in a day (Carter et al., 1997).

$$\Psi = \left[\sum_{day} n_i \, \sigma_i^m \right]^{1/m}$$

Whalen et al. (1988) substituted an external measure of ground reaction force (GRF) for the effective stress term (σ) and proposed that the daily stress stimulus could be effectively estimated from GRF history. Unfortunately, accurate and continuous measurement of GRF is technically difficult. Accurate GRF measurements require stationary ground-based force platforms. Portable in-shoe systems have been developed but these devices tend to have low frequency responses and yield inconsistent results. Portable and continuous measurement of acceleration may be a more practical approach in humans because accelerometers have a high frequency response and are small and relatively unobtrusive. The goal of this study was to determine if accelerations measured at the distal tibia correlate with GRFs, in the hope that they might provide a useful index of skeletal loading.

PROCEDURES

Vertical ground reaction forces, and accelerations of the distal tibia were measured using a force platform (Kistler Model 9287A) and a uniaxial accelerometer (Kistler Model 802BD) respectively. A custom holder and Velcro™ strap, secured as tightly as possible without causing discomfort, were used to mount the accelerometer just proximal to the ankle, with its axis aligned with the long axis of the tibia. Ten healthy female subjects between the ages of 17 and 30 were tested while performing the following activities: walking, running, cutting at a 45-degree angle while running, and jumping down from heights of 20cm (8"), 40cm (16"), and 60cm (24"). All subjects wore athletic shoes. Each subject executed three trials of each activity while GRFs and accelerations were recorded at 1000 Hz using a portable PC, a National Instruments PCMCIA data acquisition card, and LABVIEW software.

All forces were normalized to body weight and data were compiled for all activities. Regression analyses were then performed to determine the relationships between distal tibial acceleration and peak vertical ground reaction force, initial vertical loading rate (slope to first peak of the vertical GRF profile), and initial impulse (area under the first peak).

RESULTS

Average tibial accelerations ranged from 2.9g for walking to 48.2g for jumping from a 60cm (24") height (Fig. 1). Within-subject accelerations were consistent for each activity but varied considerably across subjects. For example, tibial accelerations for jumping from a 40cm (16") height was subject dependent and ranged from 11.0g to 53.3g.
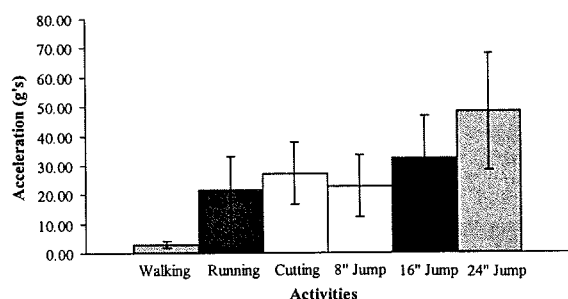
Figure 1: Average peak accelerations at the distal tibia during different activities (n=10; error bars = 1 SD)

Significant but weak correlations were found between acceleration and GRF. The most promising linear analyses were between acceleration and peak vertical GRF ($R^2 = 0.45$, Fig.2) or acceleration and initial vertical loading rate ($R^2 = 0.46$).

DISCUSSION

We found that accelerations at the distal tibia during walking, running, cutting, and jumping were significantly correlated to both the initial peak in vertical GRF (normalized to body weight) and the initial vertical loading rate. Though these

relationships were highly significant ($p < 0.001$) they indicate that tibial accelerations can only explain about one-half of the variance in ground reaction forces. This finding is not surprising given that GRFs are dependent on the accelerations and mass of the whole body, whereas our acceleration measurements consider some unknown fraction of that mass. Clearly, other factors, such as body mass distribution, footwear, and motor coordination also influence the accelerations measured at the distal tibia.
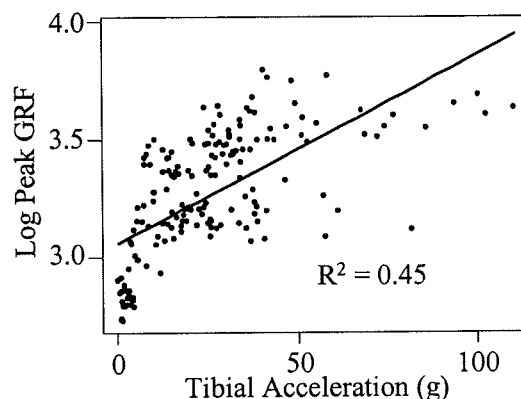
Figure 2: Linear regression of tibial acceleration vs. log peak GRF.

CONCLUSION

Our data suggest that monitoring tibial accelarations may be useful for tracking skeletal loading but it is by no means ideal. Further research and development of other more predictive technologies appears to be warranted.

REFERENCES

Carter, D.R., et al. (1987). *J Biomechanics*, **20**:785-794.

Friedlander, A, et al. (1995). *J Bone Mineral Res*, **10**: 574-585.

Whalen, R.T. and Carter, D.R. (1988). *J Biomechanics*, **21**:825-837.

Linear Power Flow in Voluntary Toe-Walking

Patrick O. Riley and D. Casey Kerrigan

Department of Physical Medicine and Rehabilitation, Harvard Medical School, Boston, MA
and
Center for Rehabilitation Science, Spaulding Rehabilitation Hospital, Boston, MA
Email: patriley@thelma.mgh.harvard.edu

Introduction

Toe walking is common among patients with upper motor neuron pathologies such as stroke and cerebral palsy. A variety of surgical and orthotic interventions is employed to eliminate toe-walking. Toe-walking is believed to impair the mechanics of gait. This belief stems primarily from the analysis of joint powers. Joint powers, as measured in clinical gait analysis, are the product of the net joint moment and angular velocity about the flexion/extension axis. Ankle joint power at push-off is significantly reduced in toe-walking (Olney, MacPhail et al. 1990).

As toe-walking is quite common in nature, far more common than heel-toe walking, even among bipeds, it seems unlikely that it is inherently mechanically disadvantageous. We chose to study the kinetics of toe-walking by comparing the linear power transmitted to the upper-body at the hip joint in heel-toe and toe-walking gait. Further, we employed a novel form of power analysis that allows us to determine the contribution of each joint's moment to the total linear power at the hip.

Procedures

We evaluated the heel-toe and toe-walking gait of 10 healthy young adults (27±5yrs, 60±10kg, 1.7±0.1m). Informed consent was obtained and the protocol was approved by the hospital IRB. Gait laboratory kinematic and kinetic data were obtained for the subjects walking at their chosen speed (1.2±0.1m/s) and toe-walking at nearly the same speed (1.1±0.1m/s). Individual models of each subject's right lower extremity were developed using SIMM/Dynamic Pipeline (Musculo-Graphics, Evanston, IL). Inverse dynamic analysis was then performed using SD/Fast (Symbolic Dynamics, Mountain View, CA). At each instant, the net joint moments were calculated and the instantaneous velocity and contact force at the hip joint were determined. Each net joint moment was then applied individually and the resulting joint velocity and contact force were determined. This permitted us to determine the total hip joint linear power throughout the gait cycle and each joint torque's contribution to the total power. Three trials of each form of gait were analyzed for each subject.

Results

Throughout the gait cycle the net linear power at the hip joint in toe-walking was similar to that in heel-toe walking (Figure 1). There is a large positive component just after heel strike and a smaller component just before toe-off in stance. The average peak hip linear power in toe-walking was 99.3(28.5) watts and 100.1(33.9) watts for heel-toe walking. In late swing, there is also a large positive power flow from the leg to the upper-body.

The ankle moment contribution to the total power showed two positive peaks in stance. The first peak occurred in early stance. The peak ankle moment contribution (the second peak for toe-walking) occurred prior to toe-off in both cases and was not significantly different in magnitude. The first ankle moment associated positive power peak was offset by compensations in the knee moment associated induce power. Knee moment associated linear power becomes positive in early stance in heel-toe gait. In toe-walking, it remains negative throughout stance.

The ankle moment makes no significant contribution in swing. In late swing, the hip moment (extending the thigh) produces a positive power contribution that is precisely offset by the knee moment, which is extending the knee at this stage. Thus, the net positive power flow at the hip in late swing is not due to the action of any joint moment. Rather it is energy flowing from the slowing lower limb to the upper-body.

Figure 1a. Linear power at the hip joint in heel-toe gait.
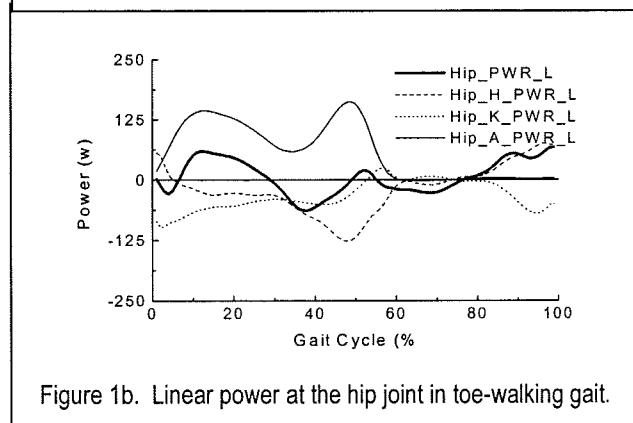
Figure 1b. Linear power at the hip joint in toe-walking gait.

Discussion

Linear power analysis reveals that only a small portion of ankle push-off power directly propels or supports the upper-body. The majority of the power generated by the ankle moment is absorbed in the segments of the lower limb. A portion of the energy absorbed by the lower limb is passively transferred to the upper-body in late stance. This result is consistent with the findings of Meinders et al. (Meinders, Gitter et al. 1998). Thus, calculations of linear power and power flow analyses based on joint powers yield consistent results, as they should.

Calculation of the contribution of each joint moment to the total linear power provides valuable insight into inter-segmental coordination. Toe-walking requires increased knee compliance in early stance.

In healthy young subjects, this is provided by precise modulation of the knee moments. Among patients with neuromuscular pathologies, we would expect to see different compensating mechanisms or failure to compensate, compromising upper-body propulsion or support.

References

Meinders, M., A. Gitter, et al. (1998). "The role of ankle plantar flexor muscle work during walking." Scandinavian Journal of Rehabilitation Medicine 30(1): 39-46.

Olney, S. J., H. E. MacPhail, et al. (1990). "Work and power in hemiplegic cerebral palsy gait." Physical Therapy 70(7): 431-8.

STATIC AND DYNAMIC OPTIMIZATION SOLUTIONS FOR GAIT ARE PRACTICALLY EQUIVALENT

Frank C. Anderson[1] and Marcus G. Pandy[1,2]

[1]Dept. of Mechanical Engineering and [2]Dept. of Kinesiology and Health Education
The University of Texas at Austin, Austin, Texas, USA
Email: fca@mail.utexas.edu

INTRODUCTION

Static optimization has been the method of choice for estimating muscle and joint contact forces during gait (Brand et al, 1994). Although the relatively small computational demands of this approach have allowed very detailed musculoskeletal models to be used, static optimization has been criticized in several respects: 1) the method is highly dependent on the accurate collection and processing of experimental data, 2) the physiological properties of muscle have typically not been included in the problem, and 3) the performance criterion is required to be time-independent (Hardt, 1978; Patriarco et al., 1981). Dynamic optimization addresses these shortfalls, but it incurs enormous computational cost. As a result, dynamic optimization solutions for gait have been few and have lagged behind their static optimization counterparts in terms of model complexity (Yamaguchi and Zajac, 1990), so much so that a meaningful comparison of the two methods as they apply to gait has not been possible. In this study, a dynamic and a static optimization problem for gait were solved. The musculoskeletal model used was similar in complexity to previous static optimization models and considerably more detailed than previous dynamic optimization models. A direct comparison of the two methods was made possible by using as inputs to the static optimization problem the joint moments computed from the dynamic optimization solution.
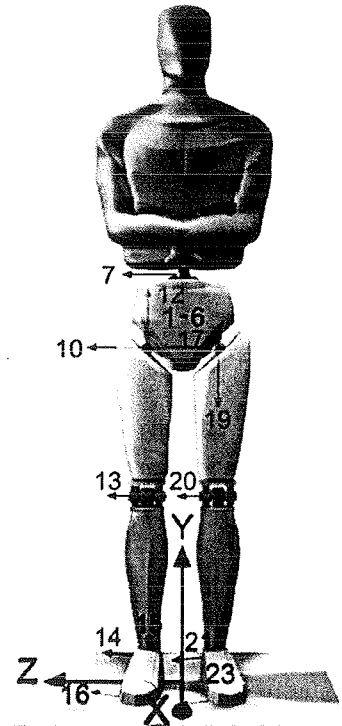
Figure 1: Model of the body.

METHODS

The body was modeled as a 10-segment, 23-degree-of-freedom linkage (Fig. 1). Each leg was actuated by 24 muscles. Relative movements of the pelvis and upper body were controlled by 6 abdominal and back muscles. Interaction of the feet with the ground was modeled using a series of spring-damper units distributed under the sole of each foot. Details of the model are given in Anderson and Pandy (in press). In the static optimization problem, the physiological properties of the muscles were

taken into account by limiting muscle force in accordance with the force-length-velocity property of muscle; however, muscle activation dynamics was neglected. The performance criterion was the minimization of the sum of the square of muscle activations. For the dynamic optimization problem, the performance criterion was the minimization of the total amount of metabolic energy expended per unit distance traveled.

RESULTS

In general, the time histories of muscle force predicted by the static and dynamic optimization solutions were very similar. Consequently, the contact forces at the hip, knee, and ankle were also similar (Fig. 2).
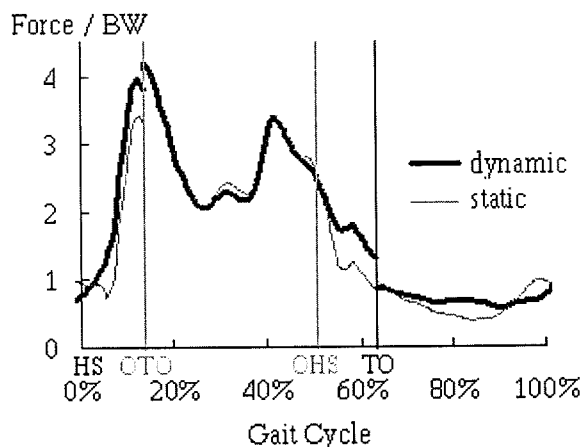
Figure 2: Resultant joint contact force at the hip normalized by body weight.

DISCUSSION

The striking similarity between the dynamic and static optimization solutions provides strong evidence that static optimization is entirely adequate for predicting joint contact forces during gait, provided that the net joint torques exerted by the muscles are known with confidence. Similarity between the two solutions implies that 1) activation dynamics may be neglected in the static optimization

problem for gait and 2) there is a functional equivalence between minimizing metabolic energy over the entire gait cycle (a time-dependent performance criterion) and minimizing the sum of muscle forces squared at any instant (a time-independent performance criterion). Accurately estimating the net joint torques exerted by the muscles remains a critical element of the static optimization approach (Patriarco et al., 1981). It is suggested that dynamic optimization should be used when 1) accurate experimental data cannot be obtained, 2) activation dynamics is suspected to play a significant role during the activity, or 3) one would like to use simulation as a tool for predicting how changes in musculoskeletal structure might affect function.

REFERENCES

Anderson, F.C., Pandy, M.G. (in press). *Comp. Meth. Biomech. Biomed. Engng.*

Brand, R.A. et al. (1994). *J. Arthroplasty*, **9**, 45-51.

Hardt, D.E. (1978). *J. Biomech. Engng.*, **100**, 72-78.

Patriarco, A.G. et al. (1981). *J. Biomech.*, **14**, 513-525.

Yamaguchi, G.T., Zajac, F.E. (1990). *IEEE Trans. Biomed. Engng.*, **37**, 886-902.

ACKNOWLEDGEMENTS

A Comparison of Between Day Reliability of Different Types of Lower Extremity Kinematic Variables in Runners

D. Williams[1], I. McClay[1,2] and C. Laughton[1]

[1]Motion Analysis Laboratory, University of Delaware, Newark, DE 19716
[2]Joyner Sportsmedicine Institute, Harrisburg, PA 17111
e-mail: blaise@udel.edu

INTRODUCTION

Three-dimensional motion analysis has become a valuable tool for research and clinical assessments over the past ten years. One commonly recognized problem is the day to day variability that may be present due to placement of markers over the skin. This variability is especially important when the same subject is being tested on more than one occasion and comparisons are made between the two sessions.

Kadaba et al (1989) have demonstrated relatively low between day reliability in walking in the frontal and transverse plane angles and attributed these results to replacement of markers between days. Coefficients of multiple correlation were used to compare similarities in the overall patterns of motion. However, distinct points such as peak angles, peak velocities and angular excursions are often the variables of interest used when making statistical comparisons. It is important to understand the magnitude of change that is attributed to simply repositioning the markers when interpreting statistical results. Therefore the purpose of this study is to compare the three-dimensional kinematics of the hip, knee and rearfoot in runners in two separate data collections. It was anticipated that excursion and velocities would be less sensitive to marker placements and result in higher reliability values than peak values.

PROCEDURES

Twenty recreational runners volunteered for this study. The right leg was tested in all individuals and subjects had no lower extremity injuries at the time of testing.

Four retroreflective markers were affixed to a velcro-backed polyform shell and attached to the thigh via a neoprene wrap. In addition, four markers were attached to the shank via neoprene wrap and three markers were attached to the heel counter of the shoe. Additional markers were placed over various body landmarks to establish the anatomical coordinate systems in which the motion would be described. After a standing calibration trial was collected, the anatomical markers were removed.

Subjects then ran along a 75-ft. runway at a speed of 3.35 m/s ($\pm 10\%$). Five trials were collected. Subjects then returned for a second data collection in which the same procedure was employed. The same tester attached the markers on all subjects. Data were sampled at 120 Hz with a 6 camera VICON (Oxford Metrics, UK) motion analysis system. GRF were collected with a Bertec (BERTEC Corp, OH) forceplate being sampled at 480 Hz. Three-dimensional joint kinematics were calculated using MOVE3D software (NIH Biomechanics Laboratory). The variables of interest were three-dimensional angular peaks, excursions and velocities at the hip, knee and ankle. Additionally, ground reaction forces were evaluated. Intraclass correlation coefficients (ICC(2,k)) were used for the chosen variables to compare reliability between days.

RESULTS

Table 1: ICC(2,k) for rearfoot

	DF (Sag)	EV (Frt)	AB (Trans)
Peak	0.287	0.472	0.778
Excurs	0.804	0.898	0.895
Veloc	0.919	0.905	0.740
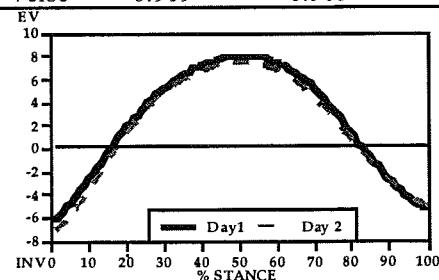
Figure 1: Rearfoot Frontal Angles

Table 2: ICC(2,k) for knee

	Flx (Sag)	Add (Frt)	IR (Trans)
Peak	0.743	0.767	0.939
Excurs	0.914	0.799	0.790
Veloc	0.961	0.922	0.900
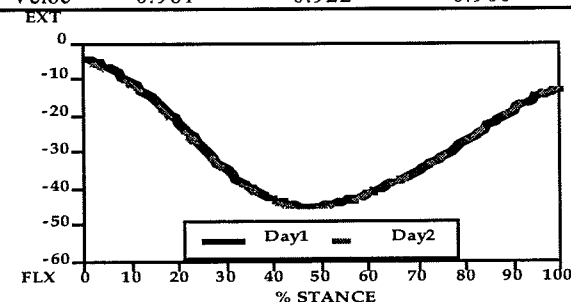
Figure 2: Knee Sagittal Angles

Table 3: ICC(2,k) for hip

	Flx (Sag)	Add (Frt)	IR (Trans)
Peak	0.863	0.737	0.591
Excurs	0.787	0.768	0.764
Veloc	0.594	0.774	0.843
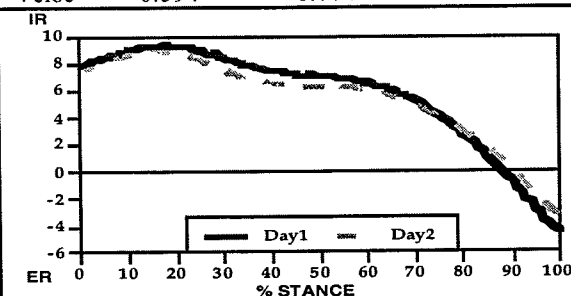
Figure 3: Hip Transverse Angles

Table 4: ICC(2,k) for GRFs

	ICC(2,k)
Peak lateral GRF	0.460
Peak medial GRF	0.918
Peak braking GRF	0.718
Peak propulsive GRF	0.777
Peak vertical GRF	0.743

DISCUSSION

There was remarkable agreement in the averaged curves between days for all variables as represented in Figs. 1 -3. This suggests that when looking at averaged group curves, there is good agreement. However, the ICC(2,k) values which are associated with peaks are lower which suggests higher within subject variability between days (shaded in Tables 1-3). For instance one subject exhibited a difference in peak eversion of 10.1° between days.

Anatomical marker placement is most crucial as this establishes the anatomical coordinate system (ACS) about which axes the angles are decomposed. Slight changes in marker positions would result in different peak angle values. As expected, excursions and velocities had higher ICC values than the peaks did. Peak values are absolute measures and more likely affected by alterations in the ACS alignments than the relative measures of velocity and excursion.

The relatively high reliability in the secondary planes was surprising in light of previous reports. The lower ICCs for the peak rearfoot values suggest more attention should be paid to the placement of the foot markers. Finally, ground reaction force ICCs (Table 4) suggest some of the between day variability may be due to true mechanical differences.

SUMMARY

These data suggest that when marker placement is carefully standardized, average patterns of motion are very consistent. However, when assessing individual subjects across days, ICC(2,k) values are more variable. Velocities and excursions are more reliable from day to day and these values may be more useful than peaks in interpreting changes. This is important when these parameters are being compared before and after treatment interventions.

REFERENCES

Kadaba et al. J Orthop Res., 1989.

GAIT CHARACTERISTICS OF PATIENTS WITH PROGRESSIVE MULTIPLE SCLEROSIS

Ann E. Walker[1], John H. Noseworthy[2], and Kenton R. Kaufman[1]

[1]Biomechanics Laboratory, Dept. of Orthopedics, [2]Dept. of Neurology
Mayo Clinic, Rochester, Minnesota
Email: kaufman.kenton@mayo.edu

INTRODUCTION

Individuals affected with progressive multiple sclerosis (MS) have complex, multi-system pathologies. Clinical evaluation of gait is difficult because systems including muscle function, motor control and integration of movement may be affected by MS leading to subtle and obvious changes in locomotion capabilities. Identification of effective therapies for MS have been significantly hindered due to the largely unpredictable clinical course of the disease and the limited understanding of its etiology and pathogenesis. The purpose of this study is to determine if the gait characteristics of patients with progressive MS may be used to differentiate their ambulation characteristics from subjects with normal gait.

PROCEDURES

Eighteen patients, seven women and eleven men, identified with progressive MS were selected to participate in the study. The patients had a mean age of 49 ± 8.5 years. Each patient was evaluated by a neurologist to confirm the diagnosis of progressive MS. The gait of 19 normal subjects, ten women and nine men, was also analyzed. The normal subjects had a mean age of 32 ± 6.9 years. All subjects were studied during level walking. A set of 24 reflective markers were placed on bony landmarks as described by Kadaba et al. (1989). Data from at least three complete gait cycles was collected for both the right and left side of the body. A

six camera ExpertVision System (Motion Analysis Corporation, Santa Rosa, CA) was used to collect three-dimensional trajectory data of the reflective markers at a sampling rate of 60 frames per second. Data analysis was performed using Analyze software (Meglan, 19910.) to obtain temporal-distance (TD) parameters. A two-sample t-test was used for inter-group comparison. A paired t-test was used for inter-visit comparison if the data was normally distributed, otherwise a Wilcoxon signed-rank test for non-normally distributed data was used.

RESULTS

The TD parameters for patients with MS and normal subjects are presented in Table 1. During normal walking, the MS patients exhibited a 35% reduction in velocity compared to normals. The decreased velocity is the result of a 25% decrease in stride length, and a decrease in cadence of 22% as compared to the normals. Step width showed a 23% increase over normal subjects.

Table 1 Comparison of gait parameters.

	Normal		MS		p-level
Parameter	Mean	±SD	Mean	±SD	
Velocity(m/s)	1.22	0.12	0.78	0.30	0.0001
Stride(m)	1.32	0.14	0.99	0.29	0.0004
R_Step(m)	0.66	0.08	0.51	0.14	0.0006
L_Step(m)	0.66	0.09	0.49	0.14	0.0002
Step Width(m)	0.13	0.03	0.16	0.05	0.0555
Cadence (steps/min)	115.81	9.51	90.43	14.8	0.0001

In order to test the reproducibility of the gait analysis, each MS patient was retested one week following their initial gait evaluation. Comparison of visit 1 and visit 2 for the MS patients are presented in Table 2. There was no statistical difference found in the TD parameters between visit 1 and visit 2 therefore it can be concluded that gait analysis is reproducible in the MS patients.

Table 2 Gait reproducibility in patients with MS.

	Visit 1		Visit 2		p-level
Parameter	Mean	±SD	Mean	±SD	
Velocity(m/s)	0.78	0.3	0.81	0.3	0.54
Stride(m)	0.99	0.29	1.02	0.3	0.23
R_Step(m)	0.51	0.14	0.52	0.15	0.57
L_Step(m)	0.48	0.14	0.49	0.14	0.35
Step Width(m)	0.16	0.05	0.16	0.05	0.47
Cadence (steps/min)	90.4	15	92.5	16.6	0.92

DISCUSSION

The gait of the MS patients in this study was quantitatively different from the gait of normal subjects. Two likely contributing factors to the observed changes in gait are ataxia and spasticity, both of which depend on the progression of the disease. These neurological impairments affect the patient's muscular coordination during walking and therefore may manifest themselves in terms of decreased stride length and increased step width to maintain a stable base of support during gait. Results of the current study of patients with MS are similar to those reported by Holden (1986) and less than those reported by Gehlson (1986). These differences are likely due to variations in the severity of the disease in the subject pools.

Both the current literature and our data show that TD parameters displayed by the MS patients are clearly different from those displayed by healthy subjects. Measurement of normal gait is reproducible (Growney et al., 1997). Similarly, this study demonstrates that measurement of gait parameters in patients with MS is reproducible. Therefore, it's possible to use TD parameters to develop a reliable differentiation between normal and MS pathological gait. Gait analysis may be a useful tool for quantifying functional changes associated with the disease progression of MS allowing for earlier clinical treatment.

REFERENCES

Holden et al. (1986). *Physical Therapy*, 64: 35-40.

Gehlsen et al. (1986). *Archives of Physical Medicine Rehabilitation*, 67: 536-539.

Growney et al. (1997). *Gait and Posture*, 6: 147-162.

Kadaba et al. (1990). *Journal of Orthopaedic Research*, 8: 383-392.

Meglan, DA. PhD Dissertation, *Enhanced Analysis of Human Locomotion*. The Ohio State University, 1991.

ACKNOWLEDGEMENTS

UPPER EXTREMITY MUSCULOSKELETAL LOADS WHEN USING A WALKER FOR AMBULATION

Guy G. Simoneau[1], George W. Hambrook[2], Gerald F. Harris[2]

[1] Dept. of Physical Therapy, Marquette University, Milwaukee, Wisconsin
[2] Dept. of Biomedical Engineering, Marquette University, Milwaukee, WI
e-mail: simoneaug@vms.csd.mu.edu

INTRODUCTION

In 1990, there were over 1.7 millions non-institutionalized walker users in the United States. While walkers are often used to provide stability and prevent falls, they are also commonly used to help alleviate weightbearing loads on the lower extremities. Individuals who had a recent lower extremity fracture, a joint replacement or a lower extremity amputation are all likely to rely on a standard walker to relieve loads on the affected limb. In addition, the frail elderly may also require assistance from a walker due to generalized weakness of the lower extremity musculature.

Currently, there are no data that fully quantify the loads applied to the upper extremities during walker ambulation. In addition, there are no data that validate a particular walker height and pattern of use to minimize these loads. The purpose of this study was to perform a comprehensive kinematic and kinetic analysis of the upper extremities during walker ambulation. Furthermore, we documented how walker height and placement influence upper extremity kinematics and kinetics.

PROCEDURES

A standard walker was instrumented with strain gages to provide six degree-of-freedom load measurements at each of the hands. Bilateral upper body joint kinematic data were acquired with a six camera Vicon motion analysis system. Shoulder, elbow and wrist joint kinetics were calculated in the three planes using the inverse dynamics method. Moments were normalized to body weight and arm length.

Ten male subjects between the ages of 22 and 33 years participated in this study (mean = 24.4 ± 3.6 years). All subjects were right hand dominant and were tested with the right lower limb being non-weightbearing.

The five walker conditions were as follows: 1) standard walker height and placement (walker height set at the level of the subject's ulnar styloid process, walker placement such that the back legs of the walker were placed level with the tip of the left big toe when positioned on the ground for the next step), 2) walker height 5.08 cm (2 inches) above standard height and standard walker placement, 3) walker height 5.08 cm below standard height and standard walker placement, 4) forward walker placement (standard walker height and back legs of walker positioned 15.2 cm (6 inches) in front of the big toe) and 5) walking into the walker (standard walker height and back legs of walker positioned 15.2 cm behind the big toe). Five gait cycles were analyzed for each subject and each condition.

RESULTS AND DISCUSSION

Gait pattern: The average walking velocities for the five walker conditions ranged from 0.11 to 0.13 m/sec. Stride lengths for the five conditions were between 0.34 and 0.37 meters. Walking velocity and stride length were not statistically different among the five conditions ($p > 0.01$).

The full gait cycle is described from walker contact to the next walker contact. The average time for a full gait cycle was between 3.0 to 3.4 seconds depending on the walker condition. After walker contact, the weight is progressively transferred to the upper extremities until the left foot is lifted

off the ground. This event, described as foot off, occurs at approximately 40% of the gait cycle. After a short time when both feet are off the ground, the left foot is returned to the ground. This event is called foot contact and occurs at about 60% of the gait cycle. Shortly after foot contact (at approximately 72% of the gait cycle), the walker is picked up (event called walker off) to be advanced to its next location. Recall, the right foot is off the ground during the entire gait cycle.

Data for the left and right upper extremities were very similar. Therefore, only right upper extremity data will be presented here.

Sagittal plane upper extremity kinematics (standard condition): Approximately 20° of shoulder flexion is present at walker contact. The shoulder moves toward extension as the weight is progressively applied to the upper extremities. Maximum shoulder extension of approximately 10° is reached in the foot contact-walker off interval of the gait cycle. Approximately 40° of elbow flexion is present at walker contact. The elbow extends to an angle of approximately 30° in the foot off-foot contact interval. Maximum elbow flexion occurs when the walker is lifted off the ground to be advanced forward. Approximately 12° of wrist extension is present at walker contact. The wrist extends to a maximum of about 35° in the foot off - foot contact interval.

Sagittal plane upper extremity kinetics: For the standard walker condition, the peak shoulder flexion moment (generated by the shoulder flexors) is 0.16 ± 0.06 Nm/Kgm. This peak moment occurs before foot off. Maximum elbow extension moment is 0.18 ± 0.08 Nm/Kgm. This peak moment occurs at just about foot off. The maximum wrist flexion moment of 0.09 ± 0.04 Nm/kgm occurs in the foot off to foot contact interval.

Influence of walker height on joint kinetics: Walker height had a statistically (p < 0.05) significant influence on peak torque values at the shoulder, elbow and wrist. Raising the walker by 2 inches increased the peak shoulder flexion moment to 0.19 ± 0.04 Nm/kgm (a 19% increase). Lowering the walker by 2 inches lowered the peak

shoulder flexion moment to 0.13 ± 0.03 Nm/kgm (a 19% decrease). Peak elbow extension moments were 0.27 ± 0.11 and 0.13 ± 0.05 for the higher and lower walker settings, respectively (a 50% increase and 28% decrease). The higher walker setting increased peak flexion moment at the wrist to 0.12 ± 0.05 Nm/kgm (33% increase). The lower setting decreased the peak flexion moment to 0.07 ± 0.02 Nm/kgm (22% decrease).

Influence of walker placement on joint kinetics: Walker placement also had a significant (p < 0.05) influence on peak torque values at the three joints. Placing the walker 6 inches in front of the toes increased the peak shoulder flexion moment to 0.32 ± 0.14 Nm/kgm (a 100% increase). Walking more into the walker lowered the peak shoulder flexion moment to 0.07 ± 0.03 Nm/kgm (a 56% decrease). Peak elbow extension moments were 0.32 ± 0.12 for the more forward placement and 0.11 ± 0.05 for walking more into the walker (a 77% increase and 39% decrease). The forward walker placement increased peak wrist flexion moment to 0.12 ± 0.06 Nm/kgm (a 33% increase). Walking into the walker decreased the peak wrist flexion moment to 0.06 ± 0.02 Nm/kgm (a 33% decrease).

SUMMARY

To our knowledge, this study provides the first detailed analysis of the kinematics and kinetics of the upper extremities during walker ambulation. Our results provide evidence that walker settings (such as height) and walker placement have a statistically and likely clinically significant influence on the musculoskeletal demands of the upper extremities. While young healthy subjects (as tested here) have no difficulty dealing with these changes, walker settings may be critical in maximizing walker usage for frail elderly men and women.

ACKNOWLEDGMENTS

USE OF A DIGITAL INCLINOMETER TO ASSESS SCAPULAR UPWARD ROTATION: A RELIABILITY AND VALIDITY STUDY

Michael P. Johnson [1], Phil W. McClure [2] and Andrew R. Karduna [1]

[1] Department of Rehabilitation Sciences, MCP Hahnemann University, Philadelphia, Pennsylvania
[2] Department of Physical Therapy, Beaver College, Glenside, Pennsylvania

E-mail: johnsonm1@mcphu.edu

INTRODUCTION

Evidence exists that the scapula plays a role in shoulder pathology. However, clinical evaluation of patients with shoulder dysfunction often fails to include an objective assessment of scapular motion. The purpose of this study was to examine the reliability and validity of an inexpensive inclinometer to assess scapular upward rotation during humeral elevation in the scapular plane.

REVIEW AND THEORY

Scapulohumeral rhythm is defined as the coordinated glenohumeral and scapulothoracic movements during arm elevation. Scapular upward rotation occurs simultaneously with humeral elevation. Changes in the scapulohumeral rhythm are associated with various shoulder pathologies (Warner et al., 1992).

Researchers have been studying motion of the shoulder complex for more than 50 years. Early research performed two-dimensional (2-D) static analysis using various methods (Poppen, Walker, 1976). More recent studies used three-dimensional (3-D) static and dynamic motion analysis (McQuade, Smidt, 1998). However, these methods are impractical for use in clinical research and practice.

Recently, 2-D clinical methods have been used to assess scapular positions (Gibson et al., 1995). None of the 2-D clinical methods 1) assesses scapular upward rotation or 2) has been validated with a 3-D motion analysis system.

PROCEDURES

Proposed New Method: A Pro 360 digital inclinometer (Macklanburg Duncan, Oklahoma City, OK) was used for 2-D static measurements of scapular upward rotation during humeral elevation. The instrument was modified by adding two wooden locator rods to its inferior surface. These rods had Y shaped ends, which were placed over the root of the scapular spine and the posterolateral acromion during each measurement session. A guide angled 40° from the frontal plane was used to insure positioning of the arm in the scapular plane. Thirty-nine subjects with (n=16) and without (n=23) shoulder pathology participated in the study.

Reliability: The Pro 360 was used to assess scapular upward rotation positions with the arm at rest, 60°, 90°, and 120° of humeral elevation in the scapular plane. In this study, we assessed seventy-five scapulae for reliability. Intra-rater reliability was determined using repeated measurements from the Pro 360 taken at each static arm position, 10 minutes apart.

Validity: 3-D measurements of scapular

motion were taken using a Polhemus 3Space FasTrak (Polhemus 3Space FasTrak, Colchester, VT). Karduna and associates previously developed a methodology for using this system to accurately measure 3-D scapular kinematics (Karduna et al., 1998). Scapular upward rotation data were statically collected with the arm at rest, 60°, 90°, and 120° of humeral elevation in the scapular plane. Data were also collected during dynamic humeral elevation in the scapular plane.

We assessed fifty-nine scapulae for validity. Validity was determined, at the four arm positions, using the following comparisons: (1) Pro 360 and Polhemus under <u>static</u> arm conditions and (2) Pro 360 and Polhemus during <u>dynamic</u> arm elevation in the scapular plane (see Figure 1).
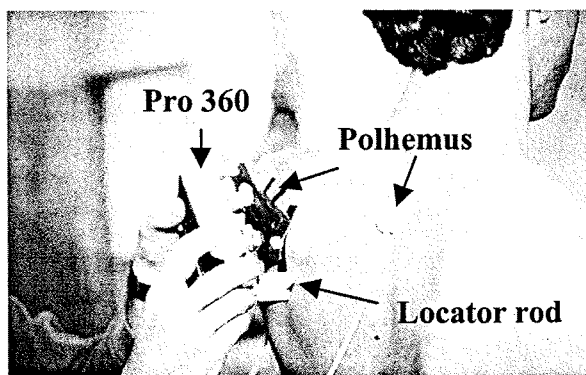
Figure 1: Concurrent measurements of scapular upward rotation using the Pro 360 and Polhemus with the arm held at 90°.

RESULTS AND DISCUSSION

Intra-class correlation coefficients [ICC 3,1], shown in Table 1, indicated excellent reliability. Our results compared favorably with previous literature regarding intra-rater reliability of assessing scapular positions using 2-D methods (Gibson et al., 1995). Pearson product-moment correlation coefficients were used to assess validity and are shown in Table 1. Concurrent validity

was excellent comparing scapular positions using the Pro 360 and the Polhemus under static conditions. Validity was good comparing the Pro 360 and the Polhemus during dynamic arm elevation.

SUMMARY

This is the first study to address validation of a simple, clinical measurement with a 3-D measurement system. The 2-D method described is quick and easy to perform. It is plausible for clinical use and may provide useful objective data regarding scapular motion, which is presently unavailable to the clinician. Future research should address inter-rater reliability and between groups comparisons using a digital inclinometer.

Table 1: Results of reliability and validity testing at all four arm positions.

Arm Position	Reliability ICC (3,1)	Validity (1) r	Validity (2) r
rest	0.90	0.85*	0.68 *
60°	0.90	0.86*	0.65 *
90°	0.93	0.85*	0.67 *
120°	0.94	0.91*	0.71 *

* $p < 0.001$

REFERENCES

Gibson, M.H. et al. (1995). *JOSPT*, 21(2), 100-6.

Karduna A.R. et al. (1998) *Proceedings of NACOB '98*, 575-6.

McQuade K.J., Smidt G.L. (1998). *JOSPT*, 27(2), 125-33.

Poppen N.K., Walker P.S. (1976). *JBJS*, 58-A(2), 195-201.

Warner J.J.P., et al. (1992) *Clin Orthop and Related Research*, 85, 191-9.

STRIDE-TO-STRIDE VARIABILITY IN HUMAN WALKING IS NOT "NOISE"

Jonathan B. Dingwell[1,2], Joseph P. Cusumano[3], Dagmar Sternad[2], Peter R. Cavanagh[1,2,4]

[1]The Center for Locomotion Studies, [2]Department of Kinesiology, [3]Department of Engineering Science and Mechanics, [4]Departments of Biobehavioral Health, Medicine, and Orthopaedics and Rehabilitation, Penn State University, University Park, PA
Email: j-dingwell@nwu.edu   Web: http://www.celos.psu.edu/

INTRODUCTION

Traditional methods of gait analysis typically assume that stride-to-stride variations in walking are random. Potentially important information about spatio-temporal structure in these fluctuations is lost in these analyses. Sensory feedback may play a role in adjusting step-to-step limb trajectories (Nashner, 1980) and/or in smoothing unintended irregularities that occur during unperturbed walking (Gandevia and Burke, 1992). Thus, stride-to-stride fluctuations may contain information about deterministic neuromuscular processes contributing to the generation of normal and pathological gait. This study directly challenges the assumption that stride-to-stride fluctuations in unobstructed overground walking are purely random.

METHODS

Fourteen diabetic patients with significant neuropathy (NP) and twelve gender-, age-, height-, and weight-matched controls (CO) participated. A self-contained "DataLogger" was built to collect kinematic data during continuous walking (Fig. 1). Electrogoniometers measured sagittal plane motions of the hip, knee, and ankle. A tri-axial accelerometer mounted at the base of the sternum measured upper body motions. Ten minutes of data were collected at 66.7 Hz while subjects walked around a 200m open level indoor walking track at their natural pace.

To analyze the nature of walking variability in each time series, average stride profiles were subtracted from each stride of the original data, leaving only the stride-to-stride fluctuations. The method of surrogate data was used to test the null hypothesis that these fluctuations could have been generated by a linearly correlated Gaussian noise process (Theiler et al., 1992). Phase randomized surrogates of the fluctuation signals were generated by computing Fourier transforms (FFT) of the original fluctuation signals, randomizing the phase spectra, and computing inverse FFTs (Theiler et al., 1992). Randomized fluctuation signals were added back onto the original mean periodic signals to generate the final surrogate data. These surrogate signals had the same underlying periodicity, mean, variance, power spectrum, and autocorrelation as the original time series, except that the stride-to-stride fluctuations about their means were randomized.
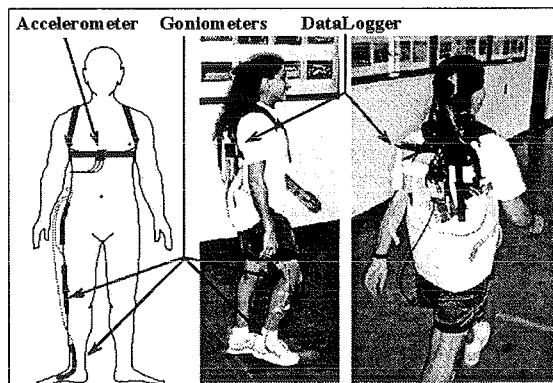
Fig. 1: Setup of data collection instrumentation.

State space reconstructions of all original and surrogate time series were performed using standard embedding techniques (Takens, 1981; Fraser and Swinney, 1986; Sauer et al., 1991; Kennel et al., 1992). Each time series was then divided into five equal sub-series to calculate within-subject variance. For each time series, the magnitude of the estimated

local maximum finite time Lyapunov (MFTL) exponent (Rosenstein et al., 1993) was calculated and used as the nonlinear statistic used to test the null hypothesis (Theiler et al., 1992). MFTL exponents were statistically compared using a two-factor repeated measures ANOVA to test for differences between original and surrogate data types and between subject groups.

RESULTS

Figure 2 shows MFTL exponents for the anterior-posterior (Ax) acceleration data. There was a clear and consistent trend towards decreased exponents for surrogate data compared to original data for all subjects. This same trend was seen for all variables quantified. These differences were statistically significant ($p \leq 0.02$) for all 12 variables measured. Therefore, the stride-to-stride fluctuations in these human walking data could be clearly distinguished from linearly correlated Gaussian noise.

Additionally, there were significant group × data type interaction effects for short-term MFTL exponents for all three acceleration variables (Fig. 3). Overall differences between original and surrogate time series were slightly (but significantly) greater for the NP subjects than for the CO subjects. This suggests that the nature of the stochasticity observed in the stride-to-stride fluctuations in the NP subjects was different from that observed from the CO subjects.

DISCUSSION

The present results demonstrate that stride-to-stride fluctuations can be clearly distinguished from correlated Gaussian noise. This suggests, contrary to the assumption of most gait analyses that stride-to-stride fluctuations are merely random, that potentially important information regarding the state of the underlying neuromuscular control sys-

tem is reflected in the dynamical structure of these fluctuations. The differences between the stochastic structure of the walking data for the NP and CO subjects further support the hypothesis that peripheral sensory feedback plays a role in adjusting step-to-step limb trajectories and to smooth unintended irregularities (Nashner, 1980; Gandevia and Burke, 1992) during walking.
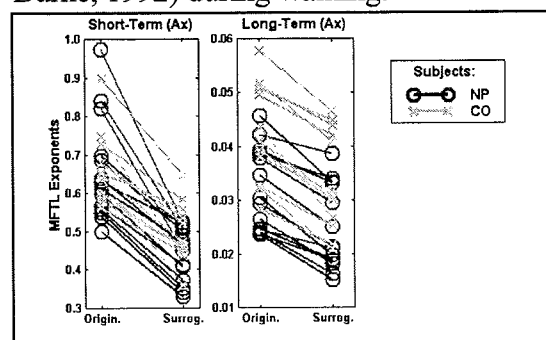
Fig. 2: Original and surrogate MFTL exponents for all subjects in both groups.
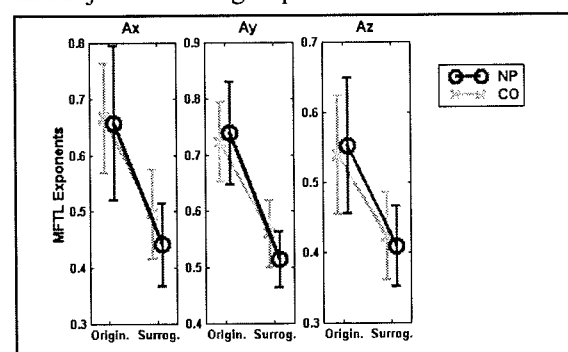
Fig. 3: Group × data type interaction effect for short-term exponents of trunk accelerations.

ACKNOWLEDGEMENTS

REFERENCES

Fraser, A.M. and Swinney, H.L. (1986). *Phys. Rev. A* **33**: 134-1140.

Gandevia, S.C. and Burke, D. (1992). *Behav. Brain Sci.* **15**: 614-632.

Kennel, M.B. et al., (1992). *Phys. Rev. A* **45**: 3403-3411.

Nashner, L.M. (1980). *J. Neurophysiol.* **44** (4): 650-664.

Rosenstein, M.T. et al., (1993). *Physica D* **65**: 117-134.

Sauer, T. et al., (1991). *J. Stat. Phys.* **65** (3/4): 579-616.

Takens, F. (1981). *Dynamical Systems and Turbulence.* Springer-Verlag, pp. 366-381.

Theiler, J. et al., (1992). *Physica D* **58**: 77-94.

WALKING VARIABILITY AND STABILITY IN DIABETIC NEUROPATHY

Jonathan B. Dingwell[1,2], Joseph P. Cusumano[3], Dagmar Sternad[2], Peter R. Cavanagh[1,2,4]

[1]The Center for Locomotion Studies, [2]Department of Kinesiology, [3]Department of Engineering Science and Mechanics, [4]Departments of Biobehavioral Health, Medicine, and Orthopaedics and Rehabilitation, Penn State University, University Park, PA
Email: j-dingwell@nwu.edu   Web: http://www.celos.psu.edu/

INTRODUCTION

Quantifying dynamic stability of walking is important for assessing people who are at risk of falling. Patients with peripheral neuropathy lose sensation in their distal extremities as a consequence of long-term diabetes. These patients are as much as fifteen times more likely to report an injury during walking than healthy subjects (Cavanagh et al., 1992). It was hypothesized that the greatest effects of neuropathy would be seen in the spatio-temporal structure of the stride-to-stride variability in the walking kinematics of these patients. Methods from nonlinear time series analysis were used to provide a mathematically precise means of quantifying local dynamical stability in gait.

METHODS

Fourteen diabetic patients with significant peripheral neuropathy (NP) and twelve gender-, age-, height-, and weight-matched controls (CO) participated. A self-contained "DataLogger" was built to collect kinematic data during continuous walking (Fig. 1). Electrogoniometers measured sagittal plane motions of the hip, knee, and ankle. A tri-axial accelerometer mounted at the base of the sternum measured upper body motions. Ten minutes of data were collected at 66.7 Hz while subjects walked around a 200m open level indoor walking track at their own freely chosen pace.

Average stride-to-stride standard deviations were calculated to quantify the variability of each subject's walking patterns. Dynamic stability was quantified by estimating maximum finite-time Lyapunov (MFTL) exponents from a state space analysis of the raw data (Rosenstein et al., 1993). Lyapunov exponents directly quantify the long-term sensitivity of a system to small local perturbations in state space, and are thus a direct measure of intrinsic local dynamic stability.
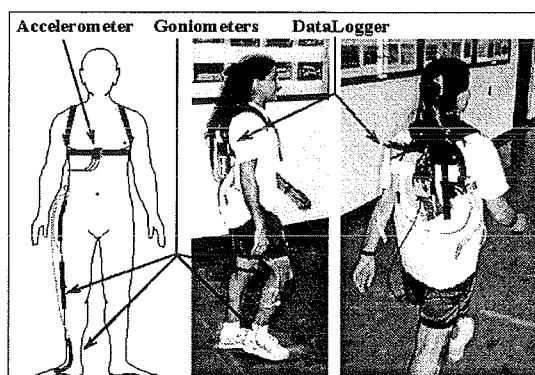
Fig. 1: Setup of data collection instrumentation.

Multi-dimensional state spaces were reconstructed from each original time series and its time-delayed copies (Takens, 1981; Sauer et al., 1991). Time lags for the reconstructions were calculated from the first minimum of the Average Mutual Information function (Fraser and Swinney, 1986). Embedding dimensions were computed from a Global False Nearest Neighbors analysis (Kennel et al., 1992). Sensitivity to local perturbations was quantified by calculating the average logarithm of the divergence (Euclidean distances) of neighboring orbits in the embedded state spaces as a function of time (Rosenstein et al., 1993). MFTL exponents were estimated from the slopes of linear fits to each of these curves (Rosenstein et al., 1993) in the range between 4 and 10 strides (see Fig. 3).

RESULTS

NP subjects walked more slowly and exhibited greater variability in lower extremity kinematics than did CO subjects (Fig. 2). Differences in variability of upper body accelerations were not significant. Multiple regression analysis showed that significant differences in ankle joint variability were significantly predicted by differences in sensory status, even after accounting for group differences in walking speed, passive range of motion, and lower extremity strength.
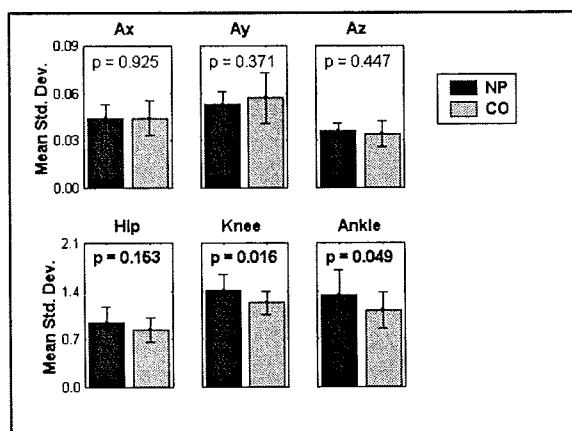
Fig. 2: Mean standard deviations for trunk accelerations and joint angle excursions.

MFTL exponents were all greater for the CO group than for the NP group, indicating that the NP subjects in fact showed better long-term dynamical stability than controls. Differences were statistically significant for upper body accelerations in the horizontal plane in both the anterior-posterior (Ax, p = 0.001) and mediolateral (Az, p = 0.007, Fig. 3) directions, and for knee joint movements (p = 0.022). These results were significantly predicted by differences in walking velocity.

DISCUSSION

The most surprising finding in this study was that of better long-term dynamical stability in the NP subjects, which seems contrary to clinical findings (Cavanagh et al., 1992; Richardson et al., 1992). However, these NP subjects had been living with significant sensory loss for many years and the present results support the hypothesis that

decreases in walking speed are a compensatory strategy used by NP subjects to maximize local dynamic stability of the upper body during unperturbed level walking (Courtemanche et al. 1996). Figure 3 shows, however, that while the divergence rates were lower for NP subjects in the long-term range (strides 4 to 10), the initial divergence (< 1 stride) was in fact greater for NP subjects than for CO subjects. This suggests that these NP were still not able to fully compensate for local instabilities in the short term. A reasonable interpretation is that the increased risk of falling in these subjects is not due to their inability to generate normal and stable locomotor rhythms, but is due to their inability to develop and execute appropriate response strategies when faced with unexpected obstacles or large-scale perturbations encountered during locomotion.
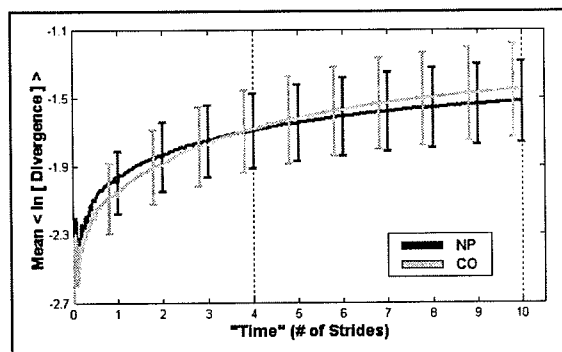
Fig. 3: Stability of mediolateral accelerations.

REFERENCES
Cavanagh, P.R. et al., (1992). *Diabet. Med.* 9: 469-474.
Courtemanche, R. et al. (1996). *Arch. Phys. Med. Rehabil.* 77(9): 849-855.
Fraser, A.M. and Swinney, H.L. (1986). *Phys. Rev. A* 33: 134-1140.
Kennel, M.B. et al., (1992). *Phys. Rev. A* 45: 3403-3411.
Rosenstein, M.T. et al., (1993). *Physica D* 65: 117-134.
Sauer, T. et al., (1991). *J. Stat. Phys.* 65 (3/4): 579-616.
Takens, F. (1981). *Dynamical Systems and Turbulence.* Springer-Verlag, pp. 366-381.

THREE-DIMENSIONAL QUANTIFICATION OF CONCOMITANT CHANGES IN KNEE FLEXION-EXTENSION AND QUADRICEPS ANGLES

L.A. Livingston[1] and S.J. Spaulding[2]

Dept. of Kinesiology and Physical Education, Wilfrid Laurier University, Waterloo, ON[1]
Faculty of Health Sciences, University of Western Ontario, London, ON[2]
Email: llivings@wlu.ca   Web: www.wlu.ca/~wwwk+pe

INTRODUCTION

The quadriceps (Q) angle is typically measured in a static supine or standing position (Horton & Hall, 1989; Insall et al., 1976). To improve upon the ecological validity of the measure, some have suggested that the Q angle should be measured when weight bearing (Holmes & Clancy, 1998) or while the knee is flexing (Livingston, 1998). However, attempts to quantify changes in the Q angle with increasing knee flexion have yielded conflicting results.

Some (Hehne, 1990; Huberti & Hayes, 1984) assert that the Q angle decreases, while others report no change (Caylor et al., 1993) or a rise (Chen, 1997) in the Q angle with increases in knee flexion. Inadequate control over foot position during measurement, and reliance on inappropriate two-dimensional measurement techniques (Ando et al., 1993; Olerud & Berg, 1984) provide the most plausible explanations for this lack of consensus. The purpose of this investigation, therefore, was to examine changes in the Q angle with increasing knee flexion under self-selected versus standardized foot positions using a three-dimensional measurement system.

PROCEDURES

Twenty males and females (19-30 years) volunteered to participate in this study. Individuals with a history of lower limb injury or dysfunction were excluded. Left Q angles were defined by placing LEDs on the anterior superior iliac spine, the midpoint of the patella, and the center of the tibial tubercle. Three-dimensional data were then collected using an OPTOTRAK motion measurement system while each participant performed five trials of a shallow knee bend exercise (ie, from knee extended to knee flexed to knee extended position) with their feet positioned as follows: Romberg stance (ie, medial borders of the feet touching), mean stance (ie, 0.17 m between heel centers, with an angle of 14° between the long axes of the feet) (McIlroy & Maki, 1997), and self-selected stance.

RESULTS AND DISCUSSION

The averaged data for one representative subject are presented (Figure 1). Patterns of change in the Q angle (ie, magnitude, direction, and timing) varied depending upon the foot position adopted. When measured with feet in the Romberg or self-selected position, decreases in the Q angle with knee flexion were followed by increases with continued flexion. Q angles measured with feet in mean stance, however, steadily increased with continued knee flexion. The greatest inter-subject variation in Q angle patterns was observed for data derived under the self-selected stance condition.
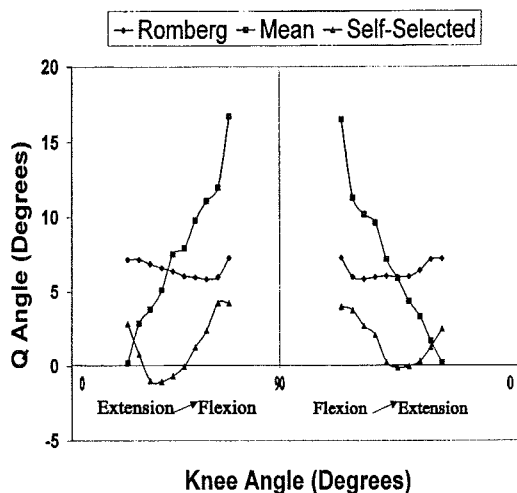
Figure 1: Variations in Q angle magnitude with changes in the knee flexion-extension angle while adopting different stances. The data depicted are for one representative subject only.

The observed differences may be attributed to the transverse plane positioning (ie, internal or external rotation) of the femur and tibia relative to each stance. The Romberg position, for example, required greater internal rotation of the lower limb, while the mean stance position required greater external rotation of the lower limb. For the majority of subjects, the self-selected foot position was represented by a stance position that fell between these two extremes. A rise in Q angle values when knee flexion increased beyond 25-30° for two of the three stance positions, moreover, suggests that the screw home mechanism (Nordin & Frankel, 1980) may play a role in reversing the direction of Q angle change with increased knee flexion.

Interestingly, the changes in Q angle magnitude observed as the knee moves from extension to flexion are not exactly mirrored when the knee reverses direction and moves from flexion to extension. These differences may be explained, in part, by a change from an eccentric to a concentric mechanism of

contraction within the quadriceps musculature.

SUMMARY

When investigating changes in the Q angle under dynamic conditions, future investigators would be well advised to rely on three-dimensional measurement techniques and to take foot position into account when explaining their results.

REFERENCES

Ando T. et al. (1993). *Clin Orthop*, **289**, 213-219.
Caylor D. et al (1993). *JOSPT*, **17**, 11-16.
Chen, S. (1997). *Chinese J Sports Med*, **16**, 91-94.
Hehne, H-J. (1990). *Clin Orthop*, **258**, 73-85.
Holmes, Jr., S.W., & Clancy, Jr., W.G. (1998). *JOSPT*, **28**, 299-306.
Horton, M.G., & Hall, T.L. (1989). *Phys Ther*, **69**, 897-901.
Huberti, H.H., & Hayes, W.C. (1984). *J Bone Joint Surg*, **66A**, 715-724.
Insall, J. et al. (1976). *J Bone Joint Surg*, **58A**, 1-8.
Livingston, L.A. (1998). *JOSPT*, **28**, 105-109.
McIlroy, W.E., & Maki, B.E. (1997). *Clin Biomech*, **12**, 66-70.
Nordin, M., & Frankel, V. (1980). *Biomechanics of the Skeletal System*. Lea & Febiger.
Olerud, C., & Berg, P. (1984). *Clin Orthop*, **191**, 162-164.

BILATERAL IMBALANCES IN Q ANGLES AND QUADRICEPS PEAK TORQUE MEASUREMENTS

T. Byl and L.A. Livingston

Dept. of Kinesiology and Physical Education, Wilfrid Laurier University, Waterloo, ON
Email: llivings@wlu.ca   Web: www.wlu.ca/~wwwk+pe

INTRODUCTION

The quadriceps (Q) angle is that angle formed between the vectors for the combined pull of the quadriceps femoris muscle and the patellar tendon (Hungerford et al., 1979). It is delineated by drawing an imaginary line from the anterior superior iliac spine to the center of the patella, and from the center of the patella to the midpoint of the tibial tubercle.

The common assumption of bilateral lower limb within-subject symmetry in this measure has been challenged by the results of recent investigations. Hahn and Foldspang's (1997) study of 339 athletes found right Q angles to be on average 3° greater in magnitude than, and significantly different from, those in the left lower limb. More recently, Livingston and Mandigo (1999) observed bilateral imbalances in Q angle measures amongst those asymptomatic versus symptomatic for anterior knee pain, with almost half (47%) of the individuals studied demonstrating a minimum 4° difference between right and left Q angles. These studies did not directly address the question of why such imbalances exist, yet it was hypothesized that bilateral Q angle asymmetry may be related to bilateral strength imbalances in the quadriceps musculature. The purpose of this study, therefore, was to determine if Q angle magnitude is related to quadriceps musculature strength by gathering peak torque measurements during the completion of a dynamic knee extension exercise.

PROCEDURES

Thirty-four males (n=16) and females (n=18), from 18 to 34 years of age (M=20.9, SD=2.7), volunteered to participate in this study. The participants had no history of lower limb injury or dysfunction.

Bilateral goniometric measurements of the Q angle were taken with individuals in a standing position with knees extended and the medial borders of the feet touching, using the standard clinical method of measurement (Horton et al., 1989). All measurements were taken by the same investigator. Intertester reliability was established by measuring the Q angle in a group of 10 subjects. An r=0.80 (ICC(2,1) (Shrout et al., 1979) determined that intertester reliability was excellent (Fleiss, 1986). Peak torque measurements were gathered using a CYBEX II® Isokinetic Dynamometer in conjunction with an MS-DOS computer. Following three warm up trials, subjects performed three trials of a dynamic knee extension movement at a velocity of 60°/s. Peak torque was recorded as the largest single score obtained during the three trials.

Q angle and peak torque data were analyzed using separate 2 X 2 analysis-of-variance

(ANOVA) procedures with gender (male, female) and limb (right, left) as the independent variables. Pearson product moment correlation coefficients were generated to examine the relationship between Q angle and peak torque.

RESULTS AND DISCUSSION

Significant differences in Q angle magnitude $(F(1,2)=9.83, p<0.003)$ and peak torque values $(F(1,2)=90.05, p<0.001)$ were observed between males and females, but not between limbs (Table 1) even though more than one-third (ie, 35%) of the subjects displayed a minimum 4° difference in left versus right Q angles. Significant interaction effects were not observed. Pearson product-moment correlation coefficients between the Q angle and peak torque measures were weak but significant, with values of $r=-0.41$ $(p<0.01)$ and $r=-0.45$ $(p<0.01)$ for the right and left limbs, respectively.

Table 1: Mean Q angle and peak torque values by limb and gender.

	Q Angle (°)	Peak Torque (Nm)
Right		
Female	10.1	109.4
Male	6.3	189.5
Left		
Female	9.7	113.2
Male	5.9	184.7

Given that the patella is embedded in the tendon of the quadriceps femoris complex, it is logical that the magnitude of the Q angle will vary with changes in the strength and tonus of the musculature. The findings of this study support this notion. The observation of a weak, yet significant correlation, between Q angle and peak torque values indirectly supports the hypothesis that Q angle magnitude decreases as quadriceps strength and tonus increases. The generalizability of this observation is limited, however, by our consideration of the influence of moment arm length in combination with, rather than in isolation from, the force generated by the quadriceps musculature.

SUMMARY

Three skeletal landmarks define the Q angle, yet the location of the patella within the quadriceps tendon leads to alteration in the magnitude of the angle when the characteristics of the quadriceps musculature change.

REFERENCES

Fleiss, J.L. (1986). *Reliability of Measurement*. Wiley & Sons..

Hahn, T., Foldspang, A. (1997). *Scand J Med Sci Sports*, 7, 43-48.

Horton, M.G., Hall, T. (1989). *Phys Ther*, **69**, 897-901.

Hungerford, D.S., Barry, M. (1979). *Clin Orthop*, **144**, 9-15.

Livingston, L.A., Mandigo, J.L. (1999). *Clin Biomech*, **14**, 7-13.

Shrout, P.E., Fleiss, J.L. (1979). *Psych Bull*, **86**, 420-428.

CERVICAL POLAR FORCE AND ELECTROMYOGRAPHIC ACTIVITY

[1]D.A. Gabriel, [2]J.Y. Matsumoto, [3]D.H. Davis, [4]B.L. Currier, [4]K.-N. An, Ph.D.

[1]Physical Therapy Department, East Carolina University, Greenville, NC 27858, Email: gabrield@mail.ecu.edu, Departments of [2]Neurology, [3]Neurosurgey, and [4]Orthopedics, and Mayo Clinic/Mayo Foundation, Rochester, MN 55905

INTRODUCTION

Cervical dystonia is a neurodegenerative disorder that results in focal contractions of the neck muscles, forcing its victims into painful postures of the head and neck. Treatment involves chemical or surgical denervation of the driving muscles (Braun et al. 1995). However, successful muscle reorganization also depends on approxi-mating the normal balance between muscles that cross the joint. This is important for maintaining normal joint kinematics, and for preventing inappropriate moments of force which may lead to degenerative joint disease (Lindscheid 1982). If the pattern of moments of force at the neck can be used as a measure of muscle balance, then denervation therapy should also focus on approximating a normal pattern in the patient. This paper presents the force and EMG patterns throughout the polar range of motion in normal controls from which to compare patients before and after denervation therapy.

PROCEDURES

Recording Force and EMG. A load cell (JR3) was centered and secured over a clamp for the head. This unit was attached to a jig to adjust for subject height and head position. The arms of the jig were integrated into a testing chair. The electrodes were 25-micron diameter Teflon-coated stainless-steel wires, with 5 mm of insulation stripped from the tips. Two fine-wires were placed in a bipolar configuration. The sternocleidomastoid; the trapezius; the splenius capitis; the semispinalis capitis; and the scalenus were recorded bilaterally. The EMG activity was amplified (MA 100) and band-passed filtered from 20 to 600 Hz. All signals were digitized (CODAS) at 5 kHz on an IBM computer, and stored on hard-disk for later off-line processing.

Task. Subjects (N=18) were secured in the testing chair and they produced a maximal isometric force in twelve directions in the horizontal plane. There was a 30° interval between each direction of force which was marked on an x-y oscilloscope with a tem-plate. The center of the oscilloscope screen was defined as the origin (i.e., the relaxed position), and subjects learned to produce a force which appeared on screen as a vector with a magnitude and direction related to tension at the load cell. Subjects produced three maximal voluntary contractions in the desired direction of force. There were four test sessions. The first three days served as training sessions while the last day was used for data collection.

RESULTS AND DISCUSSION

The normalized force in the 90° direction corresponded to flexion while the 270° direction was extension (Figure 1). The 0° and 180° directions were right and left lateral bending, respectively. Strength in extension was greater ($p<0.05$) than in flexion while right and left lateral bending strengths were quite comparable ($p>0.05$). The normalzed neck strength values for the 300 and 330° directions were greater than those for the 210 and 240° directions ($p<0.05$). Thus, neck strength exhibited a right lateral dominance. This extends

previous findings for studies in which the neck strength was only examined in the flexion, extension, and lateral bending directions (Moroney et al. 1988).

Normalized Polar Neck Strength
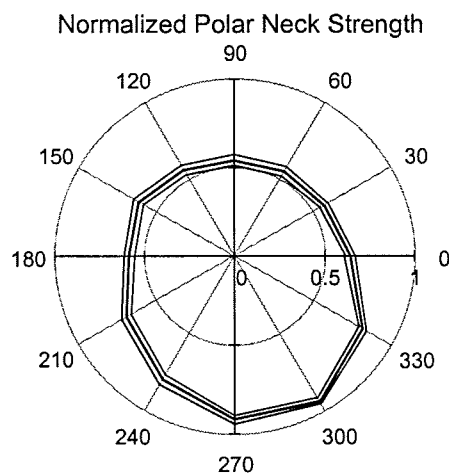
Figure 1: The mean normalized force (thick line) and standard deviation (thin lines).

Figure 2 shows normalized EMG from the right splenius capitus (RSPLEN). Peak EMG was centered at 330°. Based on the work of Dempster and Finerty (1949), this muscle served as an agonist between the 0 and 270° directions of force ($p<0.05$). Synergistic muscle activity occurred between the directions of 0-90° and 180-270° where the EMG magnitude was still appreciable ($p<0.05$). Antagonistic activity between the 90 and 180° directions of force was minimal. There was an identifiable direction of force for which each muscle served as either an agonist, synergist, or antagonist. The polar patterns of EMG for each muscle were stereotyped across subjects. However, the direction of greatest EMG activity was not bilaterally symmetric. For example, the direction of greatest EMG magnitude for left splenius capitus was 240°, not 210° as might be expected. These data extend the findings of Keshner et al. (1989) to maximal voluntary contractions.

Normalized RSPLEN EMG
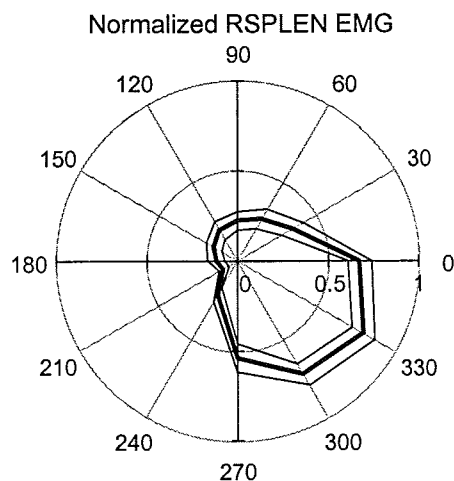
Figure 2: The mean (thick line) normalized EMG and standard deviation (thin lines).

CONCLUSION

The consistent patterns of force and EMG throughout the polar range of motion offer a basis of comparison for a patient population.

REFERENCES

Braun et al. (1995). *J. Neurol.*, **242**, 504-507.

Dempster, W.T., Finerty, J.C. (1947). *Am. J. Physiol.*, **150**, 596-606.

Keshner, E.A. et al. (1989). *Exp. Brain Res.*, **75**, 335-44.

Lindscheid, R.L. (1982). *Difficult problems in hand surgery*. (pp. 169-172). Saint Louis: C.V. Mosby.

Moroney, S.P. et al. (1988). *J. Orth. Res.*, **6**, 713-720.

ACKNOWLEDGMENTS

EXTERNAL FOOT SHAPE DIFFERENCES BETWEEN
MALES AND FEMALES AND AMONG RACES

Roshna E. Wunderlich[1] and Peter R. Cavanagh[1,2]
[1]The Center for Locomotion Studies and [2] Departments of Biobehavioral Health, Medicine, and
Orthopaedics and Rehabilitiation, Penn State University, University Park, PA
Email: celos@psu.edu Web: www.celos.psu.edu

INTRODUCTION

Traditionally, the literature on shape differences among human feet has focused on osteological differences between men and women (Smith, 1997). A few studies have also compared populations who habitually use different types of footwear, but these studies have been limited in the variables examined and rarely considered ethnic differences unrelated to footwear (Ashizawa et al., 1997).

As correct shoe fit is commonly recognized to be attained by matching shoe shape to foot shape, appreciation of the sexual dimorphism of foot shape is essential to the proper design of women's shoes. Traditionally many women's shoes have been made using a small version of a men's last with all dimensions proportionally scaled according to foot length. However, if women's feet differ in *shape* from men's feet, this is an inappropriate model for a women's shoe last and could lead to improper shoe fit in women.

An understanding of morphological and functional responses to variation in footwear among ethnically different populations necessitates a basic understanding of racial variation among populations using *similar* footwear. Information on gender and racial differences in foot shape is also useful to forensic scientists identifying isolated remains.

METHODS

The U.S. Army foot and leg anthropometric data set (Parham et al., 1992) was used to analyze sexual dimorphism as well as racial differences in foot shape. Univariate t-tests were used to assess differences between males and females and among races for each right foot and leg dimension standardized to foot length. Multivariate discriminant analyses were used to test the reliability of classification into sex and race classes and the relative importance of each variable to the discrimination among sex and race classes. Both absolute variables and those standardized to foot length were used in these analyses. Analysis of covariance and multivariate allometric analyses were used to assess sex-specific differences independent of size and to compare size-related shape changes within sexes.

RESULTS

The results indicate that, for a given stature, males have significantly longer and broader feet than females. After normalization of the measurements by foot length, males and females were found to differ significantly in two calf, five ankle, and four foot shape variables. Classification by sex alone using absolute values was correct at least 93% of the

time, whereas classification by race alone was correct only 80% of the time, and by race and sex together only 78% of the time. Using the variables standardized to foot length, sex and race together could be classified correctly 71.3% of the time, sex alone 85%, and race alone 81%.

DISCUSSION

These findings have implications for forensic science as well as for footwear. The results indicate that the reliability of classification of isolated foot and lower leg specimens to sex and race categories is high. This study also demonstrates that female feet are not simply scaled-down isometric versions of male feet but rather differ in a number of shape characteristics. A woman's foot has a higher arch, a shallower first toe, a smaller ball of foot circumference, a shorter ankle length, a shorter length of the outside ball of foot, and a smaller instep circumference. The last on which a women's shoe is built should reflect these differences. It remains to be seen, however, whether a shoe designed for women that incorporates the many small differences suggested here would be perceived subjectively as being a better fit and, therefore, more comfortable.

REFERENCES

Ashizawa K. et al. (1997) *Ann. Hum. Biol.* **24**:117-129.

Parham K. et al. (1992) U.S. Army Natick Research, Development and Engineering Center Technical Report #92/028, Natick, MA.

Smith S.L. (1997) *J. Forensic Sci.* **42**:186-195.

ACKNOWLEDGEMENTS
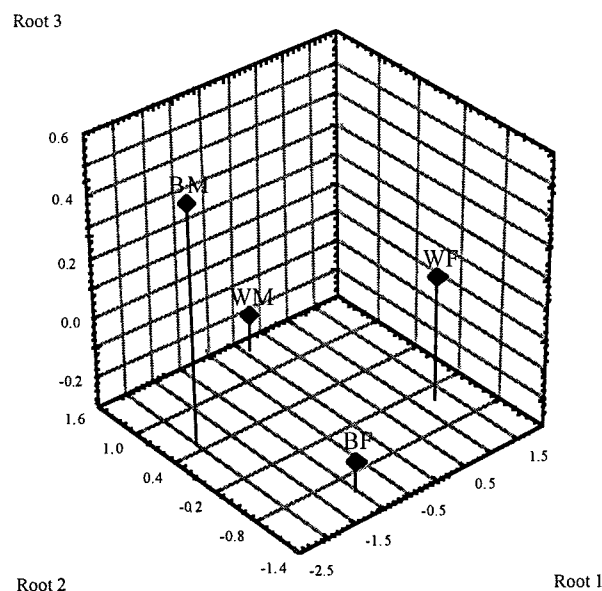
Figure 1. Plot of centroids of first three roots of the canonical variates analysis by sex and race. WM – White males; BM – Black males; WF – White Females; BF – Black Females.

THE EFFECT OF A SHOCK-ABSORBABLE POLYMER MEMBRANE ON THE MECHANICAL BEHAVIOR OF DENTAL IMPLANTS

K. Choi[1], W. Joo[1], I. C. Kwon[1], J. B. Choi[2], H. J. Moon[3], J. W. Shin[3], Y. C. Lee[4]
[1]Biomedical Research Center, Korea Institute of Science and Technology, Seoul Korea
[2]Dept. of Mechanical Systems Engineering, Hansung Univ., Seoul Korea
[3]Dept. of Oral Anatomy, Dental School, Kyoung Hee Univ., Seoul Korea
[4]Dept. of Oral and Maxillofacial Surgery, Medical School, Hallym Univ., Seoul Korea
E-mail: choi@kistmail.kist.re.kr Web: www.kist.re.kr

INTRODUCTION

Dental implant has been increasingly used to recover the masticatory function of lost tooth. It has been well known that the success of dental implant is heavily dependent on initial stability and long-term osseointegration due to optimal stress distribution in the surrounding bones. Most important role of periodontal ligament, removed during operation, is to absorb impact force and to distribute them to alveolar bone. Therefore, removal of periodontal ligament caused stress concentration and micro-fractures in alveolar bone. For this reason, the study for artificial periodontal ligament has become an important issue in this field. Thus, a new concept of coating an implant's surface with a natural polymer membrane was introduced in order to provide the viscoelastic characteristic of the periodontal ligament to implant system. In this study, chitosan was coated on Bränemark type dental implant for replacing the role of intact periodontal ligament.

METHODS

1. Initial stability test

This experiment was aimed at improving the stability of the dental implant by coating the implant with the polymer membrane, which was designed to function like a normal periodontal ligament. After coating the Bränemark type implants with Chitosan, it was mechanically tested and then initial stability between the coated and uncoated implants was compared.

For this study, dental implants with 30 50 membrane of Chitosan thickness were used and they were operated into the fresh patella bones from porcine knees because their structure is similar to the alveolar cancellous bone. To test initial stability, load was applied to the upper part of an implant in a shear direction (right angles to an implant) with constant speed until the surrounding bone was destroyed. The shear stiffness was derived by regression analysis in the linear region of the load-displacement curve.
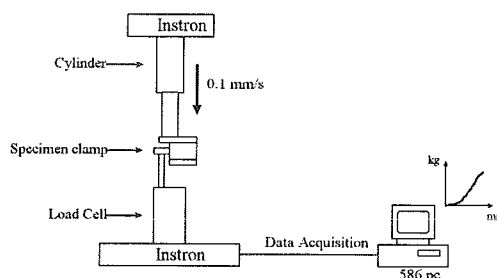
Figure1. Schematic diagram of testing set-up

2. Numerical analysis of the impact loading on dental implants.

In order to study the effect of the polymer membrane on a dental implant, four cases of 3-dimensional FE model were developed. Case 1 modeled a control case with natural periodontal ligament a 100-microns thickness. Case 2 modeled an implant with a 50-micron gap between the alveolar bone and implant. Cases 3 and 4 modeled coated implants with a 50 and 100-micron layer of polymer material. To shorten analysis time of the finite element model and to simplify modeling, a cylindrical implant was modeled and the form of an alveolar bone, based on the structure of a mandible, was simplified. The finite element model had 4919 nodal points and 4276 eight node brick elements. All materials were assumed isotopic and homogeneous.

Pam-Crash[TM] V96.1 program was used for dynamic analysis with elasto-plastic material. It was assumed that an interface between the Chitosan membrane and bone tissues was perfectly bonded. To apply the impact load on the dental implant, a rigid

body weighing 0.3kg was made to collide at a speed of 0.3m/s in a lateral direction to the tip of the dental implant.

RESULTS AND DISCUSSION

1. The results of the mechanical experiment on the initial stability of dental implants

The results was obtained from the mechanical test of uncoated and Chitosan coated implants were shown in Table 1. The uncoated implants had an average shear stiffness of 34.728kg/mm and the coated implants 47.108kg/mm.

Table 1. Shear stiffness of chitosan coated and uncoated dental implant

	Uncoated implant	Coated implant
Average	34.728	47.108
S.D.	11.668	14.956
T-test	p=1.07E-02 < 0.05	

Dimension [kg/mm]

2. The results of 3-dimensional finite element analysis for dental implants
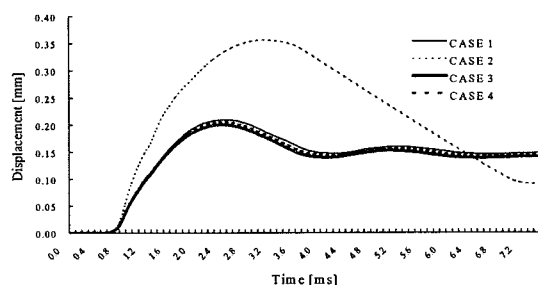
Figure 2. Transient response of displacement at implant tip
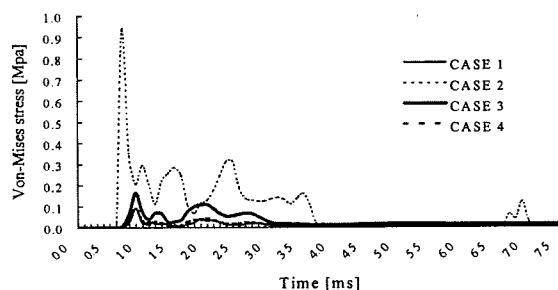
Figure. 3 Transient response of von-Mises Stress at cortical bone.

Fig. 2 represents the displacement on the tip of a dental implant after the rigid body's impact in each case. The graph shows that the displacement of case 2 was greater than case 1 because the periodontal ligament absorbed the impact force in case 1. By coating Chitosan on the implant in cases 3 and 4, a displacement curve line similar to case 1 could be obtained. Fig. 3 represents

the change of stress in the cortical bone. At point A, the maximum stress generated in case 2 was 9 times greater than case 1. The reason was that case 2 generated the stress by direct transmission from the implant to the surrounding bone without any reduction in impact, whereas in case 1 the periodontal ligament absorbed the impact.

SUMMARY

After the operation, the membrane would be 50 100 microns thick, similar to a periodontal ligament's thickness. The histological observation showed Chitosan infiltrated into the inner cancellous. Shear stiffness of coated implant is increased by 35.64% because Chitosan expanded from its pre-operated dry situation, increasing the stability of implant by filling the gap between the implant and alveolar bone during the implant operation. Furthermore, Chitosan substituted the function of the periodontal ligament in the natural tooth, mitigated the load that pressed on the implant, and prevented the yield of surrounding bone.

The results of impact analysis showed that stress on the cortical bone was 10 times greater than stress on the cancellous bone because impact stress was concentrated on the cortical bone and less time was needed to generate maximum stress. In cases 3 and 4, when maximum stress generated in every observational point was decreased, it resembled the stress change in case 1. Therefore, methodically coating an implant with a visco-elastic polymer material can reproduce the periodontal ligament's function to absorb the shock of impact reducing the stress convergence generated around the surrounding bone.

REFERENCE

Albrekttsson T., Zarb G., Worthington P., Eriksson A.R. (1986). The long term efficience of currently used dental implants : A review and proposed criteria of success. Int J Oral and Maxillofac Implants 1:1-25

Brunski J.B., Skalak R. (1993). Biomechanics of osseointegration and dental prostheses. In osseointegration in oral rehabilitation, pp. 133-156, Quintessence Publishing Co., London,

Kinzel G.L., and Brose M.O.(1990). Finite element analysis of bone-adapted and bone bonded prosthetic endosseous implant. J Prothet Dent 62:671

Rieger M.R., Mayberry M., Brose M.O. (1990). Finite element analysis of six endosseous. J Prothet Dent 63:671

A 3-D CONTACT PROBLEM FINITE ELEMENT MODEL FOR BREAST SHAPE DEFORMATION DERIVED FROM MRI DATA

A. Samani , J. Bishop , E. Ramsay , D. Plewes
Dept. of Medical Biophysics, University of Toronto, Toronto, Ontario, Canada
Email: asamani@sten.sunnybrook.utoronto.ca

INTRODUCTION

Multi-modality imaging of the breast obtained by mammography, MRI and PET is thought to be best achieved through some form of data fusion technique. However, images taken by these various techniques are often obtained under entirely different tissue configurations of compression, orientation or body position. In these cases some form of spatial transformation of image data from one geometry to another is required such that the tissues are represented in an equivalent configuration. While many investigators have studied the use of ad-hoc geometric transformations, they ignore the different elastic properties of the various tissue components such as fat, fibroglandular tissue and skin. We have been exploring the use of finite element method (FEM) for this purpose which reflects the biomechanical characteristics of the complex distribution of these components derived from MRI images of the breast. The problem of calculating breast tissue deformation is associated with difficulties such as complex geometry, large number of unknowns, nonlinear and visco-elastic behavior. An interesting application of this problem is MRI to mammography modality conversion. In mammography, the breast is placed and aggressively compressed between two rigid plates. In this case breast shape deformation is modeled as a contact problem. In this article, we discuss a three dimensional nonlinear FE model which we use to calculate shape deformation of breast tissue under mammography. In this model, we assume that the breast consists of fat, fibroglandular and skin.

METHODS

We use a 3-d FE model to simulate tissue deformation of breast under mammography. This is a contact problem where the boundary conditions change continuously until equilibrium is reached. Therefore, irrespective of the materials mechanical properties the problem is nonlinear. We assume that the fat, fibroglandular tissue and skin are elastic and incompressible materials. The first step in the implementation of the FEM is mesh generation. Here, because there is not a simple, analytical representation that can be used for surfaces and interfaces of the breast soft tissues, meshing is not a straight forward task. For mesh generation, we use 3-d MR images to find these surfaces and interfaces. We first apply a segmentation algorithm on the MR images to separate different materials within the breast, then use a meshing code which we have developed to read in the segmented images and produce the 3-d mesh. This mesh generation code is fully automatic and is based on the algorithms presented by Keyak et. al. 1990. We use ABAQUS (Hibbit et. al. 1998): a nonlinear finite element package to solve the contact problem. We first mesh the breast using the three dimensional mesh generation code which outputs a three dimensional mesh compatible ABAQUS preprocessor. We use eight nodded hexahedral elements which are known as well behaved type of elements to mesh the fat and fibroglandular tissue, and four nodded membrane elements to mesh the skin. After preprocessing, ABAQUS solves the nonlinear contact problem incrementally.

RESULTS

To demonstrate the capability of this model in predicting breast shape deformation, we used two sets of MR images of a breast. The first set was obtained from a breast of a female volunteer before compression and the second was obtained after applying a 48 mm (50%) compression to the breast using two rigid plates. We used the first set to obtain the mesh shown in Figure 1-a and the second one for verifying the results. Figure 1-a depicts the mesh of the breast tissues that are covered by the skin. In this mesh, there are approximately 18500 elements and 33000 nodes each of which has 3 degrees of freedom. We assume that Young's modulus of fat, fibroglandular tissue and skin are 5.0 kpa, 50.0 kpa and 500.0 kpa respectively (Sarvazian et. al. 1995). The deformed shape of the breast obtained from ABAQUS is shown in Figure 1-b. To verify the results, we present a calculated and real images of a sagittal section of the breast. These images are depicted in Figure 2. In this figure the white and dark regions represent the fat and fibroglandular tissues respectively.

a)   b)
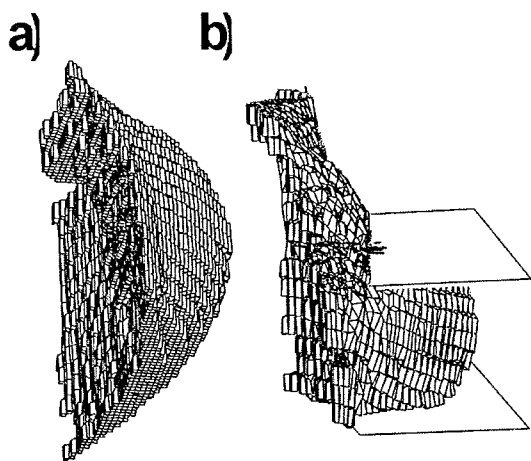
Figure 1: a) 3-d mesh of the breast.
b) deformed shape of the breast after 50% compression applied by two rigid plates

a)   b)
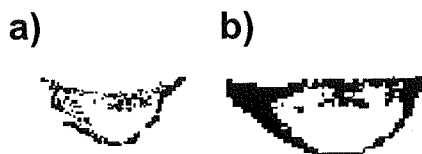
Figure 2: a) calculated image of a breast section
b) MRI sagittal image of the same section.

CONCLUSIONS

We developed and implemented a 3-d FE model to predict breast tissue deformation under given loads or boundary conditions. This model is capable of handling large scale calculations and complicated nonlinearities such as that of contact problems. The preliminary results of this model, considering the lack of accurate information about breast tissue elastic parameters is encouraging. To improve the results we will do more research to obtain more accurate elastic parameters of the breast tissue components. The results demonstrate that this model is capable of predicting breast tissue deformation; therefore it can be used as an effective tool in data fusion techniques.

REFERENCES

Hibbit, Karlson, and Sorenson Inc. (1998). *ABAQUS, User's Manual.*

Keyak, J. H. et al. (1990). *Automated three-dimensional Finite Element Modelling of Bone: a New Method.* J. Biomed. Eng., **12**, 389-397.

Sarvazyan A. P. et al. (1995). *Biophysical Bases of Elasticity Imaging.* Acoust. Imag., **21**, 223-240.

ACKNOWLEDGEMENT

DEVELOPMENT OF PATIENT-SPECIFIC FULLY HEXAHEDRAL 3D ANATOMIC MESHES USING ORTHOGONAL GRIDS

Branislav Jaramaz[1,2], Volkan Akcelik[2], Omar Ghattas[2], Anthony M. DiGioia III[1,2]

[1]Center for Orthopaedic Research, UPMC Shadyside, Pittsburgh, Pennsylvania
[2]Department of Civil and Environmental Engineering, Carnegie Mellon University, Pittsburgh, Pennsylvania
Email: branko@cor.ssh.edu

INTRODUCTION

Development of computational models for patient-specific simulation is an important step in further advancing the predictive capacities of biomechanical simulation. Patient-specific preoperative planning and simulation could be tailored for specific needs of an individual patient. It could better prepare the surgeon for specific requirements of the surgical task and allow the examination of potential outcome and the optimization of the surgical plan.

In this paper we introduce an alternative method of developing three dimensional anatomical meshes fully constructed of hexahedral elements. The method is based on orthogonal grid generation by the solution of elliptical partial differential equations [1]. In addition to some innovative aspects of the grid generation process, the method is adapted for semi-automatic development of patient-specific models from three-dimensional medical images.

METHODS

A structured grid can be interpreted as a mapping from a computational region to a physical space. In the index space the grid is defined as a lattice of points in a rectangular region. The continuum transformation in 2D can be written as:

$$x = x(\xi, \eta), \quad y = y(\xi, \eta) \tag{1}$$

where variables x, y describe physical space and ξ, η describe logical space. The boundary fitting transformation map that satisfies Laplace-Beltrami partial differential equation (PDE) is performed from a computational to a physical space [2]. The PDE has the form:

$$\frac{\partial}{\partial \xi}\left(f \frac{\partial x}{\partial \xi}\right) + \frac{\partial}{\partial \eta}\left(\frac{1}{f}\frac{\partial x}{\partial \eta}\right) = 0$$

$$\frac{\partial}{\partial \xi}\left(f \frac{\partial y}{\partial \xi}\right) + \frac{\partial}{\partial \eta}\left(\frac{1}{f}\frac{\partial y}{\partial \eta}\right) = 0 \tag{2}$$

where f is the so-called distortion function:

$$f = \left(\frac{\left(\frac{\partial x}{\partial \eta}\right)^2 + \left(\frac{\partial y}{\partial \eta}\right)^2}{\left(\frac{\partial x}{\partial \xi}\right)^2 + \left(\frac{\partial y}{\partial \xi}\right)^2}\right)^{\frac{1}{2}} \tag{3}$$

Equations (2) are nonlinear and need to be solved iteratively. The problem can be solved using either Dirichlet boundary conditions, with the boundary points fixed, or with the Neumann-Dirichlet boundary condition with the boundary points sliding along the boundary. The method produces a nearly orthogonal grid but can create elements with very large aspect ratios. In order to limit the aspect ratio and produce a more uniform grid, we have introduced a pseudoforce that acts between adjacent nodes of the grid. The pseudoforce is prescribed as a function of normalized distance between adjacent nodes, and can be attractive or repulsive depending on the distance between nodes. By varying the intensity of the force, the uniformity of the mesh can be controlled, and balanced with the requirements of mesh orthogonality. The outlined methodology is implemented in the interactive computer program that takes as

an input a set of contours extracted from a CT scan (generated by a threshold-based contour extraction program). The user assigns the corner points of the grid to the contour, and the other boundary points of the grid are uniformly distributed along the contour. The orthogonal grid is then generated and the next contour is read in. The corners of the grid can be assigned either manually or automatically to the nearest neighbors of the preceding slice's corners. The additional inter-layer forces are assigned to minimize distortion relative to the previous slice. The mesh quality is monitored, by displaying both the pseudo-colored values of the Jacobian and the warping index of every element.

RESULTS

The performance of the hexahedral mesher is illustrated in the examples of anatomic meshes of the pelvis and femur. Figure 1 shows the mesh of the pelvis derived from a CT scan. Meshing of the pelvis presents us
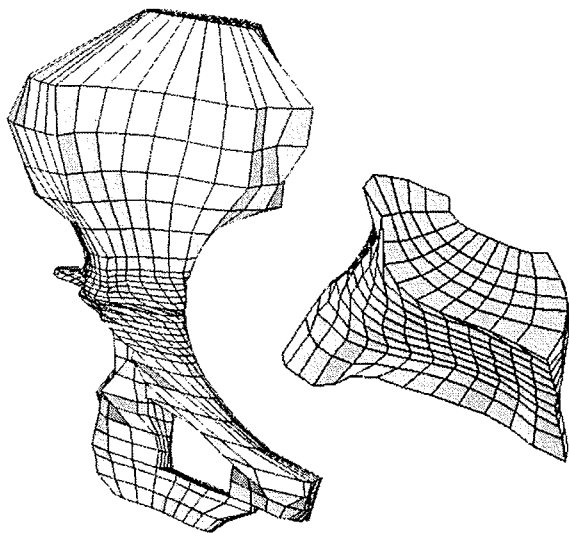
Figure 1. Hexahedral mesh of a pelvis.

with problems such as branching, change of dimensions, excessive distortion, change of dominant dimension, and warping of the surface. To successfully develop a mesh one has to take into account changes of the contour as a function of scanning direction,

placing the grid corners accordingly. The mesh shown in Figure 1 is comprised of 2224 nodes and 1600 elements. A particular difficulty in development of this mesh was in the area superior to the acetabulum, where the shape changes in direction of the longitudinal body axis are extreme.

Figure 2 shows an example of a mesh of the femur. The geometry is simpler than that of the pelvis, with relatively simple convex contours in each scanning plane and a gradual transition from one CT plane to the next.
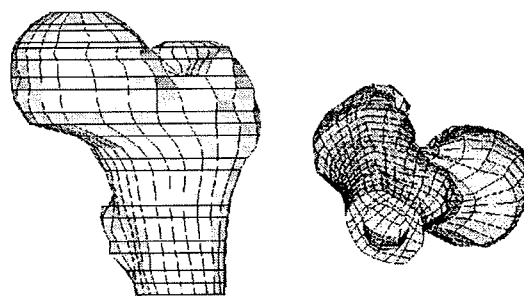
Figure 2. Hexahedral mesh of a femur.

DISCUSSION

The presented method of meshing the anatomic structures using orthogonal grids results in fully hexahedral three-dimensional finite element meshes, suitable for biomechanical analysis and patient-specific simulations. Because of their numerical performance these meshes are advantageous over those built with tetrahedral elements of the same order and element size. Progressive refinement of the meshes is simple and results in a slower increase of number of degrees of freedom than a similar refinement of tetrahedral meshes. The meshing is semiautomatic and can be done relatively quickly, even for complex anatomic structures.

REFERENCES: 1. Castillo, J.E. (ed.) Math. Aspects of Numerical Grid Generation, SIAM, 1991. 2. Eca, L., J. Comput. Phys., Vol. 125, 440-453, 1996.

MODELING MULTI-JOINT CONTROL IN LANDINGS

Philip S. Requejo[1], Jill McNitt-Gray[1], Henryk Flashner[2]
[1]Biomechanics Research Lab, University of Southern California
[2]Department of Mechanical Engineering, University of Southern California
Email: requejo@rcf.usc.edu   Web: biomech1.usc.edu

INTRODUCTION

In multi-joint motions, a stereotypical pattern is often seen despite the variety of ways a movement may be executed. In landing tasks the aim of the neuromuscular system is to control the lower extremity joint motion to decrease the total body center of mass velocity. During a landing impact the human body is exposed to large forces that create the potential for lower extremity musculoskeletal injury. Due to the highly practiced nature of this ballistic task, joint motion is likely to be executed in a stereotypical pattern. Flashner et al., (1987) proposed a movement control structure which combines open and closed loop control strategies derived from stereotype joint kinematics. Beuter and Flashner (1991) determined that joint kinematics can be characterized by a small number of basis functions yielding a simple analytical description of open and closed loop control. The present study applies the movement control model by Flashner et al.(1987) to study control in the contact phase of landing from multiple tasks. We hypothesize that the lower extremity joint motion during drop, front, and back salto landing can be adequately represented by a set of basis functions, and a finite number of task dependent coefficients. The existence of such joint control model is important to the identification and understanding of the mechanisms underlying human movement.

PROCEDURES

Experimental data were collected from collegiate gymnasts (n=6, Age: 21.1±1.8 years, height:1.68±.05m, mass: 61.52±5.42kg) performing drop, front, and backward salto landings. A Kistler force plate (800 Hz) and high-speed video (200 fps; NAC Motion Analysis System) as described in McNitt-Gray (1993) was used. Analysis of the experimental data was limited to the contact phase of landing in the sagittal plane. A 3-D, 12 segment, 11 joint dynamical model (ADAMS, Mechanical Dynamics, Ann Arbor MI) was developed (Requejo et al., 1999). The control module in ADAMS was used to represent the dynamics of the physical plant into a Matlab/Simulink (Mathworks, Natick MA) block element developed to simulate the movement control system (Figure 1). Mean hip, knee, and ankle angle was determined for all subjects and subsequently used to derive a series of equations using least squares regression method used by Flashner et al. (1988). The joint trajectory functions were input to the open-loop controller.

RESULTS AND DISCUSSION

It was determined that a polynomial basis function can be used to model the joint trajectory during the contact phase of landing. The ankle, knee, and hip joint trajectory for the drop, back, and front salto landing is described using the general equation:

$$\theta(t) = \sum_{i=0}^{n} C_i * t^n$$

where C_i is a task specific coefficient. Comparison between estimated and experimental data of the drop, front, and back salto landing of one subject shows a high degree of agreement ($R^2 > .95$) (Figure 2).

Due to the highly practiced nature of the experimental tasks, small variability was observed between landing trials. These results support the findings of Beuter and Flashner (1991). Our experimental result suggests that there are invariant features in joint trajectories between multiple landing tasks. In addition, the shape of the joint trajectories also suggests that movement planning takes place at the joint level.

These results suggest the presence of a common control model for multiple tasks that may incorporate mechanically and physiologically relevant coefficient modification to adjust for variations between tasks.

REFERENCES

Beuter A., Flashner H. (1991), *Trends in Biol. Cyber.*, 59-77.

Flashner H., Beuter, A., Arabyan A., (1987), *Biol. Cyber.* 387-395.

Flashner H., Beuter, A., Arabyan A. (1988). *Biol. Cyber.* 91-99.

McNitt-Gray (1993). *J. Biomech.* 1037-1046.

Requejo P., McNitt-Gray, Flashner H. (1999). *Proceedings of SCCB.*
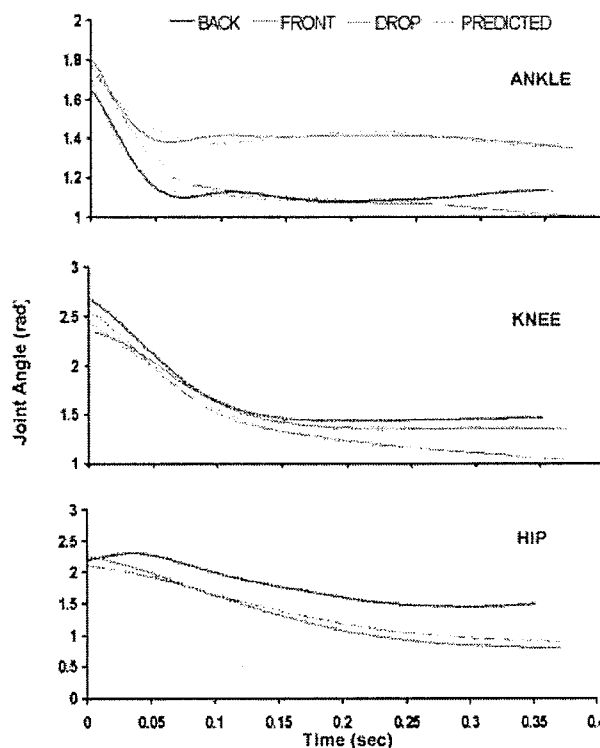
Figure 2: Experimental and predicted joint
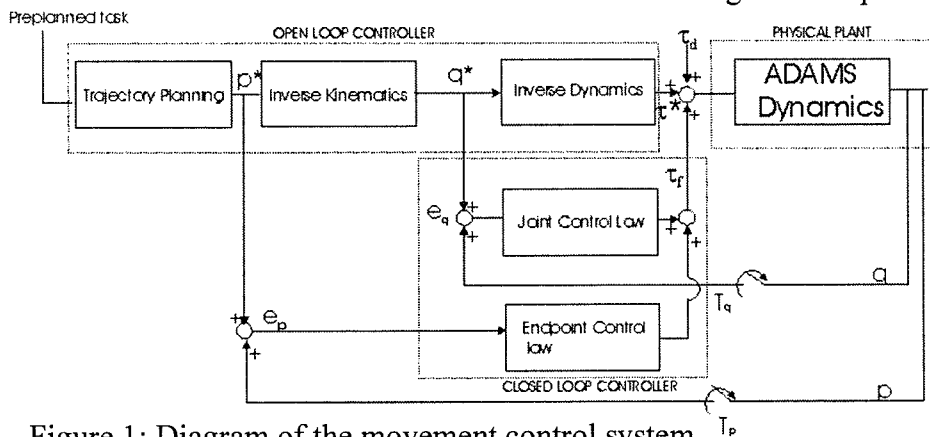
Figure 1: Diagram of the movement control system

DESIGN OF A REAL TIME EMG-DRIVEN VIRTUAL ARM

Xiaofeng Shen, Jianyu Cheng, Kurt Manal, and Thomas S. Buchanan
Center for Biomedical Engineering Research, University of Delaware, Newark, Delaware
Email: xshen@me.udel.edu, Web: http://www.cber.udel.edu/~shen

INTRODUCTION

An EMG-driven virtual arm (VA) is being developed in our laboratory for the purposes of studying neuromuscular control of arm movements. Specifically, we are interested in control of the muscular system during the transition from static arm postures to movement. The VA incorporates the major muscles spanning the elbow joint and is used to estimate tension developed by *individual* muscles based on recorded EMGs. For the muscle tensions, it is able to estimate joint moments and the corresponding virtual movements, which it displays in real-time. In addition, the VA offers artificial control over a variety of physiological and environmental conditions. For example, it is possible to modify the tension a muscle generates by adjusting parameters in the model. This approach can been used to examine how the neuromuscular system compensates for the partial or total loss of a muscle's ability to generate force as might result due to trauma or pathology.

PROCEDURES

The VA is comprised of six distinct, but highly integrated components. The organization of these components is summarized in Figure1. Data collection is performed in two phases. In Phase I, the model is trained so as to adjust the parameters of the model to fit the subject. This training and parameter optimization is not performed in real-time. In Phase II (once the optimal parameters are obtained), the optimal controller is no longer used, but the model is operated in real-time

with a graphical interface that displays the current state of the model. The six components of the VA are as follows.

1. Data collection. EMG data are collected for 7 muscles (2 heads of biceps, brachialis, brachioradialis & 3 heads of triceps) during *isometric* unidirectional and sinusoidal flexion/extension time varying loads. Elbow torque is recorded from a six degree of freedom load cell rigidly attached to the distal forearm.

2. EMG-to-activation model. EMG data are processed (filtered, full wave rectified) and passed to the EMG-to-activation model. This transforms processed EMG to an activation time series. The model is similar to the linear discrete time dynamic model proposed by Thelen et al. (1994), but differs in that it accounts for the non-linearities of the isometric EMG to force relationship (Buchanan et al., 1997).

3. Anatomical model. Moment arms are estimated from the anatomical model and used to calculate a net joint moment based on

EMG-Driven Virtual Arm
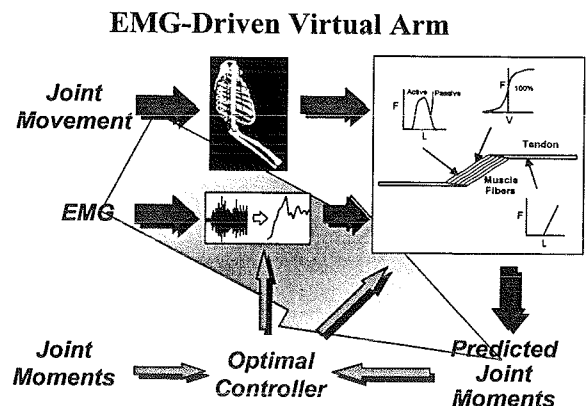
Figure 1: Diagram of Phase I (the training phase) of the Virtual Arm. In Phase II, the optimal controller is eliminated and the VA works in real-time.

force contributions from individual muscles.

4. Hill-type muscle model. The output of the EMG-to-activation model along with the musculotendon lengths and velocities as determined by the anatomical model are used as input to a Hill-type muscle model as described by Zajac (1989).

5. Optimal Controller. Non-linear optimization is used to adjust coefficients in the EMG-to-activation model and input parameters to the muscle model (optimal fiber length, resting tendon length, maximum contraction velocity) such that the elbow moment of the VA fits the experimental data. This process is performed off-line. A Levenberg-Marquardt, quasi-Newton method is used to determine activation parameters and Hill-based muscle parameters. Bounds imposed on muscle parameters are introduced to ensure the parameters are consistent with values reported in the literature. The entire process of training the VA (including data collection) can be completed in approximately 10 minutes. The optimized parameters are unique to each subject and are used during the real time experiments.

6. Graphical display. A 3D graphics model of the ulna, radius, humerus, scapula, rib cage and major muscles spanning the elbow is displayed on the computer screen. The subject controls movement of the VA via EMG even though the subject's arm is fixed in the load cell. The subject is instructed to move the VA throughout the workspace in an effort to acquire specific targets.
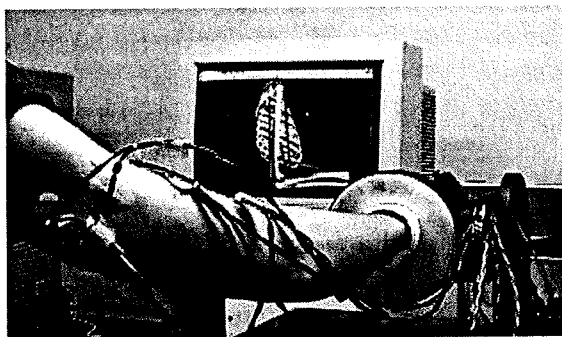
Figure 2: A photograph of a subject controlling the virtual arm.

In Phase II of the model, EMGs are recorded and processed (filtered, full wave rectified) *on-line* as the subject performs unidirectional and sinusoidal elbow movements with the arm fixed in the load cell. The processed EMGs and activation coefficients determined during training are used as inputs to the EMG to activation model. The output of this component and the optimized muscle parameters are used to calculate elbow torque of the VA. The torque and inertial properties of the subject's arm are used as inputs to a dynamic model which returns the angular position of the VA.

RESULTS AND DISCUSSION

Shown in Figure 2 is a subject preparing to flex the elbow of the VA by contracting his muscles. Preliminary results suggest that consistent neuromuscular patterns emerge as a subject controls elbow flexion of the VA. Particularly interesting was the observation that a different neuromuscular pattern was adopted when the brachialis of the VA was incapacitated. That is, the subject altered his control strategy to effect elbow flexion to rely more on the biceps muscle.

It is our belief that the VA can be used to better understand the neuromuscular control process of healthy and impaired individuals.

RFERENCES

Buchanan, T.S. et al. (1997) *Int Soc Biomech*, **16**, 330.
Thelen, D.G., et al. (1994) *J. Biomech.*, **27**, 907-919.
Zajac, F. E. (1989) *Critical Reviews in Biomedical Engineering.*, **17**, 359-411.

ACKNOWLEDGEMENMTS

Finite Element Modeling of Load Transmission Through the Calcaneus

Susan E. D'Andrea[1], David Thompson[2], Dongbu Cao[2] and Brian Davis[2]

[1] Graduate Medical Sciences, Barry University, Miami Shores, FL
[2] Biomedical Engineering, The Cleveland Clinic Foundation, Cleveland, OH
Email: sdandrea@mail.barry.edu

INTRODUCTION

The calcaneus is the largest and strongest tarsal bone of the foot composed of a thin, hard cortical shell surrounding a core of trabecular bone. It is a critical link between the body and the ground and serves as a lever for many of the extrinsic muscles of the lower limb. Because of its shape and size, the calcaneus provides the foot with strength, stability and an ability to withstand high compressive and tensile forces.

Determination of the forces acting on bone is a common problem in the field of orthopaedics. Finite element analysis (FEA) affords the biomedical researcher a unique opportunity to study complex anatomical structures such as the foot, to measure its interaction with the environment and assess the relationship between load and morphology of biological tissue.

In order to understand the force transmission thorough the calcaneus during high impact situations, finite element analysis techniques were used to determine the relationship between external force, internal calcaneal strain and bone mineral density.

PROCEDURES

A two-dimensional finite element model of the foot was developed which included a sagittal view of the second metatarsal, proximal phalanx; the intermediate cuneiform, talus and calcaneus; the plantar aponeurosis; the calcaneal and metatarsal fat pads and the skin on the plantar surface of the foot (Figure 1).
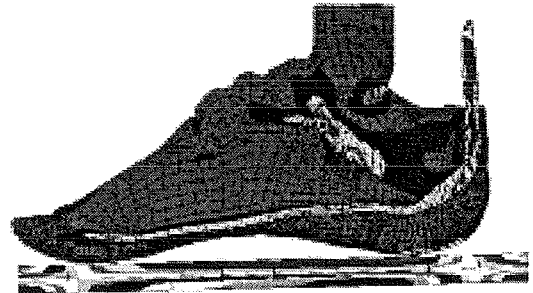
Figure 1: Finite Element Model of the Foot

Each surface was meshed using Patran® (MacNeal-Schwendler Corporation) with eight noded quadrilateral or six noded triangular elements depending on the geometry. Linear elastic properties were assigned to the cartilage, bone, muscle (soft tissue), aponeurosis, tendon and ligament (Nakamura, et al., 1981; Kitaoka et al., 1994). The calcaneal and metatarsal fat pads and the skin on the plantar surface of the foot were given non-linear properties using a standard hyperelastic constitutive relation. Bone was assumed to behave in an isotropically linear manner and the elastic moduli were varied with position in the calcaneus based upon imaging and regression techniques (Davis and Hanson, 1995; Keaveny and Hayes, 1993). Other tarsal bones and the metatarsal were assigned a moduli of 250 MPa and Poisson's ratio of 0.3 (Shorten, 1993). The proximal talus was constrained to mimic the physiologic conditions of a vertical impact.

Custom software was utilized to a high impact force imparted to the foot by displacing the metal plate into the foot a maximum of 1.4 cm. Four conditions were tested by altering the loading rates (78 and 150 cm/sec) and calcaneal bone density distributions (average and low). Stress distribution was plotted for the entire foot and the third principal strain patterns in the calcaneus were analyzed along predefined axes in the calcaneus (Figure 2).

_ _ **Vertical Axis**   ◄—► **Post. Vert. Axis**
——**Neutral Axis**   ◆—◆**Ant. Vert. Axis**
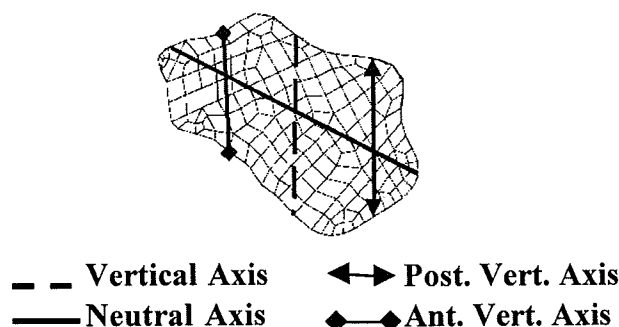
Figure 2: Strain Axes in the Calcaneus

RESULTS
Strain results for the calcaneus differed depending on the location in the bone.
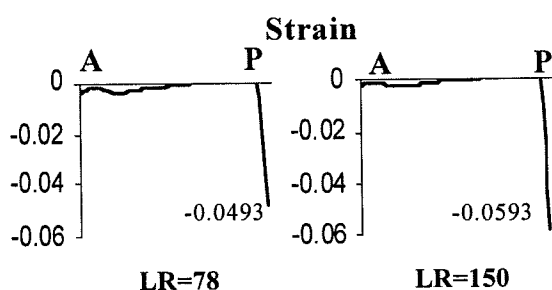
Figure 3: Neutral Axis Strain
A= Anterior Surface; P= Posterior Surface
LR = Loading Rate
*Values represent peak compressive strain

An increase in compressive strain accompanied the increase in loading rate (from 78 to 150 cm/sec) for all strain axes. For the neutral axis, the maximum compressive strain increased in magnitude by a value of 0.01 (Figure 3). Little or no

effect on the magnitude or distribution of the

High   Low
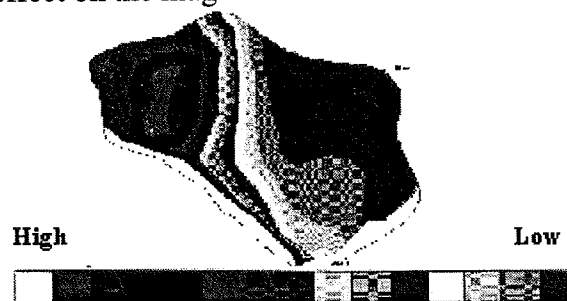
strain was evident in the model when the bone mineral density was decreased.

The compressive strain distribution in the calcaneus increased anteriorly and inferiorly with the higher strains occurring at the inferior surface of the bone due to bending (Figure 4).

Figure 4: Strain Distribution in Calcaneus

DISCUSSION
The finite element model has shown to be a powerful tool to investigate the relationship between load carrying capabilities and morphology of tissue in the foot. In the current state, the foot model can differentiate the effects of loading rate. With modifications in the material characteristics and the inclusion of a more viscoelastic properties for the fatpad, skin and bone, the model will be capable of identifying the effects of bone mineral density or any pathologic alteration in the foot structure.

REFERENCES
Davis and Hanson (1995). Combined ORS Meeting, 249.
Keaveny and Hayes (1993). J. Biomech. Eng., 115: 534-542.
Kitaoka et al.(1994). Foot and Ankle International, 15(10): 557-560.
Nakamura et al.(1981). Bulletin of Prosthetic Research, 18: 27-34.
Shorten, MR (1993). Proceedings of the Int. Society of Biomechanics, 114.

FORCE TRANSMISSION IN THE JUVENILE RHEUMATOID ARTHRITIS WRIST

Xiaopeng Lu, Kurt Manal and Thomas S. Buchanan
Center for Biomedical Engineering Research, University of Delaware, Newark, Delaware
E-mail: lu@me.udel.edu

INTRODUCTION

The wrist is a complex biomechanical structure comprised of carpal bones and the ulna and radius. Juvenile rheumatoid arthritis (JRA) is a common pathology that can lead to osseous deformation resulting in malalignment of the joint and functional impairment. The proximal carpal bones of the JRA wrist tend to deviate toward the ulna (Sennwald & Segmuller, '86). Re-establishing normal alignment of the bones is a necessary step in improving function and restoring natural development of the joint. Static and dynamic orthoses have been used as treatment modalities when malalignment of the joint is indicated. Design of an effective orthosis requires knowledge of the contact forces between the many joints of the wrist and hand. Several studies have examined joint contact forces and pressure distributions using a variety of techniques. To our knowledge, no study has examined contact forces between the articulating surfaces of the JRA wrist.

The purpose of this study therefore was to estimate contact forces between the proximal carpal bones and their articulations with the ulna and radius during a simulated gripping task.

PROCEDURES

Two-dimensional bone geometries for 1 normal and 3 JRA wrists were obtained by digitizing postero-anterior X-rays using IMOD modeling software (Figure 1). The trapezoid and trapezium were treated as a single body because their borders overlap in the X-ray view. Rigid body spring modeling (RBSM) was used to estimate joint contact forces and tension in the major ligaments of the hand and wrist. Cartilage and ligament were modeled using compressive and tensile springs. In excess of 300 springs were used in each of the 4 wrists modeled. Compressive springs were set at a stiffness of 17 N-mm resulting in an average cartilage stiffness of approximately 200 N-mm between each joint. Stiffness values for the tensile springs were identical to values reported in the literature (Schuind et al., 1995). The compressive and tensile springs were not allowed to carry load if they were longer / shorter than their respective resting lengths. The following

Figure 1. Postero-anterior X-ray of a normal wrist. The digitized geometry of the bones is shown in the schematic. R=radius, U=ulna, S=scaphoid, L=lunate, T=triquetrum, TT=trapezium & trapezoid, C=capitate, H=hamate, 1-5 denote metacarpals.

Table 1. Proportion of the applied force transmitted through the radio-ulnar-carpal joints of the normal wrist. A similar force of 142 N was applied in all 3 studies.

%Force	Schuind	Iwasaki	Lu
Radioscaphoid	55	55	51
Radiolunate	35	28	25
Ulnolunate	8	13	14
Ulnotriquetral	2	4	10

forces were applied to metacarpals 1 through 5 respectively: 22, 34, 42, 26 & 18 N. SD-Fast dynamic analysis software was used to solve the equilibrium equations for the perturbed model of the wrist.

RESULTS & DISCUSSION

Our method of solving the equilibrium equations differs from the method used in other studies (Schuind et al., 1995; Iwasaki et al., 1998). In theory, both methods should yield similar results. We report data for our 1 normal subject for two reasons: (1) justify our approach by comparing our results with values reported in the literature, (2) allow us to compare the JRA data to a larger population since our 1 normal wrist is consistent with values reported in the literature.

The proportion of force transmitted through the radio-scaphoid joint of the JRA wrist was less than noted in the normal wrists. Conversely, the contact force between the radio-lunate joint appears to be larger than normal in the JRA wrist. Contact forces between the articulating surfaces of the ulna-carpal joints were similar for both the normal and JRA wrists. Statistical comparisons were not possible given our small sample size (n=3). An increase in force transmitted across the radio-lunate joint and a decrease across the radio-scaphoid joint is consistent with ulnar deviation of the proximal carpal bones characteristic of a malaligned JRA wrist.

Table 2. Proportion of the applied force transmitted through the radio-ulnar-carpal joints of the JRA wrists (n=3). Standard deviations reported in parentheses.

%Force	JRA
Radioscaphoid	37.5 (11.9)
Radiolunate	37.2 (7.8)
Ulnolunate	16.2 (2.4)
Ulnotriquetral	9.2 (3.5)
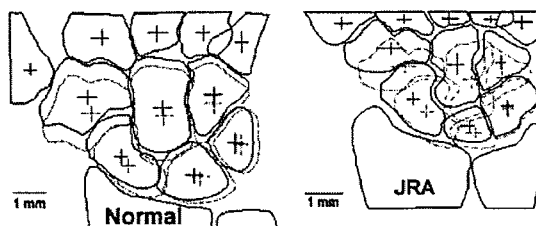
Figure 2. Initial and final equilibrium positions of the carpal bones.

Initial and final positions of the carpal bones for the 1 normal wrist and 1 JRA wrist are shown in Figure 2. Note how the scaphoid and lunate of the JRA wrist undergo greater ulnar deviation than in the normal wrist.

These data represent our initial efforts to estimate joint contact forces in the JRA wrist. The data suggest a larger proportion of force is transferred through the radio-lunate joint than normal. The actual force may be greater than predicted by our model since we assume the ligaments are fully functional. Loss of ligamentous integrity is common of JRA (Findley et al., 1983). Future work is needed to better model this characteristic of the disease.

REFERENCES

Findley, T. W. et al., G. (1983). *Archives of Phys. Med. & Rehab.*, **64**, 69-74.
Iwasaki, N. et al. (1998). *J. Hand Surgery*, **23A**, 415-424.
Sennwald, G., Segmuller, G. (1986). *International Orthopaedics*, **10**, 25-30.
Schuind, F. et al. (1995). *J. Biomechanics*, **28**, 587-601.

ACKNOWLEDGEMENMTS

INVESTIGATING NONLINEAR VISCOELASTIC PROPERTIES OF BRAIN TISSUE USING THE FORCED VIBRATION METHOD

Kurosh Darvish and Jeff R. Crandall

Automobile Safety Laboratory, University of Virginia, Charlottesville, Virginia
Email: kurosh@virginia.edu   Web: cinderella.mech.virginia.edu

INTRODUCTION

The objective of this study was to develop a method for characterizing nonlinear viscoelastic properties of brain tissue using the forced vibration method. Understanding nonlinearity of brain material is crucial in studying the effects of *a*) finite deformation, *b*) multiple impacts and *c*) shock and acceleration waves in traumatic brain injury.

Brain tissue, like most other soft tissues, exhibits viscoelastic behavior. Traumatic brain injury is generally caused by deformation impulses with duration of a few milliseconds. Therefore, it is necessary to use dynamic test methods for characterizing the brain material. The study of dynamic viscoelasticity of brain tissue began in late 1960's. The reader should see Arbogast and Margulies (1998) for a brief review of the previous dynamic test results. In previous studies the brain material is assumed to be linearly viscoelastic. However, the more recent results of stress relaxation tests on human and bovine brain (Takhounts, 1998) and on porcine brain (Prange *et al.*, 1998) show that the material instantaneous and time dependent responses are generally nonlinear. In addition injury tolerance of neural fibers is about 15% to 20% tensile strain or 20% to 30% shear strain (Thibault *et al.*, 1990). The study presented in this paper accounts for both material and geometric nonlinearities in characterizing brain tissue.

BRIEF THEORY

In the Green-Rivlin model with multiple hereditary integrals, the stress response is considered to be nonlinear with respect to both strain and time. Developing a fully nonlinear model provides a basis for evaluating simpler models such as linear and quasilinear viscoelastic models. In this study the brain material was assumed to be isotropic, homogeneous and incompressible and a third order Green-Rivlin constitutive relation following Pipkin (1964) was used. Assuming simple shear deformation with $x_1 = X_1 + K(t)X_2$, $x_2 = X_2$, $x_3 = X_3$, the sample shear stress can be written as:

$$\Sigma_{12} = \frac{1}{2}\int_0^t \psi_2 \dot{K}(\tau_1)d\tau_{(1)} +$$
$$\frac{1}{2}\int_0^t\int_0^t \psi_6 \dot{K}(\tau_1)K(\tau_2)\dot{K}(\tau_2)d\tau_{(2)} + \quad (1)$$
$$\frac{1}{8}\int_0^t\int_0^t\int_0^t \psi_{III} \dot{K}(\tau_1)\dot{K}(\tau_2)\dot{K}(\tau_3)d\tau_{(3)}$$

where $\Sigma_{12} = \sigma_{12} + \frac{1}{2} K \Delta\sigma_n - \frac{1}{2} K^2 \sigma_{12} - \frac{1}{8} K^3 \Delta\sigma_n$, with $\Delta\sigma_n = \sigma_{11} - \sigma_{22}$, σ_{ij} is the Cauchy stress tensor, and ψ_2, ψ_6, and ψ_{III} are the time dependent material kernel functions to be determined.

MATERIAL AND METHOD

Small cylindrical samples (about 10 mm to 15 mm diameter and 2 mm to 5 mm length)

of white and gray matters of fresh bovine brain tissues were tested using the experimental apparatus developed for this purpose and described in Darvish et al. (1998). Samples were cut along the superior-inferior direction of the head. During all tests, samples were immersed in artificial cerebrospinal fluid that was kept at the body temperature. In order to investigate nonlinearity of the constitutive relation (1), the input excitation was selected as a superposition of three harmonic inputs:

$$K(t) = K_I \sin(\omega_I t) + K_{II} \sin(\omega_{II} t) + K_{III} \sin(\omega_{III} t) \qquad (2)$$

with a total shear strain level up to 30%. In the frequency range below the first natural frequency (about 400-450 Hz) where the inertial effect is small, the output force signals were used to measure σ_{12} and σ_{22} ($\sigma_{11} = 0$) and subsequently to derive the shear complex moduli $G_n(\omega_1,..,\omega_n)$ for $n = 1$, 2, 3 (Lockett, 1972). Due to nonlinearity, the force responses had frequency components in addition to the fundamental frequencies ω_I, ω_{II}, and ω_{III}. By performing spectral analysis on the force signals and using the magnitude and phase of the first three harmonics and two-term and three-term combinations of the fundamental frequencies, the first-, second- and third-order complex shear moduli were determined. The presence of non-integer harmonics in the force signals could not be modeled with single hereditary integral models and confirmed the Green-Rivlin model assumption. In order to determine the kernel functions in time domain that can be used in explicit numerical algorithms a product form was assumed for the second- and third-order relaxation kernels (Nakada.1960). The first-order relaxation functions were fitted to discrete spectrum approximation in the form of 4-term Prony series with short-, intermediate-, and long-time decay rates in the order of magnitude of 10 ms, 100 ms, and 1.0 s respectively in addition to a constant term.

SUMMARY

In this study, a method was presented to develop nonlinear viscoelastic model of brain tissue in the form of multiple hereditary integrals using the forced vibration method. The results show that a third-order Green-Rivlin material model sufficiently describes the nonlinearity of the brain material subject to finite shear deformation.

REFERENCES

Arbogast, K. B., and Margulies, S. S. (1998) "Material Characterization of Brainstem from Oscillatory Shear Tests," *J. Biomechanics*, **31**, 801-807.

Darvish K., Takhounts E. G., and Crandall J. R. (1998) "A Dynamic Method to Develop Nonlinear Viscoelastic Model of Brain Tissue", *Advances in Bioengineering*, ASME, BED-VOL. 39.

Lockett, F. J. (1972) *Nonlinear Viscoelastic Solids*, Academic Press.

Nakada, O. (1960) "Theory of Nonlinear Responses," J. Physical Society of Japan, **15**, 228.

Pipkin, A. C. (1964) "Small Finite Deformation of Viscoelastic Solids," *Rev. Mod. Phys. Solids*, **36**, 1034-1041.

Prange M. T., Meany, D. F., and Marguiles, S. S. (1998) "Directional Properties of Gray and White Brain Tissue Undergoing Large Deformation", *Advances in Bioengineering*, ASME, BED-VOL. 39

Takhounts, E. G. (1998) "The Experimental Determination of Constitutive Equations of Human and Bovine Brain Tissue," Ph.D. Dissertation, University of Virginia, Charlottesville, VA.

Thibault, L. E., Gennarelli, T. A., Margulies, S., Marcus, J., and Eppinger, R., (1990) "The strain dependent pathological consequences of inertial loading on central nervous system tissue," in: *Proceedings of the 1990 International IRCOBI conference on the Biomechanics of Impacts.*

AN ASSESSMENT OF THE PULL-THROUGH STRENGTH AND FATIGUE PROPERTIES OF A NEW STERNAL CLOSURE TECHNIQUE

Joseph E. Hale[1], Donald D. Anderson[1], Greg A. Johnson[2], and James A. Magovern[3]

[1]Biomechanics Laboratory, Minneapolis Sports Medicine Center, Minneapolis, MN
[2]Cardiac Assist Technologies, Inc., Pittsburgh, PA
[3]Department of Thoracic Surgery, Allegheny General Hospital, Pittsburgh, PA
e-mail: jhale1@fairview.org   web: msmc.org

INTRODUCTION

Median sternotomy is the most commonly used surgical approach in cardiothoracic surgery. Complications associated with the traditional use of parasternal stainless steel sutures for sternal closure, although infrequent, result in significant morbidity and mortality. Sternal dehiscence occurs when the two edges of the sternum separate, typically as the sutures pull through the bone.

The objective of this study was to assess the pull-through strength and fatigue properties of a new sternal closure technique. The CAT Sternal Closure System (Cardiac Assist Technologies, Pittsburgh, PA) attempts to distribute stresses exerted by the stainless steel sutures on the sternum by threading them through grommets placed within pre-drilled holes in the sternum.

MATERIALS AND METHODS

Due to the high degree of inter-specimen variability and the scarcity of human cadaveric sterna, mechanical testing was performed using a low density polyurethane (LDPU) foam (0.24 g/cc). This density value was chosen to represent a low to mid-range value for cancellous bone (0.09-1.26 g/cc; Gibson and Ashby, 1988). The use of polyurethane foam as a bone analogue was validated for this study (Hale et al., 1999). Uniform specimens of rectangular cross-section (8 x 19mm) were used for testing. Pull-through strength testing of six specimens with grommet and suture, and six control specimens with suture alone was performed. Since wire crimping is common to both techniques, only one side of the sternotomy was simulated to remove wire crimping as a variable. The uniaxial testing

performed was intended to reproduce the predominant lateral stresses placed on the sternum during breathing, while neglecting smaller forces applied in the anterior-posterior and rostral-caudal directions.

For tests of suture augmented with grommets, a 3.9 mm diameter hole was drilled approximately 1 cm from the lower edge of the specimen and a grommet placed as described in the Directions for Use. For the suture alone group, a 2.4 mm diameter hole was drilled. With the specimen clamped in a material testing system (MTS Model 858), a length of 0.79 mm diameter stainless steel suture was threaded through the hole. The free ends of the suture were gripped in a custom designed fixture attached to the testing machine and used to apply a tensile load perpendicular to the hole axis. Following application of a pre-load (nominally 5 N), specimens were loaded to failure at a rate of 100 mm/min.

The fatigue testing procedure followed closely that used in pull-through strength testing. Instead of a single pull, the suture was tensioned sinusoidally at 10 Hz from 10-55 N for 850,000 cycles or until failure, whichever came first.

Load-elongation data and failure mode were recorded for both procedures. Statistical comparisons were made using ANOVA techniques. Post-hoc testing was performed using correction for multiple comparisons, and significance assigned for $p < 0.05$.

RESULTS AND DISCUSSION

The stainless steel sutures augmented with the grommets demonstrated clearly superior pull-through properties compared to the sutures alone when tested in LDPU foam (Figure 1). Failure load with the grommets was nearly 270% that of the stainless steel sutures alone. Five-fold increases in secant stiffness and tangent stiffness values indicate that the grommets not only fail at a higher load, but exhibit greater resistance to pull-through in the initial loading phase as well (Table 1). It is interesting to note that once the grommets reach their failure load, a force comparable to the failure load of the suture alone is needed to continue pulling the grommets through the test specimen.

Table 1: Pull-through properties. Tabulated values are mean ± standard deviation, with six specimens per group.

	Sutures alone	With grommets
Failure Displacement (mm)	7.10 ± 0.85	3.85 ± 0.39
Failure Load (N)	62.36 ± 3.46	167.08 ± 4.94
Secant Stiffness (N/mm)	8.88 ± 1.08	43.65 ± 3.39
Tangent Stiffness (N/mm)	16.18 ± 1.66	87.45 ± 11.14

Fatigue testing revealed that all of the sutures alone pulled-through well before completion of the 850,000 cycles to be tested (Figure 2). The number of cycles required for pull-through varied widely, ranging from 15,065 to 134,082 cycles (mean ± std. dev. = 58,578 ± 40,835 cycles). Failure displacements in the group of sutures alone averaged 7.44 mm. Conversely, none of the sutures augmented with grommets pulled through. The average pull-through at 850,000 cycles was 1.96 mm, 26% of the sutures alone, a value which was statistically smaller ($p < 0.001$) than for the sutures alone.
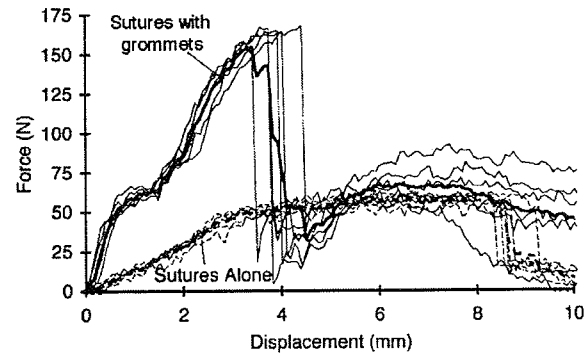
Figure 1: Pull-through response. Bold lines represent group averages.
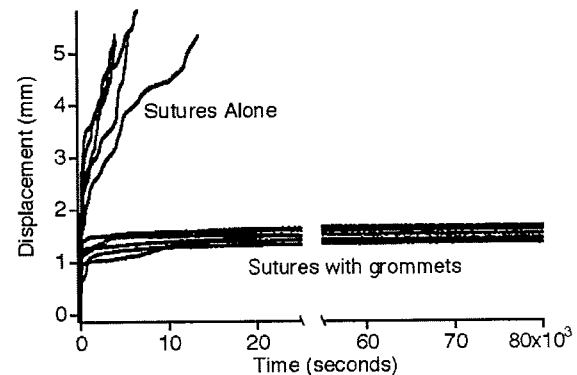
Figure 2: Fatigue testing results.

REFERENCES

Gibson, L. and Ashby, M. (1988) *Cellular Solids*, Pergamon Press, 316-331.

Hale, J. et al. (1999) *Proceedings of the '99 Bioengineering Conference*, ASME, **35**.

ACKNOWLEDGMENTS

GEOMETRIC SOLID MODELLING OF THE HUMAN FOREARM

James J. Dowling and Jennifer Durkin
Department of Kinesiology, McMaster University, Hamilton, CANADA

INTRODUCTION

The use of dual photon absorptiometry (DXA) has recently been shown to be an accurate method of calculating the mass, moment of inertia and location of the center of mass of human limb segments (Durkin, 1998). Briefly, living subjects were scanned via DXA which sent a beam consisting of photons at two energy levels through the body. The attenuation of the high energy photon as measured by the detector was proportional to the quantity of matter (mass) that the beam passed through. The scanned elements were stored in a file (see Figure 1 for a graphical representation of this file) and a computer program was written to digitally section this file such that the inertial characteristics of human limb segments could be calculated from the mass elements within the segment. While others have developed geometric shapes of the forearm (i.e. Hanavan, 1964), to our knowledge no study has validated the use of geometric shapes on measured inertial characteristics of living human subjects from various populations. The purpose of this study was to examine the characteristics of the mass distributions along human forearm segments of male and female subjects of different ages to determine the degree of geometric similarity between these populations.

METHODS

Twenty subjects were randomly selected from a pool of 100 subjects that were DXA scanned by Durkin (1998). Five subjects were taken from each of four sub-populations (males and females between 19 and 30 years of age and males and females over 55 years of age). A computer program was written to normalize the scanned mass data for each percentage of the segment length from the proximal to the distal ends.
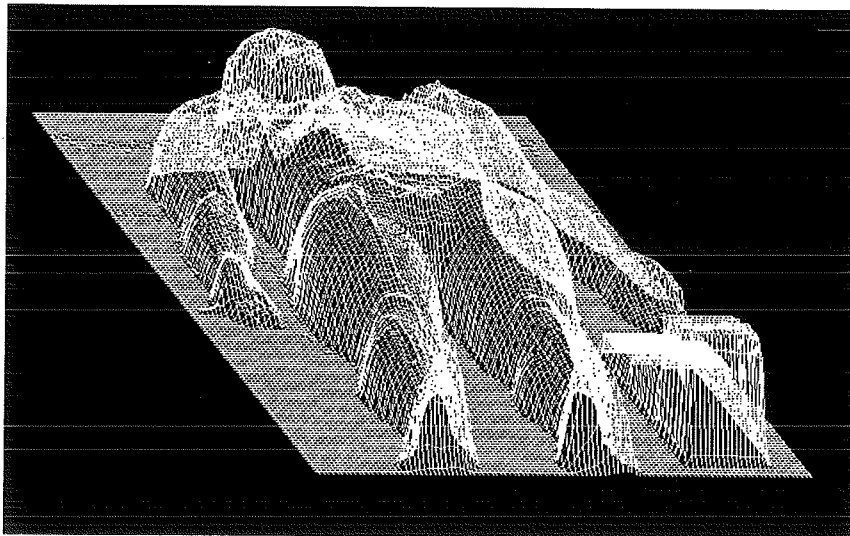
Figure 1: Mass map of the 336x730 scanned elements of a human subject. The height of the surface is proportional to the mass of each scanned element.

The amplitudes of the scanned masses were normalized to 100% of the total mass. The five subjects in each of the sub-populations were ensemble averaged and plotted. Each variance about the ensemble averages was analyzed for geometric similarity.

RESULTS AND DISCUSSION

Figure 2 shows the ensemble averages for the four populations. It can be seen that there was a similar shape for each sub-population. This indicated that a geometric solid could be defined that would estimate the inertial characteristics of human forearms regardless of age or gender. The shape of the mass distribution revealed that it was unlikely that a constant density cylinder or frustum would be a very good representation. The geometric shape that

represents this distribution would need to be a composite of at least three different shapes. However, this composite would only require one longitudinal estimate (i.e. length) and one transverse estimate (i.e. elbow circumference).

REFERENCES

Durkin, J.L. (1998) The prediction of body segment parameters using geometric modelling and dual photon absorptiometry. Master's Thesis. McMaster University. Hamilton, Ontario, Canada.

Hanavan, E.P. (1964) A mathematical model of the human body. AMRL-TR-64-102. Aerospace medical research Laboratories, Wright-Patterson Air Force Base: Ohio.
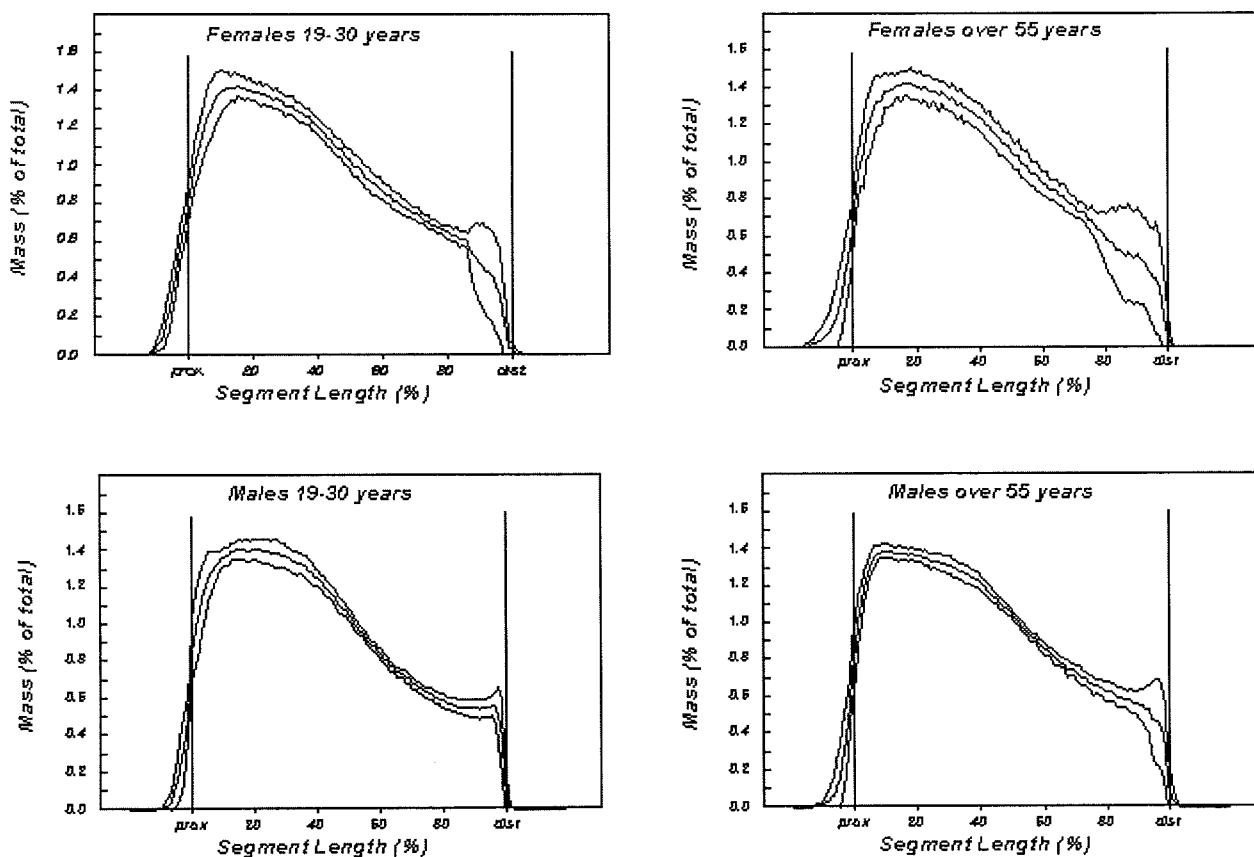
Figure 2: Ensemble averages (plus and minus one standard deviation) for the mass distributions of the four sub-populations. The area under each curve represents 100% of the total mass of each forearm.

HYDRAULIC RESISTANCE AND PERMEABILITY OF HUMAN LUMBAR VERTEBRA

Ruth S. Ochia [1] and Allan F. Tencer [2]

[1] Department of Bioengineering, University of Washington, Seattle, WA
[2] Department of Orthopaedics, Harborview Medical Center, Seattle, WA
Email: roachia@u.washington.edu

INTRODUCTION

Hydraulic resistance (HR) is a measure of resistance of viscous fluid flow through a porous matrix (Downey 1988) and is thought to be the mechanism through which marrow shares load with trabecular bone under dynamic compressive loads. HR has been calculated from pressure-flow studies, where fluid was forced through bone samples under varying conditions and the resultant steady state flow or pressure was measured (Ochoa 1992, Simkin 1985, Hong 1998). These studies determined that HR was constant and can be described according to Darcy's Law (Eqn. 1):

$$HR = \frac{\Delta P}{Q} = \frac{h}{A*k} \quad \textbf{Equation 1}$$

where ΔP is the change in pressure, Q is volumetric flow, h is specimen height, A is cross-sectional area of the specimen, and k is permeability of the porous material. Darcy's Law assumes use of a homogeneous fluid and a uniform pressure across the sample area. Due to these assumptions, previous studies have used bone plugs with the marrow removed and homogeneous fluids, such as saline, in their experiments.

The current research determines HR in whole human lumbar vertebrae and explores the use of Darcy's Law for intact bone.

PROCEDURES

Specimen Preparation: Eleven human cadaveric lumbar vertebrae (L3 and L4) were used (mean age 69.3 ± 13.0 years).

These specimens were determined to be free of pre-existing pathologies and fractures using visual and radiographic inspections. Bone mineral density (BMD) was determined for each specimen using dual x-ray absorptiometry (DXA) (Hologic Inc., Waltham, MA). The soft tissue, disk material and posterior elements were removed. Specimen cross-sectional area and volume were determined from superior-inferior and lateral radiographs, which were imported into a graphics program (NIH Image, Bethesda, MD) and measured against a known standard. Then the superior endplate was removed with a low speed diamond saw (Buehler, Lake Bluff, IL) exposing the trabecular bone matrix.

Mechanical Testing: The cephald end of each specimen was potted with a thin layer of polymethalmethacrylate (PMMA) to create a seal between the specimen and potting plate. The specimens were then heated to 39°C in a water bath for about 1-hour until testing began. The chosen heating temperature allowed for the specimen to cool during the testing without falling below 37°C.

The experimental assembly consisted of a piston with an attached pressure transducer (Eaton Lebow, Troy, MI) and the potted specimen (Fig. 1). This set up allowed for fluid to be introduced into the specimen without imposing other external loads. The piston was filled with olive oil heated to 39°C. Olive oil was used since it has a viscosity comparable to marrow at

physiological body temperature (Bryant 1989).

The assembly was then positioned in a materials testing machine (MTS Systems, Minneapolis, MN). The displacement rate used was 10mm/sec, which produced a constant flow rate. The total displacement of the piston ram was calculated to inject a fluid volume equivalent to 8.2% of the original specimen volume into the vertebra. The oil and marrow were allowed to egress through natural orifices in the cortical wall, as would be seen *in vivo*.

Analysis: A linear regression analysis was used to determine correlation for hydraulic resistance and permeability.
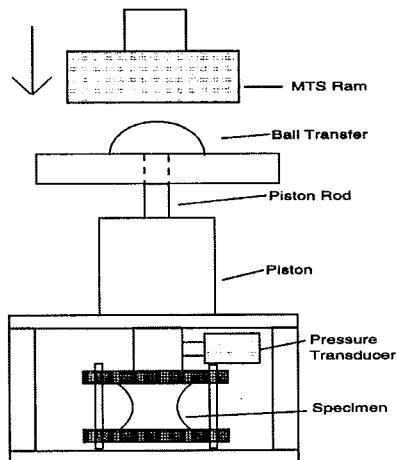
Figure 1: Schematic of resistance to flow apparatus

RESULTS AND DISSCUSSION

The mean BMD was 0.777 ± 0.105 g/cm^2 (mean $\pm$ standard deviation). The average flow was 11.74 ± 0.29 ml/sec and the peak pressure was 46.83 ± 40.32 kPa. HR was calculated to be 4.04 ± 3.64 kPa·sec/ml. Permeability (Eqn. 1) was strongly related to HR with a power relationship ($p < 0.05$) (Fig. 2).

In previous studies, HR was calculated from pressure-flow studies and was determined to be constant. Thus Darcy's Law has been used to predict pressure-flow relationships in trabecular bone samples under low flow-rate conditions. In this study, flow rate was kept constant but the measured peak pressure, and thus HR, varied substantially. Trabecular bone permeability greatly affected the resultant HR and did have an inverse relationship with HR (Fig. 2) as would be expected using Darcy's Law (Eqn. 1). Although the oil and marrow mixture was not homogeneous, nor was the pressure area uniform in this study, Darcy's Law still accurately described the HR–permeability relationship in whole vertebral bodies.

HR, as well as bone density, contributes to vertebral compressive strength and both should be considered in the prediction of vertebral compressive failure load.
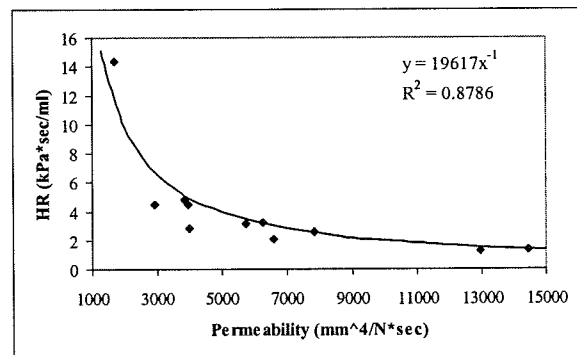
Figure 2: Permeability versus HR

REFERENCES

Bryant, J.D. et al. (1989). *Proc. Inst. Mech. Eng. H.* **203** (2), 71-75.

Hong, J.H. et al. (1998). *Transactions of the 44th Annual Meeting of the Orthopaedic Research Society,* 117.

Ochoa, J.A., Hillberry, B. (1992). *Transactions of the 38th Annual Meeting of the Orthopaedic Research Society,* 162.

Simkin, P.A. et al. (1985). *J. Biomechanics.* **18** (9), 657-663.

ACKNOWLEDGMENTS

CAN RADIOGRAMMETRY PREDICT THE MECHANICAL STRENGTH OF THE PROXIMAL FEMUR? AN IN VITRO COMPARISON WITH BONE MINERAL DENSITOMETRY.

Thomas A. Gruen[1], Carter A. Kenamond[2], Keith T. Hustosky[1,3]
and Timothy L. Norman,[1,3]

[1]Department of Orthopedics, [2]School of Medicine, [3]Department of Mechanical and Aerospace Engineering
West Virginia University, Morgantown, West Virginia
Email: tgruen@wvu.edu

INTRODUCTION

Numerous anthropometric studies from radiographs of normal femurs have been used for design analysis of implants to be used in patients with different musculo-skeletal disorders of the hip (Noble et al., 1988). Similarly, in-vitro biomechanical testing and finite element modelling of the proximal femur with or without implant often have involved the use of either a single normal femur (Couteau et al., 1998), or many femurs (e.g. 36 used by Keyak et al., 1998), or of a single synthetic composite (analog) femur (Cristofolini et al., 1996; McKellop et al., 1991). Few papers have demonstrated validation of the material properties used in composite bones, but almost none for structural properties (Cristofolini et al., 1996; McNamara et al., 1998). However, in few biomechanical research studies radiographs are taken of the proximal femur to screen out pathological specimens to minimize variability associated with the diversity of femurs with different intrinsic (material) and extrinsic (structural) properties among normal femurs and particularly among femurs with musculo-skeletal pathology. The purpose of this investigation is to assess the feasibility of radiographic characterization of extrinsic (structural) properties related to the mecha-nical strength of the proximal femur and to compare the results with intrinsic (e.g. bone mineral density (BMD)) properties as measured with dual-energy x-ray absorptio-metry (DEXA).

PROCEDURES

Comparative in-vitro analysis of femoral strength was performed in thirty-eight unilateral (right-sided) femurs (13 females, 25 males) with an average age being 61.7 ± 20.3 years at the time of death. The analysis included biplanar orthogonal radiogram-metry, bone mineral densitometry using DEXA, and mechanical testing (simulating a fall on the greater trochanter as per Courtney et al., 1995). Radiogrammetric indices of the proximal femur included external cortical dimensions (width of the femoral head, neck and shaft as a measure of bone size), femoral cortical index (Gruen, 1997), cortical cross-sectional area (as a measure of axial stiff-ness) and cross-sectional moments of inertia (as a measure of flexural stiffness). All cross-sectional geometric properties were derived from external and internal cortical dimensions made at the site for measure-ment of the cortical index. All bone mineral densitometry measurements, with a Lunar DPX-α system by an experienced observer at another hospital, were made with the three standard regions of interest as well as at a customized region at the level of measure-ments for radiogrammetry. The mechanical

test done on each femur was performed using the protocol of Courtney et al., 1995.

RESULTS AND DISCUSSION

Strong significant correlation was found between measured load at fracture of the femur and femoral BMD measurements ($0.94 > r > 0.78$; $p < 0.0001$). This corroborates the well-known relationship between the in-vitro strength and BMD of the proximal femur. Moderate to good relationships were noted for all radiogrammetric indices ($0.82 > r > 0.42$; $p < 0.01$) except for the external (size) dimensions of the femoral head, neck, and shaft ($r = 0.29$, 0.24, and 0.29 respectively). The correlation between fracture load and femoral cortical index as measured in the anterior-posterior and lateral films was highly significant (r-values of 0.73 and 0.75 respectively; $p < 0.0001$). As expected a moderately good inverse significant relationship was found between measured fractured load, BMD, and cortical index with age (Table 1)

Table 1. Relationship between mechanical strength, bone densitometry, and cortical index with age.

	r-value	p-value
Mechanical strength	-0.615	<0.001
Femoral neck BMD	-0.52	<0.01
Femoral shaft BMD	-0.48	<0.01
Cortical index(AP)	-0.44	<0.01

A strong relationship was also noted between cortical index and femoral BMD with $r = 0.811$ and 0.866 for the femoral neck and femoral shaft respectively ($p < 0.0001$).

SUMMARY

Overall, the results of this study suggest a strong biomechanical interdependency between the extrinsic (cortical geometry) and intrinsic properties (bone mineral density) for the proximal femur. It is apparent that the structural characteristics of the femoral cortical bone can contribute to the strength of the proximal femur. This includes the use of the cortical index, a dimensionless ratio, as a first-order approximation of structural strength, which unlike other radiogrammetric parameters is relatively insensitive to problems inherent with clinical radiography, i.e. magnification as well as rotational and obliquity variation due to specimen positioning.

This biomechanical study corroborates previous studies suggesting that cortical bone is important to its strength and resistance to loading (Courtney et al., 1995). It is acknowledged that radiogrammetry is not recommended for monitoring longitudinal studies of changes in either material or structural properties of a single patient, but it does appear to be practical for cross-sectional population-based studies. This would then allow better characterization of normal and abnormal femoral specimens with pathologies associated with different musculo-skeletal disorders.

REFERENCES

Courtney, A. et al. (1995). *Calc. Tiss. Int.*, **55**, 53-58.

Couteau, B. et al. (1998). *J. Biomech.*, **31**, 383-386.

Cristofolini, L., et al. (1996). *J. Biomech.*, **29**, 525-535.

Gruen, T. (1997). *Acta Orthop. Belg.*, **63**(Suppl. I), 20-27.

Keyak, J.H. (1998). *J. Biomech.*, **31**, 125-133.

McNamara, B.P. et al. (1997). *J. Biomech.*, **30**, 621-630.

McKellop, H.A. et al. (1991). *J. Orthop. Res.*, **9**, 297-305.

Noble et al. (1988). *Clin. Orthop.*, **235**, 148-165.

MICRODAMAGE ACCUMULATIONS AT STRESS FRACTURE SITES IN HUMAN METATARSALS

Seth W. Donahue[1], Neil A. Sharkey[2], and R. Bruce Martin[1]

[1]Orthopaedic Research Laboratory, University of California, Davis, Sacramento, CA
[2]Center for Locomotion Studies, Pennsylvania State University, University Park, PA

INTRODUCTION

Bone microdamage accumulation has been implicated in increasing skeletal fragility, and in the pathomechanics of osteoporotic and stress fractures (Burr et al., 1997). *In vitro,* bone fatigue life exponentially decreases with increasing strains, this behavior is also attributed to microdamage accumulation. However, the roles of bone microdamage and strain in the development of stress fractures is still unclear. It has been postulated that strain, damage, and remodeling interact in a positive feedback mechanism that can become unstable and result in a stress fracture (Martin, 1995).

In spinal trabecular bone, damage was not significantly related to age (Wenzel et al., 1996). Microcrack density in femoral neck trabecular bone was significantly ($p = 0.032$) higher in women over 70 years (Mori et al., 1997).

Both fatigue and insufficiency type stress fractures occur more frequently in second than fifth metatarsals. The goals of this work were to assess microdamage accumulations in regions where stress fractures are common (second metatarsal diaphysis) and rare (fifth metatarsal diaphysis), and investigate how damage accumulation is influenced by age and strain.

PROCEDURES

A dynamic gait simulator loaded nine cadaver feet with physiologic muscle and ground reaction forces over the entire stance phase of gait for conditions simulating normal walking (Sharkey and Hamel, 1998). Diaphyseal strains were measured on the second and fifth metatarsals using axial strain gauges. The contralateral second and fifth metatarsals were assessed histologically at the same location the strain gages were mounted on the experimental bones.

Metatarsals were stained *en bloc* in basic fuchsin to label microcracks and embedded in methacrylate. Three 120 micron thick cross-sections were taken from the strain gage location of each control metatarsal; cross-sectional areas were measured at 23x magnification using a light microscope video imaging system. Linear microcracks were counted and measured at 200x magnification. The crack density (Cr.Dn: $\#/mm^2$) and crack length density (Cr.Le.Dn: $\mu m/mm^2$) were averaged for the three cross-sections. ANOVA's were used to assess differences in Cr.Dn and Cr.Le.Dn between second and fifth metatarsals. Regressions were used to explore relationships between the damage parameters, age, and peak metatarsal strain.

RESULTS AND DISCUSSION

Cr.Dn and Cr.Le.Dn were higher in the fifth metatarsal than in the second, but the differences were not significant ($p > 0.1$), (Figure 1). Both Cr.Dn and Cr.Le.Dn significantly ($p < 0.023$) increased with age in the second metatarsal, but not in the fifth ($p > 0.2$), (Figure 2). Neither Cr.Dn nor

Cr.Le.Dn were significantly (p > 0.3) related to peak strain in either metatarsal.
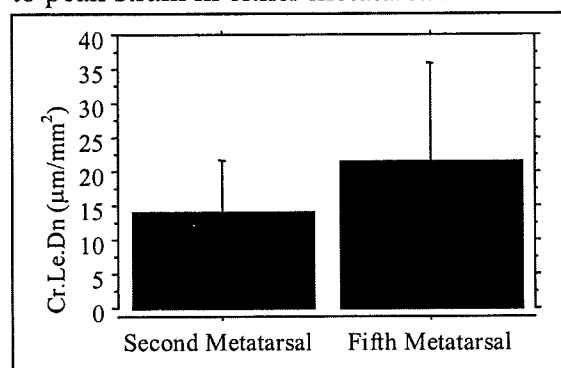
Figure 1: Second vs. fifth metatarsal crack length density.
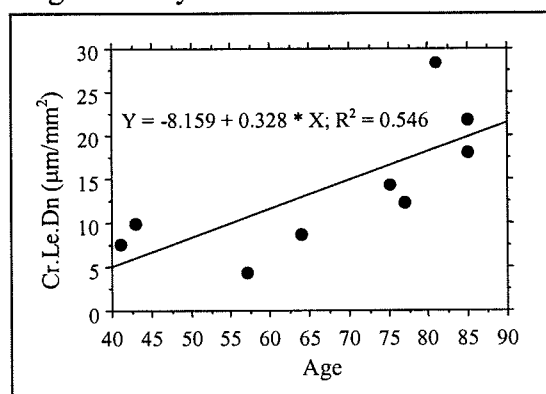
Figure 2: Second metatarsal crack length density regressed against age (p = 0.023).

Cr.Dn and Cr.Le.Dn were expected to be higher in second than in fifth metatarsals since stress fractures are more common in the second. A homeostatic level of damage may have been maintained in these bones by the removal of microcracks by bone remodeling, explaining why there were no significant differences in the damage parameters between metatarsals.

Over a wide range of ages, 41 to 85 years, strain alone was not a good predictor of *in vivo* metatarsal microdamage accumulation. Although higher bone strains are likely to result in higher microdamage accumulations, it is also likely that remodeling is activated at higher rates to repair the damaged bone (Burr and Mori, 1993). An increased number of resorption spaces will reduce the stiffness of a bone causing strains to be higher under habitual loading conditions. If this feedback mechanism becomes unstable (i.e. damage exceeds repair) a stress fracture may occur.

SUMMARY

Cr.Dn and Cr.Le.Dn were unable to explain the greater incidence of second metatarsal stress fractures, supporting the theory that resorption spaces caused by remodeling play a critical role in stress fracture etiology. Second metatarsal Cr.Dn and Cr.Le.Dn significantly increased with age which may explain why insufficiency stress fractures are more common in the second metatarsal. Contrary to laboratory studies, bone strain may not be a good predictor of *in vivo* fatigue damage accumulation or fatigue life because of the repair capabilities of bone remodeling.

REFERENCES

Burr, D. B. et al. (1997). *J. Bone Miner. Res.*, **12(1)**, 6-15.

Burr, D. B. and Mori, S. (1993). *Bone*, **14**, 103-109.

Martin, B. (1995). *J. Orthop. Res.*, **13(3)**, 309-316.

Mori, S. et al. (1997). *Bone.*, **21(6)**, 521-526.

Sharkey, N. A. and Hamel, A. J. (1998). *Clin. Biomech.*, **13**, 420-433.

Wenzel, T. E. et al. (1996). *Bone,* **19(2)**, 89-95.

ACKNOWLEDGEMENTS

DIFFERENCES IN INTERCONDYLAR NOTCH GEOMETRY BETWEEN MALES AND FEMALES

Mark D. Tillman[1], Kendra R. Smith[2], Judith L. Pattishall[1],
Jeffrey A. Bauer[1], Anthony B. Falsetti[2]

[1]Biomechanics Lab, University of Florida, Gainesville, Florida
[2]C.A. Pound Human ID Lab, University of Florida, Gainesville, Florida
Email: tillman@ufl.edu   Web: www.hhp.ufl.edu/ess/biomech

INTRODUCTION

The geometry of the intercondylar notch has been implicated as a possible risk factor related to ACL injury. ACL injuries are a common source of disability in the United States and often lead to instability, further ligamentous injury, meniscal injury, and arthritis. Females are substantially more susceptible than males to suffer acute noncontact injury of the ACL. Although the cause of disparity in injury rate is not fully understood, numerous extrinsic and intrinsic factors are believed to be associated with ACL injury. Intercondylar notch geometry is one of the intrinsic factors suspected of predisposing individuals to ACL injury. Some data indicate that females have a more narrow intercondylar notch than males, while other data show that no difference exists between females and males. Orthopedic surgeons have also observed that the shape of the intercondylar notch varies between females and males. However, their subjective commentary has not been confirmed. The purpose of this study was to compare intercondylar notch geometry between males and females.

PROCEDURES

One hundred male skeletons (age at death 33.0±10.3) and one hundred female skeletons (age at death 36.7±11.8) from the Terry Collection (a 20th century autopsy store) housed at the National Museum of Natural History, Smithsonian Institution in Washington, D.C., were evaluated relative to intercondylar notch geometry. The individuals were free from any orthopedic disorder as listed in medical records or observed upon inspection.

Digital photographs were taken of the distal end of the left femur of each individual. Three indices related to intercondylar notch geometry were calculated using MATLAB: notch width index (NWI), notch area index (NAI), and notch shape index (NSI). NWI was calculated by dividing the width of the intercondylar notch by the width of the femoral condyles. NAI was computed by creating a ratio of the area encompassed by the intercondylar notch to the area of the femoral condyles. NSI was determined by dividing the width of the intercondylar notch by the height of the notch.

Descriptive statistics (means and standard deviations) were calculated for each of the three dependent variables. Independent t-tests were used to detect any differences between males and females across the dependent variables. The Bonferroni adjustment for multiple comparisons was used to decrease the likelihood of making a Type I error.

RESULTS AND DISCUSSION

Previous data are somewhat inconclusive concerning differences in notch width

between injured and healthy individuals, as well as, males and females. In this study, no differences were detected between males and females for NWI and NAI. NSI for males exceeded NSI for females (p=0.003). See Table 1.

Narrow notches have been subjectively identified as being shaped like a cresting wave and wider notches appear as an inverted U. No attempts have been made to objectively quantify the shape of the intercondylar notch. Our data indicate that no differences exist between males and females concerning notch width or the two dimensional area that the cruciate ligaments pass through. However, males and females do differ when compared with a general measure of intercondylar notch shape. The results demonstrate that males may have a proportionately wider intercondylar notch when normalized by the anterior/posterior height of the notch.

SUMMARY

This study is a unique evaluation of cadaveric skeletal geometry. Previous research has yielded inconclusive results regarding intercondylar notch width and little or no information regarding the area and shape of the notch. The shape of the intercondylar notch may play an important role in causing ACL injuries and apparently varies between males and females.

The present work is a part of a larger project designed to evaluate skeletal alignment and its affect on knee mechanics. The larger NSI present in males may partially explain the discrepancy in ACL injury rates between males and females. Further quantification of the shape of the notch is recommended.

REFERENCES

Anderson, A.F., Lipscomp, A.B., Liudahl, K.J., Addlestone, R.B. (1987). *Am J Sports Med,* 15(6), 547-52.

Arendt, E.A., Dick, R. (1995). *Am. J. Sports Med,* 23, 694-704.

Markolf, K.L., Burchfield, D.M., Shapiro, M.M., Shepard, M.F., Finerman, G.A.M., Slauterbeck, J.L. (1995). *J Ortho Res,* 13, 930-935.

Table 1: Intercondylar notch geometry indices (mean ± SD).

Index	Male	Female
NWI	0.255±0.03	0.249±0.03
NAI	0.173±0.02	0.170±0.02
NSI*	0.638±0.09	0.599±0.09

MECHANICAL CHARACTERIZATION OF A BONE FRACTURE SURROGATE

Christina L. Beardsley[1], Anneliese D. Heiner[2], J. Lawrence Marsh[2], Thomas D. Brown[1,2]

[1] Department of Biomedical Engineering, University of Iowa, Iowa City, IA
[2] Department of Orthopaedic Surgery, University of Iowa, Iowa City, IA
Email: tom-brown@uiowa.edu

INTRODUCTION

Recently, for purposes of quantifying mechanical aspects of comminution in the fracture of bone, we reported use of a surrogate material that responds to impact in a manner analogous to bone, and that has been radiopacified to mimic the CT appearance of cortical bone (Beardsley et al, 1998). The material underwent sequentially greater comminution (as judged by the size and shape of fragments) as energy input was increased. However, no data were available on the foam's pertinent mechanical properties. In further developing this new research tool, it is worthwhile to compare the foam's modulus of elasticity, bending strength, toughness, and dynamics energy absorption with those of bone.

PROCEDURES

Eight specimens each were milled to a uniform size (45.72 x 13.72 x 5.97 mm) from barium sulfate-doped, high-density polyetherurethane foam, and from adult bovine tibial bone from a single donor. Additionally, foam specimens (n=6) 139.3 x 12.7 x 7.14 mm in size were prepared for bend testing, along with bovine cortical specimens (n=5) dimensioned to 101.6 x 12.7 x 4.76 mm. Before machining, the bones had been fresh frozen to –20° C. They were thawed at room temperature prior to testing. Bones were kept wet at all points in the preparation and testing.

Impact tests were performed at room temperature on foam and bone specimens using a Hounsfield Balanced Impact Machine (Tensometer Ltd., Croydon, England). Impact velocity was approximately 7.2 m/s. The Hounsfield Impact Machine imposes a three-point impact similar to that created by a Charpy apparatus. Due to geometric constraints of both the bovine tibiae and the specimen holder in the pendulum, specimens were tested such that impact was in the transverse direction of the bone. All impact specimens were unnotched. A tare value for free swing energy loss was subtracted.

Modulus of elasticity and bending strength were characterized via a four-point bending test. Testing and data collection were performed utilizing an MTS Bionix 858 test machine (MTS Corp., Eden Prairie, MN) with standard four-point bend fixtures (span separation of 1.5" for the foam and 1.0" for the bone). This corresponded to a span-to-depth ratio of 16:1, as per recommendations in ASTM D790. Crosshead speed was adjusted to impose a strain rate of 0.00017 sec^{-1}. Modulus (E) was computed from flexural rigidity formula:
$$E = (1 / I)*(5 / 12)*(P/y)*c^3$$
where P/y is slope of the load-deflection curve in the linear region, I is area moment of inertia, and c is the span distance. For all specimens the region of the curve taken to compute P/y was linear with $R^2 > 0.999$.

RESULTS AND DISCUSSION

In the impact test, the mean energy absorption was greater in the bone than in the foam surrogate (Table I). When data were compared with a homoscedastic, unpaired t-test, this difference was marginally significant (p = 0.065). There was considerable variation in values obtained for bone. One contributing factor here may be that specimen location was not controlled for; bone will have a somewhat different impact strength depending on whether it is from anterior, posterior, medial or lateral part of tibia (Evans, 1973).

Elastic modulus and ultimate strength measured for bovine bone (Table I) were comparable to previously reported values

(Behiri et al, 1984). The foam surrogate material is an order of magnitude lower in bending modulus and ultimate strength. Toughness was taken to be the area under the stress-strain curve (Fig. 1). The foam's quasi-static toughness is halfway between cortical and cancellous bone fracture toughness (Norman et al, 1995). In the four-point bend test, foam exhibited only one-fifth the toughness of bovine cortical bone. This may initially seem contrary to the impact test results, as one would expect correlation between impact energy absorption and quasi-static toughness. However, both the bone and the foam are viscoelastic, and thus there exists a transition in fracture characteristics associated with a change in strain rate. These rates may be different for the bone and foam, and results imply that the foam has a higher degree of viscoelasticity than bone.

Currently, we are using FR7140 foam as a calibration material in the developing CT-based image analysis routines to index injury severity in tibial pilon fractures. Energy absorption in human cortical bone *in vivo* is probably higher than what was quantified in this experiment. Aside from interspecies differences in bone properties, results are orientation-dependent. As reported by Reilly et al (1975), the ultimate stress in the longitudinal direction is one and a half times greater than that in the transverse. Furthermore, specimens have four times higher longitudinal ultimate strain compared to thetransverse direction, as well as greater plasticity, leading to average energy absorption by the bone tissue in the longitudinal direction that is an order of magnitude greater than in the transverse.

SUMMARY

Mechanical properties of polyetherurethane foam and bovine compact bone were compared. Although for our current (CT) purpose it is not necessary to match bone mechanical properties, the present data provide a good point of reference for expanding the use of this foam to other applications where energy absorption matching is desirable.

REFERENCES

Beardsley et al (1998), *NACOB*, 483-4.
Behiri et al (1984) *J Biomech*, 17, 25-34.
Evans (1973) *Mechanical Properties of Bone*, Charles C. Thomas Publisher.
Norman et al (1995), *J Biomech*, 28, 309-20.
Reilly et al (1975), *J Biomech*, 8, 393-405.

ACKNOWLEDGEMENT
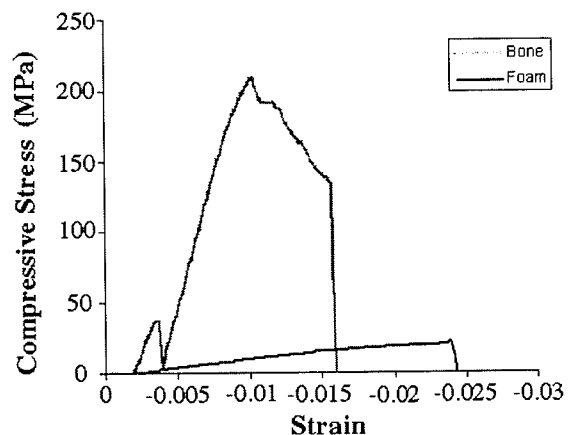
Figure 1. Typical stress-strain curves.

Table I. Elastic modulus, ultimate strength, toughness, and dynamic energy absorption

	Energy Absorbed (J/mm^2)	Modulus of Elasticity (GPa)	Quasi-static Toughness (MPa)	Ultimate Strength (MPa)
Foam	0.071 ± 0.009	0.795 ± 0.030	4.00 ± 0.24	27.34 ± 1.74
Bone	0.106 ± 0.048	13.69 ± 4.25	21.17 ± 3.48	222.00 ± 39.53

BONE FATIGUE LIFE IS ALTERED IN A CALCIUM-FREE SALINE BATH

R.B. Martin[1], V.A. Gibson[1], M.B. Gustafson[1], S.M. Stover[2], J.C. Gibeling[3]
[1]Orthopaedic Research Laboratories, School of Medicine
[2]J.D. Wheat Orthopaedic Research Laboratory, School of Veterinary Medicine
[3]Department of Chemical Engineering and Materials Science, College of Engineering
University of California, Davis, CA 95616, e-mail: rbmartin@ucdavis.edu

INTRODUCTION

The mechanical properties of bone are very sensitive to its mineral content. Currey (1988) showed that the elastic modulus of cortical bone increases as the fourth power of calcium content. Also, bone placed in a solution not properly equilibrated with respect to its mineral loses mineral and stiffness. Gustafson et al. (1996) found that soaking 4x10x100 mm beams of cortical bone in normal saline at room temperature for 6 days significantly decreased their elastic modulus by 2.4%. Buffering the saline with 57 mg/L of $CaCl_2$ prevented any modulus change. We have therefore used Ca-buffered saline baths for high cycle (long duration) fatigue testing to avoid leaching of bone mineral that could compromise test results; i.e., modulus diminishment could be due to either damage or lost mineral. However, in this paper we show that Ca-buffering of the test bath can alter the fatigue life of specimens tested to failure in less than one hour.

METHODS

We compared data from two previous fatigue studies, identical in every respect except the composition of the immersion bath (Gibson et al., 1996, 1997). Beams (4x10x100 mm) were machined from the lateral, medial, or dorsal regions of 18 third metacarpal (3MC) bones from 18 thoroughbred racehorses. The specimens were stored frozen at -4°C, and care was taken to keep them wet and cool during machining. Each beam was loaded to failure in unreversed 4 point bending using an MTS servohydraulic materials testing machine. Inner and outer supports were 32 and 64 mm apart, respectively. Beginning with an initial strain of 1.0%, specimens were tested in load control using a 2 hz sinusoidal waveform. Two groups of specimens were compared. A $CaCl_2$ Group (12 beams from 12 horses) was tested in saline buffered with 57 mg/L of $CaCl_2$. A Saline Group (18 beams from 6 horses) was tested in normal saline. In both cases the 37°C immersion bath was stirred. Fatigue life was recorded as the number of cycles to specimen fracture (N). Because fatigue life is not normally distributed, we applied a log-transformation to this variable, and used a t-test to compare the two groups. We also used Weibull analysis to compare the failure probability distributions of the two experimental groups.

Table 1: Logarithm of fatigue life

Test solution:	N	Mean	St. Dev.
Saline	18	6.440	1.063
$CaCl_2$ buffered	12	5.398	0.652
Independent t-test	t = 2.93,		p < 0.010

RESULTS

The mean fatigue life in the Saline Group was 626 cycles (range 85-6407) compared to 221 cycles (range 99-973) for the $CaCl_2$ Group. Table 1 shows that the log-

Fig. 1

Fig. 2
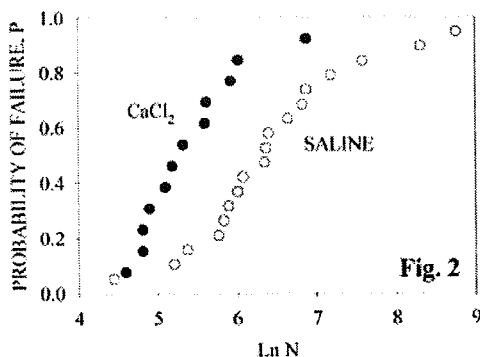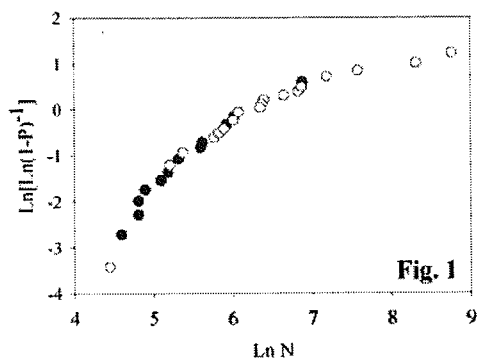
normalized mean fatigue life is significantly greater in the Saline Group. Fig. 1 shows a ln-ln plot of the 2-parameter Weibull equation

$$\ln(1-P)^{-1} = (N/N_0)^m \qquad (1)$$

for all 30 specimens treated as a single group. Here, P is the probability of failure after N cycles; N_0 and m are parameters. Clearly, specimens tested in $CaCl_2$-buffered saline (filled circles) were more likely to fail early than those tested in unbuffered saline (open circles). Fig. 2 shows this in separate probability plots for the two groups: the $CaCl_2$ Group is well-separated from the Saline Group. For any particular probability of failure P, the expected fatigue life N is less if the bath is Ca-buffered.

DISCUSSION
Gustafson's (1996) calcium leaching study was prompted by concern that mineral would dissolve from bone during prolonged fatigue tests. By contrast, the longest fatigue test shown here lasted less than an hour. In the Gustafson experiment the specimens

were soaked in a stress-free state. The present data are consistent with a hypothesis that when specimens are soaked in unbuffered saline while being fatigue-loaded, calcium leaves the bone within minutes, lengthening the fatigue life. Such a phenomenon would be consistent with two other observations. First, equine bone fatigue life is inversely related to stiffness (Gibson et al., 1996). Thus, loss of stiffness due to dissolution of mineral could be consistent with increased fatigue life. Second, mineral solubility is a function of Gibbs free energy, which includes strain energy. Thus, one would expect mineral to be more soluble in a stressed bone than a stress-free bone.

These must be considered preliminary results because the specimens were not paired. However, they were all from thoroughbred racehorse 3MC bones prepared and tested in the same way except for the immersion bath. The bones' 3 cortical regions were equally represented in each experimental group, and the initial elastic modulus of each group was similar ($CaCl_2$: 18.1 ± 2.33 GPa; Saline: 19.1 ± 2.15 GPa). Both groups of horses were between 2-5 years old.

We are presently repeating this work with paired specimens to confirm these results.

REFERENCES
Currey, JD (1988) J. of Biomechs 21:131-139.
Gibson, VA, Stover, SM, Martin, RB, et al. (1996) J. of Orthop. Res. 13:861-868.
Gibson, VA, Martin, RB, Stover, SM, et al. (1997) Trans. of the ORS. 22:41.
Gustafson, MB, Gibson, VA, Stover, SM (1996) J. of Biomechs. 29:1191-1194.

A BIPLANE "V" OSTEOTOMY OF THE TROCHANTER IMPROVES STABILITY

Carl Churchill, Simon Roe [2], Dan Albright [3] and Larry Stikeleather

Department of Biological and Agricultural Engineering and
[2] Department of Companion Animal and Special Species Medicine,
North Carolina State University, Raleigh, NC
[3] Raleigh Orthopaedic Clinic, Raleigh, NC
Email: Simon_Roe@ncsu.edu

INTRODUCTION

Delayed or nonunion of the greater trochanter can complicate the recovery of a patient from total hip arthroplasty. Although many factors may influence union, stability of the trochanter fragment is essential. The wiring technique is an important factor. Many have been suggested and some have been evaluated mechanically (Markolf et al 1979, Dall, et al, 1983) Clinical studies of osteotomy techniques suggest advantages of the "chevron", biplane "V" and dihedral configurations over a single planar cut (Berry & Muller, 1993, Weber, 1989). Elghor (1992) failed to demonstrate differences between flat and biplane osteotomies stabilized with either the Charnley wire configuration, a spring-wire system of Dall-Miles cable grip.

We hypothesized that the biplane "V" osteotomy would result in a more stable structure when loads were applied that simulated muscle force applied to the trochanter at the beginning of rising from a chair.

MATERIALS AND METHODS

Urethane models of a proximal femur prepared for total hip arthroplasty were used to ensure consistency between specimens. A single plane trochanteric osteotomy, 45° to the long axis of the femur, was made in 8 models. A biplane "V" osteotomy was made in another 8 models. A cutting jig was used to ensure consistency of osteotomy location. A second jig was used to drill holes for wire passage and for attachment of the loading cable to the trochanter fragment. The trochanter was stabilized using the Charnley wiring technique (2 vertical and 2 looped horizontal wires) using 18 gauge orthopaedic wire. The repaired model was mounted in a stabilizing frame so that the load was applied at 90° to the osteotomy (simulating gluteal loading while rising from a chair). Load was applied by pulling on the cable attached to the trochanter using a materials testing machine (Instron 1122, Canton, MA), at a loading rate of 200 mm/min, until failure of the wire was observed or the fragment had displaced greater than 10 mm. Displacement of the trochanter was measured with an extensometer attached to the femoral shaft and resting on the caudolateral aspect of the trochanter. The osteotomies were compared based on load and stiffness at 1 and 5 mm of displacement using a Student t-test ($p < 0.05$).

RESULTS

The biplane "V" osteotomy was significantly stronger and stiffer at both displacements than the planar osteotomy (Figures 1 & 2).
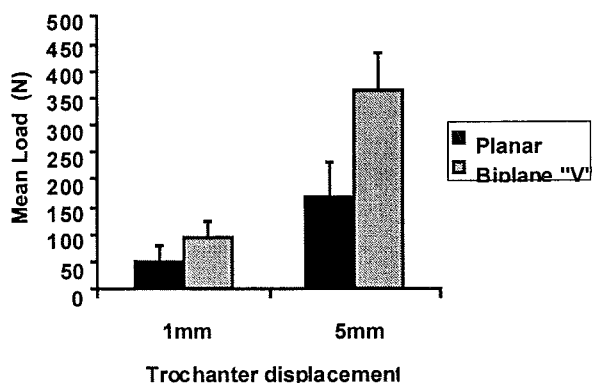
Figure 1. Mean load required to displace the trochanter 1 and 5 mm for planar or biplane "V" osteotomy
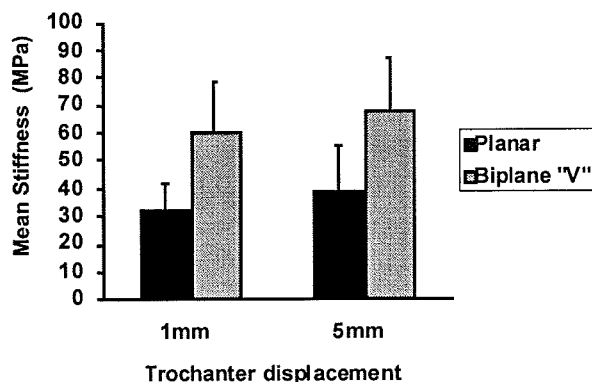
Figure 2. Mean stiffness of the repaired planar and biplane "V" osteotomies at 1 and 5 mm of displacement

DISCUSSION

When the direction of gluteal pull is forward of the line of the femur, the trochanter fragment tends to rotate. For the planar osteotomy, the wire configuration was not effective in limiting trochanter movement. For the biplane "V" osteotomy, the interlock of the trochanter in the osteotomy bed effectively countered rotation. The fragment could only move from the bed by rising upwards, and the wire configuration was effective in limiting displacement in that direction.

Of concern is the observation that, even given the ideal model, for both osteotomy configurations, the load that caused 1 mm of displacement is much lower than the predicted loads for this muscle group during many normal activities.

This study shows that a biplanar "V" osteotomy is more stable when gluteal loading from multiple directions is considered. Stabilization techniques that result in a stiffer repair are likely to improve clinical results.

REFERENCES

Berry, D.J., Muller, M.E.. Clin. Orthop., 294, 155-161.

Dall, D.M., et al (1983) J. Bone Jt. Surg., 65, 55-59.

Elghor S. (1992) M. Ch. Orthian. J. 2, 41-43

Markolf, K.L., et al (1979). Clin. Ortho. Rel. Res., 141, 111-121

Weber, B.G. (1989) Orthopade 18, 540-544

RELATIONSHIP BETWEEN IMPACT ANGLE AND DEFORMATION OF PROXIMAL FEMUR IN FALLING

Byung Soo Kim[1], Kyung Tae Kim[1], Kuiwon Choi[1], Jae Bong Choi[2], Seung Baik Kang[3], Kang Sup Yoon[3], Hee Joong Kim[3]

[1]Biomedical Research Center, Korea Institute of Science and Technology, Seoul, Korea
[2]Dept. of Mechanical Systems Engineering, Hansung University, Seoul, Korea
[3]Dept. of Orthopedic Surgery, Seoul Municipal Boramae Hospital, Seoul, Korea
E-mail: [1]choi@kistmail.kist.re.kr   Web: kist.re.kr

INTRODUCTION

Bone mineral density(BMD) has proven to be an effective predictor of fracture risk. By predicting a fracture risk from an individual's BMD, one can estimate the denominator of the risk factor. Loading angle and strain rate, which are independent of density, might also affect the structural capacity of the femur[Courtney et al., 1994; Pinilla et al., 1996]. Nonetheless, in previous studies, there have not been attempts to match these two factors in falling condition.

Therefore, the purposes of this study were (1) to develop the impact testing system to simulate the falling condition; (2) to investigate the change of deformation pattern of proximal femur considering the influence of impact angle; and (3) to conduct the traditional static test for two-legged stance to compare with the deformation pattern caused by the impact

MATERIALS and METHODS

Prior to impact test using a fresh-frozen human femur(male, 31) prepared by the procedure of Carter et al.[Carter et al., 1980], we developed surrogate-pelvis and pendulum impact tester to simulate the falling condition and then conducted the experiments changing the impact angle of proximal femur[Robinovitch et al., 1991]. Also, in order to analyze the relative risk due to falling to normal situation in proximal femur, we did the static test simulating the two-legged stance condition.(Table 1) (Figure 1)

RESULTS

The maximum impact force and velocity were 1,050±35N, and 0.91±0.04 , respectively. The axial and transverse strain patterns at each impact angle were presented in Figure 2 and 3

Table 1: Strain gage number and location

Strain gage location		
Subcapital region	Femoral neck	Femoral shaft
1. Inferior	4. Inferior	7. Posterior
2. Superior-Posterior	5. Superior-Posterior	8. Anterior
3. Superior-Anterior	6. Superior-Anterior	
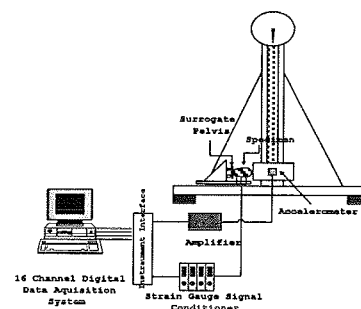
Figure 1: Schematic diagram of impact test
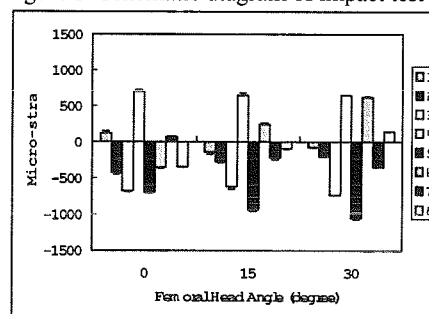
Figure 2: Axial strain patterns of each location at different impact angle

During the present experiment, the neutral axis was calculated by the simple matrix operation[Biewener, 1992]. The angle of the neutral axis to horizontal line in femoral head were 66.04°, 53.04°, 57.43°, and 29.05°for 0°,

15°, 30°impact angle, and two-legged stance, respectively(Figure 4). In femoral neck, they were -70.88°, -47.43°, -36.46°, and -80.36°, respectively(Figure 5).
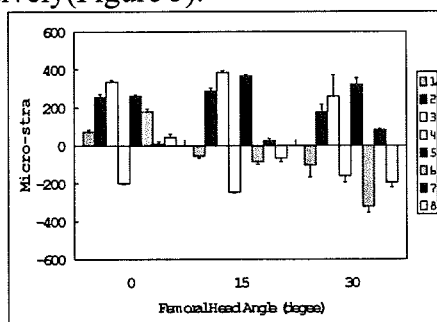
Figure 3: Transverse strain patterns of each location at different impact angle
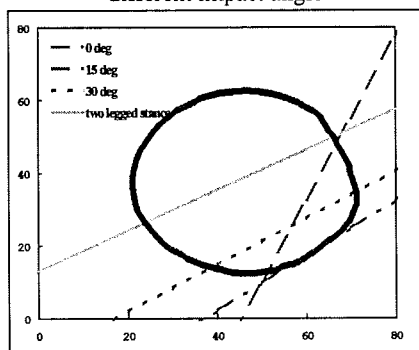
Figure 4: Changes of neutral axis in femoral head
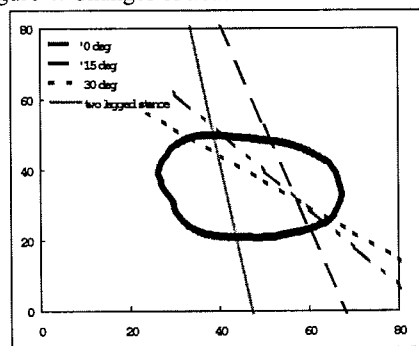
Figure 5: Changes of neutral axis in femoral neck

DISCUSSION

The object of our study is to investigate the relationship between impact angle and deformation pattern in falling. The test was conducted on the same specimen below the yield stress to prevent its permanent deformation at each impact. In spite of these limitations, we have some favorable aspects.

One of the strengths in our study is that the present impact test is to investigate the effect of impact direction on the deformation of proximal femur during fall. Unlike previous

mechanical test protocols,[Courtney et al., 1994; Pinilla et al., 1996] we developed the impact test system composed of impact pendulum and surrogate pelvis. It is an essential aspect at impact study that the impact system properly simulates the dynamic response of the hip during a falling of body. So, we adjusted our test system to simulate effective mass, stiffness, and damping of a typical male pelvis during a fall of the hip. Another strength is that based on these data, more accurate finite element model will be constructed to predict the failure of femur. Earlier computational models have not fully predicted hip fracture due to the lack of experimental data. So our findings will be helpful comparing with the previous models. Finally, the deformation patterns computed in our study are clinically useful. The computed strains are considered more useful for the comparison of injury occurrences with biomechanical responses. Furthermore, fundamental mechanics for loading and bending induced by a primary impact will be useful in regards to the various modes of femoral fracture.

SUMMARY

We have developed the impact test system and observed that a slight variation in impact angle affects deformation pattern of the proximal femur significantly. Along with bone mineral density, geometry, and trabaecular morphology, impact angle and strain rate are thus another important factors affecting the structural capacity of the proximal femur. However, unlike the intrinsic, bone-related properties, impact angle depends on the falling direction, which needs additional researches of falling itself in the etiology of hip fracture.

REFERENCES

Biewener, A.A. (1992). Biomechanics - Structures and Systems., IRL PRESS
Carter, D.R. (1980). Acta. Orthop. Scand., 51, 733-741
Courtney, A.C. et al. (1994). Calcif .Tissue Int., 55, 53-58
Pinilla, T. P. et al. (1996). Calicif. Tissue Int., 58, 231-235.
Robinovitch, S.N. et al. (1991). J. Biomech. Eng. , 113, 366-374

STRESS-BASED DESIGN OF A FEMORAL HIP PROSTHESIS

Michael H. Santare, Makarand G. Joshi, Suresh G. Advani, Shawn P. Riley, Freeman Miller

Department of Mechanical Engineering, University of Delaware, Newark, DE

Email: santare@me.udel.edu

INTRODUCTION
In the normal hip, stress is distributed over the entire crossection of the femur. Bending and axial compression are the major modes of loading. Following THA, the stress in the bone is significantly different mainly due to the manner in which the load is transferred to the femur (Huiskes, 1990, Huiskes, 1995). In this case, the load is primarily transferred through shear across the bone-cement-prostheses interfaces.

In addition, the bending displacement in the bone surrounding the stem are reduced because of the relatively high flexural stiffness of the prosthesis. This reduced bending unloads the outer fibers of femur leading to a state of stress shielding. The medial calcar, which experiences a significant reduction in stresses (stress shielding) has been commonly seen to atrophy in *in-vivo* radiological studies.

An apparent solution to this problem would be a prosthesis which loads the proximal end of the femur in a manner similar to the natural state. Recently, a stemless prosthesis design using proximal fixation was developed by Munting and Verhelpen, (1995) and has shown promising initial results. This design is fixed to the lateral side of the proximal femur by means of a bolt. Their in-vitro experiments showed minimal micromotion and the short-term clinical studies have shown low initial failure rates.

The motivating hypothesis for the current study, is that it is possible to develop a new femoral prosthesis component designed specifically to reduce the levels of stress shielding and interfacial shear stress in the femur following total hip arthroplasty.

PROCEDURES
The first stage of the current design was the development of a general geometry that restores, as much as possible, the natural load-transfer mechanism through the proximal femur. A detailed finite element model of the femur was used to calculate the stresses in the bone. The change in stress, caused by the introduction of the prosthesis, was used as a standard for comparison. The initial study indicated a significant benefit from the use of a short stem verses a long stem in terms of the interfacial shear stresses in the bone.

As a further modification, a proximal plate was added to distribute the contact load over the entire crossection of the femur and reduce stress shielding in the cortical bone. The combination of a shortened stem and a proximal plate resulted in a major reduction in both stress shielding and interfacial shear stress. Reducing stem length however, made it necessary to devise an alternate method of fixation. One example of proximal fixation is the design by Munting and Verhelpen, (1995) described in the previous section. However, to avoid the use of a stiff metal bolt through the relatively brittle lateral cortex, a cabling system was developed. The cables not only anchor the prosthesis to the bone, but they also help produce a more natural bending-load transfer over the crossection of the femur by fixing the trochanter to the implant. In the following sections, we present results of the stress analysis and discuss the preliminary *in-vitro* study of the new design.

RESULTS AND DISCUSSION
To estimate the effect of the prosthesis on the stress distribution in the bone, the stress difference for each element was calculated. Positive stress difference values indicate an increase in overall stress level due to the introduction of the prosthesis and negative values indicate a decrease. The proximal femur below the neck and above the shaft was divided into five medial (regions 3-7) and five

lateral (regions 8-12) regions numbered starting distally. Region 1 represents the proximal diaphysis and region 2 the greater trochanter. In all the regions, except region 2 (greater trochanter), the conventional prosthesis produces significant stress shielding. In region 2, the conventional prosthesis causes a 100% overstress due to the loss of bone mass in this region during surgery. Both the current design and the Munting and Verhelpen, (1995) design show far less stress shielding everywhere except region 12. In addition, both proximally fixed designs cause no noticeable change in the stresses in the diaphysis. Figure 1 compares the stress differences for the Munting et. al. and current designs. As shown, the current design produces lower magnitude stress differences in all regions.

As a preliminary test of the new design, human cadaver femora were tested in static loading before and after implantation of a prototype new prosthesis. The bone was dried, cleaned and potted in a metal cup. Strain gages were attached to the proximal femur, three around the stem on the medial calcar and one on the lateral surface below the anchoring cable. The gages were placed in locations where a conventional intramedullary prosthesis often causes significant stress shielding (see for example the summary in Huiskes and Verdonschot, 1997), but the numerical analyses predicted that the new design would not.

Load was applied to the femoral head in the axial direction through a displacement controlled Instron loading frame. These results showed that the current prosthesis produces little or no stress shielding in at least several critical areas of the proximal femur. Qualitatively therefore, the experimental results were consistent with the analytical predictions.

SUMMARY

This study presents a new design aimed at reducing stress shielding. In the numerical studies, the proposed design consistently performs better than the traditional

intramedullary design and the Munting and Verhelpen, (1995) design in the context of femoral stress differences.

The preliminary *in-vitro* study showed that the new fixation method is viable from a surgical and initial post-surgery perspective. Results show that in several critical areas of the proximal femur, the new design produces little or no stress shielding. This is consistent with the numerical models and lends evidence that the analyses can be used to give an estimate of the overall behavior for the loadings considered.

REFERENCES

Huiskes R. (1990). Clinical Orthopedics, **261**, pp. 27-38.

Huiskes R. (1995). in Total Hip Revision Surgery, Raven Press, New York, pp. 159-171.

Huiskes R, and Verdenschot N. (1997). in Basic Orthopaedic Biomechanics, 2nd. ed., Lippincott-Raven, Philadelphia.

Munting E., Verhelpen M. (1995). Journal of Biomechanics, **28**, pp. 949-961.

ACKNOWLEDGMENTS
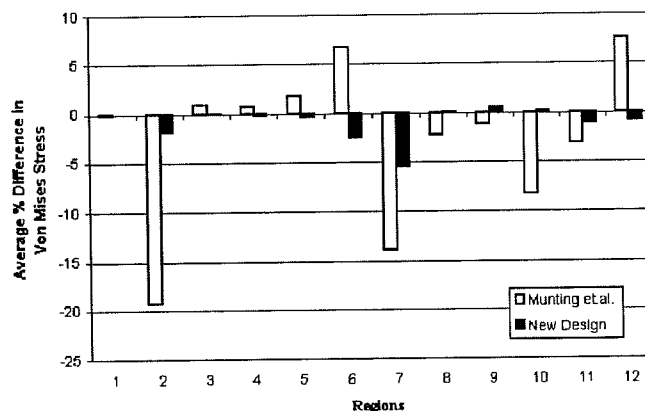
Figure 1: Stress comparison for Munting et. al. and the current design

CONSISTENCY OF RADIOGRAPHIC MEASUREMENTS OF CUP ORIENTATION

Branislav Jaramaz[1,2], Constantinos Nikou[1], Timothy J. Levison[2], Anthony M. DiGioia III[1,2]

[1]Center for Orthopaedic Research, UPMC Shadyside, Pittsburgh, Pennsylvania
[2]Robotics Institute, Carnegie Mellon University, Pittsburgh, Pennsylvania
Email: branko@cor.ssh.edu

INTRODUCTION

Radiographic measurements of cup orientation after THR surgery were analyzed to evaluate the difference in measured values of cup orientation during postoperative follow-up in order to: (1) assess the sensitivity of the measurement technique to inter- and intra-subject measurement variation, and (2) evaluate the variation in measured cup orientation from subsequent individual xrays.

METHODS

Postoperative AP radiographs were analyzed for a group of patients that underwent primary THR surgery. The cup orientation was measured from the radiographs at 1, 3, 6 and 12 months, and annually thereafter. The measurement of cup orientation was performed on digitized x-rays using a computer assisted technique, in which the cup position and orientation were reconstructed in space to match the outline of the x-ray projection. The source-to-film distance was set to 1000 mm for all supine x-rays, and the central x-ray beam was placed centrally at the level of the pubis symphysis. The transverse axis was defined using the radiographic teardrop landmarks, and the position and orientation of the cup geometric model in space were interactively manipulated until the calculated projection matched the cup outline on the radiograph [2]. All measurements were expressed using the operative definition of cup alignment, i.e. in terms of abduction and flexion. To evaluate the sensitivity of the measurement technique to subjective error, all measurements were independently performed twice by two evaluators. The two measurement sessions for each observer were spaced one week apart, in order to minimize the influence of the first session measurements upon the second session. The intra- and inter- subject variation was measured as a difference in abduction and flexion angles of the cup for each x-ray measurement. The results were then statistically analyzed. For each patient, the only difference in measurements should be primarily the result of pelvic flexion or extension and the abduction should be the same for all cup orientation measurements, provided that (a) there was no migration of the cup, (b) the transverse axis is uniquely identified, and (c) the version of the pelvis is the same for all consecutive x-rays. All measurements are converted according to the radiographic definition [2] and analyzed.

RESULTS

Measurements were performed for 23 patients, with a follow-up period between three months and one year. For most patients, a standing AP radiograph was also acquired. Of the 92 analyzed radiographs, 71 were obtained in a supine position and 21 in a standing position. The means for the inter- and intra-observer variation are presented in Table 1.

Table 2 shows the measured variation of cup abduction and flexion for each patient's set of consecutive AP radiographs. Only sets of four or more radiographs per patient were analyzed. Table 2 presents the range, mean and standard deviation for each patient's measurements. Only the measurements from supine x-rays were compared

Table 1. Mean values of intra- and inter-observer variation for cup orientation measurements expressed in cup abduction and flexion

	Observer 1				Observer 2			
	Session 1		Session 2		Session 3		Session 4	
	abd	flex	abd	flex	abd	flex	abd	flex
Session 2	1.0	1.67	-	-	-	-	-	-
Session 3	1.34	2.52	0.89	2.17	-	-	-	-
Session 4	1.12	1.92	0.68	1.63	0.72	1.53	-	-

Table 2. Variation of measured cup orientation per patient. Single observer (session 4) data.

Patient #	# of x-rays	Cup Abduction [degrees]			Cup Flexion [degrees]		
		range	μ	σ	range	μ	σ
1	5	4.0	48.9	1.8	13.2	19.3	5.2
2	7	2.7	48.1	0.9	16.8	16.2	5.8
3	4	2.1	42.8	1.0	14.1	12.0	7.6
4	4	0.8	44.9	0.4	3.2	9.5	1.3
5	4	1.4	52.7	0.7	7.1	15.8	2.9
6	4	0.7	50.5	0.4	3.2	11.9	1.5
7	5	3.2	40.8	1.3	5.3	17.1	1.9
8	4	2.2	50.3	1.0	2.3	30.2	1.1

DISCUSSION

Measurements of intra-observer variability indicate that abduction can be measured with somewhat less variation (1° for Observer 1 and 0.72° for Observer 2) than cup flexion (1.67° for observer 1 and 1.53° for observer 2). Somewhat larger variation can be observed for inter-observer comparison. Overall, it can be estimated that with some practice, the cup orientation can be measured from AP x-rays with variation in the order of 1° in abduction and 2° in flexion. Variation in measurements of the abduction angle can be attributed in part to the variation in definition of the transverse axis using radiographic landmarks. Variation in flexion measurements is primarily due to the accuracy of the approximation of the cup contour. This variation could be reduced with increased resolution of the x-ray scan and the aid of automatic contour detection and fitting algorithms.

The results from Table 2 show that although the radiographic procedure is standardized and the patient is always in the supine position, there is a wide variation in measured values of cup orientation. Cup abduction ranges from 0.8° to 4.0°. The standard deviation from the mean abduction per patient ranges from 0.4° to 1.8°. Additional study is necessary to explain this variation which is possibly due to pelvic version. The measured cup flexion, however, varies between 2.3° and 16.8°, with standard deviation from the mean value between 1.1° and 7.6°, indicating that for some patients there is a large variation of pelvic flexion when they are in a supine position. Such variation makes the comparison of consecutive x-rays, and the detection of problems such as wear and implant migration more difficult and requires additional measures to standardize the radiographic procedure.

REFERENCES: 1. Jaramaz et al. Trans. 45th ORS, 925, 1999, 2. Jaramaz et al. CORR 354, 1998.

THE ROLE OF THE CORONOID AND RADIAL HEAD IN COMPLEX ELBOW FRACTURE-DISLOCATIONS

Patricia G. Neale, Shawn W. O'Driscoll, Stephen L. Cheng, Kai-Nan An

Orthopedic Biomechanics Laboratory, Mayo Foundation, Rochester, MN
Email: an.kainan@mayo.edu

INTRODUCTION

Although it is a common, clinically-significant problem, the treatment of complex elbow fracture dislocations remains an enigma. This project models a dislocation of the elbow complicated by fractures of the radial head and the coronoid, with what is clearly a profound degree of instability in the elbow. This type of injury, due to its terrible prognosis, has been termed the terrible triad. The purpose of this biomechanical study was to test the hypothesis that *a dislocated elbow is at risk of re-dislocation in proportion to the loss of the coronoid, and this risk is greatly increased if the radial head is lost as well.*

METHODS

Seven fresh-frozen cadaveric elbow specimens were prepared. The humerus was potted and attached to a frame. The forearm was cross-pinned in neutral and amputated at the wrist. All soft tissues around the elbow were released, except for the biceps, brachialis, and triceps tendons. As a result, the elbow could be dislocated and then reduced. The triceps, biceps, brachialis tendons were placed in balanced loading.

In order to study the effects of the radial head coupled with progressive coronoid loss, a titanium plate was applied to the intact radial head and neck, and then the neck was osteotomized. This allowed the radial head to be removed and replaced to repeatably simulate the presence or absence of a radial head.

After testing the intact state and post-osteotomy, a partial coronoid resection was performed removing 25, 33, 50, 75, or 100 percent of the coronoid, corresponding to a coronoid fracture classification system devised by Regan and Morrey (1992). At each resection level, the elbow was tested with and without a radial head.

The motion of the elbow was monitored with a three-dimensional electromagnetic tracking system (Fastrak, Polhemus, Inc., Colchester, VT); a sensor was attached to the humerus, radius, and ulna.

The goal of this study was to define instability by determining the angle at which the elbow subluxed or dislocated. Due to the complex nature of this type of instability, a variety of parameters were used to define when this instability occurred. The ulnohumeral rotations about two axes, as well as translations along three axes, were used to establish when instability and dislocation occurred. Instability was defined as the point at which one parameter was $\geq 1°$ or 1 mm different from the control state. Similarly, dislocation was measured at a 2° or 2 mm increase. The angle of and mode of dislocation were noted.

RESULTS

With the radial head present or absent, an increasing loss of coronoid led to an increasing tendency for the elbow to become unstable (Table 1). Additionally, when the

radial head was absent, instability occurred with less coronoid resection.

Table 1: Number of specimens exhibiting instability at any point in the extension path. Instability is defined as showing a difference from the control of >1° or >1mm.

Coronoid Resection	RH Present	RH Absent
25%	0	6
33%	3	6
50%	5	6
75%	7	7
100%	7	7

It was noted that dislocation occurred through a variety of mechanisms (Table 2), including pronation/supination (p/s), varus/valgus (v/v), and translation of the ulnar center of rotation (trans). However, most dislocations occurred via an axial rotation motion (82% of dislocations with a radial head; 52% without a radial head).

Table 2: Number of specimens for each mechanism of dislocation (>2° or 2 mm difference from control).

%	With R. H. P/s	With R. H. v/v	With R. H. Trans	Without R.H. p/s	Without R.H. v/v	Without R.H. Trans
25	-	-	-	-	-	1
33	-	-	-	1	-	3
50	4	-	-	4	-	3
75	6	-	-	5	1	1
100	4	3	-	3	3	1

The elbow dislocated at higher flexion angles as more of the coronoid was resected. The elbow dislocated more frequently and earlier in the extension motion when the radial head was absent (Figures 1 and 2).

DISCUSSION

This developed method of measuring the exact locations of elbow instability and dislocations has shown to be repeatable among specimens. Including parameters for both ulnohumeral rotation and translation

turned out to be a sensitive method of determining the flexion angle at which subluxation or dislocation occurred.

The clinical implications are that there is minimal risk of elbow dislocation for an isolated small coronoid fracture with the radial head intact, but this risk increases in proportion to the amount of coronoid that is fractured. However, if such a dislocated elbow also has a radial head fracture, there is a larger risk of instability, even with a very small amount of coronoid loss. If there is a type II fracture with 25-50 percent of the coronoid lost, the risk of instability is high.

In conclusion, the coronoid is clearly a primary stabilizer of the elbow, with the radial head being a secondary stabilizer in this model. However, it should be recognized that if the coronoid is deficient, then the radial head becomes a critical factor in determining elbow stability.
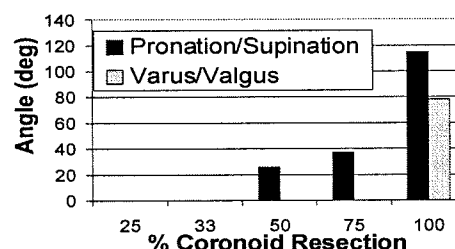
Figure 1: Angle at the start of dislocation with the radial head present.
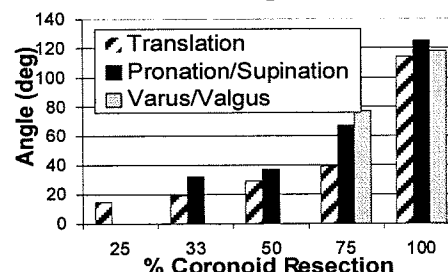
Figure 2: Angle at the start of dislocation with radial head absent.

REFERENCES
Regan, W., Morrey, B.F. (1992). *Orthopedics*, **15**, 845-8.

EVALUATION OF KNEE KINEMATICS USING
A MAGNETIC TRACKING DEVICE

W. B. McGarry, W. A. Zuelzer, J. S. Wayne

Orthopaedic Research Laboratory
Departments of Biomedical Engineering and Orthopaedic Surgery
Virginia Commonwealth University, Richmond, Virginia
Email: jswayne@ vcu.edu

INTRODUCTION

Various methods exist to measure kinematics of biological joints, each with pros and cons. Magnetic tracking devices have been shown to be accurate, are small and lightweight, and do not require intermediate steps in processing data to utilize the output. This project evaluated the feasibility of using a magnetic tracking device to measure knee kinematics by comparison to an instrumented spatial linkage.

METHODS

The magnetic tracking system used in this study is the 3Space® Tracker® from Polhemus (Colchester, VT). The receivers are approximately 1" cubes and weigh 0.6 oz. The manufacturer documents the system positional and orientation accuracy to be 0.03" and 0.15° RMS, respectively. Prior studies have reported this or similar magnetic tracking devices to have an error of less than 2% for a receiver to transmitter separation of up to 30" (1,2,4,6). However, the accuracy of the magnetic tracking device should be confirmed in each setting because different physical environments will affect the magnetic field differently.

In order to validate the positional accuracy of the magnetic tracking device, the sensor was mounted at different positions on a predrilled Plexiglas plate. The x, y, and z coordinates from the magnetic tracking system were compared to those from the Plexiglas plate. The rotational accuracy was verified using a device that allowed rotation in three dimensions. This device incorporated three potentiometers to independently measure the rotations about the axes. The Euler angles from the magnetic tracking device were then compared with angular measurements from the potentiometers.

After assessing the accuracy of the magnetic tracking device, it was used to obtain kinematic data of three porcine knees and compared to the measurements of the same knees using an instrumented spatial linkage system. The linkage system is made up of a gyroscope and a sliding link with a four-bar revolute joint to measure joint rotations and translations and uses optical encoders to measure the rotations of the linkage joints. It has an overall length of 9.5" and weighs over 2 lbs. including the attachment brackets. The linkage system has an accuracy of 0.02" and 0.1° for translations and rotations (5). To minimize slippage of the linkage, rods were placed in the intramedullary canals of the femur and tibia. The linkage was then attached to these rods using the attachment brackets on the lateral side of the knee. The femur was clamped to the table while the tibia was moved in four flexion-extension cycles. Active flexion-extension of the knee was simulated by attaching a cable to the patellar tendon of the knee and using a small motor to represent the quadriceps muscle.

Two receivers, one attached to the femoral rod and one attached to the tibial rod, were used to measure the kinematics

with the magnetic tracking device. The same rods and motor system as used for the linkage system were used for the magnetic tracking system. The data of both the linkage system and magnetic tracking device was converted into kinematic data using the Joint Coordinate System for the knee as defined by Grood and Suntay (3).

RESULTS AND DISCUSSION

The error of the magnetic tracking system was found to be less than 2% when the receiver and transmitter were within a 4-25" separation range. For clinical motions of the knee, similar trends between the linkage system and the magnetic tracking device for clinical motions were noted excluding abduction/adduction (Fig. 1). The variation in abduction/adduction is due to the weight of the linkage system which is placed on the lateral side of the knee during data collection (causing the tibia to be rotated in adduction). The accuracy and lightweight design of the magnetic tracking device make it an attractive option for studying joint kinematics.
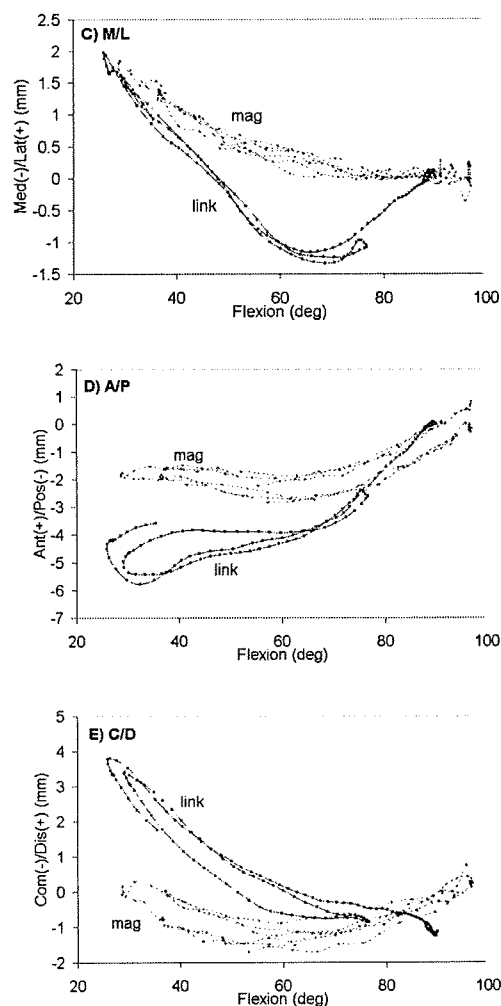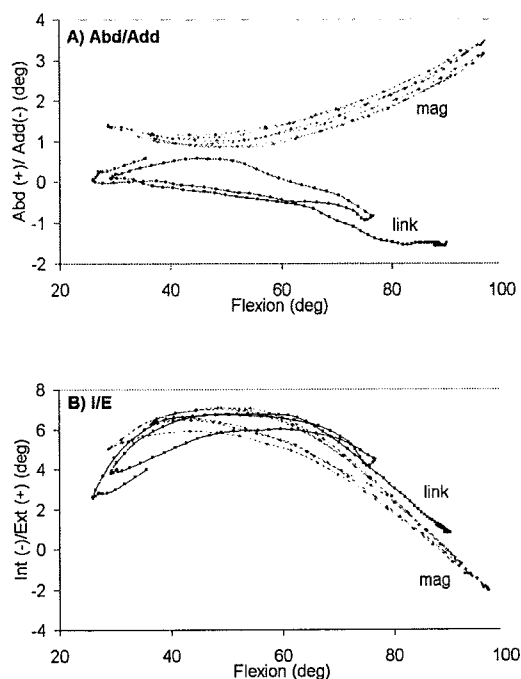
Figure 1: Clinical motions (tibia relative to femur) of a typical porcine knee during simulated active extension versus flexion of the joint: A) abduction/adduction; B) internal/external rotation; C) medial/lateral translation; D) anterior/posterior translation; E) compression/distraction.

REFERENCES

1) An, K.N., et al. (1988). *J. Biomechanics*, **21**, 613-620.
2) Day, J.S., et al. (1998). *J. Biomechanics*, **31**, 957-961.
3) Grood, E.S., Suntay, W.J. (1983). *ASME J. Biomechanical Engineering*, **105**, 136-144.
4) McKellop, H., et al. (1993). *J. Bone and Joint Surgery*, **75A**, 1019-1025.
5) Meglan, J.F. (1989). M.S. Thesis, Ohio State University, Columbus, Ohio.
6) Milne, A.D., et al. (1996). *J. Biomechanics*, **29**, 791-793.

Bone Strain is Accentuated by Ground Reaction Forces With Higher Than Normal Frequency Spectra

Schultheis, L. Rastogi S., Lee J., Annand J., Ruiz J., Schultheis A., Dept. of Biomedical Engineering, Johns Hopkins University, Phone 410 516 5112, fax 4771, email lschulth@bme.jhu.edu

Introduction

Previous work has demonstrated the efficacy of episodic dynamic loading in preventing disuse atrophy of bone. In contrast, static loading appears to lack osteogenic properties.(1) The characteristics of an optimum-loading regimen to serve as a countermeasure for reduced weightbearing activity are not clearly defined.

We independently manipulated static weightbearing and the dynamic impact forces on the forelimbs of hindquarter suspended rats using a servo-controlled forceplate.
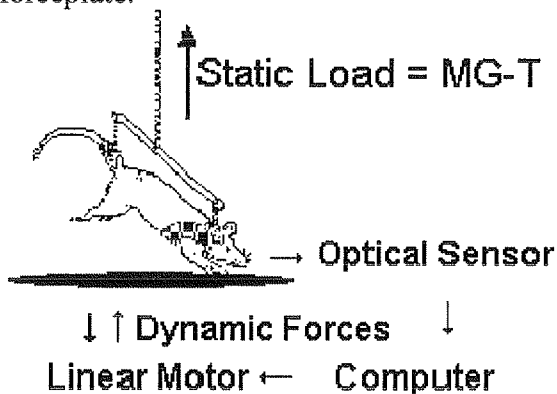
Figure 1.

The static weightbearing on the forelimbs is defined by the difference between the animal's weight (MG) and the tension (T) on the tether. We adjusted the tether tension so that the weight supported by the forelimbs is equal to weight normally supported (about 30% total body weight). By programming the computer within the feedback loop we were able to prescribe the bandwidth of ground reaction forces.

Prior work using Fourier transformation of the ambulatory ground reaction forces on individual paws indicated that 99% of the energy of an average impact was contained between 0-10 Hz and 50% was contained between 0-3Hz. (2)

Methods

100-day-old female Sprague Dawley rats were prepared with isoflurane inhalation anesthesia for surgical implantation of a calibrated C31 single axis strain gauge (Micromeasurements Inc). The musculature of the lateral upper extremity was exposed and bluntly dissected from the bone. After bonding the gauge to the mid-diaphysis, previously soldered 32 gauge braided stainless steel leads were passed from the gauge under the skin to a Teflon connector in the dorsal midline of the rat's neck.

The animal was placed in a harness on the force plate depicted in Figure 1 and allowed to recover from the procedure. The harness admitted only one foreleg so that the animal ambulated by hopping on its single exposed forelimb. The leads from the connector on the rat's neck were soldered to wires on a Wheatsone bridge. The ouput from the bridge was amplified, bandlimited by an analog prefilter and sampled by a 12 bit A/D system at 300/sec. A Faraday cage enclosed the rat and forceplate system and all electronics were shielded to yield a signal to noise ratio of 100:1.

The forceplate was calibrated dynamically by dropping clay weights from prescribed heights with the servo system engaged. The computer software enabled the forceplate to resonate at either 3 Hz or 16 Hz. An identical fall with a clay weight at either frequency produced the same peak force and peak potential energy. The resolution of the forceplate to changes in static load was 0.05 Newtons. The system

appeared to be linear with impacts between 0.1-3 Newtons.

Ground reaction forces were simultaneously recorded with bone strain while the animal moved about on the force plate. Data was stratified off-line so that bone strain could be compared when impact forces and peak work done on the leg were identical with floor resonance at either 3 or 16 Hz. Statistical comparison between similar impacts at each frequency was determined using Student's T-test and Fisher's PLD, with variation as SEM.

Results

Four rats with impacts having similar peak force and peak work profiles for impacts at both 3 and 16Hz exhibited significantly ($P<0.05$) higher peak strain at 16 Hz than 3Hz. See Figure 2.

Strain 60% Higher at 16 Hz than at 3 Hz
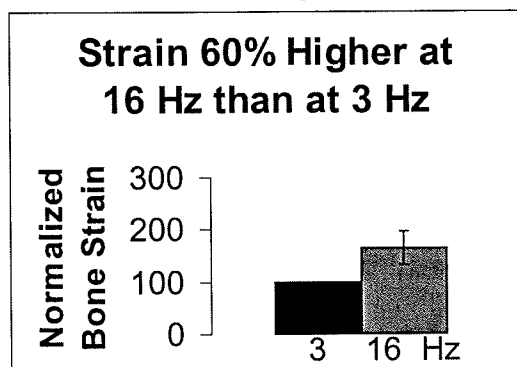
Figure 2.

Each rat behaved in a similar fashion, with peak bone strain from impacts on the forceplate resonating at 16 Hz exceeding the peak bone strain from impacts on the forceplate resonating at 3 Hz. This bias was only supported when the peak energy and peak forces of impact were controlled to be similar at each resonant frequency. See Table 1.

Rat	Hz	µstrain	Peak force (Newtons)	Peak work (µJoules)
1	3	112±6	1.1±0.01	269±11
	16	146±6	1.2±0.07	238±8.3
2	3	156±8	1.2±0.02	518±23
	16	198±13	1.3±0.03	521±50
3	3	108±8	0.9±0.01	157±1.5
	16	168±20	0.9±0.02	191±3.5
4	3	99±5	0.9±0.01	247±7
	16	253±23	0.95±.01	248±22

Table 1.

When peak force was controlled at both resonant frequencies, but peak work varied, higher peak bone strain was associated with higher peak work regardless of the resonant frequency of the platform.

Discussion

These data suggest that ground reaction forces with spectral components of higher frequency than normal are more effective in producing bone strain. If bone strain history is an effective predictor of bone modeling, shifting the spectrum of loading forces toward high frequencies may be advantageous in developing osteogenic physical countermeasures for space flight or prolonged inactivity.

References

1. Lanyon LE, Rubin CT, Static vs Dynamic Loads as an Influence on Bone Remodeling, J. Biomechanics (17) no. 12 pp 897-905, 1984.
2. Schultheis L., Schultheis A., Inoue N, Lee J., Chao EYS et al. Freq. Analysis of Ambulatory Forces on Forlimbs of Hindquater Suspended Rats in a Simulation of Reduced Gravity, ORS (23) pp135, 1998.

Acknowledgements

INTERLIMB COUPLING IS AFFECTED BY PERIPHERALLY MEDIATED FACTORS

Peter F. Vint, Susan M. Thompson and Gregory M. Harron

Department of Exercise and Sport Science, University of North Carolina at Greensboro, Greensboro, NC

E-mail: pfvint@uncg.edu   Web: http://www.uncg.edu/~pfvint

INTRODUCTION

Interlimb coupling may be an inherent tendency in human coordination. For example, bimanual tasks of varying difficulty tend to be performed together and exhibit a tight spatiotemporal coupling of the involved limbs (Kelso et al., 1979). Unfortunately, the locus of the interlimb coupling mechanism is still not understood. Results from reaction time, movement speed, and weight-matching experiments suggest that the control of bilateral motor performances is related to *centrally* mediated factors (Jeeves, 1969; McCloskey et al., 1974; Wyke, 1969). Others suggest that such inhibitory mechanisms may be reflexive in nature or may be modulated *peripherally* using feedback from the active musculature.

The primary purpose of this study was to identify the locus of the interlimb coupling mechanism by inducing acute asymmetries in muscular force during a series of simultaneous bilateral elbow flexion tasks. Neuromuscular impairments in elbow flexion force were achieved reliably using a reciprocal inhibition technique. It was hypothesized that if interlimb coupling tendencies were sensitive to peripherally mediated factors, non-impaired limb forces would gravitate toward the force level of the impaired limbs and vice-versa.

PROCEDURES

Twenty-five subjects (mean age 24.5 ± 4.8 yr., height 171.9 ± 9.5 cm; mass 76.9 ± 21.5 kg) volunteered to participate in the experiment. All subjects were right-hand dominant as indicated by writing-hand preference. Isometric elbow flexion force data were obtained from each arm separately using two independent strain gauges. Pre-amplified, bipolar electrodes were used to measure surface EMG activity of the biceps and triceps on each arm. Force and EMG data were sampled for 3 s at 1000 Hz.

Subjects were required to complete a series of maximum effort elbow flexion exertions in each of 8 experimental conditions. Unilateral exertions were performed separately with the dominant (D) and non-dominant (N) arms in either supinated (UL-S) or actively pronated (UL-P) radioulnar joint positions. Symmetric bilateral exertions were performed in both supinated (SBL-S) and actively pronated (SBL-P) positions. Asymmetric bilateral exertions were performed with one limb supinated and the other actively pronated (ABL-S/P; ABL-P/S). Conditions were counter-balanced across subjects.

Maximum elbow flexion force was defined by the average force in a 250 ms window that resulted in the greatest integrated force value. Average integrated EMG (AIEMG) values of the biceps and triceps were quantified over the same 250 ms window.

RESULTS AND DISCUSSION

Repeated measures ANOVA revealed significant main effects for arm (non-dominant < dominant), position (pronated < supinated), and condition (bilateral < unilateral). On average, active radioulnar pronation resulted in a 54.8 N (19.8%) reduction in maximum isometric elbow flexion force. Position-induced changes in force were paralleled by changes in biceps

AIEMG. However, biceps AIEMG data were not sensitive to the differences in force observed between unilateral and bilateral exertions.

Regardless of arm or radioulnar joint position, symmetric bilateral exertions resulted in significantly lower forces than unilateral exertions. Mean bilateral deficits in elbow flexion force were $-12.1 \pm 6.6\%$ while supinated and $-11.4 \pm 12.6\%$ while actively pronated. These values were both significantly less than zero ($p < .001$) but were not significantly different from each other ($p = .78$).

Asymmetric bilateral exertions resulted in arm-specific changes in force. Supinated limbs, when paired with actively pronated limbs, experienced significant *decreases* in force (see ABL-S, Figure 1). Actively pronated limbs, conversely, experienced significant *increases* in force (see ABL-P, Figure 2).
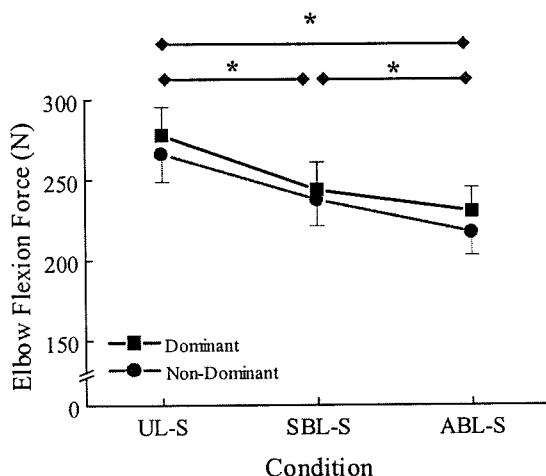
Figure 1. Elbow flexion force of supinated arm during unilateral (UL), symmetric bilateral (SBL) and asymmetric bilateral (ABL) exertions. Asterisks above horizontal bars denote statistically significant comparisons ($p < .01$).
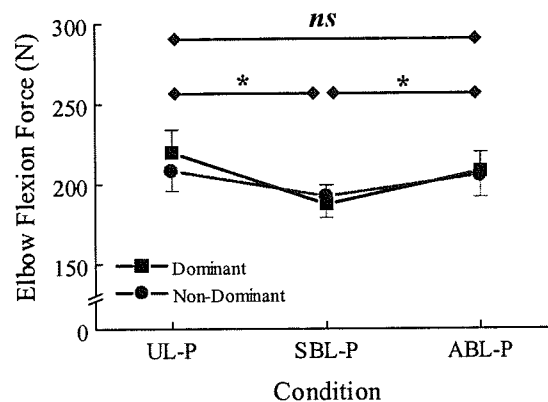
Figure 2. Elbow flexion force of actively pronated arm during unilateral (UL), symmetric bilateral (SBL) and asymmetric bilateral (ABL) exertions. Asterisks below horizontal bars denote statistically significant comparisons ($p < .05$).

The results of this study demonstrated a strong bi-directional interlimb coupling effect. During asymmetric bilateral exertions, non-impaired (supinated) limb forces declined toward the impaired (pronated) limb forces. Impaired limb forces concurrently rose toward those of the non-impaired limb. These data indicate that during asymmetric bilateral exertions, limbs tend to gravitate toward a *common* force level. We therefore conclude that interlimb coupling tendencies are sensitive to peripherally mediated factors.

REFERENCES

Jeeves, M.A. (1969). *Psych. Sci.*, **16**, 245-256.

Kelso, J.A.S., Southard, D.L., Goodman, D. (1979). *J. Exp. Psych.*, **5**, 229-238.

McCloskey D.I., Ebeling, P, Goodwin, G.M. (1974). *Exp. Neurobiol*, **42**, 220-232.

Wyke, M. (1969). *Neuropsych.*, **15**, 33-42.

ACKNOWLEDGEMENTS

COMPATIBILITY OF CONTROL THEORIES OF REACHING MOTIONS

John H. Challis and Susan C. Challis

Biomechanics Laboratory, The Pennsylvania State University, University Park,
Pennsylvania
Email: jhc10@psu.edu

INTRODUCTION

Use of the upper limb to reach a target has been studied extensively. It is a common task which is normally performed with ease. Morasso (1981) showed that during reaching the hand path is straight, whilst Hogan (1984) showed that such motion can be achieved if the jerk associated with the hand is minimized. More recent experimental work has suggested that these hand paths are slightly curved (Uno et al., 1989). Gottleib et al. (1996) suggested that during reaching motions there is a simple linear relationship between the moment at the shoulder and elbow joints, whilst Bock (1994) suggested that moment profiles are bi-phasic.

The purpose of this study was to examine the compatibility of straight line hand paths, bi-phasic moment profiles, and colinear shoulder and elbow moments, during reaching motions.

PROCEDURES

The study combined an experimental and simulation modeling approach. Four different reaching tasks in a horizontal plane were examined (see figure 1). Seven experimental subjects (mass 73.6 ± 17.0 kg; height 1.72 ± 0.08 m) gave informed consent to participate in the study. They performed 8 repeat trials for each task. The motion of the upper limb was recorded using an image based motion analysis system (ProReflex, Qualisys©). The resulting data were combined with subject specific body segment inertial parameters to determine resultant joint moments at the shoulder and elbow joints. During the

reaching tasks both shoulder joint center and wrist joint motion were negligible.
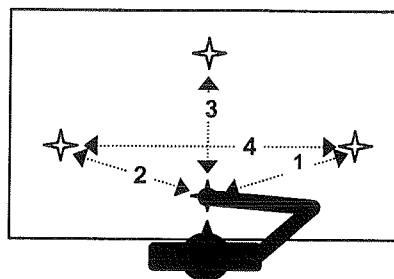
Figure 1 - Plan of reaching tasks

An optimal control direct dynamics simulation model of the upper limb motion was developed to further investigate these reaching motions. For example motion kinematics and kinetics were determined for a simulated reaching task when the mean squared jerk experienced by the hand was minimized.

RESULTS

Figure 2 shows the mean and standard deviation of the shoulder resultant joint moments for a typical subject performing a reaching task. These moments are tri-phasic. Similar profiles were obtained for the elbow joint. Figure 3 shows the relationship between shoulder and elbow resultant joint moments during a simulated reaching motion for task 3 with minimization of jerk. Clearly these moments are not a simple linear function of one another.
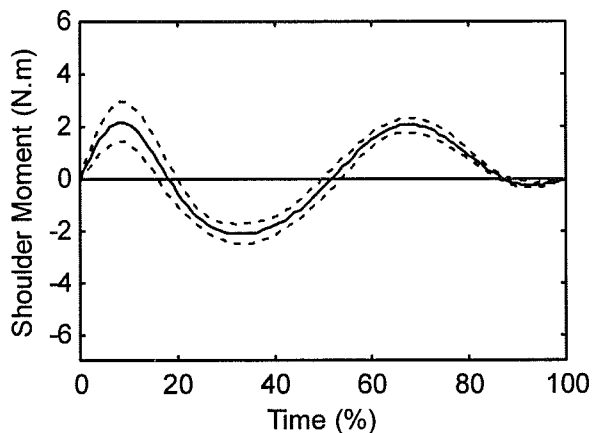
Figure 2 - Resultant shoulder moments for task 1.
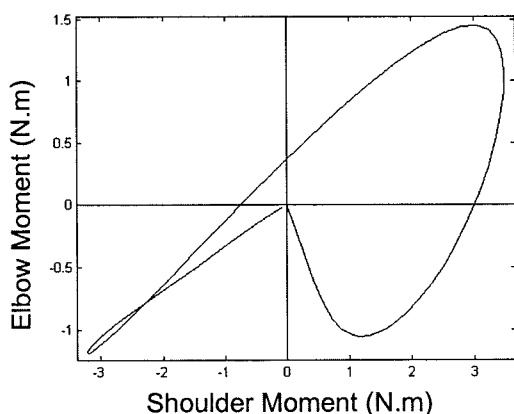
Figure 3 - Relationship between shoulder and elbow joint moments for a simulated task 1.

Figure 4 - The hand path for one subject performing task 4.

Notice that the eight trials are performed in a repeatable fashion, and that the hand path is curved.

DISCUSSION

Hand path curvature varied between subjects, some exhibited almost straight hand paths for all tasks, whilst others had curved hand paths. The minimum hand jerk model produces a straight hand path, so is not correct for all of the normal healthy subjects in this study.

Bock (1994) suggested that reaching tasks are generated by scaling bi-phasic moment profiles. Moment profiles were commonly tri-phasic, and varied wildly between subjects performing the same task.

Gottleib et al. (1996) reported that in vertical plane reaching the shoulder and elbow moments were linearly related. Linearity was numerically quantified in this study, and these horizontal plane motions did not produce a linear relationship between shoulder and elbow moments. Simulation of the reaching tasks using the minimum hand jerk model also does not produce a linear relationship between these moments.

Certain subjects produced movements which could be explained by one or other of the theories, whilst others did not. Either the hitherto considered theories do not apply for all subjects, or some control mechanism is at play which manifests itself in different movement patterns for different subjects.

REFERENCES

Bock, O. (1994). *Exp. Brain Res.*, **101**, 346-352.
Gottleib, G.L. et al. (1996). *J. Neurophys.*, **75**, 1374-1381.
Hogan, N. (1984). *J. Neurosci.*, **4**, 2745-2754.
Morasso, P. (1981). *Exp. Brain Res.*, **42**, 223-227.
Uno, Y. et al. (1989). *Biol. Cyber.*, **61**, 89-101.

USING ELECTRICAL NOISE TO REDUCE VIBROTACTILE THRESHOLDS IN HUMANS

Wen Liu[1], Kristen A. Richardson[1], Lewis A. Lipsitz[2], and James J. Collins[1]

[1]Center for BioDynamics and Department of Biomedical Engineering, Boston University,
Boston, Massachusetts

[2]Hebrew Rehabilitation Center for Aged and Harvard Medical School Division on Aging,
Boston, Massachusetts

Introduction

Cutaneous sensation plays an important role in human interaction with the environment and defense against potential harmful influences. Diminished cutaneous sensation, which occurs in older adults, stroke patients, and patients with peripheral neuropathies, may lead to impaired motor function, accidental injury, and confusion. Accordingly, there is a need to develop bioengineering techniques for improving cutaneous sensation.

Recently, it was shown that the ability of an individual to detect a subthreshold mechanical cutaneous stimulus (in the form of a ramp signal) can be significantly enhanced by introducing a particular level of mechanical noise (Collins et al., 1996, 1997) or electrical noise (Richardson et al., 1998). In this study, our objective was to extend previous work to vibrotactile stimuli. Specifically, we were interested in testing the hypothesis that an individual's vibrotactile thresholds can be significantly reduced through the application of electrical noise.

Methods

Ten healthy adults (8 males and 2 females; aged 22-40 years, mean 27 years) participated in this study. All subjects were free of any detectable neurological disorder.

Vibration stimuli were applied to the glabrous skin of the finger tip of the right middle digit of each subject using a 2-mm diameter flat cylindrical probe. The probe was mounted on an indenter arm that was actuated by a force-controlled dc motor. The subject's hand was held in a fixed position by a hand-shaped clay molding to ensure that the subject's right middle digit remained over the indenter arm of the mechanical stimulation device. The vibration stimuli (duration: 0.2 s) were repeatedly presented with and without electrical noise. A constant indentation force offset of 0.036 N was applied to maintain the contact between the fingertip and the probe. The noise signals, which were generated digitally on a PC, consisted of zero-mean Gaussian "quasi-white" noise. These signals were transmitted through a biphasic stimulus isolator into the indenter arm of the mechanical stimulation device. The associated electrical current was passed through the tip of the indenter arm into the subject's finger. Prior to data acquisition, the subject's detection threshold for electrical noise was approximated by asking the subject to adjust the level of the noise to the level that he/she could barely feel. The noise level applied during testing was 35% of the approximated threshold.

During the tests, the subjects were seated in front of a computer screen that provided cues signaling the start and end of each presentation period. Subjects were instructed to indicate whether or not they detected the vibration stimulus. A 4, 2, and 1 stepping algorithm was used to estimate vibrotactile detection thresholds (Dyck et al., 1993). Two vibration stimuli were used: a 30 Hz stimulus and a 125 HZ stimulus. These stimuli were tested independently. For each trial, two conditions — the selected vibration stimulus without electrical noise

(0% noise) and the selected vibration stimulus with 35% noise — were run in parallel. For each condition, a total of 20 vibration stimuli (of varying amplitude, depending on the subject's responses), plus 5 null stimulus randomly inserted, were presented. Thus, each trial included 50 presentations. Nine trials were conducted on each subject for each vibration stimulus (e.g., see Figure 1). A paired t-test was used to compare the results from the 0%-noise condition with those from the 35%-noise condition for each vibration stimulus.

Results

For the 30 Hz vibration stimulus, the application of electrical noise led to a lower detection threshold in 7 of the 10 subjects. Across the subject population, we found that the detection threshold for the 35%-noise condition was significantly lower ($P<0.05$) than that for the 0%-noise condition .
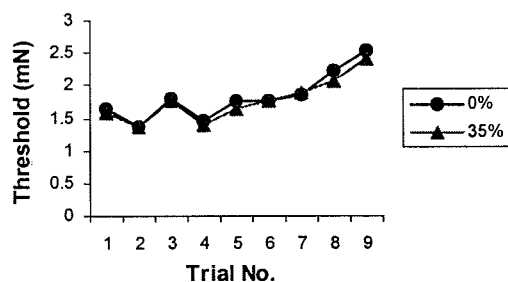
Figure 1. Detection threshold values of a representative subject for the 30 Hz vibration stimulus with electrical noise (35%) and without electrical noise (0%).

For the 125 Hz vibration stimulus, the application of electrical noise led to a lower detection threshold in 8 of the 10 subjects. Across the subject population, we found that the detection threshold for the 30%-noise condition was significantly lower ($P<0.05$) than that for the 0%-noise condition (Figure 2). As reported previously (Talbot et al., 1968), we found that the detection thresholds for the 125 Hz vibration

stimulus were considerably lower than those for the 30 Hz vibration stimulus.
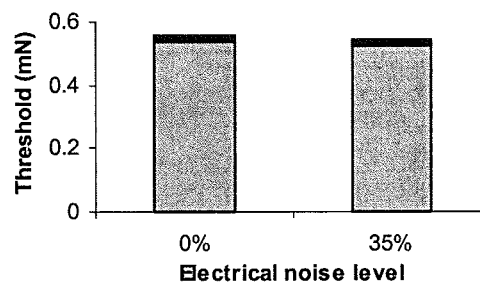
Figure 2. Group means and standard errors of the detection thresholds of the 10 subjects for the 125 Hz vibration stimulus with and without electrical noise.

Discussion

This study showed that an individual's vibrotactile thresholds can be significantly reduced through the application of electrical noise. The parallel running of the presentations in two noise conditions allowed us to detect relatively small differences in the mean threshold between the two conditions, i.e., 0% noise and 35% noise. It is possible that the small (but significant) reductions in threshold found in this study could be enhanced considerably by utilizing arrays of electrodes with distributed, independent noise sources (Collins et al., 1995).

Acknowledgements

References

Collins J.J. et al. (1995), Nature, 376, 236-238.
Collins J.J. et al. (1996), Nature, 383, 770.
Collins J.J. et al. (1997), Physical Review E, 56, 923-926.
Dyck, P.J. et al. (1993), Neurology, 43, 1508-1512.
Richardson K.A. et al. (1998), Chaos, 8, 599-603.
Talbot, W.E. et al. (1968), J. Neurophysiol., 31, 301-334.

MOTOR OUTPUT VARIABILITY DURING CONCENTRIC AND ECCENTRIC CONTRACTIONS OF THE QUADRICEPS FEMORIS MUSCLE GROUP

Evangelos A. Christou, M.S., A.T.C/L, Les G. Carlton, Ph.D.

Department of Kinesiology, University of Illinois at Urbana-Champaign
Email: christou@uiuc.edu

INTRODUCTION

Several neurophysiological and performance differences have been reported between concentric and eccentric contractions and some researchers have hypothesized that the central nervous system might regulate gradation of muscle force by a unique strategy during eccentric contractions (Enoka, 1996). Successful and consistent motor performance of the Quadriceps Femoris muscle group can be directly linked in activities of daily living such as sitting and rising from a chair and ascending and descending stairs. Traditionally the regulation of force (motor output variability) has been systematically examined under theoretical interests (Carlton and Newell, 1993). Nevertheless this systematic examination involved primarily the upper body during isometric and rapid concentric contractions. The aim of this study was to compare the ability of young adults to regulate force under rapid concentric and eccentric contractions of the knee extensor muscle group.

PROCEDURES

Ten healthy young adults with no history of previous knee pathology were recruited for this study. To assess force production and motor output variability during a leg extension task, and to provide a near constant velocity of 50°/s throughout the range of motion, a KIN-COM 500H isokinetic dynamometer was used. Each participant attended two testing sessions and performed leg extensions that ranged from 90-110° of knee flexion. Five different parabolas were displayed on the monitor of the isokinetic dynamometer with different peak forces (50N, 100N, 150N, 200N, 250N) and with a time to peak force of 200ms. Each participant was instructed to match the parabola displayed by controlling the leg extension force. To familiarize the participants with the targeted parabolas, forty practice trials were given for each target prior to the data collection. In addition to verbal feedback and encouragement, the first half of the practice trials received visual feedback. The remainder of the practice trials and the test trials were given visual feedback only after the trial was completed. All target parabolas were randomly assigned for each subject. Thirty-six trials per contraction type (eccentric and concentric) were collected for each target parabola. A brief rest period of 20-30 seconds was given between data collection trials. Means and standard deviations of variability in peak force (PF), time to peak force (TPF) and coefficient of variation for peak force and time to peak force were computed.

RESULTS AND DISCUSSION

There were no significant differences between the PF produced by concentric and eccentric contractions at each goal force. However TPF was significantly different between the two contractions (F=73.11, p<.000) and a two way interaction (force level x contraction type) was also found

(F=15.98, p<.001). Concentric contractions, with the exception of the goal of 50N (300msec) produced times to peak force of 200msec. Eccentric contractions had shorter TPF and the TPF increased as the goal force increased. Variability of PF increased as the level of force increased for both contractions in a non linear fashion. Eccentric contractions were significantly more variable than concentric contractions (F=7.27, p<.05). No significant interaction was found.
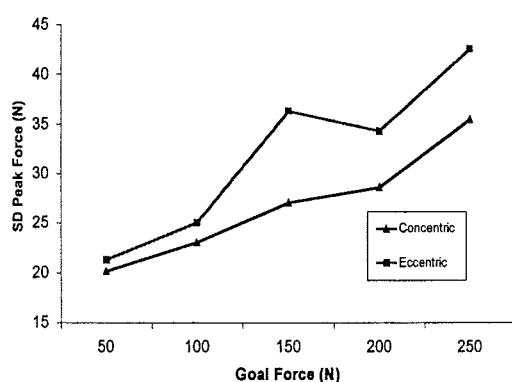
Figure 1. This graph illustrates the differences in peak force variability between concentric and eccentric contractions.

Variability of TPF revealed significant differences between eccentric and concentric contractions (F=20.58, p<.001) and a significant interaction (force level x contraction type) was also found (F=9.04, p<.000). For the concentric contractions TPF variability decreased as the level of goal force increased. However variability of eccentric contractions did not change as the goal force increased. Finally the coefficient of variation was significantly higher during eccentric contractions for the PF (F=5.74, p<.05) and for the TPF (F=14.41, p<.005) compared to concentric contractions. A two way interaction was also significant for the coefficient of variation of TPF (F=5.65, p<.001). Not surprisingly, eccentric

contractions can produce identical amounts of force at a faster pace than concentric contractions. The results of this study indicate that eccentric contractions are more variable in controlling different levels of force when compared to concentric contractions. Furthermore the coefficient of variation of peak force and time to peak force is higher for eccentric contractions.

SUMMARY

Even though both types of contractions produced similar peak forces, eccentric contractions were more variable. This increase in variability during eccentric contractions might be due to an alternative recruitment of motor units during eccentric contractions as suggested by Nardone et. al. (1989). This would also explain the faster times to peak force for eccentric contractions. The results of this study provide further evidence to support the hypothesis that eccentric contractions might be uniquely controlled by the CNS (Enoka, 1996).

REFERENCES

Carlton, L.G., & Newell, K.M. (1993). Force variability and characteristics of force production. In Newell & Cordo (Eds.), *Force Variability* (pp. 128-132). Champaign, IL: Human Kinetics.

Enoka, R. (1996). Eccentric contractions require unique activation strategies by the nervous system. *Journal of Applied Physiology*, 81, 6, 2339-2346.

Nardone, A. et. al., (1989). Selective recruitment of high-threshold human motor units during voluntary isotonic lengthening of active muscles. *Journal of Physiology London*, 409: 451-471.

TRADEOFFS BETWEEN THE ENERGETIC COST OF COLLISIONS AND CONTROL OF LATERAL MOTION IN HUMAN WALKING: AN ANALYTICAL APPROACH

Arthur D. Kuo[1], J. Maxwell Donelan[2], and Rodger Kram[2]

[1]Dept. of Mechanical Engineering & Applied Mechanics, University of Michigan, Ann Arbor, Michigan; [2]Dept. of Integrative Biology, University of California, Berkeley, California
Email: artkuo@umich.edu, mdonelan@uclink4.berkeley.edu, rkram@socrates.berkeley.edu

INTRODUCTION
We used a model of bipedal locomotion based on passive dynamic walking to study the tradeoff between collision losses and control costs during walking. We found that there should be a significant energetic loss associated with the impact of the foot with the ground, that is proportional to the square of step width. However, stabilization of lateral balance appears to be performed largely through control of lateral foot placement, requiring increasing foot motion as the step width becomes narrower. The energetically-optimal step width should be as narrow as possible while still accommodating control of foot placement for lateral balance..

MODEL
We used a previously developed model of passive dynamic walking that allows for lateral motion of the body (Kuo, 1998). The model has 3 unactuated degrees of freedom (see Fig. 1) and is powered by gravity while descending a gentle slope. No trajectory need be prescribed; the walking motion arises purely from the dynamics of the legs acting as coupled pendula (McGeer, 1990). The forward motion of the legs is passively stable and will dissipate perturbations automatically. However, the lateral motion of the model is highly unstable and requires active control. We found that the addition of a simple quasi-static, once-per-step lateral control of foot placement was sufficient to provide lateral stability, and have reported evidence that stabilization of this kind is performed by humans (Kuo & Bauby, 1998). In the present study, we considered the tradeoff between mechanical energy losses at wide step widths and control costs at narrow step widths.

COLLISION LOSSES WITH WIDE STEPS
The mechanical energetics of taking wide steps are illustrated by analysis of a point mass supported by two massless legs that rocks laterally within the frontal plane (see Fig. 2). With the angle 2α between the legs, the amount of energy dissipated at collision with the ground, assuming a perfectly inelastic impact, is

Fig. 1. Three-dimensional model of passive dynamic walking. Swing and stance legs swing freely about the hips, and the model rocks side to side about the stance foot. Step width is varied quasi-statically.
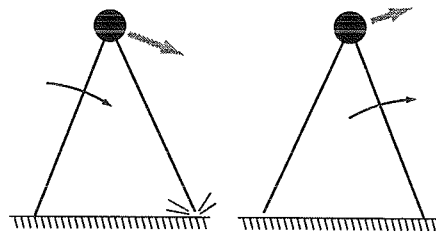
Fig. 2. Point mass model of side-to-side rocking in frontal plane predicts that mechanical energy dissipated at foot contact should be proportional to square of step width. Gray arrows show velocity of center of mass before and after impact.

$$E \sim \left(1 - \cos^2 2\alpha\right) \approx 4\alpha^2.$$

This model is very simple, but a similar quadratic dependence on step width is observed in simulations of passive dynamic walking (Fig. 3). In human walking, energy dissipation during foot contact is due to both collisions and negative work performed at the ankle joint, both of which dissipate the same amount of energy if they occur over a sufficiently short period of time. Our model predicts a significant mechanical energy loss for wide steps, regardless of which mechanism is responsible for this loss in humans.

CONTROL COSTS WITH NARROW STEPS

Another prediction made by our model is that there should be a control cost associated with taking narrow steps. When taking wide steps, the cost of stabilizing lateral motion is due to the need to make small lateral adjustments to foot position. However, for sufficiently narrow steps, it is possible for the stance foot to act as an obstacle to the swing foot. In these circumstances, the swing foot must either move around the stance foot while still landing in the proper location to provide lateral stabilization; or, step width control can be abandoned in favor of other stabilization schemes such as application of

torque about the ankle. Simulations predict a nearly constant RMS lateral foot motion for wide steps, a linear increase with decreasing step width, and a small linear transition region (Fig. 4). Although a crude measure, RMS foot motion may serve as an indicator of increased control costs.

DISCUSSION

There is likely a tradeoff in metabolic cost associated with both the energy dissipated at foot contact and with lateral motion of the feet. Energy cost should be lowest for the narrowest step width that facilitates lateral balance control through foot placement. There are many other factors affecting metabolic cost, such as the cost of force generation. However, the costs predicted here are large enough to indicate that they should be measurable in metabolic terms.

REFERENCES
Kuo, AD (1998) Int J Robot Res (submitted)
Kuo, AD & Bauby CE (1998) Proc. '98 NACOB Conf.
McGeer T (1990) Int J Robot Res 9: 68-82
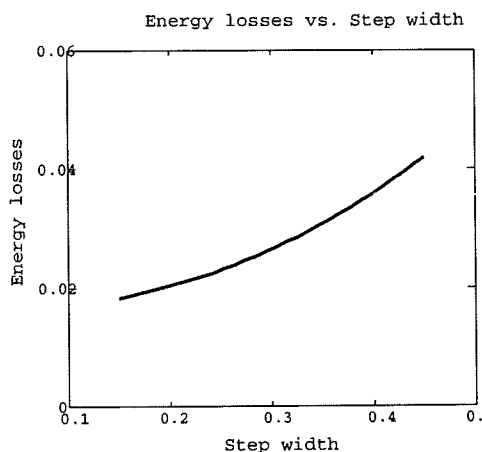
Fig. 3. Mechanical energetic losses increase with square of step width, due to energy dissipated when the swing foot contacts the ground. Energy loss is normalized by weight and distance travelled; step width is normalized by leg length.
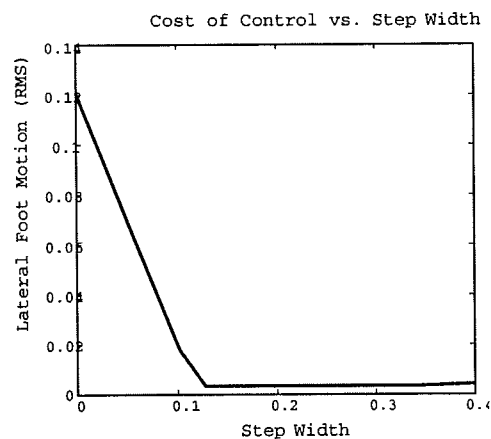
Fig. 4. For large step widths, lateral foot motion is necessary only to provide balance control. At narrow step widths with insufficient foot clearance, swing foot must also move around stance. Step width & foot motion are normalized by leg length.

TRADEOFFS BETWEEN THE ENERGETIC COST OF COLLISIONS AND CONTROL OF LATERAL MOTION IN HUMAN WALKING: AN EMPIRICAL APPROACH

J. Maxwell Donelan[1], Arthur D. Kuo[2] and Rodger Kram[1]

[1]Dept. of Integrative Biology, University of California, Berkeley, California; [2]Dept. of Mechanical Engineering & Applied Mechanics, University of Michigan, Ann Arbor, Michigan
Email: mdonelan@uclink4.berkeley.edu, artkuo@umich.edu, rkram@socrates.berkeley.edu

INTRODUCTION

Using a model of passive dynamic walking, we hypothesized that there should be substantial mechanical energy losses at ground contact for wide steps, and substantial costs to controlling lateral balance for narrow steps. We measured the metabolic costs of human walking as a function of step width. Our results support this hypothesis and showed a minimum energy cost at the preferred step width.

REVIEW AND THEORY

Passive dynamic walking refers to a model of leg dynamics in which the legs act as freely swinging, coupled pendula, and the transitions between steps are modeled as inelastic collisions between foot and ground (McGeer, 1990).

We applied our 3-D model of passive dynamic walking to study energy losses in locomotion. In passive walking, the swing phase is conservative, but at heel strike, energy is dissipated while angular momentum is conserved. We found that the mechanical energy lost at heel strike, and thus the mechanical energy required to sustain locomotion, increases substantially with step width (Kuo et al., 1999). While collision losses are minimized as step width approaches zero, walking is less stable. Controlling lateral motion can be accomplished by making small adjustments to foot placement. This strategy becomes energetically expensive at narrow widths because the stance leg becomes an obstacle to the swing foot. Lateral balance can be can be stabilized with other control strategies, but they too are energetically expensive at narrow widths.

These results led us to theorize that there is an energetically optimal step width in human walking. The mechanical energy lost due to collisions at wide widths, and the control costs associated with narrow widths are of sufficient magnitude in the model that they should be reflected in human metabolic cost. We experimentally investigated the metabolic energetic tradeoff between collisions and control of lateral motion in human walking. We hypothesized that the freely chosen step width minimizes metabolic cost.

PROCEDURES

Subjects: Four volunteer male subjects gave their informed consent (mass 81.7 ± 7.5 kg, leg length (greater trochanter height) 0.98 ± 0.02m, mean $\pm$ S.D.).

Preliminary procedures: We measured each subject's preferred stride frequency and step width using our force treadmill (Kram et al., 1998). We calculated preferred step width as the lateral distance between the centers of pressure of each foot. We familiarized the subjects with the experimental protocol by having them walk on the treadmill at normal and wide widths (10 min. each).

Data Collection: We measured the rates of oxygen consumption (VO_2) and carbon dioxide production (VCO_2) as subjects stood quietly and walked (1.25 m/s) at their nor-

mal width and at widths equal to 0, 0.1, 0.2, 0.3, 0.4 and 0.45 (normalized for leg length). Trials were 6 min. long and were randomized except for the standing trial, which was first. The stride frequency that subjects preferred at their normal width was enforced at all other widths using a metronome. We used chalk lines to ensure step width for trials between the narrowest and the preferred width. For wider widths (0.2–0.45), we used rails to physically enforce a minimum step width (Fig. 1).
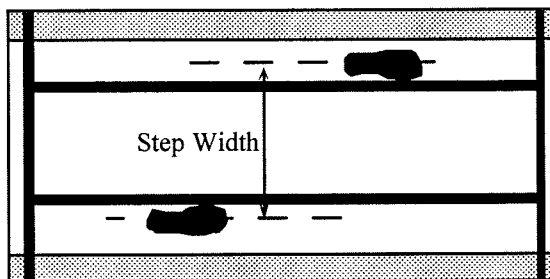
Fig. 1 *Step width enforcer*. Step widths were enforced using aluminum rails (solid black bars) mounted just above the treadmill belt. The width of the bars was adjusted for different step widths.

Data Analysis: We averaged VO_2 and VCO_2 over the last 2 min. of each trial. This elapsed time (4 min.) is sufficient for subjects to reach steady state (Poole and Richardson, 1997). We calculated metabolic power (Watts) for each trial using a standard equation (Brockway, 1997). We subtracted the metabolic power for standing from all walking values and normalized these values for body mass to derive net metabolic power (Watts/kg).

RESULTS AND DISCUSSION
In support of our hypothesis, metabolic cost was lowest at the preferred width and increased substantially for both narrow and wide walking (Fig. 2). Subjects preferred to walk with a step width of 0.15 ($\pm$ 0.01 S.D.).

Our passive dynamic walking model predicted the energetic tradeoff between collision and control of lateral motion. In human

walking, there are factors other than collisions and control affecting metabolic cost (e.g. the cost of generating force, the cost of actively swinging the limbs), but our study shows that collisions and control may be a substantial component of the total cost of walking.
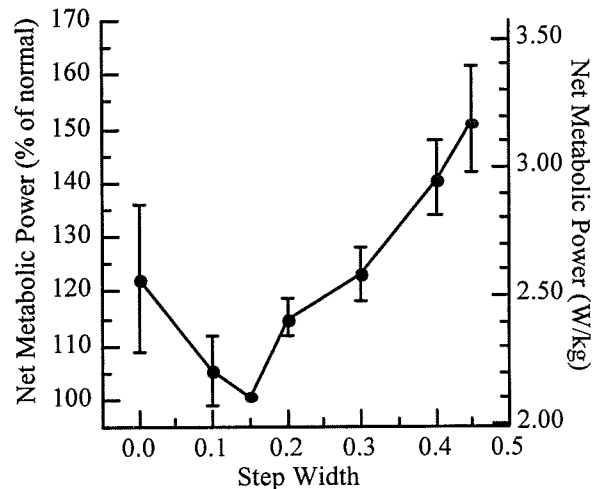
Fig. 2 Metabolic power consumption increases for wide steps due to collision losses, and increases for narrow steps due to costs related to balance control. Mean consumption ($\pm$ SEM) shown for each width. Step width is normalized for leg length.

Passive dynamic walking is relatively simple and the link between mechanical energy and metabolic cost is complex. In light of this, it is very encouraging that our analytical work predicted the large increase in metabolic cost with modest changes in step width; a non-intuitive finding.

REFERENCES
Brockway JM (1987) Hum Nutri: Clin Nutri 41C: 463-471
Kram R, Griffin TM, Donelan JM & Chang YH (1998) J Appl Physiol 85: 764-769
Kuo AD, Donelan JM & Kram R (1999) ASB Proc. Sub.
McGeer T (1990) Int J Robotic Res 9: 68-82
Poole DC & Richardson RS (1997) Sports Med 24: 308-320

A NEW ANIMAL MODEL OF FEMORAL HEAD OSTEONECROSIS, ONE THAT PROGRESSES TO HUMAN-LIKE BONY MECHANICAL FAILURE

Michael G. Conzemius[1], Thomas D. Brown[2], Yongde Zhang[2], and Robert A. Robinson[3]

[1] Department of Veterinary Clinical Sciences, Iowa State University, Ames, IA
[2] Departments of Orthopaedic Surgery, and [3]Pathology, University of Iowa, Iowa City, IA
Email: tom-brown@uiowa.edu

INTRODUCTION

Orthopaedic management of femoral head osteonecrosis (ON) remains a major surgical challenge, since most cases progress inexorably to mechanical collapse of weight-bearing cancellous bone [1]. Total hip replacement has an alarmingly high rate of late prosthesis loosening in this generally young and active patient group. Various head-preserving surgical procedures have been advocated, but remain controversial, owing substantially to the lack of controlled prospective clinical trials. Several existing animal models (sheep, pygmy goats, horses, rabbits, rats, piglets, mature miniature swine, and various canine breeds) reasonably replicate the pathogenesis of early ischemic bone repair [2]. But, none of these animal models progresses to the all-important end stage of frank mechanical collapse for which orthopaedic intervention is required in humans.

We reasoned that a key limitation of existing animal osteonecrosis models, all of which are in quadrupeds and therefore capable of limited or non-weightbearing, might be their relatively undemanding biomechanical environment, as compared to the situation prevailing in the human hip. We hypothesized that an active bipedal animal model might therefore achieve bony collapse. We here report development of such a model: surgically induced femoral head osteonecrosis in the emu (*dromaius novaehollandiae*), a flightless, ostrich-like bird native to Australia.

PROCEDURES

Since the emu is a little-studied species, a pilot series (19 birds) was first necessary to document the bony and vascular anatomy, to develop reliable anesthesia and recovery protocols, to explore the feasibility of alternative surgical approaches, and to document the efficacy of various insults in achieving focal bony ischemia. The procedure which evolved was to first sedate with Telazol® (7.5 mg/kg , IM) and xylazine (7.5 mg/kg, IM). Sedation was delivered by via blowpipe, since the birds were hazardous to handle when alert. Induction to anesthesia was performed with diazepam (1 mg/kg, IV). Following intubation, anesthesia was maintained with isoflurane in oxygen., and perioperative antibiotics (Cefazolin, 25mg/kg, IV) were started. The surgical procedure required approximately one hour, working through a ventral approach. Using careful blunt and sharp dissection, the iliacus muscle was reflected to expose the antero-medial aspect of the hip joint capsule. The capsule was incised, and a periosteal elevator was used to ablate all accessible capsular attachment to the neck. The medial circumflex femoral artery and vein (all major branches) were ligated with hemoclips. A 4.5mm serrated-tip drill guide was then used to access the infero-medial aspect of the head through a large, serendipitously located transcortical foramen. An approximately 20-second stream of pressurized liquid nitrogen was then delivered through this portal into the metaphyseal and epiphyseal cancellous bone, followed by a saline flush in order to thaw the frozen, visibly whitened bony bed.

Three repetitions of this internal freeze/thaw cycle were performed, interspersed with three episodes of delivering 20-second liquid nitrogen streams extracortically to the femoral head/neck junction. The foramen was then sealed with bone wax.

RESULTS AND DISCUSSION

Most animals were able to ambulate within 1 to 2 hours after recovery. After 2 weeks of postoperative stall confinement, they were moved to a free-roaming fenced outdoor enclosure. Both in postoperative confinement and especially in their outdoor enclosures, the birds were impressively active. No animals were lost from infection. In 16 subsequent survival birds, onset of lameness in the operated limb occurred at 11 to 16 weeks postoperatively in 13 birds, and at 21 weeks in a 14th. At necropsy, trabecular collapse and fracture were grossly evident throughout the freeze-killed region. Histologically (Fig. 1), normal marrow (NM) was replaced by fibrotic marrow (FM), with many trabeculae showing intense osteoclastic activity (scalloping), culminating in resorption and microfracture (R/Fx). On higher magnification (lower panels), empty lacunae (EL) are seen instead of the osteocyte-filled lacunae (OFL) normally present.
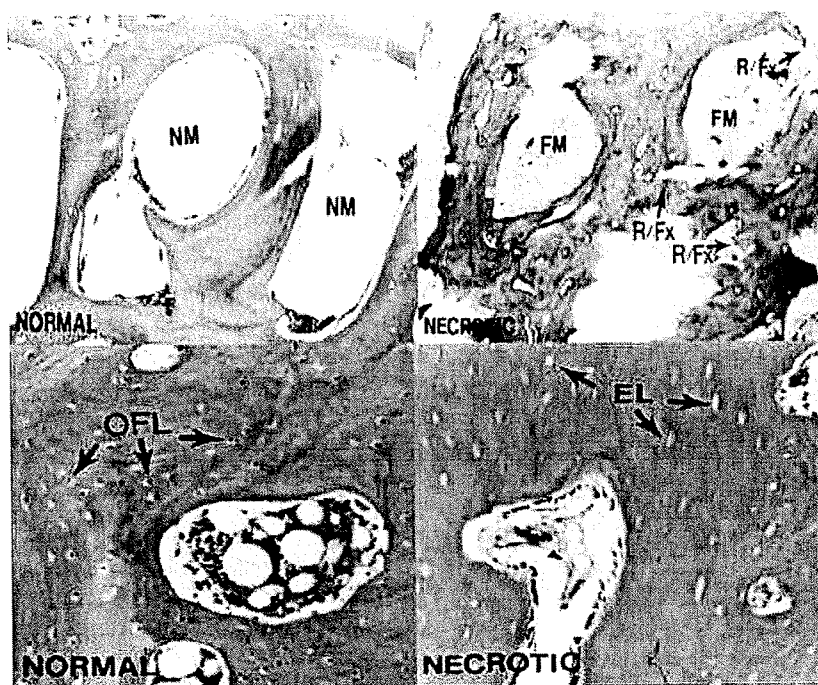
SUMMARY

The observed functional impairment and histological changes strongly support the hypothesized progression to collapse in this novel bipedal model of osteonecrosis. This success opens the way for systematic investigation of surgical interventions advocated to arrest collapse in human ON.

REFERENCES

[1] Brown, T.D. et al. (1993). *J. Bone & Joint Surg. 75A*, 1358-1367.

[2] Urbaniak, J.R., and Jones, J.P., (1997) *Osteonecrosis*, Rosemont IL (AAOS).

MECHANICAL EFFECTS OF EQUINE METACARPAL FUSION: FE PREDICTIONS

Clifford M. Les[1,2,3] and Joyce H. Keyak[4]

[1] J.D.Wheat Veterinary Orthopedic Research Laboratory, University of California, Davis
[2] NASA Ames Research Center, Moffett Field, CA
[3] Bone and Joint Center, Henry Ford Hospital, Detroit, MI
[4] Biomechanics Research Laboratory, UCI Medical Center, Orange, CA
Email: les@bjc.hfh.edu

INTRODUCTION

Bony fusion between the equine 3rd metacarpal bone and the 2nd and/or 4th metacarpal bones is a process that occurs preferentially on the medial side, is usually bilaterally symmetrical, occurs preferentially to animals in athletic occupations, and is often subclinical (Les, 1995). In this study, we modified a series of 3-D finite-element (FE) models of the metacarpus to allow for different fusion patterns, and examined the effect of fusion pattern on structural bending under several loads. Our hypothesis was that fusion would serve to limit the direction of bending under a variety of loading conditions.

METHODS

Three-dimensional FE models of the left metacarpus, previously developed and validated from QCT data of 8 horses (Les, 1994, 1997b) (1-5yr), were modified to define the lateral and medial intermetacarpal ligaments. Bone material was modeled as isotropic 3-mm cubes, with the elastic modulus computed from the K2HPO4 equivalent density of the corresponding QCT voxels (Les, 1994). Where anatomically appropriate, cubic elements were split into wedges, but the total number of nodes in each iteration of a model remained constant. Material properties of unfused ligaments were defined as a no-compression, isotropic material, G=50MPa, E=1GPa, using previous results from shear testing of the bone-

ligament-bone complex (Les, 1998). Fused ligaments were defined as an isotropic material, E=12GPa. Five fusion strategies were examined: (a) Unsplit (original model), (b) Unfused, (c) partially-fused (medially), (d) partially-fused (laterally), and (e) Fused medially and laterally (full fusion).

Models were constrained distally, and 5 different 15kN (3BW) distributed loads were placed proximally: (1) Axially-directed, (2) directed 5 degrees dorsally, (3) directed 5 degrees palmarly, (4) directed 5 degrees laterally, and (5) directed 5 degrees medially.

Maximum transverse-plane centroid displacement in the dorsal and sagittal planes was examined as a function of load and fusion status, using a 2-way repeated-measures ANOVA.

RESULTS

There was no significant effect of fusion status in structural behavior under dorsal loading, in either the dorsal or sagittal planes. Under other loading conditions, medial fusion tended to stabilize the structure, and lateral fusion tended to destabilize the structure, in the dorsal plane (Fig.1), with unfused and fully-fused models having intermediate dorsal stability. Full fusion had significant but small effects on stability of the structure in the sagittal plane over the unfused models, with partially-fused and unsplit models having intermediate sagittal effects.

DISCUSSION

The cross-sectional shape and distribution of material properties in the equine metacarpus may serve to enhance sagittal bending, and to stabilize the structure in the dorsal plane, under a variety of loads (Les, 1997a). These data suggest that one effect of bilateral medial fusions commonly seen in young athletic animals may be to further stabilize the structure in the dorsal plane. Subsequent lateral fusions, when they occur, would appear to destabilize the structure in the dorsal plane, and may result from a different biomechanical or pathological mechanism.

Limitations include the isotropic representation of material properties; the low level of mesh refinement in the ligament region (hence our approach of evaluating only the behavior of the entire structure), and the all-or-nothing fusion status of the ligament representation. The effect of the more-common localized fusion on structural bending behavior remains to be examined; these models represent a worst-case fusion scenario.

REFERENCES

Les et al. (1994), JOrthopRes 12:822-833

Les et al. (1995), AJVR 56:1421-1432

Les et al. (1997a), JBiomech 30:355-361

Les et al. (1997b), JBiomech 30:737-742

Les et al. (1998), ProcORS 44:1157

ACKNOWLEDGEMENTS
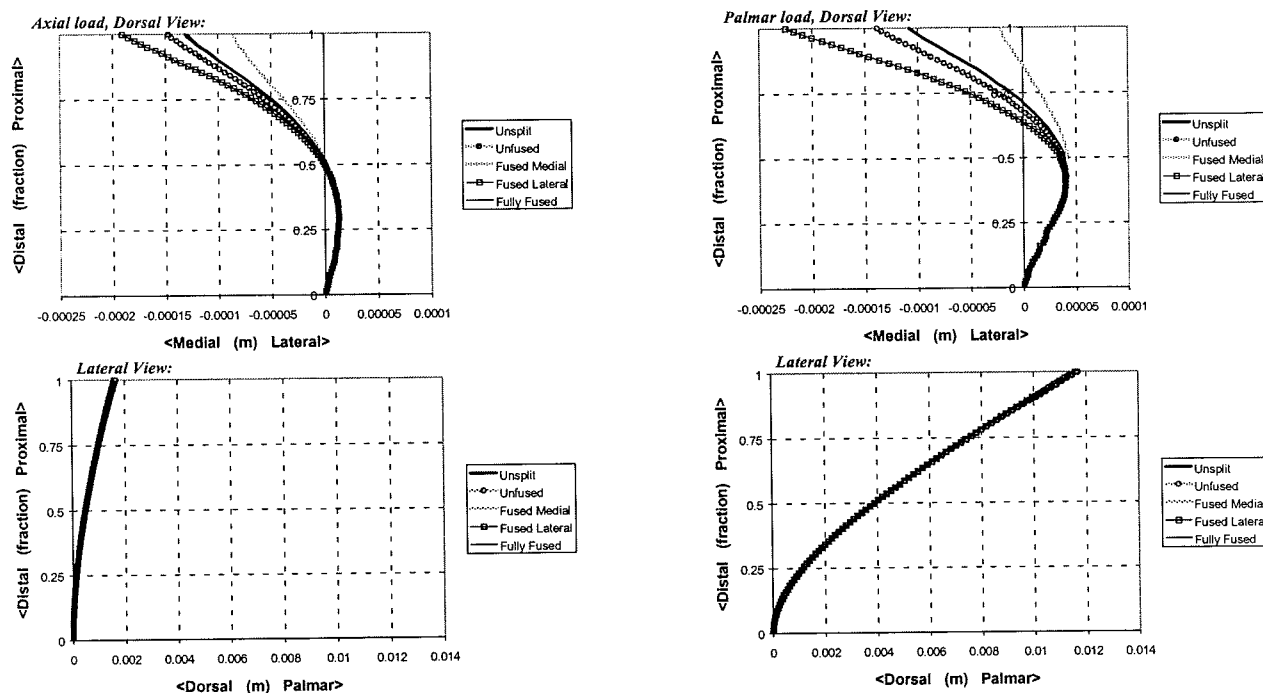
Fig.1: Centroid traces for 5yo Thoroughbred gelding under axial (left) and palmar (right) 15kN distributed load

EFFECTS OF GROUND BASED VIBRATION ON FRACTURE HEALING

S. Wolf, P. Augat, K. Eckert-Huebner, A. Laule, G. Krischak, L. Claes

Institut fuer Unfallchirurgische Forschung und Biomechanik, Universitaet Ulm, Germany

Email: steffen.wolf@medizin.uni-ulm.de Web: http://www.biomechanics.de

INTRODUCTION

Since Rubin and McLeod found an osteogenous effect for high frequency low magnitude mechanical stimuli, it's application for the external stimulation of the fracture healing process has been discussed. The stimulation system for the fractured limb should ideally be independent from the osteosynthesis system. The aim of this study was to investigate the stimulating effect of low magnitude high frequency interfragmentary movements (IFM) generated by vertical ground based vibration on the healing of experimental fractures.

PROCEDURES

A 3 mm transverse osteotomy was performed in the mid-diaphysis of the metatarsus in 12 sheep and stabilized with a custom designed, extremly rigid circular fixator frame. In 6 sheep micromovement was externally applied to the osteotomy by a vibration platform. The other sheep received no external stimulation and served as control group. Vertical displacement of the vibration platform was 1 mm, resulting in an IFM in the order of 0.02 mm, measured by a displacement transducer mounted to the fixator frame. External stimulation was performed at 20 Hz for 6,000 loading cycles each day from two weeks postoperatively to the end of the healing period of 8 weeks. Healing was assessed post mortem radiographically (bone mineral content (BMC) and cross sectional area (CSA) by peripheral quantitative computed tomography (pQCT)) and mechanically (three-point bending). To detect statistical differences between the groups a Wilcoxon test was performed.

RESULTS AND DISCUSSION

The mean values of the stimulated group for both BMC and CSA were slightly higher (17% and 11%, respectively) than those of the control group, although the radiographic results did not show significant differences between the groups. In addition, there were no statistical differences in the mechanical stability between the control group and the stimulated group.

The results of the present study showed no significant acceleration of the fracture healing process by external mechanical stimulation with low magnitude high frequency conditions. Although the fracture fixation was extremly rigid, the mechanical stimulus due to weight bearing was sufficient for an obvious callus formation even in the unstimulated control animals. The estimation of the fracture movement during weight bearing under rigid fixation resulted in IFMs in the order of the stimulation magnitude. These findings indicate that even very low magnitudes of IFM promote bone healing, that is difficult to further enhance by additional mechanical stimulation. Therefore, the indication for a clinical usage of external mechanical stimulation is limited to those patients, who can not load their limbs.

SUMMARY

In an animal experiment the hypothesis that externally applied interfragmentary movements of high frequency and low magnitude enhance fracture healing was investigated. The movements were applied externally to the fractured limb by a ground based vibration system. Healing was assessed post mortem by radiographic and mechanical investigations. The results showed no significant enhancement of the fracture healing process. Therefore, the clinical usage of external mechanical stimulation is limited.

REFERENCES

Rubin, C.T., McLeod, K.J. (1994).*Clin Orthop*, **298**, 165-174.

ACKNOWLEDGEMENTS

GAIT ADAPTATIONS IN TOTAL HIP REPLACEMENT PATIENTS ARE ASSOCIATED WITH REDUCED HIP CONTACT FORCES

Kharma C. Foucher[1,2], Debra E. Hurwitz[1], Thomas P. Andriacchi[1,3]

[1]Department of Orthopedic Surgery, Rush Medical College, Rush-Presbyterian-St. Luke's Medical Center, Chicago, Illinois
[2]Department of Bioengineering, University of Illinois at Chicago
[3]Department of Mechanical Engineering and Functional Restoration, Stanford University
Email: kfouch1@uic.edu

INTRODUCTION

Long term outcome of total hip replacement (THR) surgery is influenced by the loading environment at the hip. Despite excellent clinical results, the gait of THR patients does not return to normal, with the peak external hip adduction moment and hip range of motion significantly less than normal (Foucher et al., 1998). The external hip adduction moment is reflective of net abductor muscle activity, muscles that generate large forces during walking. This study examined the effect of these gait adaptations on the peak hip contact force with emphasis placed on relating the external adduction moment to the peak hip contact force, using a previously published analytical model (Foucher et al., 1999). The hypothesis tested was that THR patients walked with significantly reduced hip joint contact forces as compared to normal subjects, and that the forces significantly correlated with the external hip adduction moment.

PROCEDURES

To examine the effects of the gait adaptations on the hip contact force, 17 THR patients and 17 normal subjects with comparable age, height, and weight were studied. The THR patients all received a primary total hip replacement at least one year prior (15±3 months, Harris hip score

94±10). Hip joint kinematics and kinetics were calculated using data from an optoelectronic passive marker system and force plate (Andriacchi et al., 1997). A representative walking trial at 1 m/s (1.02 ± 0.08 m/s) was analyzed.

At every ten percent of stance and at the peak moments a parametric range of muscle forces and resulting contact forces were analytically modeled (Foucher et al., 1999; Foucher et al., 1998). An analytical Hill based muscle model of the lower extremity was used to simulate the maximum muscle moments (Delp et al., 1990) and the parametric model varied the individual activation levels of the muscles such that the external moments were balanced. The median value of the range of forces at each point of interest was calculated and the peak median force throughout stance was computed and expressed as multiples of the subject's body weight (BW) (Fig. 1). Student's t-tests were used to identify differences in the peak median contact force and in external moments between THR and normal groups, while Pearson correlations were used to identify significant correlations between the hip adduction moment and peak median contact force ($\alpha < .05$).

RESULTS AND DISCUSSION

The peak median hip contact force was significantly reduced in THR patients (3.1 ±

0.6 BW) as compared to normal subjects (3.6 ± 0.5 BW) (p=.016). In the THR group, the reduced contact force was significantly correlated with their adduction moment (R= .698, p<.002) (Fig. 2), which was significantly less than normal (p= .007). The adduction moment was also a significant predictor of peak contact force in the normal subjects (R=.729, p = .001).
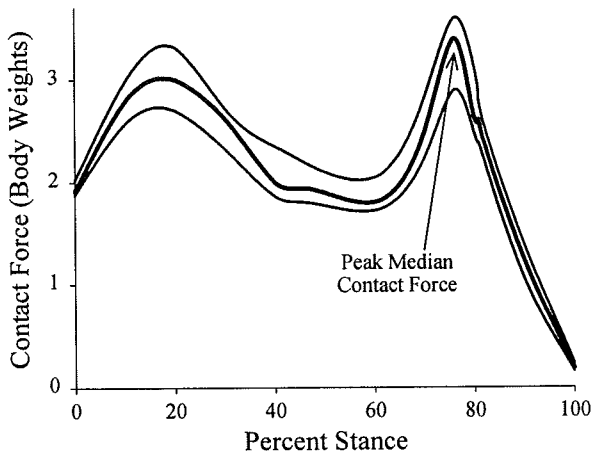
Figure 1: The median hip contact force during the stance phase of the gait cycle for a representative total hip replacement patient is shown as a thick line. Thin lines show the range of solutions obtained from the parametric model.

Analytically modeled contact forces for the THR patients (1.9 to 4.1 BW) were in close agreement with *in vivo* data from several investigators summarized by Bergmann et al. (1.5 to 4.5 BW) (1993). The reduced hip contact force was related to the reduced adduction moment in the THR patients, a common gait adaptation among THR patients. Previously we have shown that the reduced adduction moment was not related to the preoperative value and thus is not likely a learned response. We have also shown that the adduction moment was not related to the joint geometry which was not significantly altered after surgery (Foucher et al., 1998). It is possible that residual muscle weakness may be a contributing factor to this gait adaptation. Regardless of

the underlying cause, the current data show that this gait adaptation is a mechanism that reduces the forces on the implant.
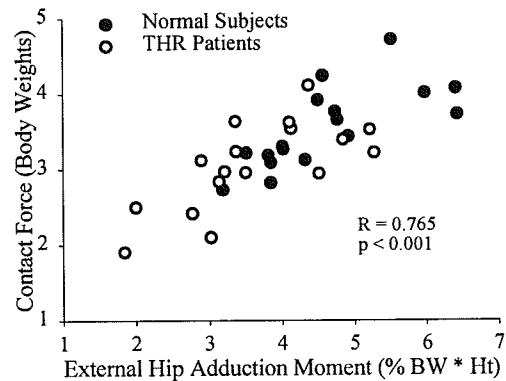
Figure 2: The peak median hip contact force was significantly correlated with the peak external hip adduction moment. The contact force and adduction moment of the THR patients (o) were both reduced compared to the normal subjects (•), p<.016.

SUMMARY
Data from this study suggest that a reduced adduction moment may be a mechanism to reduce forces at the hip joint, which at high levels, may lead to implant loosening. Finite element models and other analyses of bone remodeling, wear, or implant loosening should account for the fact that THR patients do not have normal gait and hip contact forces even among those with an excellent clinical outcome.

REFERENCES
Andriacchi, T.P. et al. (1997). Basic Orthopedic Biomechanics, 37-69.
Delp, S.L. et al. (1990). *IEEE Biomed. Eng.*, 757-67.
Foucher, K.C. et al. (1998). *Gait and Posture* 7, 158-9.
Foucher, K.C. et al. (1999) *Advances in Bioengineering ASME*.

THE EFFECT OF SURFACE FINISH ON THE BEHAVIOR OF TAPERED CEMENTED TOTAL HIP STEMS

Keith T. Hustosky [1,2], Timothy L. Norman [1,2], Vincent L. Kish [2], Thomas A. Gruen [2] and J. David Blaha [2]

[1] Department of Mechanical and Aerospace Engineering and [2] Department of Orthopedics, West Virginia University, Morgantown, West Virginia
Email: khustosk@wvu.edu   Web: www.hsc.wvu.edu/som/ortholab

INTRODUCTION

Aseptic loosening has been identified as a major threat to the long term success of cemented total hip stems (Schulte et al., 1993). Several studies have implicated debonding at the stem-cement interface as the cause of aseptic loosening (Harrigan et al., 1992; Jasty et al., 1991). Many prosthesis designs try to improve the strength of the stem-cement interface by using stems with a rough surface. Another approach is to incorporate stem-cement interface debonding into prosthesis design by using stems with a highly polished surface. The goal of this study is to compare the pull-out loads and axial displacements of stems that differ only in surface roughness to determine the effects of surface finish on total hip stem behavior.

PROCEDURES

Tapered, collarless total hip stems were inserted into nine embalmed cadaveric femora using Palacos R PMMA bone cement (Merck; Darmstadt, Germany). A plug inserted into the femoral canal prevented cement from encapsulating the distal 10 mm of the stem. Seven specimens had a polished surface finish ($R_a = 0.14$ µm) and two had a matte surface finish ($R_a = 3.3$ µm). After curing, the specimens were potted and mounted in a load frame on a servohydraulic testing machine. Each stem was subjected to a static load corresponding to single-legged stance (12° Adduction, 0° Flexion, Joint Load = 1400 N, Abductor Muscle Force = 880 N) for 24 hours. Axial displacement of the stems was measured using a miniature differential voltage displacement transducer. After loading, a tensile axial force was applied to the stems via a pull-out fixture (Hustosky et al., 1998).

RESULTS AND DISCUSSION

The mean pull-out load of the seven polished stems was 1238 N ($\pm$400 N). The polished stems were extracted from the cement mantle without damaging the cement, bone or fixture. The matte finish stems did not pull free of the cement; in both cases the femur fractured within the mounting fixture before the stem could be removed from the cement mantle. The mean failure load of these two specimens was 6743 ($\pm$654 N) (Figure 1). The mean distal displacement of the matte finish specimen after 24 hours was 0.04 mm ($\pm$0.014 mm) and the mean displacement of the polished finish stems after 24 hours was 0.33 mm ($\pm$0.064 mm).
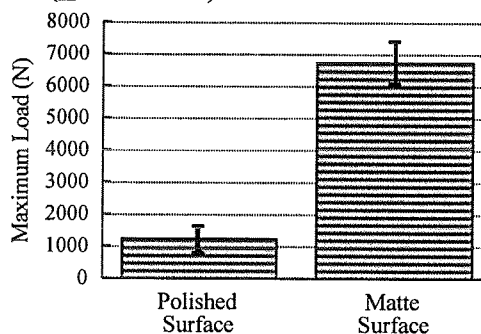
Figure 1: Mean failure loads of polished and matte finish stems. The error bars indicate standard deviation.

A finite element model of the implanted stem was generated (Saligrama et al., 1996). The model includes viscoelastic behavior of PMMA cement and load conditions identical to those applied in this study. The model also includes interface elements which are used to analyze three stem-cement interface conditions: perfect bond, debonded with a friction coefficient of 0.22 and completely debonded (friction coefficient = 0.0). The measured and calculated displacement data may include displacement due to elastic

deformation, viscoelastic behavior of the cement and slip of the prosthesis within the cement mantle. Comparison of experimental displacement data to finite element results (Figure 2) suggest that the matte finish specimens achieved a well-bonded stem-cement interface while the polished specimens had debonded at the stem-cement interface with a friction coefficient less than 0.22.
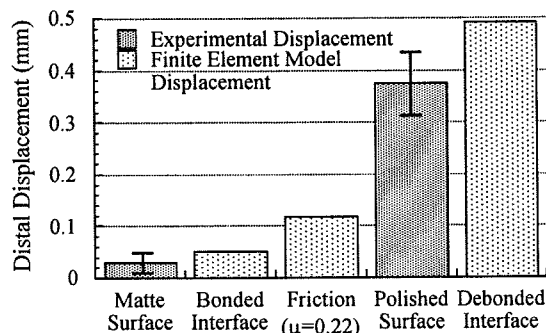
Figure 2: Comparison of experimentally measured distal displacement of matte and polished surface stems to finite element model results.

Based on the comparison of stem displacements and the mode of stem pull-out, one can deduce that the pull-out load of the polished stems is a measure of the taper-lock effect brought about by creep induced subsidence of the tapered stem within the cement mantle. Theoretically, the pull-out load of matte finish stems measures the static shear strength of the stem-cement or cement-bone interfaces. In this study, failure of the bone occurred before failure of the interfaces. Therefore, a direct comparison of pull-out strengths, while useful for investigating mechanical behavior of total hip stems, should not be the sole means of evaluating total hip stems with different surface finishes. The relatively low pull-out loads of the polished stems do not necessarily indicate poor fixation. The high radial compressive loads generated by the taper-lock effect of the stem within the cement mantle are considered beneficial to maintaining interface integrity (Miles, 1990) and act to provide implant stability (Hustosky et al., 1998; Lee, 1990). On the other hand, the high failure loads of the matte finish stems mean that the stem-cement and bone-cement interfaces are subjected to high shear loads. Ling (1992) identified this as destructive loading and clinical evidence (Gardiner and Hozack, 1994) has suggested that this may put the

implant at risk for early clinical failure. The cyclic nature of in vivo loading would most likely be more detrimental to the interfaces of the matte surface stem and may cause more subsequent debris generation compared to the polished stem.

SUMMARY

Results of this study illustrate the relationship between surface finish and interface strength using polished and matte finish stems. The polished stems debonded at the stem-cement interface and achieved fixation through a mechanical taper-lock of the stem within the cement mantle. The matte surfaced stems achieved fixation through a mechanical interlock between the stem and cement mantle. While both surface finishes seem to allow for a means of stable fixation, the long term effects of the high shear loads at the stem-cement and cement-bone interfaces of the matte surface specimens may prove detrimental to the long term success of THA.

REFERENCES

Gardiner, R.C., Hozack, W.J. (1994) *JBJS*, **76B**, 49-52.
Harrigan, T.P., et al.(1992) *JOR*, **120**, 134-144.
Hustosky K.T. et al.(1998) *44th ORS*, 761.
Jasty, M. et al.(1991) *JBJS*, **73B**, 551-558.
Lee, A.J.C. (1990) Chapter in *Implant Bone Interface*, Springer-Verlag, N.Y., 131-135.
Ling, R.S.M. (1992) *CORR*, December ,73-83.
Miles A.W.(1990) Chapter *in Implant Bone Interface*, Springer-Verlag, N.Y., 137-141.
Saligrama,V.C., et al.(1996)*42nd ORS*, 422.
Schulte, K.R., et al. (1993)*JBJS*, **75A**, 961-975.

ACKNOWLEDGMENTS

MECHANICALLY FAVORABLE BONE REMODELING IN ROTATOR CUFF ARTHROPATHY PATIENTS WITH GOOD FUNCTION

Travis J. Klein,[1] Patrick B. Ebeling,[2] Donald D. Anderson,[1,2] and Daniel D. Buss[2]

[1] Biomechanics Laboratory, Minneapolis Sports Medicine Center, Minneapolis, MN

[2] Department of Orthopaedic Surgery, University of Minnesota, Minneapolis, MN
e-mail: danders6@fairview.org web: msmc.org

INTRODUCTION

Rotator Cuff Arthropathy (RCA) is an arthritis that develops in the shoulder after a massive rotator cuff tear (Neer et al., 1983) (Figure 1). The torn cuff allows the humerus
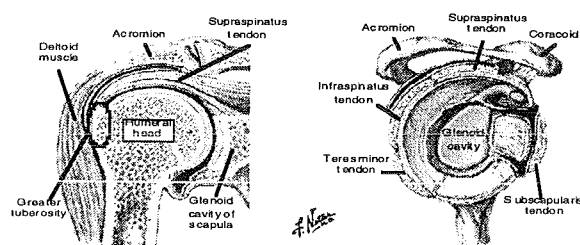
Figure 1. Anatomy of the rotator cuff.

to sublux superiorly, leading to eccentric glenoid loading and abnormal articular wear. Most RCA patients experience significant pain and shoulder dysfunction.

A subset of RCA patients retain shoulder function and experience relatively little pain in the absence of surgical intervention. It is presumed that favorable adaptive bone remodeling has contributed to this group's lack of symptoms. Our objective is to describe the changes in bony geometry that have taken place in their shoulders.

PROCEDURES

Seven shoulders in six RCA patients with good shoulder function were studied. A full radiographic evaluation was performed on each shoulder, including plain radiographs, MRI, and CT. CT scans were obtained in 1mm slice spacing through the humeral head and at 5mm through the humeral shaft.

The proximal humerus was digitized in each CT slice and reconstructed to generate a 3-D surface for each shoulder. Centroids were calculated for the proximal humeral shaft and were best-fit with a line to yield the proximal
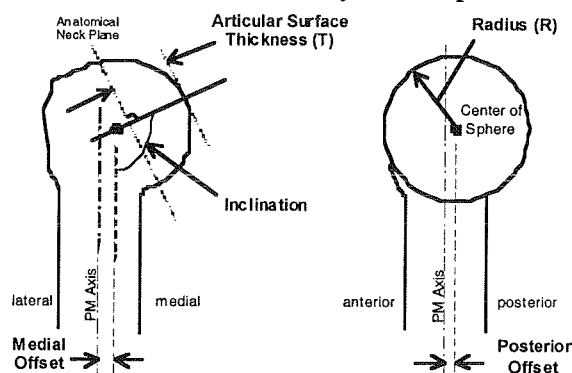
Figure 2. Schematic of humeral parameters.

metaphyseal (PM) axis (Figure 2). Articular surface edge data were best-fit to define the anatomical neck plane, whose normal defined humeral head inclination. Digitized humeral head data were best-fit to a hemisphere (Soslowsky et al., 1992). Best-fit parameters and statistical goodness-of-fit values were recorded. The origin of the fitted hemisphere was used to calculate medial and posterior offsets of the humeral head with respect to the PM-axis.

A total of five normal shoulder CT scansets were processed for comparison. A student t-test was used, with $p < 0.05$ for significance. CT scans of both humeri for the male and female of the Visible Human Project™ were obtained from the National Library of Medicine. Also, high resolution CT scans of a right humerus were obtained from the Laboratory of Human Anatomy and Embryology, University of Brussels (ULB), Belgium.

RESULTS AND DISCUSSION

An average of 1030 points were used in surface fitting each head (Figure 3). Results are summarized in Table 1. The RCA column includes data from RCA patients who have retained good function with minimal pain. The 'Our Normals' column reflects results using CT's obtained from the internet. The 'Published Normals' column presents published values for normal shoulders (all values but T/R ratio - Boileau and Walch, 1997 (n=65); T/R ratio - Pearl and Volk, 1996 (n=21)).

Table 1. Comparison of humeral head features based on hemispherical fit.

	RCA (n=7)	Our Normals (n=5)	Published Normals
Radius (mm)	28.2 ± 1.5*	24.1 ± 2.2	23.1 ± 2.7
T/R ratio	0.68 ± 0.08	0.78 ± 0.04	0.73 ± 0.04
Inclination(°)	123.1 ± 6.8	125.1 ± 8.3	129.6 ±0.9
Posterior Offset (mm)	3.3 ± 2.4	1.4 ± 0.9	2.6 ± 1.8
Medial Offset (mm)	2.7 ± 2.3	5.0 ± 2.5	6.9 ± 2.0

* Values are the mean ± standard deviation

The spherical fits had an average r^2 value of 0.90 for RCA shoulders and 0.94 for normals. These high r^2 values indicate good approximations to the surfaces, with the remodeled heads slightly lower due to osteophytic growth.

The humeral heads of the RCA study group have all remodeled, forming a larger radius of curvature for articulation compared to normal (p<0.01). This larger radius likely accommodates more stable articulation with the undersurface of the acromion. The surface models of the RCA shoulders clearly show a rounding off of the greater tuberosity as well (Figure 3).

The RCA patients' shoulders appear to have remodeled their humeral heads to be a smaller portion of a hemisphere, indicated by
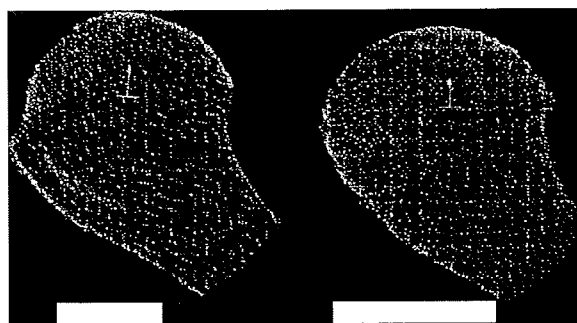
Figure 3. Surface geometry reconstructed from CT scans of humeral heads.

differences in the ratio of articular surface thickness to the radius of curvature (p<0.05). This difference in proportions could explain why the clinical practice of surgically inserting an oversized prosthetic head does not significantly improve function, but additional study is required prior to drawing this conclusion.

Possibilities for future study include analysis of the surface data for the glenoid and acromion, which have already been digitized. Extending our spherical fits to ellipsoidal surface fitting may better capture adaptive changes. Also, a larger number of RCA shoulders may be studied, including those with poorly functioning shoulders, allowing for a correlation between adaptive remodeling, pain, and function.

REFERENCES

Boileau, P. and Walch, G. (1997). *J. Bone Joint Surg. [Br]*, **79**, 857-865.

Neer, C.S. et al. (1983). *J. Bone Joint Surg. [Am]*, **65**, 1232-1244.

Pearl, M.L. and Volk, A.G. (1996). *J. Shoulder Elbow Surg.*, **5**, 320-326.

Soslowsky, L.J. et al. (1992). *Clin. Orthop. Rel. Research*, **285**, 181-190.

ACKNOWLEDGMENTS

KINEMATIC DIFFERENCES BETWEEN HIGHLY-SKILLED AND LESS-SKILLED BASEBALL PITCHERS

Glenn S. Fleisig[1], Tomoyuki Matsuo[2], Rafael F. Escamilla[3],
Steve W. Barrentine[1], and James R. Andrews[1]

[1] American Sports Medicine Institute, Birmingham, Alabama
[2] School of Health & Sports Sciences, Osaka University, Osaka, Japan
[3] Department of Surgery, Duke University, Durham, North Carolina
Email: glennf@asmi.org   Web: www.asmi.org

INTRODUCTION

A primary objective of baseball pitchers is to maximize ball velocity. In her review of throwing movements and injuries, Atwater (1979) stated that mechanical variables most likely play an important role in why some athletes throw harder than others do. In the twenty years since, this statement has been widely accepted and the throwing mechanics of elite athletes have been well-documented (Fleisig, Barrentine, et al., 1996; Morriss & Bartlett, 1996). However no study has quantified what mechanical differences, if any, exist between elite and less-skilled throwers. The purpose of this study was to investigate kinematic and temporal differences between baseball pitchers who generate high and low ball velocity.

PROCEDURES

Data were collected from a sample of 127 healthy college and professional baseball pitchers. Based upon fastball velocity generated by this sample (36.1 ± 1.9 m/s), 52 of these pitchers qualified as subjects for this study. The 52 pitchers were divided into two groups: the "FAST" group (n=29) who's ball velocity was more than one standard deviation above the sample mean, and the "SLOW" group (n=23) who threw more than one standard deviation below the sample mean. Ball speeds for the FAST and SLOW groups were 38.4 ± 0.6

m/s and 33.2 ± 0.9 m/s, respectively. Kinematic and temporal data were collected in a biomechanics laboratory with a procedure previously described (Fleisig, Escamilla, et al., 1996). With this procedure, reflective markers were attached to 14 bony landmarks on the subject. After stretching and warming up, the subject threw ten fastball pitches off an indoor pitching mound toward a strike zone ribbon. The ribbon was located over home plate at a regulation distance of 18.4 m from the pitching rubber. Ball velocity was measured with a Jugs radar gun. A four-camera 200 Hz automatic digitizing system (Motion Analysis Corporation, Santa Rosa, CA) was used to quantify each pitcher's motion. Eleven kinematic and eight temporal parameters were calculated using methods previously described (Fleisig, Escamilla, et al., 1996). Temporal variables were expressed as percent of pitch complete, scaled from the instant the front foot contacts the mound (0%) to the instant the ball is released (100%). Student's t-test (p<0.01) was used to investigate differences between the FAST and SLOW groups.

RESULTS AND DISCUSSION

Kinematic and temporal data are presented in Table 1. The FAST group achieved greater external rotation of the throwing shoulder during arm cocking. The FAST group also moved the trunk farther forward

during the delivery, demonstrated by increased knee extension and increased trunk tilt forward. Greater arm cocking coupled with greater trunk drive in the FAST group most likely created a longer path for the hand to be accelerated forward and therefore an opportunity for greater ball velocity. Another primary source of ball velocity is shoulder internal rotation velocity generated by active and passive torques about the shoulder (Feltner and Dapena, 1986). The greater external rotation produced by the FAST group may increase the stretch-shortening action of the internal rotators, and consequently contribute to greater ball velocity. Although two temporal parameters showed statistical differences between the two groups, these differences of 2% represented approximately 0.003 s. Since data were collected in 0.005 s intervals, these temporal differences have minimal practical relevance.

SUMMARY

Pitchers who generate greater ball velocity utilize greater shoulder external rotation and greater trunk drive during delivery. By emphasizing these aspects of pitching mechanics, coaches may be able to help pitchers improve their ball velocity.

REFERENCES

Atwater, A.E. (1979). *Exer Sports Sci Rev*, **7**, 43-85.

Feltner, M., Dapena, J. (1986). *Int J Sport Biomech*, **2**, 235-259.

Fleisig, G.S., Barrentine, S.W., et al. (1996). *Sports Med*, **21**, 421-437.

Fleisig, G.S., Escamilla, R.F., et al. (1996). *J Appl Biomech*, **12**, 207-224.

Morriss, C., Bartlett, R. (1996). *Sports Med*, **21**, 438-446.

Table 1: Maximum value and time of maximum value for kinematic parameters (Mean±SD). All time data expressed as percent of pitch complete.

	Maximum value		Time max. achieved	
	FAST	SLOW	FAST	SLOW
Pelvis linear velocity	2.1±0.4 m/s	2.3±0.3 m/s	-17±23 %	-15±24 %
Stride length at the instant of foot contact	87±6 %height	86±5 %height	-	-
Pelvis angular velocity	640±90 °/s	640±70 °/s	28±16 %	35±18 %
Shoulder horizontal adduction angular velocity	580±170 °/s	540±180 °/s	40±20 %	50±20 %
Upper torso angular velocity	1230±70 °/s	1180±100 °/s	51±7 %	53±12 %
Shoulder external rotation	**179±8 °**	**166±9 °**	81±5 %	81±4 %
Elbow extension angular velocity	2540±250 °/s	2350±320 °/s	**91±2 %**	**93±2 %**
Forward trunk tilt angular velocity	410±70 °/s	390±90 °/s	96±12 %	104±21 %
Lead knee extension during delivery	**17±11 °**	**3±13 °**	-	-
Forward trunk tilt at the instant of ball release	**37±7 °**	**29±11 °**	-	-
Shoulder internal rotation angular velocity	7720±1040 °/s	7350±1280 °/s	**102±2 %**	**104±2 %**

Significant differences (p<0.01) between FAST and SLOW group shown in **BOLD BLUE** and **BOLD BROWN**

HURDLE PREFLIGHT: A CASE OF DIMINISHING RETURNS?

Doris I. Miller, Aleksandra Zecevic and Graham W. Taylor

School of Kinesiology, University of Western Ontario, London, Ontario
Email: dimiller@julian.uwo.ca

INTRODUCTION

The major function of the approach and hurdle in springboard dives is to establish favorable conditions for the takeoff (board depression and recoil) that follows. Recently Boda (1996) drew attention to the fact that nontraditional techniques were being employed in an attempt to increase dive height. These techniques involve introducing a substantial period of flight immediately prior to hurdle support (Fig.1). The current study was undertaken to investigate to what extent hurdle preflight techniques (HPF) influence dive height.

PROCEDURES

The study consisted of temporal and linear kinematic comparisons of: [1] front jumps, front dives and reverse dives (3 reps each) executed by 11 collegiate level divers using both traditional (walking, running) (TRD) and HPF (leaping, jumping) approaches on 1-m; [2] front dives with limit on 3-m by 5 women using TRD and 5 employing HPF techniques in competition; and [3] dives from front and reverse groups by 1 diver who used HPF and TRD approaches in the '98 US nationals on 3-m. In all cases, standard biomechanical video data collection and analysis procedures were employed although the variables analyzed were not necessarily the same across all three parts of the study.

RESULTS AND DISCUSSION

Differences between TRD and HPF approaches in [1] based upon average values (3 reps x 3 dives x 11 divers) are presented in Table 1. The temporal advantage of HPF was ~ 3 x times greater for hurdle flight (0.077 s) than for the dive flight (0.026 s). Although all divers originally learned a TRD approach, 10 were using HPF in practice and competition at the time of the study. Therefore, the results could have been biased in favor of that technique.

Table 1. Differences in approach types [1].

	Final App. Step (m)	Hurdle		Dive Flight (s)
		Max. Dep.(m)	Flight (s)	
TRD	0.90	0.89	0.669	1.184
HPF	0.66	0.93	0.746	1.210
p <=	.01	.05	.001	.001

Although the two groups of 5 divers in [2] were not significantly different in terms of height, weight, fulcrum setting or dive score, some differences related to approach technique were found (Table 2).

Table 2. Differences in approach types in [2] based on 1 front dive with limit per diver.

	App. Max. Dep. (m)	Final App. Step (m)	Hrd. Supp. VVi (m/s)
TRD	0.04	1.21	-1.1
HPF	0.17	0.88	
p <=	.01	.001	.001

While downward velocity at the start of hurdle support (VVi) was greater for HPF divers, upward velocity at the end of this support period was the same for the two groups (3.1 and 3.0 m/s). During HPF, the board tip oscillated through 2 cycles requiring divers to 'catch' the board at the

beginning of hurdle support as well as at the beginning of the takeoff (Miller et al., 1998).

Data for the diver in [3] who used **HPF** for her front 1_ (103B) and 2_ (105B) pikes and **TRD** for her reverse dive (301B) and 2_ (305B) pike are presented in Table 3. The increased hurdle flight with **HPF** gave additional time to complete the armswing for her front 2_ pike whereas **TRD** assured greater consistency for reverse takeoffs. Vertical velocity at the end of takeoff was influenced by dive group and number of somersaults as well as approach type.

The results indicated that **HPF** techniques are characterized by greater board depression in final approach step support, a shorter final approach step and oscillation of the board tip during the actual flight prior to hurdle support. **HPF** techniques commonly produced longer hurdle flight times and thus greater downward velocities at the start of takeoff. They were also associated with short hurdles. **HPF** techniques appear to be more commonly used by female than male divers in elite competition.

Answering the challenge of comparing different techniques lies in conducting several studies with each contributing one or more pieces to the puzzle. Our results provided corner pieces to the emerging picture of **HPF**. The increase in flight time in [1] resulted in <.08 m gain in dive height. Among the divers studied, increase in vertical velocity at the start of the dive, if present, was not functionally significant. Depressing the board in the takeoff depends on a diver's ability to accelerate upward wrt the board as well as on translational KE from hurdle flight. Sanders & Wilson (1988) indicated that less than 60% of the variance in dive height could be attributed to the latter. Consistent with these observations, the present study suggested that **HPF** techniques produce diminishing returns in terms of increasing springboard dive height.

REFERENCES

Boda, W.L. (1996). *Inside USA Diving* 4(3), 8-9.
Miller, D.I. et al. (1998). *J. Sports Sciences,* **16**, 571-583.
Sanders, R.H. & Wilson, B.D. (1988). *Int. J. Sports Biomechanics,* **4**, 231-259.

ACKNOWLEDGMENTS

Table 3. Comparison of two approach techniques performed by the same diver [3].

Dive	App. Type	Step length (m)		Bd. Max. Depression (m)			Hrd. Flt. (s)	V. V. Takeoff (m/s)	
		App.	Hurdle	App.	Hurdle	Takeoff		Initial	Final
103B	**HPF**	0.76	0.24	0.23	0.50	0.71	0.717	-3.7	4.7
105B	**HPF**	0.71	0.24	0.23	0.49	0.73	0.751	-3.9	4.6
301B	**TRD**	1.00	0.40	0.04	0.41	0.70	0.634	-3.2	4.8
305B	**TRD**	0.99	0.38	0.03	0.42	0.73	0.667	-3.5	4.5
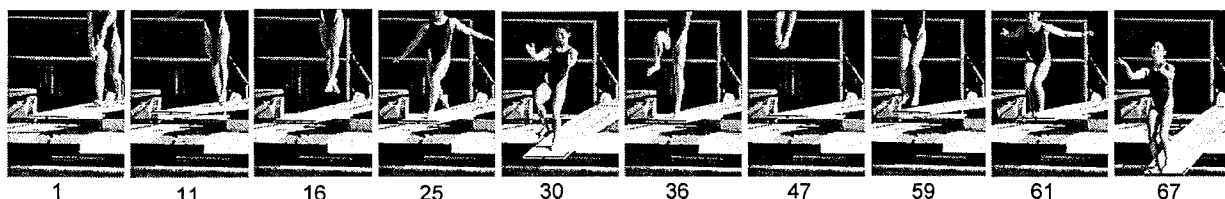
Figure 1. A leap **HPF** ((11-25)/60 s) used by an international diver preparing for a 105B on 1-m.

BIOMECHANICAL CHARACTERISTICS OF RUNNING IN ELDERLY MEN

Sicco A. Bus [1,2,3]

[1] Faculty of Human Movement Sciences, Vrije Universiteit, Amsterdam, The Netherlands
[2] TNO Institute for Industrial Technology, Eindhoven, The Netherlands
[3] The Center for Locomotion Studies, Penn State University, University Park, PA
Email: celos@psu.edu   Web: www.celos.psu.edu

INTRODUCTION
As a consequence of the running boom in the 1970's and because of the greater recent emphasis on physical activity being a contributor to a higher fitness level at older age, it is expected that the number of elderly runners (defined as >55 years of age) will grow substantially in the near future. Although considerable physiological and health related research has been done on the elderly running population, biomechanical studies on aged runners are scant. Therefore, the purpose of this study was to analyze the support phase biomechanical characteristics of running in the elderly and make a comparison with younger runners.

METHODS
Thirteen young (26.1 ± 3.9 years old, height: 1.83 ± 0.07 m, body mass: 74.9 ± 7.1 kg) and 16 elderly healthy, well trained, male runners (59.3 ± 3.2 years, 1.74 ± 0.06 m, 77.3 ± 8.0 kg, respectively) participated in the study. An infrared video based 4-camera Precision Motion Analysis System (100 Hz) was used to obtain 3 dimensional joint angular displacements of the right lower extremity and the vertical impact speed at heel strike. Simultaneously, the vertical and fore-aft ground reaction force (GRF) were determined with the use of a Kistler force plate. Running speed (RS), stride length (SL), and step frequency (SF) were also determined. Subjects were tested at two different running speeds: a preferred (PRS) and a controlled running speed (CRS) of 3.3 m/s. Subjects, wearing a standard running shoe, were instructed to run along a 17 meter long runway. t-tests compared total group means on statistical significance ($p < 0.02$, with Bonferroni adjustment). Correlation (r) values gave an indication for a relationship between two variables of interest.

RESULTS AND DISCUSSION
At the PRS, elderly subjects showed a significantly lower RS (3.34 vs. 3.77 m/s), shorter SL (2.41 vs. 2.91 m) and higher SF (1.30 vs. 1.38 Hz) than the young subjects. At the CRS, the elderly subjects still showed a significantly smaller SL (2.43 vs. 2.61) and higher SF (1.38 vs. 1.28). Differences in the anterior GRF (correlation with SL was 0.64 and 0.73 for the young and old, respectively) or the energy efficiency of running (Cavanagh & Kram, 1990) between the groups could be a cause for this.
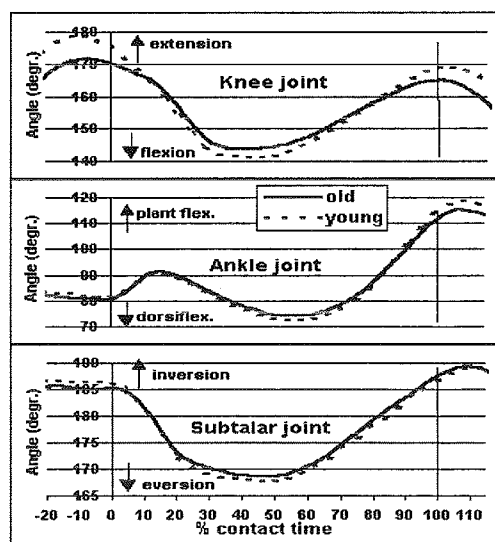
Figure 1. Knee, ankle and subtalar joint angles expressed as a function of time (in %)

The elderly runners showed significantly smaller ranges of motion and maximal and minimal values in ankle plantar/dorsiflexion and in particular in knee flexion/extension (Fig.1). A lower vertical and anterior GRF (many r's > 0.60), together with a increase in joint stiffness (Such et al.1975; Vandervoort et al.,1992) in the elderly may account for these differences. The differences in subtalar joint eversion and inversion were not significant. In contrast, the elderly runners showed a significantly higher vertical impact speed of the lower leg in the CRS condition (0.62 vs. 0.46 m/s).
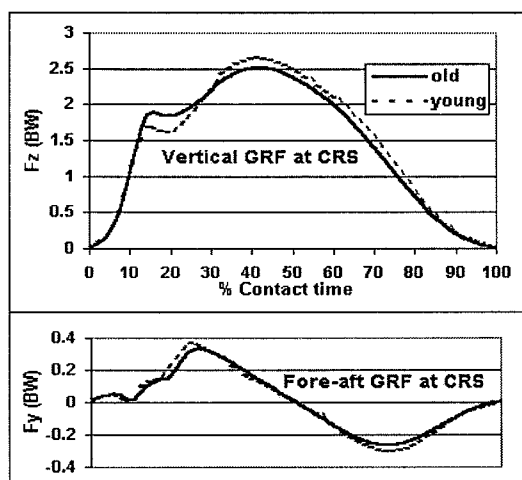
Figure 2. Vertical and fore-aft GRF expressed as a function of time (in %).

For the vertical and fore-aft shear GRF the elderly runners showed lower values on all variables except for the initial loading rate (109.5 vs. 88.4 BW/s) and impact force (1.92 vs. 1.72 BW) in the CRS condition (Fig.2). In spite of a shorter SL and a larger knee flexion angle at heel impact (both factors suggested to reduce impact), the values for these parameters were significantly higher in the elderly subjects, which means that the load on the musculo-skeletal system during running was larger for the elderly runners. The role that the higher vertical impact speed in the elderly runners could play in explaining these results (r with impact force = 0.75 and 0.38

for the young and old, respectively) needs more examination. Moreover, the reduction in shock absorbing capacity through atrophy of fat tissue underneath the heel (Edelstein, 1988; Gordon & Cuttic, 1994) and increased joint stiffness in the elderly could be major contributors.

The lower peak vertical and anterior GRF in the elderly subjects, mainly apparent at the PRS, may be related to RS, SL, SF and contact time. The role of a lower muscle strength in the leg extensors of the elderly (Murray et al.,1980; Vandervoort & McComas, 1986) in this context remains to be studied.

It was concluded that elderly and younger aged runners differ substantially in the biomechanical characteristics of running. Controlling running speed provides relevant information in this age group comparison. Future research should direct more attention to establishing direct relationships between biomechanical variables and factors such as muscle strength and joint stiffness in the elderly running population.

REFERENCES

Cavanagh, P.R., Kram, R. (1990). *Biomechanics of Distance Running*. Human Kinetics Publishers.

Edelstein, J.E. (1988). *Phys. Ther.*, **68**, 1882-1886.

Gordon, G.M., Cuttic, M.M. (1994). *South. Med. J.*, **87**, S36-S41.

Murray, M.P., et al.(1980). *Phys. Ther.*, **60**, 412-419.

Vandervoort, A.A., et al.(1992). *J. Gerontology*, **47**, M17-M21.

Vandervoort, A.A., McComas, A.J. (1986). *J Appl. Physiol.*, **61**, 361-367.

CHANGES IN VERTICAL GROUND REACTION FORCE DURING ENDURANCE RUNNING TO EXHAUSTION ON A TREADMILL

Darren Dutto and Gerald Smith
Biomechanics Laboratory, Oregon State University, Corvallis, OR 97331
Email: Gerald.Smith@orst.edu   Web: osu.orst.edu/dept/HHP/EXSS/index-biomech.html

INTRODUCTION

Several studies have measured kinematics during fatiguing runs, but there have been no studies that have measured ground reaction forces during endurance running to exhaustion, perhaps due to difficulties with force measurement during extended overground running.

There has been research investigating changes in reaction forces with fatigue. Nummela et al. (1994) found peak ground reaction force to be lower at the end of a 400 meter sprint run relative to a 20 meter sub-maximal run. Although significant differences were observed, these might be partially attributed to differences in running speed. Using upper-extremity stretch-shortening exercises, Gollhoher et al. (1987) found peak force and rate of force development to decrease and contact time to increase over 100 cycles. During running to fatigue, Verbitsky et al. (1998) found shank accelerations to increase during the run. Increased shank accelerations may be indicative of increased leg stiffness during heel strike and associated with increased impact forces.

A treadmill instrumented to measure vertical ground reaction forces provides an opportunity to examine ground reaction forces during endurance running. The treadmill allows speed control, measuring multiple, continuous steps, and sampling at specific intervals. This study will determine if vertical ground reaction forces change with endurance running to exhaustion.

PROCEDURES

Six male, trained, endurance runners (Age: 28 ± 8 yrs., VO_2 peak: 67.0 ± 3.9 ml/kg/min) performed a test run to exhaustion, at a speed approximately 80% of VO_2 peak (4.21 ± 0.35 m/s), on a treadmill instrumented to measure vertical ground reaction forces. Determination of exhaustion was subjective and left to the discretion of the runner. The average duration of the exhaustive run was 56 minutes (range: 38-78 min). Ground reaction force data were sampled for 15 seconds at 1000 Hz every five minutes, but only data from the beginning, middle, and end (last minute) are included in this report.

Individual heel strike and toe-off points were identified from the force data. Between 38 and 40 steps were identified for each sampling period. Characteristics measured from the force data include: peak impact force, loading rate, peak active force, foot contact time, and step time.

A within-subject ANOVA ($\alpha=.01$) was used to determine variable changes, and Fisher's PLSD test was used for follow-up tests. A coefficient of variation was determined for each variable and averaged across the six subjects at each time point.

RESULTS AND DISCUSSION

Response to the fatigue run tended to be highly individual. Magnitudes of the active and impact peak varied between individuals, and the changes with exhaustion were inconsistent (Table 1). Increases, decreases, and no change were observed with exhaustion in different runners.

Five of the six runners had consistent increases in loading rate over the run. Increased loading rate may be indicative of a stiffer leg at impact. This result compliments the observation of increased shank acceleration by Verbitsky et al. (1998).

Foot contact time either increased or stayed the same. Similar to the observations of Gollhofer et al. (1987) for the upper-

extremity, runners with increased foot contact time tended to have decreased peak active forces. These same runners also increased step time. These changes may be associated with the generation of vertical impulse during foot contact. With reduced force production, contact time must be increased to provide a similar vertical impulse.

With exhaustion, runners exhibited increased coefficient of variation for peak active force and loading rate (Figure 1). An increase in the coefficient of variation for the loading rate might be associated with decreased control of the leg musculature resulting in variable leg stiffness on impact, although the general trend was for the impact force to increase (implying a stiffer leg). Impact peak force coefficient of variation decreased, while force magnitude generally increased, possibly indicative of the presence of an upper boundary to impact force sustainable by the body under the given conditions.
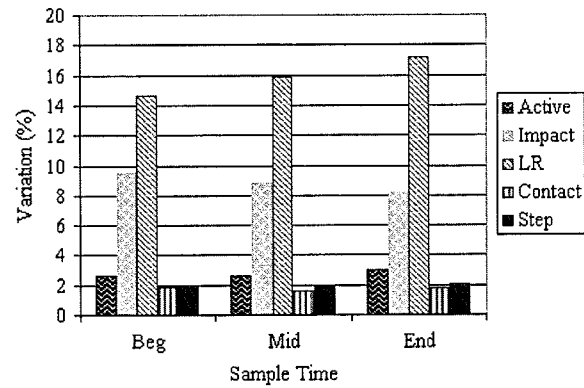
Figure 1: Average coefficient of variation for the five measured variables across sampling points.

REFERENCES

Gollhofer, A. et al. (1987). *Int. J. Sports Med.*, **8**, 71-78.

Nummela, A. et al. (1994). *Med. Sci. Sports and Exerc.*, **26**(5), 605-609.

Verbitsky, O. et al. (1998*). J. Appl Biomech.*, **14**, 300-311.

Table 1: Force and time measures for six runners. Active and impact peak (bw), loading rate (bw/s), foot contact time (s) and step time (s) are shown. (mean ± sd)

Subject		Active Peak	Impact Peak	Loading Rate	Contact Time	Step Time
1	Beg	2.47 ± 0.08	1.38 ± 0.16	50.58 ± 7.80	0.251 ± 0.006	0.361 ± 0.007
	Mid	2.41 ± 0.07*	1.24 ± 0.12*	49.75 ± 8.04	0.259 ± 0.004*	0.365 ± 0.006
	End	2.33 ± 0.08*‡	1.29 ± 0.09‡	50.72 ± 4.89	0.258 ± 0.005‡	0.363 ± 0.007
2	Beg	3.45 ± 0.08	2.53 ± 0.19	75.86 ± 13.18	0.202 ± 0.002	0.379 ± 0.009
	Mid	3.41 ± 0.07	2.52 ± 0.17	75.96 ± 10.59	0.201 ± 0.003	0.374 ± 0.008
	End	3.16 ± 0.11*‡	2.55 ± 0.15	87.85 ± 16.04*‡	0.203 ± 0.003	0.362 ± 0.012*‡
3	Beg	2.72 ± 0.07	2.43 ± 0.26	72.06 ± 7.15	0.232 ± 0.006	0.356 ± 0.006
	Mid	2.64 ± 0.05	2.60 ± 0.25	79.44 ± 11.89	0.236 ± 0.003	0.363 ± 0.008
	End	2.68 ± 0.08	2.73 ± 0.18	92.19 ± 14.46‡	0.237 ± 0.006	0.370 ± 0.007*‡
4	Beg	2.95 ± 0.09	2.13 ± 0.12	74.95 ± 11.55	0.213 ± 0.004	0.352 ± 0.005
	Mid	2.99 ± 0.12	2.18 ± 0.16	81.85 ± 11.08	0.218 ± 0.003*	0.359 ± 0.005*
	End	2.97 ± 0.10	2.32 ± 0.18*‡	85.36 ± 15.39‡	0.215 ± 0.003*	0.359 ± 0.005‡
5	Beg	2.73 ± 0.08	2.03 ± 0.21	75.19 ± 10.91	0.203 ± 0.004	0.331 ± 0.009
	Mid	2.68 ± 0.06*	1.96 ± 0.16	78.86 ± 7.92	0.209 ± 0.005*	0.337 ± 0.008*
	End	2.70 ± 0.08	2.01 ± 0.19	84.07 ± 10.98‡	0.209 ± 0.004‡	0.344 ± 0.007*‡
6	Beg	2.53 ± 0.04	1.71 ± 0.21	86.20 ± 13.32	0.232 ± 0.004	0.359 ± 0.006
	Mid	2.54 ± 0.06	1.77 ± 0.23	97.42 ± 24.05	0.231 ± 0.004	0.361 ± 0.006
	End	2.56 ± 0.05	1.83 ± 0.25	112.36 ± 26.39*‡	0.231 ± 0.04	0.361 ± 0.007

* significant from previous, $p<.01$; ‡ significant between Beg and End, $p<.01$

LOWER EXTREMITY POWER GENERATION STRATEGIES USED BY ELITE ATHLETES DURING THE TAKE-OFF PHASE OF THE LONG JUMP

Kathleen E. Costa and Jill L. McNitt-Gray

Department of Exercise Science, University of Southern California, Los Angeles, California
Email: kcosta@usc.edu

INTRODUCTION
During the take-off phase of the long jump, athletes must negotiate high loads during an impact encountered at a near maximum velocity, and precisely redirect total body momentum while in single foot contact with the ground. To date, many investigations of the long jump have focused on mechanics at the total body level (Hay et al., 1986; Hay & Nohara, 1990). Few studies have concentrated on the joint kinetics used to generate and control total body momentum during the take-off phase of the long jump (Lees et al., 1993; Witters et al., 1992; Stefanyshyn & Nigg, 1998). The purpose of this investigation was to determine how power generation across the lower extremity contributes to changes in total body center of mass (TBCM) vertical velocity during the take-off phase of the long jump.

PROCEDURES
Members of the USA Women's Heptathlon Team (n=13) and USA Men's Decathlon Team (n=8) performed a series of long jumps (LJ) into a sand pit under the direction of their coach as part of a training camp. Reaction forces during take-off were quantified using a force plate mounted at the end of the runway (600 Hz, Kistler, 0.6 x 0.9m) and sagittal plane kinematics were simultaneously videotaped (60 fps). Each body landmark coordinate was digitized (Motus, Peak Performance, Inc.) and filtered using a fourth order Butterworth Filter (Saito & Yokoi, 1982) with cut-off frequencies determined according to Jackson (1979). Kinematic and reaction force data were synchronized at force plate contact and kinetic variables of the take-off leg were determined using Newtonian mechanics. Take-off phase, defined from touchdown to departure from the plate, was normalized for each subject and divided into thirds to characterize momentum transition phases. Work done at the ankle, knee, and hip was calculated during each third of the take-off phase by integrating the net joint moment power (NJMP). NJMP was defined as the product of net joint moment (NJM) and joint angular velocity (ω). Data was sorted according to changes in TBCM vertical velocity during take-off phase. The median (M) value was used to differentiate athletes with relatively small (<M, n=10) and large (>M, n=10) changes in TBCM vertical velocity during take-off phase. Student's t-Test was used to determine significant ($p<0.05$) differences in work done by the NJM at each joint between groups.

RESULTS AND DISCUSSION
Similar ranges of TBCM horizontal velocity at contact (heptathletes: 7.35 – 8.48 m/s; decathletes: 7.83 – 9.24 m/s) and changes in TBCM vertical velocity during take-off (heptatletes: 2.23 – 3.32 m/s; decathletes: 2.71 – 3.92 m/s) were observed for men and

women. Throughout the take-off phase, athletes exhibiting a large change in TBCM vertical velocity produced significantly greater positive work at the hip (Figure 1. A: $p=0.03$, B: $p=0.03$, C: $p=0.04$) than athletes in exhibiting a relatively small change in TBCM vertical velocity. Positive work at the hip was achieved by positive hip NJM (extensor) and positive ω, whereas, negative work at the hip was achieved by a negative hip NJM (flexor) and positive ω. Athletes exhibiting a large change in TBCM vertical velocity during the take-off phase initiated

contact with a more horizontal shank angle than did the athletes exhibiting a small change in TBCM vertical velocity. The more horizontal shank angle, increased the relative angle between the net joint forces (NJF) and the segment CM, and thus resulted in greater proximal and distal moments (PM, DM) created by the NJFs at the ankle and knee. When the summed magnitude of PM and DM of the shank were equal to or slightly less than the ankle NJM, the knee NJM was small and negative which led to a positive hip NJM and positive work done at the hip.
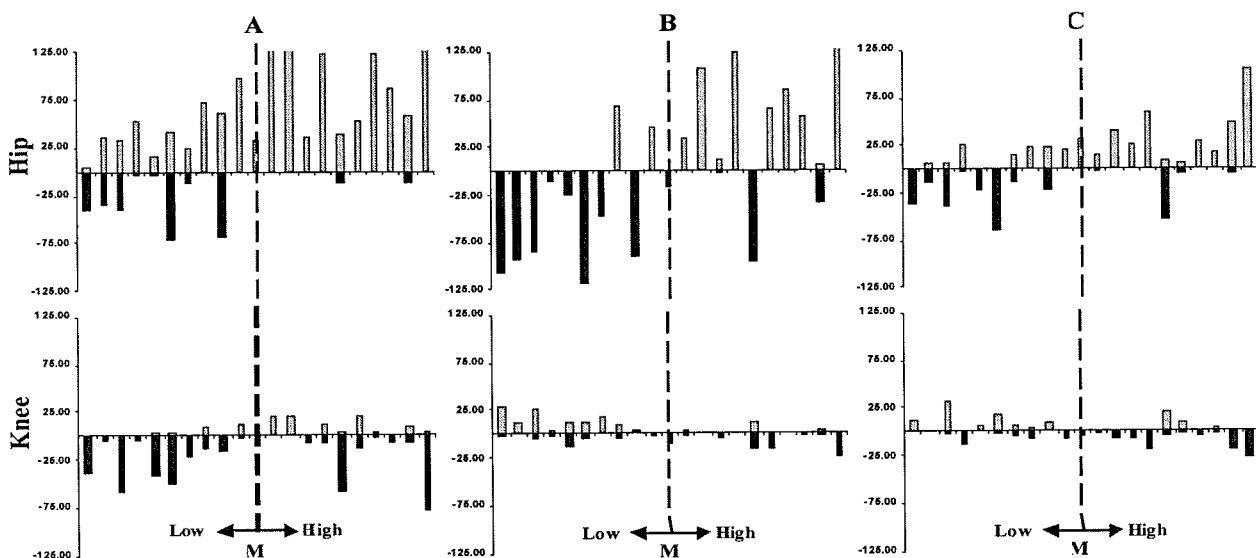
Figure 1. Work done by the net joint moment at the hip and knee during the first (A), middle (B), and last (C) third of the take-off phase. Dashed line located at the median (M) separates the athletes that had low increases in TBCM vertical velocity during take-off from those that achieved high increases in TBCM vertical velocity.

CONCLUSION

In conclusion, a significant relationship was found between positive work done at the hip and large increases in TBCM vertical velocity during the take-off phase of the long jump. Results indicate that maintaining a small negative or near zero knee NJM leads to a positive hip NJM and positive work done at the hip.

REFERENCES

Hay, J. et al. (1986) *J. Biomechanics*, **19**:10, 855-66.
Hay, J., Nohara, H. (1990) *J. Biomechanics*, **23**:3, 229-39.
Jackson, K. (1979) *IEEE Trans. BME*, **26**, 122-4.
Lees, A. et al. (1993) *J. Sports Sciences*, **11**, 303-14.
Saito, S., Yokoi, T. (1982) *Bltn. Health & Sports Sci. U of Tsukuba*, **5**, 201-6.
Stefanyshyn, D.J., Nigg, B.M. (1998) *J. Sports Sciences*, **16**, 177-86.
Witters, J. et al. (1992) *J. Sports Sciences*, **10**, 533-540.

GENERATING VERTICAL VELOCITY AND ANGULAR MOMENTUM DURING SKATING JUMPS

Deborah King

Biomechanics Lab, Montana State University, Bozeman, Montana
Email: dking@montana.edu

INTRODUCTION

As figure skaters continue to perform increasingly difficult jumps, the importance of understanding the mechanics of skating jumps increases as well. Two critical parameters to the completion of these jumps are vertical velocity and angular momentum.

Albert and Miller (1997) performed an analysis of vertical velocity and angular momentum for single and double Axels. Their results indicate that both radial and tangential motion of the skater are critical to the generation of vertical velocity throughout the take-off of single and double Axels. In generating angular momentum during the take-off, the movement of the free leg was most critical. The authors surmised that the movement of the fee leg creates an eccentric horizontal ground reaction force with a moment consistent with the rotational direction of the jump. The purpose of this study was to expand upon the study of Albert and Miller (1997) and investigate the techniques used by athletes in generating vertical velocity and angular momentum in single, double, and triple Axels.

PROCEDURES

Seventeen elite skaters gave their written informed consent to participate in this study. Video footage of the take-offs of single, double, and triple Axels were taken with three video cameras placed around the ice rink. Each jump was manually digitized at a sampling rate of 60 frames/second. The raw two-dimensional data were filtered then the Direct Linear Transform Theory was used to calculate the three-dimensional coordinates (PEAK5, Peak Performance, CO).

The primary variables of interest were vertical velocity (V_v), angular momentum about the vertical axis through the COM of the skater (H_z), and moment of inertia about the vertical axis trough the COM of the skater (I_{zz}). Vertical velocity was sub-analyzed by determining the contribution from tangential motion (angular velocity of the COM about the ankle joint of the take-off foot) and radial motion (linear velocity of the radius between the ankle and COM). Two-way analyses of variance were calculated to determined whether the differences between the two main effects, jump type and gender, were significant for the selected variables. Tukey's pairwise comparison was performed when an F-value was statistically significant ($p < 0.1$).

RESULTS AND DISCUSSION

Tangential motion contributed between 9 and 12 percent of overall V_v gain (Table 1). There was no significant difference in V_v between jump types; though, the males did have significantly greater vertical velocities than the females. These results indicate that skaters do utilize forward and upward rotation during the approach as a means for generating vertical velocity during the approach.

Neither H_z nor I_{zz} at take-off were significantly different between jump type. However, I_{zz} values at take-off were significantly smaller for females as compared to males. The average H_z and I_{zz} values are presented in Table 1. Figure 1 illustrates the typical pattern for gaining H_z throughout the approach of the jump. During the period in which the largest gains in H_z are observed, the skater is driving forward with the free leg and arms.

Typical Angular Momentum Pattern for Double Axel
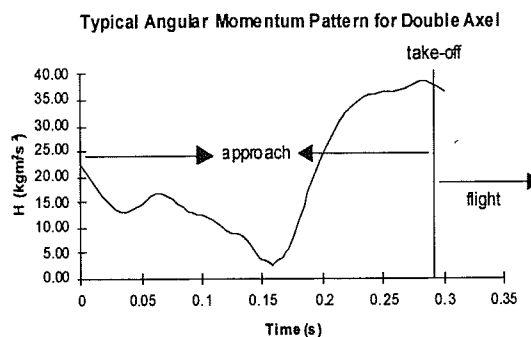
Figure 1. Characteristic angular momentum curve for a skater during the approach of a double Axel.

Table 1. Angular momentum, moment of inertia, and vertical velocity values at take-off (with percent contribution from tangential motion). Values are means ± SD.

| | Singles | | Doubles | | Triples |
	Females	Males	Females	Males	Males
V_v at take-off (m/s)	1.84 ±0.62	2.76 ±0.95	2.62 ±0.49	3.32 ±0.95	3.23 ±0.95
V_v tangential (% gain)	9 ±0.1	10 ±0.1	8 ±0.2	11 ±0.1	11 ±0.1
H_z at take-off (kgm²/s²)	18.0 ±7.8	17.7 ±6.3	13.2 ±7.0	21.0 ±6.5	21.1 ±8.9
I_{zz} at take-off (kgm²)	2.63 ±0.9	3.31 ±0.6	2.29 ±0.7	3.46 ±0.8	3.5 ±0.4

These results are similar to those found by Albert and Miller (1997), who indicated that the movement of the free leg is critical to generating necessary H_z for the jump. Interestingly, the results from this study do not support the findings of Albert and Miller (1997) that I_{zz} decreases as jump type increases. A possible explanation is the level of skaters involved in each study, with the more experienced skaters in this study maintaining larger I_{zz} at take-off during their multi-revolution jumps. These two different techniques of manipulating I_{zz} at take-off and in flight have been discussed in detail by Aleshinksy (1986, 1987).

CONCLUSIONS
The results of this study provide further insight into techniques used by skaters to generate the necessary vertical velocity and angular momentum to complete multi-revolution jumps. The primary findings indicate 1: that skaters utilize both tangential and radial motion to generate vertical velocity for take-odd, and 2) that angular momentum values are not significantly different between single, double, and triple Axels.

REFERENCES
Albert and Miller (1997). *J. Appl. Biomech.*, 12, 72-87.

Aleshinsky, S. (1986). *Skating*, 63, 11-15.

Aleshinsky, 1987). *The Professional Skater*, 18, 24-28.

A THREE DIMENSIONAL KINETIC ANALYSIS OF SUMO AND CONVENTIONAL STYLE DEADLIFTS

Rafael F. Escamilla[1], Anthony C. Francisco[1], Glenn S. Fleisig[2], Christian M. Welch[3], Steven W. Barrentine[2], Andrew V. Kayes[1], and James R. Andrews[2]

[1]Division of Orthopaedic Surgery, Duke University Medical Center, Durham, NC
[2]American Sports Medicine Institute, Birmingham, AL
[3]Human Performance Technologies, Inc., Jupiter, FL
Email: rescamil@duke.edu   Web: http://surgery.mc.duke.edu/klab

INTRODUCTION

Strength athletes and rehabilitation patients often employ the deadlift in their training and rehabilitation regimens. The deadlift is performed using either a conventional (narrow stance, feet slightly turned out) or sumo (wide stance, feet turned out $\approx 45°$) style. In the only previous kinetic analysis between sumo and conventional deadlifts [Cholewicki, 1991], lumbar spinal forces & moments and knee & hip moments were quantified using a one camera two-dimensional (2-D) analysis. Unlike trunk movements, ankle and knee movements during the deadlift occur in three-dimensions when the feet are turned out. Therefore, erroneous ankle and knee moments and moment arms may result with a 2-D analysis, especially during the sumo deadlift. Hence, it was the purpose of this study to conduct a three-dimensional (3-D) analysis of the sumo and conventional deadlifts, and compare ankle, knee, and hip moments and moment arms between these two lifting styles. Mechanical work was also compared.

MATERIALS AND METHODS

Twenty-four male powerlifters served as subjects (12 sumo and 12 conventional) during a national powerlifting championship. Two synchronized video cameras were used to collect 60 Hz video data. Three events were noted during the deadlift:1) liftoff (LO); 2) knee passing (KP); and 3) lift completion (LC). A 3-D video system was used to manually digitize joint and segmental centers of the toes, ankles, knees, hips, shoulders, hands, and bar. A 4th order, zero lag Butterworth digital filter was used to smooth the raw data with a cutoff frequency of 5 Hz . A 2 x 1.5 x 1 m volume calibration frame was positioned in the volume occupied by the lifter-barbell system. A 3-D orthogonal axes system was translated and rotated appropriately in order to calculate ankle, knee, and hip moments and moment arms. Joint moments were calculated using a quasi-static model. Body segment center of masses and weights were estimated by using appropriate anthropometric data and each lifter's known mass. Unpaired t-tests ($p < 0.01$) were used to used to compare kinetic parameters between sumo and conventional deadlift groups.

RESULTS AND DISCUSSION

When normalized by body height, the conventional group had 20-25% greater vertical bar displacements from LO to LC compared to the sumo group. This is not surprising since the sumo group had a stance width approximately three times greater than the conventional group. The lower vertical displacement by the sumo group resulted in 25-30% less mechanical work performed compared to the conventional group. Joint moments and moment arms are shown in Table 1. Since ankle and knee movements occur in the direction the feet are pointing,

ankle and knee moments and moment arms calculated from a 2-D analysis were significantly different from a 3-D analysis, especially for the sumo group. Ankle and knee moment arms for the conventional deadlift were generally only a few centimeters different between a 2-D and 3-D analysis. In contrast, ankle and knee moment arms for the sumo deadlift were generally 20-25 cm different between a 2-D and 3-D analysis. Similar to data from Cholewicki et al. [Cholewicki, 1991], there were no significant differences in hip moments and moment arms between sumo and conventional deadlifts. This was not surprising since hip flexion and extension during the deadlift occurs primarily in the sagittal plane. Hence, a 2-D analysis is adequate in calculating hip moments and moment arms. Unlike knee moments in the current study (Table 1), knee moments from Cholewicki et al. [Cholewicki, 1991] were not significantly different between sumo (18 N·m) and conventional (18 N·m) deadlifts. In addition, 2-D knee moments for the sumo (106±55 N·m) and conventional (-7±66 N·m) deadlifts were relatively similar to the 2-D knee moments from Cholewicki et al. [Cholewicki, 1991], but quite different than 3-D knee moments (Table 1).

SUMMARY

Mechanical work is greater in the conventional deadlift, which suggest a higher energy expenditure. Moderate to high hip extensor, knee extensor, and ankle dorsiflexor moments are generated during the sumo deadlift, which implies moderate to high muscle activity is needed from the hip extensors, knee extensors, and ankle dorsi flexors. In contrast, moderate to high hip extensor moments and low knee flexor, knee extensor, and ankle plantar flexor moments are generated during the conventional deadlift. This implies moderate to high muscle activity from the hip extensors, and

lower activity from the knee flexors & extensors and ankle plantar flexors. These kinetic differences result from technique differences. Hence, a electromyographic analysis should now be conducted to confirm muscle activity patterns. This would help trainers and therapists in prescribing the appropriate deadlift technique.

REFERENCES

Cholewicki, J. et al. (1991). Med. Sci. Sports Exerc., 23(10), 1179-86.

Table 1. Moments and moment arms relative to barbell load center of mass.

	Sumo	Conventional
Moment Arms at LO		
Ankle (cm)	-17.2±6.8[*]	5.1±2.5[*]
Knee (cm)	-17.8±5.0[*]	-3.9±3.6[*]
Hip (cm)	19.0±4.0	20.7±6.7
Moments at LO		
Ankle (N·m)	-359±159+[*]	109±50[*]
Knee (N·m)	-370±11[*]	-95±91[*]
Hip (N·m)	403±121	461±164
Moment Arms at KP		
Ankle (cm)	-18.6±6.1[*]	1.4±3.5[*]
Knee (cm)	-12.8±5.1[*]	2.2±2.7[*]
Hip (cm)	17.4±4	16.2±4.5
Moments at KP		
Ankle (N·m)	-389±145[*]	23±80[*]
Knee (N·m)	-266±109[*]	46±66[*]
Hip (N·m)	366±102	351±78
Moment Arms at LC		
Ankle (cm)	-17.6±6.9[*]	2.9±3.4[*]
Knee (cm)	-9.8±4.2[*]	2.4±3.5[*]
Hip (cm)	8.7±2.9	6.0±2.0
Moments at LC		
Ankle (N·m)	-369±167[*]	55±75[*]
Knee (N·m)	-204±93[*]	46±75[*]
Hip (N·m)	190±92	132±45

[*] $p < 0.01$

Note. Hip extensor, knee flexor, and ankle plantar flexor moments are positive

A FORMULATION OF THE INFLUENCE OF OSTEONS ON THE FRACTURE TOUGHNESS OF CORTICAL BONE IN LONGITUDINAL CRACK GROWTH

Yener N. Yeni[1] and Timothy L. Norman[2]

[1] Breech Research Lab, Bone and Joint Center, Henry Ford Hospital, Detroit, Michigan
[2] Departments of Mechanical and Aerospace Engineering and Orthopedics
Musculoskeletal Research Center, West Virginia University, Morgantown, West Virginia
Email: tnorman@wvu.edu   Web: www.hsc.wvu.edu/som/ortholab/

INTRODUCTION

Bone microstructure, namely porosity and osteonal features, has been demonstrated to have significant influence on the fracture resistance of cortical bone (Behiri and Bonfield, 1989; Yeni et al., 1997). Behiri and Bonfield (1989) have shown that the longitudinal plane is the weakest plane for the crack to propagate within the bovine cortical bone. Microscopic examination of in-vivo microdamage also suggests that cracks tend to propagate along the cement lines (Schaffler et al., 1995). The mechanism of this behavior is usually explained as crack deflection at the cement line that is considered to be a weak interface between the osteon and the interstitial matrix (Burr et al., 1988). The objective of this study was to formulate a fracture mechanics model to study the influence of microstructure on fracture toughness in light of previous experimental data. Using this model, the interstitial bone matrix to cement line fracture toughness ratio, k, was determined.

PROCEDURES

It was assumed that cracks tend to propagate longitudinally along cement lines of osteons (fiber/matrix debonding) when there are osteons on crack pathways and in the matrix (matrix cracking) otherwise. Using the concept of effective crack length, crack pathways around osteons were projected on the line of the main crack and the pores were homogenized (Anderson, 1991). These effects were represented by replacing the surface energy of bone with an effective surface energy in the new configuration. Then using a surface energy approach, critical strain energy release rate or fracture toughness, G, was expressed as (Yeni, 1998):

$$G = \left\{ \left(1 - \frac{2pr}{B}\right)\left(1 - \frac{2nr}{B}\right)^2 + \left(\frac{\pi}{kB} - \frac{2}{B}\left(1 - \frac{2nr}{B}\right)^2\right)nR \right\} G_m$$

where p and n are the number of non-Haversian pores and osteons in the crack pathway, r and R are radius of pores and osteons, B is the specimen thickness, G_m is the fracture toughness of bone matrix and k is the matrix to cement line fracture toughness ratio.

Since bovine bone has negligible secondary osteons compared to human bone, G_m was approximated by G_{Ic} of bovine bone (Norman et al., 1995; Feng et al., 1996). Microstructural parameters were derived from two dimensional histomorphometrical data, assuming an area of 2R x B, (Yeni et al., 1997; Yeni, 1998). Haversian to non-Haversian pore ratio was adapted from measurements of bovine bone (Martin and Ishida, 1989).

RESULTS

Matrix to cement line fracture toughness ratio, k, was optimized such that predicted and measured values of G provide the best linear fit. The optimal values of k were found to be 1.9830 and 1.8555 for G_I and G_{II}, respectively. Matrix to cement line toughness ratio, k, as determined for individual specimens had a significant

increase with age for both tension and shear (Figure 1).
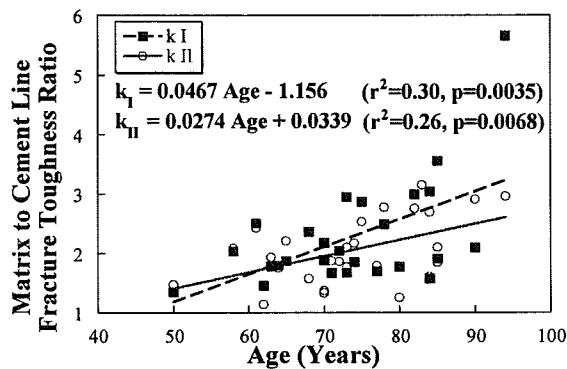
Figure 1: Calculated matrix to cement line fracture toughness ratio significantly increases with age in the human femur.

DISCUSSION

The calculated values of the matrix/cement line fracture toughness ratio are close to 2 which is consistent with the assumption that cement lines have lower resistance to crack growth than the matrix. The equation suggests that for a certain range of values for the cement line toughness, the range depending on the Haversian canal size, the effect of a Haversian canal in an osteon can be compensated by energy dissipation at the cement line of the same osteon. An implication of such a compensation mechanism is that pores at the resorption stage of remodeling may be more harmful, since resorption cavities are not encircled by the cement line until bone formation begins. For large values of k, however, the overall effect of an osteon (cement line and pore) on fracture toughness will be negative.

The calculated values of k significantly increased with increasing age suggesting that as the individual gets older, the osteons in the individual's bones become less efficient in energy dissipation. Cement lines with lower fracture toughness would also allow longer cracks than tougher cement lines for dissipation of the same amount of energy. Longer cracks may more easily

reach a critical size than short cracks, after which crack growth becomes catastrophic and more detrimental.

SUMMARY

In summary, this model formulates the influence of a major fracture mechanism, osteonal debonding, on the fracture toughness of cortical bone. Using this model we found that the toughness of the matrix was approximately twice that of the cement line, which is consistent with the assumption that the cement line traps or arrests cracks in-vivo. It was also found that k, the potential to arrest cracks, increases with age.

REFERENCES

Behiri J.C., Bonfield W. (1989). *J. Biomechanics*, **22**, 863-872.
Yeni, Y.N. et al. (1997). *Bone*, **21**, 453-459.
Schaffler, M.B. et al. (1995). *Bone*, **17**, 521-525.
Burr, D.B. et al. (1988). *J. Biomechanics*, **21**, 939-945.
Anderson, T.L. (1991). *Fracture Mechanics: Fundamentals and Applications*. CRC Press.
Norman, T.L. et al. (1995). *J. Biomechanics*, **28**, 309-320.
Feng, Z. et al. (1996). *Trans 42nd ORS*, 609.
Yeni, Y.N. (1998). Dissertation, West Virginia University.
Martin, R.B., Ishida, J. (1989). *J. Biomechanics*, **22**, 419-426.

ACKNOWLEDGEMENT

THE IMPLICATIONS OF REDUCED GROUND REACTION FORCES DURING SPACE FLIGHT FOR BONE STRAINS

[1,3]Marc M. Peterman, [1,3]Andrew J. Hamel, [1,2]Neil A. Sharkey,
[1,2,3]Stephen J. Piazza, and [1,2,4]Peter R. Cavanagh
[1]The Center for Locomotion Studies and the Departments of [2]Kinesiology; [3]Mechanical
Engineering; [4]Biobehavioral Health, Medicine, Orthopaedics and Rehabilitation;
The Pennsylvania State University, University Park and Hershey, PA
Email: celos@psu.edu   Web: www.celos.psu.edu

INTRODUCTION

The specific mechanisms regulating bone mass are not known, but most investigators agree that bone maintenance is largely dependent upon mechanical demand and the resultant local bone strains. During space flight, bone loss such as that reported by LeBlanc et al. (1996) may result from failure to effectively load the skeleton and generate sufficient localized bone strains.

In microgravity, a gravity replacement system can be used to tether an exercising subject to a treadmill (Davis et al. 1993, McCrory 1997). It follows that the ability to prevent bone loss is critically dependent upon the external ground reaction forces (GRFs) and skeletal loads imparted by the tethering system. To our knowledge, the loads during orbital flight have been measured only once (on STS 81). Based on these data and data from ground based experiments, it appears likely that interventions designed to prevent bone loss in micro-gravity generate GRFs substantially less than body weight. It is unknown to what degree reductions in external GRFs will affect internal bone strain and thus the bone maintenance response.

To better predict the efficacy of treadmill exercise in micro-gravity we used a unique cadaver model to measure localized bone strains under conditions representative of those that might be produced by a gravity replacement system in space.

METHODS

Cadaver limbs were mounted into a dynamic loading apparatus that reproduces the kinetics and kinematics of the tibia, foot, and ankle during the stance phase of gait (Sharkey and Hamel, 1998). The device is able to produce GRFs equivalent to those produced in life. Physiologic muscle actions are simulated using force feedback controlled linear actuators interfaced with the tendons of the specimen using freeze clamps.

The distal third of the tibiae were each instrumented with seven miniature strain gauge rosettes (Micro-Measurements Group, Inc. EA-06-031RB-120) oriented on a transversely co-planar section (Figure 1). Dynamic gait simulations were conducted at GRFs corresponding to 25%, 50%, 75%, and 100% of body weight (BW). Strain data were collected over the entire stance phase
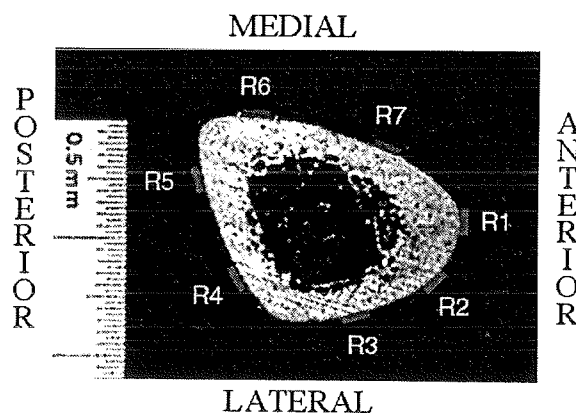
Figure 1.   Tibial cross-section showing strain gauge placement.

and the results were used as input for a computer model of bone strains over the stance phase.

RESULTS

Decreased GRFs produced proportional decrements in peak tibial strains (Figure 2). At all gauge locations, development of maximum strains within the specimen corresponded to the second peak of the GRF profile. The overall strain maxima for each condition was compressive and occurred along the posterio-medial border of the tibial cross section. Maximum tensile strains occurred anteriorly on the tibial crest. Animations of the strain profiles from heel-strike to toe-off were created using SIMM and MATLAB and will be presented.
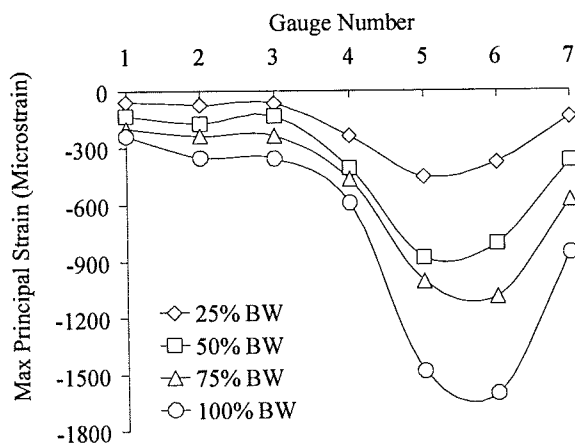
Figure 2. Peak maximum principal strains on the tibia for varying GRFs during simulated walking.

DISCUSSSION

Several investigators have attempted to measure *in vivo* strains in the human tibia, but these studies have been somewhat limited (Lanyon et al., 1975; Milgrom et al., 1996; Burr et al., 1996; Aamodt et al., 1997). *In vivo* human studies have focused on the antero-medial aspect of the tibia due to ethical concerns and technical constraints. Using a robust cadaver model we found that peak strains occur at sites other than those typically measured in live human subjects.

The strain distributions measured in the current study indicate bending as the primary mode of tibial loading and muscle force (i.e. the triceps surae) as the principal modulator of bone strain. Carter et al. (1987) and Turner (1998) have derived separate theoretical equations of bone adaptation based, among other things, on the magnitude of stress or strain experienced by the bone. Our data suggest that *in-situ* bone strains can be reliably related to the external loading environment, so that these equations can be used to calculate a theoretical stimulus using GRFs as input.

CONCLUSION

Internal tibial strains can be predicted using external GRFs. This inter-relationship is important for understanding the bone stimulating potential of various exercise interventions during space flight.

REFERENCES

Aamodt A., et al. (1997). *J Orthop Res*, 15: 927-31.
Burr D.B., et al. (1996). *Bone*, 18: 405-10.
Carter D.R., et al. (1987). *J Biomechanics*, 20: 785-94.
Davis B.L., et al. (1996). *Aviat Space Environ Med*, 67(3): 235-42.
Frost H.M. (1986). *Intermediary Organiz-ation of the Skeleton*. CRC, Boca Raton.
Lanyon L.E., et al. (1975). *Acta Orthop Scand*, 46: 256-68.
LeBlanc A., et al. (1996). *J Bone Mineral Res*, 11: S323.
McCrory J.L. (1997). *Ph.D. Thesis*. Penn State University, University Park.
Milgrom C., et al. (1996). *Foot & Ankle Int*, 17: 667-71.
Turner C.H. (1998). *Bone*, 23(5): 399-407.
Sharkey N.A., Hamel A.J. (1998). *Clin Biomech*, 13: 420-433.

ACKNOWLEDGEMENTS

MICRODAMAGE COALESCENCE MECHANISMS IN HUMAN CORTICAL BONE

Ozan Akkus, Dwight T. Davy and Clare M. Rimnac

Department of Mechanical and Aerospace Engineering, Case Western Reserve University,
Cleveland, OH, 44106, USA
Email:oxa@po.cwru.edu

INTRODUCTION

The initiation and accumulation of microdamage have been described previously (Schaffler et al., 1989). However, the interaction of microdamage patterns has not been fully elucidated. The objective of this study was to investigate microdamage growth and coalescence mechanisms during crack propagation transversely to the osteons via acoustic emission (AE) and histological examination.

MATERIAL AND METHODS

Grooved compact tension specimens (n=4) were machined from a pair of human femora (female, age=53) following the method of Behiri and Bonfield, 1989. The loading rate was 0.09mm/min. Two transducers (T1 and T2, Figure 1) detected AE waveforms associated with the initiation of cracks. Amplitude, duration, rise time and frequency of the AE waveforms were recorded. Time delay between hits, hit sequence and the wave velocity were used to locate the hits. AE data were pooled and grouped into two clusters by the K-means method. Specimens were bulk stained in basic fuchsin amd embedded in poly-methylmethacrylate. Three specimens were sectioned perpendicularly to the osteons for histological evaluation. Two sections per specimen, approximately 0.8 mm above and below the crack propagation plane were examined. The cracks in along the first 7 mm of crack propagation were counted at x200 magnification. Cracks were classified

according to their location: interstitial matrix (IM), cement lines (CL), or osteons (O). A third section was also taken as close as possible to the crack propagation plane from each specimen for qualitative evaluation of microdamage.
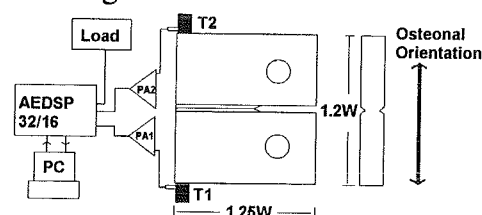
Figure 1: Experimental set up,W=14mm.

RESULTS

Crack initiation was marked by AE and followed by stable crack growth. The number of hits increased as the load decreased. The decrease in load was marked by stepwise descents (arrowheads, Figure 2). K-means clustering yielded two groups of waveforms, one with higher amplitude and duration (86.3 ± 8.5dB, $225.4\pm194.4\mu s$) than the other (61.2 ± 7.9dB, $32.0\pm25.6\mu s$). The lower energy cluster occurred first and was closely followed and augmented by the higher energy cluster. The occurrence of the higher energy clusters coincided with initiation of the stepwise load descents. The higher energy cluster emanated from the fracture plane while the lower energy cluster tended to be more diffuse. The Mann-Whitney test indicated that there were significantly more cracks per section in the interstitial matrix than in the cement lines ($p=0.0025$) and in osteons ($p=0.0025$)

(Table 1). This finding is supported by the fact that the majority of in vivo microcracks are observed in the interstitial matrix (Schaffler et al., 1995). Three coalescence cracks formed by the joining-up of the microcracks in the interstitial matrix, cement lines, and osteons are shown in Figure 3 (arrows). Figure 3 is taken from the sample whose load-time history is given in Figure 2. Qualitative observation of the crack plane sections showed completely or partially missing osteons and/or osteon bundles. The majority of osteons on the crack plane were more densely stained than the osteons in the neighboring sections.

DISCUSSION

Two clusters of AE (high energy and low energy) and the two levels of damage based on histology (ultrastructural damage on the crack plane and coalesced micro-cracks in the neighboring sections) were observed in this study of crack propagation. Based on these observations, we suggest the following sequence of microdamage initiation, accumulation, coalescence, and failure. *Initiation* on the crack plane is precipitated by damage at the ultrastructural level (low energy AE hits). At about the same time in the neighboring sections, interstitial microcracks initiate and accumulate (low energy AE hits). *Coalescence of microcracks* occurs after saturation of interstitial microcracks. Interstitial microcracks coalesce via microcracks either within osteons or along cement lines (low energy AE hits). Eventually, these visible cracks have a length scale of millimeters (Figure 3). Failure occurs when ultrastructural damage renders the osteons sufficiently weak on the crack plane and coalescence cracks render them sufficiently isolated in the neighboring sections. A further increase in stress results in transverse failure of the osteons at the crack front (high

energy AE hits) with incremental crack propagation. Presently, more than one damage pattern is assigned to the low energy AE cluster. Future analysis of the low energy AE cluster will be conducted to determine if the different failure modes can be further separated.
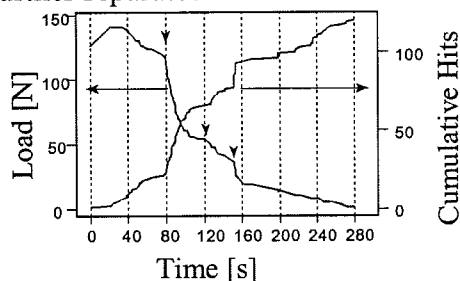
Figure 2: Typical load-cumulative hit history
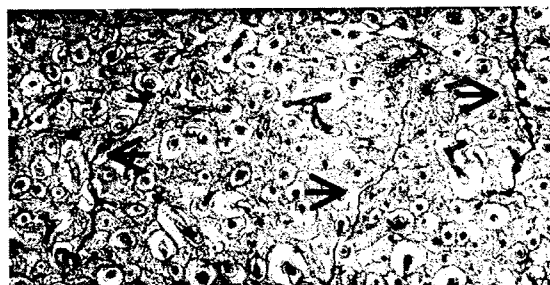
Figure 3: Coalescence cracks on a section 0.8mm away from the crack plane. The direction of propagation of the main crack is from left to right.

Table 1. Average # of microcracks/section

IM	CL	O
35.3±13.4	4.3±4.9	8.2±7.3

REFERENCES:
Behiri, J.C., Bonfield, W., (1989). *J. Biomechanics,* **22,** 863-72.

Schaffler, M.B. et al. (1989). *Bone,* **10,** 207-14.

Schaffler, M.B. et al. (1995). *Bone,* **17,** 521-25.

DETERMINATION OF MECHANICAL STIMULI SUFFICIENT TO INITIATE OSTEOBLASTIC ACTIVATION

Sundar Srinivasan and Ted S. Gross
Department of Orthopaedic Surgery, University of Cincinnati
e-mail: sprinis@email.uc.edu

INTRODUCTION

Daily mechanical loading of the skeleton serves as an anabolic influence upon bone mass. However, the cells responsible for perceiving mechanical stimuli (e.g., osteocytes or osteoblasts) and the specific stimuli capable of initiating cellular events culminating in bone formation (e.g., strain or fluid flow) are unknown. An array of experimental studies support the thesis that the larger the loading related stimulus, the more substantial the evoked response (1,2,3,4). One intriguing aspect of these studies is that in each experiment, some level of external stimulus (e.g., low strain magnitude) was not sufficient to significantly increase bone mass. These data suggests that when the response of the whole tissue is considered, a threshold must be reached in order to activate the ensuing cellular cascade and increase bone mass. We hypothesized that a similar activation threshold exists at the cellular level. Here, we test this hypothesis by subjecting an *in vivo* model of bone adaptation to a low magnitude mechanical loading regimen and assessing activation of periosteal osteoblasts in response to the regimen.

METHODS

Five adult male turkeys were included in the study (1.5 yr). Each turkey underwent the functionally isolated avian ulna procedure, in which the diaphysis of left ulna was isolated from loading via parallel metaphyseal osteotomies (2). Externally controlled loading of the diaphysis was achieved by applying loads to transcutaneous pins inserted through stainless steel caps cemented to the exposed diaphyseal bone ends. A one week protocol was used in which the turkeys underwent a brief loading regimen on days 2, 3, and 4 (100 cycles per day). A pneumatic loading apparatus loaded the left ulna in bending, with an induced normal strain distribution (i.e., neutral axis) similar to that achieved during vigorous wing flap. Calcein labels were administered i.v. on day 6 to quantify periosteal activation, and the animals were sacrificed on day 7. Transverse cross-sections were taken from the mid-diaphysis of each experimental and intact contralateral ulna and were hand ground to 80 μm. Composite digital images of each cross-section were obtained using a Polaroid digital camera mounted on an Olympus epifluorescent microscope. Activation of periosteal surface osteoblasts was assessed by determining the percent labeled surface. Mean percent labeled surface was compared between experimental and control bones using a Wilcoxon non-parametric test. End loading conditions previously established using a strain gaged calibration bone were applied to each cross-section geometry. Peak strain magnitudes induced in each animal were determined using beam theory.

RESULTS

Across animals, the short duration, low magnitude loading regimen was sufficient to activate a quiescent periosteum, though not to statistically significant levels (12.6 (6.8% vs 2.0 (0.9% for the control bones; p=0.09). Across animals, maximal induced normal strains ranged from 585 μe to 995 μe. Three turkeys demonstrated periosteal activation in

response to the loading, while two animals demonstrated no periosteal activation. Peak normal strains differed by 14% between these two groups (Figure 1). No correlation was evident between peak induced normal strains and percent labeled surface (r=0.18).
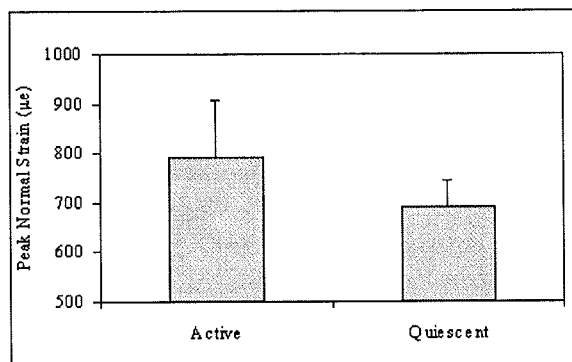
Figure 1. Mean ((s.e.) peak normal strains induced by the external loading regimen in animals in which the periosteum was activated by the loading (Active) and animals in which the periosteum remained unaffected by the loading (Quiescent).

DISCUSSION

The low magnitude loading regimen induced periosteal activation in 3 of the 5 animals in the study, suggesting that the induced strain environment closely bracketed the threshold necessary for periosteal activation in this model. The absence of periosteal activation in two animals provides convincing evidence that the invasive surgery required by the procedure does not induce periosteal activation.

The wide range of induced strain magnitudes resulted from differing cross-sectional geometry and lowered bending loads in two animals (both of which were quiescent). The poor correlation between induced strain magnitude and total labeled surface emphasizes the complexity of mechanotransduction within the tissue. Previous studies with this model emphasize

the interdependence of several mechanical parameters (e.g., magnitude, cycle number, frequency content) in eliciting an adaptive response from the tissue (2,5,6). It is therefore likely that the cellular and tissue equilibrium attained in this study could also be achieved by permutation of components within the loading waveform (e.g., frequency content vs amplitude).

While the loading protocol used here approximated the threshold for periosteal activation, the same stimuli may not be sufficient to surrogate for the role that functional strains play in maintaining a remodeling equilibrium within the cortex. These data do suggest, however, that it should be possible to identify a loading protocol that maintains a quiescent tissue at both cellular and tissue levels. Determination of a threshold between quiescence and activation will facilitate future studies targeted toward identification of cell types responsible for mechanotransduction, and the biochemical pathways initiated as a result of this process.

REFERENCES

1. O'Conner et al. (1982), *J Biom*, 15:767.
2. Rubin et al. (1985), *CTI*, 37:411.
3. Turner et al. (1994), *JBMR*, 9:87.
4. Mosley et al. (1997), *Bone*, 20:191.
5. Rubin et al. (1984), *JBJS*, 66:397.
6. Rubin et al. (1994), *Clin Orthop*, 298:165.

Primary Human Bone Cells from Older Patients Do Not Respond In Culture at Continuum Level *In Vivo* Strain Magnitudes

Clark M. Stanford, D.D.S., Ph.D.[1], Frederic Welsch, M.D.[2],
Norbert Kastner, M.D.[3], Geb Thomas Ph.D.[4], Rebecca Zaharias, BS,[1]
Kevin Holtman, BS,[1] Richard A. Brand, M.D.[2]

[1]Dows Institute for Dental Research, [2]Department of Orthopaedic Surgery, [4]Department of Industrial Engineering, The University of Iowa, Iowa City, IA 52242, U.S.A.
[3]Department of Orthopaedic Surgery, University of Graz, 8036 Graz, Austria
Email: dick-brand@uiowa.edu

INTRODUCTION

Many features of a strain history (e.g., magnitude, frequency, duration, duty cycle) influence bone adaptation, although their inter-relationships and relative importance are unknown. To explore these inter-relationships we developed a culture system allowing substrate deformation in the range of 100-3000 microstrain, 0.5-30 Hz, any programmable wave form, and any number of cycles or duty cycles (Bottlang et al., 1998). With the initial studies we intended to determine whether primary human bone-like cells responded to two specific stimuli similar to those causing *in vivo* responses.

PROCEDURES

Primary human bone-like cultures (Robey, 1985; Zaharias, 1998) were obtained from hip arthroplasty procedures performed for osteoporotic fracture (n=8) or osteoarthrosis (n=5). All patients were post-menopausal females older than 60. Cultures (96,000 cell/cm^2) were strained in rectangular optically clear silastic wells. Three periods of axial substratum strain (1000μ-strain, sine wave, 1 Hz or 20 Hz, 10,000 cycles) were provided every 24 hr using the 4-point

bending, computer-controlled device (Bottlang, et al. 1998).

We used a semiquantitative immunolabeling confocal approach to ascertain levels of bone-related proteins: Type I collagen (ColI), osteopontin (OPN), bone specific alkaline phosphatase (AP), osteonectin (OCN), bone sialoprotein (BSP), and a negative control antibody (Drosophila even-skipped protein, 3C10). Two cultures were assessed per protein per patient, using ten random data images (10x) per culture. We used NIH Image to calibrate and subtract background. Pixel density/image was calculated using a gray scale value (0-256) and averaged for semi-quantitative comparisons. We additionally determined AP activity and AP mRNA copy number using a cRNA RT-PCR approach. Strained cultures were compared to unstrained from the same donor and culture at the same time. Kruskal-Wallis analysis was performed on average percent in signal intensity of strained versus unstrained cultures. We presumed an $\alpha = 0.05$ as the level of significance.

RESULTS
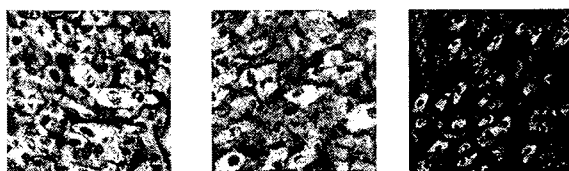
Coll   AP   BSP

All cultures qualitatively exhibited high levels of bone related proteins in most cells compared to negative controls (see above).
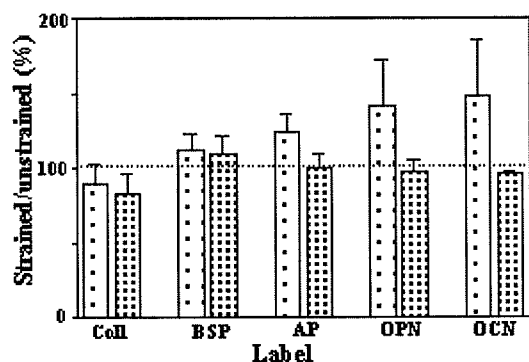
Strain did not alter (p>0.05 in all cases) levels of bone-related protein levels, enzyme activity, or steady state copy number per cell in response to strain (standard errors of the mean; shaded bars osteoporotic cells).

We observed no differences (p>0.05) in confocal imaging, AP activity, AP mRNA levels, or cellular proliferation at 1 versus 20 Hz.

DISCUSSION

Many authors have reported responses of primary and transformed bone-like cells to various strain regimens, although in all but perhaps one study the low frequency (1 Hz) strains were well above that believed physiological for bone as a tissue (i.e., over 3000 microstrain peak). Given higher frequency regimens appear to affect bone formation *in vivo*, we also used one higher frequency (20 Hz) regimen (Rubin, 1994). Only Brighton et al. (1991) have demonstrated responses below 3000

microstrain (1 Hz) and these were in newborn rat calvarial osteoblasts at 400 microstrain. The failure of our bone-like cells to respond to two strain regimens anticipated to evoke responses could be owing to a number of factors, including use of: 1.) primary human and not transformed cells; 2.) cells from older human females not on estrogens; 3.) low strain magnitudes. Perilacunar strains are as much as 10-15 times peak continuum (e.g., 1000-3000 microstrain) determined levels (Nicolella et al., 1998a&b). Thus, "sensing" cells could be those experiencing 5-20,000 microstrain (below fracture levels).

SUMMARY

This data and that from the literature showing responses at much higher strain magnitudes are consistent with the notion that sensing cells require higher levels of strain than generally appreciated, although we cannot rule out lack of responsiveness of older primary human bone-like cells.

REFERENCES

Bottlang., M. et al. (1997). Biomedizinische Technik 42, 305-309.
Brighton, C.T. et al. (1991). Journal of Bone and Joint Surgery 73A, 320-331.
Nicolella, D.P. et al. (1998a). Transactions of the Orthopaedic Research Society, 137.
Nicolella, D.P. (1998b) Personal communication.
Rubin, C.T., McLeod, K.J. (1994). Clinical Orthopaedics and Related Research 298:165-174.
Robey, P., Termine, J.D. (1985). Calcified Tissue International 37, 453-460.
Zaharias, R.S. et al. (1998). Journal of Dental Research 77, 212.

ACKNOWLEDGEMENTS

TRANSVERSE CREEP RESPONSE IN HUMAN FEMORAL BONE

Christopher U. Brown[1,2], Timothy L. Norman[1,2], Vincent L. Kish[2], Thomas A. Gruen[2]
and J. David Blaha[2]

[1] Department of Mechanical and Aerospace Engineering and [2]Department of Orthopedics,
West Virginia University, Morgantown, West Virginia
Email: cbrown@ds5500.cemr.wvu.edu Web: www.hsc.wvu.edu/som/ortholab/

INTRODUCTION

Human cortical bone is known to exhibit viscoelastic, a time-dependent, behavior in the longitudinal direction of long bones (Carter and Caler, 1983; Caler and Carter, 1989; Rimnac et al., 1993; Fondrk et al., 1988; Pattin et al., 1995). The time-dependent response of bone to transverse loads has received less attention. This response has an important role in the fixation of implants in cortical bone. Cementless total hip replacement involves the placement of an implant into the femoral canal. The prosthesis is held in place by circumferential stress generated within the cortical bone. Relaxation of the radial forces in bone may compromise the initial fixation of the implant, allowing for subsidence and the establishment of a new loading environment.

Previous work involving the transverse time-dependent response of bone has been limited to the study of bovine bone loaded in compression (Tanabe and Kobayashi, 1994) and tension (Crowninshield and Pope, 1974). Although these studies did not examine creep behavior, the results suggest that the time-dependent response of bone differs with the direction of the applied load. Further study is needed to understand the time-dependent response of bone to loads applied in the transverse direction.

Creep is a viscoelastic response defined as time-dependent strain under constant load. At low levels of constant stress, an equilibrium deformation may be attained, however, at higher stress levels, deformation may increase with time leading to creep-failure. The objective of this investigation was to study the short-term creep behavior of human bone cylinders subjected to internal pressure. A technique has been developed to apply constant radial load to right circular cylinders of human cortical bone, inducing creep in bone.

PROCEDURES

A fresh femur, with normal bone quality, was obtained from an 86 year old male cadaver. A bulk section of the mid-diaphysis of the femur was machined into a right circular cylinder 19 mm in length, with a 19 mm inner wall diameter, and a wall thickness of 2.4 mm. The specimen was kept wet with physiological saline solution throughout the machining process.

To provide a more realistic assessment of bone behavior, a technique was established to simulate the radial forces during the insertion of a maximum fit and fill press-fit implant. The test fixture applied constant internal pressure to the inner surface of the specimen through a latex hose (Figure 1). Pressurized nitrogen gas was used to internally load the specimen to a constant pressure of 2 MPa until failure. Eight strain

gages (grid dimension 1.57 x 1.57 mm) were oriented to measure hoop (circumferential) strain at equal intervals around the circumference of the cylinder. The test fixture, including the bone specimen, was submerged in a saline solution bath at body temperature for the duration of the test. Time, internal pressure, and strain were recorded.
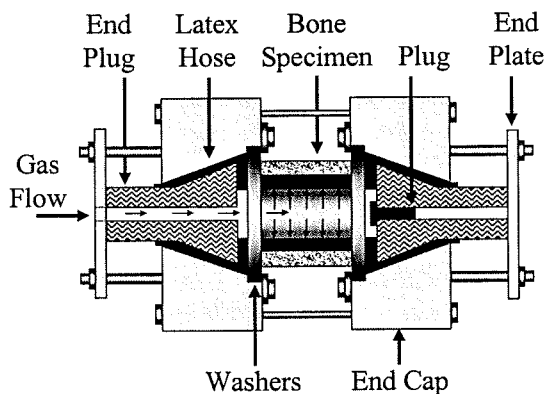
Figure 1: The test fixture for applying radial load to bone cylinders (cut-away view).

RESULTS AND DISCUSSION

The results of this study indicate that bone subjected to a transverse load exhibited the three basic characteristic stages of creep prior to fracture: primary creep where the creep rate decreased, secondary creep where the creep rate was constant, and tertiary creep where the creep rate increased until failure (Figure 2).

A technique was developed to apply internal pressure to a uniform cylinder in order to observe the creep response of femoral cortical bone to a constant radial load. The data presented in this paper are part of ongoing research to measure cortical bone creep behavior in femoral bone cylinders. This work has shown that cortical bone experiences creep as a result of transverse loads. This creep behavior occurs at the time of internal pressure application (implant insertion), and may affect the initial fixation and stability of a femoral implant. Understanding this response of bone immediately following the insertion of an implant will make it possible to improve cementless prosthetic design, improve computer models of the bone-stem system, and help to predict short and long-term stability of the stem after insertion.
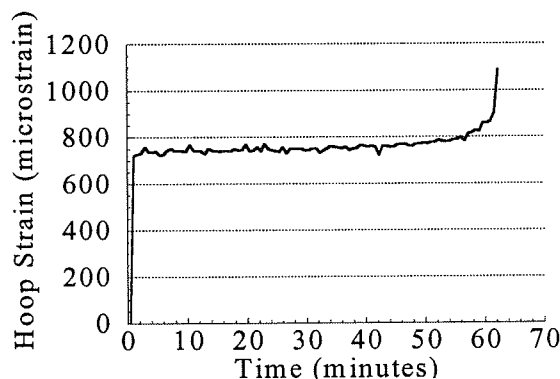
Figure 2: Transverse elastic and creep strain of cortical bone subjected to an internal pressure of 2 MPa. A cubic spline was used to fit the data.

SUMMARY

These results suggest that cortical bone exhibits creep behavior under radial loading that simulates in-vivo conditions of an intramedullary prosthesis. Results from continuing research will be used to develop numerical models that predict in-vivo stresses induced by implants in bone.

REFERENCES

Caler, W.E., Carter, D.R. (1989). *J. Biomechanics*, **22**, 625-635.

Carter, D.R., Caler, W.E. (1983). *J. Biomech. Engng.*, **105**, 166-170.

Crowninshield, R.D., Pope, M.H. (1974). *Ann. Biomed. Engng.*, **2**, 217-225.

Fondrk, M. et al. (1988). *J. Biomechanics*, **21**, 623-630.

Pattin, C.A. et al. (1995). *ASME BED*, **29**, 247-248.

Rimnac, C.M. et al. (1993). *J. Biomechanics*, **26**, 219-228.

Tanabe, Y., Kobayashi, K. (1994). *J. Mater. Sci.: Mater. Med.*, **5**, 397-401.

A BIOMECHANICAL STUDY ON THE EFFECTS OF PAMIDRONATE FOR PREVENTION OF OSTEOPOROSIS IN OVARIECTOMIZED RATS

Jung-Woog Shin[1], Su-Hyang Kim[1], Jang-Suk Choi[2], Sung-Jae Lee[1] and Min-A Ok[1]

[1]Department of Biomedical Engineering, Inje University, Korea
[2]Department of Orthopaedic Surgery, Inje University Paik Hospital, Korea
Email: sjw@bme.inje.ac.kr

INTRODUCTION

Animal studies show that pamidronate can be 10-100 times more potent than clodronate or etidronate in inhibiting bone resorption *in vivo*. The purpose of this study is to determine the effects of pamidronate on the prevention of postmenopausal osteoporosis in the femur of ovariectomized rats by conducting bio-mechanical analysis.

PROCEDURES

Forty-two female Sprague-Dawley rats were used for this study. At the beginning of the experiment, the animals were 17 weeks of age weighing approximately 244g. The animals were randomly divided into 3 groups: Group 1 (n=10) was sham-operated, Group 2 (n=12) bilateral ovariectomy, and Group 3 (n=20) bilateral ovariectomy plus intravenous injection of 0.1mg/kg pamidronate twice a week during the first 8 weeks. Animals were sacrificed 12 weeks postoperatively and stored at -20°C in a freezer. Before testing, the specimens were thawed at room temperature. The femurs from each group were tested in a 3-point bending mode with an MTS 858.20 Bionix testing machine (MTS System Corp., Minneapolis, MN, USA) to obtain bending stiffness. Load was applied to the bone at the mid-point of the femur at a deformation rate of 0.01 mm/sec. Bending stiffness was measured as the initial linear slope of the load-displacement curve. In addition, the stiffness was calculated analytically. For this, the femur was assumed

as an isotropic, homogeneous, and deformable material of a small size. Thus, the following relationship between the deflection, bending moment, moment of inertia, and Young's modulus was used for analysis of bending of the femur:

$$\frac{|v''|}{\left[1 + (v')^2\right]^{1.5}} \approx |v''| = \frac{M_b}{EI} \quad \text{...(1)}$$

where M_b is the bending moment, v is the deflection, I is the moment of inertia, and E is Young's modulus. To calculate the moment of inertia of varying cross-sections, the specimens were cut into 2 mm-thick slices with a diamond saw (ISOMET™ 1000 Precision Saw, Buehler Analyst Ltd., Lake Bluff, IL, USA). Photos of the cross-sections were taken using CCD camera (WV-BP310, Panasonic®) and the cross-sectional areas were measured using specially-developed image analysis software. Young's modulus was calculated using the moment-area method as in Equations (2) and (3):

$$E = \frac{PL^2}{576 \cdot \delta} \cdot \frac{2L}{36} \left(\frac{8}{I_1} + \frac{19}{I_2} + \frac{37}{I_3} + \frac{49}{I_4} + \frac{91}{I_5} \right) \quad \text{...(2)}$$

$$E = \frac{PL^2}{576 \cdot \delta} \cdot \frac{2L}{36} \cdot \left(\frac{8}{I_1} + \frac{19}{I_2} + \frac{37}{I_3} + \frac{152}{I_4} \right) \quad \text{...(3)}$$

where P/δ is the stiffness, L is the distance between the two supports and $I_{i(i=1...5)}$ is the moment of inertia of each segment. Equation

(2) is for specimens with 5 slices and Equation (3) is for specimens with 4 slices.

RESULTS AND DISCUSSION

Figure 1 shows the analytically calculated Young's modulus results of each group: 12.6 ± 3.5 GPa for Group 1, 9.6 ± 2.7 GPa for Group 2, and 12.0 ± 2.4 GPa for Group 3. Young's modulus of Groups 1 and 3 were each significantly larger ($p<0.1$) than that of Group 2. The difference between Group 1 and Group 3 was not significant ($p=0.4$). These results suggest that pamidronate treatments can raise the Young's modulus of osteoporotic bone to levels close to that of normal bone. Differences between the load-deflection curves from the bending tests were, however, indistinguishable among the groups (Figure 2).

SUMMARY

Our biomechanical analysis showed that the Young's modulus of the femur was increased by administration of pamidronate in a rat model of osteoporosis. This suggests that pamidronate could be effective for prevention of osteoporosis during the early period of estrogen deficiency.

REFERENCE

Fitton, A., McTavish, D. (1991). *Drugs*, **41(2)**, 289-318.
Choi, J.S. et al. (1998). *Journal of Korean Orthopaedic Research Society*, **1(1)**, 115-123.
Gere, J.M., Timoshenko, S.P. (1984). *Mechanics of Materials*. Second Edition, Brooks/Cole.
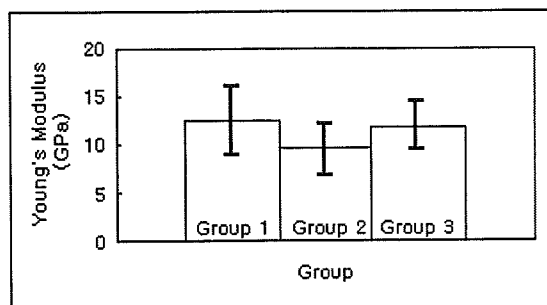
Figure 1: Comparison of Young's modulus for each group.
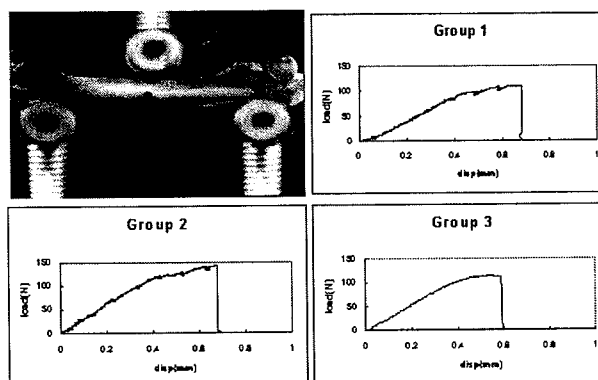
Figure 2: 3-point bending test and typical load-displacement curves for each group.

THE EFFECTS OF ADULT ACQUIRED FLATFOOT DEFORMITY ON TIBIOTALAR JOINT CONTACT CHARACTERISTICS

Mark A. Friedman, Louis F. Draganich, Brian Toolan, and Michael E. Brage

Section of Orthopaedics and Rehabilitation Medicine, Department of Surgery
The University of Chicago, Chicago, Illinois 60637
Email: ldragani@surgery.bsd.uchicago.edu

INTRODUCTION

The acquired flatfoot deformity is a condition whose principle etiologies can be traumatic, spontaneous, degenerative or neuropathic (Henceroth & Deyerle, 1982) and can severely limit a person's ability to stand or walk comfortably (Mann & Thompson, 1985). The condition arises as an insidious collapse of the longitudinal arch as a result of a progressive valgus deformity of the calcaneous, plantar flexion of the talus, and abduction of the forefoot (Mann & Thompson, 1985). One of the most commonly recognized causative factors is deficiency of the tibialis posterior or rupture of the tendon (Deland et al., 1992, Henceroth & Deyerle, 1982, Mann & Thompson, 1985) which acts as a principle inverter and adductor of the foot. This leads to increased loads in the local soft tissues which may stretch or tear and the described deformity may develop (Mann & Thompson, 1985).

Osteoarthritic changes in the ankle have been observed in patients with long term deformity (Jahss, 1991), yet little is known of the mechanical effect of acquired flatfoot deformity on the ankle joint. The objective of this study was to characterize the changes in contact pattern and load distribution of the tibiotalar joint with an acquired flat foot deformity.

The changes in the tibiotalar contact characteristics were investigated using fresh frozen cadaver ankle specimens to model the acquired flatfoot deformity. The deformity was simulated by sectioning the tendons and ligaments of the ankle and foot that normally support the longitudinal arch. The cadaver model simulates physiologic conditions by loading the ankle axially in a neutral position to two times the body weight of an average man. This load reproduces the actual forces experienced by the articular surfaces during normal gait generated by both ground reaction forces and muscle contractions (Stauffer et al., 1977). Measurements of the tibiotalar joint contact characteristics were made using pressure sensitive film.

We hypothesized that the acquired flatfoot deformity would result in significant alterations in the tibiotalar contact characteristics. Specifically, a lateral shift and reduction in area of the contact distribution was expected as a result of the everted position of the calcaneus and consequent malalignment of the joint surfaces.

PROCEDURES

Eight fresh frozen cadaver ankle specimens were obtained for testing. Each ankle had been radiologically screened and manually examined to exclude previous fractures, osteoarthritis, or other signs of defects. Threaded rods were cemented into the tibial and fibular canals with epoxy.

Hermetically sealed film packets were constructed of low pressure, Pressensor film (Inteque Resources Corp., Fort Lee, NJ,

USA). The film packets were placed into the tibiotalar joint anteriorly through an arthrotomy incision. Pins were used to place reference marks and to locate the film packet within the joint in a reproducible manner.

Loading of the specimen was performed on a materials testing device (Instron model 8500 plus, Instron Corp., Canton, MA). The tibial rod was mounted vertically in the machine and the foot rested in zero degrees of flexion on a steel plate supported by ball bearings assuring that a purely axial load was applied to the specimen. An aluminum plate was rigidly fixed to the tibial rod and was secured to the fibular rod with an adjustable nut. Bending of the plate could be adjusted to transfer 10% of the total load to the fibula during testing.

The testing procedure involved pre-loading the ankle to 50 N. Then, a 0.5 second ramp load was applied to a peak load of 1,350 N. This maximum load was held for 0.5 second, and then returned to 50 N in 0.5 second. This loading sequence was applied three times to obtain three sets of film prints for each intact specimen. An established ligamental release procedure was then employed to create a severe flatfoot deformity (Deland et al., 1992). The loading sequence was again applied three times to obtain three sets of film prints for the flatfoot specimen.

The pressure imprints were scanned forming a 600 dpi 256 gray scale image (0=black, 255=white). The images were analyzed using Global Lab Image version 2.20 (Data Translation Inc., Marlboro, MA, USA) software. Area, mean pressure, and center of contact area measurements were then made. A high pressure region was defined

as the 90th percentile of darkest pixels and was used to determine the peak pressure and location of peak pressure.

These measurements were averaged for the three film prints for each condition, intact and flatfoot. Average values of change in the measured variables were tabulated. Each specimen served as its own control and paired t-tests were performed. Differences were considered to be statistically significant at the α=0.01 level of significance.

RESULTS AND DISCUSSION
The flatfoot condition resulted in significant lateral shifts of 5.28 mm (p=0.0002) in global contact area and 11.26 mm (p=10^{-6}) in the location of peak pressure. The flatfoot condition also resulted in a significant, 35% (p=0.005), reduction in contact area.

These findings support our hypothesis and provide insight into the probable mechanism of injury to the articular cartilage in long term flatfoot deformities. This model will further provide a tool for the evaluation of various corrective measures, including reconstructive techniques.

REFERENCES
Deland, J.T. et al. (1992). *Foot and Ankle*, 13, 327-332.

Henceroth II, W.D., Deyerle W.M. (1982). *Foot and Ankle*, 2, 304-308.

Jahss, M.H. (1991). *Disorders of the Foot and Ankle*. WB Saunders Company.

Mann, R.A., Thompson, F.M. (1985). *J Bone Joint Surg*, 67A, 556-561.

Stauffer, R.N. et al. (1977). *Clin Orthop*, 127, 189-196.

UTILIZATION OF AN AUTOMATED MODEL FITTING PROCESS TO DETERMINE KINEMATICS OF TKA

[1,2]Sarojak, M.E., [2]Hoff, W.A., [1]Komistek, R.D., [1]Dennis, D.A.

[1]Rose Musculoskeletal Research Labortory, Denver, Colorado
[2]Machine Vision Lab, Colorado School of Mines, Golden, Colorado

INTRODUCTION

Recently, fluoroscopy has been utilized to capture *in vivo* images of total knee arthroplasty (TKA) during various activities Dennis, et al, 1996; Banks et al, 1993). Using these x-ray images, various techniques have been used to determine the *in vivo* kinematics of TKA with respect to flexion angle. The objective of this study was to utilize advances in computer technology and software capabilities to develop an automated process that very quickly and accurately recovers the 3D kinematics from 2D fluoroscopic images.

METHODS

Silicon Graphics computers were used in conjunction with the Open Inventor software package to recreate a fluoroscope within the computer. In a fluoroscope, the radiation source emits x-rays, which create a perspective projection of a patient's anatomy on the image intensifier. To recreate the fluoroscope within the computer, the components of the fluoroscope are replaced by their computer counter-parts. The radiation source is represented by a virtual camera, and the image intensifier is replaced by the x-ray image itself. Finally, the patient's knee is replaced by computer models of the TKA implants.

Next, a software program corrects the radial distortion of the x-ray images and then determines the positions and orientations (pose) of the TKA models within the images. This process utilizes image-processing techniques to determine how well the positions of the models correspond to those of the actual implants in the x-ray image. By manipulating the TKA models so that their projected contours align with the silhouettes of the actual implants in the x-ray image, the computer very quickly and accurately determines the correct pose of each TKA implant.
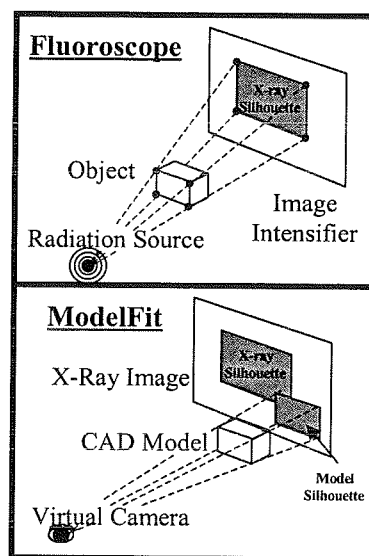
Figure 1. Actual fluoroscope geometry and the computer recreation of fluoroscope.

RESULTS

By comparing the performances of various processes, the power of the automated process becomes clear. First, three different processes (automated model fitting (1), manual model fitting (2), and library matching (3)) were implemented on 20 fluoroscopic images in order to compare their relative speeds. The automated model-fitting process was 5.54, and 28.86 times

faster than the manual model fitting and library matching techniques, respectively.
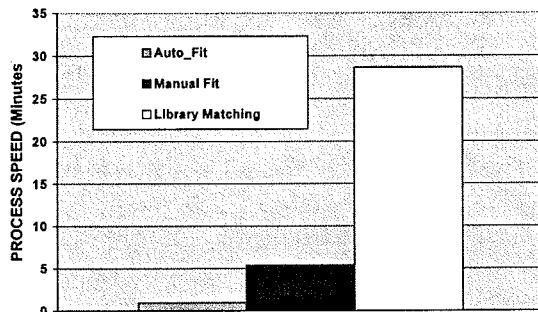
Figure 2. Average processing time of the three techniques.

Next, the repeatability of the automated process was determined for 10 dynamic fluoroscopic images. This study revealed that the automated process is repeatable to within 0.17 degrees of rotation and 0.15 mm of translation. Finally, the accuracy of the automated process was tested. On synthetic images (perfect image quality and model accuracy) the automated model-fitting algorithm achieved an accuracy of 0.009 degrees of rotation and 0.013 mm of translation. By way of comparison, the accuracy of manual model fitting averaged 0.38 degrees and 0.13 mm for the same images. On fluoroscopic images, an error analysis of the manual process revealed accuracy of 0.75 degrees for rotation and 0.75 mm for the in-plane translation. Although the results of the error analysis of the automated process are pending, the synthetic accuracy and *in vitro* repeatability studies suggest that the accuracy will be better than 0.1 degrees of rotation and 0.1 mm of translation.
Furthermore, using either library matching or manual model fitting, the out-of-plane translation error ranges from 2.4 to 5.0 mm. Using the automated system, the average error for synthetic images was 0.04 mm.
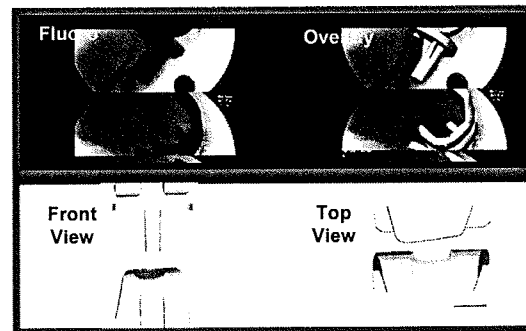
Figure 3. Model fitting process.

DISCUSSION

The automated model fitting system is faster and more accurate than either the manual fitting or library matching techniques. Additionally, the automated process removes operator bias and error from the process.
It is also important to note that, unlike template matching, the model-fitting technique is capable of handling images with partially occluded implants (not completely visible). This is possible because the automated system finds the maximum correlation between the projected contour of the TKA model and the remaining portion of the implant silhouette. Even though a portion of the x-ray silhouette is occluded, the maximum correlation still occurs in the correct pose.
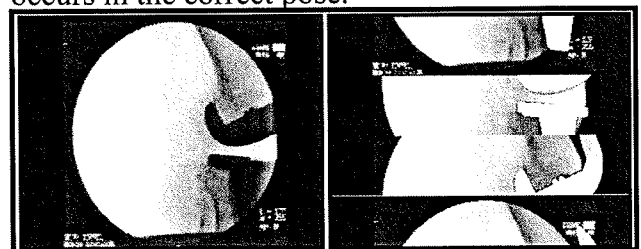
Figure 4. Occluded image and its overlay.

REFERENCES

[1] Dennis DA, et al, (1996). *Clin Orthop, 107-117*
[2] Banks SA, et al, (1993), *ORS 39th Meeting*

A QUASI-LINEAR, STRUCTURAL MODEL OF THE PLANTAR SOFT TISSUE WITH FREQUENCY DEPENDENT DAMPING PROPERTIES

William R. Ledoux, [1,2] David F. Meaney, [1] and Howard J. Hillstrom, [2,1]
[1] Department of Bioengineering, University of Pennsylvania, Philadelphia, PA
[2] Gait Study Center, Temple University School of Podiatric Medicine, Phila., PA
Email: hhillstrom@tuspm.temple.edu

INTRODUCTION

The foot is the interface between the body and ground during posture and locomotion. Although the structural properties of the subcalcaneal tissue have been explored, (Aerts, et al., 1995, Ker, 1996, Kinoshita, et al., 1996, Valiant, 1984) most of the research has concentrated on the response of the tissue to impact loads and little has been done to develop constitutive relationships. (Ledoux, et al., 1997) There are no published data for other areas on the plantar aspect of the foot. The quasi-linear viscoelastic (qlv) theory has been developed as a constitutive relationship for non-linear viscoelastic tissue. (Fung, 1993) Force is a function of an elastic function, $F^e(\varepsilon)$, which depends on strain, and a reduced relaxation function, $G(t)$, which depends on time. (Note that the qlv theory is being used as a structural model, with force rather than stress.) See equations 1 to 4.

$$F(t) = \int_0^t G(t-\tau) \frac{\partial F^e[\varepsilon(t)]}{\partial \tau} dt \qquad (1)$$

$$F(\varepsilon) = A\left(e^{B\varepsilon} - 1\right) \qquad (2)$$

$$G(\tau) = \frac{1 + \int_0^\infty S(\tau)e^{-t/\tau}d\tau}{1 + \int_0^\infty S(\tau)d\tau} \qquad (3)$$

$$S(\tau) = \begin{cases} \dfrac{c}{\tau}, & \tau_1 \leq \tau \leq \tau_2 \\ 0, & \tau < \tau_1 \ \text{and} \ \tau > \tau_2 \end{cases} \qquad (4)$$

A and B are elastic constants, c_1 is the amplitude of the viscous effects, while τ_1 and τ_2 represent the frequency limits of the relaxation spectrum, $S(\tau)$. The most common implementation of the qlv theory uses a relaxation spectrum function that shows a constant dissipation across a broad frequency range. As our data will demonstrate, the plantar soft tissue does not exhibit the common response, but shows a dissipation that changes with frequency. Recently, a linear frequency-sensitive model

has been developed. (Iatridis, et al., 1997) The investigators assumed linear elastic behavior for equation 2 and modified equation 4 as follows:

$$S(\tau) = \begin{cases} \dfrac{c_1}{\tau} + \dfrac{c_2}{\tau^2}, & \tau_1 \leq \tau \leq \tau_2 \\ 0, & \tau < \tau_1 \ \text{and} \ \tau > \tau_2 \end{cases} \qquad (5)$$

Where c_1 is the amplitude of the viscous effects and c_2 is the linear increase in amplitude with frequency. We developed a model that incorporated the nonlinear elastic function from Fung with the rate dependent reduced relaxation function from Iatridis. The model parameters A, B, c_1, c_2, and τ_1 are obtained by curve fitting the data, while τ_2 is taken as the last point in time.

PROCEDURE

Both age (Kinoshita, et al., 1996, Kuhns, 1949, Prichasuk, et al., 1994) and peripheral vascular disease (Buschmann, et al., 1995, Jahss, et al., 1992) can alter the subcalcaneal tissue. The temperature of a specimen should be considered, since adipose tissue melts near body temperature. (Phinney, et al., 1994) Eight young (average age 36.9, with a range of 18 - 58 years), healthy (no peripheral vascular disease) cadaveric feet were studied. Each foot was disarticulated at the subtalar joint, dissected down to ligament and bone, and mounted plantar side up in bone cement. The feet were heated and maintained at body temperature. Stress relaxation experiments were conducted with a protocol described previously. (Ledoux, et al., 1997) Each of the seven areas (subcalcaneal, subhallucal, and five submetatarsal) on the plantar aspect of the foot was tested. The loading of each area was based on the peak loads experienced during gait. (Ledoux, et al., 1997)

RESULTS

The force and strain data for each area were averaged over the number of feet. The resultant average data were curve fit with the

modified qlv model using a nonlinear least-squares algorithm in Igor Pro (WaveMetrics, Inc.; Lake Oswego, OR). Figure 1 is the average data for the calcaneal area (n=6) +/- 1 standard deviation. Figure 2 is the curve fit of the average data. Similar results were demonstrated for the other six areas. Table 1 summarizes the parameters from fits of the data for each of the seven areas of loading.
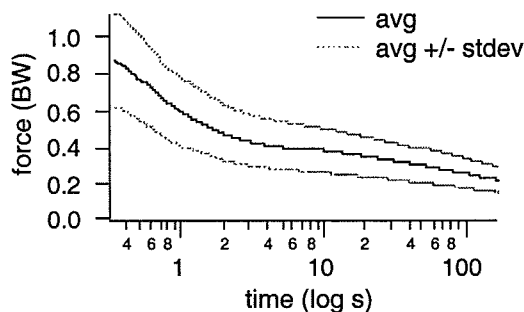
Figure 1: Average force (+/- 1 standard deviation) versus time.
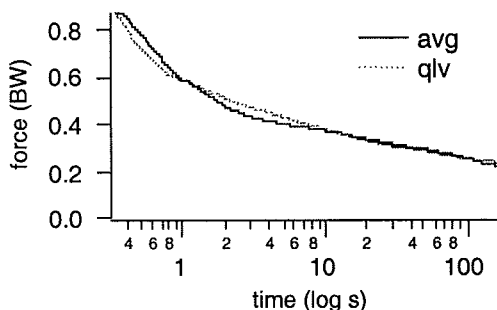
Figure 2: Curve fit of average force versus time with the modified qlv model.

DISCUSSION

This work represents the first comprehensive structural testing of the soft tissue on the plantar aspect of the foot. Stress relaxation experiments were performed on seven loading areas from eight feet. A modified quasi-linear viscoelastic model was developed by incorporating a linear elastic function and a frequency dependent reduced relaxation function. This model predicted the frequency-sensitive behavior of the plantar soft tissue. Table 1 indicates differences in the parameter (A) that determines peak forces, as well as with the damping constant, c_1. The elastic and reduced relaxation constants that describe rate (B and τ_1) as well as one of the damping constants (c_2), were similar for six out of the seven areas. Only the subcalcaneal area, with its unique anatomy, was found to have different structural properties. The other six areas may potentially be modeled with one set of values.

ACKNOWLEDGEMENTS

REFERENCES

Aerts, P., Ker, R. F., et al. (1995). *Journal Of Biomechanics* 28, 1299-1308.

Buschmann, W. R., Jahss, M. H., et al. (1995). *Foot & Ankle International* 16, 254-8.

Fung, Y. C. (1993). *Biomechanics: mechanical properties of living tissues.* Springer-Verlag.

Iatridis, J. C., Setton, L. A., et al. (1997). *Journal of Biomechanics* 30, 1005-13.

Jahss, M. H., Michelson, J. D., et al. (1992). *Foot & Ankle* 13, 233-42.

Ker, R. F. (1996). *Journal of Experimental Biology* 199, 1501-8.

Kinoshita, H., Francis, P. R., et al. (1996). *European J. of Applied Physio. & Occupational Physio.* 73, 404-9.

Kuhns, J. G. (1949). *Journal of Bone and Joint Surgery* 31-A, 541-547.

Ledoux, W. R., DeLott, J. M., et al. (1997). Proceedings The N. A. Soc. of Gait and Clinical Movement Analysis

Ledoux, W. R., Hillstrom, H. J., et al. (1997). Proceedings American Society of Biomechanics

Phinney, S. D., Stern, J. S., et al. (1994). *American Journal of Clinical Nutrition* 60, 725-9.

Prichasuk, S., Mulpruek, P., et al. (1994). *Clinical Orthopaedics & Related Research* , 197-200.

Valiant, G. A. (1984) Ph.D. Thesis, The Pennsylvania State University

Table 1: The results for the curve fit of average relaxation data.

area	no.	A	B	c_1	c_2	τ_1	τ_2
subhall	8	0.238	1.676	0.400	0.451	0.114	174.90
subcalc	6	0.451	2.299	0.311	0.146	0.087	174.92
1st submet	7	0.097	1.973	0.422	0.546	0.140	174.90
2nd submet	7	0.058	2.085	0.400	0.500	0.130	174.92
3rd submet	6	0.077	1.555	0.363	0.447	0.123	174.93
4th submet	6	0.044	1.778	0.233	0.446	0.127	174.90
5th submet	4	0.020	1.966	0.174	0.274	0.121	174.94

QUASI-LINEAR VISCOELASTICITY OF ANKLE LIGAMENTS

James R. Funk, Gregory W. Hall, Jeff R. Crandall and Walter D. Pilkey

Automobile Safety Laboratory, University of Virginia, Charlottesville, Virginia
Email: jrf4y@virginia.edu Web: http://cindarella.mech.virginia.edu/home.html

INTRODUCTION

Prior mechanical testing of ankle ligaments has focused on quantifying ligament ultimate strength (Attarian et al., 1985; Siegler et al., 1988). Few studies have attempted to model the constitutive behavior of ankle ligaments at sub-failure levels. Although the viscoelastic nature of ankle ligaments has been noted (Attarian et al., 1985), no studies have attempted to create a viscoelastic constitutive model for any ankle ligament. The purpose of this study was to create a quasi-linear viscoelastic constitutive model of eight major ankle ligaments for use in computational modeling of the human lower extremity.

METHODOLOGY

Three pairs of below-knee amputation specimens were acquired from middle-aged 50th percentile male donors. Twenty-nine (29) bone-ligament-bone specimens were harvested from the six foot/ankle complexes. For each pair, the calcaneofibular (CF), anterior tibiofibular (ATiF), posterior tibiofibular (PTiF), and tibiocalcaneal (TiC) ligaments were harvested from one ankle, and the anterior talofibular (ATaF), posterior talofibular (PTaF), anterior tibiotalar (ATT), posterior tibiotalar (PTT), ATiF and PTiF ligaments were harvested from the other ankle. The relaxed length of each ligament was measured with calipers. Specimens were potted in bone cups using a low melting point alloy and mounted to a universal test machine (MTS 858 Bionix). The zero-strain state for each ligament was defined by raising the actuator until the ligament began to resist tension with a nominal load (< 2 N).

Each ligament was preconditioned by applying ten (10) successive steps up to the 10% strain (20% in some tests), after which the ligament was allowed to recover at zero strain for at least 1000 sec. A series of step strains (180 mm/sec) were then applied and held for up to 1000 sec, allowing recovery time after each step. The steps were applied at different strain levels (2%, 4%, 6%, 8%, and 10% or 5%, 10%, 15%, and 20%). Finally, the ligaments were subjected to a failure test at 280 mm/sec.

Step relaxation data at different strain levels were averaged for each specimen and curve fit to a constant plus three exponentials. Due to vibration of the test machine, the first .1 sec of data were contaminated by a large 20 Hz shock wave. Relaxation curves were obtained by curve fitting only the data beyond .1 sec and back-extrapolating to time zero. The curves were then normalized by dividing by the peak value to obtain reduced relaxation functions (RRF) $G(t)$ of the form:

$$G(t) = G_0 + G_1 e^{-t/\tau_1} + G_2 e^{-t/\tau_2} + G_3 e^{-t/\tau_3}$$

The elastic response function (ERF) $T(\varepsilon)$ for each specimen was obtained by curve fitting the isochronous force-strain data at time zero to an exponential of the form:

$$T(\varepsilon) = a(e^{b\varepsilon} - 1)$$

The RRF's and ERF's were then averaged for each ligament type. In two cases an exponential could not fit the ERF data, so a linear form was used. For a given strain history, the force in a ligament can be

described by a quasi-linear viscoelastic constitutive equation of the form (Fung, 1981):

$$F(t) = T[\varepsilon(t)] + \int_0^t T[\varepsilon(t-\tau)]\frac{\partial G(\tau)}{\partial \tau}d\tau$$

RESULTS AND DISCUSSION

For individual specimens, curve fits of the RRF and ERF were found to have an excellent goodness of fit ($R^2 > .99$ in most cases). However, interspecimen variability was found to be generally high (Table 1 and Table 2). Because of the high number of ligament harvested from each specimen, bone ends were often small and weakened, and therefore failure tests were not always successful. The failure loads reported here (Table 2) are somewhat higher than values reported in the literature (Attarian et al., 1985; Siegler et al., 1988). This is probably because our specimens came from middle-aged males, as opposed to older or female donors.

Several aspects non-linear viscoelastic behavior were observed. Isochronous force-strain curves were found to be highly non-linear, with a soft initial toe region followed by a progressively stiffer loading region. Also, more relative relaxation (decreasing G_0) was observed at higher strains during serial testing of the same ligament.

SUMMARY

Twenty-nine (29) specimens from eight major ankle ligaments were characterized viscoelastically at sub-failure loads. Non-linear behavior was observed and modeled using a quasi-linear viscoelastic constitutive equation.

Table 2: Elastic Response Function Curve Fit Data and Failure Test Data

Ligament	a	b	R^2	Failure load (N)
ATaF	18.78	8.50	0.945	297 (n=2)
ATiF	0.98	41.22	0.541	708 (n=1)
ATT	2.12	19.90	0.979	131 (n=2)
CF	0.08	58.84	0.852	598 (n=2)
PTaF	0.15	43.96	0.970	554 (n=2)
PTiF	403.34	linear	0.238	n/a
PTT	1.05	29.94	0.999	n/a
TiC	438.35	linear	0.513	403 (n=1)

REFERENCES

Attarian, D.E. et al. (1985). *Foot & Ankle* 6(2), 54-58.

Fung, Y.C. *Biomechanics: Mechanical Properties of Living Tissues*. Springer-Verlag, New York.

Siegler, S. et al. (1988). *Foot & Ankle* 8(5), 234-242.

Table 1: Reduced Relaxation Function Curve Fit Data

Ligament	sample size	G_0	G_1	τ_1 (sec)	G_2	τ_2 (sec)	G_3	τ_3 (sec)	R^2
ATaF	n=3	0.661	0.092	0.558	0.104	8.51	0.144	132.8	0.536
ATiF	n=6	0.651	0.091	0.627	0.100	11.11	0.158	217.1	0.603
ATT	n=3	0.729	0.091	0.465	0.084	6.95	0.097	131.8	0.422
CF	n=3	0.649	0.069	0.605	0.073	12.72	0.209	244.1	0.680
PTaF	n=3	0.695	0.078	0.472	0.081	9.48	0.146	185.2	0.620
PTiF	n=5	0.602	0.097	0.765	0.112	12.86	0.189	161.1	0.793
PTT	n=3	0.438	0.127	0.832	0.152	14.75	0.284	216.9	0.918
TiC	n=3	0.514	0.125	0.704	0.152	11.16	0.209	164.6	0.664

PROPER FORCE TRANSMISSION THROUGH THE TOES AND FOREFOOT IS DEPENDENT ON THE PLANTAR FASCIA

Andrew J. Hamel[1,2] and Neil A. Sharkey[1,3]

[1]The Center for Locomotion Studies, [2]Department of Mechanical Engineering,
[3]Department of Kinesiology, Pennsylvania State University, University Park, PA
Email: celos@psu.edu Web: www.celos.psu.edu

INTRODUCTION

During terminal stance, as push-off occurs, the extrinsic toe flexor muscles (flexor digitorum longus and flexor hallucis longus) are activated to resist the dorsally directed forces imposed on the toes by the ground, thereby enhancing their ability to bear weight. At the same time, the taut plantar fascia helps maintain effective force transmission through the remainder of the foot by preventing collapse of the longitudinal arch.

Previous work using a quasi-static cadaver model of the foot suggests that the plantar fascia may also play an important role in stabilizing the toes and maintaining proper pressure distributions in the forefoot (Sharkey et al., 1998 & 1999). The goal of this study was to determine the relative contributions of the extrinsic toe flexors and the plantar fascia in maintaining balanced pressure distributions and proper force transmission through the toes and forefoot.

PROCEDURES

Nine unpaired cadaver feet were tested in a dynamic gait simulator that reproduces the kinetics and kinematics of the tibia, foot, and ankle during the stance phase of gait (Sharkey and Hamel, 1998). The device is able to produce ground reaction forces and plantar pressures equivalent to those measured in healthy human subjects. Physiologic muscle actions are simulated using force feedback controlled linear actuators interfaced to the tendons of the specimen with freeze clamps. Donors included five men and four women from 41 to 86 years old (mean age 67 years).

Plantar pressure distributions were determined for the instant in terminal stance corresponding to the second peak of the vertical ground reaction force profile. Instantaneous pressure maps were obtained using a Pedobarograph (Baltimore Therapeutic) retrofitted with a high resolution CCD camera. Contact area and mean pressure was measured using NIH Image software in each of 5 regions: the entire forefoot, the metatarsal region, the great toe, the second toe, and the lesser toes. The force imposed on each region was subsequently calculated as the product of area and mean pressure.

Three conditions were tested: the intact foot loaded under normal muscle activity (forces), the intact foot without toe flexor activity, and the foot following plantar fasciotomy but with normal muscle activity. Repeated-measures analyses of variance, followed by Bonferroni multiple comparisons were used to assess the effects of toe flexor dysfunction and fascial division on the dependent pressure parameters.

RESULTS AND DISCUSSION

In the absence of toe flexor activity and following plantar fasciotomy, plantar contact area and force under the toes decreased significantly, while these same parameters increased significantly in the metatarsal region (Figure 1, Tables 1 and 2).

Normal   No Flexors   Fasciotomy

Figure 1
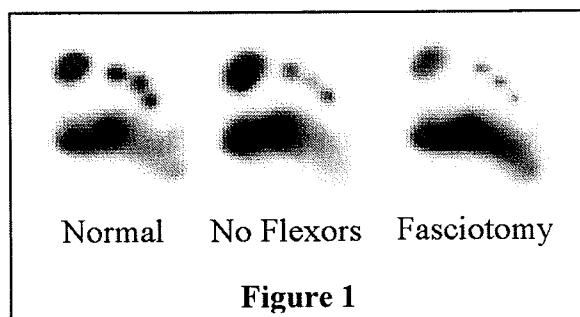
The extrinsic plantar flexors of the toes, by virtue of their tendinous pathways and insertions on the distal phalanges, contribute to force generation during terminal stance. Consistent with this function, we found that loss of digital flexor activity during terminal stance transfers forces normally carried by the toes posteriorly to the region of the metatarsal heads.

More interestingly, loss of plantar fascial integrity produced comparable alterations in force distribution, even with the toe flexors functioning normally. The "windlass" mechanism first proposed by Hicks offers the most logical explanation. Because of its insertion on the proximal phalanges, the plantar fascia helps to prevent excessive extension (dorsiflexion) of the metatarso-phalangeal joints (MP). In the absence of an intact plantar fascia, tensioning the flexor tendons that insert on the more distal phalanges will produce spontaneous extension at the MP joints. This configuration causes the toes to lose their mechanical advantage and force is transferred posteriorly.

SUMMARY

Without the tethering effect of the plantar fascia on the proximal phalanges, the toes are pulled into a clawed position and lose their ability to effectively transmit plantar force, which is necessarily transferred to the metatarsal heads.

REFERENCES

Sharkey, N.A. et al. (1998). *Foot and Ankle* **19** (12) 812-820.

Sharkey, N.A. et al. (1999). *Foot and Ankle* **20** (2) 86-96.

Sharkey, N.A. and Hamel, A.J. (1998). *Clinical Biomechanics* **13**:420-433.

ACKNOWLEDGEMENTS

Table 1: Force (Newtons) for the Five Regions of the Forefoot at Terminal Stance Under Three Different Conditions (mean ± SD).

Condition	Entire Forefoot	Metatarsal Region	Great Toe	Second Toe	Toes 3-5
Intact	716 ± 117	521 ± 137	139 ± 38	20 ± 13	37 ± 33
No Toe Flexors	726 ± 118	591 ± 114*	104 ± 35	12 ± 11*	19 ± 25*
Fasciotomy	706 ± 131	581 ± 116*	103 ± 36*	8 ± 6*	15 ± 14*

Table 2: Area (sq. cm) for the Five Regions of the Forefoot at Terminal Stance Under Three Different Conditions (mean ± SD).

Condition	Entire Forefoot	Metatarsal Region	Great Toe	Second Toe	Toes 3-5
Intact	51 ± 10	33 ± 10	10 ± 1	2.6 ± 1.4	5.5 ± 2.8
No Toe Flexors	51 ± 10	37 ± 8	8 ± 2*	2.0 ± 1.4	3.1 ± 2.6*
Fasciotomy	49 ± 8	36 ± 6	9 ± 2	1.6 ± 0.8*	2.9 ± 2.1*

*Asterisks represent a significant (p<0.05) difference from the intact condition.

EFFECTS OF RESTRICTED ANKLE DORSIFLEXION ON PLANTAR PRESSURE DISTRIBUTIONS

Paul M. Malloy, Mary B. Becker, and Neil A. Sharkey

Center for Locomotion Studies and Department of Kinesiology
The Pennsylvania State University, University Park, PA
Email: celos@psu.edu   Web: www.celos.psu.edu

INTRODUCTION

Foot ulceration in patients with peripheral neuropathy due to diabetes mellitus produces significant morbidity. In addition to loss of protective sensation, limited joint mobility and motor neuropathy may also play important pathogenic roles by increasing the plantar pressure exerted on the forefoot during gait. Specifically, we hypothesize that restricted ankle dorsiflexion will increase the magnitude and duration of plantar pressure in the forefoot. To examine this hypothesis, we measured dynamic plantar pressures during walking in normal healthy subjects with the ankle unconstrained and under conditions of limited dorsiflexion.

PROCEDURES

Ten subjects participated in this study; 5 females and 5 males, mean age of 30.7. The subjects had no history of lower extremity pathologies.

Two identical, mechanical ankle - foot orthoses (AFOs) were specifically designed and fabricated to manipulate and set maximum ankle dorsiflexion to pre-selected limits. The AFOs consisted of an anterior tibial brace and a dorsal midtarsal brace that were mechanically linked via a sliding crank mechanism. The linkage was freely adjustable to allow for unlimited positioning of the midtarsal brace against the dorsum of the foot, after which it could be rigidly locked to prevent further dorsiflexion. The anterior tibial brace was secured to the subject with Coban™ (3M Health Care, St. Paul, MN). Identical AFOs were secured to both anterior tibial borders of each subject.

Six conditions of restricted ankle dorsiflexion were examined in randomized sequence: unconstrained (AFOs attached but not set to limit dorsiflexion), 10 degrees dorsiflexion, 5 degrees dorsiflexion, 0 degrees (neutral), 5 degrees plantarflexion, and 10 degrees plantarflexion.

Right foot plantar pressures were measured with an in floor EMed SF plantar pressure plate (Novel Elect. Inc., St. Paul, MN). Five trials per condition were performed for a total of 30 trials per subject. Relative normal gait speed was determined beforehand with the AFOs secured in the unconstrained position. Subject gait speed was maintained throughout the experiment within ± 5% of the mean normal gait speed.

Plantar pressure data was collected at 67 Hz and processed using software provided by the manufacturer. Analyses of variance were used to examine the effect of limited dorsiflexion on plantar pressures.

RESULTS

Restricting maximum ankle dorsiflexion to the neutral or dorsiflexed positions did not have a significant effect on plantar pressure. Limiting dorsiflexion to 5 and 10 degrees of plantarflexion significantly altered the magnitude, distribution, and temporal progression of plantar pressure from heel to forefoot. The inability to produce a plantargrade foot shifted pressure laterally,

and from the heel into the midfoot and forefoot. These overall shifts are illustrated by the changes in the pressure-time integrals at the lateral heel and lateral metatarsal region (Fig. 1) and the peak pressures at the midfoot (Fig. 2).
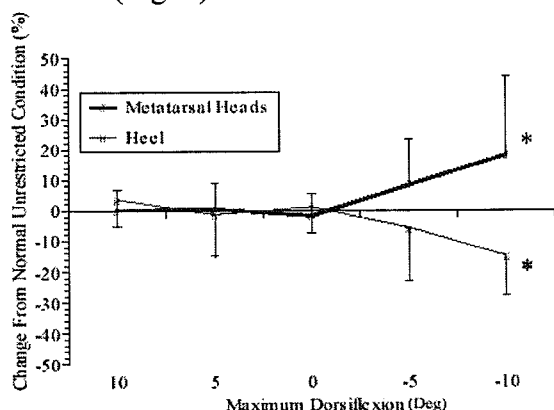
Figure 1: Mean plots of the changes in the pressure time integrals for the lateral heel and three lateral metatarsal heads as a consequence of limited dorsiflexion (n = 10, error bars = 1 SD).
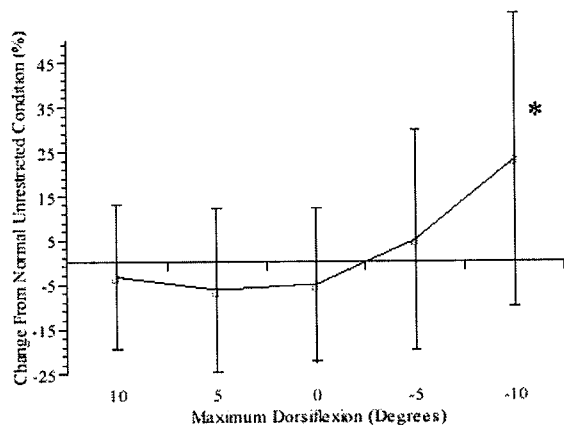
Figure 2: The change in peak pressure exerted on the lateral midfoot as a consequence of limiting dorsiflexion (n = 10, error bars = 1 SD).

DISCUSSION

Limited joint mobility leading to diabetic foot pathology is often relieved surgically by a tendo-Achilles lengthening (TAL). Anecdotal data exists supporting the procedure but little systematic research has been conducted to elucidate the effectiveness of TAL, or delineate its indications for use in the diabetic patient. Baseline information on the effects of limited joint mobility on forefoot pressure is necessary to determine the significance of this condition on diabetic forefoot ulcerations and the utility of TAL.

Our data indicate that limited ankle dorsiflexion produces significant shifts in the distribution of plantar pressure during gait. In particular, it was found that pressure was shifted laterally and dwelled for more time in the forefoot rather than the heel. Increasing the time integral of pressure at the metatarsal heads may further predispose patients already at risk for plantar ulceration due loss of protective sensation. These findings indicate that tendo-Achilles lengthening may be indicated in patients with recurrent ulceration of the lateral forefoot who are unable to achieve neutral dorsiflexion due a contracted heel cord. Investigations of the affects of limited dorsiflexion on temporal and kinetic parameters of ground reaction force are underway.

REFERENCES

Barry, D.C. et al. (1993). *J. American Pod. Med. Assoc.*, **83**: 96-100.

Boulton, A.J.M. et al. (1983). *Diabetes Care.* **6**: 26-33

Cavanagh, P.R. et al. (1991). *Diabetes.* **40**(Suppl 1): 531A

Delbridge, L. et al. (1988). *Diabetic Medicine.* **5**: 333-337

Lin, S.S., et al. (1996). *Orthopedics.* **19**: 465-475

ACKNOWLEDGEMENTS

CONTROL OF THE CENTER OF MASS DURING A FORWARD REACHING TASK PERFORMED AT TWO SPEEDS

Ksenia Kozak[1], James A. Ashton-Miller[1-2] and Kendra D. Lohrmeyer[2]

[1]Department of Biomedical Engineering and [2]Department of Mechanical Engineering
University of Michigan, Ann Arbor, MI 48109
Email: ksenia@umich.edu

INTRODUCTION

Falls from elevated surfaces are a recognized cause of injury at any age (Baker et al., 1992). Because the underlying causes of these falls are largely unknown, we chose to study the control of balance while standing and reaching at the edge of a rigid, horizontal, support surface.

The maximal distance a person can reach forward while maintaining a fixed base of support in the standing position is a recognized clinical measure of balance (Duncan et al., 1990). The quasistatic maintenance of balance generally involves maintaining the vertical projection of the whole body center of mass (COM) within the existing base of support (BOS), usually defined by the area and position of the feet. Pai et al. (1992) demonstrated, in a sit-to-stand task, that when the COM has momentum the horizontal velocity of the COM also influences the range of feasible movements for which control of balance may be maintained. In the case of the present reaching task, reaches performed quickly not only involve relatively large displacements of the COM, but can also generate significant momentum which may be difficult to arrest without falling.

This study was undertaken to examine how speed affects reach task performance and specifically the control of COM movement when healthy young adults are confronted with having to reach forward as far as possible and as fast as possible while standing on the edge of an elevated surface.

PROCEDURES

Ten young females (mean age 23.7 years) participated in this study. Wearing a full body ceiling-supported safety harness, subjects stood with the tips of their toes aligned with the front edge of a 43 cm high platform. Subjects were instructed to reach forward and touch a target with both hands simultaneously. With the target set at the subject's maximum reach distance, reaches were performed at both a comfortable speed and as fast as possible. Body segment kinematics were measured at 100 Hz using an Optotrak® optoelectronic camera system and 12 infrared emitting marker. Reactions between the feet and support surface were measured at 100 Hz using an AMTI® force platform. The coordinates of the markers and standard anthropometric data from the literature were used to estimate the COM of 7 body segments (head, trunk, upper arms, lower arms, thighs, shanks, feet) and the position of the whole body COM in the sagittal plane (Winter, 1990).

Two-sided paired t-tests were used to test the effect of reaching speed with $p < 0.05$ being considered statistically significant.

RESULTS AND DISCUSSION

Subjects reached 6% less far (37.8 vs. 35.6 cm, $p < 0.05$) when asked to reach as fast as possible compared to reaching at a comfortable speed. That they did indeed

increase their reaching speed is evident in the maximum value of their horizontal COM velocity which increased by 21% (10.6 cm/s vs. 12.8 cm/s, $p<0.05$). The maximum values of the horizontal component of linear momentum and the angular momentum increased by 22% (6.2 vs. 7.6 kg m/s, $p<0.05$) and 25% (7.2 vs. 9.0 kg m^2/s, $p<0.05$), respectively.

Phase plane plots of COM angular velocity vs. COM angular position (subtended at the ankle joint) indicated that COM displacement was controlled in a stepwise manner (Fig. 1). The dynamics of the final increment of COM angular displacement just prior to the attainment of maximum reach were compared for the two reaching speeds. The peak COM angular velocity for this final increment increased by 23% (2.6 deg/s vs. 3.2 deg/s, $p<0.05$) when reaching as fast as possible. The final deceleration prior to the occurrence of maximum COM anterior displacement increased more than two-fold (12.8 deg/s^2 vs. 31.2 deg/s^2, $p<0.01$). The 'safety margin' between the projection of the COM onto the base of support and the edge of the platform significantly increased by 42% (17.6 vs. 25.0 % BOS, $p<0.05$). This indicates the priority placed on arresting momentum when reaching as far and as fast as possible.

SUMMARY

Results show that reaching speed affected maximum reach distance, with a faster speed associated with a shorter reach distance. The COM movements were also different for the two speeds. A greater 'safety margin' was achieved by using a higher deceleration of momentum during fast reaches. These findings suggest that timing of the COM momentum arrest is critical to avoiding loss of balance at the limit of a fast reach.
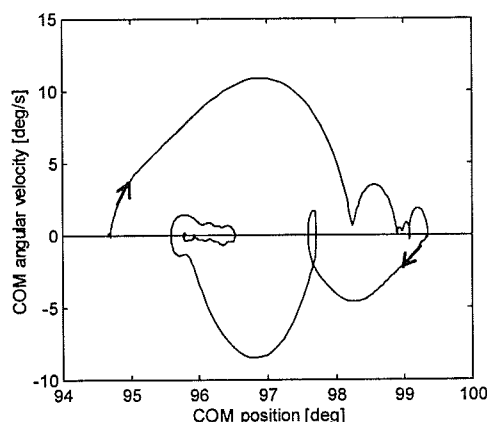
Figure 1. Phase plane plot of COM angular velocity vs. position for a trial performed at a comfortable speed. Arrows indicate direction of movement. A COM position of 90° places the COM directly above the ankles.

REFERENCES

Baker, S.P. et al. (1992). *The Injury Fact Book,* 134-148.

Duncan, P.W. et al. (1990). *J. Gerontol.,* **45,** M192-197.

Pai, Y.-C. et al. (1992). *Posture and Gait: Control Mechanisms,* **2,** 301-304.

Winter, D.A. (1990). *Biomechanics and Motor Control of Human Movement,* 54-63.

ACKNOWLEDGMENTS

A NEW METHOD TO QUANTIFY DEMAND ON THE UPPER EXTREMITY IN MANUAL WHEELCHAIR PROPULSION

Michelle B. Sabick[1] and Kai-Nan An[2]

[1]Biomechanics Research & Consulting, Inc., Evergreen, Colorado
[2]Orthopedic Biomechanics Laboratory, Mayo Clinic, Rochester, Minnesota
Email: michelle@brcinc.com

INTRODUCTION

Chaffin et al. (1978) demonstrated that when a person is performing an exertion close to his or her maximum strength, movements may cause tissue failure. They defined the job strength rating (JSR) for investigation of job related injuries. The JSR was defined as the ratio of the maximum strength requirement of a job to the average isometric strengths of the workers placed in the job. Subsequent research has confirmed that neither isometric strength nor job demand are sensitive predictors of job-related injuries by themsleves, but job demands relative to the maximum isometric strength of the worker is a sensitive predictor (Mostardi et al., 1992; Batti'e et al., 1989).

Overuse injuries are common in manual wheelchair users. To date, no study has compared strength requirements in manual wheelchair propulsion to the isometric strength of the user. The purposes of the current study were: (1) to propose a rating called the Wheelchair Propulsion Strength Rating (WPSR) for assessing the likelihood of injury in manual wheelchair propulsion; and (2) to compare WPSR values for the joints of the upper extremity when ascending ramps with increasing slopes.

PROCEDURES

Ten ambulatory physical therapists with wheelchair experience and no history of serious upper extremity injury propelled a wheelchair up a 3.66 m ramp which could be adjusted to provide four different grades (level, 20:1, 12:1, and 8:1 run:rise, Fig. 1). The wheelchair was equipped with an instrumented handrim and portable data logger that recorded the three-dimensional forces and moments applied to the handrim at a sampling frequency of 100 Hz. The positions of the trunk and upper extremity were recorded at 60 Hz using a motion analysis system (Motion Analysis Corp., Santa Rosa, CA). Subjects propelled the wheelchair up each slope five times. The order in which the conditions were performed was randomized.
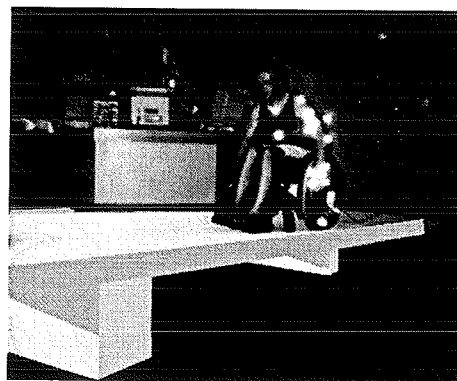
Figure 1. A subject propelling the instrumented wheelchair up the ramp.

For each isolated joint motion, the maximum isometric functional strength (torque) was measured using a Cybex II isokinetic dynamometer (Cybex, Ronkonkoma, NY) or custom torque dynamometers. Subjects performed three maximum voluntary isometric contractions 3s in duration for each joint motion. The

average peak torque calculated from three trials for each joint function was used for analysis. The peak joint moments generated in wheelchair propulsion were normalized to those generated in isolated isometric maximum strength tests. Each of these normalized joint moments, expressed as a percentage, was called the WPSR.

RESULTS AND DISCUSSION

WPSR values for the level condition ranged from 2.6 to 33.2%. Shoulder flexion had the highest mean WPSR value, at 33.2±13.25%. Pronation also had a relatively high mean WPSR, at 31.5±13.59%. Mean WPSR values for all upper extemity joint functions tended to increase with ramp slope (Figure 2). Increases in mean WPSR from level ground to the lowest ramp (20:1) were dramatic for most joint motions. Shoulder abduction and adduction were the only values that did not increase markedly from level ground values. Mean WPSR values for shoulder flexion exceeded 100% for the steepest ramp (117±44%).
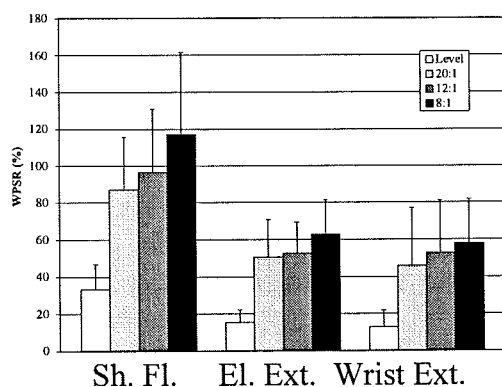
Figure 2. WPSR values for the major upper extremity joint motions (Sh=Shoulder, El=Elbow, Fl=Flexion, Ext=Extension).

The data collected in the current study demonstrates why shoulder injury is a common complaint among manual wheelchair users. Mean shoulder WPSR

values reached 96±35% when propelling up the 12:1 ramp, and exceeded 100% for five of the ten subjects on the 8:1 ramp. Mean WPSR values did not exceed 100% for any other joint function.

Joint strength varies with joint angle and angular velocity. Therefore, an ideal strength rating would take into account these factors. Future studies are necessary to ascertain whether calculating WPSR using isometric strength can be used to predict the likelihood of overuse injuries of the upper extremity in wheelchair propulsion, like its counterpart the JSR has been shown to predict low back injuries.

SUMMARY

Mean WPSR values increased dramatically from level ground to the 20:1 ramp. Demands on the shoulder joint approach or exceed maximum isometric strength for many individuals when ascending 12:1 and 8:1 ramps. WPSR values for the wrist and elbow were generally less than those at the shoulder, and rarely exceeded 100%. This data supports previous findings of high incidence of overuse injury in the shoulders of manual wheelchair users.

REFERENCES

Batti'e, M.C., et al. (1989). *Spine* 14(8), 851-856.

Chaffin, D.B., et al. (1978). *J. Occup. Med.* 20(6), 403-408.

Mostardi, R.A., et al. (1992). *Spine* 17(2), 189-193.

ACKNOWLEDGMENTS

GAIT CHARACTERISTICS DURING STAIR CLIMBING IN ADULTS WITH OSTEOARTHRITIS OF THE KNEE

Christine Hughes, Kenton Kaufman, Bernard Morrey, Michael Morrey and Kai-Nan An

Orthopedic Biomechanics Laboratory, Mayo Clinic/Foundation, Rochester, Minnesota
Email: kaufman.kenton@mayo.edu

INTRODUCTION

Osteoarthritis (OA) affects nearly everyone past age 60. Symptoms of knee OA include pain, stiffness, and decreased range of motion of the joints. One of the common complaints of an individual suffering from OA of the knee joint is pain while climbing stairs. Therefore, this study was performed to quantify the gait characteristics of adults with OA of the knee while ascending and descending stairs.

PROCEDURES

Knee kinematics and kinetics during stair climbing were collected from 139 adults, 47 males and 92 females, diagnosed with OA of the knee. The subjects ranged in age from 30 to 82 and had a mean age of 57 (±12.5). Their mean weight was 85 kg (±17) and their mean height was 167 cm (±9.7). The subjects reported having pain in one or both knees on most days and showed radiographic signs of OA, including hypertrophic changes, marginal spur formation, subchondral schlerosis or cyst formation, or nonuniform joint space narrowing.

A set of 24 reflective markers (Helen Hayes set) were placed on bony landmarks of the subject before the gait trials. A six camera ExpertVision system (Motion Analysis Corp, Santa Rosa, CA) recording at 60 Hz was used to collect 3-D marker trajectory during gait. The kinetic data was time-synchronized with the cameras by a trigger.

All joint angles and moments were calculated using Orthotrak 4.0 software (Motion Analysis Corp, Santa Rosa, CA). Kinematic and kinetic data were collected during stair climbing as described previously (Yu et al., 1996, 1997). The stairs consisted of four steps, each with a rise of 18 cm and a run of 25 cm. Handrailings were not used by the subjects. A BERTEC (type 4060A, Bertec Corp, Worthington, OH) force plate was positioned in front of the stairs to measure the ground reaction forces immediately before or after stair climbing. The first and second stairs were independently attached to two separate KISTLER (type 9281B, Kistler Instrumente AG, Winterthur, Switzerland) force plates without touching any other parts of the stairway or floor.

Results were averaged from three trials for both ascending and descending the stairs. While ascending the stairs, data was analyzed from the foot strike of the first stair through the toe off of the second stair. While descending the stairs, data was analyzed from the foot strike of the second stair through the foot strike on the floor.

RESULTS

We evaluated the knee joint under two circumstances: at the occurrence of the maximum external knee flexion moment and the maximum knee flexion angle. The maximum knee flexion moment occurred during stance phase and the maximum knee

flexion angle occurred during swing phase of gait. The maximum knee flexion moment when descending stairs was near six times that when ascending stairs (Fig. 1). The corresponding knee flexion angles at the peak joint moment were 59.5° ±16.8° while ascending the stairs and 49.2° ±9.5° while descending the stairs. The maximum knee flexion angles during both ascending and descending stairs were similar (Fig. 2).

DISCUSSION

Knee flexion angles and moments during stair climbing in subjects with OA have not been reported previously. Andriacchi et al. (1980) analyzed knee joint moments and angles in 10 young male subjects, with a mean age of 28 years, with no history of disease or injury of the locomotor system. They reported a maximum knee flexion angle of 73.4° (±12.4°) when ascending stairs, and a maximum knee flexion angle of 81.6° (±11.3°) when descending stairs (Fig. 2). These values are slightly lower than the values we reported. A possible reason for this difference could be that although their stairs were slightly higher (rise of 21 cm and a run of 25.5 cm), their subjects were significantly taller (mean height of 179 cm).

The maximum knee flexion moment was similar when ascending stairs, but when descending stairs it was significantly higher for the population diagnosed with OA of the knee compared to healthy subjects (Fig. 1). Andriacchi et al. (1980) reported the knee moments for ascending stairs at 54.2 Nm (±17.2) and descending the stairs at 146.6 Nm (±48.0). This may be partly due to the fact that our subjects with OA had an average weight (85 kg) that was greater than that of the healthy subjects (71 kg). Due to associated pain and subsequent decreased activity levels, it is not uncommon for people with OA of the knee to have greater

body mass which places extra stress on the joints. OA subjects often report pain when utilizing the stairs with a greater incident of discomfort when descending. In order to accomplish this common functional activity of daily living, people learn to compensate by altering their gait or discontinue taking the stairs altogether to reduce or alleviate the pain.

Fig. 1 MAXIMUM KNEE FLEXION MOMENT
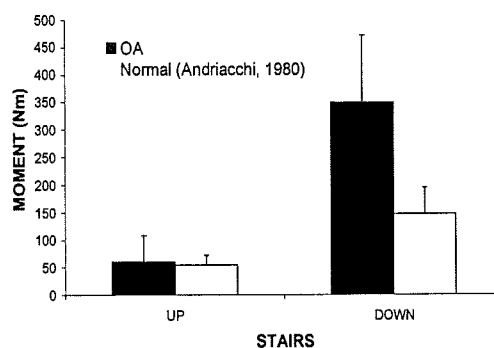
Fig. 2 MAXIMUM KNEE FLEXION ANGLE
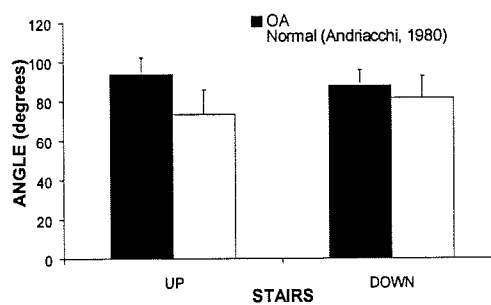
REFERENCES

Andriacchi, T.P. et al. (1980). *J. Bone Joint Surgery*, **62-A**, 749-757.
Yu, B. et al. (1996). *J. Biomechanics*, **29**, 1625-1628.
Yu, B. et al. (1997). *Journal of Orthopaedic Research*, **15**, 348-352.

ACKNOWLEDGEMENTS

A NEW METHOD FOR OBJECTIVE QUANTIFICATION OF TREMOR

Duane Morrow[1], Joseph Matsumoto[2], Ann Walker[1], and Kenton Kaufman[1]

[1] Orthopedic Biomechanics Laboratory and [2] Department of Neurology,
Mayo Clinic/ Foundation, Rochester, Minnesota
Email: kaufman.kenton@mayo.edu

INTRODUCTION

Current techniques for assessing tremor in multiple sclerosis (MS) patients involve use of clinical scales, which can be both subjective and unreliable. In order to more completely understand and assess treatments for MS patients, the tremor needs to be more objectively quantified. Methods for tremor measurement proposed to date typically have constrained the observed limb (Liu et al, 1997 and Elble et al, 1996). The purpose of this study was to develop a method for quantifying unconstrained tremor.

PROCEDURES

Ten outpatients (mean age = 44) diagnosed with either clinically definite MS or laboratory-supported definite MS were used in this study. Additionally, eight healthy subjects (mean age = 34) free from neurological deficits were also evaluated to assess the reliability of the technique and establish baseline numbers for "normal" amounts of tremor. All subjects were tested on two separate days. A three-dimensional magnetic tracking device (Flock of Birds, Ascension Technologies, Burlington, VT, USA) was attached to the subject's dominant hand. Subjects were seated at a table with four target markers (the Left, Right and Far markers were on the tabletop, while the Near marker was elevated above the surface to chin-level). Position data was recorded at 144 Hz as a subject reached in turn between the left and right markers (LR reaches), as well as the far and near markers (FN reaches). Each reach was performed and recorded ten times.

Hand position data was filtered with a fourth-order low-pass butterworth filter with a cutoff frequency of 10 Hz. Hand velocity was calculated using a central-difference formula. A 512-point Fast Fourier Transform (FFT) was calculated for each of the three orthogonal directions (with zero padding for files that required it). Power Spectral Densities (PSDs) were calculated from the FFTs. Mean spectra were calculated by averaging the PSDs for ten trials from each direction of reach, and the peak power of the modal frequency was extracted. The power level for each velocity component was then categorized as being either Intended (in the direction of the reach defined by the target markers) or Unintended (in the plane normal to the Intended direction). The total Unintended Velocity Power (UVP) was given by the vector summation of the modal frequency powers of both Unintended directions.

RESULTS

Figure 1 shows characteristic PSDs for A) Normal and B) MS subjects. UVP was between 20 and 40 times larger on average for MS patients than for normal controls.

Intravisit comparisons for both normal controls and MS patients revealed no significant differences in the UVPs (see Table 1), proving the repeatability of the test.

UVPs for the MS patients were compared to those of the normal subjects for each direction of reach using all responses. As shown by Figure 2, the groups are clearly separable, exhibiting large significant differences for both LR and FN reaches (Wilcoxon Rank Sums test, p<0.0001 and p=0.0001, respectively).

A) Normal
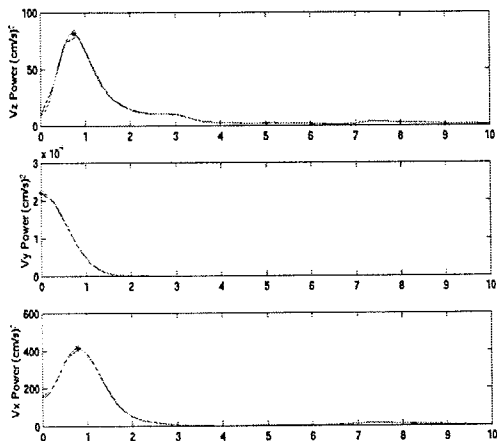
B) MS
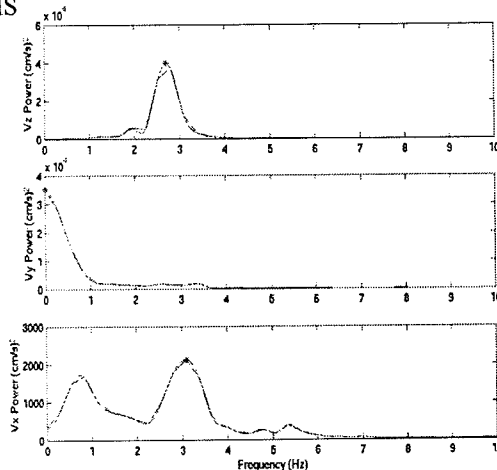
Figure 1: 3-orthogonal PSD components of velocity for A) normal and B) MS subjects.

Table 1: Intratest significance results for repeatability of reaching tests (Wilcoxon's matched pairs rank sums test)

Group	Reach	P value
Normal	LR	0.84
	FN	0.55
MS	LR	0.82
	FN	0.50

A) LR reach
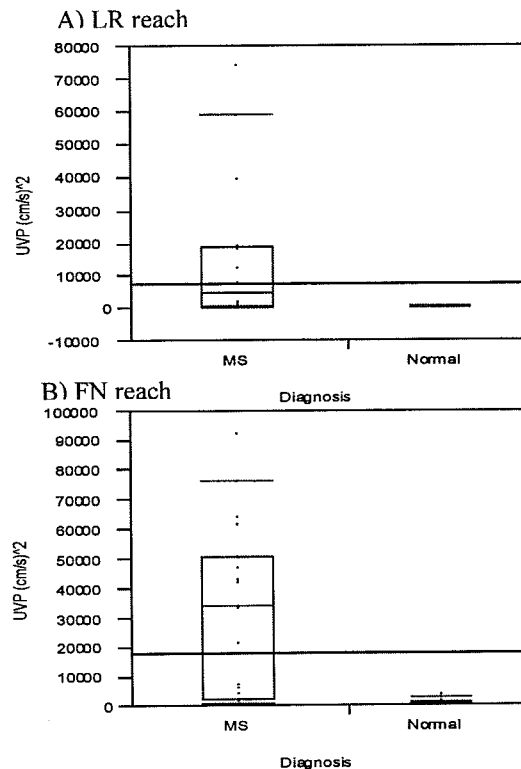
B) FN reach

Figure 2: Quantile box plots depicting the differences in UVP of MS and normal subjects for A) LR and B) FN reaching.

DISCUSSION

Vector summation of the peak powers of the modal frequency of hand velocity data is capable of quantifying the levels of patient tremor. Testing is repeatable and shows significant differences where they exist. This type of evaluation will be useful in more completely and precisely defining the severity of tremor, while avoiding error due to observational subjectivity.

REFERENCES

Liu et al. (1997). *Mov Disord*, 12, 992-999.

Elble, et al. (1996). *Mov Disord*, 11, 70-78.

ACKNOWLEDGEMENT

KINEMATIC CHARACTERISTICS OF UPHILL WHEELCHAIR PROPULSION FOR YOUNG MALES

John W. Chow[1], Tim A. Millikan[2], Les G. Carlton[1], Woen-Sik Chae[1], and Marty I. Morse[2]
[1]Dept. of Kinesiology and [2]Div. of Rehabilitation Education, Univ. of Illinois, Urbana, IL 61801

INTRODUCTION

Most studies investigating the kinematics of wheelchair propulsion have been conducted using wheelchair ergometers, treadmills, or rollers. Very few studies examined the stroking kinematics overground. Also, no attempt has been made to examine systemically the characteristics of uphill stroking. To fill the void, the purpose of this study was to quantify the wheelchair stroking kinematics over ramps of different slopes performed by young males.

PROCEDURES

Ten male wheelchair users (age 22.3±5.3 yrs) of different functional levels served as the subjects. A wooden ramp [7.3 m (24') long and 1.1 m (3.5') wide] of adjustable slopes – 0° to 12° at intervals of 2° – was constructed. Using his own wheelchair, each subject pushed up the ramp three times for each slope condition at a self-selected normal speed. The sagittal view (right-hand side) of the stroking movement was recorded by a S-VHS camcorder (60Hz).

One stroke (from the instant of initial hand contact (HC) to the instant immediately before the next HC) was selected from each trial for analysis. The coordinates of different body landmarks defining the trunk and right arm and the wheel center were extracted using a Peak Motion Measurement System. For each subject, the average profile over three strokes (one from each trial) were used in subsequent analysis.

In addition to segment inclinations and angular velocities at the instants of HC and hand release (the instant the hand breaks contact with the pushrim, HR), contact, release, and push angles (Figure 1) were determined for each stroke. For each slope condition, mean and standard deviation were computed for each kinematic parameter. For each parameter, a one-way ANOVA with repeated measures was used to test for the significant difference for the factor of slope. When a significant difference was found, post hoc analyses were performed using the Tukey-Kramer procedure.
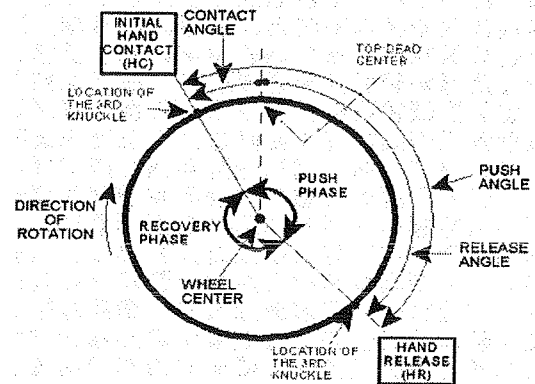
RESULTS AND DISCUSSION

The average stroking speeds (stroke distance divided by stroke time) ranged from 0.94 m/s (12° slope) to 1.29 m/s (0°). The post hoc analysis indicated that there were significant differences in speed between adjacent slopes except between 0 and 2° and 8 and 10°. The decrease in speed with increasing slope was due to the greater decrease in stroke distance (distance traveled per stroke) rather than in the decrease in stroke time (time to complete a stroke).

Hand Position Relative to Wheel Center. Significant differences among slopes were found in contact, release, and push angles (Table 1). The increase in contact angle (increase in absolute value but decrease in magnitude) with increasing slope indicated that the hand contact occurred closer to the top dead center (Figure 1) as the slope increased. The decrease in push angle with increasing slope was due to the greater

increase in contact angle than in the decrease in release angle. Significant differences were found between all adjacent slopes in all three angles.

Segment Inclinations. The inclination (the smallest angle between a segment and the horizontal, the angle is positive if the distal endpoint is higher than the proximal endpoint) of the trunk and upper arm at HC increased steadily as the slope increased (Table 1). No significant difference was found in the inclination of forearm at HC. These suggest that the major adjustments in body position at HC were in the trunk and upper arm.

The inclination of the trunk at HR was slightly greater than the corresponding values at HC for all slope conditions. The differences in the inclinations of upper arm and forearm at HR indicated that the arm was not fully extended at HR. Although the post hoc analysis showed that there were significant differences in these three segment inclinations at HR, the average values (Table 1) seem to suggest that minimal changes occurred until the slope reached 4 to 8°.

Segment Angular Velocities. Both positive and negative angular velocities of the trunk at HC were found in 0 and 2° slopes. In the other slopes, the trunk was rotating forward (negative direction) at HC and the speed of rotation increased steadily with increasing slope. The direction of upper arm and forearm rotations at HC were not consistent among subjects, especially for lower slopes.

In all but few instances in level stroking, the trunk was rotating backward (positive direction) at HR and the speed of rotation increased steadily with increasing slope. The upper arm was rotating in the clockwise direction at HR in most cases. As reflected in the SD values, a large range of forearm angular velocity at HR was recorded for each slope condition.

Conclusion. The subjects started to lean forward during the push phase when the slope increased to 6-8°. The trunk also became actively involved in wheelchair propulsion at this slope range.

Table 1: Kinematic characteristics of wheelchair stroking at different slopes (mean±SD).

Angle (°)	0°	2°	4°	6°	8°	10°	12°
Contact*	-16.2±12.0	-20.3±9.9	-16.6±9.1	-12.5±4.3	-9.8±5.7	-8.4±8.7	-5.9±6.6
Release (°)*	31.3±6.3	31.7±5.2	33.0±5.9	33.5±6.9	34.7±4.9	36.9±5.6	36.0±5.9
Push (°)§	46.8±7.6	50.7±7.5	49.2±7.6	47.9±7.6	45.5±5.7	45.3±8.6	42.1±7.0
Inclination at HC (°)							
Trunk*	82.0±5.6	82.7±4.8	81.0±4.4	79.1±6.4	74.4±8.5	72.9±8.6	66.1±9.0
Upper Arm*	-36.1±6.3	-32.3±6.1	-27.3±5.9	-25.7±5.5	-21.6±6.5	-21.6±7.7	-19.2±10.2
Forearm	-73.5±15.9	-75.9±11.1	-78.0±10.5	-77.4±8.6	-73.9±9.1	-69.6±10.8	-68.2±10.2
Inclination at HR (°)							
Trunk*	84.7±4.9	84.7±3.8	84.7±4.2	81.5±5.2	76.9±6.4	74.8±8.1	72.6±7.4
Upper Arm*	-75.4±8.1	-75.9±6.4	-75.6±6.7	-75.8±5.6	-78.8±7.3	-77.3±6.2	-79.6±6.6
Forearm*	-47.7±7.2	-48.3±5.2	-48.6±5.0	-52.6±6.6	-55.8±7.0	-57.2±7.9	-55.9±9.2
Angular Velocity at HC (°/s)							
Trunk*	-1±26	-19±17	-20±13	-33±17	-51±22	-59±17	-83±36
Upper Arm	-39±73	-56±110	-53±72	-45±76	-72±94	-114±87	-142±83
Forearm*	50±102	-30±124	22±127	-40±99	-122±87	-160±94	-161±97
Angular Velocity at HR (°/s)							
Trunk*	7±17	33±25	50±35	71±43	100±44	109±55	120±53
Upper Arm*	136±64	178±122	189±148	232±141	233±169	279±160	219±174
Forearm	-75±73	-80±91	-73±135	-64±118	-61±105	-58±98	-19±142

Significant difference at p ≤ 0.05 (§) or p ≤ 0.01 (*)

KINEMATIC ANALYSIS OF THE JAVELIN THROW PERFORMED BY WHEELCHAIR ATHLETES OF DIFFERENT MEDICAL CLASSES

Ann Frances Kuenster and John W. Chow
Department of Kinesiology, University of Illinois, Urbana, Illinois, 61801
Email: akuenste@uiuc.edu

INTRODUCTION

Previous studies have investigated the kinematics of racing wheelchair propulsion, but very few have focused on the kinematics of field events such as shot put, discus, and javelin . There are eight medical classes for wheelchair field athletes, F1-F8. However, there is no javelin competition for the F1 class. The growing popularity of these events have illuminated the need for kinematic analyses to provide baseline data for coaching and instructional purposes.

The purposes of this study were to evaluate selected kinematic parameters of the javelin throw performed by skilled wheelchair field athletes and to identify those kinematic parameters that are significantly correlated to the medical classification of the athlete and the measured distance of the throw.

PROCEDURES

Subjects. The subjects were 15 male participants (2 F2, 1 F3, 2 F4, 5 F5, 1 F6, 3 F7, and 1 F8) of a training camp organized by the Wheelchair Sports, USA (WSUSA). All but two subjects were right-handed. The data for the left-handed subjects were transposed and were treated as right-handed.

Protocol. Javelin throw performances were recorded using two S-VHS video cameras (Panasonic AG-455, 60 fields s^{-1}). Each subject performed 6 trials, and the best two trials were selected for subsequent analysis.

Data Reduction. The direct linear transformation (DLT) procedure was used to obtain 3D coordinates of selected landmarks of the body and javelin. The horizontal, vertical, and resultant velocities at release, the angle of release, and the attack angle of the javelin were calculated. Inclination angles and angular speeds at release, and the range of motion (ROM) and average angular speeds during the forward thrust were computed for the trunk, shoulder girdle, and right upper arm, forearm, and hand.

Data Analysis. The mean and standard deviation of each parameter were computed for each medical class. Pearson product moment coefficients of correlation were computed between selected parameters and the medical classification, and between selected parameters and the measured distances. Correlation coefficients of $|r| \geq 0.46$ and $|r| \geq 0.57$ were required to attain statistical significance at the 0.01 and 0.001 levels of probability, respectively (n=30, df=28).

RESULTS AND DISCUSSION

Kinematic Characteristics of Javelin at Release. Due to their anatomical and functional limitations, wheelchair athletes are unable to make use of the full kinetic chain. As a result, the kinematics of a javelin throw performed by a wheelchair athlete differ from those of the able-bodied. The distances of throws performed by our subjects ranged from 8.77 to 26.44 m. In comparison, able-bodied athletes can throw up to four times as far (Komi and Mero, 1985).

The average speeds of release for different classes, ranging from 9.1 to 14.7 m s^{-1}, are considerably smaller than those reported for the javelin throws performed by male able-bodied athletes, 25.78 to 20.12 m s^{-1}. The

average angles of release for different classes, ranging from 29.6° to 35.8°, are smaller than those performed by male able-bodied athletes, 34° - 42° (Komi and Mero, 1985).

The average angular speeds at release for different classes ranged from: 1.52 to 2.16 rad s⁻¹ for the trunk; 1.41 to 7.78 rad s⁻¹ for the shoulder girdle; 2.90 to 13.38 rad s⁻¹ for the upper arm; 10.63 to 25.98 rad s⁻¹ for the forearm; and 6.14 to 30.88 rad s⁻¹ for the hand. The range of average angular speeds during forward thrust for different classes were: 1.23 to 2.40 rad s⁻¹ for the trunk; 2.64 to 5.34 rad s⁻¹ for the shoulder girdle; 3.01 to 6.05 rad s⁻¹ for the upper arm; 3.24 to 6.56 rad s⁻¹ for the forearm; and 4.12 to 8.32 rad s⁻¹ for the hand. The range in speeds increased as the segments became more distal. This demonstrates that the functional differences among different classes are more evident in the distal body segments than the proximal ones.

Correlation Coefficients. The correlation coefficients for selected parameters are given in Table 1. The high correlation coefficients for the velocities of the javelin at release indicate that the speed of release is the most important determinant of measured distance and is highly correlated to the classification. The speed of release is determined by the motions of the upper body segments during the forward thrust. The high correlation between speed of release and classification signifies the overall fairness of the classification system.

The height of release of the javelin is significantly correlated to both the classification and the measured distance. This suggests that all else being equal, the thrower who has a higher release height will have a longer throw. The release height is limited by the maximum chair height of 75 cm allowed by the rules. Wheelchair athletes will often use a chair that is lower than the maximum height to better accomodate their disabilities.

The angular speed at release, ROM (during the forward thrust), and average angular speed during the forward thrust of the shoulder girdle are all significantly correlated to both the classification and the measured distance. These results imply that wheelchair athletes should strive to maximize their potential in their trunk movements.

Table 1: Pearson Product Correlation Coefficients (r)

Parameter	r-Class	r-Dist
Javelin at Release (Rel)		
Horizontal Velocity	0.73[#]	0.84[#]
Vertical Velocity	0.50[*]	0.84[#]
Resultant Velocity	0.70[#]	0.92[#]
Angle of Release	-0.02	0.28
Release Height	0.65[#]	0.62[#]
Inclinations at Rel.		
Trunk	0.58[#]	0.14
Shoulder Girdle	0.14	0.21
Upper Arm	0.14	0.29
Forearm	0.03	0.29
Hand	-0.34	-0.24
Angular Speeds at Rel.		
Trunk	-0.17	-0.01
Shoulder Girdle	0.60[#]	0.58[#]
Upper Arm	0.13	0.34
Forearm	0.35	0.31
Hand	0.15	0.24
Range of Motion		
Trunk	0.28	0.46[*]
Shoulder Girdle	0.50[*]	0.60[#]
Upper Arm	0.28	0.03
Forearm	0.15	0.08
Hand	0.21	0.11
Average Angular Speeds		
Trunk	0.33	0.47[*]
Shoulder Girdle	0.56[*]	0.59[#]
Upper Arm	0.26	0.08
Forearm	0.17	0.15
Hand	0.34	0.24

[*] Significant at the 0.01 level
[#] Significant at the 0.001 level

REFERENCES
Komi, P., Mero, A. (1985). *Int. J. of Sport Biomechanics*, **1**, 139-150.

A STUDY OF ISOMETRIC REGIONS IN ANTERIOR CRUCIATE LIGAMENT INTACT AND DEFICIENT KNEES UNDER CLINICALLY SIGNIFICANT LOADING CONDITIONS

Brian S. Coan and Louis F. Draganich[1]
[1]Section of Orthopaedics and Rehabilitation Medicine
Department of Surgery, University of Chicago, IL
Email: ldragani@surgery.bsd.uchicago.edu

INTRODUCTION

Surgeons attempt to optimally reconstruct the anterior cruciate ligament (ACL) by placing a tissue graft isometrically according to manatomical landmarks. (Sapega, et al., 1990) The magnitude of the change in distance between two points, one located on the ACL insertion on the tibia and the second on the medial surface of the lateral femoral condyle, can be measured. Ideally this distance change is zero, making the set of points isometric. It has been determined however that there are no truly isometric points in the knee, (Hefzy and Grood et al., 1989) so maps have been made depicting the level of isometry of various regions on the medial aspect of the lateral femoral condyle.

Ideal graft placement should function to restrict abnormal motion without preventing normal kinematics. Additionally, isometric placement should protect the graft and improve outcomes by minimizing strain. Since removal of the ACL changes the kinematics of the knee in a characteristic and predictable way, it was hypothesized that ACL excision would also result in a predictable and statistically significant change in isometry. If such a relationship could be determined, then a method might be developed to better restore normal isometric relationships in the reconstructed knee. Five knees were tested under two physiologic loading conditions, passive flexion and anterior drawer, with and without the ACL (20 cases total). The kinematics of the bone surfaces were collected using the 3-Space digitizing and tracking system to map the relative positions of the regions of isometry.

MATERIALS AND METHODS

Five unembalmed cadaveric knees were tested under passive flexion and 100N of anterior drawer between full extension and ninety degrees of flexion in fifteen degree increments. Using a Polhemus 3-Space Digitizer, the three-dimensional kinematics of the tibia and the femur were acquired. Next, a medial para-patellar incision was made, the ACL was excised, and 2050 points covering the medial surface of the lateral femoral condyle were digitized. The incision was sutured and the kinematics under both loading conditions were recorded again. Using coordinate transformations, the relative motions of the condylar surfaces were determined with and without the ACL. Next, the most isometric regions and the most isometric point (MIP) were identified for each case. The MIP was localized in 3D space for each case and its position was compared between the excised and intact knees. Statistical significance was determined with the paired-t test at the a <.01 level. These methods have been reported. (Draganich et al. 1995; Draganich et al. 1996)

RESULTS

The average of the peak anterior-posterior displacements for the five knees was 6mm in the intact case and 16mm for ACL excised case. As an example of the isometric maps generated, two of the twenty cases are depicted (Figure 1). Shown is the outline of the medial surface of the lateral femoral condyle. The roughly circular inscription represents the margin of the ACL insertion. The black dot represents the most isometric point (MIP) located within the most isometric region (MIR). Each image is annotated with the level of isometry in the MIR. Each successive topographical line represents a decrease in isometry of 1mm (i.e. an increase in magnitude with respect to the region encircling the MIP). Figure 1A represents a knee under anterior drawer with the ACL intact. Figure 1B represents the same knee in anterior drawer after the ACL was excised. The decrease in isometry and the translation of both the MIP and MIR are apparent.
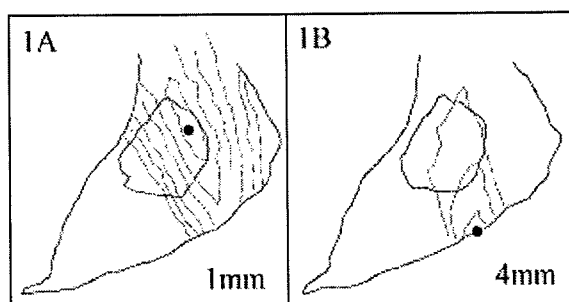
Figure 1: Isometry maps for the A) ACL intact and B) excised knee under anterior drawer. The numbers in the lower right corners represent the level of isometry for the MIR (i.e. the change in graft through the range of motion).

The average change in the magnitude for the MIR was 1.5 mm between the intact and excised cases. The three-dimensional distance between the MIPs for the two cases was significantly different from zero for both loading conditions (P<.01). For anterior drawer, the average distance was 9.3 mm (95%CI: 9.1mm, 28.2mm). For passive flexion, the average distance was 7.8mm (95%CI: 11.1mm, 20.2mm).

DISCUSSION

It was hypothesized that under clinically significant loading conditions the most isometric region would be translated in a predictable way after excision of the ACL allowing prediction of the MIR in the intact case given only the ACL-deficient knee. This study demonstrated that isometric measurements in the ACL-deficient knee under anterior drawer and passive flexion are not directly beneficial to graft placement, because they are not representative of isometry in the native ACL intact knee. This is supported by the change in kinematics after loss of the ACL.

It was previously demonstrated that placing a graft based on the average location of the MIP (measured in normal knees) restored normal kinematics on average, but left some knees over-constrained and others under constrained (Draganich,et al, In Press). This study aimed at individualizing graft placement. Under the loading conditions in this study, the 95% CI was too large to attribute clinical significance to the positions of the MIP and MIR.

REFERENCES

1. Draganich L.F. et al. (1995), Am J Sports Med, 23, 424-430.
2. Draganich L.F. et al. (1996), Am J Sports Med, 24, 342-349.
3. Draganich L.F. et al. (In Press), Am J Sports Med.
4. Hefzy M.S. et al. (1989). Am J Sports Med, 17, 208-216.
5. Sapega et al. (1990), J Bone Joint Surg Am, 72, 259-262.

THE EFFECT OF WEIGHT BEARING ON
ANTERIOR CRUCIATE LIGAMENT (ACL) STRAIN

Braden C. Fleming [1], Bruce D. Beynnon [1], Per A. Renstrom [2],
Bjorn Engstrom [2] and Glenn D. Peura [1]

[1] Dept of Orthopaedics & Rehabilitation, University of Vermont, Burlington, VT
[2] Section of Sports Medicine, Karolinska Institute, Stockholm, Sweden
Email: fleming@salus.mcd.uvm.edu   Web: www.vtmednet.org/~g136911/

INTRODUCTION

Knee joint stability is maintained by a force balance between the ligaments, muscles, articulating surfaces, and body weight. One of the most important ligaments to knee stability, and yet most frequently ruptured is the ACL. To gain insight into ACL function and its interaction with other factors that maintain joint stability, its strain response should be evaluated under both non-weight bearing and weight bearing conditions. The objective of this study was to evaluate the ACL strain response during non-weight bearing and weight bearing in combination with three clinically relevant externally applied loadings; 1) anterior-posterior (A-P) shear, 2) internal-external (I-E) torques, and 3) varus-valgus (V-V) moments.

PROCEDURES

Eleven subjects who were candidates for arthroscopic meniscectomy under local anesthesia participated in the study. Following the routine surgical procedure, a Differential Variable Reluctance Transducer (DVRT; MicroStrain, Inc. Burlington VT) was implanted in the anteromedial bundle of the ACL. The wounds were closed and the subject's foot was positioned in a custom designed loading fixture that allowed independent application of A-P shear forces, I-E torques, and V-V moments to the knee.

The subject was placed in a position similar to that of a squat, with their knee flexed at $20°$ and the trunk flexed to $10°$. The magnitude of the applied loads were measured using a 6 DOF load cell (SRMC3A-6-250; AMTI, Watertown MA) at the foot in combination with a custom designed load cell at the tibiofemoral joint. For the weight bearing condition, the compressive force was applied to the foot and directed along the axis defined by the center of the ankle and hip joints. A compressive load equal to 40% of body weight was applied simulating the weight of the torso and upper leg. The external loading conditions were then applied in a random order. A 2 x 3 factorial ANOVA was employed where each subject served as their own control. The independent variables were the external loading regimes (A-P, I-E, & V-V) and the dependent variable was ACL strain. The two factors investigated were the weight bearing status and selected externally applied load levels (A-P forces: 0, 90 & 130 N; I-E torques: -9, 0, and 9 Nm; and V-V moments: -10, 0, and 10 Nm).

RESULTS AND DISCUSSION

For all three loading conditions, there were significant changes in ACL strain values due to weight bearing status ($p<0.01$) and the externally applied load levels ($p<0.01$). Significant interactions were found between

weight bearing status and ACL load (p<0.01). An increase in ACL strain values was produced by an increase in anterior shear load for both weight bearing and non-weight bearing conditions (Fig. 1). With no shear force applied to the tibia, application of body weight alone produced a significant increase in ACL strain. At high anterior shear loads (130 N), ACL strain values during weight bearing became similar to the non-weight bearing condition (Fig. 1). An internal torque of −10 Nm strained the ACL with the knee non-weight bearing while an external torque of 10 Nm did not (Figure 2). Weight bearing significantly increased ACL strain values with the application of external torques and low internal torque values. At −10 Nm of internal torque, no difference was found between weight bearing and non-weight bearing conditions. For V-V loading, the ACL was not strain when the knee was non-weight bearing. Weight bearing increased ACL strain values significantly across the range of V-V moments tested.

SUMMARY

This investigation provides new insight into the function of the ACL, *in vivo*, during two clinically relevant conditions. The first condition included evaluation of ACL strain without body weight and muscle contraction. The non-weight bearing data is clinically relevant for the evaluation of ligament integrity. The second was the response of the ACL in the presence of body weight and associated muscle activity, and provides insight into ACL function during activities of daily living and rehabilitation. In the absence of body weight, ACL strain values were increased only in response to externally applied anterior shear loads and internal torques of the tibia. In contrast, weight bearing, even in the absence of externally applied loads, increased ACL strain values. Similar findings were

observed with the addition of the externally applied loads in combination with weight bearing. The observed increase in ACL strain is important from a clinical perspective. Previous cadaveric studies have suggested that the compressive load produced by body weight reduced the A-P displacement response of the tibia with respect to the femur as well as ACL load. Our in vivo study contradicts the decrease in ACL load observed in cadavers and emphasizes the need to quantify ACL function in the presence of body weight.

ACKNOWLEDGEMENTS

FIG. 1: ACL strain vs A-P shear loading.
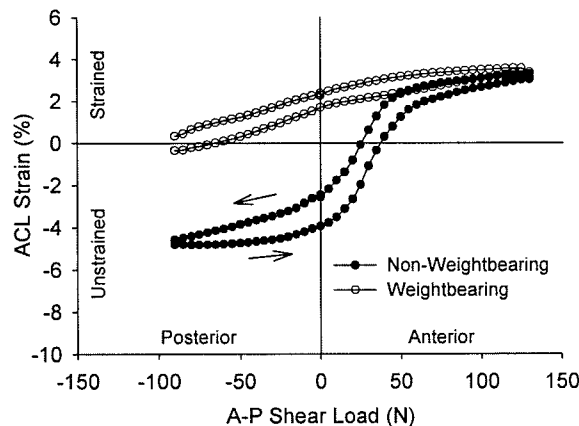
FIG. 2: ACL strain vs I-E torque.
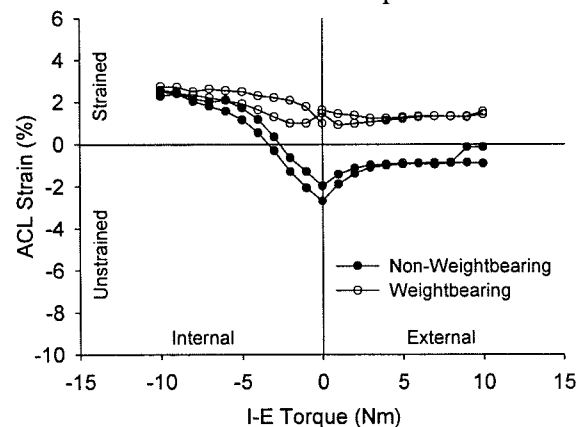
RELIABILITY OF A 3D FINITE ELEMENT MODEL CONSTRUCTED USING MAGNETIC RESONANCE IMAGES OF A KNEE FOR JOINT CONTACT STRESS ANALYSIS

Guoan Li, Orlando Lopez

Orthopedic Biomechanics Lab, Massachusetts General Hopital/ Beth Israel Deaconess Medical Center, Harvard Medical School, Boston, MA
Email: gli@obl.caregroup.harvard.edu

INTRODUCTION

3D FE modeling is a useful tool for understanding of the stress distributions within articular cartilage in response to external loads and investigating both the prevention of injury and the pathological degeneration of the joints. Various computational models of the human knee have been constructed. However, more accurate cartilage models are required to enable reliable predictions of stress-strain distributions within the cartilage. MR imaging provides multiplanar and 3D image data with high spatial resolution. It is therefore feasible to construct 3D FE models using MR images of the knee joint. However, the processing of MR images, either by manual digitization or by the threshold method, might cause certain variations in cartilage thickness. This paper investigated the effect of thickness variation of the cartilage on contact stress analysis when the knee is subjected to axial compressive loads.

PROCEDURES

Magnetic resonance images of a human cadaveric knee specimen in the sagittal plane were obtained with the knee at full extension position. The scan consisted of 128 parallel digital images with a resolution of 512x512 pixels. The contours of the femoral and tibial cartilage were manually digitized within each image. The digitized data was then used to construct the inner and outer surfaces of the cartilage. The 3D cartilage thickness was defined as the shortest distance from one point of the outer surface of the cartilage to the inner surface. Solid models of the cartilage were then constructed from the inner and outer surfaces of the cartilage using the MSC/Patran® software.

The inter-observer variability in delineation of cartilage boundaries was estimated by asking five independent investigators to define the boundaries of cartilage from the same set of MR images. The data demonstrated a variation of thickness by less than 8% in both femoral and tibial cartilage. A 3D cartilage model (named the "average" model) of the knee was then constructed using the mean digitized contours (Fig. 1). In order to examine the effect of variation of cartilage thickness on the prediction of joint contact pressure, four additional cartilage models were constructed for the knee joint at various thicknesses for the cartilage layers: 1) both femoral and tibial cartilage being 10% thinner; 2) 5% thinner; 3) 5% thicker; and 4) 10% thicker than the average model. This range of cartilage thickness was selected to cover the spectrum of variations in cartilage thickness imposed by subjective error attributed to the inter-observer variability during the cartilage digitization procedure. Both the femoral and tibial cartilage were modeled as linear elastic materials with a Young's modulus of 5 Mpa and Poisson's ratio of 0.45. These material properties were chosen in order to represent the cartilage behavior between short and long term responses to functional loads (Blankevoort et al., 1991). Cartilage contact was simulated with a friction coefficient of 0.02 (Mow et al.,
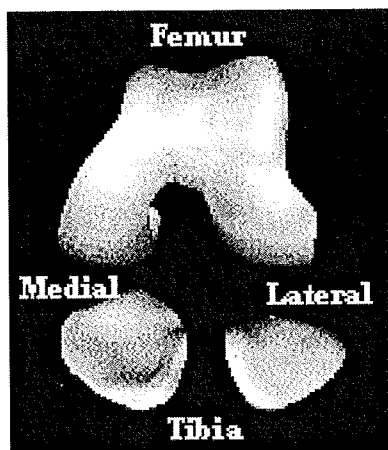
Fig. 1 The finite element cartilage model of the knee constructed using MR images.

1993). Large deformation was included in the stress-strain analysis. The models were analyzed at full extension position and under moderate axial tibial compressive loads (up to 400 N, a load that represents approximately 50% of ones body weight) (Li et al., 1998). Maximal contact pressure, von Mises stress and hydrostatic pressure in the cartilage were compared among the five knee models to evaluate the effect of thickness variation on stress distributions within the cartilage.

RESULTS
Maximal contact pressure in response to an axial compressive load of 400 N is shown in Table 1. Reduction in thickness of the cartilage caused increases in both von Mises stresses and hydrostatic pressure, and increases in cartilage thickness caused decreases in the two stress values. For example, a 10% reduction in cartilage thickness generated a 10% increase in maximal von Mises stress and an 11% increase in maximal hydrostatic pressure within the cartilage. However, a 10% increase in cartilage thickness only caused a 6% reduction in maximal von Mises stress and a 9% decrease in hydrostatic pressure.

DISCUSSION AND SUMMARY
Necessary preliminaries for the construction of 3D finite element cartilage models are

image processing and the digitization of cartilage contours from MR images. Currently, using the threshold method for automated digitization is still difficult to accurately extract geometric boundary information from MR images. This study examined the effect of thickness variation of the cartilage on the contact stress analysis using 3D finite element knee models. Results of this study demonstrated that the contact stress is more sensitive to thinning rather than thickening of the cartilage. The finite element model constructed from MR images is reliable for stress analysis of the cartilage under the condition that an anticipated 10% variation in results might be attributed to the manual digitization procedure.

Table 1. Maximal surface contact pressure, von Mises stress and hydrostatic pressure (Mpa) in the cartilage

FE Model	Surface pressure	Von Misess Stress	Hydrostatic Pressure
-10%	1.895	1.081	1.335
-5%	1.783	1.031	1.262
0%	1.7	0.9796	1.199
5%	1.622	0.9461	1.142
10%	1.555	0.9177	1.092

Reference:
Blankevoort, L., et al. (1991). "Articular Contact in a Three Dimensional Model of the Knee." *J. Biomech*, 24, pp. 1019-1031.
Mow, V., et al. (1993). "Biomechanics of Diarthrodial Joints: A Review of Twenty Years of Progress." *J Biomech Eng*, 115, pp. 460-467.
Li, G., (1998). "Prediction of muscle recruitment and its effect on joint reaction forces during knee exercises." *Ann Biomed Eng*, 26, pp. 725-7

MAGNETIC RESONANCE IMAGE BASED 3D POROELASTIC FINITE ELEMENT MODEL OF TIBIO-MENISCO-FEMORAL CONTACT

Heng Zhang [1], Saara M.S. Totterman [2], Renato Perucchio [1], Amy L. Lerner [1]

[1] Department of Mechanical Engineering, University of Rochester, Rochester, NY 14627
[2] Department of Radiology, University of Rochester Medical Center, Rochester, NY 14620
Email: jade@me.rochester.edu

INTRODUCTION

The importance of the biomechanical functions of the meniscus is becoming widely recognized. However, the interaction between the fluid and solid matrix of the meniscus during total knee load transmission and the kinematic characteristics of the meniscus are not yet well understood. Three-dimensional FE models become necessary to obtain quantitative insight of these mechanical behaviors. The objective of this study is to develop a 3D FE model for the knee joint that allows investigation of the transient effects of kinematic loading conditions.

PROCEDURES

Two orthogonal sets of magnetic resonance (MR) images of the left knee of a 36 yr. old normal male volunteer were acquired on a 1.5T clinical imaging unit (GE Signa Horizon, Milwaukee, Wisconsin). T2 weighted 3D gradient recall echo and 3D chemical shift gradient recall echo imaging sequences were used to optimize the visibility of different tissues. A set of 60 sagittal images with 400μm×400μm in plane resolution and 1.5mm slice thickness was used to reconstruct the geometry of the tibio-menisco-femoral joint contact area. On each image, control points for meniscus boundary, cartilage surface and cartilage-bone interface were carefully digitized. These control points were imported to ACIS Solid Modeler and interpolated into cross-sectional curves. All cross-sectional curves were then interpolated into six-faced ACIS solids with B-spline surfaces. An in-house meshing code was developed based on the

ACIS open data structure of the solids and an elliptic p.d.e. algorithm (Knupp, 1994). This customized code was used to generate a mesh of 840 hexahedral elements for femur (354) and tibia (150) cartilage layers and both menisci (236) (Fig. 1). Ligamentous attachments of the menisci were modeled by uniaxial elements. The insertion area on the tibia was carefully identified on the MR images. Cruciate and collateral ligaments can be modeled in a similar fashion. All finite element analyses were performed in MARC 7.2 FE analysis software. The bone surface of the tibia cartilage was assumed to be fully fixed, while the bone surface of the femur cartilage was prescribed a ramp of vertical displacement up to 1mm in 5 seconds and hold for another 100 seconds.
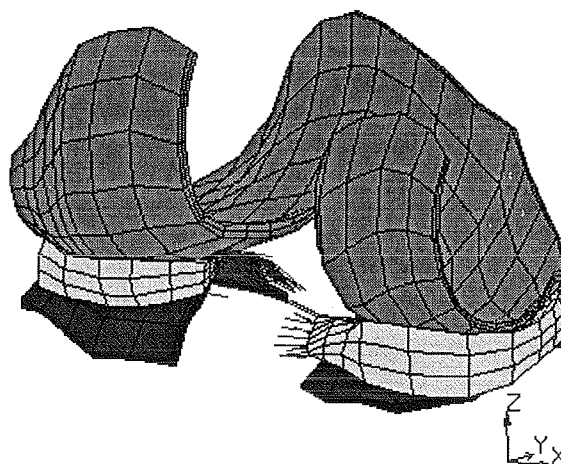
Fig.1. Three-dimensional finite element model of tibio-menisco-femoral contact with 840 quadratic hexahedral elements.

All articular cartilage and menisci are modeled as isotropic poroelastic materials (E_c=0.7MPa, v_c=0.1, k_c=2.17×10^{-15} m^4/Ns; E_m=20MPa, v_m=0.1, k_m=1.26×10^{-15} m^4/Ns;

Athanasiou, 1991). Since there are no published material properties available for meniscus attachments, they are treated as linear elastic with modulus of circumferencial meniscus specimen at anterior and posterior region in tensile testing (Tissakht,1995; E between 80MPa and 120MPa). Contact surfaces between femur cartilage, menisci, and tibia cartilage were defined in MARC 7.2, and assumed to be frictionless. Fluid was allowed to escape only out of the sides of the meniscus and surfaces of cartilage not in contact.

RESULTS AND DISCUSSION

The distribution of minimum principal stress and pore pressure (Fig. 2, 3) suggests that fluid in the articular cartilage carries a larger amount of the load during the loading period. As fluid gradually flows out, the stress in the solid matrix increases with time, indicating that the solid matrix supports more and more of the load. This transient effect is due to the high percentage of fluid and low compressive modulus and permeability of the solid matrix in cartilage and meniscus.

At present, the Young's modulus used in this study is a compromise between compressive and tensile properties measured in all directions. Anisotropic properties will be incorporated into the model in the near future to represent the circumferentially oriented collagen fibers in the meniscus.
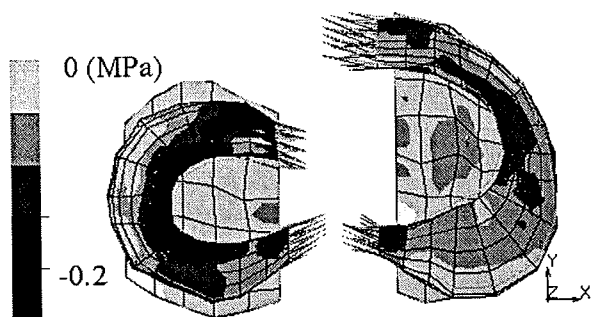
Fig.2. Minimum principal stress distribution in meniscus and tibia cartilage at peak of the displacement (t=5s).
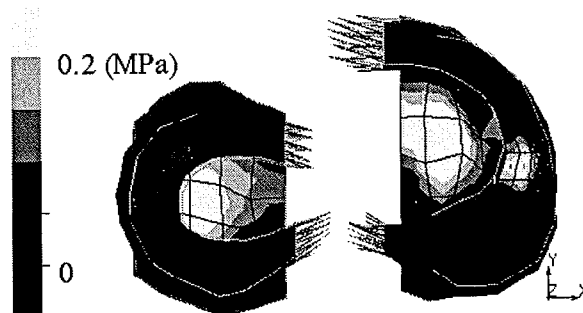
Fig.3. Pore pressure distribution in meniscus and tibia cartilage at peak of the displacement (t=5s).

SUMMARY

This 3D FE model is an accurate representation of the knee geometry and provides us with a framework to study the interaction between fluid and the solid matrix of the meniscus under kinematic loading conditions. In addition, rotational kinematic boundary conditions can also be incorporated into the present model to investigate the motion pathway of the menisci.

REFERENCES

Athanasiou et al. (1991) *J. Orthop Res*, **9**, 330-340.

Knupp P. and Steinberg S. (1994) *Fundamentals of Grid Generation*. CRC Press, Inc.

Tissakht M. and Ahmed, A.M. (1995). *J. Biomech.*, **28** (4), 411-422.

ACKNOWLEDGEMENTS

MEASUREMENT OF THE SCREW-HOME MOTION OF THE KNEE IS SENSITIVE TO ERRORS IN AXIS ALIGNMENT

S. J. Piazza[1] and P. R. Cavanagh[2]

The Center for Locomotion Studies and [1]Depts. of Kinesiology and Mech. & Nuclear Eng.,
[2]Depts. of Kinesiology, Biobehavioral Health, Medicine, and Orthopaedics and Rehab., Penn
State University, University Park and Hershey, PA
Email: sjp12@psu.edu   Web: www.celos.psu.edu

INTRODUCTION

Several authors have reported on the "screw-home" motion of the knee joint (external rotation of the tibia with respect to the femur during extension) with varying results (Kurosawa et al., 1985; Lafortune et al., 1992). These discrepancies in measurements of axial knee rotation may be due to errors caused by kinematic "crosstalk". Such errors arise when the chosen knee joint coordinate system is not aligned with anatomical axes (e.g., when the flexion-extension axis is not aligned in the mediolateral direction).

The purpose of the present study is to investigate the possibility that screw-home motion of the knee is a manifestation of kinematic crosstalk. It may be that external rotation of the tibia does not *accompany* knee extension but rather *is* knee extension that appears as rotation about a different axis. We hypothesize that small misalignments of the knee joint coordinate system may result in knee extension being misinterpreted as external rotation of a magnitude consistent with reports of measured screw-home motion. Specifically, we will test (1) whether a screw-home motion can be measured where none exists, and (2) whether kinematic crosstalk can hide a screw-home motion that is known to occur. Unlike the sensitivity analyses of Blankevoort et al. (1988) and Kadaba et al. (1990), in which the effects of crosstalk were examined by reinterpreting motion data collected in actual knees, the present study concerns the motion of mechanical linkages with known kinematics.

METHODS

A Vicon 370 motion analysis system (Oxford Metrics; U.K.) was used to measure the motions of two mechanical linkages (NSH and SH). The linkages had "thigh" and "shank" segments connected either by a simple revolute joint (NSH) or by a geared joint that produced 15° screw-home over 90° knee extension (SH). Local coordinate systems were determined for each segment from the measured locations of anatomical control points (ACPs) using a method similar to that of Cappozzo et al. (1995). The transformation between segment coordinate systems was determined for each linkage as it was manually flexed to 90° and returned to full extension. These transformations were converted into joint angles using the decomposition proposed by Grood and Suntay (1983).

Kinematic crosstalk was apparent in these joint angles and was removed by adjusting the position of one of the ACPs that defined the flexion axis (Woltring, 1994). This first adjustment was made by performing a systematic grid point search for an ACP position that achieved abduction, rotation, and flexion angles that corresponded to the known mechanical behavior of each linkage. The ACP positions were then adjusted a second time to attempt to produce an apparent screw-home rotation in linkage NSH and to remove screw-home from linkage SH.

Measurements of anatomical landmarks on human subjects were made to determine inter-observer variability in knee flexion axis orientation. The femoral epicondyles of

a single subject were palpated and identified by five experienced observers, and flexion axes were determined that passed through these points.

RESULTS

A flexion axis was found for each linkage that resulted in measurement of joint angles that corresponded to its known motion (Figure 1). Further displacement of the flexion axis by 19.5° in linkage NSH resulted in an apparent screw-home pattern (Figure 2, left). Displacing the flexion axis of linkage SH by 8.5° resulted in the screw-home behavior of this linkage being obscured (Figure 2, right). The apical angle of the cone subtended by the flexion axes determined from anatomical landmarks by the five observers was 13.3°.
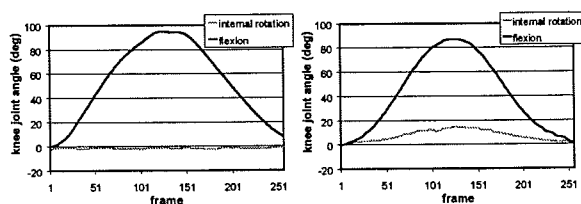
Figure 1: Rotation and flexion angles for linkages NSH (left) and SH (right) following removal of kinematic crosstalk effects.
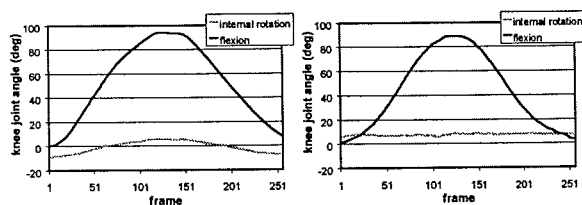
Figure 2: Rotation and flexion angles for linkages NSH (left) and SH (right) subject to crosstalk induced by reorienting the flexion axis. Linkage NSH (which featured a simple hinge) seemingly exhibited a screw-home rotation, and the screw-home rotation of linkage SH was made to disappear.

DISCUSSION

The results of this study demonstrate that kinematic crosstalk resulting from joint axis misalignment can cause screw-home motion to be measured where none exists and can

prevent a true screw-home motion from being measured. The angular displacements of the flexion axis necessary to effect these changes were consistent with the inter-observer range of flexion axis orientations found by palpating the femoral epicondyles. Any technique that relies on accurate estimation of joint axes is subject to these crosstalk errors, including video-based motion analysis, roentgen stereophotogrammetry, and electrogoniometry. Small out-of-plane rotations measured along with large flexion angles should be examined carefully by clinicians to ensure that they are not the product of kinematic crosstalk.

The conclusions drawn from this study are based on the motions of mechanical linkages, not human knees. As such, they provide no insight into whether screw-home motion normally occurs in actual knees. Knowledge of the motion of the mechanical linkages did, however, allow crosstalk errors to be separated from the true motion being measured. Mechanical models such as these provide reference motions useful for the study of errors in the measurement of joint rotations.

REFERENCES

Blankevoort, L. et al. (1988), *J. Biomech.*, **21**, 705-20.

Cappozzo, A. et al. (1995). *Clin. Biomech.*, **10**, 171-8.

Grood, E. S., W. J. Suntay (1983). *J Biomech. Eng.*, **105**, 136-44.

Kadaba, M. P. et al. (1990). *JOR*, **8**, 383-92.

Kurosawa, H. et al. (1985). *J. Biomech.*, **18**, 487-99.

Lafortune, M. A. et al. (1992). *J. Biomech.*, **25**, 347-57.

Woltring, H. J. (1994). *J. Biomech.*, **27**, 1399-414.

ACKNOWLEDGEMENTS

BIOMECHANICAL PROPERTIES OF HEALING GOAT MEDIAL COLLATERAL LIGAMENTS

John D. Withrow, Theodore D. Clineff, Steve D. Abramowitch,
Christos D. Papageorgiou, Savio L-Y Woo

Musculoskeletal Research Center, Department of Orthopaedic Surgery
University of Pittsburgh, P.O. Box 71199, Pittsburgh, PA 15213, (412) 648-2000
Email: ddecenzo@uoi.upmc.pitt.edu   Web: www.ortho.pitt.edu

INTRODUCTION

Isolated medial collateral ligament (MCL) injuries have been shown to heal with conservative treatments [Woo, 1987], but the biomechanical properties of the healing MCL at 6 and 12 weeks have been reported to be inferior to the intact MCL [Weiss, 1991]. However, clinical studies have demonstrated that athletes return to full activity 4-12 weeks after an isolated MCL rupture [Reider, 1994]. The apparent discrepancy suggests that quantitative data on knee kinematics and *in situ* forces of the healing MCL are needed to further understand the healing process. Thus, the objectives of this study were to elucidate the relationship between knee kinematics and tensile properties of healing MCLs at 6 and 12 weeks after isolated rupture using a goat model.

METHODS

Twelve skeletally mature female Saanen breed goats, weighing 44.9 ± 9.6 (mean ± SD) kg were used. The MCL of the right knee (experimental) of each goat was ruptured by pulling medially with a 2.4 mm diameter stainless steel rod passed beneath the ligament creating a "mop-end" tear [Weiss, 1991]. In the contralateral knee, the MCL was exposed and undermined but not ruptured and served as a control.

Post-operatively the goats were allowed free cage activity. The animals were euthanized 6 or 12 weeks after injury. Both hind limbs of each animal were disarticulated from the hip and fixed in specially designed clamps using epoxy putty.

Each knee was mounted on a robotic/universal force-moment sensor testing system. The path of passive flexion/extension of the knee was first determined through the range of knee flexion (30° to 90°). Those positions at 30°, 60°, and 90° were used as starting points for the 4-DOF knee kinematics measured in response to a valgus moment up to 5 N-m. Subsequently, all periarticular soft-tissue structures, except the MCL, were removed leaving only a femur-MCL-tibia complex (FMTC). With the MCL as the only remaining structure, the resulting *in situ* forces in the MCL were determined by repeating the previously recorded kinematics and measuring the new set of force and moment data [Rudy 1996].

Afterwards, the cross-sectional area of the MCL mid-substance was measured using a laser micrometer system [Woo, 1990]. Each FMTC was mounted at 60° of flexion onto customized clamps in a uni-axial testing machine and placed in a saline bath at 32° C. After application of a 2 N preload the ligament was preconditioned for 20 cycles between 0-1mm. The FMTC then underwent a load to failure test at 10 mm/min. Structural properties were calculated from

the load-elongation curve. Simultaneously, strain was determined using a Motion Analysis system which tracked 2 reflective tape markers glued to the surface of the midsubstance of the MCL 1 cm apart. Mechanical properties were analyzed from the stress-strain curves.

Statistical analysis was performed using analysis of variance, followed by multiple contrasts. Statistical significance was set at $p < 0.05$.

RESULTS

Each of the healing MCLs showed some signs of inflammatory response. Valgus rotations of the both experimental groups were ≈50% larger than the controls at 30°, 60°, and 90° of knee flexion. Similar valgus rotations were observed for the 6 and 12 weeks groups at all knee flexion angles tested. At 30° of flexion, the in situ force in the 6 weeks healing MCLs was 40% lower than the controls and the 12 weeks healing MCLs.

Table 1. E/C under 5 N-m valgus moment (n=6). *$p < 0.05$ w.r.t. 1, †$p < 0.05$ w.r.t. 12 wk

E/C	wks	30°	60°	90°
valgus	6	1.4±0.2*	1.6±0.5*	1.5±0.7
rotation	12	1.5±0.3*	1.4±0.2*	1.5±0.2*
in situ	6	0.6±0.3*†	0.8±0.2	0.8±0.3
force	12	1.0±0.2	1.0±0.2	0.9±0.3

The cross-sectional areas were similar for the 6 and 12 weeks groups, but both were significantly larger than their controls. However, the ultimate load was significantly lower in the experimental groups at 6 and 12 weeks compared to the controls. At 6 weeks, stiffness and modulus were significantly lower in the experimental group. By 12 weeks, these properties were not shown to be statistically different from the controls.

Table 2. Biomechanical properties of the FMTC (n=6). *$p < 0.05$ w.r.t. experimental

	wks	Healing	Control
X-Area (mm²)	6	18.0 ± 6.1	11.1 ± 2.4 *
	12	19.2 ± 3.5	11.6 ± 1.9 *
Ult. Load (N)	6	331 ± 130	655 ± 190 *
	12	450 ± 146	717 ± 49 *
Stiffness (N/mm)	6	52.5 ± 19.4	80.3 ± 26.4 *
	12	61.7 ± 19.5	72.6 ± 9.1
Modulus (MPa)	6	205 ± 109	529 ± 293 *
	12	228 ± 119	516 ± 158

DISCUSSION

In this study, knee kinematics, in situ forces in the MCL, and tensile properties of the healing MCL were measured. The lack of significant differences for the knee kinematics and in situ forces in the MCL between 6 and 12 weeks suggests that only minimal improvement occurred in knee function to resist valgus loading. However, tensile properties at 12 weeks of healing were significantly improved compared to those at 6 weeks of healing but did not completely return to normal. This study suggests that knee function may recover as early as 6 weeks, while the tensile properties of the healing MCL are still improving up to 12 weeks after an isolated MCL injury [Scheffler, 1999].

REFERENCES

Reider et al. (1994). AJSM, 22:470-477.
Rudy et al. (1996). J Biomech, 29:1357-60.
Scheffler et. al (1999). Trans. ORS, 45:1052.
Weiss et al. (1991). JOR, 9:516-528.
Woo et al. (1987). AJSM, 15:22-29.
Woo et al. (1990). JBME, 112:426-431.

ACKNOWLEDGEMENTS

BIOMECHANICAL ANALYSIS OF THE CERVICAL DISCECTOMY AND FUSION USING A THREE SEGMENT MODEL

R.N. Natarajan, B.H. Chen*, H.S. An, and G.B.J. Andersson
Department of Orthopedic Surgery, Rush-Presbyterian-St.Luke's Medical Center, Chicago
*Department of Orthopedic Surgery, Qingdao University, Qingdao, P.R. China.
E-mail : rnataraj@rpslmc.edu

INTRODUCTION: Anterior discectomy and fusion (ACDF) is the main surgical procedure for the patients with cervical disc diseases and spondylosis. The Smith-Robinson technique has been a common procedure of the ACDF since 1950. However, the biomechanical effect of the stability of the segment which has undergone fusion as well as the change in flexibility in the adjacent segments have not been well defined in the literature. The present study attempts to quantify percentage changes in flexibility in the fusion segment (C5-C6) and the adjacent segments (C4-C5 and C6-C7) under moment loadings using three segments (C4-C7) finite element model. It is hypothesized that (1) change in stiffness in the fused segment would be much greater than the stiffness changes in adjacent segments and (2) the overall change in stiffness over the three segments due to fusion in the mid segment is small as compared to the change in fused segment stiffness.

MATERIAL & METHOD: Finite element modeling was used for this study. The Smith-Robinson procedure with fusion was modeled for the experiment. A three dimensional non-linear finite element model of an intact C4-C7 cervical spine segment was developed using CT scans of 38-year-old female normal subject. The CT slices were digitized using CAD programs to construct three-dimensional model of the vertebrae, uncinate processes and the intervening discs. The model included fiber reinforced annular fibers represented by cable elements whose cross-sectional area decreased along radial direction from outer portion of annulus. The nucleus was modeled by fluid elements. Ligaments were modeled using non-linear "no compression" uni-axial elements (cable elements). Insertion points of various ligaments were determined from the CT scans. Facet joints assumed inclined at an angle of 45 degrees to transverse plane were modeled by three-dimensional moving contact surface elements. To simulate cartilage layers at the facet joints, three-dimensional elements with cartilage properties were attached to facet contact surfaces. Initially the facet contact surfaces were assumed to be in contact (gap=0.02 mm) with each other. Material properties for the current model were taken from the literature. The analyses were conducted using large displacements small strains theory since it is known that the cervical spine undergoes large displacements due to applied loads. For all the load cases, nodes in the inferior surface of C7 were assigned zero displacements in all directions. Moment load was generated by applying equal and opposite forces at the anterior most and posterior most nodes on the superior surface of C4 vertebra. The ACDF model (the Smith-Robinson procedure) was generated from the intact model by replacing the annulus and the disc of C5-C6 segment by fitting tight graft between the superior and inferior vertebra of C56. A graft of mean cross-sectional area equal to 75% of end plate area was used. The elastic property of the graft was taken as 3500Mpa to simulate iliac crest bone. The predicted responses due to moment loads

(0.6 Nm) along with a pre-load (40N) as a result of the model variations due to the Smith-Robinson procedure was studied to provide all the three displacements and rotations of C4 with respect to C5, C5 with respect to C6, C6 with respect to C7 and C4 with respect to C7 vertebrae.

RESULT: The present study showed that the anterior discectomy and fusion produced large decrease in motion as compared to intact segment at the fused segment level for all moment loads. An ACDF produced a reduction in flexion motion (Figure) of 68%, a 52% reduction in extension motion, a maximum of 91% reduction in lateral bending motion, and a 77% reduction in its principal motion under torsion. The adjacent disc motions increased in response to all the four-moment loads. Lateral bending produced an increase in motion of 25% at C6/C7 level and 18% at C4/C5 level. A 10% increase in motion was seen at C4/C5 level under torsion and at C6/C7 level under extension. All other increases at adjacent levels were less than 5%.

An overall (motion of C4 with respect to C7) increase in motion of less than or equal to 5% was observed under extension and lateral bending moment loads. Flexion and torsion moment loads produced a decrease in overall motion of 10% to 15% due to fusion at C5-C6 level.

CONCLUSION: The present study showed that the ACDF produced a stable segment at the fused level while increasing the flexibility of the adjacent segments nominally. The fused segment was more stable under torsion and lateral bending moment loads as compared to flexion/extension bending loading modes. The interbody graft effectively reduced the motion of all the three motion segments taken together under all the four-moment loadings. From the biomechanical point of view, the interbody fusion is more reliable for reconstructing the stability of the cervical spine after anterior decompression.
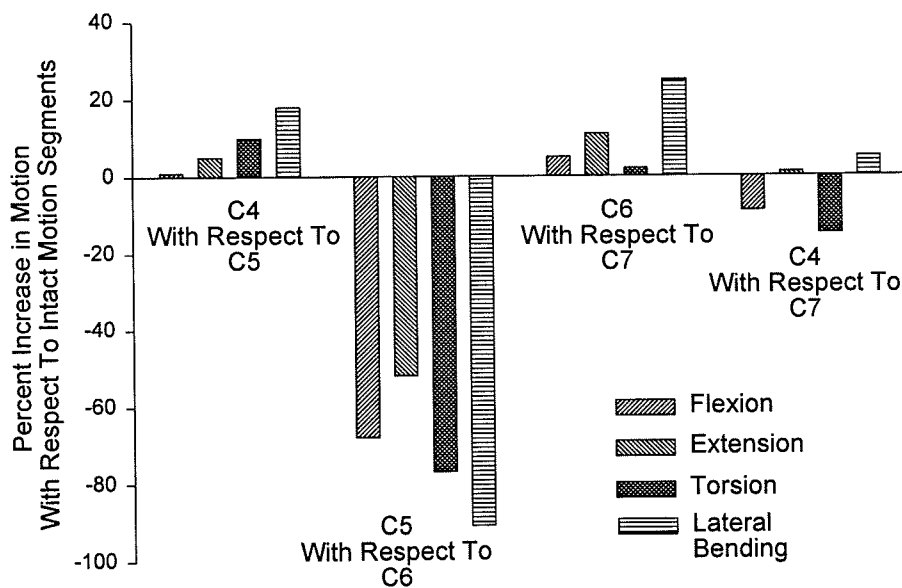
PERCENT INCREASE IN MOTION AT EACH THREE LEVELS
AS WELL AS INCREASE IN MOTION OF C4/C7
DUE TO FUSION AT C5-C6 LEVEL

THE EFFICACY OF DC STIMULATION ON LUMBAR INTERTRANSVERSE FUSION

[1]John C. France, [1,2]Timothy L. Norman and [1]Robert D. Santrock

[1] Department of Orthopedics, West Virginia University, Morgantown, West Virginia
[2]Department of Mechanical and Aerospace Engineering, West Virginia University, Morgantown, West Virginia
Email: jfrance@wvuortho1.hsc.wvu.edu   Web: www.hsc.wvu.edu/som/ortholab/

INTRODUCTION

A variety of studies have been done regarding direct current electrical stimulation and its effect on bone healing. Kahanovitz et al. (1990) have been able to demonstrate significant efficacy in facet fusions using a canine model. Additionally, a variety of clinical studies are available supporting its use in human intertransverse process fusions, but many of these lack adequate controls. Human *in vivo* studies limit the ability to perform adequate biomechanical and histological investigation regarding adequacy of the fusion mass. All of these studies have been done utilizing the standard lower amperage stimulator with 20 microamps. The purpose of this study was to better understand and assess the effect of direct current stimulation on a more commonly utilized intertransverse process fusion utilizing a rabbit model. In addition, we compared the low amperage (20 microamps) to a newly developed higher amperage (60 microamps) stimulator.

PROCEDURE

Thirty-one mature New Zealand white rabbits were randomly divided into three groups and the investigators remained blinded throughout the study. All rabbits underwent a L5-6 intertransverse process fusion using a standard muscle splitting approach and autologous bone graft as outlined by Boden et al. (1995). All rabbits were harvested at five weeks for testing.

Group I was done with a sham (inactive) implanted stimulator battery; Group II utilized the currently available 20 microamp stimulator and Group III was implanted with a 60 microamp stimulator. Lastly, an additional unfused adjacent segment was harvested at the time of the testing to act as a control group for the biomechanical testing. Following harvesting, all rabbits underwent radiographic evaluation for assessment of fusion. This was done by assigning a grade of one to three. Four rabbits were sent for histological evaluation and the remainder of the rabbits underwent additional testing using a gross palpation analysis and biomechanical testing for stiffness and load to failure.

RESULTS AND DISCUSSION

The mean radiographic grade for Group I (sham) was 1.91, Group II (20 microamp active battery) was 2.22 and Group III (60 microamp active battery) was 2.58. The difference between the higher amperage battery and the sham group was statistically significant ($p < 0.04$). A trend towards stronger fusion on manual palpation was also noted in the higher amperage battery group, though this did not quite reach statistical significance. On biomechanical testing, the higher amperage group was found to be significantly stiffer ($p < 0.05$) (Fig. 1) and had a significantly higher load to failure ($p < 0.02$) (Fig. 2) than the unfused control segments. In each mode of analysis, it appeared that there was a consistent trend

in that the lower amperage stimulated models had a better fusion mass than the sham group and the higher amperage group had even better overall testing results than the lower amperage battery. We did not identify any complications that could be attributed to the difference in the electrical stimulator amperage strength.

The results of this study offer strong evidence that direct current electrical stimulation enhances intertransverse process fusions at least in the early phases of healing. One criticism of the Kahanovitz study in canine facet fusions has been that the more current and common anatomic location for lumbar fusion is the intertransverse region. Our study utilized a model more accurately simulating this technique and has been widely utilized by others to evaluate efficacy of methods to enhance fusion.

The maximal amount of amperage distributed by DC batteries has not been accurately determined. Studies to date have all used 20 microamp stimulators. The efficacy of such stimulators is again demonstrated in this study, but by increasing amperage to 60 microamps, the beneficial effect was enhanced in all tested parameters. Thus, the newly developed higher amperage (60 microamps) battery appears to have an enhanced effect even above and beyond the previously utilized lower amperage (20 microamps) batteries. Further investigation on the effect of stimulation in a more compromised model such as smoking chamber or the longer term effect on the strength of fusion mass may be warranted.

SUMMARY

The effect of direct current stimulation on an intertransverse process fusion rabbit model was assessed using low and a new higher amperage stimulator. Results offered strong evidence that direct current stimulation enhances intertransverse process fusion, and that the healing effect was enhanced by increasing the amperage to 60 microamps.

REFERENCES

Kahanovitz N, Arnoczky SP (1990). *Clin. Orthop.* **251**, 295-299.

Boden SD, Schimandle JH, Hutton WC (1995). *Spine* **20**, 412-420.

ACKNOWLEDGEMENTS
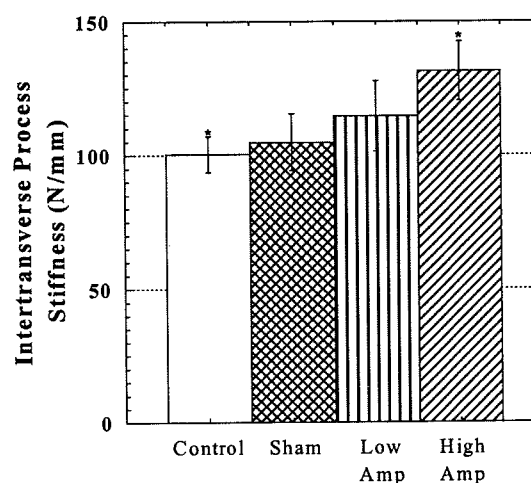
Figure 1: The higher amperage group had significantly greater stiffness than the control group (p < 0.05).
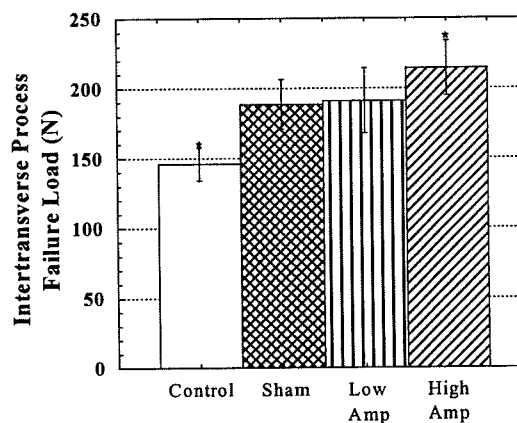
Figure 2: The higher amperage group had significantly greater failure load than the control group (p < 0.02).

ANTERIOR PLATE AND BONE GRAFT LOAD SHARING IN THE CERVICAL SPINE -- A FINITE ELEMENT INVESTIGATION

Jeffrey L. Scifert[1], Vijay K. Goel[1], Nicole M. Grosland[1],
Christian M. Puttlitz[1], Koji Totoribe[1], Vincent C. Traynelis[2]

[1]Departments of Biomedical Engineering & Orthopaedics
[2]Division of Neurosurgery
University of Iowa, Iowa City, IA
E-mail: Vijay-Goel@uiowa.edu

INTRODUCTION

Graft healing and subsidence are both clinically relevant issues related to the use of an anterior plate with bone graft. Our hypothesis is that these issues are related to load sharing and stresses observed among the plate, graft, and endplates. The reported load sharing data between the plate and bone graft using the in vitro approach is sparse and in vitro protocols are not well suited to address this issue. The finite element (FE) technique can be exploited for an in depth understanding of load sharing between plate and graft and potential sites for graft subsidence.

PROCEDURES

A ligamentous, non-linear, three-dimensional FE model of the C4-C6 motion segments was developed from 1.5 mm thick serial computed tomography (CT) scans. Material properties for the intact model were taken from our previously validated C5-C6 FE model (Goel and Clausen, 1998). Validation of the intact model was performed by comparing model predictions to published cadaveric load-displacement characteristics and our own in vitro experiments. The intact model was modified at the C4-C5 level to simulate an anterior plate and bone graft. The bone graft was assigned three different material properties: cancellous bone, cortical bone, and titanium. A bone graft healed (BGHL) case and bone graft not healed (BGNH) case were

simulated. All models were subjected to compressive loading of 73.6 Nm with and without flexion/extension, right lateral bending (RLB), and left axial rotation (LAR) moments of 1.5 Nm. C4-C5 and C5-C6 rotations were determined for all cases. Loads in the plate and graft were computed. Von Mises stresses were observed to identify loading patterns and possible subsidencelocations.

RESULTS AND DISCUSSION

Model predictions demonstrated good agreement with the in vitro data. C4-C5 rotations in the stabilized models were an order of magnitude lower than intact rotations.

In BGHL and BGNH compression, the graft took a majority of the load in all simulations while the anterior plate and facets were minimally loaded, Figure 1A, 1B. In BGHL flexion, the plate was in compression, while the graft was in tension. In BGNH flexion, the plate was in compression and the graft was unloaded. In BGHL and BHNH extension, the plate was in tension, while the graft was in compression. In BGHL RLB the graft and plate were in compression, while in BGNH RLB the graft was in compression and the plate was in compression or tension, depending upon graft type. In both BGHL and BGNH LAR the graft and plate were in compression.

The Von Mises stress patterns observed at the endplates equaled the load distribution and followed the load sharing mechanism. In cases of no or minimal load transfer through the graft (ie. flexion), endplate stresses were decreased compared to the intact case. In cases where the graft load increased greatly (ie. extension), the maximum endplate stresses increased by as much as 425% compared to the intact case (21.8 MPa in BGHL titanium graft case versus 5.12 MPa in the intact case), Figure 2. Trends indicated higher stresses in the BGHL cases than in the BGNH cases and stresses tended to increase with increasing graft modulus. The higher endplate stresses tended to occur in the inferior endplate.

The data indicate that the plate load is very sensitive to motion segment rotations. The graft will experience high compressive loads in extension. The plate will stress shield the graft in flexion. Model predictions indicate that the magnitude and nature of loads (tensile or compressive) seen by the plate and graft is dependent upon several factors: the axial compressive load that simulates the head weight and the accompanying flexion/extension rotation, the degree of lordosis, compression induced on the graft via distraction, graft stiffness, and degree of graft consolidation. Higher stresses are expected to occur after fusion, with increasing graft modulus, and at the inferior endplate region. Stress patterns can also be expected to change with endplate bone quality, thickness, and morphology. Under distraction and re-compression, these stresses can be expected to be increased, possibly enough to cause subsidence or pistoning of the graft, both of which are observed clinically.

SUMMARY
Using an FE model of C4-C6, the load sharing between an anterior plate and bone

graft was investigated. Endplate stress patterns under various loading modes were investigated to determine locations of graft subsidence. Results indicated that the graft will experience high compressive loads in extension and the plate will stress shield the graft in flexion. Endplate stress patterns indicated potential subsidence would occur at different endplate locations, depending upon loading modality.

(+ve indicates compression, -ve indicates tension)

(A)

(B)
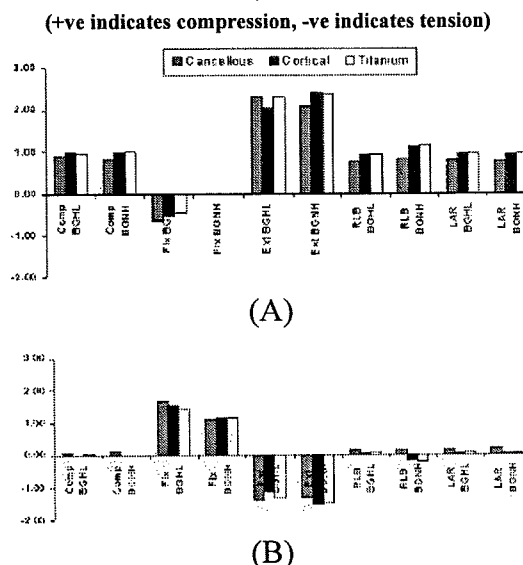
Figure 1: (A) Ratio between predicted load in the graft vs. applied compressive load (B) Ratio between predicted load in the plate vs. applied compressive load
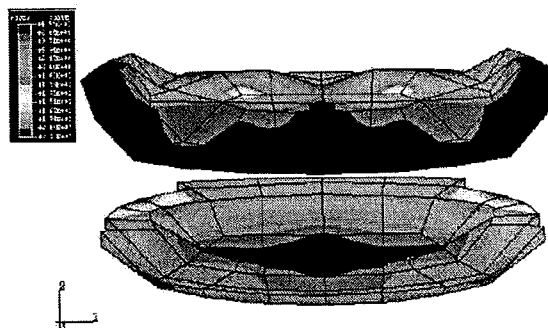
Figure 2: Von Mises stress plot of stresses observed in the C4-C5 endplates during extension with a titanium graft (BGHL)

REFERENCES
Goel V and Clausen J. (1998). Spine, 23, 648-691.

IMPACT DYNAMICS OF THE SPINE AND THE EFFECT OF DEGENERATION

Sara E. Wilson [1], Thomas A. McMahon [2] and Elizabeth R. Myers [3]

[1] Orthopedic Biomechanics Laboratory,
Beth Israel Deaconess Medical Center, Boston, MA
[2] Division of Engineering and Applied Sciences, Harvard University
[3] Hospital for Special Surgery, New York, N.Y.
Email: sew@obl.bidmc.harvard.edu

INTRODUCTION

It has been estimated that Caucasian women have a 16% lifetime risk of a vertebral fracture by the age of 50 (Melton, 1997). Studies of vertebral fracture patients with acute symptoms have shown that 30 to 50% of these patients associate a fall with their fracture (Cooper, 1992, Myers, 1996). This has led to the development of models to examine the loads on the spine during falls (Wilson, 1998). These models require an accurate assessment of the stiffness and damping properties of the spine. The variability in these properties among the elderly is also important to assess. In this study, the stiffness and damping properties of elderly spine segments were measured and the effect of MRI based measurements of degenerative changes was assessed.

PROCEDURES

Five male and fourteen female, cadeveric, L1 to L3 spine segments over the age of 60 (62 to 85 years) were dissected, preserving the posterior elements and ligaments. The spines were imaged using T2 weighted magnetic resonance images (2000/80). Geometry of the intervertebral disks and signal intensity relative to heavy water phantoms were obtained.

The L1 and L3 vertebrae were potted in polymethylmethacrylate. Spines were precompressed in a saline bath for an hour. They were then tested mechanically in a pendulum impact apparatus (Fig. 1). Preload was applied using elastic straps and the resulting impact force transmission was measured. The frequency of the post-impact force vibrations was found by the fast Fourier transform of the data. The data were then low pass filtered and the damping ratio was found by measuring the peak-to-peak signal decay. Stiffness and damping coefficients were found using a Kelvin model. Analysis of variance
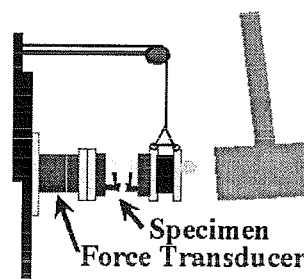
Figure 1. The pendulum apparatus consisted of a pendulum arm that struck an end mass (20.9 kg). The end mass was attached to the posterior potted end of the spine segment. The anterior, potted end was attached to a force transducer that was mounted to the wall.

was used to examine the influence of preload on the stiffness and damping coefficients. Linear regression correlation coefficients were used to examine the relation of stiffness and damping constants to MRI-based measurements.

RESULTS AND DISCUSSION

Spine segments without osteophytes were found to exhibit second-order, underdamped oscillations when attached to an end mass of 20.9 kg (Fig. 2). Predicted stiffness and damping fits matched closely with the original force signal.
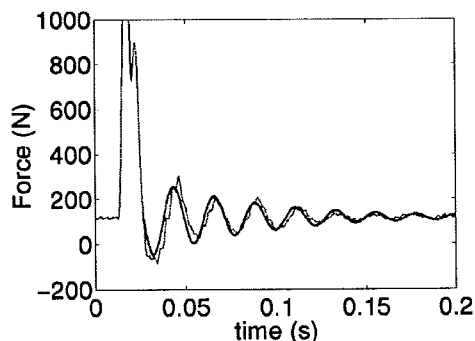
Figure 2. Force transmission after impact exhibits underdamped oscillations. Fit of the oscillations is shown as a dark, thick line.

Stiffness values were found to range between 17.9 and 754.5 kN/m with a mean of 264.9 ± 194.0 kN/m. Damping values were found to range between 133.6 and 905.3 Ns/m with a mean of 265 ± 193.9 Ns/m. Stiffness was found to increase with preload ($p < 0.001$). Mean spine segment MRI T2 signal intensity was found to correlate significantly with stiffness at a preload of 0 N with a decreased signal corresponding to an increased stiffness. At higher preloads this trend was less pronounced. A decreased signal is often used in clinical settings as a sign of degeneration. Damping constant values were not found to significantly correlate with either preload or MRI based measurements. Using the mean stiffness and damping found here, changes in stiffness and damping by one standard deviation could change the predicted force in models of the impact phase of a backwards fall by as much as 17%.

SUMMARY

In summary, stiffness increased with increasing preload. Stiffness was also predicted to increase with decreasing MRI T2 signal intensity at low preloads. Damping was not shown to change either with preload or with other measures. Variations of one standard deviation in stiffness and damping result in considerable changes in the force applied to the spine as the result of a backwards fall.

REFERENCES

Melton, L.J. (1997). *Spine*, 22(24S), 2S-11S.
Cooper, C.C. et al. (1992*). J. Bone Min. Res.*, 7(2), 221-227.
Myers, E.R., Wilson, S.E. (1996). *Spine* 22(24S), 25S-31S, 1997.
Wilson, S.E., Myers, E.R. (1998). *Proceedings of the PreORS Symp. on Comp. Methods in Orthop. Biomech.*

ACKNOWLEDGEMENTS

QUANTIFICATION OF LUMBAR-PELVIC COORDINATION IN HEALTHY ADULTS

Kevin P. Granata[1] and Adam H. Sanford[2]

[1] Department of Orthopedic Surgery, University of Virginia, Charlottesville, Virginia
[2] Department of Biomedical Engineering, University of Virginia, Charlottesville, Virginia
E-mail: ahs8t@virginia.edu Web: www.med.virginia.edu/medcntr/gaitlab/

INTRODUCTION

Sagittal trunk motion is accomplished through a coordination of pelvic rotation and lumbar spine flexion/extension. As trunk range of motion in healthy subjects is not fundamentally different to persons with low-back pain (LBP), other means of discriminating the two populations must be used. Research suggests that lumbar-pelvic (LP) coordination could be a potential diagnostic metric for LBP. Though LP coordination has been studied at length, there is little consensus regarding the gross contributions of the lumbar spine and pelvis to total trunk motion; literature values for lumbar to pelvic (L/P) ratios range from 0.4 to 1.97. Such a spread of literature values would pose difficulties for the comparison of healthy and LBP populations. Previous studies have not controlled lifting parameters such as weight or trunk extension velocity as possible influences of LP coordination. A study of the effect of lifting parameters upon LP coordination was performed to provide a complete description of lifting behavior and to assess possible sources of error in previous quantifications of LP coordination.

PROCEDURES

18 subjects (13 M, 5 F) with no prior history of LBP volunteered to participate in the study. Subjects performed lifting exertions at 15, 30 and 60 deg./s trunk extension velocity with 0 and 10 kg loads carried in the hands. To control trunk extension velocity, subjects were required to follow a target region in a real time display that was pre-programmed to travel at the desired trial velocity. Spinal motions were recorded from six degree of freedom electromagnetic sensors placed over the spinous processes of the S1 and T10 vertebrae. The shape and magnitude of the LP coordination was quantified using principal component analysis (PCA). For direct comparison to literature values, L/P ratios were calculated over three 30° windows as reported in previous studies. A repeated measures ANOVA was performed on all findings, and significance was noted for all effects with $\alpha < 0.05$.

RESULTS AND DISCUSSION

PCA results show that the weighting coefficient of the most powerful eigenvector was significantly affected by task weight. This eigenvector describes the basic lifting behavior of all subjects, so significance with weight describes a gross effect upon the lumbar and pelvic contributions to total trunk motion.
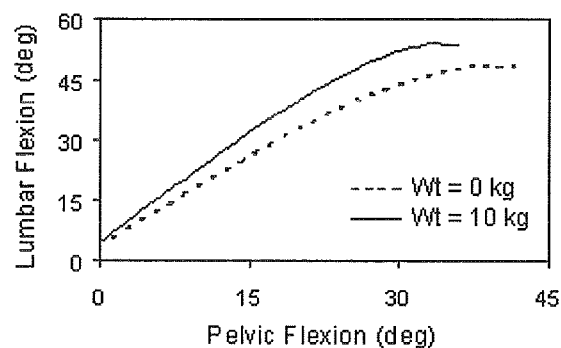
Fig. 1: Weight effect on LP Coordination

The weighting coefficient of the third most powerful eigenvector was significantly affected by the trunk extension velocity. This eigenvector describes a time dependent shift in the L/P ratio, so significance with velocity describes a timing effect on the LP coordination.
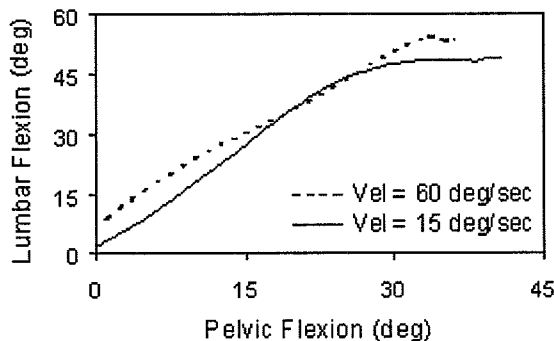
Fig. 2: Velocity effect on LP Coordination

Calculated L/P ratios agree to some extent with literature values, but previous studies did not control the aforementioned lifting parameters. The average L/P ratio was approximately 2.25, describing the lumbar spine as responsible for roughly 70% of the total motion.

Marras reported that lifting parameters influenced lumbar spine behavior. As the lumbar and pelvic angles recorded in this study describe the shape of the lumbar spine, the lifting parameter effects on LP coordination found in this study are consistent with his findings. Minitski found that weight affected lumbar timing and not lordotic magnitude, suggesting L/P ratio was not affected as was found in this study. However, Davis found that lumbar timing was affected by weight with the bent-knee lifting method, but not with the straight-leg lifting method. Given that Minitski's study did not limit knee flexion, Davis' finding could well explain how Minitski's study contradicts the findings of this study.

SUMMARY

LP coordination is statistically different under differing lifting parameters. Task weight affects the magnitude of the gross LP contributions to trunk extension, while trunk extension velocity affects the timing of the lumbar and pelvic contributions to trunk extension. As previous research did not take these lifting parameters into account, these findings could explain the wide range of L/P ratios previously reported. Given this, if LP coordination is to be used to compare healthy and LBP populations, lifting parameters such as weight and trunk extension velocity must be carefully controlled. Now that the LP coordination has been quantified for healthy subject population, future work can be done to compare this data set with persons with LBP. A similarly performed PCA could yield a physiologic eigenvector describing LBP behavior as statistically different from that of healthy subjects. Another future direction of LP coordination research is to employ it as measure of spinal stability.

REFERENCES

Esola, M.A. et al. (1996) *Spine*, **21**: 71-78.

Marras, W.S. et al. (1994) *IEEE Trans. Rehab. Eng.*, **2**: 137-146.

Davis P.R. et al. (1965) *J. Anat.*, **99**:13-26.

Minitski, A.B. et al. (1998) *Clin. Biomech.*, **13**:121-127.

McClure, P.W. et al. (1997) *Spine*, **22**: 552-555.

Porter, J.L., Wilkinson, A.(1998) *Spine*, **22**: 1508-1514.

ACKNOWLEDGEMENTS

BASIC SCIENCE AND CLINICAL APPLICATIONS OF
A MAGNETIC TRACKING/VIRTUAL REALITY BASED SYSTEM
FOR ASSESSMENT OF OVERALL CERVICAL SPINE KINEMATICS

Jonathan L. Sakai, B.S., Lars G. Gilbertson, Ph.D., Louis E. DeFrate, B.S.,
Seong-Hwan Moon, M.D., William F. Donaldson III, M.D.,
James D. Kang, M.D., Savio L-Y. Woo, Ph.D.

Musculoskeletal Research Center
The University of Pittsburgh
Pittsburgh, Pennsylvania 15213

INTRODUCTION

Delineation of in-vivo cervical spine kinematics can provide clinically valuable benchmarks for quantifying biomechanical effects of aging, degeneration, injury, surgery, rehabilitation, and other agents. Active kinematic assessments typically involve the measurement of overall cervical spine mobility as a volunteer/patient actively performs selected spinal movements. A disadvantage of active assessments is their dependence on the ability and willingness of the volunteer or patient to control his overall movements—mandating development of methods for enabling improved control.

The magnetic tracking/virtual reality (VR) based system has recently been developed for measurement, description, and control of movements of the head relative to the torso. The objective of this study was to test the efficacy of VR-assisted visual feedback of overall cervical spine kinematics for improving control of voluntary cervical spine movements in the assessment of the active kinematics of normal volunteers and spinal surgery patients.

MATERIALS AND METHODS

The magnetic tracking/VR-based system consists of a magnetic tracking system, head mounted display, and programmable visual interface, operating under the control of a personal computer. The magnetic tracking system Flock of Birds™ (Ascension Technologies, Inc., Burlington, VT 05402) was used to measure the translational and rotational movements of the head and torso within a global coordinate system defined by the position and orientation of a stationary transmitter placed behind a seated subject. Ten healthy male volunteers (with no history of spinal problems), and three cervical fusion patients performed maximal cervical spine active range-of-motion (AROM) maneuvers in flexion/extension, axial rotation, and lateral bending, both without and with VR-assisted visual feedback of their overall rotations. The primary and secondary rotations at the extremes of primary movement were analyzed to determine normative baseline values (controls) and effect of fusion surgery (patients).

RESULTS AND DISCUSSION

For the control group, the mean overall cervical spine primary rotations at the extremes of primary movement for AROM maneuvers with VR feedback were statistically no different from those without VR feedback—supporting use of VR feedback for acquiring physiologic range-of-motion data (Table 1).

Figure 1 illustrates the improved quality of spinal movement control achieved

with VR feedback by the 10 control subjects during lateral bending. Secondary rotations with VR feedback spanned a much narrower range than those without VR feedback—indicating that the subjects were successful in reducing secondary rotations, resulting in a "purer" overall rotation—thereby improving the consistency of the AROM maneuver.

Table 2 compiles the ranges-of-motion (ROM) of the three cervical spine fusion patients, achieved with VR feedback. Patient 1 had received a one-level (C5-6) fusion surgery, while patients 2 and 3 received two-level (C5-7) surgeries. Although Patient 1 had one more mobile level (C6-7) than the other patients, range-of-motion was much less than attained by the two-level fusion patients—possibly due to presence of pain in Patient 1.

Comparison of data from Tables 1 and 2 reveal that the ROM of the patients was less than that of the control subjects in each of the primary rotational degrees-of-freedom studied. Considering only the two-level fusion patients (who were pain-free at the time of the kinematic assessment), the decreased range of motion of Patient 2 (with respect to control group) was consistent with the loss of mobility of the C5-6 and C6-7 segments. The ROM of Patient 3, however, was considerably less than expected based solely on loss of mobility of C5-7—pointing to the presence of other factors.

In summary, a magnetic tracking/VR-based system for comprehensive kinematic assessment of the cervical spine has been developed and tested on 10 asymptomatic volunteers and 3 spinal fusion patients, and has been found to aid subjects in control of active range-of-motion maneuvers. Our long-term objective is to explore the potential use of this system as a basis for standardized, more objective testing of normal volunteers and clinical patients.

Table 1. Mean (±SD) range of motion of control subjects, without and with VR feedback (n=10).

Primary Movement	Primary Rotation (degrees)	
	Without VR	With VR
Flexion	62.9 ± 8.5	64.0 ± 10.1
Extension	-57.4 ± 11.9	-58.3 ± 12.9
Left AR	70.4 ± 6.0	72.9 ± 7.0
Right AR	-72.1 ± 6.1	-74.2 ± 6.6
Left LB	-37.8 ± 9.0	-38.2 ± 8.7
Right LB	38.8 ± 9.3	39.4 ± 10.0
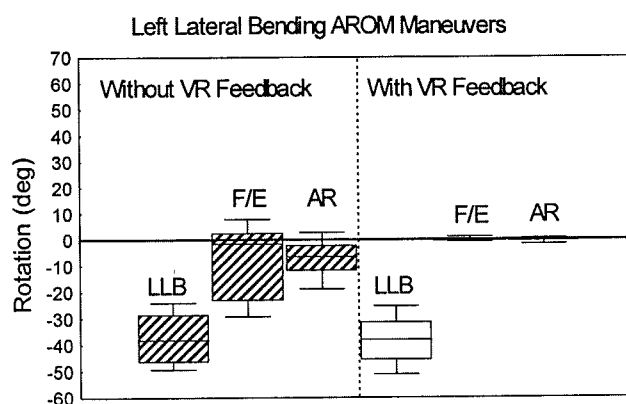
Figure 1. Box plot showing range and distribution of primary and secondary rotations during left lateral bending AROM maneuvers by the 10 control subjects, without and with VR feedback.

Table 2. Overall cervical spine rotations for three fusion patients.

Primary Movement	Rotation (deg)		
	Patient 1*	Patient 2**	Patient 3**
FE	32.8	109.6	64.7
AR	59.3	125.4	93.5
LB	28.3	64.8	36.0

FE = flexion/extension, AR = axial rotation, LB = lateral bending.
* 1-level fusion; ** 2-level fusion

ACKNOWLEDGMENTS

AN IMPROVED EXERCISE COUNTERMEASURE
TO PROVIDE ENHANCED VERTICAL IMPACT LOADS IN LOW GRAVITY

Young-Hui Chang, Chris M. Hamerski, and Rodger Kram

Department of Integrative Biology, University of California, Berkeley, CA
Email: younghui@uclink4.berkeley.edu   Web: socrates.berkeley.edu/~hbbiomxl/

INTRODUCTION

Chronic exposure to microgravity causes a variety of physiological changes within the human body. The loss of bone mineral is one change that adversely affects the bio-mechanical integrity of the musculoskeletal system. To successfully accomplish long-term human space exploration, an effective countermeasure must be devised to minimize this effect (Baldwin, et al., 1996). We investigated the use of applied horizontal aiding forces (AHF) as a possible countermeasure against bone mineral loss.

Impact loading rates of bone from normal daily activity is correlated with the retention of bone mineral density (Cavanagh, et al., 1992; Lanyon and Rubin, 1984). Current countermeasures use elastic cords to apply a downward force to the shoulders and hips of a running astronaut to simulate Earth-like forces. This method, however, causes discomfort due to the high downward forces (McCrory, et al., 1996) and results in unsatisfactory forces generated against the ground (Boda, et al., 1998).

We previously saw that externally-applied, horizontal aiding forces caused vertical impact peaks generated against the ground to increase when running at Earth,s gravity (Chang & Kram, 1999). We hypothesized that impact forces generated against the ground during running would increase with AHF even at simulated reduced gravity.

PROCEDURES

Four male subjects (27 ± 7 yr., 69.6 ± 8.3 kg, mean ± SD) gave their informed consent to run normally at 3 m/s on a force-measuring treadmill (Kram, et al., 1998) and at simulated gravity levels of 0.25, 0.38, and 0.50G (where G is 9.81 m/s2). We simulated reduced gravity by pulling up on the subject's torso via a harness attached to a series of stretched latex springs. Applied horizontal aiding forces (AHF) were produced in a similar manner via a belt worn about the waist (Chang & Kram, 1999). For each gravity level, an AHF of 0%, 10%, 15%, and 20% of the gravity-specific body weight was applied. The order of trials at each gravity level was randomized. Vertical ground reaction force data were sampled at 1kHz and low-pass filtered (100 Hz cutoff).

We compared the vertical impact peaks generated on the ground at each condition to those for running at 1G with no AHF (control). We used a repeated measures ANOVA with a criteria of $p < 0.05$ and Tukey's HSD post-hoc test to compare across conditions. Impact peaks were deemed "desirable" if they met or exceeded impact peaks measured for normal running at 1G.

RESULTS AND DISCUSSION

Running normally at 1G, subjects generated impact peaks of 1.6x body weight at 1G (BW). Impact peaks increased with AHF at each gravity level (Fig. 1). With a 20% AHF, subjects produced desirable impact peaks at all gravity levels. At 20% AHF, impact peaks were 2.2x BW at 0.50G (a 32% increase above the 1G control). Impact

peaks increased with gravity for each level of AHF (Fig.1).

Vertical impact force peaks generated on the ground during running increased with horizontal aiding forces and, with sufficient AHF, actually surpassed those experienced normally at 1G.
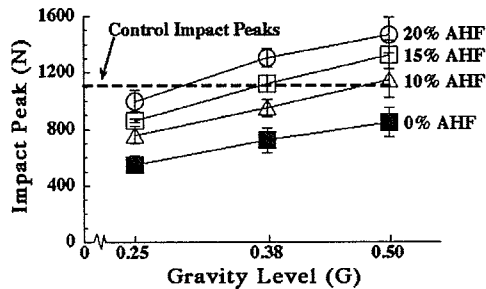
Figure 1: Vertical force impact peaks for different AHF at each gravity level. Dashed line indicates mean impact peak at 1G with no AHF (control). Data are mean ± SE.

Although the actively generated peak forces decreased with gravity (A), passive impact peaks (I) were highly sensitive to AHF and increased with AHF despite decreases in the active vertical force peak (Fig.2).
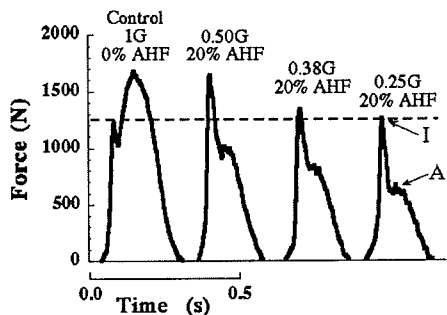
Figure 2: Typical vertical ground reaction forces at four gravity levels. Dashed line indicates impact peak for control condition. I is passive impact peak; A is active peak.

Our previous research has shown that both vertical and horizontal components of the forces generated on the ground during running are tightly coupled (Chang, et al., 1998). When one component of force is altered, people adjust their gait such that the other component changes in proportion.

Adding horizontal aiding forces to proposed exercise countermeasures (i.e. motorized treadmill running with simulated partial gravity) would improve impact loading on the musculoskeletal system. This technique would likely be a more effective countermeasure against the bone mineral loss from chronic exposure to weightlessness. This method can provide desirable impact loads and can do so at a much lower partial gravity level, which may provide a more comfortable alternative to currently used countermeasures.

REFERENCES

Baldwin, K. M., et al. (1996). Med. Sci. Sports Exercise, **28**, 1247-1253.

Boda, W. L., et al. (1998). Proceedings from Experimental Biology 98, 5547.

Cavanagh, P. R., et al. (1992). Aviat. Space Environ. Med., **63**, 482-485.

Chang, Y.-H., et al. (1998). Proceedings of NACOB'98, 309-310.

Chang, Y.-H. and Kram, R. (1999). J. Appl. Physiol., **86**, 1657-1662.

Kram, R., et al. (1998). J. Appl. Physiol., **85**, 764-769.

Lanyon, L. E. and Rubin, C. T. (1984). J. Biom. **17**, 897-905.

McCrory, J. L. et al., (1996). Proceedings of ASB,**96**, 235-236.

ACKNOWLEDGEMENTS

Can Gait be Retrained to Prevent Injury in Runners?

I.S.McClay[1,2] , DS Williams[2] and CA Laughton[2]

[1]Joyner Sportsmedicine Institute, Harrisburg, PA 17111
[2]Motion Analysis Laboratory, University of Delaware, Newark, DE 19716
email: mcclay@udel.edu

INTRODUCTION

Abnormal mechanics are recognized as a factor in the etiology of running-related injuries. Foot orthotic devices are sometimes prescribed to address excessive foot pronation. However, in general, running gait is thought to be relatively automatic and unchangeable. Treatments are most often aimed at decreasing symptoms with medication and palliative therapeutic intervention. However, if improper mechanics are the cause, once the patient returns to running, the problem is likely to reoccur. If a runner is able to modify his gait pattern and correct the abnormal mechanics, the risk for further injury is likely to be reduced.

Therefore, the purpose of this study was to assess the lower extremity mechanics of an injured runner and investigate the effect of a gait retraining program on their running pattern.

PROCEDURES

One 40 yr old female recreational runner who presented with running-related injuries served as the subject for this study. Prior to her injuries, she had been running approximately 15-20 miles per week. At the time of her evaluation, she had discontinued running as a result of right plantar fasciitis and a left tibial stress fracture (which was healed at the time of the study). Further attempts at running resulted in a return of symptoms. A visual analysis of the patient's running revealed the following. On the right, the hip was in excessive internal rotation and the knee in genu valgum throughout the support phase. While the rearfoot motion appeared normal, excessive midfoot pronation was observed. On the left, a scuffing sound was noted with each footstrike.

The patient's running gait was evaluated with instrumented gait analysis in order to objectively quantify the gait deviations that were noted visually. Four retroreflective markers were affixed to a velcro-backed polyform shell and attached to the thigh via a neoprene wrap. A similar marker set was attached to the shank. Three markers were attached directly to the heel counter of the shoe. Additionally, markers were placed over various anatomical landmarks in order to define the anatomical coordinate system. After a standing calibration trial was collected and the anatomical transformations calculated, these markers were removed.

The subject then ran along a 75-ft runway at a speed of 3.35 m/s ($\pm$10%) striking a forceplate at its center. Speed was monitored with a photoelectric timing system. Data were sampled at 120 hz with a 6 camera VICON (Oxford Metrics, UK) Motion Analysis System. Ground reaction forces (GRF) were collected from a Bertec (BERTEC Corp, OH) forceplate being sampled at 480 hz. 5 trials were collected and averaged. The three-dimensional joint kinematics were resolved about a joint coordinate system using MOVE3D software (NIH Biomechanics Laboratory). Data were compared to a database of non-injured runners collected in this laboratory. Attention was focused on values that fell outside of 1sd of this dataset.

Based upon the findings of the gait evaluation, the subject agreed to undergo an 8-week, 3 times per week gait retraining program. All training took place on a treadmill running at 3.35 m/s. A mirror was used to provide feedback initially, but was gradually removed after the initial 3 weeks of training. The subject began running for 10 minutes and gradually progressed to 32 minutes by the end of the 8-week session. The subject then underwent another instrumented gait analysis to assess any changes that occurred as a result of the training.

RESULTS

Results of the initial gait analysis are presented in table 1. As can be seen, on the right, the subject landed with increased hip adduction and internal rotation and reached greater peak values compared to normals. In addition, excessive knee abduction (at footstrike and peak) was seen suggesting a knee in greater valgus. Greater knee flexion

was noted (fs and peak) bilaterally. On the left, similar findings were seen at the hip, but to a lesser degree. In addition, the peak braking forces were higher than normal.

Table 1. Initial Right and Left Variables of Interest (EXT, ADD & IR are positive)(*=outside 1 sd of NL)

	Right	Left	Normal (+/-sd)
Hip (deg)			
fs ADD	11.6*	9.8*	4.1 (5.0)
pk ADD	11.6	10.8	10.1 (4.9)
fs IR	16.9*	13.2*	7.5 (5.3)
pk IR	20.4*	13.9	10.4 (4.72)
Knee (deg)			
fs FL	-15.6*	-20.8*	-5.6 (6.1)
pk FL	-52.7*	-55.1*	-45.6 (3.4)
fs ABD	-9.0*	-3.2	-3.1 (2.6)
pk ADD	-3.2*	8.2	0.523 (4.3)
AP GRF			
peak (bw)	-0.37	-0.49*	-0.32 (0.04)
load rate (bw/s)	-8.99	-9.57	-10.25 (5.24)

As a result of the initial evaluation, the subject was instructed to realign her right hip during support by contracting her abductors and external rotators without rotating her foot outward. She was verbally cued to keep her knee facing forward. In addition, she was instructed to extend her left leg further forward before heel striking in order to decrease the scuffing of her foot.

Figure 1 below demonstrates the changes seen following gait retraining.

Hip Frontal

Hip Transverse

Knee Frontal

% STANCE
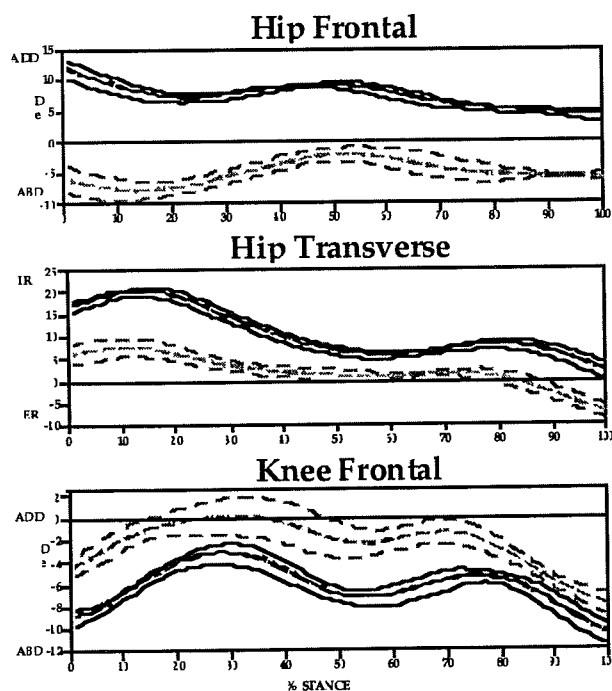
Figure 1. Pre (solid) and post (dashed) training data (+/- sd). Note the significant reduction in hip IR, ADD and knee ABD following training.
In addition, left peak braking force was reduced by 15% to 0.42 bw and loading rate was reduced to a third of its original value to -2.18 bw/s.

DISCUSSION
Results of this study clearly suggest that the patterns of running gait can be modified as noted by the reduction of hip internal rotation and adduction and knee abduction on the right and reduction in peak braking force and loading rates on the left.

This runner exhibited the miserable malalignment syndrome described by James (1978) composed of excessive hip internal rotation, genu valgus and foot pronation. It was hypothesized that the plantar fasciitis this runner was experiencing was related to the internally and medially deviated postures of the right lower extremity placing greater stress to the arch of the foot. The subject reported initial soreness in the external rotators and abductors of her right hip during the initial training that resolved with time. She also reported a reduction in the effort required to maintain the aligned posture of her right lower extremity with time. Finally, she noted that when she became fatigued and reverted to old habits, the plantar fascial pain began to recur.

With the improved alignment of the right hip, the subject felt it was easier to reach out with her left leg and reduce the frictional forces she initially demonstrated. Hennig et al. (1993) reported a strong correlation between peak GRFs and loading rates and peak tibial acceleration during running. Loading rates and peak accelerations have been suggested to play a role in stress related injuries.

SUMMARY
Results suggest it is possible to alter gait mechanics in runners and potentially reduce one's risk for injury. Further followup of this patient is needed to determine whether she has maintained this gait pattern and remained injury-free. Additionally, larger scale studies are needed to establish relationships between mechanics and injury.

REFERENCES
Hennig, EM et al, 1993. *J. App. Biom* 9:306-314.
James, S et al, 1978. *AJSM* 6(2)40-50.

FOOTSTRIKE PATTERNS DURING RUNNING OVER OBSTACLES OF DIFFERENT HEIGHTS

Shane D. Scholten, Nick Stergiou, Jeremy Houser and Daniel Blanke
Biomechanics Lab, University of Nebraska at Omaha, Omaha, Nebraska
Email: Nick_Stergiou@unomaha.edu Web: www.unocoe.unomaha.edu/hper/hper.htm

INTRODUCTION

Previous research has focused on mechanisms to safely overcome obstacles and how vision can influence the locomotor act (Patla et al, 1996). Less attention has been directed towards the landing of the leading leg after obstacle clearance while running. Research on running has evaluated the ground reaction forces (GRF) of foot strike patterns (Cavanagh & Lafortune, 1980), and suggested that 90% of the population use a heel-to-toe landing pattern. However, during sprinting many of these runners will change to a toe only (forefoot) strike. Research on landing after vertical jumps has identified a toe-to-heel type of landing which was attributed to increased GRF (Dufek & Bates, 1990). Much research has been produced on changes such as the walk-to-run or run-to-sprint. However, limited research exists on running over high enough obstacles to cause a change of the footstrike pattern. Thus, the purpose of this study was to examine the different footstrike patterns and strategies used during running over obstacles of various heights.

PROCEDURES

Ten heelstrike subjects ran at a self-selected pace under seven conditions: unperturbed running (no obstacle present) and over obstacles of six different heights (10%, 12.5%, 15%, 17.5%, 20%, and 22.5% of their standing height). The obstacle was placed directly before a Kistler force platform so that the subject had to clear the obstacle with the right leg and land on the platform. Ground markers ensured that stride length was kept the same for all conditions. GRF data from 10 trials per condition were sampled at 900Hz. Parameters analyzed were the heel impact peak from the vertical GRF (Fh), times for braking (TB) and propulsion (TS) periods, minimum braking (FY1) and maximum propulsion (FY2) peaks from the anterior posterior GRF, and an index of the anterior posterior position of the center of pressure (ICOP). One-way repeated measures ANOVAs were performed on the subject means for all parameters. A Tukey test was performed in comparisons that resulted in a significant F-ratio ($p < 0.05$).

RESULTS AND DISCUSSION

The group analysis results are presented in Table 1. ANOVAs identified significant differences for all parameters. TB had an inverse linear relationship with obstacle height and 12 out of 21 possible post-hoc comparisons were significant, while TP was less affected (1/21). However, opposite to TB, TP inceased which was expected since the speed was kept constant between conditions. FY2 revealed a direct linear relationship with obstacle height (20/21), while FY2 showed less changes (2/21). After clearing an obstacle, both braking and propulsion are more demanding which explains the above results. The ICOP had an inverse linear relationship with obstacle height (13/21), while the opposite was true for Fh (14/21). The Fz curves illustrated that the increase in obstacle height resulted in the appearance of an additional impact peak
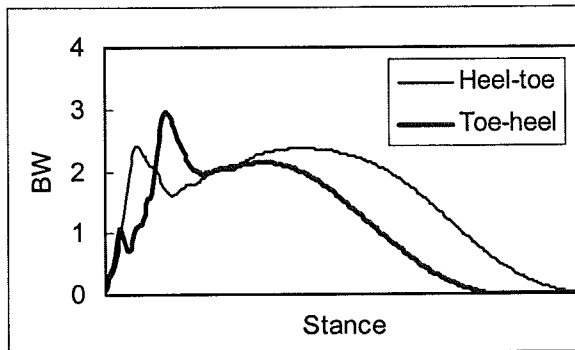
Figure 1: Representative Fz curves.

prior to Fh (Figure 1). This peak was caused by the change to a toe-to-heel landing. The group changed at a height of 15%. At that height the ICOP decreased below 0.07 m indicating a more closed path for the COP. The new pattern was similar to the footstrike patterns found in jumping activities. Thus, the subjects eventually changed from running over the obstacles to jumping. This new strategy might have helped them to absorb the increased impact forces. The toe-to-heel pattern might have increased the involvement of the ankle joint and the calf muscles in shock absorption. Even that Fh increased with obstacle height, these increases might have been larger and possibly injurious if the subjects were forced to run over the obstacles and land on their heels. Lastly, not all subjects changed at the same height. Differential strategies were revealed as an earlier or later change, underlining the importance of individual variability (Dufek & Bates, 1990).

SUMMARY

Running over high enough obstacles can cause a behavioral change of the footstrike pattern from heel-to-toe to toe-to-heel. The obstacle height for this change seems to be 15% of the runner's standing height. Individual differences however, do exist.

REFERENCES

Patla, A.E. et al. (1996). *J Motor Behavior*, **28**, 35-47.

Cavanagh, P.R., Lafortune, M.A. (1980). *J Biomechanics*, **13**, 397-406.

Dufek, J.S. Bates, B.T. (1990). *Medicine Science Sports Exercise*, **22**, 370-376.

ACKNOWLEDGMENTS

Table 1: Parameters evaluated with superscripts indicating post-hoc differences ($p<0.05$).

Variables	0%	10%	12.50%	15%	17.50%	20%	22.5%
FY1	$0.424^{17.5\%,20\%}$	0.516	0.509	0.507	0.533	0.534	0.522
(BW)	0.074	0.163	0.177	0.173	0.189	0.177	0.220
FY2	$0.278^{10\%\text{-}22.5\%}$	$0.330^{12.5\%\text{-}22.5\%}$	$0.339^{15\%\text{-}22.5\%}$	$0.355^{20\%,22.5\%}$	$0.355^{20\%,22.5\%}$	$0.369^{22.5\%}$	0.389
(BW)	0.027	0.045	0.059	0.053	0.069	0.060	0.064
TB	$0.139^{10\%\text{-}22.5\%}$	$0.122^{20\%\text{-}22.5\%}$	$0.121^{20\%\text{-}22.5\%}$	$0.113^{22.5\%}$	$0.114^{22.5\%}$	0.110	0.104
(sec)	0.023	0.023	0.023	0.025	0.025	0.023	0.021
TP	$0.132^{22.5\%}$	0.135	0.137	0.138	0.136	0.141	0.142
(sec)	0.020	0.018	0.019	0.022	0.020	0.023	0.022
Fh	$1.715^{10\%\text{-}22.5\%}$	$2.490^{17.5\%\text{-}22.5\%}$	$2.482^{17.5\%\text{-}22.5\%}$	$2.668^{20\%,22.5\%}$	2.914	3.037	3.098
(BW)	0.276	0.539	0.526	0.469	0.511	0.395	0.433
ICOP	$0.111^{10\%\text{-}22.5\%}$	$0.088^{15\%\text{-}22.5\%}$	$0.083^{17.5\%\text{-}22.5\%}$	0.066	0.062	0.060	0.054
(m)	0.016	0.034	0.033	0.032	0.030	0.030	0.024

THE SYMMETRY OF THE HUMAN LEG SPRING:

SPRING COEFFICIENTS BETWEEN RIGHT AND LEFT LEGS DURING RUNNING

Greg Bachman, Gary D. Heise, and Eadric Bressel

Biomechanics Laboratory, University of Northern Colorado, Greeley, CO 80639
Email: gsbachman@yahoo.com

INTRODUCTION

Various authors have investigated the dynamics of running gait by using a model of the leg as a simple linear spring based on the work of McMahon and colleagues (Farley et al., 1993; He et al., 1991; McMahon & Cheng, 1990). In the model, the leg and body are represented as a simple linear spring and as a point mass, respectively (Figure 1).
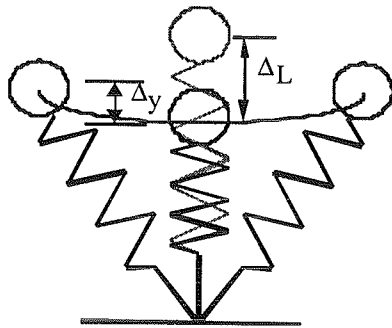
Figure 1: Leg spring model (adapted from McMahon & Cheng, 1990).

Using this model, researchers have shown that leg spring stiffness (k_{leg}), the ratio of maximum force during foot contact to deformation of the leg spring (ΔL), remains constant as humans run faster (He et al., 1991) and as various species of animals, representing a wide range of sizes, trot and hop faster (Farley et al., 1993). Consequently, constant leg spring stiffness has been proposed as an invariant feature of bouncing-type locomotion (McMahon & Cheng, 1990; Farley et al., 1993) and deemed significant for understanding gait dynamics.

An analysis of limb symmetry, using the leg spring model, would address the validity of presuming an overall symmetrical gait pattern for human locomotion (Sanderson & Martin, 1996). The relevance of the present investigation is that symmetry may be an important factor in the study of amputee gait and the subsequent design of prostheses. The issue of leg spring symmetry may have implications for active amputees (e.g., running). The purpose of the present investigation was to determine if leg spring stiffness was symmetrical for two self-selected speeds of running. Specifically, we hypothesized that both k_{leg} and k_{vert} would be similar for right and left legs.

PROCEDURES

Eight healthy women and thirteen healthy men volunteered as subjects (Body Mass$_W$ = 57.1 ± 8.1 kg; Leg Length$_W$ = 84.0 ± 7.0 cm; Body Mass$_M$ = 93.6 ± 15.0 kg; Leg Length$_M$ = 90.0 ± 6.5 cm). None of the subjects exhibited any obvious leg length asymmetry. Each subject attended one test session. After a 10-min warm-up, during which subjects practiced striking the force plate, instructions were given concerning the speed of running which consisted of telling each subject to run at a preferred "slow " or "fast" pace. A 25 m runway with a force plate flush mounted in the middle was used. Acceptable trials (minimum 2 for each leg and each speed = 8 total) were selected based on total foot contact with the force plate and no apparent aberrations in running gait. Forward running

speed was calculated from a video record of the sagittal plane movement. Standing leg length was measured from the greater trochanter of the femur to the floor. Time of contact, peak vertical ground reaction force (F_z), and peak vertical center of mass displacement (Δy) were obtained from force records. The stiffness of the leg spring, k_{leg}, was defined as the ratio of F_z to ΔL, and the effective vertical stiffness, k_{vert}, was defined as the ratio of F_z to Δy (see Fig. 1). Stiffness measures between right and left legs for the two running speed conditions were tested with repeated measures ANOVA with the probability of Type I error set apriori at .05.

RESULTS AND DISCUSSION

No significant differences were found for k_{leg} or k_{vert} between right and left legs within the two speed conditions (Table 1). Significantly higher values of k_{vert} were found between running conditions (Table 1). Mean values of k_{leg} were similar to those reported previously (He et al., 1991; Farley et al., 1993). Our findings also agree with those presented for running at one speed (Heise & Martin, 1998) and for preferred speed of running (Farley & Gonzalez, 1996). The increases in the mean values of k_{vert} with increased forward running speeds are in agreement with previous studies reporting k_{vert} for normal running (He et al., 1991; Farley et al., 1993; McMahon et al., 1987). These findings validate the assumption of gait symmetry for running in terms of the

leg spring model. This expectation may now be applied to active amputee populations and may impact future prosthetic limb design.

SUMMARY

Healthy individuals exhibit leg spring symmetry in terms of leg spring stiffness and effective vertical stiffness. As expected, k_{leg} stayed constant between speeds and k_{vert} increased at the fast speed of running. These results would proffer that leg stiffness is a symmetrical feature of the musculoskeletal system which may have a direct impact on the design of prostheses. This investigation proved that the invariance of k_{leg}, in healthy individuals with changing speed of running, holds regardless of which limb is examined.

REFERENCES

Farley, C. T. et al. (1993) *J. of Exp. Biol.* **185**, 71-86.
Farley, C. T., Gonzalez, O. (1996) *J. Biomechanics*, **29**, 181-186.
He, J. et al.(1991) *J. of App. Physiol.* **71**, 863-870.
Heise G.D., Martin, P.E. (1998) *Med. Sci. Sports Exerc.* **30**, 750-754.
McMahon, T.A., Cheng, G.C. (1990) *J. of Biomech.* **23**(Supp), 65-78.
McMahon, T.A. et al. (1987) *J. of App. Physiol.* **62**, 2326-2337.
Sanderson, D.J., Martin, P.E. (1996). *Arch. Phys. Med. Rehabil.* **77**,1279-1285.

Leg:	Right	Left	Right	Left
Speed:	(3.5 ± 0.4 m·s⁻¹)	(3.5 ± 0.3 m·s⁻¹)	(5.3 ± 0.6 m·s⁻¹)	(5.3 ± 0.6 m·s⁻¹)
k_{leg} (kN·m⁻¹):	12.4 ± 3.5	11.3 ± 3.1	11.1 ± 3.5	11.1 ± 3.7
k_{vert} (kN·m⁻¹):	44.6 ± 15.7	39.6 ± 15.0	69.1 ± 33.7*	63.5 ± 29.6*

Table 1: All numbers expressed mean $\pm$ SD. *Significantly greater than slow speed ($p < .0001$)

MOTOR CONTROL AND THE CEREBELLUM: ADAPTIVE CHANGES IN FASTIGIAL NEURONS TO SURGICALLY INDUCED EYE MOVEMENT DYSMETRIA

D. M. McGee[1] and C. A. Scudder[1,2]
[1]Department of Neurobiology [2]Department of Otolaryngology
University of Pittsburgh, School of Medicine

INTRODUCTION: How does the nervous system modify itself to support motor learning and control? Few answers to this question have been found, partly because the basic circuit underlying a particular behavior must be understood before it is possible to identify the changes in the circuit accompanying learning. Lesions of the cerebellum produce muscular uncoordination by creating timing and force abnormalities devastatingly affecting movement. The question then is: How does the cerebellum maintain such control over the motor system? In this research the oculomotor system, specifically that of saccadic eye movements, is used as a model to study motor control and neural plasticity. Saccadic adaptation is proposed to be accomplished via the direct aid of the cerebellum. The cerebellum is considered to gather and integrate information about the saccadic command and the current situation (e.g., eye position) and compute an appropriate correction signal to ensure that the resultant saccade is accurate. The enduring saccadic dysmetrias produced from cerebellar lesions demonstrate that the cerebellum plays an important and possible essential role in the adaptation of saccadic accuracy. The long-term goal of this research is to determine how the brainstem and cerebellum collectively act to generate accurate saccadic eye movements. This particular experiment was designed to study how cerebellar neurons, specifically those from the fastigial nucleus, behave before, during and after an adaptive modification of saccade size.

METHODS/PROCEDURES: Adolescent Rhesus macaques were used to examine the neural mechanisms that underlie the regulation of saccade gain (saccade size/target amplitude) by the cerebellum. The primates were trained to make accurate saccades to a moveable target. Eye movements were measured in both eyes by a standard electromagnetic search coil technique. A recording chamber was installed and electrodes were passed into the fastigial nucleus in order to obtain extracellular recordings from single neurons. Characteristics of saccadic gain adaptation in these monkeys were monitored along with fastigial nucleus neuron activity by recording before as adaptation proceeded.

During the experiments the monkeys were seated in a primate chair with their heads immobilized. A "paretic paradigm" was established through an extraocular tenectomy of the lateral and medial recti muscles, i.e., the surgical shortening of these muscles in one eye. In this paradigm vision was restricted to monocular viewing. Initially saccades measured in the paretic, operated eye fall short of the target, but over time increase in size to become orthometric when allowed to be the viewing eye. Subsequent monocular vision using the unoperated eye restores saccades to the unadapted state.

RESULTS/DISCUSSION: Recordings have shown 2 different firing rates, 2 different number of spikes, and 2 different latencies for ipsiversive as opposed to contraversive saccades. During contraversive saccades, fastigial neurons

firing initiates prior to saccadic movement (figure 1) which is thought to cause an indirect excitatory stimulation to agonistic motoneurons and to promote agonistic muscle contraction throughout the course of the saccade. Fastigial neuron activity during an ipsiversive saccade demonstrated a later discharge correlated with saccade termination, producing an excitatory stimulation to antagonistic motor units. This verifies condition specific firing patterns for these neurons. Thus, contraversive saccades are under early control, which facilitate the agonist muscles, while ipsiversive saccades are under late change control and mostly facilitate antagonists. The putative connection of cells would predict that changes in either ipsiversive or contraversive discharge parameters could bring about a change of gain in saccades.

Saccade size changed as a function of adaptation trial numbers (figure 2). To date, 25 fastigial saccadic related cells have been recorded during adaptation. Evaluation of recorded cells revealed an increase in fastigial latency for ipsiversive saccades amounting to 17 msec per 10-deg increase in saccade size. There was also a change in the number of spikes for contraversive saccades amounting to 5.5 spikes per 10-deg increase. The analysis of data has demonstrated fastigial neuron alteration from saccadic gain adaptation. These experiments do not show that the plastic neuronal changes were in the fastigial nucleus, but in conjunction with other experiments, we believe that the changes were within the cerebellum.

In summary, understanding the function of saccade related cells in the fastigial nuclei have given insight towards elucidating the overall role of the cerebellum in saccadic control and provide a model for somatic motor control in other areas.
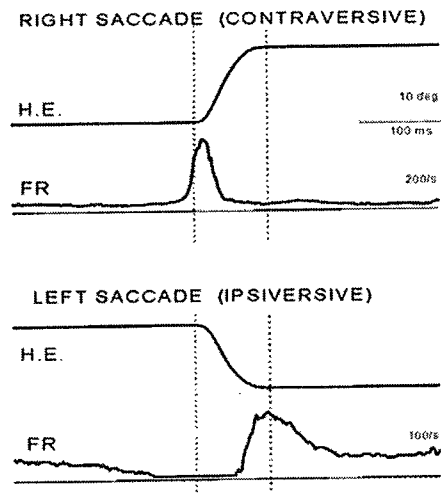
Figure 1: Single unit extracellular recording of a fastigial neuron during saccadic movement. H.E.=horizontal eye movements; FR=neurons firing rate; upward direction is right; down is left.
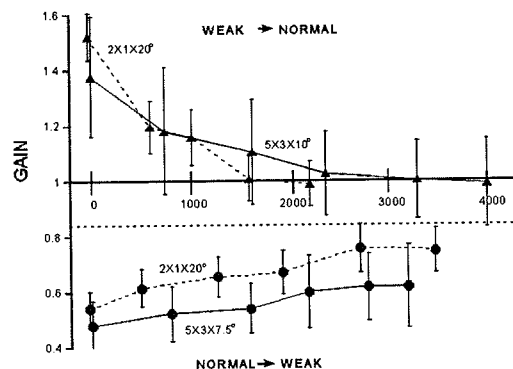
Figure 2: Saccade side decreases (top) or increases (bottom) as a function of adaptation trial numbers. The rate depends on the pattern of available target positions; 2x1x20° = 2-horizontal by 1-vertical, 20° separation; 5x3x10° = 5-horizontal by 3-vertical, 10° separation. Significant changes can be achieved within one session. WEAK-> NORMAL = viewing with the normal eye after long-term viewing with the weakened eye. NORMAL->WEAK = viewing with the surgically weakened eye after long-term viewing with the normal eye.

TEMPORAL DECOUPLING IMPROVES FORCE PRODUCTION DURING SINGLE- AND MULTIPLE-FINGER, BILATERAL KEY-PRESSING TASKS

Peter F. Vint, Susan M. Thompson, and Donovan A. Shaw
Department of Exercise and Sport Science, University of North Carolina at Greensboro, Greensboro, NC
E-mail: pfvint@uncg.edu   Web: http://www.uncg.edu/~pfvint

INTRODUCTION

In their studies of bimanual coordination, Swinnen et al. (1988) reported that subjects were more successful in "decoupling" limb movements when bilateral reaching tasks were initiated asynchronously. It was suggested that this temporal decoupling strategy lead to improvements in the required motor performances because each limb was able to function more independently. These results were recently extended to include maximum effort isometric knee extension tasks and two-legged vertical jumping performances (Vint & Hinrichs, 1997, 1998). Collectively, these data suggest that tasks initiated simultaneously appear to be constrained by a mechanism that inhibits the expression of maximum voluntary muscular force. Tasks initiated asynchronously, however, are apparently less susceptible to this inhibitory mechanism and result in greater muscular forces.

The primary purpose of this study was to validate the temporal decoupling mechanism during single- and multiple-finger bilateral key-pressing tasks. It was hypothesized that multiple-finger bilateral key-pressing tasks initiated asynchronously would elicit significantly greater forces than analogous tasks initiated simultaneously.

PROCEDURES

Twenty subjects (mean age 24.7 ± 4.7 yr., height 169.0 ± 10.7 cm; mass 71.5 ± 16.1 kg) volunteered to participate in the experiment. Isometric key-pressing forces were obtained from four independent piezoelectric sensors placed beneath the index (I) and middle (M) fingers of the right (R) and left (L) hands. Force data were sampled at 1000 Hz for 5 seconds.

Following a series of sub-maximal practice exertions, each subject was required to complete three maximum effort key-pressing trials in each of the following conditions:
1. unilateral single-finger efforts (RI, RM, LI, LM);
2. unilateral multiple-finger efforts (RIM; LIM);
3. simultaneous bilateral (SBI) and decoupled bilateral (DBI) single-finger efforts;
4. simultaneous bilateral (SBIM) and decoupled bilateral (DBIM) multiple-finger efforts.

During simultaneous bilateral tasks, subjects were specifically instructed to initiate all key-pressing actions at *exactly* the same time. During "decoupled" bilateral tasks, however, subjects were asked to initiate key-pressing force with fingers on the non-dominant hand only. Then, after a short, self-selected time, subjects added fingers on the dominant hand. Therefore, although decoupled bilateral exertions were initiated asynchronously, subjects eventually developed and maintained key-pressing forces from fingers on both hands throughout the remainder of the exertion.

Test order was counter-balanced across subjects and a minimum of 2 minutes was allowed between successive trials to minimize the effects of fatigue.

Calibrated force data were smoothed with a fourth-order, zero-lag Butterworth digital filter operating at a nominal cutoff frequency of 5 Hz. Maximum isometric key-pressing force was found by extracting the maximum value from the summed instantaneous key-pressing force array.

RESULTS AND DISCUSSION

Mean force data for single- and multiple-finger key-pressing tasks are summarized below (Figures 1 & 2). One-way repeated measures ANOVA and subsequent post-hoc analyses revealed that forces produced during unilateral single-finger key-pressing tasks were significantly greater than those produced during simultaneous bilateral key-pressing tasks. No significant differences were observed between forces produced during unilateral and decoupled bilateral single-finger key-pressing tasks ($p = 1.0$). Forces produced during unilateral multiple-finger key-pressing tasks were significantly higher than those produced during either simultaneous or decoupled bilateral key-pressing tasks. However, decoupled bilateral forces were significantly greater than simultaneous bilateral forces.
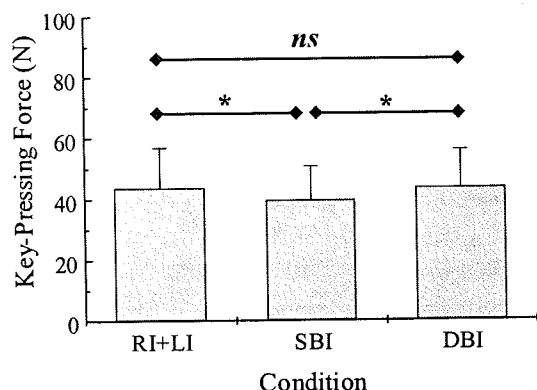
Figure 1. Single-finger key-pressing forces during unilateral (RI+LI), simultaneous bilateral (SBI) and decoupled bilateral (DBI) exertions. Asterisks above horizontal bars denote statistically significant comparisons ($p < .01$).
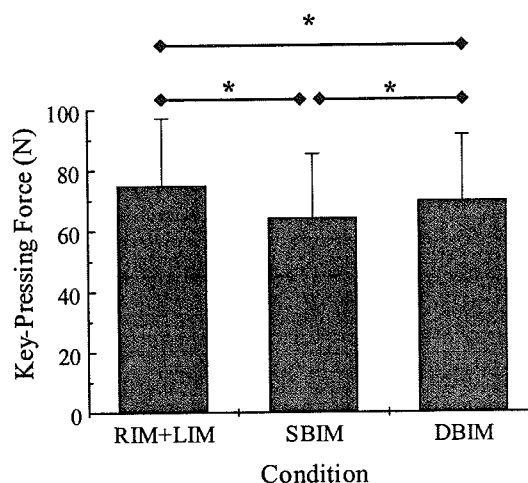
Figure 2. Multiple-finger key-pressing forces during unilateral (RIM+LIM), simultaneous bilateral (SBIM) and decoupled bilateral (DBIM) exertions. Asterisks above horizontal bars denote statistically significant comparisons ($p < .01$).

Compared to simultaneous bilateral exertions, temporal decoupling improved force production by 8.7% and 7.3% during single- and multiple-finger key-pressing tasks, respectively. The magnitudes of these improvements were not significantly different ($p = .395$). It is therefore concluded that temporal decoupling is an effective strategy in reducing the inhibitory influences that are associated with interlimb coupling.

REFERENCES

Swinnen, S., Walter, C.B., Shapiro, D.C. (1988). *Brain Cogn.,* **8**, 326-347.
Vint, P.F., Hinrichs, R.N. (1997). *ASB Proceedings*, 194-195.
Vint, P.F., Hinrichs, R.N. (1998). *NACOB Proceedings*, 475-476.

ACKNOWLEDGEMENTS

UNIQUE ECCENTRIC ACTIVATION PATTERNS ARE OBSERVABLE ACROSS UNI- AND MULTI-ARTICULAR COMPONENTS OF QUADRICEPS FEMORIS

Tammy M. Owings, Kristy Ebinger, Alex Hamilton, Mark D. Grabiner
Department of Biomedical Engineering, The Cleveland Clinic, Cleveland, Ohio
Email: grabiner@bme.ri.ccf.org

INTRODUCTION

There is increasing evidence that the central nervous system can use different activation strategies to control concentric and eccentric contractions (Enoka, 1996). Previously, we demonstrated that differences between the activation level of vastus lateralis during concentric and eccentric isokinetic contractions were evident from the onset of muscle activation and prior to the time after which differences in muscle lengthening or shortening may have contributed (Grabiner et al, 1995). Further, during this period, the significantly smaller activation level during eccentric contractions was not associated with a change in the rate of knee extension force generation. We concluded that the central command includes information about the type of muscle contraction to be performed and that the descending signals distinguish between eccentric and concentric contractions. However, we could not discount the possibility that activation of other quadriceps femoris components was concomitantly increased to accommodate the significantly lower activation of vastus lateralis.

This study extended the experimental method to include analysis of the vastus medialis and biarticular rectus femoris muscles. Despite the uni- vs. biarticular between-muscle differences and based on the common neural innervation, we hypothesized that the previously observed trends in activation level would be shown to be similar across quadriceps femoris components.

METHODS

Nine healthy subjects (6 males) participated in the study. Concentric and eccentric isokinetic knee extension contractions were performed on a Kin-Com isokinetic dynamometer at 60 deg·s^{-1}. Concentric and eccentric contractions were performed through a 30 deg range of motion and were initiated from a 30 deg knee flexion angle. A knee extension force threshold value of 30% of the subject's isometric MVC was required to initiate motion of the dynamometer. EMG was collected from the rectus femoris, the vastus lateralis, and the hamstrings using bipolar surface electrodes. The detected EMG signals and the force, position and velocity signals from the Kin-Com were digitized at 1 kHz.

EMG was rectified and integrated over a 100 ms window extending backwards from the instant at which the onset of dynamometer motion occurred. The rate of knee extension force generation was represented as the slope coefficient derived from a linear regression computed using the force data acquired during the same 100 ms window.

The slope coefficients derived from the concentric and eccentric contraction trials, and the hamstrings coactivation levels during the concentric and eccentric contraction trials were compared using a paired t-test. The activation levels of the vastus lateralis, vastus medialis and rectus femoris were analyzed using a 3 by 2 (muscle by contraction) repeated measures ANOVA.

RESULTS AND DISCUSSION

The difference between the activation level of the hamstrings muscles during the concentric (38.1±27.7 mv·s) and eccentric (34.7±20.2 mv·s) knee extensions was not significant (p=0.34). This suggests that the antagonist muscles were not an influential factor in the outcome of the study.

The differences between the rate of knee extension force generation during the concentric and eccentric knee extension contractions, 0.95±0.40 Nm·s and 0.86±0.42 Nm·s, respectively, approached, but did not achieve statistical significance (p=0.06). Therefore, this result is statistically similar to that of our previous study.

The ANOVA revealed that differences between the activation levels during concentric and eccentric contractions were significant (p<0.001, Figure 1). This finding indicates that independent of the specific quadriceps component, eccentric contractions were associated with significantly lower activation levels. The main effect of *muscle* and the muscle by contraction interaction were not significant (p=0.16 and 0.55, respectively). Collectively, these findings indicate that individual quadriceps components were similarly affected by the contraction conditions. The mean decreases in activation level from concentric contraction to eccentric contraction were −12.1, −12.9 and −14.5 percent, respectively.
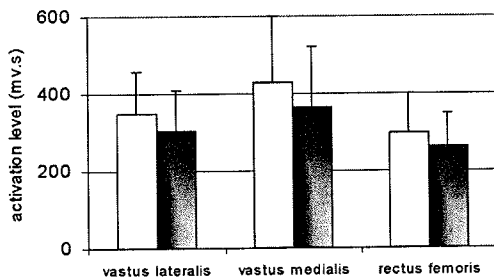
Figure 1: Activation levels of quadriceps femoris components during concentric (white bars) and eccentric (gray bars) contractions. The contractions were initiated from the same knee joint flexion angle. Activation was quantified during a 100 ms period prior to the onset of dynamometer motion.

Two results from the present study are considered important. First, the results confirm the findings of our previous study. The data suggest activation strategies associated with concentric and eccentric contractions are selected *a priori* by the CNS. Second, these differences are similarly distributed to the muscle group as opposed to simply one component. This is further support for the contention that the CNS activation strategies for eccentric and concentric contractions can be disparate.

REFERENCES

Enoka, R.M. (1996) *J Appl Physiol*, 81:2339-2346.
Grabiner, M.D. et al. (1995). *Proceedings of ISB*, 338-339.

MUSCULOSKELETAL BASIS FOR THE SCALING OF LEG STIFFNESS WITH BODY MASS IN HUMANS

Claire T. Farley and Wyatt L. Korff

Locomotion Laboratory, Dept. of Integrative Biology, University of California, Berkeley
Email: cfarley@socrates.berkeley.edu, Web: http://socrates.berkeley.edu/~hbbiomxl/

INTRODUCTION

Running, hopping and trotting animals can be modeled as spring-mass systems in which the mechanical behavior of the musculoskeletal system is represented as a leg spring. The stiffness of the leg spring is the primary determinant of the dynamics of running. Biomechanical studies have revealed that larger mammalian species have stiffer legs (Farley et al., 1993). Similarly, large adult humans have stiffer legs than small adult humans (Carruthers & Farley, 1998).

Our goal was to gain insight into the neuromuscular determinants of leg stiffness by examining why leg stiffness is greater in larger humans. We examined the roles of changes in joint stiffness and limb dimensions in determining the changes in leg stiffness with body mass.

METHODS

Eighteen male subjects (65-117kg) performed two-legged hopping at 2.2 Hz on a force platform while being videotaped (200 Hz) in sagittal view. All subjects had reciprocal pondural indices (height / $mass^{0.33}$) between 12.0 and 13.7 (Frederick, 1990).

We calculated leg stiffness from the ratio of peak ground reaction force to leg compression during ground contact (Fig. 1A). Leg compression was equal to the vertical displacement of the center of mass, calculated by double integration of the vertical acceleration with respect to time. We determined the average joint stiffness from the ratio of the change in net muscle moment (deter-mined from inverse dynamics analysis) to the joint angular displacement during ground contact (Fig. 2A). All stiffness values are for the two limbs combined.

We examined the sensitivity of leg stiffness to changes in each joint stiffness by using a computer model consisting of four segments (foot, shank, thigh, head-arms-trunk) interconnected by torsional springs (ankle, knee, hip) (Working Model 4.0).

RESULTS

The average slope of the leg's force vs. displacement relationship, and thus leg stiffness, was greater in larger subjects during hopping in place. Leg stiffness was directly proportional to body mass ($k_{leg} \propto M^{1.00 \pm 0.23}$, M = body mass; p < 0.001; Fig. 1).
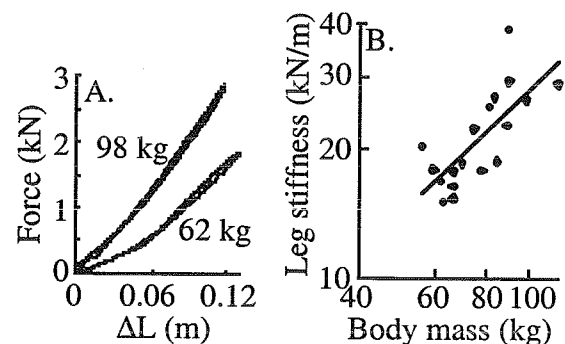
Figure 1. A. Ground reaction force versus leg compression (ΔL) during ground contact for a 98 kg subject and a 62 kg subject. **B.** Average leg stiffness versus body mass, plotted on log-log axes.

Leg stiffness primarily depended on ankle stiffness. We altered each joint stiffness in our torsional spring model while keeping all

other factors constant and measured the effect on leg stiffness. Doubling ankle stiffness caused leg stiffness to double. Doubling knee or hip stiffness caused leg stiffness to increase by less than 2 percent.

Ankle stiffness increased dramatically with body mass in our subjects ($k_{ank} \propto M^{1.22 \pm 0.31}$, $p = 0.001$; Fig. 2). According to the results of the computer simulation, leg stiffness is proportional to ankle stiffness. Therefore, based on the scaling of ankle stiffness, leg stiffness should be proportional to $M^{1.22}$.
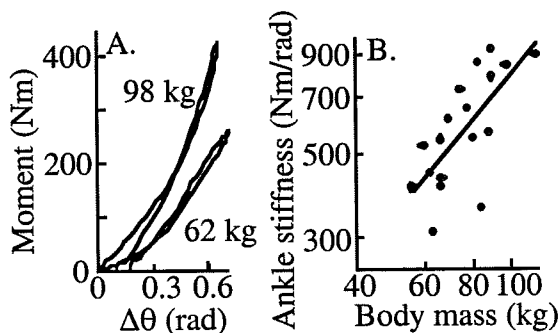
Figure 2. A. Moment versus angular displacement ($\Delta\theta$) of the ankle during the contact phase for a 98 kg subject and a 62 kg subject. **B.** Average ankle stiffness versus body mass plotted on log-log axes.

The longer limb segments in larger subjects caused leg stiffness to decrease. We built torsional spring models based on anthropomorphic measurements from subjects ranging from the smallest to the largest subjects. When all models had the same joint stiffnesses, the largest model had the lowest leg stiffness ($k_{leg} \propto M^{-0.30}$). This decrease in leg stiffness probably was caused by the ground reaction force having a greater moment arm about the joints in larger subjects.

DISCUSSION
The observed scaling, $k_{leg} \propto M^{1.00}$, results from two offsetting factors. First, ankle stiffness increases dramatically in larger

humans ($k_{ank} \propto M^{1.22}$). Second, the longer limb segments of larger humans cause a reduction in leg stiffness ($M^{-0.30}$).

We examined whether the size-dependent change in ankle stiffness could be due to a size-dependent change in Achilles tendon stiffness. Achilles tendon stiffness can be estimated as EA/L, where E is elastic modulus, A is tendon cross-sectional area, and L is tendon length. Elastic modulus is similar for a variety of mammals (Alexander, 1988). Thus, based on geometric scaling of tendon dimensions (Pollock & Shadwick, 1994), Achilles tendon stiffness (k_{Ach}) is predicted to scale as $M^{0.33}$.

If Achilles tendon stiffness determines ankle stiffness, ankle stiffness should scale as $k_{Ach} \cdot r_{ank}^2$, where r_{ank} is the moment arm of the Achilles tendon about the ankle. If r_{ank} scales geometrically as do other segment lengths ($L \propto M^{0.33}$), the ankle stiffness resulting from the Achilles tendon alone should be proportional to $M^{1.00}$. This prediction suggests that size-dependent changes in tendon stiffness contribute to the increased ankle stiffness, and thus leg stiffness, in larger humans.

REFERENCES
Alexander, R. McN. *Elastic Mechanisms in Animal Movement.* Cambridge University Press, 1988.
Carruthers, A.C. and C.T. Farley. *Proceedings of NACOB.* 307-308, 1998.
Farley, C.T., J. Glasheen, T. A. McMahon. *J. Exp. Biol.* **185**, 71-86, 1993.
Frederick, E.C. In Cavanagh, P.R. *Biomechanics of Running.* Human Kinetics, 307-320, 1990.
C.M. Pollock and R.E. Shadwick. *Am. J. Physiol.* **266**, R1022-R1031, 1994.

ACKNOWLEDGEMENTS

MAXIMAL AND SUBMAXIMAL EXPRESSIONS OF THE BILATERAL DEFICIT PHENOMENON

Peter F. Vint and Scott P. McLean
Department of Exercise and Sport Science, University of North Carolina at Greensboro, Greensboro, NC
E-mail: pfvint@uncg.edu   Web: http://www.uncg.edu/~pfvint

INTRODUCTION

Muscular forces produced during maximum voluntary contractions are typically 3-20% smaller during simultaneous bilateral exertions than during independent unilateral exertions. This result describes the traditional manifestation of the bilateral deficit phenomenon. However, there is evidence to suggest that bilateral deficits may also exist for motor tasks performed at submaximal intensities (Oda & Moritani, 1996; Seki & Ohtsuki, 1990). The purpose of this experiment was to test the hypothesis that a significant bilateral deficit in isometric elbow flexion force would be found at both maximal and submaximal intensities. It was expected that any reductions in simultaneous bilateral force would be paralleled by reductions in agonist EMG activity and would not be associated with increases in antagonist EMG activity.

PROCEDURES

Twenty right-handed college students volunteered to participate in the experiment (mean age 23.2 ± 3.9 yr., height 168.6 ± 9.5 cm, and mass 71.9 ± 13.0 kg). Isometric elbow flexion force data were obtained from each arm separately using two independent strain gauges. Bipolar surface electrodes were used to measure EMG activity of the biceps and triceps on each arm. Force and EMG data were sampled for 3 s at 1000 Hz. Subjects completed a series of maximum effort elbow flexion tasks, which were followed by a series of submaximal exertions at 25%, 50%, and 75% of their perceived maximum effort. Subjects

received no feedback regarding the actual levels of force that were produced. All exertions were performed unilaterally with the right (RUL) and left arms (LUL) separately, and bilaterally with both arms together (BL). Three trials were completed for each condition and for each intensity level. Maximum and submaximum elbow flexion forces were defined by the average force in a 250 ms window that resulted in the greatest integrated force and minimum RMS error values, respectively. Average integrated EMG (AIEMG) values were quantified over the 250 ms windows that were defined by the force-time criteria. For each subject and for each arm, relative forces were expressed as percentages of either the UL maximum or mode (UL or BL) maximum. Bilateral deficits in relative force were calculated using the bilateral deficit index (Howard & Enoka, 1991).

$$[(RBL+LBL)/(RUL+LUL)*100-100]$$

RESULTS AND DISCUSSION

Bilateral deficits in force were observed at both maximal and submaximal intensities (Fig. 1). A $2\times2\times4$ repeated measures ANOVA of the isometric force data revealed significant main effects ($p < .05$) between arms ($L < R$), modes ($BL < UL$), and levels ($25\% < 50\% < 75\% < 100\%$). Doubly-multivariate repeated measures analyses of variance of both triceps and biceps AIEMG data revealed significant differences between levels. However, despite trends to the contrary (Fig. 2), AIEMG were not different between modes (biceps, $p = .12$; triceps, $p = .06$).
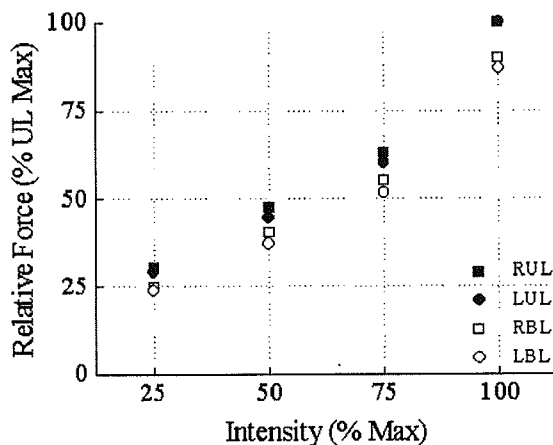
Figure 1. Maximum and submaximum isometric elbow flexion force expressed as a percent of the unilateral maximum (n = 20).
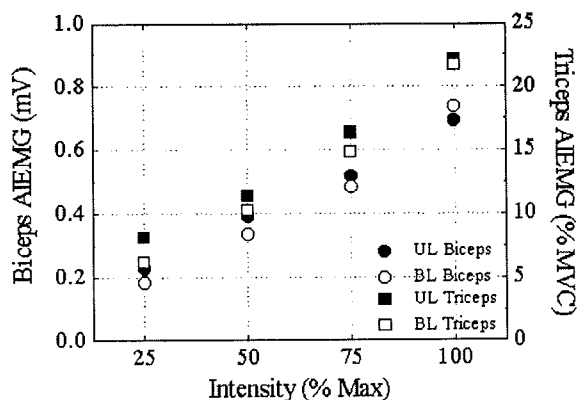
Figure 2. Average integrated EMG (AIEMG) from biceps and triceps brachii during maximum and submaximum isometric elbow flexion tasks (n = 20).

Bilateral forces were significantly less than unilateral forces across maximal and submaximal intensities. When all forces were expressed as percentages of UL maximum forces, bilateral deficits ranged from -18.3% at 25% max to -11.4% at 100% max. When forces were expressed as percentages of either the UL or BL mode maximum, bilateral deficits ranged from -8.1% at 25% to 0% at 100% max. The difference between these relative expressions of UL and BL force was nearly constant (-11%) across intensity levels (Fig. 3) which indicated that a significant component of the bilateral deficit was

independent of consciousness. The remaining component of the bilateral deficit, indicated by the deficit band on the % mode maximum data, was attributable to perceptual differences between UL and BL tasks. The magnitude of this "perceptual" component was inversely related to the level of intensity and therefore contributed more significantly to the bilateral deficit at lower submaximal intensities.
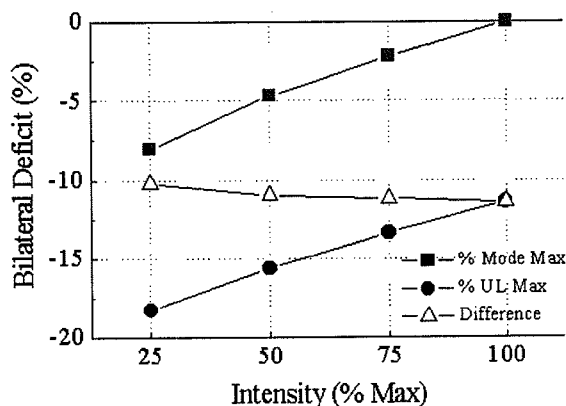
Figure 3. Solid circles: traditional bilateral deficit. Solid squares: "perceptual" component of bilateral deficit. Open triangles: component of deficit that is independent of consciousness (n = 20).

In conclusion, the bilateral deficit appears to be manifest at both maximal and submaximal intensities. At decreasing submaximal intensities, perceptual differences between unilateral and bilateral exertions appear to contribute significantly to the magnitude of the bilateral deficit phenomenon.

REFERENCES

Howard, J.D., Enoka, R.M. (1991). *J. Appl. Physiol.*, **70**, 306-316.

Oda, S., Moritani, T. (1996). *Eur. J. Appl. Physiol.*, **74**, 8-12.

Seki, T., Ohtsuki, T. (1990). *Ergonomics*, **33**, 1131-1142.

MOTOR UNIT ACTIVATION VARIABILITY AND RELIABILITY DURING MAXIMAL VOLUNTARY QUADRICEPS CONTRACTIONS

Danny M. Pincivero[1], Richard C. Green[2], and Jason D. Mark[2]

[1]Department of Physical Therapy, Eastern Washington University, Cheney, WA
[2]Department of Exercise Science, Gonzaga University, Spokane, WA
E-mail: dpincivero@mail.ewu.edu

INTRODUCTION

The ability of an individual to generate maximal quadriceps torque is dependent mainly upon motor unit activation characteristics. This assessment can often be considered invalid should its reproducibility be in question. Furthermore, the median frequency (MF) of sampled EMG signals during maximal voluntary efforts is inherently variable both within and between multiple trials. The purpose of the present investigation was to assess MF variability and reliability of the quadriceps during multiple trials of maximal voluntary efforts. A second purpose of this study was to examine MF differences between the 3 superficial portions of the quadriceps femoris muscles.

PROCEDURES

Subjects for this study consisted of 30 healthy male and female volunteers (mean age=23.1 ± 2.2 yr, mean hgt=170.8 ± 9.8 cm, mean wgt=68.8 ± 13.2 kg). Motor unit activation variability and reliability, as well as muscle differences in MF, were assessed in all subjects during 3 maximal isometric voluntary contractions. Isometric torque was measured on the Biodex System II Isokinetic Dynamometer while subjects were in a comfortable, upright seated position. The subjects were secured using thigh, pelvic and torso straps in order to minimize extraneous body movements. Gravity correction was obtained by measuring the torque exerted on the dynamometer resistance adapter with the knee in a relaxed state at full knee extension. During the contractions, each subject folded their arms and was given verbal encouragement and visual feedback from a computer monitor in an attempt to achieve a maximal torque level. Once the knee of each subject was fixed at a 60 deg flexion angle, 2-3 sub-maximal followed by 2-3 maximal contractions for familiarization purposes were performed. Subjects were then asked to contract their quadriceps as hard as they could and to sustain the contraction for 5 sec. This contraction was repeated 2 more times with a minimal rest of 2 min in between each contraction.

Motor unit activation was assessed via the frequency spectrum for the vastus medialis (VM), vastus lateralis (VL), and rectus femoris (RF) muscles. Pre-amplified bi-polar circular surface electrodes (Ag/AgCl) was placed on pre-determined areas of each muscle with a fixed inter-electrode distance (center to center) of 2 cm. The reference electrode was placed over the medial shaft of the tibia. EMG activity was collected at 1000 Hertz (CMRR = 87 dB at 60 Hertz, input impedance of >25 Mohms at dc) with a gain of 10K. The signals collected within the first and last second of each 5 sec MVC was not used for analysis. A power spectral analysis was then performed on the resultant 3 sec window for each muscle. A fast Fourier transformation of 512 points (Hanning window processing) was

performed on 11 consecutive, 512 msec segments, overlapping each other by half their length (256 msec), for each 3 second contraction. The MF was determined from each of the 11 overlapping windows. The mean and standard deviation (SD) of the 11 windows during each contraction was then calculated, for each muscle. These 2 values were then used for statistical analyses.

To determine reliability of the MF (mean and SD), intraclass correlation (ICC-2,1) coefficients were calculated for each muscle across the 3 trials. The standard errors of measurement (SEMs) and 95% confidence intervals (CI) were then calculated and subsequently expressed in units of each variable to estimate the expected trial-by-trial variability range for MF. To assess any muscle or trail differences or interactions, a 2 factor ANOVA with repeated measures was performed on the calculated mean values from the 11 overlapping windows. In order to evaluate differences in MF variability, a 2 factor ANOVA was also performed on the calculated SD from the 11 overlapping windows. Analysis of the SD in this manner was based mainly upon the assumption that these data display ratio characteristics. Therefore, trial-to-trial variability differences that may be inherent to this method of using overlapping windows to average MF could be determined. All tests of significance were performed at an alpha of $p<0.05$.

RESULTS AND DISCUSSION

The mean absolute torque level ($\pm$SD) for each of the 3 MVCs were as follows: MVC_1 – 214.3$\pm$63.3 N•m, MVC_2 – 218.9$\pm$62.6 N•m, and MVC_3 – 218.8$\pm$ 63.4 N•m. The calculated ICC between the 3 MVC's was 0.98, and the SEM was 8.9 N•m (4.1% of the mean). The 95% CI for the SEM value was found to be 3.4%-4.8%. The results

from this study demonstrated a significant muscle main effect for the mean MF across the 3 MVCs ($F_{2,58}$=66.5, $p<0.05$). Specifically, pair-wise contrasts showed that MF was highest for the VL (157.9$\pm$23.9 Hz), followed by the RF (120.2$\pm$19.9 Hz) and VM (105.7$\pm$21.4 Hz) muscles. The results also demonstrated that the variability associated with calculating an average MF from a series of overlapping windows was different among the 3 muscles (muscle main effect: $F_{2,58}$=8.0, $p=0.001$). Pair-wise contrasts revealed that variability was highest for the VL (10.4$\pm$3.4 Hz) followed by both the VM (8.0$\pm$4.2 Hz) and RF (7.8$\pm$3.6 Hz). Variability for the latter 2 muscles was not significantly different. Reliability for the calculated MF mean for the 11 windows was found to be high (ICC= 0.85-0.96) with relatively low SEMs (4.2-8.3 Hz) and 95% CIs. Conversely, reliability of the SD of the 11 overlapping windows was found to be low (ICC=0.13 –0.45) with relatively high SEMs (2.7-3.3 Hz) and CIs. The findings from this study demonstrates that inter-trial MF reliability for the superficial quadriceps muscles is high, while within-trial variability measures display low inter-trial reliability estimates. These findings also show higher MF for the VL than the other 2 muscles, and higher MF for the RF than the VM muscle.

SUMMARY

The surface EMG signal sampled from the quadriceps muscles during maximal effort contractions can be considered "quasi-random" in nature. High and low reliability estimates for between trial MF mean and variability, respectively, supports this contention. Furthermore, relatively higher MF observed for the VL suggests that future inquiry focus on a possible adaptation response of this muscle as a result of habitual reliance during daily activities.

LOWER-EXTREMITY KINETICS
WHILE WALKING WITH A WEIGHTED VEST

George Salem[1], Man-Ying Wang[1], Jean Young[2], and Gail Greendale[2]

[1]Musculoskeletal Biomechanics Research Laboratory, University of Southern California,
Department of Biokinesiology & Physical Therapy, Los Angeles, CA
[2]UCLA School of Medicine, Division of Geriatrics, Los Angeles, CA
Email: gsalem@hsc.usc.edu   Web: www.usc.edu/go/mbrl

INTRODUCTION

Aging-related lower extremity weakness is associated with a greater risk of falls and fractures, lower functional ability, and loss of independence. Researchers have reported that resistance training produces substantial muscular strengthening in older adults; however, most of these programs require specialized equipment, close supervision, and participant travel. In an effort to minimize the intrusiveness of these programs and increase the accessibility of physical activity to older persons, we developed an intervention using a weighted vest. We hypothesized that wearing a weighted vest during routine activities (eg. walking) would increase the musculoskeletal loading associated with those activities. Increases in musculoskeletal loading could potentially alter bone metabolism, limit aging-related bone loss, and preserve functional strength. This paper reports the acute alterations in lower-extremity joint moments associated with walking with a weighted vest.

PROCEDURES

- Data were collected from 51 participants (74 ± 7 years of age) enrolled in a six-month physical activity study.
- Participants were randomly enrolled into three groups based upon applied vest weight: controls (N=16) wore a vest with no added weight, a second group (N=13) wore a vest with 3% of their body weight (BW), and a third group (N=22) wore a vest with 5% BW.
- Reflective markers were applied to bony landmarks and participants performed 6 walking trials at their "normal" pace. Baseline trials 1-3 were performed without a vest; experimental trials 4-6 were performed with a vest.
- Three-dimensional coordinates of the foot, leg, thigh, and pelvis were recorded from a six-camera (60 frames/sec) motion analysis system (Vicon 370, Oxford Metrics, Oxford, UK).
- Ground-reaction forces were collected from two force platforms (AMTI, Watertown, MA) at 600Hz.
- Data processing software (Vicon Clinical Manager, Oxford Metrics, Oxford, UK) was used to calculate the *net* ankle, knee, and hip moments during the stance phase of gait (Kabada et al. 1989). A support moment was calculated as the sum of the three joint moments (Winter, 1989).
- A repeated-measures analysis of variance model (SPSS Professional Statistics 7.5, Chicago, IL) was used to test for significant differences between the peak joint moments produced during the baseline and experimental trials. Comparisons were performed for the right leg only.

RESULTS

- Significant differences in peak joint moments between baseline (non-vest-wearing) and experimental (vest-wearing) trials were found at the ankle in the 3%

vest-group only and at the knee in the 3% and 5% vest groups (table 1).

- Peak ankle moments increased by 13% in the 3% vest group (p=0.03) but only 5% in the 5% vest group (p=0.44) during vest-wearing trials.
- Peak knee moments increased by 19% in the 3% vest group and 18% in the 5% vest group during vest-wearing trials. (figures 1 and 2).
- Significant differences in peak joint moments between baseline and experimental trials were not found in the control group.
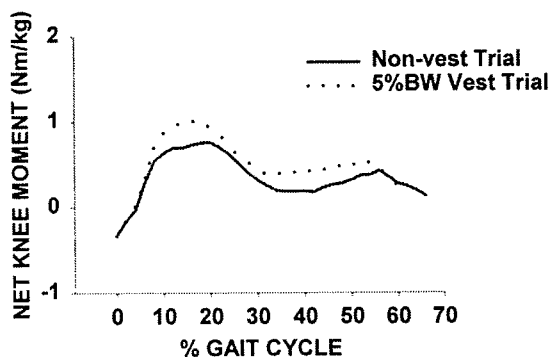
Figure 1: Representative *net* knee-moment/gait cycle curves for a single subject.

DISCUSSION & SUMMARY

These results suggest that acute applications of a weighted vest between 3% BW and 5% BW significantly increase the peak knee moments associated with normal walking in older adults. Alterations in peak ankle moments appear to be more variable. Still to be determined is whether these alterations persist over time and if they are of sufficient magnitude to effect musculoskeletal adaptation. Future analyses should examine the efficacy of vest use for the prevention of muscle weakening and bone loss in elders, and contrast this intervention with other exercise programs using biomechanical and clinical investigations.
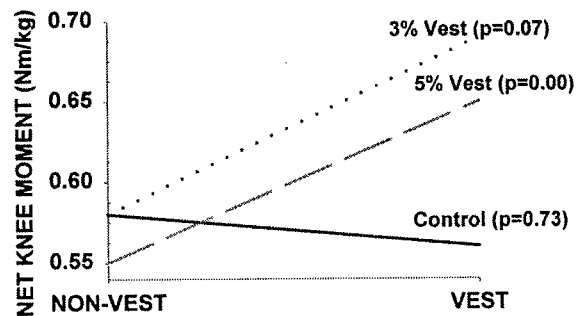
Figure 2: Change in peak knee moments with vest use.

REFERENCES

1. Kadaba MP, Ramakrishnan HK, Wootten ME, Gainey J, Gorton G, and Cochran GV. Repeatability of kinematic, kinetic, and electromyographic data in normal adult gait. J Orth. Res. 7: 849-860, 1989.
2. Winter, DA. Biomechanics of normal and pathological gait: implications for understanding human locomotor control J. Motor Behave. 4: 337-355, 1989

ACKNOWLEDGEMENTS

Table 1: Peak ankle, knee, hip, and support net-moments during the stance phase of gait.

Group	Control		3%		5%	
Trials	no vest	vest	no vest	vest	no vest	vest
Ankle	1.35 ± 0.42	1.19 ± 0.50	1.48 ± 0.47	1.67 ± 0.30	1.72 ± 0.82	1.81 ± 0.80
Hip	0.73 ± 0.22	0.71 ± 0.27	0.90 ± 0.33	0.95 ± 0.36	1.07 ± 0.38	1.04 ± 0.43
Support	1.59 ± 0.57	1.45 ± 0.64	1.79 ± 0.67	1.88 ± 0.61	2.35 ± 1.27	2.23 ± 1.15

BODY MASS DISTRIBUTION INFLUENCES
THE OUTCOME OF A TRIP IN OLDER ADULTS

Michael J. Pavol [1,2], Tammy M. Owings [2], Mark D. Grabiner [2]

[1] Biomedical Engineering Center, The Ohio State University, Columbus, Ohio
[2] Department of Biomedical Engineering, The Cleveland Clinic Foundation, Cleveland, Ohio
Email: grabiner@bme.ri.ccf.org

INTRODUCTION

Falls are a major source of injury in older adults and trips are a leading cause of these falls (Tinetti et al., 1988). Strategies used in recovering from a trip have been identified (Eng et al., 1994). However, hypothesized mechanisms whereby a trip results in a fall have not been confirmed directly. The present study therefore sought to identify the mechanisms whereby selected older adults fell following an induced trip.

METHODS

Seventy-nine healthy, community-dwelling, older adults were placed in a safety harness and tripped during normal gait using a concealed mechanical obstacle (Pavol et al., 1999). Trip outcomes were graded as falls or recoveries. A load cell in the safety harness was used to exclude subjects who were assisted by the harness in their recovery. The present analysis is limited to subjects whose

Figure 1: Descriptive variables for the trip responses. All values shown are positive.

response to the trip was a lowering strategy: the tripped limb is immediately lowered to become the support limb and the initial recovery step across the obstacle is executed by the contralateral limb. This strategy was used in 26 recoveries (17 women) and 8 falls (8 women). This analysis includes only the three fallers who did not place half their body weight (bw) on the safety harness until at least 0.45 sec after step foot ground contact.

Motions of the bilateral upper and lower limbs, torso, and head were recorded using a six-camera motion capture system (Motion Analysis). Ground reactions were recorded from two force plates (AMTI), located before and after the obstacle, respectively. The kinematic and kinetic variables in Figure and Table 1 were computed from this data.

The ankles were represented by the lateral malleoli. The hip midpoint location was computed from the greater trochanters and sacrum. Trunk flexion from vertical was computed from the sacrum and shoulders. The head-arms-torso (HAT) center of mass location was calculated from anthropometric and kinematic data using a custom algorithm. All times of interest were determined from force plate data. Body weight was subtracted from the vertical ground reaction force (Fz) before computing the impulse. All distances were normalized to body height (bh).

The recovery and fall groups were compared with the Mann-Whitney test using p<0.06.

RESULTS AND DISCUSSION

It can be argued that the outcome of a trip is determined, to a large extent, by the time of step foot ground contact. Recovery requires an appropriate positioning of the step foot and a return to dynamic stability thereafter.

Table 1: Descriptives (mean ± SD) for the trip responses of the outcome groups

Variable		Recovery	Fall
At trip:			
dx(hip)/dt	(%bh/s)	66±12	66±22
θ(hip-HAT)	(deg)	0±4	8±2 ‡
θ(trunk)	(deg)	7±4	4±4
Time (msec) from trip to:			
support foot loading		160±39	144±35
step foot toe-off		257±27	244±10
step foot grnd contact		523±44	505±54
At support foot loading:			
θ(ankle-hip)	(deg)	10±4	9±3
θ(hip-HAT)	(deg)	4±5	12±3 †
Trip to support foot toe-off:			
Fz impulse	(%bw·s)	-6±4	-9±4
net θ(Fxz)	(deg)	11±2	12±2
Trip to step foot ground contact:			
dz(hip)/dt max.	(%bh/s)	21±9	6±7 *
Step foot toe-off to ground contact:			
l(ankle-hip) min.	(%bh)	33±4	29±1 *
z(ankle) max.	(%bh)	25±4	26±3
dx(ankle)/dt avg.	(%bh/s)	115±15	117±16
dl(ankle-hip)/dt:			
min.	(%bh/s)	-144±29	-140±23
max.	(%bh/s)	171±29	177±8
step length	(%bh)	49±6	49±8
At step foot ground contact:			
θ(ankle-hip)	(deg)	-10±4	-8±6
z(hip)	(%bh)	54±2	51±3 *
θ(hip-HAT)	(deg)	25±12	40±3 *
dθ(hip-HAT)/dt	(deg/s)	-43±53	36±40 *
x(ankle-HAT)	(%bh)	-2±5	4±5 *

* p<.06, † p<.01, ‡ p<.001 vs. Recovery

However, as seen in Table 1, recovery is also significantly influenced by the ability to elevate the hips and slow the forward rotation of the HAT prior to ground contact.

The recovery step did not differ notably between falls and recoveries. Nevertheless, the hips of the fallers were lower at ground contact, while the HAT center of mass was more forward of the hips and foot and rotating forwards instead of backwards. This would reflect a decreased ability to control the hips and HAT through the support limb. Yet, the support ground reactions did not differ significantly in the fallers, indicating normal support limb function.

The fallers were, however, characterized by a more anterior HAT center of mass. In fact, at the time of trip, the fallers had the three greatest θ(hip-HAT) observed. This difference was not due to greater trunk flexion, thus reflects a differing HAT mass distribution. This difference translated into a more forward-rotated HAT center of mass at support limb loading, which appears to have sufficed to reverse the direction of moments produced by the support ground reaction forces, resulting in increased HAT forward rotation. The falls of the present analysis thus appear to have resulted, at least in part, due to a difference in body mass distribution.

REFERENCES

Eng, J.J. et al. (1994). *Exp Brain Res*, **102**, 339-349.
Pavol et al. (1999). *J Gerontol Med Sci*, **54A**, M103-M108.
Tinetti et al. (1988). *N Engl J Med*, **319**, 1701-1707.

ACKNOWLEDGMENTS

A MECHANISM OF FALLING FROM A TRIP IN OLDER ADULTS RELATED TO WALKING SPEED AND THE SUPPORT LIMB

Michael J. Pavol [1,2], Tammy M. Owings [2], Mark D. Grabiner [2]

[1] Biomedical Engineering Center, The Ohio State University, Columbus, Ohio
[2] Department of Biomedical Engineering, The Cleveland Clinic Foundation, Cleveland, Ohio
Email: grabiner@bme.ri.ccf.org

INTRODUCTION

Falls are a major source of injury in older adults and trips are a leading cause of these falls (Tinetti et al.,1988). Strategies used in recovering from a trip have been identified (Eng et al., 1994). However, the actual mechanisms whereby a trip results in a fall have not been determined. Such knowledge is needed in reducing the incidence of trip-related falls. The present study thus aimed to identify the mechanisms whereby selected older adults fell following an induced trip.

METHODS

Seventy-nine healthy, community-dwelling, older adults were placed in a safety harness and tripped during normal gait using a concealed mechanical obstacle (Pavol et al., 1999). Trip outcomes were visually graded as recoveries or falls. A load cell in the safety harness was also used to identify and exclude subjects who were assisted by the harness in their recovery. The present analysis is limited to subjects who responded to the trip with a lowering strategy: the tripped limb is immediately lowered to become the support limb and the contralateral limb executes the initial recovery step across the obstacle. This strategy was employed in 26 recoveries (17 women). Of the eight fallers (8 women) who used this strategy, this analysis includes only the subgroup of five who placed over half their body weight (bw) on the safety harness before or near step foot ground contact.

The motion of the bilateral upper and lower limbs, torso, and head during the tripping response was recorded using a six-camera motion capture system (Motion Analysis). Ground reactions were recorded from two force plates (AMTI), located before and after the obstacle, respectively. From this data, the kinematic and kinetic variables in Figure 1 and Table 1 were computed.

The ankles were represented by the lateral malleoli. The hip midpoint location was computed from the greater trochanters and sacrum. The head-arms-torso (HAT) center of mass location was calculated from kinematic and anthropometric data using a custom algorithm. All times of interest were determined from force plate data, with support foot loading identified as the start of a large medial-lateral shift in center of pressure. Body weight was subtracted from the vertical ground reaction force (F_z) before computing the impulse. All distances were normalized to body height (bh).
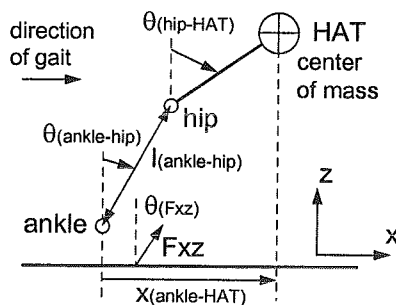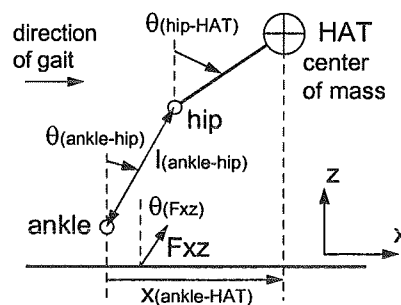

Figure 1: Descriptive variables for the trip responses. All values shown are positive.

The recovery and fall groups were compared with the Mann-Whitney test using $p < 0.05$.

RESULTS AND DISCUSSION

In the lowering strategy, the support limb has the tasks of elevating the hips to enable an effective recovery step and controlling the forward rotation of the HAT until step foot

Table 1: Descriptives (mean ± SD) for the trip responses of the outcome groups

Variable		Recovery	Fall
dx(hip)/dt at trip (%bh/s)		66±12	83±10 [†]
at +100msec (%bh/s)		73±11	94±5 [‡]
Time (msec) from trip to:			
support foot loading		160±39	267±49 [‡]
step foot toe-off		257±27	280±28
step foot grnd contact		523±44	493±25
At support foot loading:			
θ(ankle-hip)	(deg)	10±4	24±9 [‡]
θ(hip-HAT)	(deg)	4±5	17±8 [‡]
x(ankle-HAT)	(%bh)	9±4	23±10 [‡]
Trip to support foot toe-off:			
Fz impulse	(%bw·s)	-6±4	-14±6 [†]
net θ(Fxz)	(deg)	11±2	14±2 [*]
Trip to step foot ground contact:			
dz(hip)/dt max.	(%bh/s)	21±9	4±2 [‡]
Step foot toe-off to ground contact:			
l(ankle-hip) min.	(%bh)	33±4	32±4
z(ankle) max.	(%bh)	25±4	24±5
dx(ankle)/dt avg.	(%bh/s)	115±15	109±17
-dl(ankle-hip)/dt max.			
	(%bh/s)	144±29	137±19
step length	(%bh)	49±6	37±8 [‡]
At step foot ground contact:			
θ(ankle-hip)	(deg)	-10±4	13±6 [‡]
z(hip)	(%bh)	54±2	47±4 [†]
θ(hip-HAT)	(deg)	25±12	41±5 [*]
dθ(hip-HAT)/dt	(deg/s)	-43±53	79±37 [‡]
x(ankle-HAT)	(%bh)	-2±5	19±5 [‡]

[*] $p < .01$, [†] $p < .005$, [‡] $p < .001$ vs. Recovery

ground contact. As seen in Table 1, fallers were significantly less successful in executing these support limb functions. Consequently, although the gross stepping mechanics did not differ between falls and recoveries, the resulting step was shorter in the fallers and ground contact was well behind the hips and HAT center of mass, making a fall inevitable.

Fallers were walking faster when tripped, which translated into a greater forward hip velocity post-trip. Fallers also took longer to lower and start loading the support foot. The net result of these factors was that, at the start of support limb loading, the fallers' hips and HAT center of mass were rotated significantly further ahead of the support foot. The delayed support foot loading and more rotated body position appear to have resulted in a decreased vertical reaction force impulse, explaining the reduced ability to elevate the hips. The data also indicate that the net support ground reaction force was directed behind the HAT center of mass in the fallers, serving to increase HAT forward rotation, whereas the opposite appeared to be true in those who recovered.

The falls in the present analysis can thus be attributed to a faster walking speed and a delay in lowering the support foot. These factors represent targets for intervention.

REFERENCES

Eng, J.J. et al. (1994). *Exp Brain Res*, **102**, 339-349.
Pavol et al. (1999). *J Gerontol Med Sci*, **54A**, M103-M108.
Tinetti et al. (1988). *N Engl J Med*, **319**, 1701-1707.

ACKNOWLEDGMENTS

HEAD MOVEMENT DURING SUPPORTING BASE TRANSLATION IN YOUNG AND OLD ADULTS

Ge Wu
Department of Physical Therapy, University of Vermont, Burlington, VT 05405
E-mail: gwu@zoo.uvm.edu

INTRODUCTION

Falls in the elderly are a major health problem for the nation. An individual's susceptibility to falls is often related to the inability to maintain a balanced upright orientation when balance is disturbed so that the center of gravity of the whole body is within the base of support [Massion, 1994]. In particular, the head orientation in space has been considered as a primary reference frame for upright posture in healthy young adults [Pozzo et al., 1995]. However, limited studies have been done to examine the control of head orientation in the old adults.

Currently, the role of load receptors under the feet in the regulation of body orientation is still under debate. A question that remains to be explored is how the head orientation is affected when the input to the load receptors is changed under a normal weight-bearing condition. Therefore, this study was to examine the head orientation changes in response to an unexpected horizontal movement of the supporting surface when standing on different surfaces in both healthy young and healthy old subjects. It was hypothesized that (1) standing on either soft or reduced surface would not affect the head orientation; and (2) the old adults would react similarly as the young people to the supporting base movement when standing on different surfaces.

METHOD

A total of 9 healthy, young subject (mean age 24±2yrs) and 10 healthy old subjects (mean age 73±2 yrs) were tested. All subjects did not have any apparent impairment in vestibular, visual and neuro-muscular-skeletal functions, and previous history of fall-related injuries. Before testing, each subject was asked to read and sign a consent form.

Each subject was asked to stand, with shoes, on a movable platform of 3 different surfaces: normal (hard and wide), soft (foam, 5 cm tall and wide), and reduced (hard, half of shoe size, 3.6 cm tall) surface. When standing on each surface, subjects were tested eyes open or closed, and with the initial base movement in either forward or backward directions, respectively, 4 times each, for a total of 16 trials. All these conditions were provided randomly in a 4-block design for each of the three surfaces.

The sagittal plane movement of the head was measured by a Kinematometer [Wu and Ladin, 1993]. Another accelerometer was attached to the movable platform to measure its acceleration in the moving direction. The base platform moved for a total of $4cm$ with peak acceleration of $6m/s^2$, speed of $35cm/s$ and. The outputs from the Kinematometers and the platform accelerometer were collected at $120Hz$ for 3s.

The perturbation onset time was first determined based on the first point at which the platform acceleration was above the mean plus three times the standard deviation of the baseline level. Following parameters were extracted from the head movement trajectory: onset time, peak-to-peak magnitude, and frequency. ANOVA was used to determine the significant differences ($p < 0.05$) among the surfaces and between the groups.

RESULTS

The means and standard deviations of the three head movement parameters are shown in Tables 1 to 3. For the peak magnitude, there was no significant difference among 3 surfaces for both groups, but the older group had significantly larger movement than the young group. For the onset time and frequency, there was no significant difference among 3 surfaces and between 2 groups.

DISCUSSION AND SUMMARY

There are two main findings in this study. First, despite age-related changes in leg proprioception in the old adults [Wu, 1998], and the sensory changes at the feet by standing on different supporting surfaces, the head movement trajectories in response to a large movement at the base remained unchanged within each of the groups. Secondly, although the head movement was relatively small in the young adults, which is consistent with previous studies [Pozzo et al., 1995], the head movement of the old adults was significantly larger than the young adults.

Based on these two findings, it is postulated that this group difference is most likely not due to the sensory changes in the feet. Several possibilities for the group difference are: (1) due to age-related changes in the neuro-muscular-skeletal systems around the head-neck structure [Viviani and Berthoz, 1975]; (2) due to a change in strategy that old subjects compensate for the loss of sensations in the feet, because, by increasing the head movement, the stimulation to both visual and vestibular systems will be augmented which may enhance the postural control action [Pozzo et al., 1995]. Nevertheless, the changes in the head orientation control in the old adults deserve further investigation in its role in postural stability.

REFERENCES

Massion J (1994) Curr Opin Neurobiol 4: 877-887

Pozzo T et al. (1995) Exp Brain Res 106: 327-338

Viviani P, Berthoz A (1975) Biol Cybern 19:19-37

Wu G Ladin Z (1993) ASME Trans Biomech Eng 115(1): 53-62

Wu G (1998) Clin Biomech. J. Geront. 53A(4):M320-M326

Table 1: Means and standard deviations of peak head movement (Forward, EO)

Angle [rad]	Young subjects		Old subjects*	
	mean	stdev	mean	stdev
Normal	0.08	0.03	0.17	0.08
Soft	0.11	0.09	0.15	0.09
Reduced	0.11	0.07	0.17	0.07

- $p < 0.0006$ between two groups

Table 2: Means and standard deviations of head movement onset (Forward, EO)

Time [s]	Young subjects		Old subjects	
	mean	stdev	mean	stdev
Normal	0.27	0.09	0.28	0.04
Soft	0.26	0.06	0.26	0.04
Reduced	0.30	0.10	0.22	0.05

Table 3: Means and standard deviations of head movement frequency (Forward, EO)

Freq [Hz]	Young subjects		Old subjects	
	mean	stdev	mean	stdev
Normal	9.58	8.63	10.17	8.81
Soft	6.35	7.5	9.98	8.67
Reduced	12.24	11.14	17.11	15.12

EFFECT OF PERIPHERAL NEUROPATHY ON CENTER-OF-PRESSURE MEASURES

Mark Musolino[1], Mark Redfern, Ph.D.[1], Michael L. Boninger, M.D.[2,3]

[1]Dept of Otolaryngology, University of Pittsburgh
[2]Division of Physical Medicine and Rehabilitation, Dept of Orthopaedic Surgery, University of Pittsburgh
[3]Dept of Rehabilitation Science and Technology, University of Pittsburgh
Email: markmuso+@pitt.edu

INTRODUCTION

Each year, almost one-third of community dwelling people over age 65 fall. These falls are a significant source of morbidity and mortality, with serious injuries reported in up to 24 % of the cases. Recently, peripheral neuropathy (PN), which may contribute to decreased proprioception and/or increased reflex reaction time, has been implicated as a possible risk factor for falling (Richardson, 1992 ; Cavanagh, 1992). The purpose of the present study was to (1) determine the prevalence of PN in a population of known fallers (F), as compared to non-fallers (NF), and (2) examine the effect of PN on static center-of-pressure (COP) measures.

METHODS

Thirteen F and 23 NF between the ages of 55 and 80 were studied. Subjects whom had fallen at least 2 times in the 6 months just prior to testing were considered fallers, with a fall defined as an unintentional change in body position that resulted in the faller being on a lower level. For inclusion in this study, subjects had to be able to stand without support, to walk household distances independently, and to have no known history or evidence upon physical examination of CNS disease or dysfunction.

Nerve Conduction

The presence of PN was determined through nerve conduction studies, which were performed by a single author who is board certified in electromyography using a Dantek Cantata®. The sural sensory nerve on the right lower extremity was stimulated at the calf and recorded 14 cm distally, beneath the medial malleolus. Sural nerve latencies of between 0.1 and 4.6 ms were considered indicative of PN. If abnormalities were observed on the right side, the left leg was examined as well. The dorsal foot surface was checked to ensure a temperature of at least 32° C, and warmed if necessary.

COP Measures

Balance during quiet stance was tested using an Equitest platform (Neurocom, Inc). Subjects were asked to stand still, with arms at their sides, for two conditions: eyes open (EO) and eyes closed (EC). Three 20 second trials were run for each condition; data were collected at 100 Hz. Peak-to-peak amplitude (AMP), Root mean square (RMS), and Velocity (VEL) of COP sway were calculated for the anterior-posterior (A-P) and lateral (M-L) directions.

RESULTS

Incidence of PN

There were no statistical differences between F and NF groups with regards to age or

gender. Thirty percent (4/13) of fallers, and 9% (2/23) of non-fallers, met criteria for PN, based on nerve conduction studies (Table 1).

Table 1: Subject Characteristics

Group	n	w/ PN	Mean Age	Sex (M/F)
F	13	30 %	68 (56-80)	6/7
NF	23	9 %	72 (60-80)	10/13

Effect of PN on COP Measures

Clear differences, though not statistically significant, were observed between PN and NoPN groups for all measured COP variables; the differences were more pronounced in F, as compared to NF, and appear to have been influenced by visual condition as well. AMP and RMS measures were similar in that for the EO condition and in both A-P and M-L directions, values for PN subjects were consistently *lower* than those for the NoPN group (Table 2). An opposite trend was observed in the EC trials: AMP and RMS values were consistently *higher* in the PN group, indicating increased sway. VEL values, higher in PN than in NoPN for both visual conditions and in both directions, are indicative of heightened sway in PN subjects as well.

DISCUSSION

The large number (30%) of fallers found to have PN lends further creedence to previous work that has shown individuals with PN are more prone to falls than those without PN (Richardson, 1992; Cavanagh, 1992). The differences in AMP and RMS values between EO and EC suggest that those with PN relied on visual input more than NoPN subjects did. Also, the fact that the trend in VEL values (i.e. PN > NoPN) did not change across visual conditions is intriguing, and deserves further investigation. Finally, the effect of the interaction between fall status and PN on COP measures is not surprising, considering that PN is a risk factor for falling.

CONCLUSIONS

PN appears to (1) have elicited an increased quiet stance sway response, and (2) be associated with a higher incidence of falls in the population examined in this study.

REFERENCES

Cavanagh PR, et al. (1992). *Diabetic Med,* 9, 469-474.
Richardson JK, et al. (1992). *J Am Geriatr Soc,* 40, 1008-1012.

Table 2: COP Measures for PN and NoPN (control) groups

AMP (cm)				RMS				VEL (cm/s)			
A-P		M-L		A-P		M-L		A-P		M-L	
EO	EC	EO	EC	EO	EC	EO	EC	EO	EC	EO	EC
1.72 (.66)	2.69 (1.06)	0.47 (.21)	0.61 (.20)	0.37 (.13)	0.56 (.21)	0.09 (.04)	0.12 (.05)	1.44 (.33)	1.78 (.53)	1.10 (.30)	1.16 (.31)
1.83 (.61)	2.39 (.60)	0.56 (.26)	0.67 (.27)	0.39 (.14)	0.51 (.13)	0.11 (.05)	0.13 (.06)	1.41 (.21)	1.72 (.23)	1.05 (.16)	1.15 (.13)

{ shaded row = PN group ; values expressed as **mean (sd)** ; EO *eyes open,* EC *eyes closed* ; *p<0.05 }

BALANCE RECOVERY BY STEPPING DURING BACKWARD FALLS

Elizabeth T. Hsiao and Stephen N. Robinovitch
Biomechanics Laboratory, Department of Orthopaedic Surgery, San Francisco General Hospital
and University of California, San Francisco, San Francisco CA 94110
snr@itsa.ucsf.edu   http://biomechanics.ucsf.edu

INTRODUCTION

Stepping represents a primary means for balance recovery after a large unexpected perturbation, such as a slip or trip. However, little understanding exists of the biomechanical factors which govern this task. Previous studies have shown that elderly are less able than young to recover balance with a single step [Luchies, 1994; McIlroy, 1996; Thelen, 1997]. Yet, these studies have found little or no significant difference in step size or step contact time when age is considered. Therefore, from a biomechanical perspective, additional factors separating young, elderly, and the ability to recover balance with a single step, may be the capacity to develop sufficient "stiffness" in the stepping leg and the ability to position the leg such that it has an adequate mechanical advantage. In this study, the "stiffness" of the stepping leg after contact is reflected by the magnitudes and times to peak lower extremity joint torques. The mechanical advantage, or effective lever arm, of the stepping leg during step contact is defined by the ratio of the stepping angle at the instant of contact (α_C) and the body lean angle at contact (θ_C), which are related to the combined effect of step size and step contact time.

Accordingly, we tested the hypothesis that elderly subjects' ability to recover balance with a single step is better explained by the stiffness and mechanical advantage of the stepping leg during step contact, than by step size and step contact time. To test this hypothesis, we conducted simulated backward slipping experiments on elderly subjects aged 70 years and over.

METHODS

Twenty-six (12 female, 14 male) healthy, community-dwelling elderly adults, of mean age 75 ± 4 (S.D.) yrs, height 1.66 ± 0.11 m, and body mass 72 ± 15 kg, participated in the study. During the experiment, subjects were unexpectedly released by means of a tether and electromagnet from a backward inclination of seven degrees and instructed to recover balance with a single step (Fig.1(a)). During each trial, three-dimensional body segment positions and foot contact forces of the stepping leg were acquired via a 6-camera 60 Hz motion capture system and a force plate, respectively. Step contact time, stepping angle α_C (which reflects a normalized step size), and mechanical advantage α_C / θ_C were determined from the recorded motion data. Magnitudes and times to peak ankle plantarflexor, knee extensor, and hip flexor torques were estimated from the motion and force data by using inverse dynamics (Fig.1(b)). For each subject, average values based on five trials were included for analysis. Subjects were classified into three recovery ability categories: "single-steppers", who were successful at recovering balance with a single step in four or more trials, "multi-steppers", who were only successful in one or less trials, and "mixed" otherwise. Ensemble-average values were computed for each category based on subject averages.

RESULTS

Fifty percent of the subjects were single-steppers. The remaining subjects were split between being multi-steppers (27%) and mixed (23%). α_C / θ_C was the only factor which significantly associated with recovery ability ($p = 0.003$; via ANOVA). On average, single-steppers had the largest value of α_C / θ_C, 1.4 ± 0.5, while multi-steppers had the smallest, 0.6 ± 0.5 (Fig. 2). There were no significant differences with respect to recovery ability in step contact times (which

averaged 360 ± 60 ms) or stepping angles (13° ± 7°). Contrary to our hypothesis, no joint torque parameters were significantly different among the three categories. Average peak torques, normalized by body weight and height, at the hip, knee, and ankle were 0.066 ± 0.021, 0.062 ± 0.017, and 0.058 ± 0.17, respectively, while the average times to peak torque after contact were 100 ± 50 ms, 160 ± 90 ms, and 130 ±40 ms, respectively.

DISCUSSION AND CONCLUSIONS

Although we had hypothesized that both the "mechanical advantage" and "stiffness" of the stepping leg during the contact phase would associate with the ability to recover balance with a single step, we found that only the mechanical advantage, as measured by the ratio α_C / θ_C, was significantly related to recovery ability in elderly individuals. As expected, step contact time and step size, alone, did not associate with recovery ability.

We found that subjects who predominately recovered their balance with a single step had a much larger value of α_C / θ_C than subjects who used multiple steps. Therefore, single-steppers placed their stepping leg in a position which provided a better mechanical advantage for halting the body's downward movement. Biomechanically, it would appear that one can compensate for a leg placement with a poor mechanical advantage by using a greater leg stiffness, or larger joint torques. Multi-steppers, however, used similar joint torques as single-steppers. These results may suggest that, while multi-steppers were performing at their maximum strength capacity, it was an inadequate leg placement that rendered their trials unsuccessful. Therefore, the ability to assess an individual's performance based on this new parameter α_C / θ_C may be very useful in determining her/his ability to succeed in restoring upright stance by stepping.

REFERENCES
Luchies, C.W. et al. (1994) *J Am Geriatr Soc*, 42, 506-512.
McIlroy, W.E. and Maki, B.E. (1996) *J Gerontol: Med Sci*, 51A, M289-M296.
Thelen, D.G. et al.(1997) *J Gerontol: Med Sci*, 52A, M8-M13.
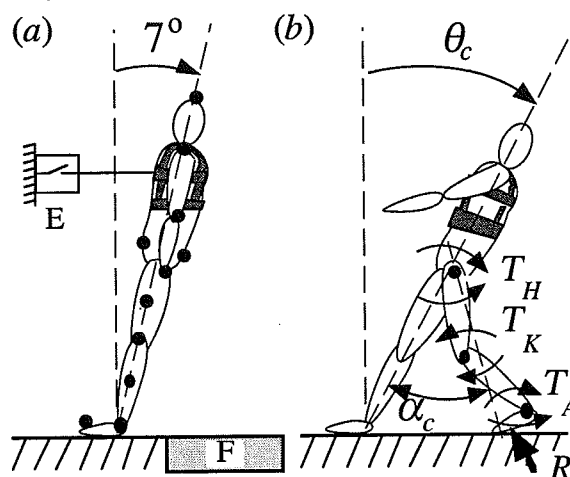
Figure 1. Backward slipping experiment. (a) The subject was held in a 7° inclination until the electromagnet (E) was released. Ground reaction forces on the stepping foot were recorded by the force plate (F). (b) The stepping angle (α_C) and body lean angle (θ_C) were determined at the instant of contact. Torques at the hip, knee, and ankle (T_H, T_K, T_A) were computed by inverse dynamics routines, starting from the reaction force R on the stepping foot upwards.
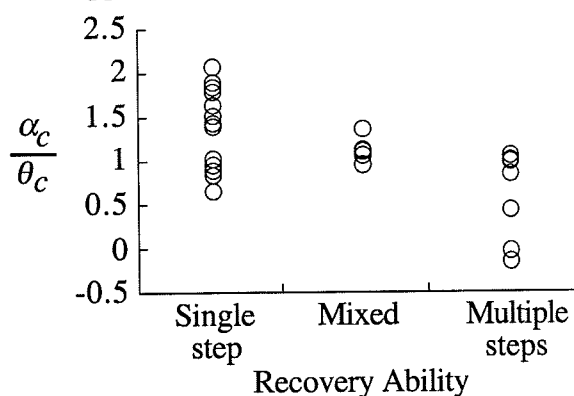
Figure 2. Subjects who recovered balance with a single step tended to position the stepping leg, during the contact phase of the step, such that it had a greater mechanical advantage (α_C / θ_C) than subjects who needed to take multiple steps.

ACKNOWLEDGMENTS

INFLUENCE OF FLOORING ON OBJECTIVE STANDING FATIGUE MEASURES

Rakié Cham, M.S. and Mark S. Redfern, Ph.D.
Department of BioEngineering, University of Pittsburgh, Pittsburgh, PA
Email: racst46+@pitt.edu

INTRODUCTION

Standing for long periods of time has been directly associated with lower extremity discomfort, pain and fatigue and low back pain (Redfern and Chaffin, 1995). These problems are particularly prevalent among workers who stand for long periods of time in restricted areas, such as checkout supermarket workers, assembly and quality control inspection workers.

Flooring may play a role in standing fatigue, however previous studies of flooring on subjective and objective measures thought to be related to fatigue/discomfort, have had mixed results. The majority of the differences in the reported results are probably due to differences in procedures and analysis methods, particularly variations in testing duration and exposure time. The impact of flooring on discomfort/pain is still largely unknown.

The first aim of this study was to examine the effect of different floors on subjective measures of fatigue and discomfort, and some related objective measures, using a longer testing session. The second aim was to investigate the relationship between these measures and material properties of the mats. This paper reports the objective measures recorded during the experiments. Tiredness/discomfort ratings findings are reported elsewhere (Cham and Redfern, 1999).

PROCEDURES

The flooring conditions included a hard vinyl tile floor and 6 floor mats placed over a force plate. During a 4-hour testing interval, subjects stood on the force plate and performed 12 series of computer tasks. Center of pressure (COP) position and electromyographic recordings (EMG's from soleus, tibialis anterior and erector spinae) were collected for 10 minutes and 1 minute every 20 minutes at a sampling rate of 20 Hz and 1 kHz, respectively. Skin temperature over a number of leg muscles and elbow (control) was recorded every 15-17 minutes. Every 30 minutes, subjects were allowed to walk back and forth on a runway (covered with the same floor they stood on) for 2 minutes. Leg volume was measured pre and post standing. All subjects wore the same brand of shoes and socks.

RESULTS AND DISCUSSION

Of the 4 measures collected (COP, EMG, skin temperature and leg volume), only COP and skin temperature showed statistically significant differences among flooring and times. During the 4th hour of the experiment, the change in the normalized (to the elbow control temperature) skin temperature (over the soleus, tibialis anterior, quadriceps and hamstrings) was significantly ($p < 0.05$) affected by floor conditions. The greatest changes in the normalized temperature were recorded over the soleus when standing on the hard floor (Table 1). Post-hoc analyses revealed not only significant differences between a number of mats and the hard floor, but also significant differences among several mats. COP measurements were used to compute the number of lateral weight shifts as subjects stood on the floors. The hypothesis

was that a greater amount of weight shifting may indicate an attempt to reduce increasing body stress and fatigue. ANOVA showed that, in the 4th hour, the number of weight shifts was significantly different ($p < 0.05$) among floors. Again, the hard surface had the greatest number of shifts (Table 1).

EMG's showed no statistically significant spectral change differences. Changes in lower leg volume were found not to be statistically significant among flooring conditions. However, interesting trends showed that leg swelling was greatest for the hard floor.

Comparisons of floor material properties to the objectives measures were performed. Floor properties were evaluated through specific measurements including stress-strain tests and a drop test. The stress-strain tests yielded the stiffness, work-lost and load-decay measures, while the drop test yielded the drop-max-g accelerations. (see Cham and Redfern, 1999 for details of material tests.) Increased stiffness and drop-max-g and decreased work lost (Table 1) were found to be associated with significant decreases in COP weight-shift and reduced changes in the normalized skin temperature, both of which can be used as an indication of a good floor performance.

Table 1: Material properties, skin temperature and center of pressure findings (4th hour)

Floor	Stiffness[i] (N/mm)	Worklost[ii] (N.mm)	Drop-Max-G acceleration[iii] (g)	Load decay[iv] (N)	Normalized skin temperature changes over soleus (°C)	Normalized number of weight shifts
A (hard floor)	NA	NA	NA	NA	1.01	175.56
B	6732.8	1408	6.66	269	0.09	166.19
C	4463.1	303	8.49	437	0.55	174.85
D	3040.0	992	5.98	462	0.28	170.50
E	2443.6	3348	4.72	982	0.35	173.87
F	2252.4	3392	3.06	686	0.79	186.41
G	1814.0	1600	4.88	468	0.33	174.80

[i] Stiffness modulus evaluated at a load level of 4000 N.
[ii] Worklost is the area enclosed in the load/unload-deformation hysteresis curve.
[iii] Drop-Max-g is the maximum deceleration of a 10 pound weight dropped on the mat from a 0.124 inch height.
[iv] Load-decay required to maintain a given displacement (corresponding to a load level of 2000 N) for 2 minutes.

SUMMARY

This 4-hour experiment indicated a significant flooring effect on skin temperature changes and lateral COP weight shifts. The hard floor and floor mat F consistently yielded worse performance. The relationships between the mat material properties and fatigue measures suggest that floor performance increased with greater elasticity and stiffness, and lower energy absorption. This study suggests that 1) floor materials can affect objective parameters, 2) these parameters may be useful in evaluating

floors and 3) a minimum of 4-hour testing period should be used in future laboratory studies.

REFERENCES

Cham R., Redfern M.S. (1999); The influence of flooring on standing comfort and fatigue; to be published in *Human Factors Proceedings*.

Redfern M.S., Chaffin D.B. (1995); Influence of Flooring on standing fatigue; *Human Factors, 37(3):570-581.*

ANTICIPATORY POSTURAL ADJUSTMENTS IN CONDITIONS OF POSTURAL INSTABILITY AND MANUAL SUPPORT

[1]Harm Slijper, Mark Latash
Motor Control laboratory, Penn State University Park, Pennsylvania
[1]Email:hps5@psu.edu

INTRODUCTION

It has been shown that anticipatory postural adjustments (APAs) display non-monotonic changes with stability, i.e. they are attenuated during both very stable and unstable standing (Aruin et al., 1998, Nardone and Shieppati, 1988). Maintaining a stable upright posture has two components; one is reflected in the postural sway during quiet standing, while the other is reflected in the ability to maintain balance in the presence of perturbations. It has been shown that a light touch by a finger leads to a dramatic decrease in postural sway (Jeka et al., 1998), which may be viewed as very stable standing. On the other hand, such a touch is apparently ineffective as a balance-keeping factor in the presence of mechanical perturbations.

The purpose of the present study has been to investigate changes in APA in unstable conditions, with and without the presence of an additional finger touch or hand grasp support.

METHODS

Eight healthy adults (aged 26-52 yr.) participated in the experiment. Subjects performed a fast unilateral shoulder flexion (focal movement) during quiet standing, while balancing on a special board (with instability in the sagittal or frontal plane). The manual support was provided by having the subject hold on to a solid support surface with a light touch with the index finger or a firm grasp to a handle. EMG activity of postural muscles (rectus abdominis (RA), erector spinae (ES), rectus femoris (RF), biceps femoris (BF), tibialis anterior (TA) and soleus (SOL)) as well as arm muscles (biceps brachii (BIC), triceps brachii (TRIC), flexor carpi ulnaris (Wrfl) and extensor carpi ulnaris (Wrex)) were recorded. From force platform data the center of pressure (COP) displacements in anterior-posterior (a-p) and medial-lateral (m-l) directions were calculated. Also the forces exerted by the supporting arm were registered. Statistical methods included repeated measures analysis of variance (ANOVA) and Student's t-test.

RESULTS

COP: Instability in sagittal or frontal planes decreased in COP excursions in corresponding (a-p and m-l) directions. The influence of manual support was not reflected in significant changes in COP displacement.

Forces: Applied forces were about 2.9 times higher in grasp than in touch, but independent of stability conditions.

EMG: Unstable conditions caused an attenuation of the APA activity, as expressed by the integrated EMG activity from 100 ms prior to till 50 ms after the focal movement. APAs were lower for RF and BF, other postural muscles showed also a decrease but it was non-significant. Furthermore, normalized APA integrals for muscle pairs were summed and subtracted from each other to characterize their overall effects at the joint level (cf. Feldman et al., 1998).

The main findings of this study are:

1) In unstable conditions, there were different changes in APAs in arm and trunk/leg muscles with a touch and a grasp.

Figure 1 shows that APAs in leg and trunk muscles (ES, BF, RF, and TA) decreased with touch and did not show further changes when a touch was substituted with a grasp.

APAs in arm muscles (Wrfl, BIC) showed a drop or no changes in the presence of touch and a substantial increase when touch was substituted with a grasp. Shown are means with standard error bars.

Arm muscles
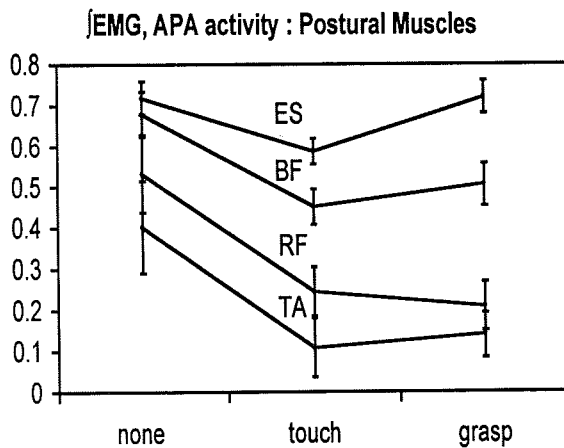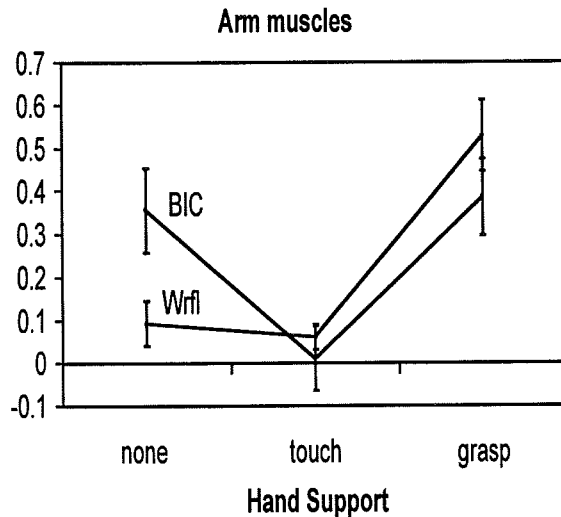
Hand Support

2) With changes in hand support only summed integrated activity of muscle pairs showed significant changes while no changes were found for the difference in EMG integrals between the agonist and antagonist. Changes in the summed activity in all five muscle pairs showed the same patterns as those illustrated in Figure 1.

DISCUSSION

These findings can be interpreted as suggesting that the decreased postural sway in the presence of a touch was associated with a subjective perception of more stable standing leading to a decrease in APAs, as in the presence of a firm external support. However, the touch could not be used for body stabilization, which is shown in the basically unchanged or decreased APAs in the arm muscles. As suggested by the significant results for the summed activity in muscle pairs, this pattern is reflected in parallel changes in the activity of antagonist muscle pairs.

SUMMARY

We observed different changes in APAs in the arm and the leg/ trunk muscles under manipulations of postural instability and additional hand support. Changes in postural sway may be dissociated from changes in APAs under manipulations of stability, so the magnitude of APA is at least partly defined by the subjective perception of the stability in the postural task. Parallel changes in APA activity at the joints seem to be associated with this pattern.

REFERENCES

Aruin, A.S. Forrest, W.R. Latash, M.L. (1998). *Electroencephalog Clin Neurophysol*, 109, 350-359.

Nardone, A Schieppati, M. (1988) *Exp. Brain Res*, 69, 469-480.

Jeka, J. Oie, K. Shoner, G. Dijkstra, T. Henson, E. (1998) *J. Neurophysiology*, 79, 1661-674.

Feldman, A.G. Levin, M.F. Mitinski, A.M Archambault, P. (1998) *J. of Electromyography Kinesiology*, 8, 383-390.

EFFECT OF COM ACCELERATION ON DYNAMIC STABILITY LIMIT

Huei-Ming Chai[1] and M. Melissa Gross[2]

[1]School of Physical Therapy, National Taiwan University, Taipei, Taiwan
[2]Department of Movement Science, University of Michigan, Ann Arbor, Michigan
Email: mgross@umich.edu

INTRODUCTION

Dynamic stability limit is typically expressed as the excursion of the center of pressure (COP) (Blaszczyk et al., 1994) or functional reach distance (Duncan et al., 1992) because of their high correlation during the forward reach test (Duncan et al., 1990). Assuming an inverted pendulum model, however, the difference between the COP and the COM positions is a function of the COM acceleration (Jian et al., 1993). Thus, it is important to know whether the COM acceleration affects the relationship between functional reach distance and COP excursion. Knowledge of these quantitative measures is essential not only for better understanding of human movement, but also for investigation of dynamic balance control. In this study, we examined the effect of COM acceleration on dynamic stability limit by studying balance measures during two reach tasks with different acceleration profiles: reach-hold and reach-reversal task.

PROCEDURES

Seventeen young adults (9 male, 8 female; 21.2 ± 1.4 yrs) participated in the study. The participants were asked to perform fast maximum reach movements under two different conditions: reach-hold and reach-reversal. For reach-hold, the arm was held at maximum reach for one second. For reach-reversal, the participants returned to their starting position immediately after obtaining maximum reach. Testing order was randomized.

Three video cameras (60 Hz) were used to capture joint motion. Reflective markers were placed over six body landmarks to construct a five-segment rigid-body model. Kinematic data were low-passed filtered at 8 Hz. Functional reach distance was the difference between maximum reach and arm length reach. COP excursion was the distance between the initial and maximum positions of the COP. Safety margin was the distance from the COP position at maximum reach to the edge of the base of support. COP-COM difference was the maximum difference between the COP and COM locations during the reach-forward period. A 2 x 2 (gender by reach task) ANOVA with repeated measures was used to test for differences between the reach tasks ($p < 0.05$).

RESULTS

Reach kinematics were different between reach-hold and reach-reversal tasks (Fig. 1). The COM initially accelerated forward in both tasks, but before the maximum reach was achieved in the reach-reversal task, the COM accelerated backwards to bring the trunk back to starting position. A second positive acceleration peak arrested the backward motion prior to motion cessation in the upright position. Gender did not affect reach kinematics.
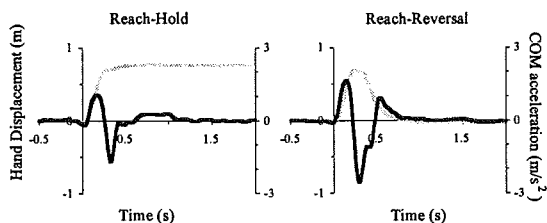
Figure 1: COM acceleration of a representative participant during the reach-hold and reach-reversal tasks. The dark lines indicate the COM acceleration and the light lines indicate hand displacement. Positive values indicate forward motion.

The reach task affected all dynamic balance measures (Table 1). Functional reach distance was significantly smaller for the reach-reversal task than for the reach-hold task. Unlike functional reach distance, COP excursion significantly increased but safety margin significantly decreased for the reach-reversal task compared to the reach-hold task. The COP-COM difference was significantly smaller for the reach-reversal than for the reach-hold task.

Table 1: Dynamic balance measures for the reach-hold and reach-reversal tasks.

	Reach-Hold	Reach-Reversal
Functional Reach (% body ht)	18.8±2.0	16.9±2.7
COP Excursion (% base of support)	30.4±8.5	34.7±7.8
Safety Margin (% base of support)	30.8±8.6	26.7±9.1
COP-COM (% base of support)	15.7±6.0	21.2±5.2

DISCUSSION

Functional reach distance was smaller but COP excursion was larger for the reach-reversal task than for the reach-hold task,

suggesting that a larger COP excursion or a smaller safety margin does not necessarily indicate better reach performance for the same individual. Young adults had to generate a large backward acceleration at maximum reach by pushing their COP closer to the edge of the base of support in order to bring their body back to the original standing posture. Since the COP motion was confined within the stability limit and a large COP excursion was required to generate backward acceleration during the reach-reversal task, the potential range for the COP to generate motion was limited, leading to a smaller functional reach distance.

The high correlation between functional reach distance and COP excursion was not maintained in the reach-reversal task when a large COM acceleration occurred. Functional reach distance significantly decreased but COP excursion significantly increased for the reach-reversal task compared to the reach-hold task. The functional reach distance does not measure the same aspect of dynamic balance as the COP excursion. Differences between the functional reach distance and the COP excursion in dynamic tasks need to be further investigated.

REFERENCES

Blaszczyk, J.W. et al., *Gait & Posture*, 2, 11-17, 1994.

Duncan, P.W. et al., *J. Gerontology Medical Sciences*, 47, M93-M98, 1992.

Duncan, P.W. et al., *J. Gerontology Medical Sciences.*, 45, M192-M197, 1990.

Jian, Y. et al., *Gait & Posture*, 1, 9-22, 1993.

POSTURAL ANTICIPATION IN CATCHING SELF- AND EXTERNALLY-RELEASED LOADS

Takako Shiratori and Mark Latash

Department of Kinesiology, Pennsylvania State University, University Park, Pennsylvania

Email: txs192@psu.edu

INTRODUCTION

The purpose of anticipatory postural adjustments (APA) are hypothesized to counteract the expected effects of reactive forces with changes in the body geometry and to keep the projection of the center of gravity of the body within the base of support (1,2). Loading or unloading the hand with an object while standing produces perturbations to posture due to quick changes in body mass distribution. In a catching task, APAs has shown to scale with linear momentum of load impact when experimenter released the load (3). However, another study showed that APAs were scaled with momentum of the object only when the subject released the load (4). In this study, we were interested in the APAs during catching an object when the load was self-released or experimenter-released. Our hypothesis was that there would be precise scaling of APAs when load was self released as a function of momentum of load impact and less precise when the load was experimenter-released.

PROCEDURES

Ten healthy adults were recruited for this study. The subjects were asked to stand on a force platform and perform 2 different tasks: 1) to catch a load released by the experimenter with the left hand, and 2) release the load from the right hand and catch the load with the left hand. Each tasks consisted of 7 series where the impact of

catch was manipulated by varying the mass of the load (1.1 to 2.2 kg) and the release height (0 to 0.4 m)so that momentum of the object at impact will change or stay the same. The release height was determined as the vertical height with respect to the catching hand, which was placed in mid-front of the body with 90 degrees elbow flexion. Surface EMGs were recorded on the following muscles: tibialis anterior, soleus, rectus femoris, biceps femoris, rectus abdominis, erector spinae, wrist flexor, wrist extensor, biceps, triceps, anterior deltoid, and posterior deltoid on the catching side of the body. From the force platform, anterior-posterior and medial-lateral COP trajectories were calculated. An accelerometer was attached to the catching hand to detect instant of load contact and was used for trial alignment (time-zero). Anticipatory activity of the muscles was calculated taking the integrals of rectified EMGs from -100 to 0 ms with respect to t_0 ($\int EMG$). COP displacements were quantified within the time interval from -500 ms to t_0. Repeated measures analysis of variance was used for statistical analysis.

RESULTS AND DISCUSSION

Self-Released Load Catch

$\int EMG$ for most muscles increased as a function of momentum of load impact. This was accompanied with COP displacement in the direction posterior and contralateral to the

side of the catching hand as the force of impact increased. There were no significant differences in $\int EMG$ for most muscles and COP displacements when mass and height were manipulated for the same momentum at instant of catch. This suggests that subjects were able to estimate similarity and differences in magnitude of the perturbation and scale APAs accordingly when loads were self-released.

Experimenter-Released Load Catch
When the same load were released at different heights, increased $\int EMGS$ were observed as a function of momentum at load. However, when the release height and mass of load was manipulated for same momentum, most muscles again showed an increase in $\int EMG$ as an increase with the release height. This indicates that APAs were not able to predict the forthcoming perturbation when the momentum at impact was the same.

This suggests that magnitude of the perturbations are scaled with APAs when the perturbation is self inflicted, probably due to handling the object prior to catching. When the perturbation was externally applied, the subjects predicted the magnitude of the forthcoming perturbation in a consistent manner although this prediction was not necessarily related to the perturbation. When one is unclear about the magnitude of the forthcoming perturbation, one may still use reasonable but 'incorrect' variable(s) that provide indication about the magnitude of future perturbations to scale APAs.

SUMMARY

APAs in catching a load was studied under two different conditions: self-released and experimenter-released load using varying the

momentum at instant of catch. Results show that APAs scale as a function of momentum of the load impact when load was self-released. When the experimenter released the loads manipulating for the same momentum at impact, subjects scaled APAs which did not pertain to the magnitude of perturbation to the body.

REFERENCES

1. Bouisset. S., Zattara. M. (1981) *Neurosci Lett*, **22**, 263-270.
2. Massion. J. (1992) *Prog Neurobiol*, **38**: 35-56
3. Lacquaniti. F., Maioli. C. (1989) *J.Neurosci*, **9**, 134-148.
4. Bennis.N.,et al. (1996) *J Physiol(Paris)*, **90**, 27-42.

ACKNOWLEDGEMENTS

VERTEBRAL KINEMATICS AND MUSCLE ACTIVATION PATTERNS IN PRIMATE HEAD-NECK SYSTEM DURING CONTROLLED HEAD MOVEMENTS

Hyeonki Choi[1], Emily A. Keshner[2], and Barry W. Peterson[1]

[1] Department of Physiology, Northwestern University, Chicago, IL
[2] Sensory Motor Performance Program, Rehabilitation Institute of Chicago, Chicago, IL
Email: h-choi@nwu.edu   Web: dept-www.physio.nwu.edu/physiology/physiofr.htm

INTRODUCTION

The head-neck system is a complex biomechanical linkage with multiple degrees of freedom of movement. Mammals hold the cervical vertebral column nearly vertical at rest. Movements are made primarily by motions about a restricted set of joint axes: yaw about C_1-C_2, pitch about either C-skull or C_7-T_1 and roll by combined lateral bending of C_2-C_5. Cats have been used to understand the relationship between head movement, neck muscle activation, and cervical vertebral movements (Keshner, 1994; Keshner et al., 1997). But, use of cats has been less than ideal since the structure and function of the cat neck differ significantly from those in humans and since it is difficult to train cats to perform tasks analogous to those we humans employ humans. In this study we examined the connections between the kinematics of the cervical vertebrae and activation of neck muscles during voluntary head tracking movements in rhesus monkey. Phase relations between the input stimulus motion, the sinusoidal motion of the vertebral column, and peak activation of neck muscles were calculated.

PROCEDURES

A rhesus monkey seated in an upright posture was trained to follow moving visual target to receive a liquid reward so that we could study voluntary sinusoidal movements of the head in the sagittal plane. Visual stimuli consist of a projected laser crosshair, spot, and line. A servo-controlled projector generated a green laser crosshair target which followed a sinusoidal vertical trajectory (0.1Hz, 0.25Hz, and 0.5Hz sine waves) during head-neck tracking runs so that the monkey could produce $\pm 20°$ range of pitch head tracking motion from the neutral posture. A red laser spot and line were projected from a light weight head-mounted laser pointer to provide the monkey with feedback regarding his head position. The laser line was used for checking the tilt of the monkey's head. Video-opaque markers were placed on C1, C2, C5 and C7 vertebrae, and intramuscular electrodes were implanted in twelve muscles of the neck. 30 Hz cine fluoroscopic images of head and cervical vertebral motion and electro-myographic responses were simultaneously collected as the monkey tracked the moving target with its head. A timer was used to synchronize the collection of movement video data and EMG data. Motion of the head was measured by 3 orthogonal angular velocity sensors (Watson Industries). Eight channels of rectified, low-pass filtered EMG data, the target position signal, and angular rate signals of the head were collected at 200 Hz on a Macintosh computer using custom data collecting software.

RESULTS AND DISCUSSION

Experimental results demonstrated that head and cervical vertebrae moved synchronously and that the vertebral movements were quite constant and showed primary movement about skull-C1 and C6-C7 joint axes during pitch motion (Table 1). The cervical spine and head led the input stimulus signal between 30° to 50°. Most of the muscles, lagged the input signal. SCM was consistently close to in-phase with the input signal (Figure 1). Muscle activation patterns varied considerably across the trials. Variability in muscle responses did not seem to affect the vertebral motion even though the muscles are the primary actuators of the joint movement. This result suggests that the central nervous system can choose multiple strategies to achieve a single movement. We are now examining the relationship between muscle activity patterns and the distribution of movement among the seven joints.

REFERENCES

Keshner, E.A. (1994). *Exp Brain Res*, **98**, 546-550.

Keshner E.A., Statler, K.D., Delp, S.L. (1995). *Exp. Brain Res*, **115**, 257-266

ACKNOWLEDGMENTS

Table 1: Angular excursion of head-neck segments with respect to C7 (mean±SD)

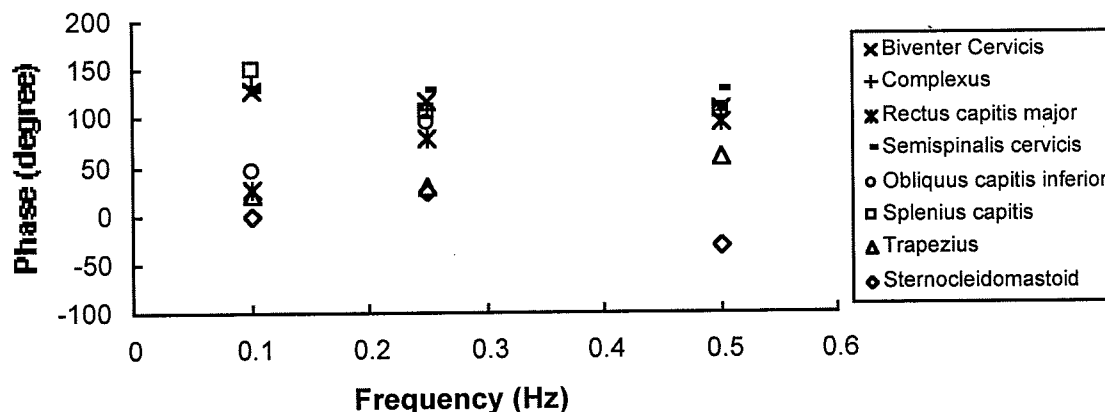|	0.1 Hz	0.25 Hz	0.5 Hz
Skull/C7	25.4±2.4	23.4±4.3	23.8±1.8
C1/C7	17.4±2.6	14.5±1.5	18.4±3.2
C2/C7	16.4±2.6	15.2±0.5	15.5±3.0
C3/C7	16.9±3.0	15.3±1.7	16.5±2.4
C4/C7	14.5±2.0	10.9±1.9	15.5±3.0
C5/C7	13.2±2.0	11.0±1.8	10.2±1.2
C6/C7	9.1±1.9	8.5±2.8	8.0±0.8

Figure 1: Plot of phases of selected muscles with respect to input simulating signal against head tracking frequencies. Data were averaged over five trials from at least three different days.

SUPPORT EFFECTS ON STANDING POSTURE

Cheryl A. Pattin [1], Amy T. Lehman [2], and Emily A. Keshner [1]

[1] Sensory Motor Performance Program,
Rehabilitation Institute of Chicago, Chicago, Illinois
[2] Northwestern University, Evanston, Illinois
Email: cheryl-ric@nwu.edu Web: http://www.smpp.nwu.edu

INTRODUCTION

Examination of postural sway using assistive supports is particularly important when attempting to enhance the balance of a clinical population. Postural stability has been measured in a variety of ways (e.g., sway area and anterior-posterior (AP) and medial-lateral (ML) sway), and tests have been performed both with the force plate under the cane and feet (Milczarek et al, 1993; Lu et al, 1997) and with the force plate under the feet only (Nandapalan et al, 1995; Maeda et al, 1998; Jeka, 1997). Enhanced support has been demonstrated by decreased postural sway in subjects stabilized with canes and from touch. Jeka and colleagues have conducted a large body of work on the efficacy of light touch (less than 1 N) to restore postural stability. He shows light touch to be comparable to force touch (with a higher contact force) in reducing postural sway measured by the ML center of pressure (COP) excursion (Jeka, 1997). We explore the question of how effective light touch is in reducing sway as the contact surfaces vary in stability. We hypothesize that light touch may prove less effective on a less stable surface.

PROCEDURES

The results reported here are from three healthy subjects. Tests were of thirty (30) seconds duration and were conducted using a 46 cm X 51 cm AMTI (model OR6-7) force plate. The sway variables measured in this study were: the sway area (the 95% confidence ellipse determined by BioSoft software from AMTI, Watertown, MA), COP path length, and AP and ML sway.

The first series consisted of trials with eyes open (EO) and eyes closed (EC) unsupported (US) and with support provided through the left hand using each of the following: 1) Regular single-point, swan-neck cane (LC) at the height of the wrist crease of each subject (WC) and 2) Standard quad, or four-footed cane (LQ) at WC. Tests using canes were conducted under both ON (feet and cane on the force plate) and OFF (feet only on the force plate, cane next to the force plate) conditions. Finally, a second set of US EO and EC tests were performed. Each test series was repeated twice to determine fatigue effects and repeatability.

A second series of tests was conducted with support provided OFF the force plate in all cases. Each subject performed the following tests under both EO and EC conditions: 1) Unsupported (US), 2) Standard one-point cane in the left hand (LC), 3) Standard quad cane in the left hand (LQ), 4) Large quad cane (feet spacing: 28 cm (AP) X 17 cm (ML)), or about 50% larger than a standard quad cane), 5) Walker providing ample stability gripped with the left hand (LW), and 6) Wall. Tests on each of the five mobility aids above (2-6) were performed both using natural touch (NT) and fingertip (or light) touch (LT). Finally, there was a

second set (EO and EC) of US tests. Both unsupported tests were averaged and used to normalize other support conditions.

RESULTS AND DISCUSSION

Our three subjects obtained varying levels of sway reduction from the regular single point cane (LC). Use of the single point cane by Subject 2 (s2) did not reduce sway area, AP or ML sway. Subjects 1 and 3 (with EO) showed decreased sway areas and decreases in AP and ML sway (but not sway path length); this finding was more obvious in the tests in which the cane was OFF the force plate and after repeated testing. All three of our subjects were able to decrease sway area and AP and ML sway with the quad cane. Results OFF the force plate showed a larger effect.

Although we tested our subjects with eyes open and closed, we found the ratio between these two conditions to be largely unaffected by the nature of the support provided (not significant using a paired t-test on the ratios of EC/EO for all tests on LQ or LXQ as opposed to the two tests (LW and Lwall) on stable objects. The percentage reduction in sway area is thus reported as the average over our three subjects of all 6 tests with EO or EC. Figure 1 shows a plot of this average percentage reduction for NT and LT (fingertip touch) under LQ, LXQ, LW, and Lwall support conditions. The mean sway area difference between the NT and LT tests was significant (p=0.026) when the support surface was a quad cane or an extended quad cane. This difference was not significant (p=0.08) when the support surface was stable, as in the LW and Lwall tests. This finding suggests that light touch may be modified by the support provided by the object being touched. If the object is not stable, as in the easily-tipped quad canes, the

subject may not be able to use haptic cues as effectively.
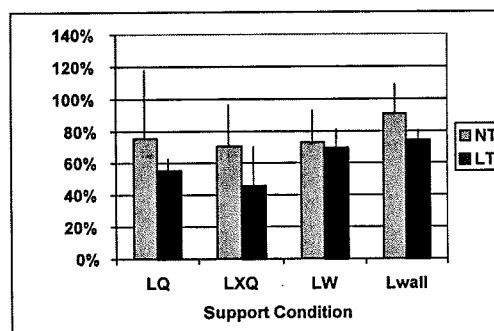
Figure 1: This figure shows the greater gap between NT and LT with the relatively unstable quad canes (LQ and LXQ) compared to (LW and Lwall).Error bars are one standard deviation above the average.

REFERENCES

Maeda, A., et al. (1998). "Body support effect on standing balance in the visually impaired elderly." *Archives of Phys. Med. & Rehab.,,*79, 994-7.
Milczarek, J. J., et al. (1993). "Standard and four-footed canes: their effect on the standing balance of patients with hemiparesis." *Archives of Phys. Med. & Rehab..,* **74**, 281-5.
Nandapalan, V., et al. (1995). "Objective measurement of the benefit of walking sticks in peripheral vestibular balance disorders, using the Sway Weigh balance platform." *J. Laryngology & Otology* **109**, 836-40.
Jeka, J. J. (1997). "Light touch contact as a balance aid." *Physical Therapy* **77**, 476-87.
Lu, C. L., et al. (1997). "Influences of cane length on the stability of stroke patients." *J. Rehab. Res. & Development,* **34**, 91-100.

ACKNOWLEDGEMENTS

EFFECTS OF DIFFERENT BASES OF SUPPORT ON POSTURAL SWAY

Mochizuki, L.[2], Duarte, M[2]., Zatsiorsky, V.M.[1], Amadio, A.C[2]., Latash, M.L.[1]
1 Department of Kinesiology , Pennsylvania State University, University Park, Pennsylvania
mll11@psu.edu
2 Department of Biodynamics of Human Movement, School of Physical Education and Sport,
University of Sao Paulo, Brazil
mochi@usp.br

INTRODUCTION. Human standing is characterized by spontaneous changes in the projection of the center of pressure (COP) commonly addressed as postural sway. The components of sway in the anterior-posterior direction, AP, or medio-lateral direction, ML, have been reported to be relatively independent. It has observed [1] that changes in the dimension of the support surface in one direction could affect stability when the other dimension of the support surface was much smaller and kept constant. These observations have suggested that AP and ML sways can become interdependent in conditions of postural instability. The aim of this study was to investigate changes in postural sway induced by manipulations of the dimensions of the supporting surface and presence of a light touch.

PROCEDURES. Ground reaction force and moments applied by each foot to force platform (Bertec, Inc.) were collected at 40 Hz during 40 s task, to calculate COP trajectory. A 12 bit AD converter was used. Then, those signals were low-pass filtered at 10Hz using a 2nd order Butterworth filter. The subjects were 9 healthy adults (32 ± 8 years old, 76 ± 10 kg weight, 1.80 ± 0.09 m height). They were instructed to stand as still as possible on three different unsteady boards with a narrow beam attached to the bottom and placed on the force plate. Those boards had the same dimension as the force plate. Each one had a rectangular supporting surface, which was 4.3 cm wide, and 8.6 cm, 17.2 cm or 50 cm long. During the trials, subjects stood on the top of each board

facing along the beam's axis (instability in the frontal plane) or perpendicular to that axis (instability in the sagittal plane). A light touch of the right index finger to a fixed surface placed at the subject's right side was used in half of the trials. The combination of those factors and normal standing with and without touch resulted in 14 different tasks performed. The following mean measurements were taken from COP for both AP and ML direction: maximum amplitude (*max*), standard deviation (*std*), mean velocity ($\bar{v}$), and excursion area (e-area) [2]. Statistical methods included repeated measures analysis of variance (ANOVA) with direction of instability and touch as factors.

RESULTS AND DISCUSSION. During normal standing, AP *std* was smaller than ML *std*; *max* and $\bar{v}$ were higher at AP-COP, and the use of light touch decreased *max* for both AP and ML directions. During standing on unstable boards, both *max* and $\bar{v}$ became much larger for ML than for AP direction. Besides, *std* had bigger values in AP direction than ML. Instability in the sagittal plane produced higher *std* than in the frontal plane. Those results point that, when an instability is added to a standing task, sway constrains may be changed, even when subjects are standing on a board whose support dimensions are much larger than typical sway characteristics.

The direction of instability (sagittal or frontal) did not influence the size of COP excursion area, but all means of other

variables in unstable conditions were bigger than in normal standing. During sagittal instability, *std*, *max* and $\bar{v}$ were bigger (p<0.02) than during frontal instability.

The addition of a light touch led to a decrease in e-area (p<0.03), but no changes in such indexes as *max* and *std* were observed. An interesting effect was observed: in no touch condition the excursion area in frontal instability was higher than during sagittal instability, but the inverse result was observed when the subjects were touching the support. The mean velocity increased with touch during instability conditions (sagittal instability had higher values than frontal instability, and $\bar{v}$ in AP direction was slower than in ML direction); on the other hand, the same variable was decreased during normal standing. The instability when the subjects were asked to stay as quiet as possible on different boards did not change *max* due to physical constraints: If the amplitude were increased in the direction of instability, COP could go beyond the boundaries of the support causing a fall. The increased $\bar{v}$ combined with the effect of touch during unstable conditions was probably reflective of a strategy used to reach a more stable equilibrium. An evidence for such an argument is the fact that the use of a light touch during normal standing decreased $\bar{v}$.

CONCLUSIONS. Postural instability during standing on unstable boards is a mechanical challenge that produces different patterns in COP, particularly increasing constraints in ML direction of sway. Frontal stability increased COP sway excursion and velocity more than for sagittal direction stability as compared to normal standing. The addition of touch decreased only the area of sway, but increased the mean COP velocity in postural instability, opposite to what was observed during normal standing.

REFERENCES.

[1] Aruin, A.S.; Forrest, W.R. Latash, M.L. (1998) Electroenceph Clin Neurophysiol, 109:305-359.

[2] Oliveira, L.F. Simpson, D.M. Nadal, J. (1996) Physiol Meas, 17:305-312.

THE MEASUREMENT OF TRUNK EXTERNAL FORCES AND MOMENTS DURING ISOMETRIC TRUNK MUSCLE EXERTIONS

C. Larivière[1], D. Gravel[2], D. Gagnon[3], J.-P. Dumas[1], M. Goyette[1], M. Leblanc[1],
A. B. Arsenault[2], P. Loisel[4], Y. Lepage[5]

[1] Research Center, Montreal Rehabilitation Institute, Montreal, Canada; [2] School of Rehabilitation & [5] Dept. of Mathematics and Statistics, University of Montreal; [3] Faculty of Physical Education and [4] Dept. of Surgery, University of Sherbrooke.
Email: bertrand.arsenault@umontreal.ca

INTRODUCTION

Spectral electromyographic (EMG) analysis is a modern approach to assess low back impairments such as fatigue. Even if it is recognized that load sharing between muscle groups (van Dieen et al., 1993) may impair the clinical interpretation of these measures, most studies have not controlled all the forces and moments generated by the subject during trunk exertions. To measure these forces and moments, a new static triaxial dynamometer based on a force platform was designed. The aim of this paper was to describe the external forces and moments recorded by the dynamometer for trunk efforts directed in different planes.

PROCEDURES

Description of the dynamometer: A triaxial force platform (Advanced Mechanical Technology Inc., model MC6-6-1000) was mounted on a steel frame allowing lower limb, pelvis, and thorax stabilization (Fig. 1A & B). The subjects stood in the dynamometer that measures the triaxial net loading at the L5/S1 joint. The thorax stabilization system was bolted on the force platform (Fig. 1B) and could be adjusted vertically at the shoulder level. The vertical lever arm of the system (Lz in Fig. 1A) was the difference between the L5/S1 joint and platform positions.

Subjects & Tasks: Fifteen males (Age: 32 ± 11 yr; Height: 1.77 ± 0.05 m; Weight: 74 ± 12 kg) with no back problems participated to the study. To obtain a reference target value for the ramp contractions, a single 5 s static maximal voluntary contraction (MVC) was obtained about each anatomical axis (flexion, extension, lateral bending and axial rotation on both sides). After a 10 min. rest, three 7 s static ramp contractions from 0 to 100% MVC were performed in all

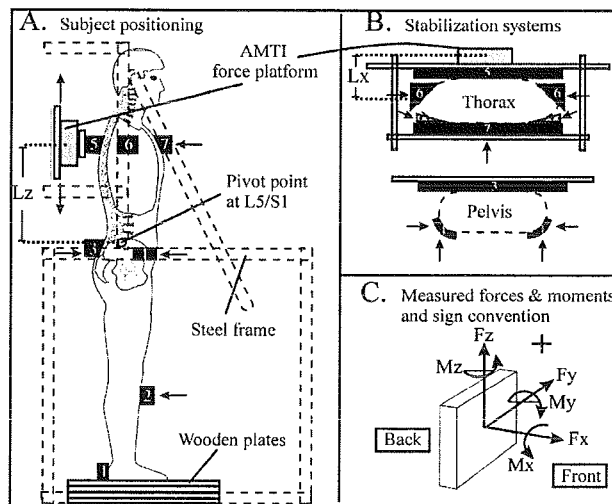Fig. 1. Illustration of the dynamometer. Adjustable elements (platform and pads) in A and B are depicted by arrows.

directions. Based on a free-body diagram analysis of the forces and moments applied to the force platform (Fig. 1C), L5/S1 moments were calculated to provide one real time visual feedback moment (tolerance = ±10%) during the ramp contractions in each specific effort direction. The order of

contractions was counterbalanced for both MVC and ramp contractions. A 90 s rest period was given between efforts.

Data analysis: Because external forces depend on the absolute moment values generated at L5/S1, a similar moment level was selected on each ramp (80% of the highest moment calculated). At this level, external forces and moments were averaged across the 3 trials.

RESULTS AND DISCUSSION

The highest L5/S1 moment ($\pm$SD) values in flexion, extension, and lateral bending to the left and to the right reached 170 ± 33, -243 ± 57, -152 ± 44, and 157 ± 38 Nm respectively (mean Lz value: 35.6 ± 2.9 cm). These values are similar to those reported in the literature (Gravel et al., 1997). The results in axial rotation are not reported because the algorithm used to generate the visual feedback moment at L5/S1 was erroneous. Work is in progress to solve this problem.

In the table, the values appear in bold characters with the corresponding sign when forces and moments were in the same direction for all subjects. In the other cases, average absolute values are given with the standard deviation.

During flexion and extension, large Fx forces were observed in the expected direction. The Fy and Fz forces were low but, due to the fact that these forces were applied at a distance from the

surface of the force platform, they are partly responsible for the external moments Mz and My respectively.

During lateral bending, high forces were measured along the y axis. At the same time, consistent Mz moments were observed. The latter result can be largely explained by the effect of the Fy forces that were applied on the lateral pads with a lever arm Lx (Fig. 1B) of about 19 cm. Moderate forces were also recorded along the x axis.

SUMMARY

In summary, the results revealed that complex forces and moments are generated during trunk exertions. They can be explained by the design of the dynamometer and/or by the coupled L5/S1 moment exerted by the subject in other directions than the main attempted effort (Parnianpour et al., 1991).

REFERENCES

Gravel et al. (1997). *Clin. Biomech.*, **12**, 314-324
Parnianpour et al. (1991). *Int. J. Indust. Ergonomics*, **8**, 279-287
van Dieen et al. (1993). *Eur. J. Appl. Physiol.*, **66**, 70-75.

ACKNOWLEDGEMENTS

Table. Force platform measures at 80% of the highest L5/S1 moment [mean (SD)]

Direction of effort	Fx (N)	Fy (N)	Fz (N)	Mx (Nm)	My (Nm)	Mz (Nm)
1. Flexion	**396 (89)**	19 (21)	46 (42)	2 (1)	15 (15)	13 (10)
2. Extension	**-549 (103)**	34 (29)	21 (19)	4 (3)	6 (5)	10 (8)
3. Left lateral bending	166 (122)	**356 (63)**	55 (32)	10 (7)	14 (12)	**91 (24)**
4. Right lateral bending	161 (100)	**-353 (74)**	62 (42)	10 (9)	14 (11)	**-102 (26)**

KINEMATIC ANALYSIS OF THE CERVICAL SPINE

James T. Brumley II[1], Richard D. Komistek[1], A. Alexander M. Jones[1], Mary E. Hajner[1]

[1]Rose Musculoskeletal Research Laboratory, Denver, Colorado
Email: jbrumley@rmmrl.org

INTRODUCTION

Neck pain can be debilitating, significantly reducing a patient's range of motion and his/her ability to perform normal neck motions. Degeneration of the intervertebral disks is found to be one of the major factors leading to severe neck pain. Commonly, the lower levels of the cervical spine are susceptible to disc degeneration. It has been hypothesized that the fusion process, while successful, may change the normal motion patterns of the cervical spine. Previous kinematic studies on the human spine have been conducted under in vitro conditions, but recently fluoroscopy has been used on other joints to determine in vivo kinematics (Dennis et al, 1996; Dennis et al, 1998; Komistek et al, 1998). This study focuses on the determination of the in vivo cervical spine kinematics during active neck flexion.

PROCEDURES

Six subjects (two normal cervical spines, two degenerative cervical spines, and two 2-level fused cervical spines) were analyzed under fluoroscopic surveillance. The subjects having a fused spine were fused at the C5-C6 and C6-C7 levels. Both two-level fusion cases were deemed successful by the surgeon who performed the surgery. Fluoroscopic images were downloaded directly to a workstation computer to maintain the high resolution of each image. Each patient was analyzed at ten various increments of spinal flexion/extension (Figure1).
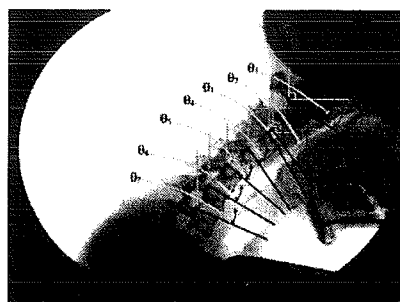

Figure.1 Digitization Method

These images where analyzed using a two-dimensional digitization technique (Komistek, et al, 1998). During the digitization process constant points on each of the seven cervical spine vertebrae were tracked throughout the range of motion. The points were analyzed to determine the rotation angle of each individual vertebra. The rotation of each vertebra relative to the subsequent vertebra was plotted with respect to time and the data was curve-fit to obtain a temporal function that represented the motion pattern. Using a mathematical model, the relative velocities were obtained and used to determine the partial angular and linear velocities. These velocities lead to the determination of generalized speeds and relative interaction forces (Komistek, et al, 1998). Subjects having similar cervical spine conditions were compared to each other. Once this comparison was made, subjects having different cervical spine conditions were then compared against each other.

RESULTS AND DISCUSSION

As hypothesized, motion patterns varied between the normal, degenerative, and fused cervical spines. Normal cervical spines showed a smooth, arc like motion depicting proper function of the articulating surfaces (Figure 2). In contrast, degenerative cervical
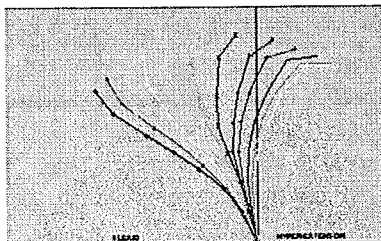

Figure.2 Normal Spine Motions

spines demonstrated inconsistent motion patterns especially at the C5, C6, and C7 vertebrae (location of the degeneration) (Figure 3).
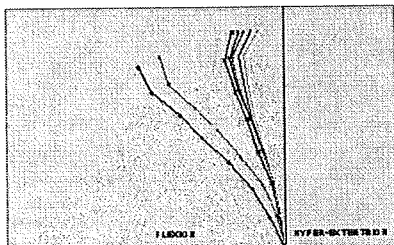

Figure.3 Degenerative Spine Motions

It should be noted that both of the degenerative patients expressed extreme levels of pain. This pain could be one of the factors contributing to the inconsistent motion.
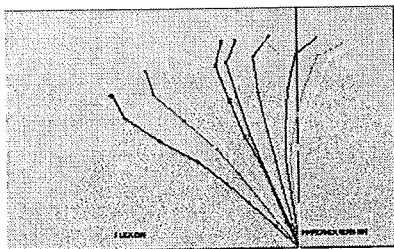

Figure. 4 Fused Spine Motion

The two-level fusion patients demonstrated similar motion patterns to those of the

normal patients except in the C5-C6 and C6-C7 levels (Figure 4). No motion was observed between the fused vertebrae, but there were variations at the C4-C5 level (level above fusion). Using the angular motion data, the relative angular velocities demonstrated significant differences between the normal, degenerative and fused subjects. As hypothesized, the subjects having a fused spine experienced a significant change in the relative angular velocities above the fused joint, which may lead to an increase in the reaction force at this joint.

SUMMARY

This present study has shown that fluoroscopy can be used to determine the in vivo motions of the cervical spine. This analysis determined that there is a significant difference in the normal cervical spine motion compared to a degenerative or fused cervical spine. Quite possibly, this change in motion may lead to increased forces at the articulate, degenerative disk, which may attribute to cervical disk failure. Further work needs to be conducted before a definitive conclusion can be made. Therefore, our future work will include the analysis of more subjects, and the determination of the 3D cervical spine kinematics using our previously accepted 3D model-fitting software package.

REFERENCES

Dennis, et al, (1996). *Clin Orthop*, 107-117.

Dennis, et al, (1998). *Clin Orthop*, 47-57.

Komistek, et al. (1998). *Clin Biomech*, (in print).

Komistek, et al. (1998). *J Biomech*, 185-189.

FORCES ON THE SPINE DURING A FALL IN WHICH TORSO MUSCLES ARE ACTIVE

Sara E. Wilson[1] and Elizabeth R. Myers[2]

[1] Orthopedic Biomechanics Laboratory,
Beth Israel Deaconess Medical Center, Boston, MA
[2] Hospital for Special Surgery, New York, N.Y.
Email: sew@obl.bidmc.harvard.edu

INTRODUCTION

Studies of vertebral fracture patients have shown that 30 to 50 percent of these patients associate a fall with their fracture (Cooper, 1992, Myers, 1996). Previous work has examined the forces on the spine during the impact phase of a backwards fall in order to estimate risk of fracture (Wilson, 1998). These models have, however, only examined passive falls. Muscle forces could potentially increase the forces applied to the spine during impact.

Other models of the dynamics of the torso musculature have examined the issues of stability in the spine (Cholewicki, 1997, Gardner-Morse, 1998, Crisco, 1991, Bergmark, 1989). These efforts used a linear relation of the muscle stiffness to active muscle tension proposed by Morgan (1977). This relation has, however, not been assessed adequately for the torso musculature (Crisco, 1991).

Our research question was: What are the effects of muscle tension and associated stiffness on the predicted forces on the spine during an impact from a backwards fall? Several tension-stiffness relations were examined to assess the sensitivity of these predictions to the muscle model used.

PROCEDURES

Previously developed, one and two-dimensional models of the impact phase of a backwards fall were used as the base model for this analysis (Wilson, 1998) (Fig. 1). The models contain masses representing the upper body, pelvis, and abdominal mass and parallel spring-dashpot pairs representing the spine, pelvis soft tissue, and abdominal contents. These models have been validated against literature vibration experiments in which volunteers sat on vibrating platforms, and the transmission of vibration was measured (Panjabi, 1986). Two muscle tension springs were added to these models (Fig. 1). These springs, which represent the abdominal wall and erector spinae musculature, were placed 11.24 cm anterior and 5.32 cm posterior to the spine. The models were run with initial equal tensions of 0 to 1500 N.
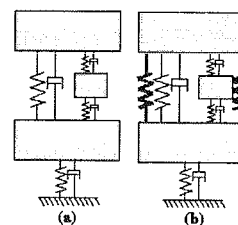

Figure 1. One-dimensional model of the impact phase of a fall (a) Muscle stiffness (b) was added by adding variable stiffness springs.

The tension-stiffness proportionality constant was varied from 50 to 250 (Cholewicki (1997) used 150). Stiffness was assigned based on the initial tension and was assumed to remain constant during the impact.

RESULTS AND DISCUSSION

In the one-dimensional model, the axial spine force peaked at about 0.05s into the impact and then settled to a compression value equal to the total muscle tension (Fig. 2).
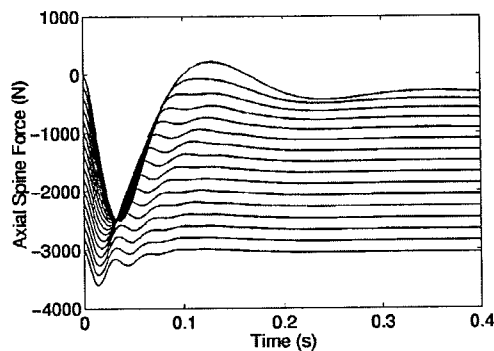

Figure 2. Axial spine element compression as a function of time (stiffness function K = 150 F). Uppermost line represents no muscle tension, the lowest line, tensions of 1500 N in both muscle groups.
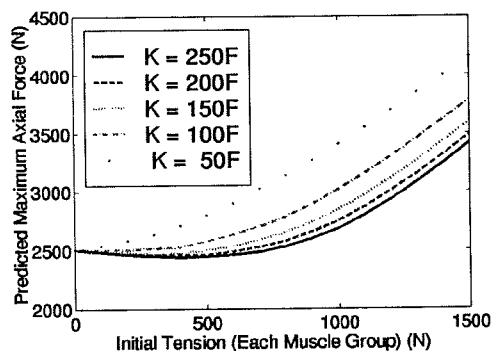

Figure 3. Peak spine compression force exhibits a toe-region that changes for different muscle tension-stiffness relations.

The peak axial spine force did not change with initial muscle tension for low muscle tensions but increased proportionally to the total muscle tensions at high muscle tensions (Figure 3). This initial toe-region varied depending on which tension-stiffness relation was used.

SUMMARY

The peak spine compression force was shown to increase from 2500 N to as much as 4000 N. This can be compared to the average elderly cadaveric vertebra failure force of approximately 2000 N (Myers, 1996). Muscle tension in the torso could, therefore, increase fracture risk. The actual force values depend on the tension-stiffness relation used. This relation needs to be studied further.

REFERENCES

Bergmark, A. (1989). *Acta Orthop. Scand.*, 230S(60), 1-54.
Cholewicki, J. et al. (1997). *Spine*, 22(19), 2207-2212.
Cooper, C.C. et al. (1992*). J. Bone Min. Res.*, 7(2), 221-227.
Crisco, J.J, Panjabi, M.M. (1991), *Spine*, 16(7), 793-799.
Gardner-Morse, M.G., Stokes, I.A.F.. *Spine*, 23(1), 86-92.
Myers, E.R., Wilson, S.E. (1996). *Spine*, 22(24S), 25S-31S, 1997.
Panjabi, M.M. et al. (1986). *J. Bone Jnt. Surg.*, 68-A(4), 695-702.
Wilson, S.E., Myers, E.R. (1998). *Proceedings of the PreORS Symp. on Comp. Methods in Orthop. Biomech.*

ACKNOWLEDGEMENTS

The Study of Adhesive Properties of Hepatocellular Carcinoma Cells to Collagen Type I

Xian-hang Wang[1] Mian Long[2] Ze-zhi Wu[2] Shao-xi Cai[2] Yun-peng Wu[2]

[1] Huawei Technology C.O. Ltd.
[2] Bioengineering Center , Chongqing University , Chongqing
Email: wangxianhang@huawei.com.cn or Email: xrzeng@cqu.edu.cn

1. INTRODUCTION

Malignant tumors are a serious disease about human health and life. The clinical treatment about malignant tumors is one of difficult medical problems all over the world. The present work focuses on the hepatic tumor invasion and metastasis in clinical treatment, and select the hepatocytes(HTCs) or hepatocellular carcinoma cells (HCCs) as study objects firstly. The studies about adhesive properties of HCCs to one of main components of liver—collagen type I are little[1,2]. The main aim is at finding out a satisfactory experimental method , so as quantitatively to discuss the adhesive property of hepatocytes or HCCs to collagen type I. A micropipette aspiration technique that is a very mature biomechnical experimental technique[3] was employed to investigate the adhesive properties of hepatocellular carcinoma cells (HCCs) to collagen type I , based on the isolation and primary culture of hepatocytes(HTCs) and the culture of HCCs . This investigation suggested a quantitative analysis methodology for the metastasis of hepatocellular carcinoma .

2. EXPERIMENTAL METHOD

The paper developed a new, a simple, low cost, and rapid method for the isolation and purification and cultivation of primary human liver sinusoidal endothelial cells (LECs) and hepatic parenchymal cells. The two cells were isolated by collagenase IV perfusion of the liver, and separated by speed gradient centrifugal method. After getting liver, it was possible to insert the plastic tube further in the portal vein without rupture of the vessel. The inferior vena cava beneath the liver was immediately cut and preperfusion started with 37° balanced salt solution . About 50ml of balanced salt solution was flushed repeatedly through the liver at a flow rate of 10ml/minute, during which the inferior vena cava above the liver was ligated with a clamp. Directly after the preperfusion , 40ml of 37° collagenase solution was pumped repeatedly through the liver at a flow rate of 5ml/minute. After 20 minutes, the cell suspension was then filtered through nylon gauze to remove undigested tissue. The cell suspension was centrifuged at 50g for 3 minutes to isolate most of parenchymal cells in the bottom of pipette. After washing and purification of parenchymal cells at 50g, its can be inoculated in culture dish[4]. The supernatant enriched in sinusoidal cells was then centrifuged for 10 minutes at 500g. The pellet was resuspended and centrifuged alternately for 5 minutes at 50g or 500g, in order to purify the liver sinusoidal cells. After inoculation of LECs suspension for 2 hours, inoculated supernatant again to remove Kupffer's cells. In the meantime, the problem of the anchorage of LECs in a chamber using PDL and collagen type I was solved.

The collagen type I-coated technology is described firstly in this paper. The matrix was coated with PDL(Poly-D-lysine), collagen type I and BSA(Bovine Serum albumin). Firstly, 200 µl of PDL(2µg/ml) was perfused in the marked circle area of chamber to help collagen type I adhesion to substrate. After incubation for 30 minutes, remove PDL solution from chamber. PBS solution wash chamber twice. Secondly, 200 µl of collagen type I solution was perfused in same area of chamber. After incubation for 40 minutes, remove collagen type I solution from chamber. The 200 µl of 0.5% BSA solution was perfused in same area for filling a vacant position after collagen type I-coated. After incubation for 15 minutes, it was washed by PBS solution and put on the stage for experiment. The coated method was tested and verified about methodology at same time and presented that collagen type I was the most important role. The paper researched the adhesive properties of hepatocytes or HCCs to PDL, collagen type I and BSA. The result denoted that PDL and BSA would benefit collagen type I-coated process. We developed one quantitative method to measure the adhesive property of HCCs or hepatocytes to collagen type I-coated surface based on cell culture technology and micropipette aspiration technology. The cells were inoculate in chamber with collagen type I. The chamber was incubated for 30 minutes in 37° incubator. After 30 minutes, it was put on the

37° stage. Regulate the microscope so as to focus on the cells. Remove manipulator in order that the micropipette appeared in field of microscope vision. The pressure system produced negative pressure to grasp a cell. We increase the negative pressure to remove a cell critically from bottom of chamber and record the pressure value.

3. RESULTS AND DISCUSSION

Cell-substrate adhesive model is showed in Fig.1. Different diameter of micropipette and cells will produce different relative adhesive stress. We defined the relative adhesive force(RAF) Fa and relative adhesive stress(RAS) Sa in Fig.1 in order to compare the changes of RAF or RAS for different experimental groups.

$$Fa = \Delta P * \cos\theta * \pi R_p^2 \quad (1)$$

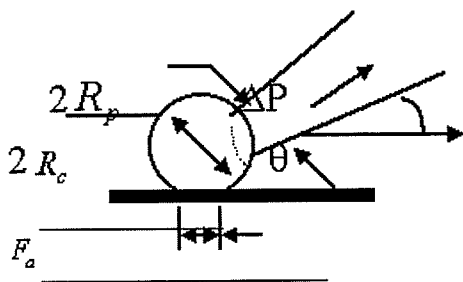$$Sa = \Delta P * \cos\theta * (R_p/R_a)^2 \quad (2)$$

Fig. 1 Geometry of adhesive model

Changed the pressure value to critical value and analyzed the data with mathematical statistics theory and equation (1) or (2). In the meantime, we will research the dependence of adhesive duration(0-59min, 60-89min, 90-120 min) and collagen type I concentration(1μg/ml, 2μg/ml, 5μg/ml) for experimental groups adhesion to collagen type I. Fig.2 and Fig.3 show the experimental results of adhesive duration and collagen type I concentration dependence of RAS.
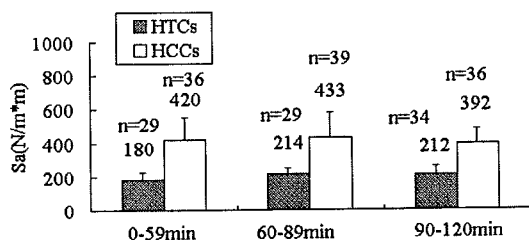
PDL:2μg/ml ,collagenI: 1μg/ml , 0.5%BSA , n:sample number

Fig.2 Adhesive duration dependence of relative adhesive stress.
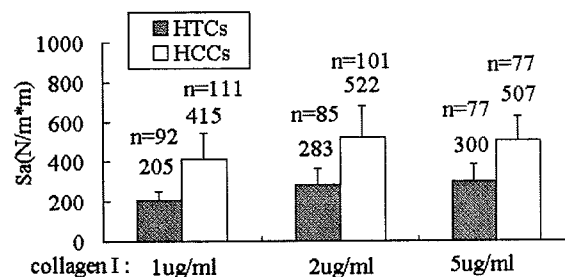
0-120min , PDL: 2μg/ml , 0.5%BSA , n : sample number

Fig. 3 Collagen type I concentration dependence of relative adhesive stress.

The experimental results that were dealt with mathematics method presented that the normal hepatocellular carcinoma cells showed stronger relative adhesive force and relative adhesive stress in contrast to hepatocytes under every time duration or concentration. The time and density dependence of HCCs showed that the relative stress or force would increase to the saturation value with increasing of time and density. The relative force and stress of HCCs decreased after increase with time increase, and showed different adhesive properties during invasion and metastasis process. Therefore we obtained a new view about adhesive properties of HCCs to collagen type I using quantitative mechanics method. The results will benefit to explain some questions on biomechanical views about how the HCCs peeled off primary position and how the HCCs invaded to secondary position.

4. CONCLUSION

The adhesive experimental results presented show that relative adhesive stress of HCCs is so stronger than HTCs that HCCs could adhere to tissues or cells around it as well as possible. It will provide better condition for HCCs crawling , spreading and infiltrative growth during cancer invasion or metastasis. The conclusion could give a better theory basement for clinical medicine treatment.

REFERENCES

[1] Okuda. K. "Hepatocellular carcinoma: Recent progress." Hepatology , 1590(5) : 948-963 (1992)

[2] R. Hughes, S. C. Stamataglou "Adhesive interaction and the metabolic activity of hepatocyte." J.Cell Sci. Supply. 8,273-291(1987)

[3] M. Long, X. H. Wang et al.:"Experimental investigation on viscoelasticity of hepatocytes" ACTA Biophysica Sinica, Vol12, No.1 (1996)

[4] Braet. F. et al. "Assessment of a method of isolation, purification, and cultivation of rat liver sinusoidal endothelial cells.": Lab. invest. Vol.70 No.6 : 944, (1994)

A MULTI-FREQUENCY SPECTROMETER FOR FAST ASSESSMENT OF THE DYNAMIC PROPERTIES OF CARTILAGE EXPLANTS

Chih-Tung Chen [†], John E. Bertram [§], Jennifer Wurster [†],
Nancy I. Burton-Wurster [†], and George Lust [†]
[†] James A. Baker Institute for Animal Health and [§] Department of Anatomy,
Cornell College of Veterinary Medicine, Cornell University, Ithaca, NY, 14853
Email: cc116@cornell.edu   Web: bakerinstitute.vet.cornell.edu

INTRODUCTION

The ability of cartilage to transmit or withstand loads depends on the integrity of its extracellular matrix (Grodzinsky, 1983; Mow et al., 1984). This ability is commonly defined by its dynamic stiffness and phase-shift (Frank and Grodzinsky, 1987). The spectra of dynamic characteristics provide useful insights into matrix integrity and its resistance to damage (Ishihara et al., 1992).

Traditional testing using single harmonic waveform to determine the dynamic properties of cartilage (Frank and Grodzinsky, 1987; Schmidt et al., 1990) was a time-consuming procedure. With a multi-frequency waveform, the total testing time, and thus risk of contamination, can be significantly reduced. Benefiting from modern DAQ technique, we designed a spectrometer using the multi-frequency waveform (0.1-200 Hz) as an input for fast assessing the dynamic properties of normal and degenerative cartilage.

MATERIALS AND METHODS

Normal cartilage was excised from the skeletally mature humeral joint with a 4 mm biopsy punch. Cartilage disks was subjected to repetitive impacts 5MPa of at 0.3 Hz with 30% loading cycle for 120min (previously described in Farquhar et al., 1996). Cartilage with osteoarthritic lesion was obtained from two-year-old canine dysplastic hips.

A spectrometer was designed to characterize the matrix changes in the a wide spectrum of frequencies (0.1-200 Hz). System consisted of amplifier, signal conditioning system, electrodynamic vibrator, and a specially designed loading frame (Fig. 1) with resolution of 0.2μm and 0.01N. Facilitated with inboard control, this spectrometer was capable to test tissue with multiple frequencies or user-defined waveforms. Load control and post-testing analyses were achieved with a commercially available programmable software, LabVIEW 4.1 (National Instruments), operating on a Power Macintosh 8100/80 computer.

Explant was subjected to a multi-frequency (0.1-200Hz) diagnosis waveform. The total diagnosis time was less than 30 sec to minimize possible loading stimulation. The maximum stress, 0.1 MPa, was within the linear region of stress-strain curve. Dynamic moduli and phase-shift at each frequency were calculated from the responding stress and strain after decomposition with fast Fourier Transform. Compositional analyses included water content, hypotonic swelling, and glycosaminoglycan content (via DMMB assay). Non-paired Student's t-test was perform to determine the statistical significance ($P<0.05$).

RESULTS

Results were highly repeatable ($R^2>99\%$) and consistent with single harmonic loads ($R^2>95\%$). Dynamic properties of degenerative tissues were found to be significantly different from normal tissues. Phase-shift of injured explant was increased by 0.6-1.1° while the dynamic stiffness (30%) was decreased (Fig. 2). Phase-shift of OA lesion had higher increases (4.1-1.3°), and dynamic moduli were decreased 76%. A hypotonic swelling (4.6%), increase of water content (9.2%), and decrease of GAG content (Fig 3) were found in the OA tissues. But, the hypotonic swelling and GAG content of impact-injured cartilage was not significantly different from normal.

DISCUSSIONS

This study showed that using the multiple frequency waveform as an input significantly

reduce the total time of testing, and thus the risk of contamination. This technique can potentially be applied to a servo-hydraulic system. Degenerative cartilage showed the low dynamic moduli and high phase-shifts that were consistent with compositional analyses. Since the maximum stress was in the linear region of strain-stress curve, the viscoelastic effect was minimal and decomposition was in good approximation (Fung, 1993). This spectrometer is also small enough to operate inside an incubator, thus can monitor the progression of dynamic properties of *in vitro* injured cartilage.

ACKNOWLEDGEMENTS

REFERECNCES

Farquhar, T. et al., (1996). J. Ortho. Res. 14, 417-423.

Fung, Y.C. (1993). Biomechanics. New York, Springer-Verlag press.

Frank, E. and Grodzinsky, A. J., (1987). J. Biomech. 20, 439-447.

Grodzinsky, A. J. (1983). CRC Rev. Biomed. Eng. 9, 133-199.

Ishihara, H. et al. (1992). Spine 17, S7-S12.

Mow, V. C. et al. (1984). J. Biomech. 17, 377-394.

Schmidt, M. B. et al., (1990). J. Ortho. Res. 8, 353-363.

Fig. 2 The dynamic stiffness of normal and degenerative cartilage at 0.1-200 Hz

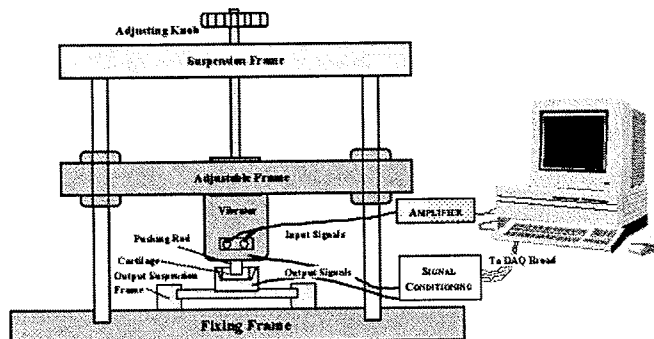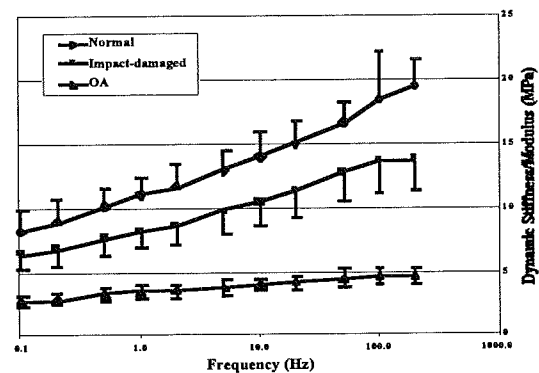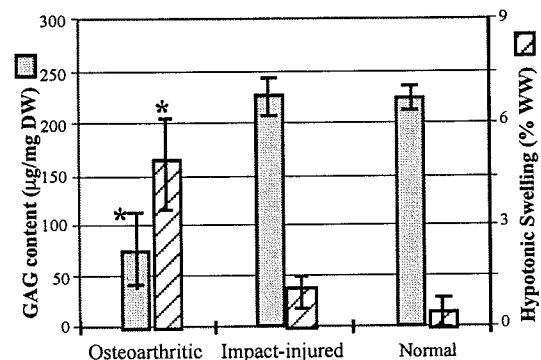Fig. 3 GAG content and hypotonic swelling of normal and degenerated cartilage

Fig. 1 A diagram of the spectrometer consisting amplifier, signal conditioning, electrodynamic vibreator, and a specially designed loading frame.

NECROSIS FOLLOWED BY APOPTOSIS IN ARTICULAR CARTILAGE AFTER REPETITIVE IMPACTS

Chih-Tung Chen, Nancy I. Burton-Wurster, Caroline Borden, and George Lust
James A. Baker Institute for Animal Health, Cornell University, Ithaca, NY, 14853
Email: cc116@cornell.edu   Web: bakerinstitute.vet.cornell.edu

INTRODUCTION

Reductions in cartilage collagen/GAG deposition and in chondrocyte numbers (Burton-Wurster *et al.*, 1982) are hallmarks of osteoarthritis (OA). A recent study (Blanco *et al.*, 1998) suggests these changes in OA lesions are closely related to *in situ* apoptosis. Apoptosis (cell suicide) is characterized by chromatin condensation, DNA fragmentation, and budded cell membranes. This contrasts with necrosis, another type of cell death (cell murder), characterized by ruptured cell membranes and swollen nuclei, (Majno and Joris, 1995; DeFrancesco, 1999).

Excessive loading occurs in unstable joints. *In vitro* cartilage studies show that excessive load/impact can produce structural damage and OA–like changes including tissue swelling (Borelli, *et al.*, 1997; Farquhar *et al.*, 1996), increased collagen denaturation (Chen *et al.*, 1999) and reduced GAG synthesis (Farquhar *et al.*, 1996). It is important to know 1) if cell death occurs in impact-damaged cartilage; 2) the relationship between cell death and the severity of impact damage; and 3) the mode of cell death. Recently, apoptosis (Leoning *et al.* 1999) was shown in excessive sinusoidal loaded cartilage. We hypothesized that impact damage also would induce apoptosis in cartilage explants and that the number of dead cells would increase with the severity of injury.

MATERIALS AND METHODS

Cartilage: Normal cartilage was excised from the canine humeral joint with a 4 mm biopsy punch. Damage to normal cartilage was induced by 5MPa cyclic impacts at 0.3 Hz with a 30% loading cycle for 2, 20, or 120min (described in Chen *et al.*, 1999), and incubated for 4, 48 or 144hr. Necrosis was induced in cartilage by four freeze (liquid N_2) / thaw cycles. Apoptosis was induced by treatment with 50µg/ml mitomycin C (MMC) for 48hrs. Cartilage with OA lesions was obtained from 2-year-old canine dysplastic hips.

Cell Viability: Necrosis in normal, loaded, and freeze/thawed cartilage was evaluated less than 2hr post treatment by uptake of the cell membrane impermeable dye, propidium iodide (PI). The cellular hydrolysis activity dye, fluorescein diacetate (FDA), was used to assess the cell viability. The (live) explants were immersed in 40µg/ml PI and 1µM FDA for 5min before being sliced into ~200µm and viewed with a fluorescent microscope.

TUNEL and Nucleus Morphology Assay: To determine DNA fragmentation, explants were cryo-embedded in OCT and then cut into 6mm sections. The sections were then immobilized onto glass slides, air-dried, fixed, and stained with TUNEL assay (Boehringer-Mannheim, Indianpolis, IN) for DNA nicking. Since the cell membrane was compromised after TUNEL assay, the total numbers of nuclei could be determined by counter-staining with 50µg/ml PI. Fluorescence of TUNEL and PI was captured using a CCD camera. The percentage of TUNEL+ (v.s. PI+) cells was analyzed using NIH image 1.62. The adjacent slide was stained with 0.2mM Hoechst dye (#33342) for 5 min, and viewed with a fluorescent microscope at 1000x to determine the morphology of the nucleus.

Biosynthesis and Statistical Analysis: GAG synthesis in explants was measured via a 4 hr radiolabel with 40µC/ml S^{35}-sulfate. Sample was then digested with papain to determine the total DNA (flurometric assay) and GAG content (DMMB assay). The GAG synthesis in live cells was determined by normalizing to the percentage of live (non-TUNEL+) cells. Non-paired Student's t-test was performed to determine the statistical significance ($P < 0.05$).

RESULTS

When incubated for just 4 hours post loading, only a few cells in the superficial zone and fracture site of cartilage loaded for 120min were TUNEL+. But, after 48hr of incubation, TUNEL+ cells were seen in all regions (Fig. 1). TUNEL+ cells were also found in the superficial and middle zones of 2 and 20min-loaded cartilage after 48hr of incubation (Fig. 1). The percentage of TUNEL+ cells increased from 7.8% to 73.4% when the duration of loading increased from 2 to 120min. No further increase in TUNEL+ cells in loaded explants occurred between 48hr and 144hr of incubation post loading. Eighty-eight percent

of cells in a freeze/thawed cartilage after 48hrs of incubation and 28% of cells in an OA lesion (Fig. 2a) were also TUNEL+. The GAG synthesis (normalized to live cells) of loaded explants was consistently increased (Fig. 2b).

Vital stains showed that 32.4±8.3% cells in 120min-loaded cartilage and all cells in freeze/thawed cartilage were (PI+/FDA-) necrotic (Fig. 3a). Hoechst dye showed swollen nuclei in all regions of freeze/thawed explants (Fig. 3b) and many condensed and fragmented nuclei in the middle and deep zones of MMC–treated and 120min-loaded cartilage (Fig. 3c, d).

DISCUSSIONS

Although the TUNEL assay has been reported to be specific to apoptotic cells (Gold et al., 1995), at least in the early stage, in this study we found that the TUNEL assay also stained necrotic cells in freeze/thawed cartilage as evidenced by cell vital stains and swollen nuclei. To avoid false-positives in the TUNEL assay, a second independent method (nuclear morphology, cell vital stain, and DNA ladder) should be used (DeFrancesco, 1999). Since by vital staining and nuclear morphology, 40% of dead cells in the loaded tissue were necrotic, we reject our hypothesis. But, some cells in the deep zone of the loaded explant after 48hrs of incubation were TUNEL+ and showed clear features of apoptosis (nuclear fragmentation). This result indicates repetitive impacts induce necrosis (PI+/FDA-) followed by apoptosis in damaged cartilage. The percentage of dead cells increases with the severity of impact-injury. Work is in progress to determine the relative contribution of necrosis and/or apoptosis to characteristics of OA lesions.

REFERECNCES

Blanco, M et al. (1998) Arthitis Rheum 41, 284-298.
Borelli, J. et al., (1997). J Ortho Taum. 11, 319-326.
Burton-Wurster N. I. et al. (1982). Biochim Biophys Acta, 718, 74-84.
Chen, C.-T. et al. (1999) J Orthop Res (accepted).
DeFrancesco, L. (1999). The Scientist, Mar 1, 17-19.
Farquhar, T. et al, (1996). J Orthop Res 14, 417-423.
Gold et al. (1995). Lab. Invest. 71, 219-225.
Majno, G. and Joris, I. (1995). Am J Path 146, 3-15.
Loening, A.M. et al. (1999) Trans. of ORS, 45, 42.

ACKNOWLEDGEMENTS
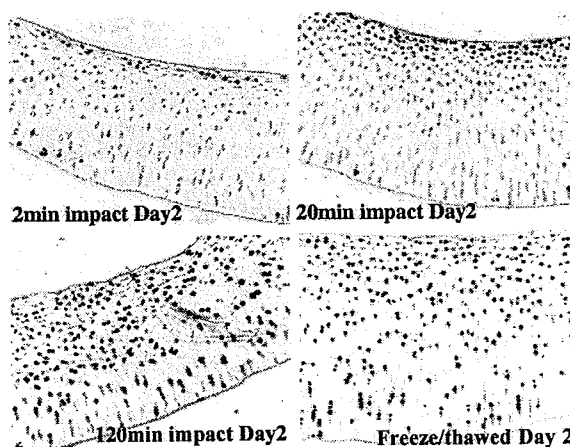
Fig. 1 Florescence of TUNEL (in black) was overlapped with a phase-contrast image. TUNEL+ cells were found in the superficial and middle zones of 2, 20min-loaded cartilage, and in all regions of 120min-loaded and freeze/thawed cartilage after 48hr of incubation.
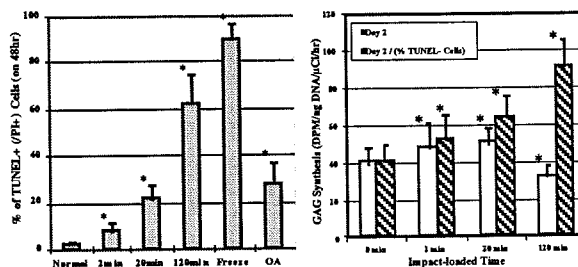
Fig. 2 (a) Increased TUNEL+ (/PI+) cells with the severity of impact damage; (b) Increase of GAG synthesis in (Day 2) impact-loaded cartilage.
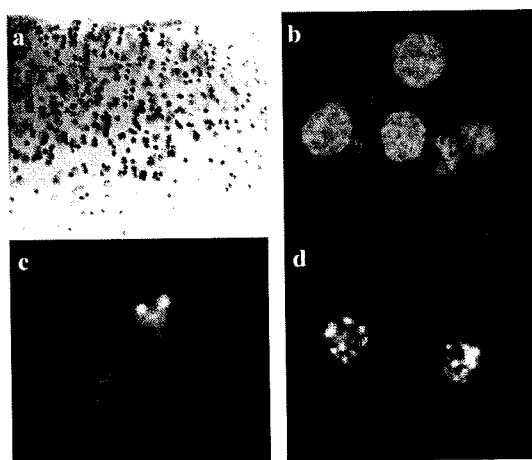
Fig. 3 (a) Membrane-impermeable dye, PI, stains cells in the live 120min-loaded explant. Fluorescence (1000X) of Hoechst dye shows (b) swollen nuclei in freeze/thawed cartilage and condensed and fragmented nuclei in (c) 50 µg/ml (48hr) MMC-treated cartilage as well as in (d) 120min-loaded cartilage (48, 144hr).

FAST BUT NOT SLOW ANKLE ROTATIONS MODIFY STRESS-RELAXATION OF ACTIVE SKELETAL MUSCLE

Mark E. T. Willems and William T. Stauber

Department of Physiology, West Virginia University, Morgantown, West Virginia
Email: willems@wvnvms.wvnet.edu

INTRODUCTION

Stretch-shorten cycles of skeletal muscles are common during human and animal movements. Following a stretch of active muscles without joint movement, muscle force decays with time (i.e. stress-relaxation) (Cook and McDonagh, 1995). Stretches of active muscles can cause injury which could alter the biomechanics of skeletal muscles to repeated stretches. The purpose of this study was to examine stress-relaxation following repeated active stretches of plantar flexor muscles during velocity-controlled ankle rotations.

PROCEDURES

Female Sprague Dawley rats (n = 6, body mass 265 ± 5 g) were positioned with flexed knee (1.57 rad) and the left foot pressing on an aluminum plate connected to a custom-built dynamometer (Cutlip et al., 1997). Plantar-flexor muscles were stimulated via a cuff electrode around the tibial nerve (200 µs width pulse; 80 Hz, 5.4 ± 0.3 V) and force was measured under the sole of the foot. The muscles were preloaded by an isometric contraction and stretched repeatedly (30) by dorsiflexion of the foot (range of motion 0.70–1.57 rad) with 0.87 rad•s^{-1} (slow stretch) or 10.47 rad•s^{-1} (fast stretch). Rest periods between contractions were 3 minutes to minimize effects of fatigue. For both velocities, stress-relaxation was analyzed for the first 300 ms following each stretch. The decay in force output

between F_{peak} (i.e. force at the end of the stretch) and $F_{post300}$ (i.e. force at 300 ms during stress-relaxation) was fit to the exponential equation, $F = A + B exp [-C(t-t_{peak})]$ ($r^2 = 0.98 \pm 0.02$), where F is the force, t is the time where force values between F_{peak} and $F_{post300}$ were reached, t_{peak} the time where F_{peak} was reached, and A, B and C are constants. C is the time-constant of force decay during stress-relaxation.

RESULTS AND DISCUSSION

Force recordings of plantar flexor muscles during the 1th and 30th contraction with slow stretches are shown in Fig. 1. Force reached a peak at the end of the movement [i.e. at the end of the active stretch (F_{peak}, Fig. 1)].
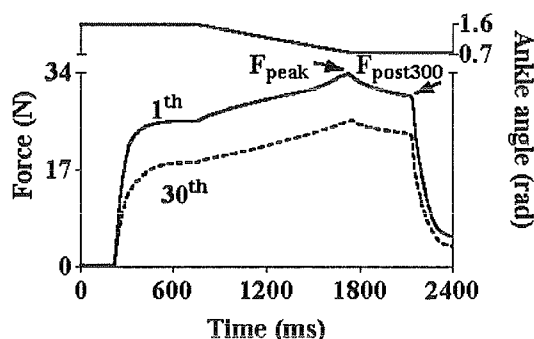

Fig. 1. Typical example of the force during the 1th (solid line) and 30th (broken line) contraction with slow ankle rotation. F_{peak}, and $F_{post300}$ represent the highest force during the stretch and the force 300ms following the stretch (arrows). Upper trace is a recording of the force-plate position (i.e. ankle angle) of the dynamometer.

Following the movement there was a non-linear decay of force with time (i.e. stress-relaxation). Repeated slow- and fast movements decreased the total force output of plantar flexor muscles measured by the isometric force preceding each stretch. The time-constant of force decay, normalized with respect to the time-constant for the first contraction in each series of slow and fast movements, decreased with fast but not with slow stretches (Fig. 2) (ANOVA, $P < 0.05$), indicating an increased stress-relaxation following fast stretches (i.e. increased relative capability of producing force).
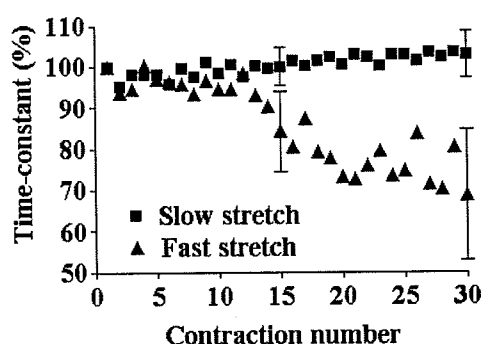

Fig. 2. The time-constant of force decay plotted as a function of contraction number for slow (■) and fast (▲) stretches. The time-constants of force decay were normalized with respect to the time-constant in the first contraction in each series of slow and fast stretches. For clarity, only SE's of contraction numbers 15 and 30 are plotted.

Morgan (1990) proposed that during active stretches a non-uniform distribution of sarcomere lengths develops likely influenced by the stretch velocity– very slow stretches could result in a more uniform distribution of sarcomere lengths. Non-uniform sarcomeres readjust their lengths during stress-relaxation, some becoming shorter and others elongating further. If the sarcomeres were uniformly distributed, the readjustment is expected to be small. If heterogeneity exists, then the readjustment could lead to some sarcomeres being pulled

further apart by the sarcomeres with greater filament overlap and resulting in an increasing force as the shortening sarcomeres move closer to optimal filament overlap. Based on this line of reasoning, the fast stretches in our study probably produced greater sarcomere heterogeneity than slow stretches with a greater population of sarcomeres with filament overlap closer to optimal overlap.

SUMMARY

Repeated fast but not slow stretches of plantar flexor muscles by dorsiflexion of the foot in intact rat produced a smaller decline in stress-relaxation. Injury, defined as an increase in sarcomere heterogeneity which develops from stretching active muscles (Morgan, 1990), may be inferred from a decrease in the time-constant for skeletal muscle stress-relaxation. The use of intact muscle tendon units under nerve stimulation to study muscle injury revealed that the unit behaves much like individual isolated muscles and relevant biomechanical information can be obtained.

REFERENCES

Cook, C.S., McDonagh, M.J. (1995). *Exp. Physiol.* **80**, 477-490.

Cutlip, R.G. et al. (1997). *Med. Biol. Eng. Comput.* **35**, 540-543.

Morgan, D.L. (1990). *Biophys. J.* **57**, 209-221.

ACKNOWLEDGEMENTS

PREDICTION OF TISSUE DIFFERENTIATION DURING
FRACTURE HEALING – INFLUENCE OF MECHANICAL LOADING

Damien Lacroix and Patrick J. Prendergast

Department of Mechanical Engineering, Trinity College, Dublin 2, Ireland
Email: pprender@tcd.ie   Web: http://www.mme.tcd.ie/Groups/Bioengineering

INTRODUCTION

After fracture of a long bone, there is initially an inflammation phase followed by periosteal lifting leading to formation of a callus filled by granulation tissue. The callus is invaded by Mesenchymal Stem Cells (MSCs). Mechanical stimuli sensitise these cells so that they will differentiate into either fibroblasts, chondrocytes or osteoblasts. After several months, the integrity and strength of the bone is restored. The success of healing is partly controlled by the mechanical loading. Perren and Cordey (1980) proposed the "interfragmentary strain theory" which stated that strains below 2% were required for bone formation.

The aim of this study was to develop a numerical model based on the concept that strain of the collagenous phase and fluid velocity of the interstitial fluid phase mechanically regulate tissue differentiation (Prendergast et al., 1996), see Fig. 1.
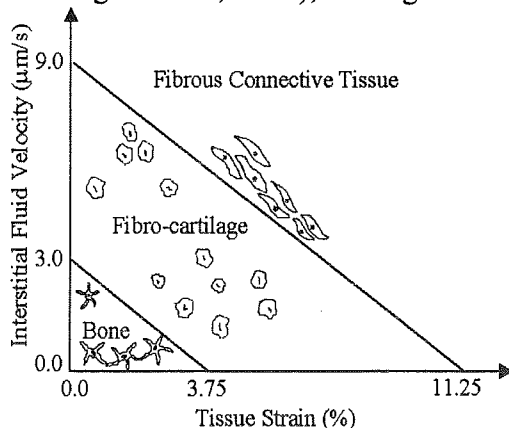
Fig. 1: Mechano-regulation diagram regulating the differentiation of cells.

METHODS AND MATERIALS

An osteotomy of a long bone was analysed using an axisymmetric finite element model (Fig. 2). All tissues were modelled as biphasic tissues (Table 1). A cyclic axial displacement was applied on the cortical bone (see inset of Fig. 2). Two loading magnitudes were investigated: 500 N and 700 N. The proliferation of MSCs in the granulation tissue was modelled as a diffusion process over a typical healing period of 16 weeks. Three origins for the cells were investigated: (1) from the surrounding tissues, (2) from the inner cambial layer of the periosteum, (3) from the marrow, see Fig. 2. Cells were capable of differentiating depending on two mechanical stimuli: octahedral shear strain and fluid velocity (Fig. 1). Material properties were updated every iteration.
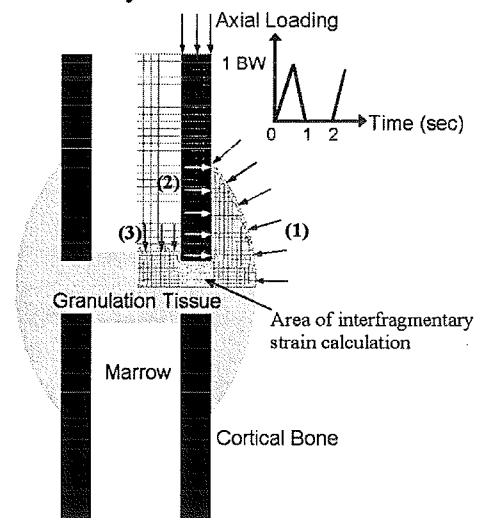
Fig. 2: Axisymmetric model with boundary conditions. (1), (2), (3) describe the three Mesenchymal Stem Cell sources.

Table 1: Biphasic material properties

	Cortical Bone	Marrow	Granula-tion Tissue	Fibrous Tissue	Fibro-cartilage	Woven Bone
Young's modulus (MPa)	4590	2	1	2	10	300
Permeability (m^4/Ns)	3.7E-13	1E-14	1E-14	1E-14	5E-15	3.7E-13
Poisson's ratio	0.30	0.47	0.47	0.47	0.47	0.30

RESULTS

It is predicted that the healing pattern and timing differ greatly depending where the MSCs originate. For case (1), cells differentiate into bone in the external callus first, forming a bridge at the lateral side of the callus as ossification progresses between bone ends. In case (2), a similar differentiation occurs. However, bridging occurs closer to bone ends without full ossification of the external callus. In case (3), an internal callus is predicted but proliferation is very slow in the external callus.

Fig. 3 shows the average interfragmentary shear strain (area indicated in Fig. 2). It is predicted that strain reduces over time as tissue stiffens. However, the strain depends on the source of the cells and on the loading applied. With 500N loading, an initial 15% strain is predicted and reduces greatly to 2% in 38 days when cells originate from the

Fig. 3: Average interfragmentary strain over time for the three different sources of cells and for 500N and 700N loading.

surrounding tissues or from the cortex. However, when cells originate from the marrow, strain decreases similarly in the first 20 days but more slowly thereafter to reach a strain of 5% after 16 weeks. At 700N loading, strain is much higher and does not decrease as fast as with 500N loading. This shows a delay in healing with higher loads. The strain after 16 weeks is about 8% for cells originating from the surrounding tissues or cortex while strain is about 14% when cells originate from the marrow.

DISCUSSION AND CONCLUSION

This study predicts that a loading of 500N leads to a bony healing with a strain of 2%, while a loading of 700N gives too high a strain for bone to form in 16 weeks. The mechanical loading has thus a major influence on the healing timing.
In this study, a model to predict tissue differentiation over time during fracture healing was proposed. The model incorporated the origins and migration of cells, which is revealed as being essential in predicting the healing pattern.

REFERENCES

Perren SM and Cordey J (1980) In *Current Concept of Internal Fixation of Fractures, Uhthoff (ed)*. Berlin, Springer-Verlag. pp 63-77
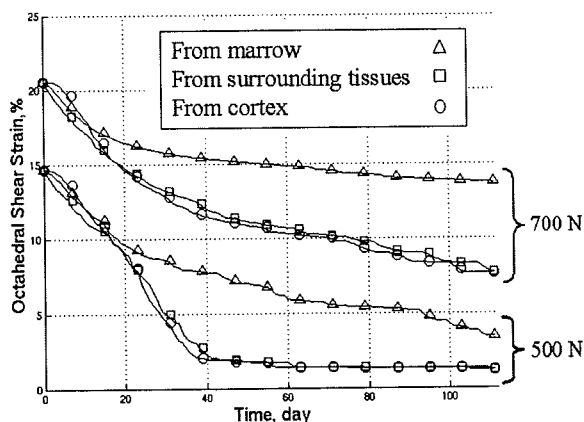
Prendergast PJ *et al.* (1996) *J. Biomech.*, 30, 539-548

THE QUASI-LINEAR VISCOELASTIC PROPERTIES OF THE HEALING GOAT MEDIAL COLLATERAL LIGAMENT: AN EXPERIMENTAL & ANALYTICAL APPROACH

Steven D. Abramowitch, Theodore D. Clineff, John D. Withrow,
Christos D. Papageorgiou, Savio L-Y. Woo

Musculoskeletal Research Center, Department of Orthopaedic Surgery
University of Pittsburgh, P.O. Box 71199, Pittsburgh, PA 15213, (412) 648-2000
Email: ddecenzo@uoi.upmc.pitt.edu   Web: www.ortho.pitt.edu

INTRODUCTION
Knowledge of the time and history dependent viscoelastic properties of healing ligamentous tissue should add insight to the quality, rate, and completeness of the healing process. The objective of this study was to use a combined experimental and analytical approach to characterize the viscoelastic properties of the healing goat MCL at 6 and 12 weeks. The quasi-linear viscoelastic theory (QLV) of Fung (2) was used in this study.

MATERIALS AND METHODS
A mop-end tear was created in the right MCL of 12 skeletally mature Saanen breed female goats (44.9 ± 9.6 Kg). The left knee was sham-operated and served as a control. Post-operatively, the goats were allowed free cage activity. Six animals each were humanely euthanized at 6 and 12 weeks. The hind limbs were disarticulated and dissected of all soft-tissue structures except the MCL, leaving a femur-MCL-tibia complex (FMTC). Using a laser micrometer system, the cross-sectional area of the MCL was measured (6). Each FMTC was then mounted onto customized clamps in an Instron testing machine and tested in a saline bath at 32° C. A cyclic preconditioning test of 20 cycles from 0-1 mm, was followed by a stress relaxation test by elongating the FMTC to 3 mm ($\neq 5\%$ strain) and held for 20 minutes. An analysis of variance was performed using one within factor (Exp. vs. Con.) and one between factor (6 vs. 12 weeks) with significance set at $p < 0.05$.

The QLV theory assumes the stress relaxation to be:

$$\sigma[\varepsilon(t);t] = G(t) * \sigma^e(\varepsilon) \quad G(0)=1 \quad (1)$$

where σ^e is the *elastic response* and $G(t)$ is the *reduced relaxation function*. Using Fung's generalized relaxation function based on the assumption of a continuous relaxation spectrum (2),

$$G(t) = \frac{[1 + C\{E_1(t/\tau_2) - E_1(t/\tau_1)\}]}{[1 + C * Ln(\tau_2/\tau_1)]} \quad (2)$$

where E_1 is the exponential integral and, C, τ_1 and τ_2 are constants with $\tau_1 \ll \tau_2$. Experimental data obtain from a static stress relaxation test satisfies three boundary conditions,

$$\frac{\_G(t)}{\_t} = k_1, \quad G(\_) = k_2, \quad \text{and} \quad G(t_0) = 1 \quad (3)$$

where k_1 and k_2 are constants. Thus, parameters C, τ_1, and τ_2 could be determined using a nonlinear regression analysis for each specimen.

RESULTS
For both experimental groups, an enlarged tissue mass was noticeable at the injury site, while controls appeared white and well-defined. The cross-sectional area of the

healing tissue was 1.7 times larger than controls at 12 weeks (p<0.05). The constants describing the *reduced relaxation function* (mean ± SD) for the control and healing groups are shown in Table 1. C was significantly larger than the control for the 12 week group. Additionally, significant differences between the two experimental groups existed only for τ_2. The percentage of stress relaxation for both experimental groups was significantly greater than their control values (Fig. 1). Similarly, the modulus of G(t) for both experimental groups was significantly less than their control values (Fig. 2).
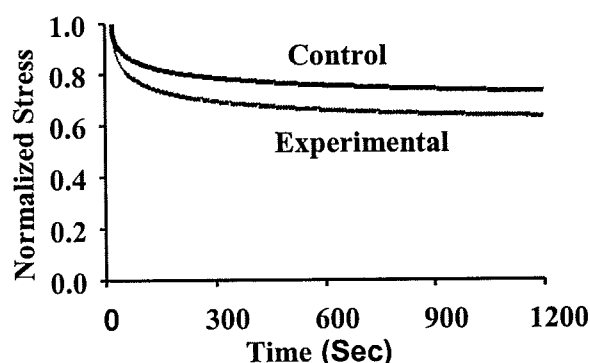

Figure 1. Stress relaxation data for a typical pair of knees at 12 weeks. Data normalized to peak stresses.

DISCUSSION

Our data reveals that the healing MCLs at 6 and 12 weeks are more viscous than the controls, i.e. values of C (4). Therefore, the healing MCL should dissipate more energy and have a longer recovery time upon

removal of load, possibly due to an increase in glycosaminoglycans (GAGs) (5). Further, the 6 weeks healing tissue has a greater initial rate of relaxation than its control, i.e. values of τ_1. The lack of significant change between 6 and 12 weeks suggests that only minimal improvement occurred in the healing process, also suggesting that the remodeling process of healing ligamentous tissue may take an extended period of time.
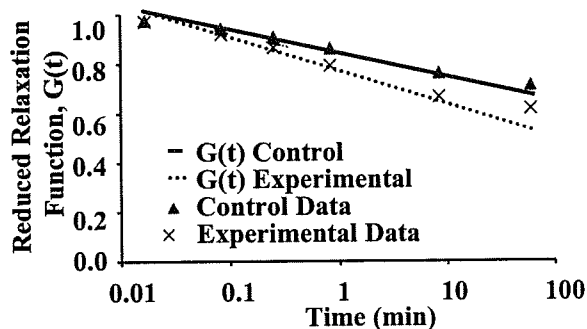
Figure 2. Experimental and analytical data of the reduced relaxation function for a typical pair of knees at 12 weeks.

REFERENCES
1. Chimich, et al., 1991, *JOR*, **9**: 37-47.
2. Fung, 1972, *Biomechanics: Its Foundations and Objectives*, 181-208.
3. Woo, et al., 1983, *JBME*, **109**:68-71
4. Sauren, et al., 1983, *JBME*, **105**: 92-95
5. Chimich, et al., 1992, *JBME*, **25**: 831-37
6. Woo, et al., 1990, *JBME*, **112**: 426- 4

Table 1. Parameters describing the viscoelastic behavior (n=12) of the experimental and control groups.

	6 WEEK EXP.	6 WEEK CON.	12 WEEK EXP.	12 WEEK CON.
C	0.254 ± 0.21	0.073 ± 0.02	$0.185 \pm 0.10^*$	0.062 ± 0.02
τ_1	$4.0 \pm 0.9^*$	3.0 ± 0.8	3.4 ± 0.8	3.5 ± 0.9
τ_2	$9.06 \pm 7.57(10^3)$	$13.1 \pm 22.7(10^3)$	$1.6 \pm 0.6(10^3)\dagger$	$2.59 \pm 3.04(10^4)$
$\partial G(t)/\partial \ln(t)$	$-0.078 \pm 0.015^*$	-0.046 ± 0.008	$-0.073 \pm 0.014^*$	-0.041 ± 0.013
Relaxation (%)	$47.0 \pm 8.5^*$	29.1 ± 5.5	$47.1 \pm 11.6^*$	25.1 ± 7.4

MECHANICAL STRENGTH CHANGES OF RABBIT PATELLAR TENDONS AFTER INJECTION OF AUTOLOGOUS BLOOD AND SALINE

[1]Mark A. Taylor, [1]Nina B. Clovis, [1,2]Timothy L. Norman, [1]J. David Blaha, [1]William R. Post
[1]Musculoskeletal Research Center, Department of Orthopedics, West Virginia University, Morgantown, West Virginia
[2]Department of Mechanical and Aerospace Engineering, West Virginia University, Morgantown, West Virginia
Email: tayfam@aol.com

INTRODUCTION

Inflammatory tendinopathy (tendonitis) is a common and often self-limiting disorder. However, sometimes the tendon will develop an area of chronic degeneration that does not heal rapidly (tendonosis). There are multiple factors that cause tendonosis (Astrom and Westlin, 1994; Leadbetter, 1992). Decreased blood supply is believed to play a role in the development of these disorders (Myerson and Biddinger, 1995). There are potent chemical factors in blood that can stimulate vascular ingrowth (Knighton et al., 1982; Pettet et al., 1996) and fibroblast activity (Arnoczky et al., 1988; Iyer et al., 1999). It is possible that injection of autologous blood can help stimulate a healing response in chronic tendon disorders. However, there are no known reliable animal models for chronic tendonosis (Backman et al., 1990; Leadbetter, 1989). This study is designed to assess the mechanical strength changes of normal rabbit tendon tissue to injected autologous blood and saline.

PROCEDURES

Adult post-breeding New Zealand white rabbits were used. In Series I, there were three groups: one control (N=7) and two test groups, six week (N=18) and 12 week (N=18). The test groups had 0.15 cc of autologous blood injected into the left patellar tendon and 0.15 cc of saline injected into the right patellar tendon. In the test groups, 13 specimens were randomly selected for mechanical testing and five for latex vascular injection and tissue clearing. In Series II, only the left tendon was injected. The right was used for control. Mechanical tests were performed on a Materials Testing System. The tendon strengths were then compared using two-tailed student t-tests.

RESULTS AND DISCUSSION

In Series I, we found at six weeks, the patellar tendon strength after injection with blood showed no statistical difference compared to the control group or the saline injection side (Table 1). At 12 weeks, both the saline and the blood injected tendons showed increased strength (p>0.001) compared to controls. However, the difference between the blood and saline injection groups was not significant. In Series II, there was no significant increase in strength at 6 weeks (Table 2). At 12 weeks the blood injected left was increased significantly compared to the untreated right.

Surgical intervention for chronic tendinosis may have the benefit of direct debridement of damaged tissue (Organ et al., 1997). However, some surgical procedures, such as longitudinal tenotomy, are aimed at trying to stimulate a healing neovascular response without tissue debridement (Maffulli et al., 1997). While not exposing the patient to surgery, there are two mechanisms by which

injecting blood may benefit a chronic, poorly healing tendon lesion. Blood clot stimulated new vascular ingrowth and fibrocyte activity (Knighton et al., 1982) and there is growing interest in the use of growth factors in promoting fibrous tissue healing. In this study, we found that saline injections alone caused significant increase in strength of the patellar tendon at three months. We speculate this is due to local tissue disruption and bleeding that stimulated a healing response. However, this increase was not as statistically significant as with the injection of blood. In Series I, some of the increased strength may be related to growth of the rabbits during the study. Series II controlled for this variable by using a matched untreated tendon to compare. No ill effects from the injection of tendons with autologous blood were noted. We found that the strength of patellar tendon complex at six weeks after treatments was not compromised by the procedure and at 12 weeks was significantly increased by 15% (Series II) to 27% (Series I).

SUMMARY

We found, in two different series, that 12 weeks after the injection of blood, the mechanical strength of rabbit patellar tendons significantly increased. In Series I, the increase was 27%. In Series II the increase was 15%. In this animal model, there were no complications to the injections.

REFERENCES
Astrom M, Westlin N (1994). *Clin. Orthop.* **308**, 166,172.
Leadbetter WB (1992). *Clin. Sports Med.* **11**, 533-578.
Myerson MS and Biddinger K (1995). *Physic. Sports Med.* **23**, 47-54.
Knighton DR et al. (1982). *Ann. Surg.* **196**, 379-387.
Pettet G et al. (1996). *Proc. R. Soc. Long. B.* **263**, 1487-1493.
Arnoczky SP et al. (1988). *J. Bone Joint Surg.* **70A**, 1209-1216.
Iyer VR et al. (1999). *Science* **283**, 83-87.
Backman C et al. (1990). *J. Orthop. Res.* **8**, 541-547.
Leadbetter WB (1989). *Sports Induced Inflammation.* American Academy of Orthopedic Surgeons, Park Ridge, IL.
Organ SW et al. (1997). *Am. J. Sports Med.* **25**, 746-750.
Maffulli N et al. (1997). *Am. J. Sports Med.* **25**, 835-840.

Table 1: Summary Series I Structural Properties of the Patella-Patellar Tendon-Tibia Complexes *Statistically significant difference from control (p<0.05)

Property	Control	6 wk Rt (saline)	6 wk Lt (blood)	12 wk Rt (saline)	12 wk Lt (blood)
Number	14	13	13	13	13
Strength (N)	649.6(±109)	649.7(±107)	698.5 (±115)	*801 (±61)	*824 (±79)
Stiffness (N/mm)	173(±33)	168(±26)	164(±18)	160(±23)	154(±24)

Table 2: Summary Series II Structural Properties of the Patella-Patellar Tendon-Tibia Complexes *Statistically significant difference from control (p<0.05)

Property	6 WEEKS (N=10)		12 WEEKS (N=11)	
	Rt (Control)	Lt (Blood)	Rt (Control)	Lt (Blood)
Strength (N)	701(±146)	734(±115)	642(±106)	*741(±98)
Stiffness (N/mm)	177(±23)	193(±21)	185(±33)	198(±25)

A METHOD FOR THE DESIGN OF HEEL CUSHIONING INSOLES

Jess G. Snedeker[1,2] and Peter R. Cavanagh[1,3,4]
[1]The Center for Locomotion Studies, [2]Bioengineering Program, and [3]Departments of
Kinesiology and Biobehavioral Health, Penn State University, University Park, PA
[4]Departments of Medicine, and Orthopaedics and Rehabilitation, Penn State University,
Hershey, PA
Email: celos@psu.edu Web: www.celos.psu.edu

INTRODUCTION

Shoe insoles with specialized heel components are often intended to supplement the inherent shock absorbency of the heel pad and the shoe during the early support phase of gait and/or to relieve focal heel pain. Little quantitative information is available to aid in the design of such devices and this study presents a method by which the heel cushioning element can be appropriately positioned to match the loading environment.

REVIEW

While a number of authors have assessed the mechanical properties of insole materials (Brodsky et al.,1988; Garcia et al.,1994; Sanfillipo et al., 1992, Sanders et al., 1998) few studies have been concerned with the efficacy and appropriate design of insole components to provide rearfoot cushioning (Gardner et al.,1988, Jones et al.,1999). Heel pain represents a significant proportion of orthopaedic complaints for which medical attention is sought (Lutter, 1986) and many over-the-counter devices are sold to provide relief. Although it is a complex and multifaceted syndrome, one design requirement for such devices is that the location of the cushioning material should match the regions of high pressure. The present study describes a method to facilitate this approach.

METHODS

Plantar pressures during walking at 1 ($\pm$ 0.05) m.s^{-1} were collected at 30 Hz using an optical pedobarograph (Baltimore Therapeutic). Seven right foot contacts in 6 young symptom free subjects (mean age 26.7 $\pm$ 5.5 yrs) with arch indices 0.21< A.I. < .26 (Cavanagh and Rodgers, 1987) were collected. Prior to data collection, unobtrusive markers (11mm OD x 1.2mm thick washers) were securely fixed with adhesive tape to the plantar surface of the foot under the first and fifth metatarsal heads.

A footprint from each subject was recorded using ink and paper, and the foot position in relation to a commercially available insole component was determined. The footprints and insole outlines were digitized using NIH Image and the location of the markers on the footprint and the pressure distribution plot (apparent as a small low pressure region corresponding to the center of the washer) allowed registration of the foot print, the insole outline, and the pressure distribution. Using MATLAB 5.2, the various images were imported, filtered, aligned, scaled and then overlaid.

Pressure distribution was plotted for each available frame in relation to the foot and insole geometry along the midline of the foot (midpoint of the heel to the second toe) based on a reference frame in units of % shoe length (%SL) with its origin at the most posterior point of the insole that was the appropriate size for each subject.

This approach is, of course, based on the assumption that the pressure distribution during barefoot walking on a rigid surface can be used as a first approximation of a template for modifications to be made inside a shoe.

RESULTS

The mean peak rearfoot pressure was 506 ± 61 kPa. The AP location of peak rearfoot pressure in relation to foot length (SL) was remarkably consistent between individuals and occurred at 10.3% ± 1.2% SL. The anterior migration of the pressure distribution along midline of the foot can be seen in the typical plot shown in Fig 1. It is notable that the location of peak pressure moves initially forward and then dwells in a region of approximately 10 % SL for a considerable period of time. During this period, there is typically a broad plateau of high pressure which extends well beyond the distal margin of the cushioning element.

DISCUSSION

The insole examined in this study is typical of many commercially available devices that are intended to improve comfort and alleviate pain in the heel. While the present study does not address the issue of focal heel pain, the application of the proposed measurement technique does demonstrate that there are regions of the rearfoot that are subjected to relatively high pressures but that receive no additional "cushioning" from the insoles examined.
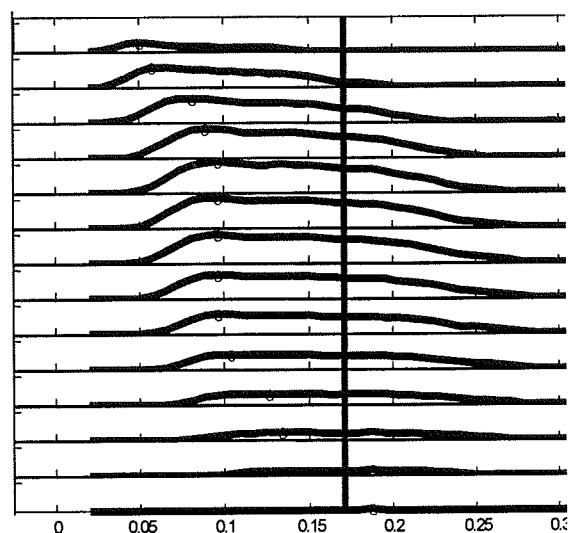

Figure 1. Successive pressure distributions for a typical subject along the midline of the foot at each 33 ms during heel contact. The peak pressure is shown as a small circle and the solid vertical line is the anterior extent of the cushioning element. The x axis is in units of SL.

REFERENCES

Brodsky, J.W.,Kourosh,S.,Stills,M. et al. (1988) *Foot Ankle Int.* 9(3), 111-116
Cavanagh, P.R. and Rodgers, M.M. (1987) *J Biomechanics* 20, 547- 51.
Garcia, A.C.,Dura,J.V.,Ramiro,J.,et al. (1994) *Foot Ankle Int.* 15(6), 311-323
Gardner, L.I. Jr., Dzadios, J.E., Jones, B.H., et al. (1988) *Am J Public Health* 78(12), 1563-1567
Jones, B.H.,Knapik,J.J., (1999) *Sports Med* 27(2), 111-125
Lutter, L.D.
Sanders, J.E. et al.(1998)*J. Rehab. R&D.,*35, 161-176
(1981) *Am J Sports Med* 14, 481-485.
Sanfillipo, P.B.,Stess,R.M.,Moss,K.M. (1992) *J.Am.Podiatric Med.*

ACKNOWLEDGMENTS

ACCURACY OF MONITORING PEAK FORCE AND TEMPORAL PARAMETERS OF GAIT USING A CAPACITANCE INSOLE SYSTEM

Susan M. Bowley[1], Gregory A. Breit[2], and Robert T. Whalen[1]

[1]Musculoskeletal Biomechanics Laboratory, NASA Ames Research Center, Moffett Field, California
[2]Qualcomm, Inc., San Diego, California
Email: sbowley@mail.arc.nasa.gov   Web: george.arc.nasa.gov/~rwhalen

INTRODUCTION

The NASA GRF Activity Monitor is used to autonomously measure vertical ground reaction forces (GRFz) in human subjects during normal daily activity (Whalen et al., 1993; Breit and Whalen, 1994). The capacitance insole sensor (E.Q., Inc.) has measurement errors during dynamic human activity loading. Bowley et al., 1998 described a non-linear calibration method to correct for these errors. The objective of this study was to examine accuracy of the activity monitor in measuring peak GRFz during walking and running following non-linear corrections. A second objective was to determine accuracy in measuring contact time (tc) and stride period (T) with the activity monitor.

PROCEDURES

Twenty-three human subjects (12 females, Average Age = 42.6 ± 13.3 yrs; 11 males, Average Age = 40.4 ± 11.5 yrs) were asked to perform a series of walking (Range: 0.637 to 2.58 m/s) and running (Range: 1.43 to 6.71 m/s) gait cycles at a range of speeds. Tests were done over a calibrated force plate (AMTI) mounted outdoors and flush with a sidewalk. This study was approved by the NASA Ames Research Center Institutional Review Board.

Subjects wore the NASA GRF Activity Monitor during gait testing, with the capacitance insole sensor in their right shoe. No control was made for the type of shoe each individual wore, although most wore tennis shoes. The insole sensor was calibrated using our non-linear calibration method prior to performing the walking and running cycles (Bowley et al., 1998).

The NASA GRF Activity Monitor containing onboard sampling and filtering algorithms (Breit et al., 1994) was carried in a fanny pack. Sampling rate for the activity monitor was 100Hz and 200Hz for the force plate. Force plate and activity monitoring data were collected autonomously. Data between monitoring systems were synchronized by the time of occurrence of a single body weight (BW) measurement event at the start of testing. Ground contact was determined from a threshold of 10% BW at initial footfall and 20% BW at lift-off on the falling edge. Impulse momentum equations were used to estimate T from force plate data.

RESULTS

The filtered GRFz peaks, contact time and stride period stored in the activity monitor compared well with force plate values (Figs 1-3 and Table 1).
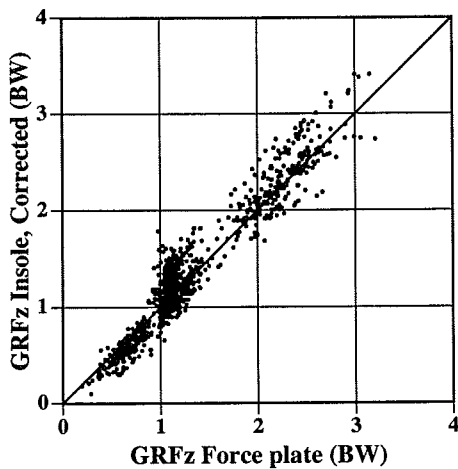
Figure 1: Comparison of corrected insole sensor filtered peaks and force plate peak GRFz generated for walking and running in 23 human subjects. Mean RMS error over all peaks was 0.185 BW (N = 980, R^2 = 0.929).
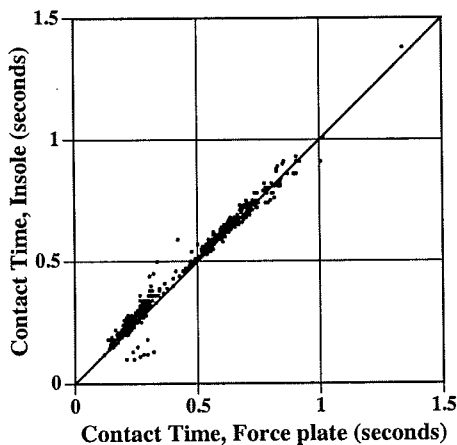

Figure 2: Comparison of insole and force plate contact times for walking and running at a range of speeds in 23 human subjects. Mean RMS error over all peaks was 0.036 seconds (N = 504, R^2 = 0.978).
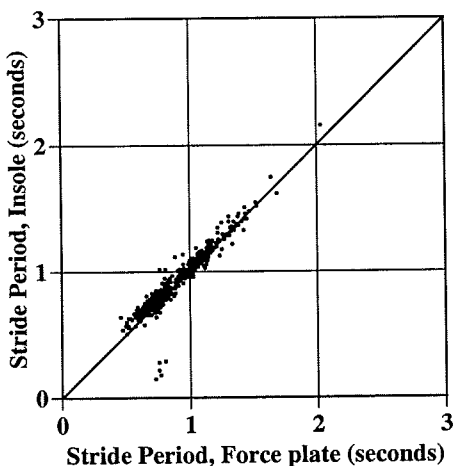

Figure 3: Comparison of insole and force plate stride periods for walking and running at a range of speeds in 23

human subjects. Mean RMS error was 0.079 seconds (N = 504, R^2 = 0.898).

	RMSE	N	R^2
Walk, Peak 1	0.126 BW	237.00	0.75
Walk, Mid	0.114 BW	236.00	0.70
Walk, Peak 2	0.249 BW	252.00	0.49
Run, Peak	0.21 BW	255.00	0.69
All peaks	0.185 BW	980.00	0.93
Walk, tc	0.025 s	254.00	0.97
Run, tc	0.044 s	250.00	0.67
All, tc	0.036 s	504.00	0.98
Walk, T	0.06 s	254.00	0.92
Run, T	0.095 s	250.00	0.28
All, T	0.079 s	504.00	0.90

Table 1: Results in RMS error found by comparing insole and force plate peak GRFz, contact time (tc), and stride period (T).

DISCUSSION

Using these data we intend to develop further correction methods to account for the observed error in insoles sensor values filtered and stored in the NASA GRF Activity Monitor. We are also interested in simplified activity monitoring techniques using tc and T as predictions and/or corrections on stored GRF data (Breit and Whalen, 1997).

REFERENCES

Whalen *et al.* (1993). *ASME BED,* **26**:535-538; Breit and Whalen (1994). *ASB,* 231-232; Bowley, Breit and Whalen (1998). *NACOB '98,* 169-170; Breit and Whalen (1997). *Med. Sci. Sports Exerc.,* **29(4)**:540-547.

ACKNOWLEDGEMENTS

SIMULATION-BASED DESIGN OF A POINTER FOR ACCURATE DETERMINATION OF ANATOMICAL LANDMARKS

A. Erdemir[1] and S. J. Piazza[1,2]

The Center for Locomotion Studies and Departments of [1]Kinesiology and [2]Mechanical & Nuclear Engineering, Penn State University, University Park, PA
Email: sjp12@psu.edu   Web: www.celos.psu.edu

INTRODUCTION

The locations of anatomical landmarks are often used during video-based motion analysis to establish local reference frames that are aligned with anatomical axes. The coordinates of such points may be determined by placing a marker on the skin above a bony prominence, but this technique is subject to errors due to skin movement (Lucchetti et al., 1998). An alternative technique was proposed by Cappozzo et al. (1995) who located anatomical landmarks using a pointer to which reflective markers were fastened. The tip of this pointer was placed at the desired point, and marker locations were then recorded using a motion analysis system. The tip point coordinates were determined from the known geometry of the pointer and the marker coordinates. While avoiding errors due to skin movement, the pointer described by Cappozzo et al (1995) is nevertheless subject to error due to inaccuracy inherent in the motion analysis system. Small errors in marker positions may combine to produce amplified error in location of the pointer tip (Figure 1).
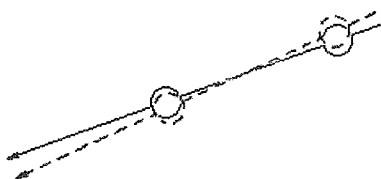

Figure 1: Pointer for locating anatomical landmarks. Errors in marker locations may cause larger errors at the tip.

The purposes of the present study were (*i*) to use a computer simulation to predict tip errors in hypothetical designs and (*ii*) to construct and test pointers suggested by the simulation results in order to compare actual tip errors.

COMPUTER SIMULATION

Computer simulation was used to predict tip location errors for various pointer designs. These errors were computed by perturbing marker coordinates and calculating the resulting change in tip location. Mean errors were computed from 1000 perturbation trials. The magnitudes of marker errors were assumed to be normally distributed (mean = 0 mm; SD = 1 mm), and the directions of marker errors were assumed to be randomly distributed in three-dimensions.

Errors associated with two pointer designs were simulated. The first design, proposed by Cappozzo et al. (1995) consisted of at least two markers arranged linearly; linear designs incorporating up to 10 markers were also considered. Tip locations were determined by fitting a line to the marker coordinates in three dimensions. Increasing the number of markers from 2 to 10 produced only a small decrease (~ 0.2 mm) in mean tip error. The second pointer design incorporated five markers arranged on a sphere whose center was the pointer tip. The tip location was determined by fitting a sphere of known radius to the measured marker locations. A t-test confirmed that the mean simulated error computed for the spherical design was significantly smaller (p < 0.0001) than that computed for the linear pointer (Table 1).

EXPERIMENTAL ANALYSIS

Physical prototypes of each pointer (Figure 2) were constructed to test for actual differences in tip location error.
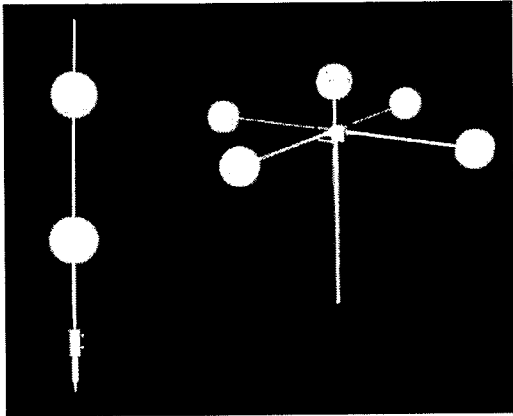

Figure 2: Linear and spherical pointer prototypes.

Four indentations were placed at known locations on a steel plate. A local coordinate system was established using markers attached to three of these points. For each of 35 trials performed using each pointer, the coordinates of the fourth point were determined using a six-camera Vicon 370 motion analysis system (Oxford Metrics, U.K.) to record marker locations for 3 seconds at 60 Hz. The measured global coordinates were averaged over each trial and then transformed into the local coordinate system. Tip errors were found by comparing the measured and known locations of this point (Table 1). As in the computer simulation results, a significant difference ($p < 0.0001$) was found between the mean errors for the two designs.

DISCUSSION

Consistent interpretation of data collected during motion analysis is dependent upon accurate measurement of anatomical landmarks. The computer simulation results of the present study suggested that a novel pointer in which markers are distributed on the surface of a sphere would exhibit less tip

location error than that of a previously proposed linear design. Experiments conducted using physical prototypes supported this conclusion.

Error magnitudes predicted using the simulation were different from those actually measured. We attribute these differences to: simulated error that does not reflect actual error in the motion analysis system; failure to account for machining errors in the simulation; and experimental error in establishing the local coordinate system.

This study demonstrates the utility of computer simulation for evaluating different pointer designs used for locating anatomical landmarks. This and previous studies (Lu and O'Connor, 1999) have shown that simulation of error that affects marker location is useful for improving the techniques and tools used to perform motion analysis.

REFERENCES

Cappozzo, A. et al. (1995). *Clin. Biomech.*, **10**, 171-8.
Lu, T.-W. and O'Connor, J.J. (1999). *J. Biomech.*, **32**, 129-34.
Lucchetti et al. (1998). *J. Biomech.*, **31**, 977-984.

ACKNOWLEDGMENTS

Table 1: Pointer tip errors (in mm) for the linear and spherical designs, both computed from 1000 simulated trials and measured in 35 experimental trials.

	simulation		experiment	
	linear	spherical	linear	spherical
mean	1.54	0.93	3.15	2.06
SD	0.99	0.54	0.74	0.50
max	6.62	3.05	4.53	3.30
min	0.08	0.05	1.70	1.25

A POLYURETHANE FOAM MODEL FOR CHARACTERIZING SUTURE PULL-THROUGH PROPERTIES IN BONE

Joseph E. Hale[1], Donald D. Anderson[1], and Greg A. Johnson[2]

[1]Biomechanics Laboratory, Minneapolis Sports Medicine Center, Minneapolis, MN
[2]Cardiac Assist Technologies, Inc., Pittsburgh, PA
Email: jhale1@fairview.org   Web: msmc.org

INTRODUCTION

Sternal closure following cardiothoracic surgery is most often performed using parasternal stainless steel sutures. Although infrequent (1-2%), complications are associated with significant morbidity and mortality. Instability and sternal dehiscence occur when the two edges of the sternum separate, typically as the sutures pull through the bone. The use of cerclage wire in orthopaedic applications gives rise to similar concerns.

Mechanical testing of new sternal closure techniques (Ozaki et al., 1998) in cadaveric tissue is problematic because of a high degree of inter-specimen variability and the scarcity of human cadaveric sterna. Synthetic foams have been used as a model of cancellous bone in other applications to increase test reliability and discrimination (Chapman et al., 1996).

The purpose of this study was to validate use of a polyurethane foam model for testing pull-through properties of stainless steel suture. Pull-through strength was tested in two densities of polyurethane foam at two different loading rates, and the results were compared to results in bone.

MATERIALS AND METHODS

Porcine ribs were chosen as a representative bone tissue based on their similarity in size and general anatomy to that of the sternum. To minimize variability, the anterior segments of six ribs were harvested from a single animal. Each rib segment was transected to yield two test specimens and both ends of each specimen were then potted in PMMA to be gripped for testing. The length of unsupported bone was 2 cm.

Two densities of polyurethane foam were evaluated. The low density (LDPU) foam had a density of 0.24 g/cc and the high density (HDPU) foam 0.48 g/cc. These values were chosen to represent low to mid-range density values for cancellous bone (0.09 to 1.26 g/cc; Gibson and Ashby, 1988). Uniform foam specimens of rectangular cross-section (8mm x 19mm) were tested in identical fashion as the porcine bone.

A 2.4 mm diameter hole was drilled through each specimen 1 cm from the lower edge. The PMMA blocks were attached to an MTS servohydraulic material testing system (Figure 1). A length of 0.79 mm diameter stainless steel suture was threaded through the test specimen, and the free ends of the suture gripped in a specially designed fixture also attached to the testing machine. Following application of a pre-load (nominally 5 N), the specimens were loaded in tension until failure of the test construct. Twelve specimens of each material were tested, six each at displacement rates of 10 and 100 mm/min. Load-elongation data, as well as failure mode, were recorded.
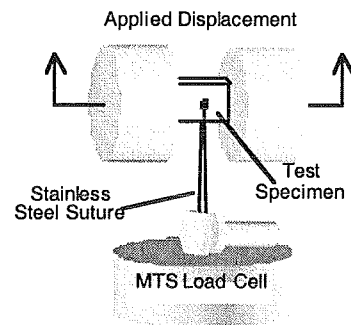

Figure 1: Suture pull-through test.

In addition to failure load and failure displacement, tangent and secant stiffness

values were computed from load-elongation data. Statistical comparisons of the means were made using ANOVA techniques. Post-hoc testing was performed using correction for multiple comparisons, and significance was assigned for $p < 0.05$.

RESULTS AND DISCUSSION

All specimens demonstrated typical load-deformation behavior (Figure 2), with bone specimens falling generally into two groups, one having a much greater stiffness and failure load than the other. This occurred despite our concerted efforts to limit tissue variability by using ribs from a single animal. The polyurethane foams, in contrast, showed a relatively small degree of variability. Loading rate did not have any significant effect upon the mechanical properties at the two rates studied.
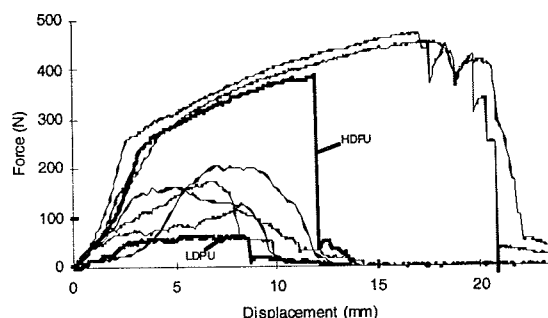

Figure 2: Representative curves for LDPU (lower bold line) and HDPU (upper bold line), in addition to six bone specimens from the 100 mm/min displacement group. Calculated mechanical parameters are

presented in Table 1, with different loading rate groups combined by test material.

Although only two densities of polyurethane foam were tested, it is clear that by varying density an acceptable match to the mechanical properties of suture pull-through in bone can be achieved. The two densities chosen effectively bracket the response seen in bone. This information allows one to study suture pull-through in both relatively strong and weak bone, depending upon the desired goal. Given that suture pull-through is principally a concern in patients with lower density cancellous bone, low density polyurethane specimens should be used to assess the pull-through properties.

REFERENCES

Chapman, J.R. et al. (1996) *Journal of Biomechanical Engineering*, **118**, 391-398.

Gibson, L. and Ashby, M. (1988) *Cellular Solids: Structure and Properties*, Pergamon Press, 316-331.

Ozaki, W. et al. (1998) *Annals of Thoracic Surgery* **65**, 1660-1665.

ACKNOWLEDGMENTS

Table 1. Mechanical properties in suture pull-through.

(n = 12 each)	Bone	LDPU	HDPU
Failure Displacement (mm)	11.0±5.0* (5.0-19.8)	6.9±0.9 (5.1-8.8)	11.3±1.3 (9.5-13.5)
Failure Load (N)	260.8 ± 157.8 (88.7-473.3)	61.6±3.2 (55.6-66.7)	372.8 ± 16.2 (349.0-397.2)
Secant Stiffness (N/mm)	23.2±8.2 (9.7-32.6)	9.0±1.3 (7.3-11.8)	33.1±2.5 (28.2-36.8)
Tangent Stiffness (N/mm)	40.3±20.5 (13.2-76.0)	16.9±2. (13.4-21.0)	54.3±7.9 (41.9-71.0)

* Tabulated values are the mean ± standard deviation and the range.

VALIDATION OF A METHOD OF TIMING FOOT CONTACT EVENTS

Jane Mickelborough[1], Marietta L. van der Linden[2], James Richards[2], Anthony R. Ennos[3]

[1] Department of Geriatric Medicine, The University of Manchester, Manchester, UK
[2] Department of Rehabilitation, The University of Salford, Salford, UK
[3] School of Biological Sciences, The University of Manchester, Manchester, UK
Email: jmickelb@fs1.ho.man.ac.uk

INTRODUCTION

Timing of foot contact events provides important information for studies of gait initiation (Jian Y et al.1993). The aim of this study is to validate the use of kinematic data, collected at 50Hz to define foot contact events during gait initiation.

PROCEDURES

Twelve normal adults, (7 men, 5 women), ages from 23 to 53 years (mean 35.6 years), were recruited. Retroreflective markers were fixed onto the swing foot shoe over the dorsum of the great toe and on the lateral heel, directly below the lateral malleolus. Subjects were requested to perform three series of ten gait initiations, in response to a cue light.

Simultaneous kinetic and kinematic data recordings of four discrete foot contact events were collected over an interval of 4 seconds. Kinematic data were collected using a five-camera 3D motion analysis system at a sampling frequency of 50 Hz, GRF was measured using a forceplate at a sampling frequency of 500 Hz. Data collection was synchronised by a trigger switch, which activated a cue light.

Four foot contact events were investigated in three series of ten tests. Each test series had a different starting position of the swing foot on or behind the forceplate:

- **Series 1.** To determine the timing of swing heel-off (SW HO), (figure 1a)
- **Series 2.** To determine the timing of swing toe-off (SW TO), (figure 1b)
- **Series 3.** To determine the timing of

swing heel contact (SW HC) and stance toe-off (ST TO), (figure 1c).

From the resultant GRF (F_R), heel contact was defined as the time of the first sample for which F_R is greater than 10N. Swing heel off, swing toe off and stance toe off were all defined as the time of the first sample (after the maximal F_R) which is smaller than 2N. The velocity of the heel or toe markers was derived from the vertical (y) displacement co-ordinates.
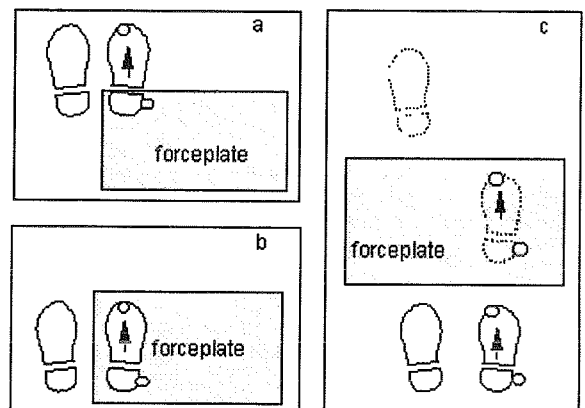
Figure 1: starting positions for a) SWHO, b) SW TO and 3 SW HC and ST TO

To test for inter-rater reliability, data were prepared for presentation to eleven raters. Four Matlab programs, one for each gait event, were written to allow a rater to determine the instant of the gait events from the kinematic data. For each subject, for each trial, both the vertical displacement (x 5) and the vertical velocity were plotted against time, and displayed on the computer screen. Raters were required to click on the velocity curve at a defined point

corresponding to each event. Raters were given a set of rules and diagrams (figure 2) that defined the specific point on the vertical velocity curve corresponding to the foot contact event being timed. The appropriate part of the displacement curve (grey) was first described. The precise point on the velocity curve (black) corresponding to the instant of the gait event was then defined. Each rater had a training session on these programs, using a full data set from a single subject, whose data was not used within the experimental series. Raters were then asked to define the times of events for the twelve experimental subjects.

kinematic rating method compared with the timing from kinetic data. Percentages for all differences that fall within the accuracy limits of the method are given in table 1. ST TO has a significantly greater incidence of all ratings of 0.02s or less, than any other event ($p \leq 0.0001$). Overall percentages for $diff_{ABS}$ ratings of 0.03s or less are 92.8% (SW HO), 91.2% (SW TO), 88.3% (SW HC) and 98.6% (ST TO).

ICC calculation for inter-rater agreement (Fleiss JL 1986) produced extremely high coefficients for inter-rater agreement ranging from 0.993 to 0.999, reflecting the precision of the instructions given.

black velocity, grey displacement toe marker, click instant of toe-off

SWING TOE-OFF
Displacement curve: toe marker is lowering slightly before going upwards. Toe-off is just before the lowest position (= zero velocity)
Velocity curve: point (one frame) before the curve goes up through the zero velocity.

Figure 2: The instructions given to raters for one foot contact event - swing toe-off.

RESULTS AND DISCUSSION

The absolute differences ($diff_{ABS}$) between the two methods (as a percentage of all ratings for12 subjects, 10 trials, 11 raters) describes the overall accuracy of the

SUMMARY

This timing method, based on kinematic data, is both valid and reliable for normal gait initiation and gait in normal adults, within the constraints imposed by the sampling frequency of 50Hz. Further work will be required to see if this method may be used directly, or may be adapted for use for pathological gaits and/or elderly subjects.

REFERENCES
Fleiss JL(1986) *The Design and Analysis of Clinical Experiments.* John Wiley and Sons.

Jian Y et al.(1993) *Gait and Posture* **1**, 9-22.

ACKNOWLEDGEMENTS

Table 1: For each rater, the % of all ratings with $diff_{ABS}$ ratings of between zero and less than/equal to 0.02s ($0 \leq 0.02s$)

	SW HO	SW TO	SW HC	ST TO
mean %	80.3	78.2	78.1	97.3

FUNCTIONAL GRIP STRENGTH: A PRELIMINARY STUDY ON THE COMPARATIVE EFFECTS OF FINE AND GROSS HANDLE SHAPE ATTRIBUTES

George B. Page & Don B. Chaffin
Center for Ergonomics, University of Michigan
Web: http://www.engin.umich.edu/dept/ioe/C4E

INTRODUCTION

As currently formulated, occupational biomechanical models like Garg and Chaffin's (1975) do not address "functional" grip strength of the hand, essentially considering the hand as a non-limiting structure in whole-body strength performance. Yet studies by Woldstad et al. (1995) and Fothergill et al. (1992) have shown that whole-body strength can be limited by hand performance in pull-type and across-hand exertions.

The bell-shaped effect of gross handle size upon clinical grip strength has been well documented (e.g., Pheasant and O'Neill, 1975), with its magnitude being 100% or greater. However, no studies have investigated whether this bell-shaped effect occurs with pull-type grip exertions or whether performance is as sensitive to gross handle size. And few since Westra (1973) have studied the effect of fine handle shape attributes, like rectangular handle edge radii. It is postulated that fine handle shape attributes may play a larger role in functional grip strength than gross handle shape, possibly due to performance inhibition associated with grip discomfort.

The purpose of this study of pull-type exertions is to: 1) investigate and compare the effect of gross and fine handle shape, 2) compare pull-type functional grip strength with "clinical" grip strength, and 3) investigate the relationship between hand discomfort, extrinsic finger flexor and extensor activity (as measured by surface EMGs), and strength performance.

PROCEDURES

Five right-handed subjects, 3 men and 2 women, ranging in age from 24 to 31 years, volunteered in this experiment. Functional grip strength was measured using a strength testing chair and handle jig system. Subjects assumed a seated posture allowing performance of a pull-type exertion with a straight-arm posture and braced feet. Pull-type strength was measured using the Caldwell et al. (1974) static strength testing regimen.

Clinical grip strength was also measured using a Jamar dynamometer and the testing methodology described by Mathiowetz et al. (1985).

Subjects' maximum pull strength also was separately measured using a wrist strap and hook that helped anchor the hand to the handle, minimizing the limiting effects of grip.

A fractional-factorial, repeated measures statistical design was employed. Rectangular-shaped handles with three levels of width and depth each (1.25, 2.5, and 10 cm) were tested along with two levels of edge radii (0.040 cm or "sharp" and 0.635 cm or "dull") on the 2.5 cm by 2.5 cm gross handle shape condition.

Hand discomfort was surveyed after each exertion using a simple rating scale. The activity of the extrinsic finger flexors and extensors were also measured using bipolar surface EMGs.

RESULTS AND DISCUSSION

Pull strength using the wrist strap exceeded all functional grip strength measurements by a range of 8 to 46%, confirming that the measured effects described below were attributable to hand performance.

Handle width significantly affected average functional grip strength ($p < 0.05$). Strength performance was greatest, but not statistically different for the 1.25 and 2.5 cm widths, 40.3 and 42.2 kg, respectively. The large, 10 cm handle width elicited a statistically significant ($p < 0.05$) lower performance of 36.2 kg. Overall, the size of the gross handle shape effect was 14%, suggesting a flat bell shape. The effect of handle depth was not significant.

For both males and females, the effect of fine handle shape was significant ($p < 0.05$). Average performance varied from 46.5 to 26.9 kg, for the "dull" and "sharp" conditions respectively for males. For females, performance varied from 38.8 to 32.5 kg for similar conditions. The magnitude of the effect was 72 % for males, 19% for females.

Average functional grip strength ranged from 81 to 147% of clinical grip strength, with performance always exceeding clinical grip strength under "dull" fine handle shape conditions.

The normalized average EMG activity of the extrinsic finger flexors and extensors behaved in a manner similar to that of average functional grip strength for males. The "sharp" edge condition had the lowest activity level (61% and 62% of MVC, respectively for flexors and extensors) and was significantly lower ($p < 0.05$) than the "dull" condition. The effect was not statistically significant for females.

Hand discomfort ratings correlated negatively with normalized finger flexor and extensor EMG activity with $r = -0.54$ and -0.44, respectively, and average functional grip strength -0.48.

SUMMARY

This study found that the effect of fine shape was much greater than the 10% reported by Westra (1973).

Strength performance decrements were associated with both discomfort ratings and extrinsic finger flexor and extensor muscle activity as measured by normalized EMGs under some circumstances. Collectively, these findings suggest that the activity of the extrinsic finger flexors the extensors may have been modulated by hand discomfort experienced by the subjects during their exertions, resulting in a reduction in functional grip strength. These findings also suggest that fine handle shape attributes may play a greater roll in pull-type grip strength performance than gross handle shape.

REFERENCES

Caldwell et all. (1974). A proposed standard procedure for static muscle strength testing. *American Industrial Hygiene Association Journal*, 35 (201-206).

Fothergill, D. M., Grieve, D. W., & Pheasant, S. T. (1992). The influence of some handle designs and handle height on the strength of the horizontal pulling action. *Ergonomics*, 35(2), 203-212.

Garg, A., & Chaffin, D. B. (1975). A biomechanical computerized simulation of human strength. *Transactions of the American Institute of Industrial Engineers*, 7, 1-15.

Mathiowetz, V., Kashman, N., Volland, G., Weber, K., Dowe, M., & Rogers, S. (1985). Grip and pinch strength: normative data for adults. *Archives of Physical Medicine and Rehabilitation*, 66(2), 69-74.

Pheasant, S. T., & O'Neill, D. (1975). Performance in gripping and turning. *Applied Ergonomics*, 6, 205-208.

Westra, L. F. (1973). *Some aspects of static and slow dynamic grip strength* Center for Ergonomics, University of Michigan.

Woldstad, J. C., McMulkin, M., Bussi, C.A. (1995). Forces applied to large hand wheels. *Applied Ergonomics*, 26(1), 55-60.

ANKLE AND FIRST METATARSOPHALANGEAL JOINT DORSIFLEXION IN CHILDREN WITH CLUBFOOT

T.C. Davies[1], G. Kiefer[3] and R.F. Zernicke[1,2]
[1]Dept. of Mechanical and Manufacturing Engineering, and [2]Dept. of Surgery,
McCaig Centre for Joint Injury and Arthritis Research, University of Calgary,
[3]Dept of Pediatric Orthopaedics, Alberta Children's Hospital, Calgary, Alberta, Canada.
Email: tcdavies@ucalgary.ca

INTRODUCTION

Clubfoot (CF) is a foot deformity due to an abnormal relation between tarsal bones, such that the navicular and the calcaneus are displaced medially around the talus (Turco, 1997). Many qualitative rating systems that have been established to measure function include a measure of ankle dorsiflexion (DF) obtained by passive motion with a goniometer or by radiographs.

CF children have abnormalities in toe-off (Hutchins, 1985) and thus the first metatarsal range of motion in addition to the lack of DF at the ankle may contribute to this lack of propulsion. The minimal range of first metatarsal DF is 60 - 65° so the hallux can act as a rigid lever for propulsion (Hetherington, 1990).

The purpose of this study was to examine the gait kinematics of bilateral CF patients who have undergone a posteromedial release to determine how active DF of the ankle and first metatarsophalangeal (MTP) joints affects DF during stance and subsequent push-off.

METHODOLOGY

Five bilateral CF subjects and five age and gender matched normal subjects participated in this study. Motion analysis using a four camera system was performed with three markers on the lower leg (head of fibula, mid-tibia, and distal fibula), three on the

foot (head of the first metatarsal, back of the calcaneus, and head of fifth metatarsal), and one on the tip of the first phalange.

Each subject was shown how to actively dorsiflex first the ankle followed by the toe. Each motion was recorded two times in a standing position with the leg extended and raised. Each subject also performed three trials at a self-selected pace along a walkway to obtain gait characteristics. Data were tracked using EVa software (Motion Analysis Corp., Santa Rosa) and analyzed using Kintrak (University of Calgary).

RESULTS

The amounts of active DF of the ankle and first MTP joints were significantly different between normals and CF patients (Table 1). These were compared to the amount of DF during the stance phase of gait (Figures 1 and 2).
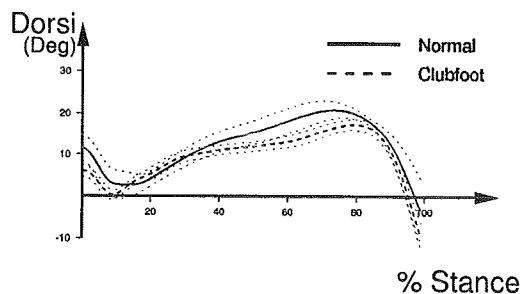

Fig. 1. DF at push-off was significantly (p ≤ 0.05) greater for normal subjects than for clubfoot by 3 °.
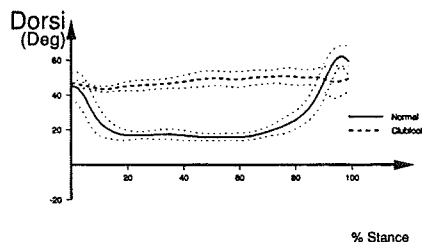
Fig. 2. DF of the MTP joint at toe-off was significantly less in the CF subjects. For two CF subjects, no DF at push-off was observed for either foot.

DISCUSSION

Karol *et al.* (1997) found no significant decrease in the range of motion of the ankle of the CF during gait as compared to the contralateral. The ankle DF of our CF subjects was significantly lower than normals when measured both during the stance phase of gait and during active motion.

It has been shown that there is a correlation between function and amount of DF of the ankle based on an outcomes questionnaire (Hutchins, 1985). We also found a correlation between the amount of DF as determined by active motion and by gait (Pearson's Coefficient= -0.393). This may have been due to the distortion of the talar dome or the navicular, but as radiographs were not used, this was not verified.

As with our study, Mann and Hagy (1979) found that the great toe was typically extended 20° from the axis of the metatarsals during the flatfoot phase of gait and was dorsiflexed 70-90° during push-off

for the normal population. Our CF subjects exhibited extension during the flatfoot phase, but did not dorsiflex to the same degree during push-off. It is possible that the windlass mechanism of the plantar aponeurosis (Hicks, 1954) was not as effective in the CF due to the abnormal musculature.

CONCLUSIONS

Abnormal propulsion of CF subjects may be due to an insufficient DF motion of the first metatarsal, preventing the hallux from acting as a rigid lever for push-off in addition to the insufficient range of DF at the ankle joint.

REFERENCES

Hetherington, V.J. (1990) *J. Foot Surgery* **29**(3), 218-222.

Hicks J.H. (1954). *J. Anat.* **88**, 25-31.

Hutchins et al. (1985) *J. Bone & Joint Surg.* **67B**:5, 791-799.

Karol L.A. et al. (1997). *J. Ped. Orthop.* **17**, 790-795.

Mann R.A., and Hagy J.L. (1979). *Clin. Orthop. & Rel. Res.* **142**, 24-49.

Turco V.J. (1981) In *Clubfoot*, Churchill Livingstone, New York.

Table 1: Dorsiflexion at the ankle during active motion. (* p≤ 0.05)

Dorsiflexion (°) (mean ± SD)	Normal Subjects n=5 / group (10 limbs)	Clubfoot Subjects n=5 / group (10 limbs)
Active Ankle	22.9 ± 7.23	5.57 ± 5.92 *
Toe	65.1 ± 12.2	54.9 ± 13.3 *

PROPULSION FORCES AND MRI EVIDENCE OF SHOULDER IMPAIRMENT

Alicia M. Koontz[1,2], Michael L. Boninger[1,2], Jeff Towers[3], Rory A. Cooper[1,2], Mark A. Baldwin[1,2]

[1]Dept. of Rehab. Science and Technology, University of Pittsburgh, Pittsburgh, PA 15261
[2]Human Engineering Research Laboratories, Highland Drive VA Medical Center, Pittsburgh, PA
[3]Dept. of Radiology, University of Pittsburgh, Medical Center, Pittsburgh, PA
Email: amkst63@pitt.edu

INTRODUCTION

The prevalence of shoulder pain and injury in manual wheelchair users (MWUs) is alarmingly high. Bayley et al. found 24% of veterans with spinal cord injury (SCI) had signs of shoulder impingement upon physical examination. Further examination using x-rays and arthrography of the veterans with signs of impingement revealed rotator cuff tears in 65% (Bayley, 1987).

While extremely mobile, the shoulder joint is relatively unstable and relies on surrounding ligaments and tendons to provide its support. During wheelchair propulsion, forces on the pushrim directed toward the hub are necessary to provide friction between the hand and pushrim. However, these forces, acting equal and opposite are transmitted up through the arm and shoulder joint. Repetitive application of large upward forces at the shoulder joint has been implicated as a causative of shoulder pain and injury.

The purpose of this study was to determine the relationship between wheelchair pushrim forces and evidence of shoulder impairment. We hypothesize that MWUs with a higher degree of shoulder impairment will propel with greater pushrim forces.

PROCEDURES

Twenty-six (16 males and 10 females) experienced MWUs with a spinal cord injury at the T-4 level or below enrolled in the study. The average age and years post injury was 34.0 ± 7.6 years and 11.6 ± 5.5 years, respectively.

A standardized MRI examination designed for detection of rotator cuff abnormalities was conducted on both shoulders. Specific sequences were designed to evaluate peritendonal edema, tendon degeneration and tendon tear. The interpretation of the images was made by a musculoskeletal radiologist who was blinded to the study.

Subjects' own personal wheelchairs were fitted bilaterally with SMART[Wheels], force and torque sensing pushrims (VanSickle, (1995). Wheelchairs were secured to a dynamometer with a resistance comparable to that of a tile floor. Participants were instructed to propel at two steady-state speeds: 0.9 m/s (2mph) and 1.8 m/s (4mph) for 20 seconds during which force data was collected.

Shoulder Magnetic Resonance Imaging (MRI) findings were assessed using a modified grading scale of pathology based on accepted radiological criteria (Kjellin, 1991). Pathology of the following anatomical structures was graded: rotator cuff tendons, acromioclavicular joint (degeneration joint disorder (ACDJD) and edema/bursitis), acromion (edema), and coracoacromial (CA) ligament (edema/thickening). In addition, MRI scores for each individual structure were totaled to

produce a single summary variable.

Three-dimensional forces, F_x, F_y, F_z, were obtained from the SMART^{Wheel}. F_x and F_y were then transformed to a force directed tangential to the pushrim, F_t, and a force radial to the pushrim, F_r. The resultant pushrim force, F, is defined as:

$$F = \sqrt{\left(F_x^2 + F_y^2 + F_z^2\right)} = \sqrt{\left(F_t^2 + F_r^2 + F_z^2\right)}$$

Peak magnitudes of the F, F_t, F_r, and F_z forces were determined for the first five strokes and then averaged across strokes. A two-tailed bivariate correlation was performed on the group to determine the relationship between pushrim forces and MRI findings. The Pearson correlation coefficients were calculated on a confidence level of $p < 0.05$.

RESULTS AND DISCUSSION

MRI results for both left and right sides were highly correlated ($r > 0.95$) and were combined to reduce the number of variables for statistical analysis. In addition, peak forces were highly correlated between right and left sides and across both speeds ($r > 0.8$). Therefore, summary force components were determined by combining side-to-side peak forces and then averaging them across speeds. Statistically significant correlations are shown in Table 1. A sample scattergram is shown in Figure 1.

The function of the CA ligament is to inhibit superior displacement of the humerus from the glenoid fossa of the scapula. Performing various upper extremity activities, like wheelchair propulsion and transfers, tend to force the head of the humerus up into the joint which can over time result in impingement under the acromioclavicular (AC) arch and subsequent inflammation. This study suggests that reducing forces during wheelchair propulsion may minimize the likelihood of developing edema and

thickening of the CA ligament as well as slow down degeneration of the AC joint.

Table 1 - Correlation Coefficients between Pushrim Forces and MRI findings

MRI Variable	Force Component	r value	Significance $p < 0.05$
ACDJD	Resultant Force (F)	0.399	0.044
CA Ligament Edema/Thickening	Tangential Force (F_t)	0.392	0.048
	Radial Force (F_r)	0.420	0.033
Total MRI	Resultant Force (F)	0.397	0.045
	Radial Force (F_r)	0.415	0.035
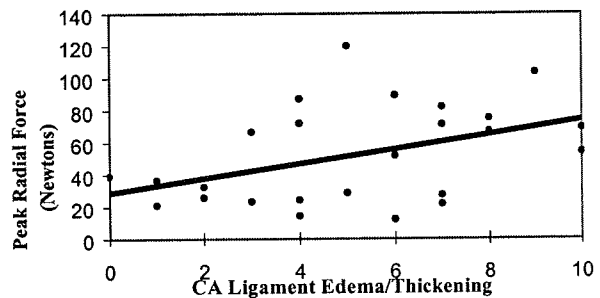
Figure 1: Scattergram of peak radial force and CA abnormality at an average velocity of 1.75 m/s

REFERENCES

Bayley J.C. et al. (1987). *J Bone Joint Surg* 69:676-678.
VanSickle, D.P. et al. (1995). *Proceedings 18th Annual RESNA Conference.* 352-354.
Kjellin I et al. (1991). *Radiology* 181:837-841.

An Investigation of Alternate ASIS Marker Placement on the Kinematics & Kinetics of Gait: A Simulation of Analysis on Obese Subjects

Gregory Rash, EdD[1], Peter Quesada, PhD[2], Craig Roberts, MD[3] & Chase Herringshaw[2]

[1]Gait & Biomechanics Laboratory, Frazier Rehab Center, Louisville, KY

[2]Department of Mechanical Engineering, University of Louisville, Louisville, KY

[3]Department of Orthopaedic Surgery, University of Louisville, Louisville, KY

Email: gsrash01@pol.net   Web: http://www.gcmas.org/frazier

INTRODUCTION

Most gait labs use either the Helen Hayes, modified Helen Hayes or Cleveland Clinic marker sets for gait analysis. These marker sets create a virtual marker for the hip joint center based on the locations of the bilateral ASIS markers and sacral marker. Typically, either the method described by Campbell, et al (1988), Davis, et al (1991), Kadaba, et al (1990) or a derivation of these techniques are used. These methods assume that you are able to place a marker directly over the bilateral ASIS, however, in the case of obese, or pregnant patients, this is impossible. Typical options are: move the marker laterally (at the same level as the ASIS), place the marker on abdomen so it is displaced anteriorly at the level of the ASIS, or place the marker on the abdomen, trying to keep the marker over the ASIS, but in the same plane formed by the bilateral ASIS and sacral markers. Another issue is if the markers are now moved away from the ASIS due to underlying tissue, should one try to correct for the displacement by changing the percentages used in the software, or by remeasuring the intra-ASIS or ASIS to trochanter distances. A survey of 10 gait labs indicated that shifting the markers laterally with no change in percentages or measurements was the most widely used, although all three described techniques were used by at least a single lab. The purpose of this study was to simulate ASIS marker placement on obese subjects and investigate which strategy would affect the kinematics and kinetics the least.

PROCEDURES

A 5 camera (60 Hz) Qualisys motion analysis system and Biopac 16 channel analog collection system were used to collect the 3D coordinate data and forceplate data. A single gait trial from three normal adult males of negligible body fat (< 6mm skinfold measurment directly over ASIS) were used in this study. After 3D coordinate data were obtained, the data were altered to yield coordinate data which displaced the ASIS markers laterally or anteriorly in the global reference frame. Trials representing lateral ASIS displacements of 2 cm, 5 cm and 10 cm and anterior displacements of 5 cm and 10 cm were manufactured. From these 3D coordinate and forceplate data AutoGait3D software was used to calculate the 3D kinematics and kinetics.

AutoGait3D gives the option of using either the Campbell, et al (1988) or Davis, et al (1991) method of determining the hip joint center. All data were ran through AutoGait3D using both methods of determining the hip joint center to see if one

was more susceptible to movement of the ASIS markers. The Campbell method needs no subject anthropometric data as it calculates the hip center based on entered percentages. These percentages relate to the calculated distances between the ASIS markers and are then used to move posterior, lateral and down from the pelvic system origin to find the hip center. Our lab uses 22%, 25% & 33% for these respectively. For the Davis method one enters the measured intra-ASIS distance, ASIS to trochanter distance and leg length of the subject in order to determine the hip center. Since we could manipulate the distances with this method, we ran the anteriorly displaced data a second time after adding the displaced amount to the measured ASIS to trochanter distance to determine if this helped in the calculations.

RESULTS AND DISCUSSION

Lateral movement of the ASIS markers, regardless of the distance, showed the least amount of change in the kinematics and kinetics for both the Campbell and Davis hip joint center methods. It was difficult to determine any difference in the overlaid plots for most of the typically viewed kinematics & kinetics plots. Both methods showed a slight reduction in the pelvic obliquity plots (2-3 degrees) and slightly less hip abduction (2-3 degrees). For sagittal plane kinetics, the hip moment and power changed very slightly for both methods, however in different directions. For the anteriorly displaced markers, the results were not as robust. Both methods were equally affected. Pelvic tilt graphs were DC shifted 2-5 degrees, Hip flexion

graphs were DC shifted 10-15 degrees, knee flexion graphs shifted 5-10 degrees, and hip and knee rotation graphs DC shifted 10-20 degrees. The hip flexion/extension moments and powers deviated in the stance phase by 50-75 Nm and 100-150 Watts respectively. For the Davis method, one can use the measured distance from the trochanter to the ASIS marker as the ASIS-trochanter input value and decrease the error significantly. There were still very slight differences in the hip and knee rotation angles, hip abduction/adduction angles. The largest differences were in the pelvic tilt and hip flexion angles as they still showed DC shifts of 2-5 degrees. The moment and power graphs became indistinguishable with respect to marker anterior displacement much like they were when the markers were displaced laterally. One should be able to fix the pelvic tilt shift by trying to align the ASIS marker so it is in the plane formed by the bilateral ASIS markers and sacral marker. However, given the robustness of the laterally displaced markers in this study with either method used, these investigators believe it would not be worth the researchers time to try to determine the pelvic system plane and then attempt to align the ASIS markers in this plane in-line with the ASIS. At best it will only be as good as the laterally displace marker on kinematics while saving the researcher valuable time and potential accuracy if the correct plane in not determine correctly.

REFERENCES
Campbell, et al., *ASB Proceedings*, 1988.
Davis, et al., *J. Human Movement Science* **10(5)**, 1991.
Kadaba, et al., *J. Orthopaedic Research* **8(3)**, 1990

PARKINSON'S DISEASE GAIT KINEMATICS: EFFECTS OF CADENCE-SETTING THROUGH RHYTHMIC AUDITORY STIMULATION

S. M. Elliott, R. W. McCoy, A. S. Joyce, and R. Kohl

Department of Kinesiology, College of William and Mary
Williamsburg, Virginia
Email: rwmcco@facstaff.wm.edu

INTRODUCTION

Significant changes in gait cycle parameters have been observed in individuals with Parkinson's Disease (PD) during walking to rhythmically accentuated music (McIntosh et al., 1997; Thaut et al., 1996). These findings are consistent with previous studies that concluded that persons with PD compensate for basal ganglia malfunction by relying more heavily on external cues to guide movement, even in patterns that are well learned (Georgiou et al., 1993). By removing the instrumental music portion of the rhythmic auditory stimulation, the metronome beat itself may be further emphasized as the salient rhythmic external cue.

Therefore, the purpose of this study was to investigate the acute effects of rhythmic auditory stimulation (metronome only) on the walking mechanics of individuals with PD.

METHODS

Seven male subjects with Parkinson's disease volunteered as subjects in this study. Their average age, height, and mass were 75.2 yrs., 1.77 m, and 79.6 kg, respectively. The subjects were tested during two morning sessions: 1) without their normal medications for PD (NO MED) and 2) with their medications (MED). The average Hoehn and Yahr scale ratings were 1.57 for the NO MED session and 1.43 for the MED session. The subjects completed three 20-m walking trials on a smooth surface per condition. The conditions consisted of self-selected cadence (SS), walking to a metronome set to the subject's self-selected cadence (SS/M), and walking to a metronome set 15% faster than the self-selected cadence (+15%/M). Four synchronized video cameras (2 per side) operating at 60 pps recorded the subjects' walking patterns. The videos were manually digitized and analyzed using the Peak Performance Technologies, Inc. Motion Measurement System. Data were smoothed using a Butterworth digital filter set at 8 Hz. to minimize high frequency noise.

Statistical analysis included two factorial MANOVAs with repeated measures (p-value of 0.05). The first MANOVA was used to examine the SS and SS/M conditions with MED and NO MED. The second MANOVA was used to examine the SS/M and +15%/M conditions with MED and NO MED.

RESULTS AND DISCUSSION

Under the +15%/M condition the subjects increased walking velocity as expected. However, stride length was increased for the left leg but not the right leg (Table 1). Additionally, an increase in shoulder range of motion indicating arm swing was observed for

the left side but not for the right side. As the majority of subjects in this study displayed decreased function on the right side, these results visually represent the unilateral effects of mild PD. A significant increase in peak anterior trunk lean was observed when the subjects walked at the +15%/M condition. This may indicate a mechanism to increase walking speed.

REFERENCES

Georgiou, N., et al. (1993). *Brain,* 116, 1575-1587.

McIntosh, G.C., et al. (1997). *Journal of Neurology, Neurosurgery, and Psychiatry,* 62, 22-26.

Thaut, M.H., et al. (1996). *Movement Disorders,* 11(2), 193-200.

ACKNOWLEDGEMENTS

Table 1: Kinematics of Parkinson's Disease Gait. Mean (SD). Values in boldface print represent significant differences between conditions.

RIGHT:	MED.			NO MED.		
	SS	SS/M	+15%/M	SS	SS/M	+15%/M
Vel. (m/s)	1.36 (.35)	**1.20 (.25)**	**1.42 (.30)**	1.16 (.27)	**1.15 (.21)**	**1.38 (.22)**
Stride Length (m)	1.35 (.19)	1.46 (.21)	1.42 (.22)	1.26 (.24)	1.27 (.22)	1.32 (.23)
Stride Rate (strides/s)	0.90 (.09)	**0.90 (.07)**	**0.99 (.10)**	0.92 (.09)	**0.91 (.06)**	**1.02 (.05)**
Maximum Ant. Trunk Angle (deg)	4.7	**4.4**	**5.6**	4.7	**5.4**	**6.9**
Shoulder ROM (deg)	27.9	28.2	28.4	25.6	23.1	23.5

LEFT:	MED.			NO MED.		
	SS	SS/M	+15%/M	SS	SS/M	+15%/M
Vel. (m/s)	1.17 (.36)	**1.18 (.31)**	**1.36 (.37)**	1.20 (.26)	**1.20 (.17)**	**1.42 (.18)**
Stride Length (m)	1.29 (.32)	**1.31 (.29)**	**1.37 (.31)**	1.30 (.19)	**1.33 (.17)**	**1.40 (.18)**
Stride Rate (strides/s)	0.90 (.08)	**0.90 (.07)**	**0.99 (.10)**	0.92 (.09)	**0.90 (.06)**	**1.02 (.05)**
Maximum Ant. Trunk Angle (deg)	5.9	**5.4**	**6.7**	4.6	**5.3**	**6.1**
Shoulder ROM (deg)	25.1	**23.1**	**23.6**	21.4	**19.4**	**23.2**

Author Index

Hughes	184	Lerner	198	Ochia	90
Hurwitz	134	Les	130	Ok	166
Hustosky	92 , 136	Levison	108	Owings	228, 238, 240
		Li	196		
Jaramaz	74, 108	Lipsitz	120	Page	292
Johnson, G.A.	86, 288	Liu	120	Pandy	48
Johnson, M.P.	56	Livingston	62, 64	Papageorgiou	202, 278
Jones	264	Lohrmeyer	180	Pattin	258
Joo	70	Loisel	262	Pattishall	96
Joshi	106	Long	268	Pavol	238, 240
Joyce	300	Lopez	196	Perucchio	198
		Lu	82	Peterman	156
Kang, J.D.	214	Lust	270, 272	Peterson	256
Kang, S.B.	104			Peura	194
Karduna	56	Magovern	86	Pfaeffle	40
Kastner	162	Malloy	178	Piazza	156, 200, 286
Kaufman	52, 184, 186	Manal	78, 82	Pilkey	34, 174
Kayes	152	Manson	40	Pincivero	234
Keith	38	Mark	234	Plewes	72
Kenamond	92	Marsh	98	Post	280
Kerrigan	46	Martin	94, 100	Prendergast	276
Keshner	256, 258	Matsumoto	66, 186	Puttlitz	208
Keyak	130	Matsuo	140		
Kiefer	294	McClay	50, 218	Quesada	298
Kilgore	38	McClure	56		
Kim, B.S.	104	McCoy	300	Ramsay	72
Kim, H.J.	104	McGarry	112	Rash	298
Kim, K.T.	104	McGee	224	Rastogi	114
Kim, S-H.	166	McLean	232	Redfern	244, 248
King	150	McMahon	210	Renstrom	194
Kish	136, 164	McMaster	34	Requejo	76
Klein	138	McNitt-Gray	76, 148	Richards	290
Kohl	300	Meaney	172	Richardson	120
Komistek	170, 264	Mickelborough	290	Riley, P.O.	46
Koontz	296	Miller, D.I.	142	Riley, S.P.	106
Korff	230	Miller, F.	106	Rimnac	158
Kozak	180	Millikan	188	Roberts	298
Kram	124, 126, 216	Mochizuki	260	Robinovitch	246
Krischak	132	Moon, H.J.	70	Robinson	128
Kuenster	190	Moon, S.H.	214	Roe	102
Kuo, A.D.	124, 126	Morrey, B.	184	Ruiz	114
Kuo, C.	42	Morrey, M.	184		
Kwon	70	Morrow	186	Sabick	182
		Morse	188	Sakai	214
Lacroix	276	Murray	38	Salem	236
Lariviere	262	Musolino	244	Samani	72
Latash	250, 254, 260	Myers	210, 266	Sanford	212
Laughton	50, 218			Santare	106
Laule	132	Natarajan	204	Santrock	206
Lawson	44	Neale	110	Sarojak	170
Leblanc	262	Neu	36	Scholten	220
Ledoux	172	Nikou	108	Schreiber	34
Lee, J.	114	Norman	92, 136, 154,	Schultheis, A.	114
Lee, S-J.	166		164, 206, 280	Schultheis, L.	114
Lee, Y.C.	70	Noseworthy	52	Scifert	208
Lehman	258			Scudder	224
Lepage	262	O'Driscoll	110		

Sharkey	44, 94, 156, 176, 178	Wu, Y.P.	268
		Wu, Z.Z.	268
Shaw	226	Wunderlich	68
Shen	78	Wurster	270
Shin, J-W.	166		
Shin, J.W.	70	Yeni	154
Shiratori	254	Yoon	104
Simoneau	54	Young	236
Slijper	250		
Smith, G.	146	Zaharias	162
Smith, K.R.	96	Zatsiorsky	260
Snedeker	282	Zecevic	142
Spaulding	62	Zernicke	294
Srinivasan	160	Zhang, H.	198
Stanford	162	Zhang, Y.	128
Stauber	274	Zuelzer	112
Stergiou	220		
Sternad	58, 60		
Stikeleather	102		
Stover	100		
Taylor, G.W.	142		
Taylor, M.A.	280		
Tencer	90		
Thomas	162		
Thompson, D.	80		
Thompson, S.M.	116, 226		
Tillman	96		
Tomaino	40		
Toolan	168		
Totoribe	208		
Totterman	198		
Towers	296		
Towles	30		
Traynelis	208		
Valero-Cuevas	30		
Van der Linden	290		
Vint	116, 226, 232		
Walker	52, 186		
Wang, M.Y.	236		
Wang, X.H.	268		
Wayne	112		
Weiss	40		
Welch	152		
Welsch	162		
Whalen	284		
Willems	274		
Williams	50, 218		
Wilson	210, 266		
Withrow	202, 278		
Wolf	132		
Wolfe	36		
Woo	40, 202, 214, 278		
Wu, G.	242		

ASB Corporate Members

Aircast, Inc.

Depuy, Inc.

Orthofix

Tekscan, Inc.

MotionAnalysis

"True" 3D Real-Time for Sports, Animation, Ergonomics, Therapy and Biofeedback